Characterisation and pharmacological regulation of GLP-1-mediated glucose homeostasis

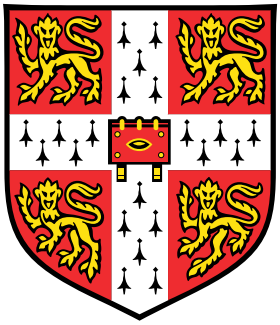

Ho Yan Yeung
Department of Pharmacology
University of Cambridge

Thesis submitted for the degree of:
Doctor of Philosophy

Supervisor:
Dr Graham Ladds

Fitzwilliam College

September 2020

Declaration

This thesis is the result of my own work and includes nothing which is the outcome of work done in collaboration except as declared in the Acknowledgements and specified in the text. It is not substantially the same as any that I have submitted, or, is being concurrently submitted for a degree or diploma or other qualification at the University of Cambridge or any other University or similar institution except as declared in the Acknowledgements and specified in the text.

I further state that no substantial part of my thesis has already been submitted, or, is being concurrently submitted for any such degree, diploma or other qualification at the University of Cambridge or any other University or similar institution except as declared in the Acknowledgements and specified in the text. It does not exceed the 60,000 word limit, exclusive of tables, footnotes, bibliography, and appendices, for the Biology Degree Committee.

Ho Yan Yeung

Abstract

Thesis title: Characterisation and pharmacological regulation of GLP-1-mediated glucose homeostasis

Author: Ho Yan Yeung

Type 2 diabetes mellitus (T2DM) is characterised by the hormonal imbalance of insulin and glucagon, leading to dysfunctional glucose homeostasis. Glucagon-like peptide 1 (GLP-1), which is an incretin hormone, activates the predominantly Gαs-coupled glucagon-like peptide 1 receptor (GLP-1R), which is a class B G protein-coupled receptor (GPCR), to mediate glucose homeostasis. It does so by promoting glucose stimulated insulin secretion (GSIS) in the pancreatic β cells and inhibiting glucagon secretion in the pancreatic α cells. Given its proven clinical efficacy in reducing long term blood glucose level, GLP-1-based treatments, such as exenatide and liraglutide, have been widely used in T2DM patients.

However, in contrast to the well-studied phenomenon of how GLP-1 enhances GSIS, the mechanism of how GLP-1 regulates glucagon secretion is still unclear. Therefore, the aim of this work is to shed new lights on how GLP-1 mediates its glucagonostatic action. To do so, the signalling properties of GLP-1 and its closely-related peptide hormones, namely oxyntomodulin (OXM), glucagon (GCG), glucose-dependent insulinotropic polypeptide (GIP), and its metabolite, GLP-1(9-36)NH_2, were examined in recombinant cell lines and rodent clonal α and β cell lines using cAMP functional assaying technique. It was demonstrated that these glucagon-like peptides, including GLP-1(9-36)NH_2 yet except GIP, can activate both GLP-1R and glucagon receptor (GCGR), which is structurally analogous to GLP-1R. Furthermore, GLP-1R, despite its very low expression in the mouse αTC1.6 cell line detected through semi-quantitative RT-PCR studies, is found to play a critical role in directly inhibiting glucagon secretion upon GLP-1 activation through performing glucagon secretion antagonism studies. More importantly, the physiologically abundant GLP-1 metabolite is discovered to play a glucagonostatic role

in the mouse glucagonoma cell line via the direct actions of GLP-1R and GCGR, an observation that has not yet been documented. Therefore, this thesis provides evidence of how GLP-1 and its metabolite are actively involved in their glucagonostatic actions via direct activations of GLP-1R and GCGR.

Another aim of this work is to identify viable pharmacological regulator of GLP-1-mediated glucose homeostasis through the action of positive allosteric modulator (PAM). Here, compound 249, which was identified previously as a small molecule GLP-1R PAM, was further pharmacologically validated using various signal transduction assaying techniques in recombinant cell lines. It was also demonstrated that compound 249 works independent of the cysteine-347 residue on the GLP-1R, an amino acid residue which has been previously shown to be instrumental for the actions of another GLP-1R agonist-PAMs. More importantly, compound 249 demonstrates robust potentiation of GLP-1 and OXM-augmented GSIS in the rat INS-1 832/3 insulinoma cell line and *ex vivo* isolated mouse islets, substantiating the potential of compound 249 to be further developed as a novel T2DM treatment.

Overall this thesis presents new evidence on the direct involvement of GLP-1R on GLP-1-regulated glucagon secretion in the pancreatic α cells and illustrates compound 249 as a PAM to promote GLP-1 mediated GSIS. The findings in this thesis will be used for future design of safer and more efficacious T2DM treatments.

Acknowledgements

The completion of this thesis could not have been possible without the help and guidance from many people. Their contributions are sincerely appreciated and gratefully acknowledged. First of all, I would like to express my deepest gratitude to my MPhil and PhD supervisor, Dr Graham Ladds, for his immense amount of help on thesis writing and guidance throughout years, showing me the fascinating wonder of GPCRs, and more importantly providing the perfect springboard for me to kickstart my career as a scientist. I would also like to thank Dr Taufiq Rahman (Department of Pharmacology, University of Cambridge) for performing the *in silico* docking studies and compound screening, as well as his continuous support throughout my PhD training. I would also like to thank Mr Kourosh Saeb-Parsy and Dr Nikola Dolezalova (Department of Surgery, University of Cambridge) and Luke Pattison (Department of Pharmacology, University of Cambridge) for their assistance with mouse pancreas dissection. The virtual screening work for compound 249 analogues by the delightful summer project student, Miss Kathleen Bowman, must also be sincerely acknowledged. Special thanks must be given to Dr Kerry Barkan for her advice on data analysis and other techical issues, and Dr Matthew Harris for his assistance with performing the NanoBiT G protein dissociation assay; their help and support, from personal to professional levels, throughout the years are sincerely appreciated. I would also like to thank Ashley Clark, Sabrina Carvalho, Abigail Pearce and Anna Suchankova for their continuous support, as well as being wonderful lunch companions. Sincerest thanks must be given to my dearest lab partner and loyal friend, Dewi Safitri, for her limitless support on going through the ups and downs throughout the PhD journey and her enjoyable companionship during Sunday and occasional evening laboratory sessions. I would also like to thank my PhD viva examiners, Dr Alejandra Tomas (Imperial College London, U.K.) and Dr Lesley MacVinish for their valuable advice and suggestions on how to further improve the scientific content and presentation of this last version of thesis. I would also like to thank my funding bodies, the Cambridge Trust and the

Rosetrees Trust, for awarding me scholarships and consumables to enable my smooth professional training as a researcher. I would also like to thank Fitzwilliam College, where I have the pleasure to call home in the past four years and for awarding me with scholarships to support my pursuit of non-academic related interests.

I would like to extend my sincerest gratitude to my parents. Without their encouragement, the dream of obtaining a doctorate from Cambridge would be out of reach. Special thanks must also be given to Marco Egle, for his patience and relentless support throughout my PhD journey, and his family, especially Uli and Marie-Luise, whom have provided me with a warm shelter and immense support during my write-up period in Freiburg, Germany. I would also like to thank all my friends whom I am fortunate enough to have met in Cambridge, especially to Camilla Ascenelli and Ru Wang, for their support, tolerance and wisdom. Last but not least, I would like to dedicate this thesis to my grandpa, whom would have loved to witness the birth of this work in person.

Contents

List of Figures

List of Tables

List of Abbreviations

1D	One-dimensional
2D	Two-dimensional
3D	Three-dimensional
ADP	Adenosine diphosphate
ATCM	Allosteric ternary complex model
ATP	Adenosine triphosphate
b-cAMP	Biotin-cAMP
C11	Compound 11
C2	Compound 2
cAMP	3′-5′-cyclic adenosine monophosphate
CHO	Chinese hamster ovary K1 cells
CHO-GLP-1R	CHO cells stably expressing GLP-1R
clogP	Log of partition coefficient
CRE	cAMP response element
DAG	Diacylglycerol
DMSO	Dimethyl sulfoxide
DPP-IV	Dipeptidyl peptidase-IV
E_{max}	Maximum response of an agonist

E_{min}	Minimum response of an agonist
EC_{50}	Concentration at which 50% of the maximal response is reached
ECL	Extracellular loop
EPAC2	Exchange protein activated by cAMP 2
ERK1/2	Extracellular signal-regulated kinase 2
ET_{combo}	Electrostatic combo score
Eu-SA	Eu-W8044 labelled streptavidin
FBS	Fetal bovine serum
FDA	Food and Drug Administration (U.S.)
GCGR	Glucagon receptors
GDP	Guanosine diphosphate
GEF	cAMP-guanine nucleotide exchange factor
GIP	Glucose-dependent insulinotropic peptide
GLP-1	Glucagon-like peptide-1
GLP-1 RA	Glucagon-like peptide-1 receptor agonists
GLP-1R	Glucagon-like peptide-1 receptors
GLP-2	Glucagon-like peptide-2
GLUT-2	Glucose-transporter 2
GPCR	G protein-coupled receptors
GRK	G protein-coupled receptor kinase 2
GSH	Glutathione
GSIS	Glucose-stimulated insulin secretion
GTP	Guanosine-5′-triphosphate
Hb	Haemoglobin

HEK	Human embryonic kidney cells
HTS	High throughput screening
IBMX	3-isobutyl-1-methylxanthine
ICL	Intracellular loop
IP_3	Inositol triphosphate
IVGTT	Intravenous glucose tolerance test
J	Juxtamembrane
K_{ATP}	ATP-sensitive potassium channel
K_A	Dissociation constants of the orthosteric ligand
K_B	Dissociation constants of the allosteric ligand
K_v	Delayed rectifying K^+ channel
LBVS	Ligand-based virtual screening
MEK	Mitogen-activated protein kinase kinase
NAL	Neutral allosteric ligand
NAM	Negative allosteric modulator
NHS	National Health Services (U.K.)
NICE	National Institute for Health and Care Excellence (U.K.)
NTD	N-terminal domain
OXM	Oxyntomodulin
p	Probability
PAM	Positive allosteric modulator
PAM-ago	Agonist-positive allosteric modulator
PBS	Phosphate buffered saline
PC	Prohormone convertase

PDE	Phosphodiesterase
pERK1/2	Phosphorylation of ERK1/2
PI-3K	Phosphoinositide 3-kinase
PKA	Protein kinase A
PKC	Protein kinase C
PLC	Phospholipase C
ROCS	Rapid Overlay of Chemical Structures
SAR	Structure-activity relationship
SBVS	Structure-based virtual screening
SGLT-2	Sodium-dependent glucose cotransporters-2
SUR1	Sulfonylurea receptor 1
T1DM	Type 1 diabetes mellitus
T2DM	Type 2 diabetes mellitus
TM	Transmembrane
TPSA	Topological polar surface area
TR-FRET	Time-resolved fluorescence resonance energy transfer
TZD	Thiazolidinediones
VDCC	Voltage-gated Ca^{2+} channel
W.H.O.	World Health Organisation

Chapter 1

Introduction

1.1 Type 2 diabetes mellitus

Type 2 diabetes mellitus (T2DM), which is a chronic metabolic disease that is clinically characterised by a consistently elevated fasting blood glucose level [Owens et al., 2017], has now become a worldwide epidemic. According to the latest International Diabetes Federation (IDF) Diabetes Atlas 2019 [International Diabetes Federation, 2019], there are 463 million adults diagnosed with T2DM, which is equivalent to 9.3% of the world's total adult population. The IDF further estimates that there will be 578 million adults with diabetes by 2030. Given the considerable health, social and economic burden which cost up to US$760 billion, which is equivalent to 12% of total world health expenditure, on treating T2DM and its complications [International Diabetes Federation, 2019], there is an urgent need to develop novel T2DM treatments to tackle the growing epidemic [Thomas et al., 2015, Defronzo et al., 2015, Zheng et al., 2018].

1.1.1 Pathogenesis of T2DM and incretin-based therapies

T2DM is a complex endocrine and metabolic disorder and involves the interplay between genetic and environmental factors. Therefore, it generates a progressive and heterogeneous pathology, with varying degrees of insulin resistance and dysfunction of pancreatic α and β cells, as well as other endocrine disturbances [Tahrani et al., 2016]. Thanks to the better understanding of the multifactorial pathogenesis of T2DM which affects the liver, the brain, the kidney, the skeletal muscles, the gut as well as the adipocytes, several new classes of glucose-lowering therapies have been developed [Defronzo, 2009, DeFronzo et al., 2013, Chowdhury et al., 2013, Bailey, 2015, Tahrani

et al., 2016]. Their mechanisms of actions are summarised in Fig. 1.1.

1.1.2 Incretin-based T2DM therapies

The incretin-based therapies (the concept of incretins will be discussed next), which are exenatide (Ex-4) [Eng et al., 1992], lixisenatide, liraglutide, albiglutide, dulaglutide and semaglutide, have been widely used in recent years [Oh and Olefsky, 2016]. There are several reasons for their surges in use among T2DM patients: 1) the proven clinical efficacy in lowering blood glucose long term [Aroda et al., 2012, Smits et al., 2016, Honigberg et al., 2020, Rosenstock et al., 2020]; 2) the apparent weight loss side effect which is beneficial to T2DM-obese co-morbid patients [Heppner and Perez-Tilve, 2015, Ghanim et al., 2020, Grill, 2020]; 3) a lower risk of hypoglycaemia [Tahrani et al., 2016]; 4) the sustained long-term blood glucose level reduction [Aroda et al., 2012, Honigberg et al., 2020]. Apart from their blood glucose lowering effect, there are also evidences suggesting their cognitive preservative and cardioprotective effects [Ravassa et al., 2017, Honigberg et al., 2020]. All these advantageous clinical effects make incretin-based therapies an attractive drug treatment.

In spite of their beneficial effects, there are several drawbacks to their uses. Firstly, most of the incretin-based therapies are injection-based, which hinder patient compliance [Spain et al., 2016]. Even though oral form of semaglutide has been developed lately, since semaglutide, together with other incretin-based therapies, are peptide-based treatments, their costs to be used on a regular basis are extortionately high [Hansen et al., 2020]. Furthermore, gastrointestinal disturbances, most commonly nauseas and vomiting, have been reported frequently in patients receiving incretin-based therapies [Meier, 2012]. Lastly, increased risk of potentially fatal pancreatitis has been reported, further limiting their uses in certain patients' subgroups who are vulnerable to developing pancreatitis [Meier, 2012]. All these disadvantages prompted the development of safer and more cost-effective incretin-based treatments.

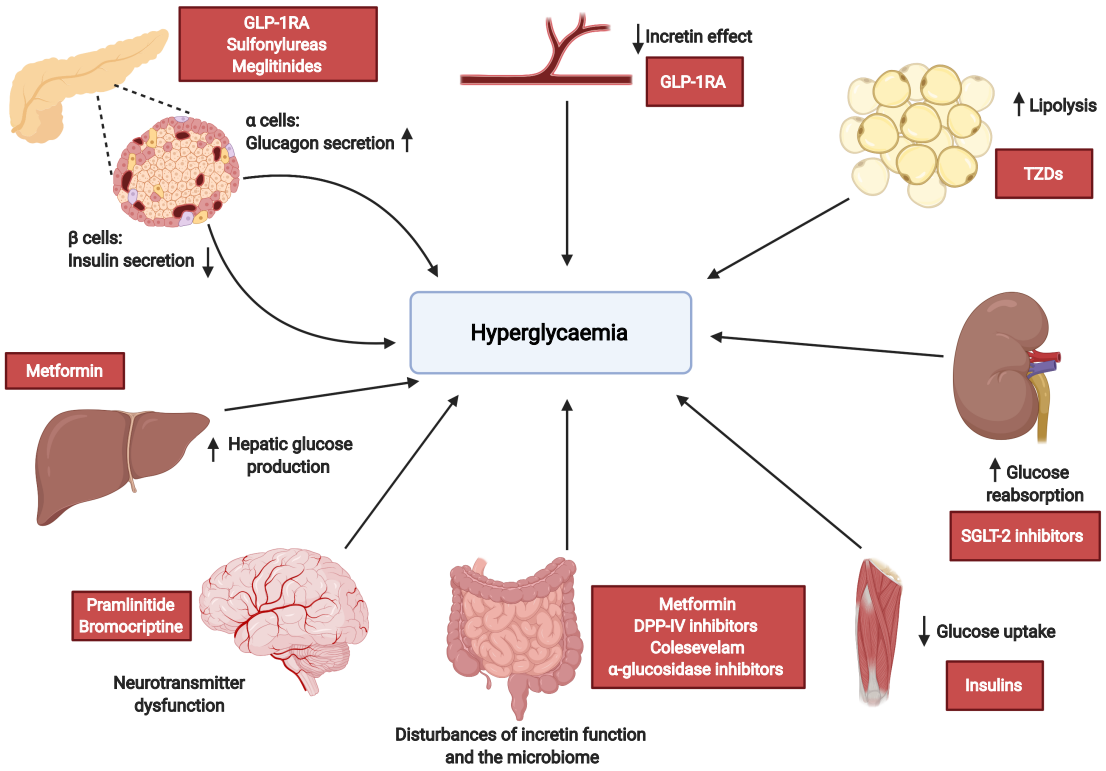

Figure 1.1: **Summary of the pathogenesis and current drug treatments of T2DM.** Heterogenous pathology have been observed in various organs, which include the pancreas, the liver, the brain, the gut, the muscles, the kidneys as well as the adipocytes. A number of T2DM therapies, such as incretin-based therapies, sulfonylureas, meglitinides, metformin, pramlinitide, bromocriptine, DPP-IV inhibitors, SGLT2 inhibitors, TZDs and insulins have been developed to target the dysfunctions in these organs which ultimately contribute to hyperglycaemia. Abbreviations: GLP-1RA: glucagon-like 1 receptor agonists; DPP-IV: dipeptide peptidase-4; SGLT-2: sodium/glucose co-transporter 2; TZDs; thiazolidinediones. Diagram modified from [Tahrani et al., 2016, Campbell and Drucker, 2015]. Diagram created with BioRender.com.

1.2 The pancreatic islets of Langerhans: the key regulator of glucose homeostasis

1.2.1 Architecture of the pancreatic islets of Langerhans

The islets of Langerhans in the pancreas have been long identified for their importance in mediating glucose homeostasis [von Mering and Minkowski, 1889]. Human islets consist of various endocrine cell types, which include a majority (approximately 60%) of insulin-secreting β cells and the glucagon-secreting α cells (around 30%). The remaining 10% endocrine cell types are the somatostatin-secreting δ cells, pancreatic polypeptide-secreting (PP) cells and ghrelin-producing ϵ cells (Fig. 1.2) [Cabrera et al., 2006, Kelly et al., 2011, Brereton et al., 2015, Da Silva Xavier, 2018]. The central cores of the islets are formed by a majority of β cells, surrounded randomly by α and ϵ cells (Fig. 1.2) [Cabrera et al., 2006, Ionescu-Tirgoviste et al., 2015]. The structural localisation of the islets is largely similar between human and mouse islets, yet the ratio of β to α cells is shown to be higher in humans, while the cell numbers of ϵ and PP are similar in both species [Gromada et al., 2018].

1.2.2 Aetiology of T2DM: the glucagonocentric hypothesis

T2DM has long been postulated to be a bihormonal dysfunction, as a result of hypoinsulinemia and hyperglucagonemia with elevated blood levels of glucose [Unger et al., 1963]. However, recent evidences suggested that inappropriate glucagon secretion may be the sole contributor for the onset of T2DM [Unger and Cherrington, 2012]. First, hyperglucagonemia is a common clinical feature in untreated type 1 diabetic mellitus (T1DM) patients and in animal models [Müller et al., 1973]. Furthermore, exogenous glucagon was found to be responsible for the restoration of hyperglycaemia, but not insulin in dogs who received surgical removal of pancreas [Stevenson et al., 1987]. To further validate the glucagonocentric hypothesis, one landmark study conducted experiments on glucagon receptor (GCGR) null mice and found that these mice manifested normal oral glucose tolerance, regardless of the presence or absence of insulin deficiency due to β cell destruction induced by streptozotocin. The authors thus further concluded that glucagon antagonism is the key to preventing the metabolic and clinical manifestation of T1DM [Lee et al., 2011]. These evidences collectively substantiate the 'glucagonocentric' hypothesis for the aetiology of T2DM [Unger and Cherrington, 2012, Campbell and Drucker, 2015]. Given the proposed gravity of glucagon secretion

in maintaining glucose homeostasis, the regulation of glucagon secretion is still not well established. Therefore, there is a need to fill in the knowledge gap.

1.2.3 Regulation of glucose-inhibition of glucagon secretion

The mechanism of glucose-regulated glucagon secretion is still under debate [Walker et al., 2011]. Based on current studies, three different hypotheses are proposed (Fig. 1.2). The first hypothesis suggests that glucose can have direct effect on glucagon secretion inhibition in the pancreatic α cells via direct signalling mechanisms upon its uptake [De Marinis et al., 2010, Sandoval and D'Alessio, 2015, Ramracheya et al., 2018, Yu et al., 2019] (which will be further explained in later section). Furthermore, it has been shown using electrophysiological studies that isolated α cells are electrically excitable, and that glucagon secretion can be stimulated via enhancing action potential and elevating intracellular Ca^{2+} (iCa^{2+}) level [Gromada et al., 2007].

The second theory suggests that glucagon secretion can be indirectly inhibited through the paracrine suppressive actions of insulin and somatostatin, secreted from neighbouring endocrine β and δ cells in the islets. This hypothesis is based on the studies which show isolated α cells respond inappropriately to glucose stimulation in terms of glucagon secretion in the absence of the insulin-secreting β cells and the somatostatin-secreting δ cells [Hauge-Evans et al., 1999]. Moreover, it has been shown that upon insulin secretion in response to high glucose, insulin receptors present on the α cells are activated [Briant et al., 2017]. Furthermore, the secretion of insulin also indirectly stimulates the production of somatostatin in the δ cells [Briant et al., 2017]. The somatostatin produced hence activates the somatostatin receptors, also present in the α cells. The activation of both receptors leads to a reduction of cAMP production, triggering protein kinase A (PKA) downstream signalling, resulting in a suppression of glucagon secretion [Briant et al., 2017].

The third hypothesis argues that glucagon secretion is regulated through the mixed mechanism of actions from the intrinsic regulation in the α cells together with the paracrine effect from β and δ cells [Johansson et al., 1989]. Given the importance of glucagon in regulating glucose homeostasis and that there is an outstanding consensus on the mechanism of how glucagon secretion is controlled, there is an urgent need to thoroughly understand such a physiologically important function. However, apart from insulin and somatostatin, incretins, namely glucagon-like peptide-1 (GLP-1), as well as glucose-dependent insulinotropic peptide or gastric inhibitory polypeptide (GIP), have been shown to also regulate glucagon secretion [Ding et al., 1997, De Marinis et al.,

2010, Campbell and Drucker, 2013, Piro et al., 2014, Ramracheya et al., 2018]. How incretins regulate glucagon secretion in the pancreatic α cells will be part of the main focuses of this thesis and the concept of incretins will be explained in the following sections.

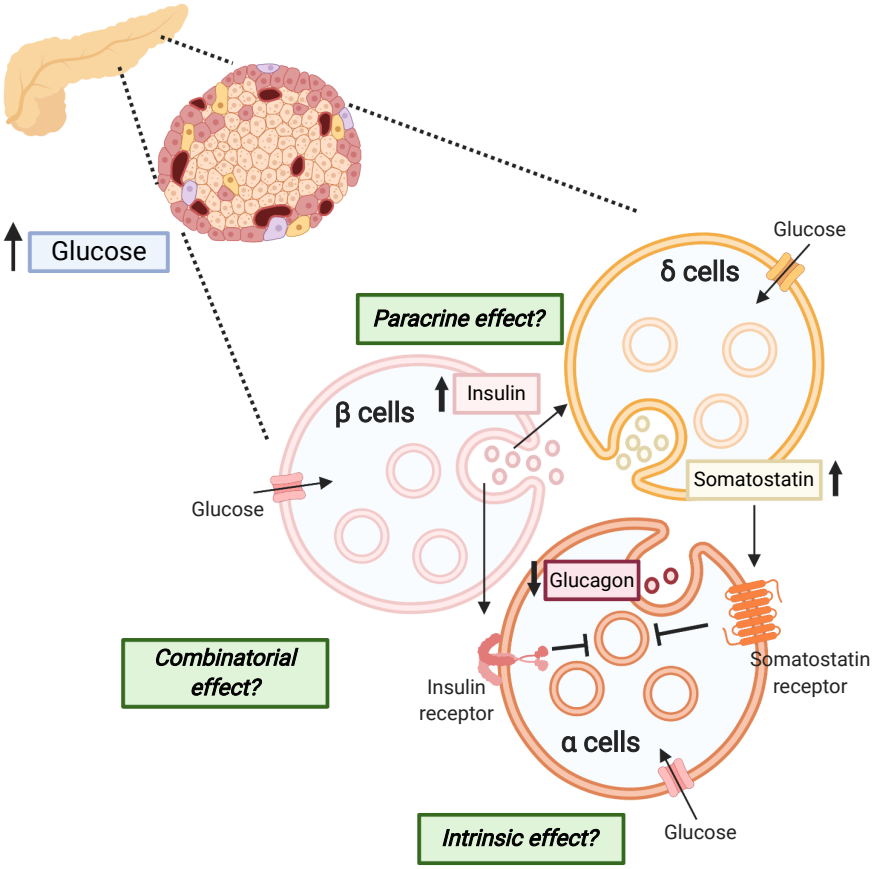

Figure 1.2: **Structural arrangement and regulation of glucose homeostasis in the pancreatic islets of Langerhans.** The above figure shows that a single islet is made up of a mixture of different endocrine cells, with a majority of β cells at its core, surrounded randomly by α and δ cells. Three mechanisms have been proposed for the glucose-inhibited glucagon secretion: through the direct effect in the pancreatic α cells, through the paracrine effect from the insulin and somatostatin-secreting β and δ cells; or a mechanism of both. Diagram modified from [Gromada et al., 2018] and re-created with BioRender.com.

1.3 Incretins: the key mediators of glucose homeostasis

1.3.1 The incretin effect

GLP-1 and GIP are the two major incretin hormones in humans [Seino et al., 2010] and are responsible for 50 to 70% of the postprandial insulin responses in healthy individuals

[Meier and Nauck, 2010]. These two hormones contribute to normoglycaemia by enhancing insulin secretion, producing the so-called 'incretin effect'. The incretin effect is a unique phenomenon of which greater insulin secretion is observed following oral glucose administration compared to intravenous glucose administration [Elrick et al., 1964] (Fig. 1.3). This phenomenon is exploited therapeutically, giving rise to current clinically efficacious incretin-based treatments, such as Ex-4, as discussed in previous section 1.1.2. However, the incretin effect is less prominent in T2DM patients [Knop et al., 2007], presumably due to the decline of β cell function; however, the exact reason for this apparent reduction of incretin effect is unknown [Meier and Nauck, 2010].

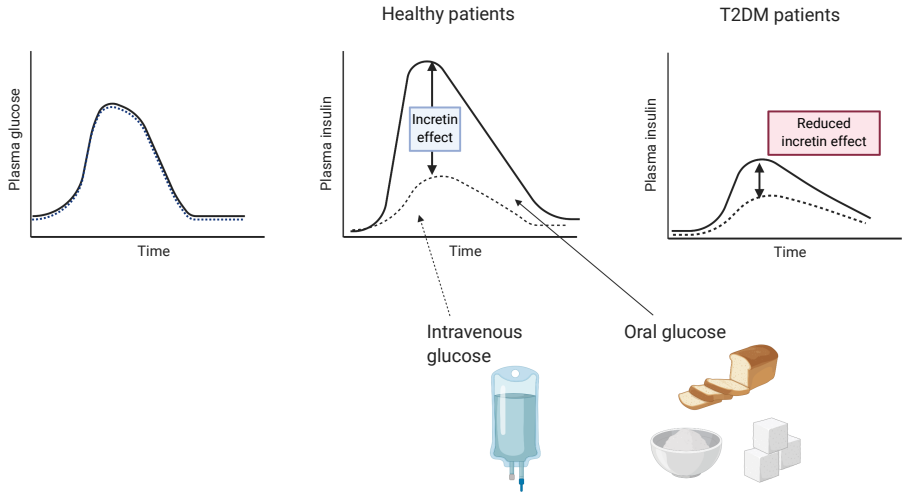

Figure 1.3: **The incretin effect of GLP-1 and GIP.** The incretin effect is defined as the observation of a greater surge of insulin secretion followed by oral glucose administration compared to intravenous glucose administration. However, the incretin effect is diminished in T2DM patients. Diagram created with BioRender.com.

1.3.2 Products of the post-translational processing of proglucagon and proGIP precursor proteins

1.3.2.1 Post-translational processing of preproglucagon gene

The preproglucagon (Gcg) gene has been found to be widely expressed in a specific population of the enteroendocrine L cells of the intestinal mucosa, pancreatic α cells as well as a discrete set of neurons within the nucleus of the solitary tract (NTS) [Sandoval and D'Alessio, 2015]. The Gcg gene encodes the 160-amino acid proglucagon (ProG) peptide, which the relative amount and forms of the ProG peptide are cell-type dependent, regulated by specific prohormone convertases (PC) that are present in specific cell

types [Cho et al., 2014] (Fig. 1.4). In particular, PC2 has been found to be predominant in pancreatic α cells, hence giving rise to glucagon (GCG) as the major bioactive product; while PC1/3 are the most dominant forms in the intestinal L cells and the NTS, producing the most prevalent bioactive products, namly GLP-1, oxyntomodulin (OXM) and glucagon-like peptide 2 (GLP-2) [Holst, 2007]. Notably, there is increasing amount of evidence illustrating the presence of PC1/3 in the pancreatic α cells, albeit at a much lower concentration compared to PC2 [Whalley et al., 2011, Sandoval and D'Alessio, 2015]. Hence, intra-islet production of GLP-1 has been shown [Fava et al., 2016], which has been postulated to play an important role in mediating its insulinotropic action in the β cells [Svendsen et al., 2018]. The properties of the major insulinotropic products of ProG peptide, which are GLP-1, GCG and OXM, will be further discussed in the following sections.

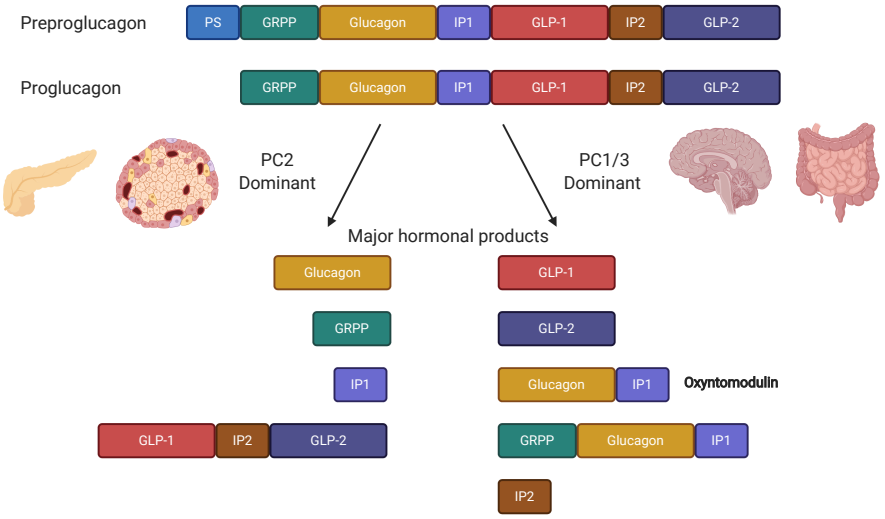

Figure 1.4: **Post-translational processing of proglucagon gene.** The proglucagon peptide (ProG), which forms are cell-type dependent, gives rise to different bioactive products upon the actions of PC2 and PC1/3, which are predominantly found in the pancreatic α cells or the intestinal L cells respectively. Diagram adopted from [Sandoval and D'Alessio, 2015]. Diagram created with BioRender.com. Abbreviations: PC: prohormone convertase; GRPP: glicentin-related pancreatic polypeptide; IP1: intervening peptide 1; IP2: intervening peptide 2; PS: precursor.

1.3.2.2 GLP-1

GLP-1(7-36)NH_2 (thereafter referred to as GLP-1) is the biologically active form which accounts for all of the major physiological activities [Deacon, 2004]. Two forms of GLP-1, namely the non-amidated GLP-1(7-37) and amidated GLP-1(7-36)NH_2, are secreted by the enteroendocrine L cells in the low intestine after proteolytic degradation by PC 1/3

(Fig.1.4) in response to feeding [Holst, 2007]. However, GLP-1 has a very short half-life ($t_{1/2}$: 1-2 minutes), as a result of the proteolytic cleavage of alanine at position 8 at the NH_2 terminal by dipeptidyl peptidase-IV (DPP-IV) enzymes to give an abundant metabolite, GLP-1(9-36)NH_2 (which will be further described next) [Eng et al., 2014] (Fig. 1.5). Hence, DPP-IV inhibitors such as sitagliptin were developed to enhance the actions of GLP-1 [Drucker and Nauck, 2006, Verspohl, 2009]. GLP-1 mediates its full agonism via the class B G protein-coupled receptor (GPCR), GLP-1 receptor (GLP-1R) [Seino et al., 2010, Graaf et al., 2016], which will be further discussed in later section. Apart from its insulinotropic action, GLP-1 also suppresses glucagon secretion in the pancreatic α cells, which is equally important in maintaining glucose homeostasis [Dunning et al., 2005, Holst, 2006, Lund et al., 2011, Sandoval and D'Alessio, 2015] (the mechanisms of which will be discussed in section 1.4.2). GLP-1 also possesses other non-glucoregulatory functions, such as neuronal protection against apoptosis in Alzheimer's disease, gastro-intestinal motility and reduction of cardiac contractility [Seino et al., 2010].

1.3.2.3 GLP-1(9-36)NH_2

The aforementioned GLP-1(9-36)NH_2 is a metabolite of the active GLP-1 [Deacon, 2004]. GLP-1(9-36)NH_2 has a relatively long half-life compared to GLP-1 ($t_{1/2}$: 8-10 minutes) and is the predominant circulatory form (around 80-90%) of the total GLP-1 forms [Sharma et al., 2013, Eng et al., 2014]. It acts as a partial agonist at the GLP-1R [Wootten et al., 2012, Nakane et al., 2015, Bueno et al., 2016] and it has weak insulinotropic effect in *in vivo* human subjects [Elahi et al., 2008]. However, the mediation of its physiological actions through the canonical GLP-1R is still debatable [Guida et al., 2020]. Therefore, 'dual receptor' hypothesis arose [Tomas-Falco and Habener, 2010, Guglielmi and Sbraccia, 2017] due to evidence showing that the cardioprotective properties of GLP-1(9-36)NH_2 are retained even in GLP-1R knock-out mouse system [Ban et al., 2010], prompting the theory that GLP-1(9-36)NH_2 acts at an alternative receptor to mediate its physiological functions. Apart from its weak insulinotropic and cardioprotective effect *in vivo* [Elahi et al., 2008], the administration of GLP-1(9-36)NH_2 has shown various other advantageous effects, such as vasodilation, hepatic glucose production suppression and neuroprotection [Guglielmi and Sbraccia, 2017, Li et al., 2017].

1.3.2.4 GCG

GCG, which consists of 29 amino acids, mediates its glucose-enhancing effect predominantly via the action in the liver, where it stimulates both glycogenolysis and gluconeogenesis, rapidly increasing glucose output [Briant et al., 2016]. GCG acts on another class B GPCR, glucagon receptor (GCGR) to mediate its action [Ahrén, 2009]. Apart from regulating hepatic glucose metabolism, glucagon also decreases food intake, promotes weight loss, affects lipid metabolism and enhances cardiac output [Müller et al., 2017].

While antagonising GCGR has been proposed to be a novel treatment of T2DM given the glucose-enhancing effect and the observed clinical effect in reducing hyperglycaemia upon administration of glucagon [Grøndahl et al., 2017], the antagonism of GCGR has been shown to lead to undesirable side effects such as weight gain, elevation of hepatic enzymes and liver fat content and α cells hyperplasia [Patil et al., 2020]. Therefore, alternative T2DM treatments, such as combining the action of GCGR with GLP-1R or GIPR [Pocai et al., 2009, Day et al., 2012, Capozzi et al., 2018], have been proposed in order to provide better control of glucose homeostasis, eliminating any potential undesirable side effects.

1.3.2.5 OXM

OXM is a C-terminal extended form of GCG with an addition of 8 amino acids [Sandoval and D'Alessio, 2015]. It is a full dual agonist of GLP-1R and GCGR, but with lower potencies and affinities compared to GLP-1 and GCG [Fehmann et al., 1994, Pocai, 2012, Willard and Sloop, 2012]. Moreover, a study shows that the glutamine (Q) residue at position 3 of the OXM amino sequence confers its GCGR specificity [Kosinski et al., 2012]. OXM has also been shown to possess glucose-lowering and weight loss effects [Holst et al., 2018]. The intravenous glucose tolerance test (IVGTT) in Wistar rats shows that OXM and GLP-1 stimulate insulin secretion at equal efficacies [Koole et al., 2010]. Apart from its insulinotropic action, OXM has been found to increase glucagon secretion in the pancreatic α cells both *in vitro* and *in vivo* [Holst et al., 2018]. OXM is also able to induce weight loss in humans when administered three times daily before meals [Wynne et al., 2010]. In addition, OXM has a longer half-life ($t_{1/2}$: 6-12 minutes) compared to GLP-1 ($t_{1/2}$: 1-2 minutes) [Pocai, 2012], and hence is also proposed to be a novel T2DM and obesity drug target [Wynne et al., 2010].

1.3.2.6 GIP

GIP(1-42) (thereafter referred to as GIP), which is another major incretin hormone comprising of 42 amino acids, is secreted by the enteroendocrine K cells of the upper small intestines in response to feeding [Seino et al., 2010, Baggio and Drucker, 2007, Gabe et al., 2019]. It is processed from the precursor protein, proGIP, via the action of PC1/3 [Baggio and Drucker, 2007, Gabe et al., 2019]. Furthermore, the presence of the PC2 motif on the proGIP protein allows the C-terminal truncation to give GIP(1-30)NH_2. Both GIP and GIP(1-30)NH_2 possess similar agonistic actions, yet the concentration of GIP(1-30)NH_2 is at a very low physiological level (i.e. at picomolar range) [Gabe et al., 2019]. Hence, it is postulated that GIP(1-30)NH_2 plays minimal physiological significance [Seino et al., 2010]. Similar to GLP-1, GIP has a relatively short half-life of 5 mins [Deacon, 2004]; both GIP and GIP(1-30)NH_2 are also susceptible to the N-terminal truncation by the DPP-IV enzymes, resulting in the metabolite GIP(3-42) and GIP(3-30)NH_2 [Deacon, 2004]. Similar to GLP-1(9-36)NH_2, GIP(3-42) is believed to have no physiological effect, while GIP(3-30)NH_2 has been used as a GIP receptor (GIPR) antagonist to study the physiological effect of GIP [Sparre-Ulrich et al., 2016].

GIP mediates its action via the class B GPCR, GIPR [Baggio and Drucker, 2007], which will be further described in later section. Unlike GLP-1, GIP has been shown to promote glucagon secretion in pancreatic α cells, nutrient uptake into adipose tissues, bone metabolism, as well as neurogenesis and memory formation [Baggio and Drucker, 2007, De Heer et al., 2008, Seino et al., 2010, Holst et al., 2011b, Khan et al., 2020].

The amino acid alignments of each proglucagon peptide product are shown in Fig. 1.5.

Amino acid position	1	11	21	31	41
GLP-1(7-36)NH_2	HAEGTFTSDV	SSYLEGQAAK	EFIAWLVKGR	$CONH_2$	
GLP-1(9-36)NH_2	EGTFTSDV	SSYLEGQAAK	EFIAWLVKGR	$CONH_2$	
Exendin-4	HGEGTFTSDL	SKQMEEEAVR	LFIEWLKNGG	PSSGAPPPS	
Glucagon	HSQGTFTSDY	SKYLDSRRAQ	DFVQWLMNT		
Oxyntomodulin	HSQGTFTSDY	SKYLDSRRAQ	DFVQWLMNT	RNRNNIA	
GIP	YAEGTFISDY	SIAMDKIHQQ	DFVNWLLAQK	GKKNDWKHNI	TQ

Figure 1.5: **Amino acid alignments of products of glucagon-like peptides.** The amino acid sequences of GLP-1(7-36)NH_2, GLP-1(9-36)NH_2, Exendin-4, glucagon, OXM and GIP are aligned as above. The dash line across the amino acid sequences of GLP-1(7-36)NH_2 and GLP-1(9-36)NH_2 represent the N-terminal truncation by the DPP-IV enzyme.

1.4 Molecular mechanisms of GLP-1-regulated glucose homeostasis

1.4.1 Insulinotropic action of GLP-1 and GIP

Glucose-stimulated insulin secretion (GSIS) is a well-characterised mechanism in the pancreatic β cells [Seino, 2012, Drucker, 2018]. During hyperglycaemia, glucose is transported into the pancreatic β cells facilitated by the glucose transporter 2 (GLUT2) and undergoes glycolysis to give pyruvate. Through oxidative phosphorylation of pyruvate in the mitochondria, the ratio of cytosolic adenosine triphosphate: adenosine diphosphate (ATP:ADP) is increased. This increase in ATP subsequently leads to the inhibition of the ATP-sensitive potassium (K_{ATP}) channel, resulting in membrane depolarisation, subsequently causing the opening of the L-type voltage-dependent calcium channel (VDCC). The opening of the VDCC leads to an intracellular influx of Ca^{2+}, further promoting the release of Ca^{2+} from intracellular stores through Ca^{2+}-induced Ca^{2+} release (CICR) in the endoplasmic reticulum (ER). This augmentation of iCa^{2+} stimulates the exocytosis of insulin-containing granules, leading to insulin release from the β cells [Graaf et al., 2016] (Fig. 1.6).

GSIS can be further promoted with the actions of incretins [Seino et al., 2010, Cho et al., 2014, Graaf et al., 2016] (Fig. 1.6). Upon binding to their canonical receptors, GLP-1R and GIPR, the Gαs subunits are activated, facilitating the adenylyl cyclase activity, leading to an increase in the production of 3',5'-cyclic adenosine monophosphate (cAMP), which is an important secondary messenger responsible for the subsequent signal transduction processes. Upon increasing cAMP production, PKA-dependent and PKA-independent pathways, via the actions of exchange protein activated by cAMP (EPAC), are mediated. The PKA-dependent pathway leads to the inhibition of the K_{ATP} channel, via the phosphorylation of the sulfonylurea receptor (SUR) unit (which is the target of another important class of T2DM drug, sulfonylurea) on the K_{ATP} channel, leading to membrane depolarisation. PKA, together with protein kinase C (PKC), also inhibit the activity of voltage gated potassium (K_V) channel, which repolarizes the membrane potential through allowing the efflux of K^+. This delays repolarization, leading to an increase in intracellular influx of Ca^{2+} via VDCC. Compared to the PKA-dependent pathway, the PKA-independent pathway leading to insulin secretion is not yet well defined. However, it is postulated that EPAC also inhibits the K_{ATP} channel via increasing its sensitivity towards ATP. Together with PKA, EPAC enhances CICR

through the actions of inositol 1,4,5- trisphosphate (IP_3) receptor and ryanodine (Ry) receptors. These collective enhancement of iCa^{2+} level promotes the exocytosis of the insulin-containing granules, therefore enhancing GSIS in the β cells. Furthermore, CICR has also been shown to directly enhance the production of ATP in the mitochondria; and that PKA and EPAC have direct effect on the exocytosis of insulin-containing vesicles. These series of downstream signalling pathways demonstrate the intricacy and complexity of incretin-regulated GSIS in the β cells [Graaf et al., 2016] (Fig. 1.6).

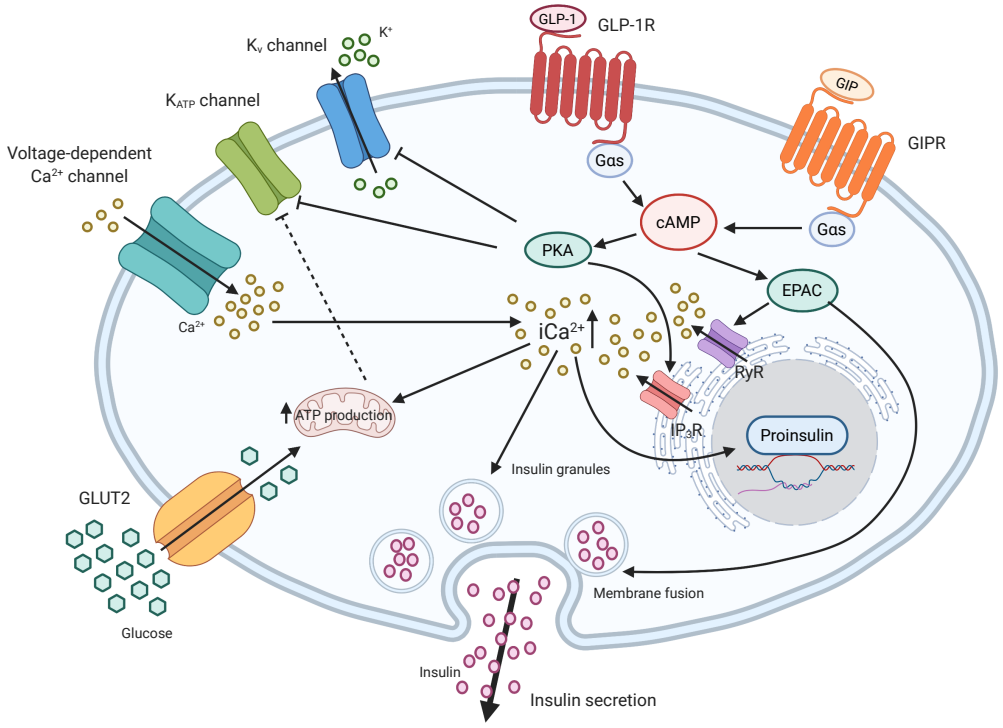

Figure 1.6: **Mechanisms of GLP-1 and GIP-facilitated glucose-stimulated insulin secretion.** GSIS is regulated under hyperglycaemic condition according to the following mechanisms: 1) glucose is transported into the β cells via GLUT2; through oxidative phosphorylation, the ratio of ATP:ADP increases; 2) the increase in ATP leads to the inhibition of K_{ATP} channel, resulting in membrane depolarisation; 3) the inhibition of K_{ATP} channel subsequently leads to the opening of L-type VDCC, leading to an influx of Ca^{2+} into the cytoplasm; 4) the increase in iCa^{2+} further promotes Ca^{2+}-induced Ca^{2+} release, ultimately stimulating the exocytosis of insulin vesicles. Incretins, namely GLP-1 and GIP, facilitate GSIS via the activation of their canonical receptors, GLP-1R and GIPR. Upon binding to the receptors, the Gαs subunit is activated, leading to an increase in intracellular cAMP production via the enhancement of activity of the adenylyl cyclase. The increase in cAMP level subsequently activates PKA and EPAC, which further inhibits and promotes the ion channels responsible for regulating GSIS. Diagram created by BioRender.com.

1.4.2 Glucagonostatic action of GLP-1

1.4.2.1 Glucose regulation of glucagon secretion

The mechanism of action of glucose-regulated glucagon secretion is highly similar to that of GSIS [Holst et al., 2011b]. However, under hyperglycaemia, the glucagon secretion in the α cells is inhibited rather than stimulated in contrast to the β cells. Glucose uptake into the pancreatic α cells is mediated through the glucose-transporter 1 (GLUT1), instead of GLUT2 in the pancreatic β cells, as the expression of GLUT2 has been proven to be low in mouse and human α cells [Suga et al., 2019]. Glucose is converted to pyruvate through glycolysis and further converted to ATP via oxidative phosphorylation in the mitochondria. In contrast to the β cells, the α cells require less intracellular ATP to inhibit the K_{ATP} channel, leading to depolarisation of the membrane potential. The VDCC and sodium ion channel are then closed, resulting in less Ca^{2+} and Na^{+} ions influx into the cytoplasm, therefore inhibiting the exocytosis of glucagon-containing vesicles, suppressing glucagon secretion [Dunning et al., 2005, Gylfe, 2016, Müller et al., 2017] (Fig. 1.7).

Intriguingly, similar to the mechanism of the suppression of glucagon secretion under high glucose condition and in contrast to the β cells in response to low glucose, the K_{ATP} channel remains closed under hypoglycaemia. The K_{ATP} channel then imposes a membrane potential, leading to the opening of VDCC and sodium ion channel; the subsequent intracellular influx of Ca^{2+} and Na^{+} ions result in the exocytosis of glucagon-containing vesicles, facilitating glucagon secretion [Müller et al., 2017] (Fig. 1.7). Apart from being regulated by glucose, glucagon secretion can also be controlled via incretins, GLP-1 and GIP. Yet compared to the fully characterised signalling mechanisms of GSIS facilitated by incretins, the mechanisms of how GLP-1 and GIP regulate glucagon secretion have not yet been fully understood [Walker et al., 2011]. Hence there is a need to elucidate the enigma underlying the molecular mechanisms of GCG secretions. The following sections will discuss current findings on incretin regulation of glucagon secretion.

1.4.2.2 Hypotheses for GLP-1-mediated inhibition of glucagon secretion

GLP-1 inhibitory effect on glucagon secretion in pancreatic α cells has been observed both *in vivo* and *in vitro* [Holst et al., 2011a]. The question of whether the inhibition of glucagon secretion mediated by GLP-1 is due to its direct effect on α cells (Fig. 1.7) or through the stimulation of insulin and somatostatin secreted from neighbouring β and

δ cells [De Heer et al., 2008] has long been debated. The evidence that support both sides of arguments will be presented as follows:

Paracrine effect: The postulation that GLP-1 inhibits glucagon secretion via paracrine hormones such as somatostatin arises, due to the very low, or in some cases non-existent expression of GLP-1R on the α cells [Moens et al., 1996, Kedees et al., 2009, Tornehave et al., 2008]. This observation poses further question on how GLP-1 mediates its glucagonostatic action through direct activation of the low expressing, or if at all, GLP-1R. The paracrine effect on glucagon regulation that solely mediates through insulin secreted in the β cells has been dismissed as normal oral glucose tolerance was observed in spite of insulin deficiency due to the total destruction of β cells in GCGR null mice; based on this observation, alternative hormones with insulinotropic properties were postulated to be responsible for the apparent glucoregulation [Lee et al., 2011]. Furthermore, GLP-1 has been shown to stimulate the secretion of somatostatin in the δ cells, which in turn inhibits glucagon secretion via paracrine effect [Orskov et al., 1988]. Also, the expression of GLP-1R on the δ cells has been shown to be higher than that of the α cells [Richards et al., 2014, Ramracheya et al., 2018]. Further studies using perfused isolated mouse islets suggest that in the presence of somatostatin receptor antagonist, the inhibition of GLP-1-induced glucagon secretion is abolished [Ørgaard and Holst, 2017]. However, according to the studies by our collaborators, the research group led by Prof. Patrik Rorsman and Dr Reshma Ramracheya (Oxford Centre for Diabetes, Endocrinology and Metabolism, University of Oxford), using static isolated human islets, they show that GLP-1 suppression on glucagon secretion exists despite the application of insulin receptor and somatostatin antagonists [Ramracheya et al., 2018], further illustrating the lack of consensual evidence indicating whether paracrine effect plays a key role in glucagon secretion suppression.

Direct effect: Initial studies suggest that 0 to 20% of rat α cells and islets express GLP-1R [Heller et al., 1997]. In a recent study which analysed GLP-1R expression in isolated human α cells, it was found that the expression level of the GLP-1R was only 1% of that in β cells [Ramracheya et al., 2018]. In spite of the very low expression of GLP-1R in the α cells, GLP-1 is able to mediate its glucagonostatic action via the direct activation of its canonical receptor, leading to an increase in cAMP production [Ramracheya et al., 2018]. Other studies utilising real-time RT-PCR technique, confocal laser scanning microscopy and GLP-1R specific antibodies also detected low levels of GLP-1R in the mouse clonal αTC-1.6 cells and the more physiologically relevant systems, the isolated rat and mouse islets [Piro et al., 2014, Nakashima et al., 2018, Zhang et al., 2019]. The

level of cAMP produced, coupled with the activation of the downstream PKA signalling, have been found to be adequately enough to inhibit glucagon secretion [Ding et al., 1997, De Marinis et al., 2010]. The study conducted by our collaborators also illustrates the relationship between cAMP level and glucagon secretion using forskolin, a direct adenylyl cyclase activator [Seamon et al., 1981]: low cAMP level produced by forskolin leads to the inhibition of glucagon secretion whereas high level of cAMP leads to the stimulation of glucagon secretion [De Marinis et al., 2010]. Therefore, this thesis aims to build on current evidence suggested by our collaborators, and further investigates the active role of GLP-1 in suppressing glucagon secretion in the pancreatic α cells.

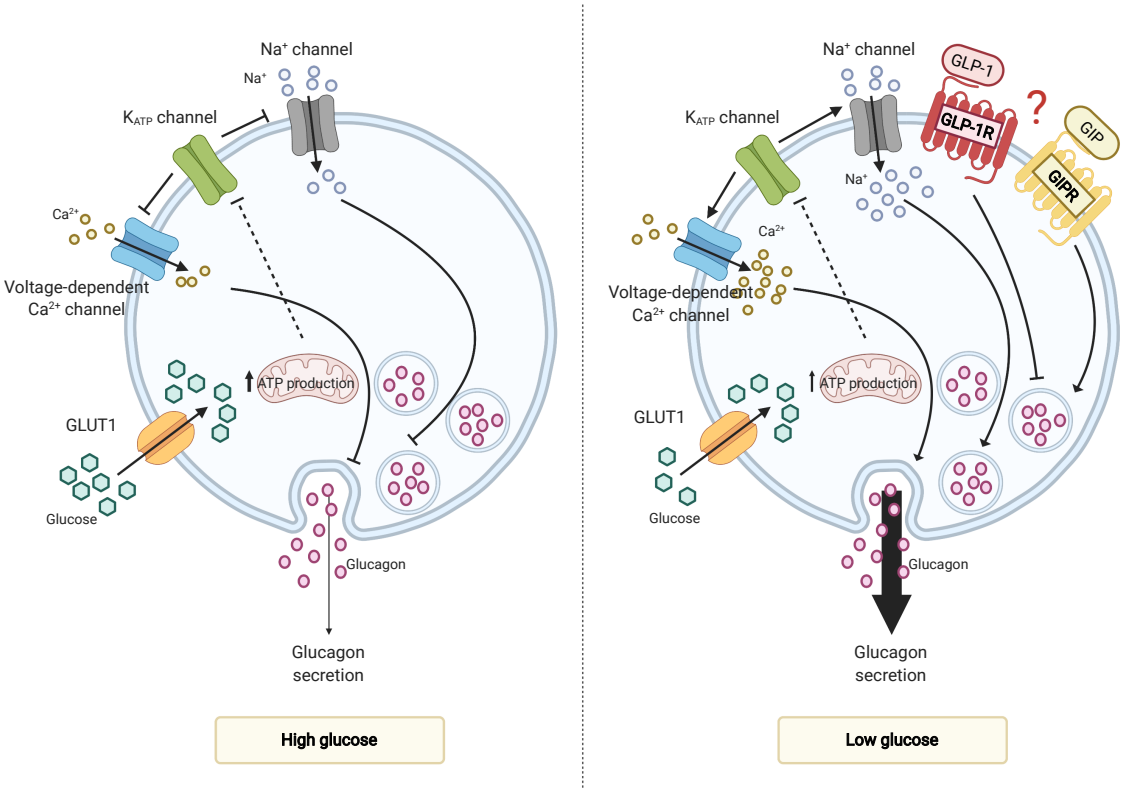

Figure 1.7: **Mechanisms of glucose-regulated glucagon secretion.** Glucagon secretion is suppressed under hyperglycaemia. This can be achieved via the following mechanisms: 1) GLUT1 (instead of GLUT2 in β cells) transports glucose into the α cells, which then leads to an increase of ATP production via the action of mitochondria; 2) this increase in ATP leads to the inhibition of K_{ATP} channel, leading to depolarisation of membrane potential; 3) the VDCC and sodium ion channel are then closed, reducing the intracellular influx of calcium and sodium ions into the cells, therefore inhibiting the exocytosis of glucagon-containing vesicles. Under low glucose condition, the K_{ATP} channel remains closed in the α cells, unlike the opening of K_{ATP} channel in the β cells. The K_{ATP} channel imposes a membrane potential, up to a point where it leads to the opening of VDCC and sodium ion channel, leading to the intracellular influx of calcium and sodium ions into the cells, thereby mediating exocytosis of glucagon-containing vesicles. Incretins are also shown to regulate glucagon secretion. Abbreviations: GLUT1: glucose transporter 1. Diagram created by BioRender.com.

1.4.2.3 GPR119: a novel regulator of GLP-1 glucagonostatic action?

GPR119, which is a class A GPCR that has recently been deorphanized [Overton et al., 2006], is postulated to play a role in GLP-1R mediated glucagonostatic action. GPR119 is activated by its endogenous agonist, the fatty acid oleoylethanolamide (OEA), as well as synthetic agonists, PSN632408 [Overton et al., 2006] and AR231453 [Semple et al., 2008]. GPR119 expresses predominantly in the pancreas and the gut in humans [Odori et al., 2013]. It has been reported that GPR119 is able to directly enhance GSIS by stimulating the production of cAMP upon receptor activation in the rat insulinoma cell line [Chu et al., 2008] and in *in vivo* mouse models [Flock et al., 2011]. GPR119 also enhances the secretion of GLP-1 and GIP in their respective enteroendocrine L and K cells, thereby indirectly facilitates glycaemia control [Chu et al., 2008]. GPR119 is also shown to enhance glucagon secretion in low glucose condition in isolated mouse islets, as well as in healthy and streptozotocin (STZ)-induced diabetic rats [Li et al., 2018], further implying its critical role in regulating glucose homeostasis. More recently, the endogenous agonist of GPR119, OEA, has been shown to potentiate GLP-1R cAMP signalling in the RINm5F rat islet cell tumour cell line and Chinese Hamster Ovary (CHO)-K1 stably expressing GLP-1R cells [Cheng et al., 2015, Brown et al., 2018], therefore posing further question if GPR119 may play a role in GLP-1 mediated glucagonostatic action. However, such notion is yet to be validated experimentally.

Following the introduction of GPR119 potential role in regulating GLP-1 glucagonostatic action and the discussion of the physiological significance of incretins, their canonical receptors, which belong to the group of GPCRs, will be discussed in the following section.

1.5 Overview of G protein-coupled receptors

GPCRs, interchangeably with other terms such as metabotropic receptors or seven transmembrane (TM) spanning receptors, are the largest superfamily of cell-surface receptors [Pavlos and Friedman, 2017]. A total of 1000 receptors have been identified. GPCRs are further classified into six different subfamilies according to their sequence homology, namely rhodopsin-like (Class A), secretin receptor family (Class B), metabotropic glutamate (Class C), fungal mating pheromone receptors (class D), cyclic AMP receptors (class E) and frizzled/smoothened (Class F) receptors [Alexander et al., 2019]. These families can be further divided into subfamilies based on sequence similarities. GPCR can be structurally categorized as having a N-terminal extracellular

domain (ECD), seven hydrophobic transmembrane helices (TM1-7) and a C-terminal intracellular domain. The seven TM are linked by three extracellular loops (ECL1-3) and three intracellular loops (ICL1-3) (Fig. 1.8).

GPCRs serve as attractive drug targets and account for 35% of total marketed drugs [Sriram and Insel, 2018]. They are considered to be an important group of cell-surface receptors as many hormones, neurotransmitters, ions, photons, odorants and other stimulus work via GPCR activation to mediate downstream signalling effect to relay their physiological functions [Chalmers and Behan, 2002, Hilger et al., 2018], including the aforementioned regulation of GSIS in the pancreatic β cells. Here, the signal transduction mechanism mediated by GPCR will be further elaborated.

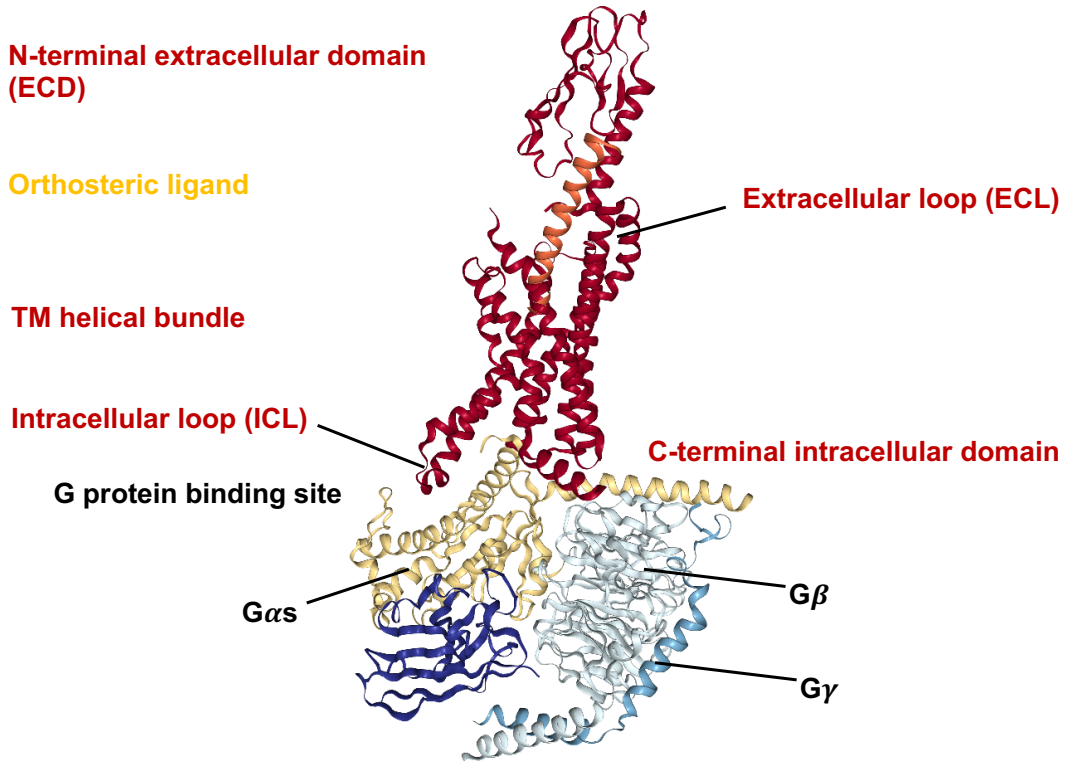

Figure 1.8: **Exemplary GPCR structure using GLP-1R cryo-EM full length structure in complex with GLP-1 and Gαs subunit as a model.** The cardinal features of GPCR include a seven transmembrane helical bundle, connected by three extracellular loops and three intracellular loops. It also has a N-terminal extracellular domain and a C-terminal intracellular domain. The full length GLP-1R structure (PDB: 5VAI) is used as a model to illustrate the common structure of GPCR.

1.5.1 GPCR-mediated signal transduction

GPCRs rely on the heterotrimeric G proteins, consisting of Gα, Gβ and Gγ subunits to relay signal transduction processes which are essential for their regulation of physiological functions [Johnson et al., 2011]. At the receptor resting state, the heterotrimeric G proteins are in close proximity with the receptor and are anchored at the plasma membrane. The Gα subunit, associating with the constitutive heterodimer G$\beta\gamma$ subunits, is also bound to the nucleotide guanosine diphosphate (GDP). Upon agonist binding, the receptor undergoes conformational changes and the heterotrimeric G protein complex, including the GDP, are recruited to the receptor. The receptor then acts as a guanine nucleotide exchange factors (GEFs), activating the release of GDP protein in exchange for the nucleotide guanosine triphosphate (GTP). This process subsequently leads to the dissociation of the Gα subunit from the G$\beta\gamma$ complex, whereby the Gα-GTP complex diffuse laterally at the cell surface, further triggering the generation of secondary messengers mediating downstream signalling transduction by activating or inhibiting other membrane proteins. The signal transduction outcome depends on the Gα subunit subgroups, which will be discussed below. The signalling process ends when GTP is hydrolysed to GDP by the intrinsic GTPase or the GTPase activating proteins (GAPs) such as regulator of G protein signalling (RGS), resulting in the association of the heterotrimeric G proteins (Fig. 1.9) [Syrovatkina et al., 2016, Campbell and Smrcka, 2018].

Apart from the canonical (G protein-dependent) signalling pathways that happen within the cell membrane surface, non-canonical (G protein-independent) signalling pathways, which rely on the actions of GPCR kinases (GRK) and β-arrestins, allowing internalisation of receptor in the endosomes, are also proven to be critical in mediating sustained signalling responses [Pavlos and Friedman, 2017]. Given the complexity of GPCR signalling, this thesis will focus primarily on the canonical signalling of GPCRs. Here, the classical downstream signalling pathway, mediated by different G protein families, will be outlined.

1.5.2 G protein subunit families

The heterotrimeric G proteins consist of a diverse family of isoforms, with a total of 20 Gα subunits, 5 Gβ subunits and 12 Gγ subunits [Milligan and Kostenis, 2006, Campbell and Smrcka, 2018]. Gα subunits, which can be further classified into 4 subfamilies, play a major role in defining the signal transduction outcomes. The G$\beta\gamma$ complex also plays

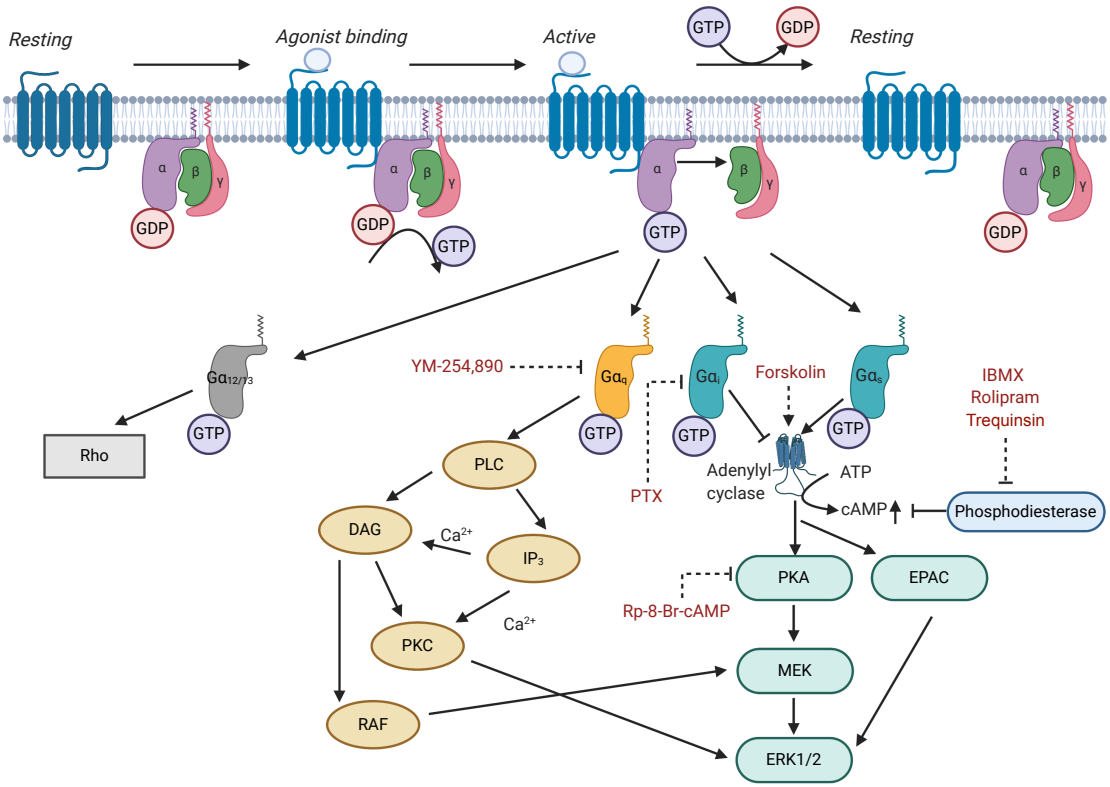

Figure 1.9: **Classical view of G protein-coupled receptor signalling.** GPCR signalling can be divided into canonical (classical) G protein-dependent signalling and non-canonical, β-arrestins/GRK dependent signalling, which results in receptor internalisation. The diagram above depicts the classical GPCR signalling, which is activated upon the dissociation of Gα subunit from the G$\beta\gamma$ subunits. Depending on the Gα subunit, different downstream signalling pathways are resulted: 1) Gα_s and Gα_i subunits stimulate and inhibits the enzymatic action of adenylyl cyclase respectively, leading to an increase or decrease in cAMP level produced. Gα_q subunit leads to the activation of PLC/DAG/IP$_3$ pathway, ultimately results in an increase in intracellular calcium mobilisation. G$\alpha_{12/13}$ subunit activates Rho, however its physiological relevance is yet unknown. Different pharmacological activator or inhibitors (in red) can be used to activate or inhibit certain signalling pathways. Diagram created by BioRender.com.

an equally important physiological role. However, the biochemical classification based on the standalone Gβ and Gγ subunits has been proven to be technically difficult to date [Smrcka, 2008]. Therefore, the G$\beta\gamma$ complex has been regarded as a single class for mediating signal transduction process [Campbell and Smrcka, 2018]. Here, the major effectors for each Gα subfamily will be discussed.

1.5.2.1 Gα_s

The Gα_s subunit was the first G protein discovered and classified based on their activities in stimulating adenylyl cyclase [Northup et al., 1980]. There are currently two main members of the Gα_s families: the Gα_s subunit, which is highly present in most cell types and the G$_{olf}$ subunit, which only presents in the olfactory sensory neurone. The Gα_s-GTP complex formed upon receptor activation binds directly to the adenylyl cyclase, catalysing the enzyme to convert ATP to cAMP (Fig. 1.9). The termination of the cAMP signalling is regulated by the phosphodiesterases (PDEs), which convert cAMP to adenosine monophosphate (AMP) [Hancock, 2010]. The increased in cAMP production further leads to the activation of the main effectors, PKA and EPAC, as discussed previously (Fig. 1.6) [Yang and Yang, 2016]. The cAMP/PKA and cAMP/EPAC pathways will be further elaborated later. Pharmacological tools, such as the direct adenylyl cyclase activator, the diterpene forskolin [Seamon et al., 1981], and PDE inhibitors, such as the pan-PDE inhibitor 3-isobutyl-1-methylxanthine (IBMX), specific PDE 4 inhibitor rolipram and specific PDE 2, 3, and 7 inhibitor trequinsin [Schmidt et al., 2020], have been used to prevent the breakdown of cAMP by inhibiting PDEs, in an attempt to aid the characterisation of Gα_s signalling pathway (Fig. 1.9).

1.5.2.2 Gα_i

The Gα_i family is the largest and most diverse Gα subfamilies, which consists of Gα_{i1}, Gα_{i2}, Gα_{i3}, Gα_o, Gα_t, Gα_g and Gα_z. Gα_o has been shown to be highly expressed in neurons while Gα_t (which t stands for transducin), which can be further divided into Gα_{t1} and Gα_{t2}, is present in the rod and cone cells of the eyes. Gα_g (which g stands for gustducin) is found in the taste receptor cells while Gα_z is present in neurones and platelets ([Kuszak et al., 2010]). Contrary to the action of the Gα_s subunit, the Gα_i subunit inhibits the adenylyl cyclase, except for Gα_o, which it shows weak inhibitory action, thereby slowing the conversion of ATP to cAMP, ultimately reducing the intracellular cAMP levels (Fig. 1.9). Furthermore, all Gα_i subunits except Gα_z can

be inhibited by pertussis toxin (PTX) [Pittman, 1979, Katada and Ui, 1982], through ADP-ribose modification of a unique cysteine at the carboxyl terminus of $G\alpha_i$ subunits, which impose steric occlusion of $G\alpha_i$ with receptors [Campbell and Smrcka, 2018].

1.5.2.3 G$\alpha_{q/11}$

The $G\alpha_q$ subfamily consists of $G\alpha_q$, G_{11}, G_{14} and G_{15} subunits, of which G_{11} shares 90% homology as $G\alpha_q$ [Campbell and Smrcka, 2018]. These subunits all have distinct tissue distributions but no specific target interactions have been identified [Kamato et al., 2015, Campbell and Smrcka, 2018]; yet most physiological studies show that $G\alpha_q$ and G_{11} share overlapping functions. All of the subunits can activate phosphate lipase Cβ (PLCβ), subsequently causing Ca^{2+} release, which is one of the major drivers of cellular body functions (the PLC pathway will be further discussed later) [Cabrera-Vera et al., 2003]. Apart from activating the PLCβ/Ca^{2+} release pathway and depending on cell type and receptor, $G\alpha_{q/11}$ has also been shown to interact with p63RhoGEF to activate Rho by converting Rho-GDP to Rho-GTP via the action of RhoGTPase [Campbell and Smrcka, 2018]. A number of $G\alpha_{q/11}$ specific small molecule inhibitors have been identified recently [Zhang et al., 2020]; YM-254,890, which is a cyclic depsipeptide isolated from the culture broth of *Chromobacterum sp.*, is one of the examples [Takasaki et al., 2004] (Fig. 1.9).

1.5.2.4 G$\alpha_{12/13}$

$G\alpha_{12/13}$ subunits were identified in a homology screening for novel G protein subunits [Kozasa et al., 2011]. They were later characterised by their interaction with p115RhoGEF protein, thereby activating Rho via the catalysis of Rho-GDP to Rho-GTP through RhoGTPase (Fig. 1.9). $G\alpha_{12/13}$ subunits are expressed ubiquitously in humans. Notably, most GPCRs which couple to G_q subunits can also bind to $G\alpha_{12/13}$ subunits, however its physiological significance is unknown [Kozasa et al., 2011].

1.5.2.5 G$\beta\gamma$

5 Gβ subunits and 12 Gγ subunits are reported to date, and the Gβ subunits are deemed to be the major determinator of the G$\beta\gamma$ subunit cellular effects. The $G\beta_{1-4}$ subunits show 80% structural homology while the $G\beta_5$ subunit only shows 50% structural similarities with the rest of the Gβ subfamily; there are less structural similarities among Gγ subunits [Milligan and Kostenis, 2006]. Furthermore, the functional significance of

each unique combination of the G$\beta\gamma$ subunit is less understood. G$\beta\gamma$ subunit has been identified to be able to mediate signal transduction on its own as well as interact with other protein kinases to further relay signal transduction [Cabrera-Vera et al., 2003]. Examples of which include the interaction with phosducin, the activation of GPCR kinase 2 (GRK2) as well as the activation of G protein gated inwardly rectifying K^+ channel (GIRK) [Smrcka, 2008].

1.5.3 Major secondary messengers for relaying signalling cascades

A number of important secondary messengers are produced upon G protein activations. These secondary messengers trigger downstream signalling cascades, controlling important physiological functions via transcription, translation or metabolism. Due to the complex nature of intracellular signalling upon GPCR activation, here three signalling pathways which are involved in the regulation of glucose homeostasis will be discussed in greater details.

1.5.3.1 cAMP/PKA pathway

The activation of the Gα_s subunit catalyses adenylyl cyclase, increasing cAMP production. cAMP acts as an important secondary messenger which further activates PKA. PKA is a serine/threonine kinase and is a holoenzyme formed by a dimer of two regulatory (R) subunits that each bind to a catalytic (C) subunit. Each R subunit contains two cAMP binding sites [Murray, 2008, McClendon et al., 2014]. Upon cAMP binding, conformation changes are induced, which release the active C subunit. There are four types of R subunits, namely RIα, RIβ, RIIα and RIIβ and two types of C subunits (Cα and Cβ) [McClendon et al., 2014]. In general, RIα, RIIα and the two types of C subunits are expressed in all tissues whereas the expressions of RIβ and RIIβ are restricted to certain tissues [Stratakis and Cho-Chung, 2002]. Notably, the type I PKA, which contains the RIα and RIβ subunits, requires less intracellular cAMP level for its activation compared to the type II PKA, which consists of RIIα and RIIβ subunits [Yang and Yang, 2016]. PKA can be inhibited by the cAMP analogue, Rp-8-Br-cAMP [Gjertsen et al., 1995], which acts as an invaluable pharmacological tool in investigating PKA-mediated downstream signalling pathway (Fig. 1.9).

The cAMP-mediated activation of PKA has also been shown to be critical in phosphorylation of the extracellular signal-regulated kinases (ERK) 1/2, which is a member of the mitogen-activated protein kinase (MAPK) family. It does so by activating the

Rap1-GTPase, which acts on the protein kinase Raf, which further stimulates the mitogen-activated protein kinase (MAPK) kinase (MEK). MEK then phosphorylates ERK1/2, which are implicated in cellular growth and differentiation, including the pancreatic β cells [Werry et al., 2005, Goldsmith and Dhanasekaran, 2007] (Fig. 1.9).

1.5.3.2 cAMP/EPAC pathway

Alternatively, EPAC, which has been recently discovered, is also activated upon the increasing cAMP level via $G\alpha_s$-activation. EPAC exists in two isoforms, the ubiquitously expressed EPAC1 and EPAC2, which is predominantly expressed in brain, liver, pancreas, and adrenal gland [Seino, 2012]. As highlighted in section 1.4.1, EPAC2 plays an important role in facilitating the exocytosis of insulin-containing vesicles, leading to an increase in insulin secretion [Tengholm, 2012, Almahariq et al., 2014].

EPAC1 and EPAC2 act on the same downstream effectors, small GTPase Rap1 and Rap2. It has also been postulated that through the action of Rap1, PKA-independent phosphorylation of ERK1/2 can be mediated through the activation of EPAC, however, its mechanism of action is still under debate [Werry et al., 2005](Fig. 1.9).

1.5.3.3 PLCβ/Ca^{2+} pathway

The activation of the $G\alpha_{q/11}$ subunit leads to the activation of PLCβ. PLC hydrolyses the membrane lipid, phosphatidylinositol 4,5-bisphosphate (PIP_2) to IP_3 and diacylglycerol (DAG), which both act as important secondary messengers, initiating their individual signalling cascades. The cytosol soluble IP_3 causes the release of Ca^{2+} into the cytoplasm via the action of IP_3R on the endoplasmic reticulum [Putney and Tomita, 2012, Islam, 2019]. The membrane bound DAG further activates PKC. DAG is also known to activate the GTPase Raf, which then leads to the activation of MEK (although the mechanism is less defined), ultimately phosphorylating ERK1/2 (Fig. 1.9) [Werry et al., 2005].

1.5.4 GPCR desensitisation and internalisation

As alluded previously, GPCRs are involved in the mediation of a range of highly physiologically relevant signal transduction process at a cellular level. However, continuous signalling or excessive stimulation can be harmful to cells, and may even lead to uncontrolled cell growth. Therefore, receptor desensitisation is an important mechanism of which healthy cells employ to blunt GPCR signalling transiently or over

a period of time to sustain normal physiology [Rajagopal and Shenoy, 2018]. Traditional receptor desensitisation is regulated through the phosphorylation of the active receptor via the action of GRKs (mainly GRK2/3 and GRK5/6) and/or other protein kinases, leading to subsequent high affinity binding of β-arrestins (mainly β-arrestin 1 and 2) at the cytosolic side of the receptor [Gurevich and Gurevich, 2019]; the arrestins then enhance the receptor endocytic trafficking machinery. The internalisation of receptor facilitates signal termination through subsequent degradative lysosomal pathway or disassembly of the active receptor complex in early endosomes to enhance recruitment of receptors to cell surface via recycling endosomes [Carbone et al., 2019]. However, several recent reports have also shown β-arrestin-independent receptor internalisation, via the clathrin and dynamin-dependent mechanisms [Wolfe and Trejo, 2007], further illustrating the diverse array of regulatory means of GPCR internalisation.

Interestingly, instead of signal termination, recent evidences suggest a few receptors generate sustained signalling responses within the endosomal compartment [Ferrandon et al., 2009, Feinstein et al., 2013]. Therefore, a new mean to improve the efficacy and to reduce side effects of existing drug treatments via the control of spatiotemporal properties of GPCRs has been proposed [Hothersall et al., 2016, Retamal et al., 2019]. GLP-1R (the properties of GLP-1R will be further discussed in section 1.5.5.2) is regarded as one of the highly physiologically relevant examples [Roed et al., 2014, Roed et al., 2015, Thompson and Kanamarlapudi, 2015, Thompson et al., 2016, Fletcher et al., 2018]. Studies have shown that the receptor-agonist complex can co-localise with adenylyl cyclase in the endosomes, triggering the production of cAMP within the endosomal compartment [Kuna et al., 2013]. Furthermore, targeting GLP-1R trafficking has been shown to enhance the efficacy of current incretin T2DM treatments [Jones et al., 2018], thereby illustrating the possibility of the delivery of a more efficacious T2DM treatment, while limiting its potential side effects, via manipulating receptor interaction with β-arrestins with the use of specific biased agonists.

1.5.5 Class B GPCRs

There are currently 6 major families of GPCRs, of which class B GPCRs are highly physiologically relevant. The 15 members of the Class B secretin-like GPCRs, and their moderate length (27 to 44 amino acids) peptide-based natural hormones [Wootten and Miller, 2020], include [Alexander et al., 2019] (Table 1.1):

Table 1.1: **List of Class B GPCRs and their endogenous hormones.**

Class B GPCR members	Endogenous hormone
CTR	Calcitonin
AMY1 (CTR:RAMP1), AMY2 (CTR:RAMP2), AMY3 (CTR:RAMP3)	Amylin
CGRPR (CLR:RAMP1)	Calcitonin gene-related peptide
AM1 (CLR:RAMP2), AM2 (CLR:RAMP3)	Adrenomedullin
CRF1R, CRF2R	Corticotropin-releasing factor
GCGR	GCG and OXM
GLP-1R	GLP-1, GCG, OXM, GLP-1(9-36)NH_2
GLP-2R	GLP-2
GIPR	GIP
SCTR	Secretin
GHRHR	Growth hormone-releasing hormone
PTH1R, PTH2R	Parathyroid hormone
PTH1R	Parathyroid hormone-related peptide
PAC1R	Pituitary adenylate cyclase activating peptide
VPAC1R, VPAC2R	Vasoactive intestinal polypeptide

Collectively belong to the glucagon receptor family

Abbreviations: Calcitonin receptor (CTR); receptor activity modifying proteins (RAMPs); amylin 1 (AMY1), amylin 2 (AMY2) and amylin 3 (AMY3) receptors; calcitonin-receptor like receptor (CLR); calcitonin gene-related peptide receptor (CGRPR); adrenomedullin 1 (AM1) and adrenomedullin 2 (AM2) receptors; corticotropin-releasing factor 1 (CRF1) and corticotropin-releasing factor 2 (CRF2) receptors; growth hormone-releasing hormone receptor (GHRHR); secretin receptor (SCTR); parathyroid hormone 1 (PTH1) and parathyroid hormone 2 (PTH2) receptors; vasoactive intestinal polypeptide 1 (VPAC1) and vasoactive intestinal polypeptide 2 (VPAC2) receptors; pituitary adenylate cyclase-activating polypeptide type I (PAC1) receptor.

1.5.5.1 Therapeutic implications of Class B GPCRs

Class B GPCRs are known to play an important role in regulating key physiological functions including satiety and glucose homeostasis, cardiovascular system, gastrointestinal functions, bone metabolism, and immune responses [Karageorgos et al., 2018]. They mediate their physiological function via cognate peptide hormones, which are currently drug targets for many diseases such as diabetes, osteoporosis, cancer, neurodegeneration, cardiovascular disease, headache and psychiatric disorders. Notable marketed therapeutic examples of Class B GPCR drug treatments include the aforementioned exenatide, which is a GLP-1R-targeted T2DM treatment, teduglutide, which is a GLP-2R-based treatment for short bowel syndrome as well as teriparatide, which is a PTH analogue for the treatment of osteoporosis [Hollenstein et al., 2014]. Given the importance of glucagon receptor family in regulating glucose homeostasis, the receptors from this subclass of Class B GPCRs will be discussed in details as follow.

1.5.5.2 Class B subfamily: glucagon receptor family

Glucagon receptor family comprises of GLP-1R, GIPR, GCGR, GLP-2R and SCTR [Alexander et al., 2019], of which GLP-1R, GIPR and GCGR have been extensively shown to be involved in glucose homeostasis, and therefore will be the main focus of this thesis.

GLP-1R: GLP-1R shares 45% primary sequence with GCGR [Song et al., 2017] and can be activated by a range of cognate ligands such as GLP-1 and its metabolite, GLP-1(9-36)NH_2, which is a very weak partial agonist [Koole et al., 2013]. Apart from being activated by its endogenous agonists, GLP-1R can also be activated by synthetic peptide agonists, such as Ex-4, and GCGR cognate ligands namely GCG and OXM [Koole et al., 2013]. GLP-1R is expressed in a wide range of tissues, such as pancreas, lung, brain, stomach, heart, and kidney, but interestingly not in tissues involved in glucose metabolism, such as the skeletal muscle and adipocytes [Janssen et al., 2013].

GLP-1R is preferentially $G\alpha_s$ coupled leading to the production of cAMP and the activation of PKA to regulate insulin secretion in β cells [Montrose-rafizadeh et al., 1999]. Recent reports also demonstrate its ability to pleiotropically couple to both G_i [Weston et al., 2014] and G_q subunits [Shigeto et al., 2015]. Furthermore, GLP-1R recruits GRK and interacts with β-arrestins 1 and 2 [Graaf et al., 2016]; β-arrestin-1 attenuates cAMP responses at the GLP-1R, inhibiting insulin secretion [Sonoda et al., 2008]. These examples illustrate the complexity of GLP-1R signalling, which encompass

both G protein-dependent and independent pathways. Moreover, GLP-1R has been shown to possess no interactions with any receptor activity modifying proteins (RAMPs) accessory proteins [Weston et al., 2015].

GCGR: Given its structural resemblance to GLP-1R, GCGR can be activated by GLP-1R cognate ligands, such as GLP-1 and liraglutide [Weston et al., 2015], in addition to its endogenous agonists, GCG and OXM. GCGR is primarily expressed in the liver, but also to some extents in the central nervous system, kidneys, gastro-intestinal tract, heart and pancreas [Galsgaard et al., 2019].

GCG activates GCGR predominantly through $G\alpha_s$ coupled pathways, which in turn stimulates adenylate cyclase, leading to the production of cAMP and the activation of PKA, thereby activating gluconeogenic enzymes which then increase gluconeogenesis and glycogenolysis [Ahrén, 2009, Wewer Albrechtsen et al., 2016]. GCG also activates G_q and G_i coupled pathways, which regulate the iCa^{2+} level, leading to glucagon-induced inhibition of glycolysis [Xu and Xie, 2009]. Furthermore, the interaction with RAMP2 alters G protein preference and ligand selectivity, of which this interaction abolishes GLP-1 activation of GCGR, further illustrating the complexity of GCGR signalling upon the interplay among agonists, receptors and RAMPs [Weston et al., 2015, Cegla et al., 2017] (the significance of RAMPs will be further elaborated later).

GIPR: GIPR has been shown to be activated by its endogenous agonists, GIP(1-42) and GIP(1-30)NH_2 (see section 1.3.2.6). GIPR has been shown to be highly expressed in the pancreas, and also with broad expressions in the gut, adipose tissue, heart, endothelial cells, pituitary gland, adrenal cortex, osteoblasts, and in regions of the central nervous system [Greenwell et al., 2020]. GIPR also predominantly couples to the $G\alpha_s$ subunit, leading to the downstream cAMP/PKA/EPAC signalling pathways, which has been shown critical for the insulin secretion [Seino, 2012]. GIPR can also pleiotropically couple to G_q and G_i subunits, leading to the downstream activation of PLC/iCa^{2+} release and inhibition of the adenylyl cyclase activity [Harris et al., 2017]. In addition, GIPR interacts with all three RAMPs, modulating its cell surface expression, iCa^{2+} mobilisation and phosphorylation of ERK1/2 [Harris et al., 2017].

1.5.6 Recent understanding towards GLP-1R structure

Compared to the class A GPCRs, the class B GPCRs are known to possess large, flexible N-terminus ECDs which hindered the structural determination of the secretin-like receptors in the past decades [Krumm and Roth, 2020, Wootten and Miller, 2020]. However, thanks to recent breakthroughs in the development of nanobodies and

antibodies, GPCRs complexes can be stabilised, allowing high-resolution structural determination via cryo-electron microscopy (EM) of a number of class B GPCRs [Liang et al., 2017, Zhang et al., 2017a, Zhang et al., 2018, Hilger et al., 2020, Qiao et al., 2020, Garelja et al., 2020, Chang et al., 2020, Liang et al., 2020b, Ma et al., 2020b]. The structures of GPCRs complexed with cognate agonists, antagonists and/or G protein provide a mechanical glimpse towards the mechanisms of activation and biased signalling of class B GPCRs. In particular, there are a number of GLP-1R full-length high-resolution structures determined by cryo-EM [Jazayeri et al., 2017, Zhang et al., 2017a, Liang et al., 2018b, Wu et al., 2020] (Fig. 1.10), which undoubtedly facilitate drug design. The significance of which will be further discussed in this section.

1.5.6.1 Structural similarities among class B GPCRs

The class B GPCRs generally have distinctly large ECDs which are composed of 120 to 160 residues. Their ECDs are comprised of two anti-parallel β-sheets and an amino-terminal α-helix, connected by series of loops and stabilised by three disulphide bonds [Graaf et al., 2017]. Compared to the class A GPCRs, their upper TM-regions are more open towards the extracellular side of the membrane and pockets where small molecules can bind to are apparently absent [Wootten and Miller, 2020]. However, their TM regions are highly conserved across class B GPCRs. Upon receptor activation, deep V cavities are formed, which are considerably wider than the rest of the other classes of GPCRs [Graaf et al., 2017]. In terms of G protein binding site, similar conformational changes at helix 6 are observed and analogous intracellular binding sites are found in class A and class B GPCRs. However, the helix 5 of the $G\alpha_s$ subunit protrudes deeper into the intracellular binding sites for the secretin-like GPCRs compared to the class A GPCRs and are stabilised by the polar interaction mediated by a conserved amino acid. This conserved amino acid has also been found to be implicated in negative allosteric modulator binding [Graaf et al., 2017].

1.5.6.2 Two-domain model of activation

Given the highly conserved amino acid sequences of the ECDs among class B GPCRs, it is postulated that the secretin-like receptors adopt similar mechanism of actions for their activation. In fact, two-domain model of activation has been proposed [Hoare, 2005]. The peptide ligands of secretin-like receptors often show little ordered structures in aqueous solutions [Parthier et al., 2009]. However once the C-terminus of the peptide

ligand interacts with the N-terminal ECD of the receptor, the peptide ligand adopts an α-helical conformation, allowing itself to penetrate deeply into the upper half of the TM domain (also termed as junction domain). In fact, recent reports of crystal structures of these class B GPCRs in complex with cognate ligands have substantiated the two-domain model of activation, which show that the peptide ligands penetrate deeply into the core and sit above the central polar network [Liang et al., 2017, Zhang et al., 2018]).

1.5.6.3 GLP-1R orthosteric agonist binding and receptor activation

Thanks to the recent structure that reveals GLP-1R in complex with GLP-1, defining features of the GLP-1R orthosteric binding pocket (i.e. the binding site of the recognised endogenous ligands of the receptors to produce biological responses) are identified [Zhang et al., 2017a], as well as providing a mechanistic comparison between its active and inactivate states [Wu et al., 2020] (Fig. 1.10). When GLP-1R is in its inactive state, its ECL1 and ECL3 form an α-helical conformation similar to that of the GLP-1-bound GLP-1R structure [Wu et al., 2020]. Furthermore, the peptide-binding groove of the ECD is juxtaposed with the TM domain interacting with ECL1 and ECL3 [Wu et al., 2020]. Also, the ECD is found to be dynamic in its inactive form as suggested in the molecular dynamic (MD) stimulation. However, closed conformation of the ECD is preferred, stabilised by the weak interaction between ECL1 and ECL3 [Wu et al., 2020].

According to the report on the active GLP-1R in complex with GLP-1 and Gα_s subunit [Zhang et al., 2017a], GLP-1 forms an extensive network of interactions involving TM1, TM2, TM5, TM7, ECL1 and ECL2, as well as ECD [Zhang et al., 2017a]. Consistent with the two-domain model of activation, the N-terminus of GLP-1 penetrates into the receptor core, particularly through the interaction of the Histidine residue at position 7 at the GLP-1 peptide to interact with Arginine-229 residue on the ECL2 at the GLP-1R, as well as the glutamic acid residue at position 9 at the GLP-1 that interacts with Leucine-388 and Serine-392 of TM7 via van der Waals' forces [Zhang et al., 2017a]. In addition, ECL1 and ECL2 have been found to be implicated in GLP-1 binding with the GLP-1R [Zhang et al., 2017a]. The precise Gα_s binding site has also been validated to be at the cytoplasmic half of TM6, with limited associated movement of TM5 to form a cavity together with TM2, TM3 and TM7 [Zhang et al., 2017a].

1.5.6.4 GLP-1R biased signalling

The availability of crystal structures of GLP-1R in complex with various ligands, namely peptide 5 (a GLP-1 nanopeptide) [Jazayeri et al., 2017] and Exendin-P5 (ExP5) (a biased GLP-1R agonist with diminished coupling with β-arrestins) [Zhang et al., 2015, Liang et al., 2018b], facilitates the molecular understanding of GLP-1R biased signalling. Firstly, the ECDs of GLP-1R bound to peptide 5 and ExP5 display different conformations when comparing that to GLP-1 bound to its endogenous agonist. The ECD is fully opened in the presence of GLP-1, whereas the ECD is only partially extended in the presence of ExP5 [Liang et al., 2017]. Secondly, TM1, the extracellular portions of TM6 and TM7, and the ECL3 conformation are different between the binding modes of GLP-1 and ExP5 at the GLP-1R [Liang et al., 2017], which suggest these regions are responsible for regulating biased signalling and are indeed substantiated by an earlier study which shows that the ECLs are responsible for triggering biased agonism [Wootten et al., 2016a].

In fact, two distinct regions that are critical for biased agonisms of GLP-1, OXM and Ex-4 have been identified in a series of mutagenesis studies; these mutations were further mapped into the reported GLP-1R structures [Lei et al., 2018]. According to the authors, the first region involves the interface between TM5 and 6 and is linked to the reorganization of ECL2 into a structured network that is required for propagation of signalling linked to $G\alpha_s$ and $G\alpha_q$-dependent pathways at the GLP-1R. The second is the interface between TM1 and 7 that is the key driver of pERK1/2 (at least mediated through $G\alpha_i$-activation) at the GLP-1R. They also identified key amino acid residues within these regions that are critical for peptide binding and their functional signalling [Lei et al., 2018].

In their study, they also identified a shallower binding orientation of OXM in the orthosteric binding pocket. They attributed the observation to the fact that OXM contains an uncharged glutamine (Gln) residue, which is equivalent to a charged residue glutamic acid (Glu) at position 9 at GLP-1 peptide. The uncharged Gln residue therefore cannot form a salt bridge with Arg-190 residue at the GLP-1R. Indeed, compared to the loss of affinity of GLP-1 and Ex-4 in the presence of the mutation of Trp-297 and the adjacent Cys-296, the attenuation of OXM affinity only occurs when a different set of amino acid mutation (F381A, L142A, and K202A, R380A) are involved. These all imply OXM binds to the GLP-1R in a different manner compared to GLP-1 and Ex-4 [Lei et al., 2018].

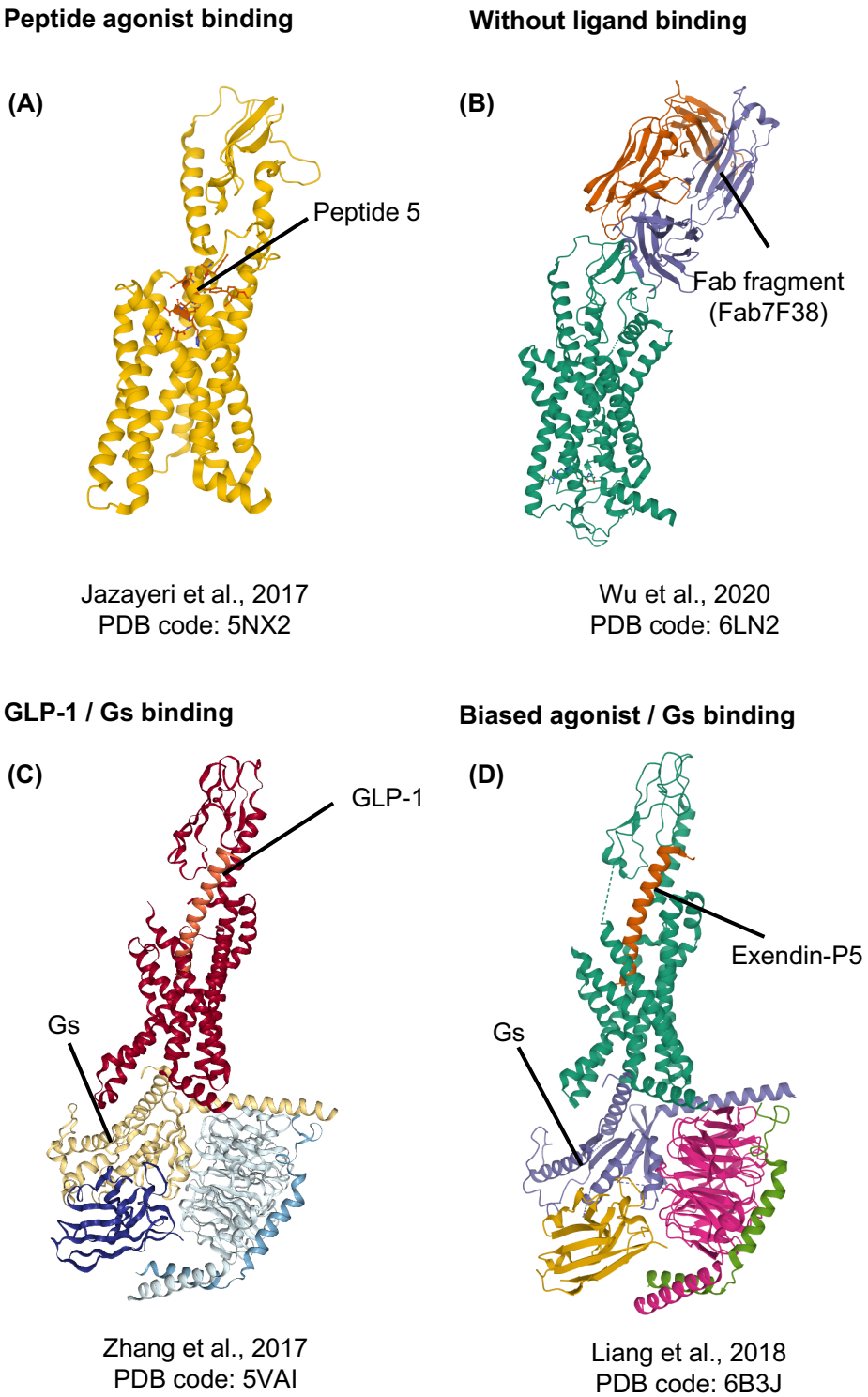

Figure 1.10: **GLP-1R full length crystal structures determined by cryo-electron microscopy.** (A) shows the full GLP-1R structure in complex with peptide 5; (B) shows the GLP-1R structure without orthosteric ligand binding and stabilised by a Fab fragment; (C) shows the GLP-1R structure in complex with GLP-1 and Gα_s; (D) shows the structure in complex with the biased agonist Exendin-P5 and Gα_s.

1.5.7 Accessory proteins: endogenous allosteric modulators of GPCR signalling

Accessory proteins are proteins that are distinct from GPCR and G protein. They are also known to be effectors that regulate the specificity, efficacy or potency of signal transduction upon receptor activation [Sato et al., 2006]. They are now known to modulate receptor trafficking in both class A and class B GPCRs [Couvineau and Laburthe, 2012]. Numerous accessory proteins have been reported ever since their discovery in the 90s [Sato et al., 2006]. Here, only the accessory proteins which are reported to modulate the functions of class B GPCRs, which are RAMPs and receptor component protein (RCP) will be discussed in more details.

1.5.7.1 Receptor activity modifying proteins (RAMPs)

RAMPs, a class of single-TM accessory proteins with three cardinal members: RAMP1, RAMP2 and RAMP3, have been first discovered to be essential for the signal transduction of CLR, giving rise to different signalling outcomes depending on the modulation by the partnering RAMPs [McLatchie et al., 1998]. RAMPs consist of N-terminal ECDs with approximately 100 amino acids and short C-terminal intracellular domains of around 9 amino acids [Hay et al., 2016]. Furthermore, the three RAMPs share 31% structural homology and 56% similarity, as determined by amino acid multiple alignments [Serafin et al., 2020]. The differences in their N and C-terminus, such as the addition of 28-amino acid in the ECD for RAMP2, and the presence of the PDZ motif in the C-terminal for RAMP3, have been thought to attribute to their functional differences [Serafin et al., 2020].

1.5.7.2 RAMPs modulation of GPCR signalling

RAMPs interact with GPCRs to regulate their binding, signalling and trafficking in ligand, receptor, and cell-type dependent manners [Hay et al., 2016]. In fact, RAMPs themselves act as an example of endogenous allosteric modulators, whereby they require a spatially different binding site to the orthosteric binding site at the GPCR (the concept of allosterism will be explained in more detail later). Recent investigations have reported a wide array of GPCR-RAMPs interactions, which mainly involve the class B GPCRs, namely CTR, CLR, CRF receptors, GCGR, PTH receptors, SCTR, GLP-2R and PACAP receptors [Routledge et al., 2017]. G protein-coupled estrogen receptor 1 (GPER/GPR30) (class A GPCR) and calcium-sensing receptor (CasR) (class C GPCR),

as well as chemokine receptors are also shown to interact with RAMPs [Serafin et al., 2020].

CLR is one of the well-studied GPCR:RAMPs interactions [Hay et al., 2016]. RAMPs are shown to act as chaperones to facilitate CLR surface expression [Hay et al., 2016]. CLR requires the coupling of RAMP1, RAMP2 and RAMP3 to form the functional CGRP receptor, AM1 receptor and AM2 receptor respectively. CLR signalling is also highly modulated by RAMPs, which RAMP1 facilitates the Gα_s signalling of CGRP and Gα_i coupling of AM1 and AM2, while RAMP2 enhances the Gα_s signalling of AM1 [Routledge et al., 2017]. RAMP3 has also been shown to modulate CLR internalisation [Hay et al., 2016].

The recent reports on the cryo-EM structures of CLR in complex with RAMP1 [Liang et al., 2018a], RAMP2 and RAMP3 [Liang et al., 2020a] have shone new insight into the structural determinant of GPCR-RAMP interaction (Fig. 1.11). According to the published structures, the RAMPs induce distinct orientations of the ECDs, which coordinate the motions of the G protein, ultimately influencing G protein interactions with the receptors [Liang et al., 2020a]. Furthermore, unique position of the ECL3 depending on the RAMP:CLR complex has been discovered, and the observation was further supported by the results from the chimeric exchange of the linker region of the RAMPs connecting the TM helix [Liang et al., 2020a]. These reports of the cryo-EM structures of full length GPCRs in complex with different RAMPs have undoubtedly advanced the understanding towards how RAMPs allosterically modulate GPCR functions.

1.5.7.3 Physiological significance of RAMPs expression

The current understanding of RAMPs functional significance has been envisaged through the use of global genetic RAMP-knock-out mice [Serafin et al., 2020]. These reports have shown significant impact of RAMPs on regulating cardiovascular, lymphatic, immune, endocrine, and central and peripheral nervous systems. In particular, global knock-out of RAMP2 has been shown to affect embryonic lethality, resulting in endocrine and skeletal muscles disorders while genetic knock-out of RAMP1 and RAMP3 leads to mild excessive fluid accumulation in embryos; yet the RAMP3-knock out has been proven to be viable in mice [Serafin et al., 2020]. Furthermore, there has been a downregulation of RAMP3 mRNA in non-diabetic obesity patients [Dong et al., 2017], further supporting the role of RAMPs in regulating physiological functions.

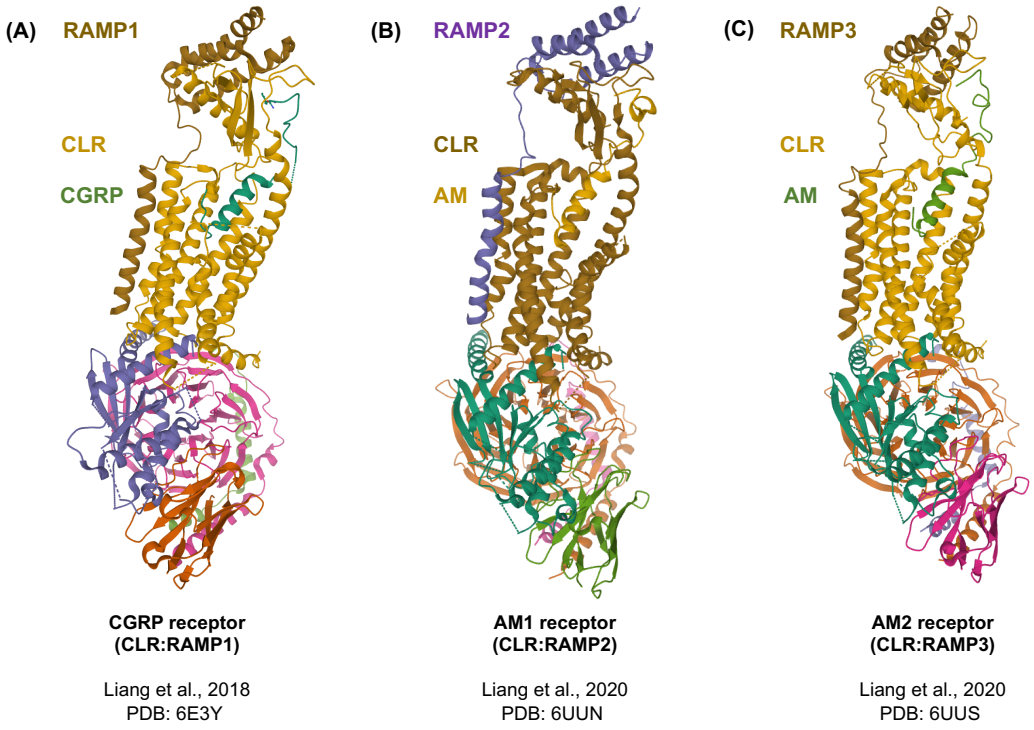

Figure 1.11: **Cryo-EM full length structures of CLR in complex with RAMP1, RAMP2 and RAMP3.** (A) depicts CLR:RAMP1:CGRP complex [Liang et al., 2018a]; PDB code: 6E3Y. (B) and (C) depict CLR:RAMP2:AM (PDB code: 6UUN) and CLR:RAMP3:AM (PDB code: 6UUS) complexes [Liang et al., 2020a].

1.5.7.4 Receptor component protein (RCP)

Receptor component protein (RCP) is a 148 amino acid intracellular peripheral protein and is found in the brain, spinal cord, uterus and blood vessels [Prado et al., 2002]. RCP is part of the human RNA polymerase II and is found to play a role in RNA synthesis [Dickerson, 2013]. However, apart from its role in RNA synthesis, RCP is shown to be essential for the effective coupling of $G\alpha_s$ subunit to the CGRP receptor to mediate cAMP responses through interacting with the ICL2 at the receptor [Dickerson, 2013]. However, the binding of CGRP to the CGRP receptor and CGRP receptor trafficking are not affected in the absence of RCP [Dickerson, 2013]. On a physiological level, the reduction in RCP expression has been shown to correlate with less sensitivity towards CGRP. Apart from CGRP receptor, a recent paper illustrates that RCP impairs the cAMP responses in other class B GPCRs, namely CTR, CRF1R and GLP-2R, but not GLP-1R, GIPR and AM1 receptor [Routledge et al., 2020].

1.6 Allosteric modulation

Developing ligands which bind to the orthosteric sites has been the mainstay of drug discovery. In recent decades, the notion of developing allosteric ligands that bind to the allosteric site (i.e the binding site that is topographically distinct to the orthosteric site of the same receptor) (Fig. 1.12A) has opened up a whole new avenue for developing novel drug treatments [Christopoulos, 2002]. The prominent examples of allosteric modulators approved by the Food and Drug Administration (FDA) include: the anti-viral agent, maraviroc, which is a negative allosteric modulator (NAM) of the class A GPCR chemokine receptor type 5 (CC5), the anti-thrombotic agent, ticagrelor, which is an allosteric antagonist of the P2Y receptor and cinacalet, a positive allosteric modulator (PAM) for the CasR for hyperparathyroidism.

1.6.1 Therapeutic advantages of allosteric modulators

The therapeutic uses of allosteric modulators confer a number of advantages. First, allosteric modulators have a high receptor subtype selectivity due to the low conservation within the allosteric sites in comparison to the orthosteric sites, which allow the discovery of novel allosteric sites. Hence selective cooperativity (the concept of cooperativity will be explained later) may exert on one subtype expressing the distinct allosteric site but not the other [Kenakin, 2012, Thal et al., 2018]. Secondly, the effect of

the allosteric ligands reaches saturation based on the existing reserve of the orthosteric ligands, therefore providing a mean to fine tune the natural hormone activity via the use of the allosteric drug adjunctive, thereby reducing the potential dose-dependent side effects mediated by traditional drug therapies [Wootten et al., 2016a]. Thirdly, allosteric ligands cannot exert their modulation in the absence of the orthosteric ligands. This may provide a tissue-specific effect as the activity of the allosteric modulation depends on the local release of the native hormone. However, certain diseases, such as late stage neurodegeneration, may limit the use of such allosteric modulation as the endogenous hormonal release has been depleted [Wootten and Miller, 2020]. Lastly, allosteric modulators have the potential to exert biased signalling on the actions of the endogenous orthosteric agonists. Yet such observations are yet to be validated clinically [May et al., 2007]. In short, the potential of delivering a safer and more efficacious drug treatment via the use of allosteric modulators provides a new mean in advancing existing drug treatments [Christopoulos, 2014, Thal et al., 2018].

1.6.2 Cooperativity and probe dependence

As previously mentioned, the allosteric site is spatially distinct from the orthosteric site, such that both allosteric modulator and orthosteric ligand can bind simultaneously to the same receptor. Each of these ligands can bind to the receptor at different affinity and can alter the function of the receptor at varying efficacies for the activation or recruitment of signal transduction proteins (Fig. 1.12). However, the simultaneous binding of both the orthosteric ligand and the allosteric modulator can influence the behaviour of each other, which is thus termed as cooperativity [Leach et al., 2007]. The quantification of cooperativity (see section 1.6.4) thus allows the classification of the allosteric modulation based on their actions on the orthosteric ligand [Leach et al., 2007, Kenakin, 2012], which will be discussed later.

Furthermore, probe dependence, a phenomenon which exists when the effect of the allosteric modulator is specific to a particular orthosteric ligand and depends on the cooperativity between the orthosteric ligand and the allosteric modulator. This phenomenon is particularly important for class B GPCRs as this class of GPCRs more often possess more than one endogenous agonists and offers a unique way to sculpt the desirable signalling outcome [Wootten et al., 2016a] (Fig. 1.12).

1.6.3 Biased agonism and biased modulation

Biased agonism (also termed as ligand-directed signalling bias or functional selectivity) has become a major paradigm in designing new drugs which through sculpting certain desirable signalling outcome, treatment efficacies can be enhanced and side effects can be eliminated [Kenakin and Christopoulos, 2013]. The phenomenon of biased agonism occurs when various ligands bind to the same orthosteric binding pocket of a GPCR, distinct responses are resulted (Fig. 1.12). It can be explained by the fact that the orthosteric ligands, each of which is a unique chemical entity, interact with the receptor in distinct ways that unique receptor conformations are resulted [Wootten et al., 2018]. Each of the unique receptor conformation upon orthosteric ligand binding governs the kinetics of binding and how the receptor interacts with the regulatory and effector proteins [Kenakin, 2012]. Examples of biased GLP-1R peptide agonists relative to the cognate endogenous agonist GLP-1 include ExP5 (as aforementioned in section 1.5.6.4) and OXM. ExP5 shows relatively limited β-arrestins recruitment compared to GLP-1, yet it displays a faster G protein dissociation, particularly the Gα_s subunit dissociation, in comparison to GLP-1 [Liang et al., 2018b]. While OXM is a full agonist in mediating cAMP response, it is a partial agonist of β-arrestin 2 and GRK2 recruitment relative to GLP-1 [Jorgensen et al., 2007]. These all supports the notions that upon ligand binding at the receptor, multiple conformations can be resulted, which all lead to distinct signalling outcomes [Thal et al., 2018].

As allosteric ligands bind to spatially distinct sites other than the orthosteric sites, these ligands often display distinct signalling relative to the orthosteric ligand. Distinctive signalling outcome arises as the allosteric ligands alter the conformational landscape of the receptor, thereby changing the signalling profile of the orthosteric ligand. Such phenomenon is known as 'biased modulation' [Wootten et al., 2016c] (Fig. 1.12).

1.6.4 Operational model of agonism and allosterism

The allosteric ternary complex model (ATCM) has been used initially to quantify the affinities (defined by the equilibrium constants, K_A and K_B of the orthosteric and allosteric ligands respectively) of both the orthosteric (represented by A) and allosteric (represented by B) ligands when binding to the receptor. The key parameter of the ATCM is the cooperativity factor (α), which is a measure of the strength and direction of the allosteric effect on affinity for one binding site when the other is occupied. However,

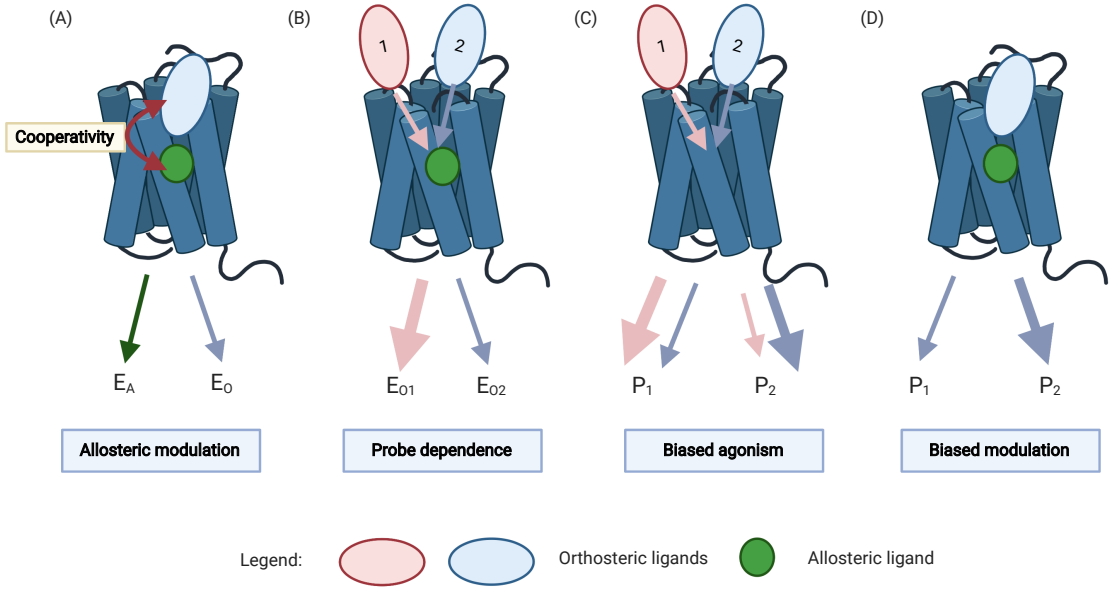

Figure 1.12: **Illustrations of allosteric modulation, probe dependence, biased agonism and biased modulation.** (A) shows that the allosteric modulator and orthosteric ligand both bind to the receptor, resulting in different efficacies of the signalling outcome (E_A and E_O denote the efficacies mediated by the allosteric ligand and the orthosteric ligand respectively). The influence of the allosteric modulator on the orthosteric ligand is termed as 'cooperativity'. (B) shows the probe dependence phenomenon which is observed when a specific signalling outcome is enhanced in the presence of the interaction of the allosteric ligand with a specific orthosteric ligand. (E_{O1} and E_{O2} denote the efficacies of signalling outcome 1 and 2 respectively). (C) shows the concept of biased agonism while (D) illustrates the concept of biased modulation (P_1 and P_2 indicate the biased signalling of pathway 1 and 2 respectively). Diagram created with BioRender.com.

the ATCM cannot account the allosteric effect on efficacy. Hence, the ATCM has been extended into the operational model of agonism and allosterism (Fig. 1.13) [Leach et al., 2007], which now enables the quantification of the allosteric effect on efficacy, which is denoted by β.

The operational model of agonism and allosterism now describes that upon stimulation by a stimuli (S), three different species are resulted, which are AR (orthosteric drug-receptor complex), RB (allosteric drug-receptor complex) and ARB (the ternary complex). The parameters τ_A and τ_B denote the capacity of agonism exhibited by the orthosteric and allosteric ligands respectively. The τ_A and τ_B values also incorporate the intrinsic efficacy of each ligand, the total density of receptors and the efficiency of stimulus-response coupling. The terms E_m and n indicate the maximal possible system response and the slope factor of the transducer function that links occupancy to response respectively [Leach et al., 2007]. Therefore, with the aid of the operational model, the key parameter, which is the cooperativity factor can be represented by the $\log\alpha\beta$ value, which incorporates both the allosteric effect of the affinity (α) and efficacy (β) on the orthosteric ligand. The mode of allosteric modulation can be classified as follow [Kenakin and Miller, 2010, Lane et al., 2017]:

- Positive allosteric modulation (PAM): $\log\alpha\beta > 1$
- Negative allosteric modulation (NAM): $\log\alpha\beta < 1$
- Neutral allosteric ligand (NAL): $0 < \log\alpha\beta < 1$

Apart from possessing pure positive allosterism, certain allosteric ligands can also exhibit intrinsic agonism independent of the presence of orthosteric ligand. These compounds are so-called 'agonist-positive allosteric modulator' (ago-PAM) [Kenakin, 2012]. Compound 2 [Knudsen et al., 2007] is a representative example for such a unique class of allosteric modulator, which will be further discussed in the following sections.

1.6.5 Challenges of developing GLP-1R small molecule PAMs

T2DM treatments that target GLP-1R are highly sought after as GLP-1R regulates blood glucose homeostasis through the action of GLP-1 [Seino et al., 2010]. In fact, a number of GLP-1R based peptide treatments exhibit superior efficacies compared to standard oral T2DM treatments, yet their uses are limited by their gastrointestinal side effects and subcutaneous administration, which largely hinder patient compliance [Defronzo et al., 2015]. Hence, tremendous amount of effort was made in recent years in an

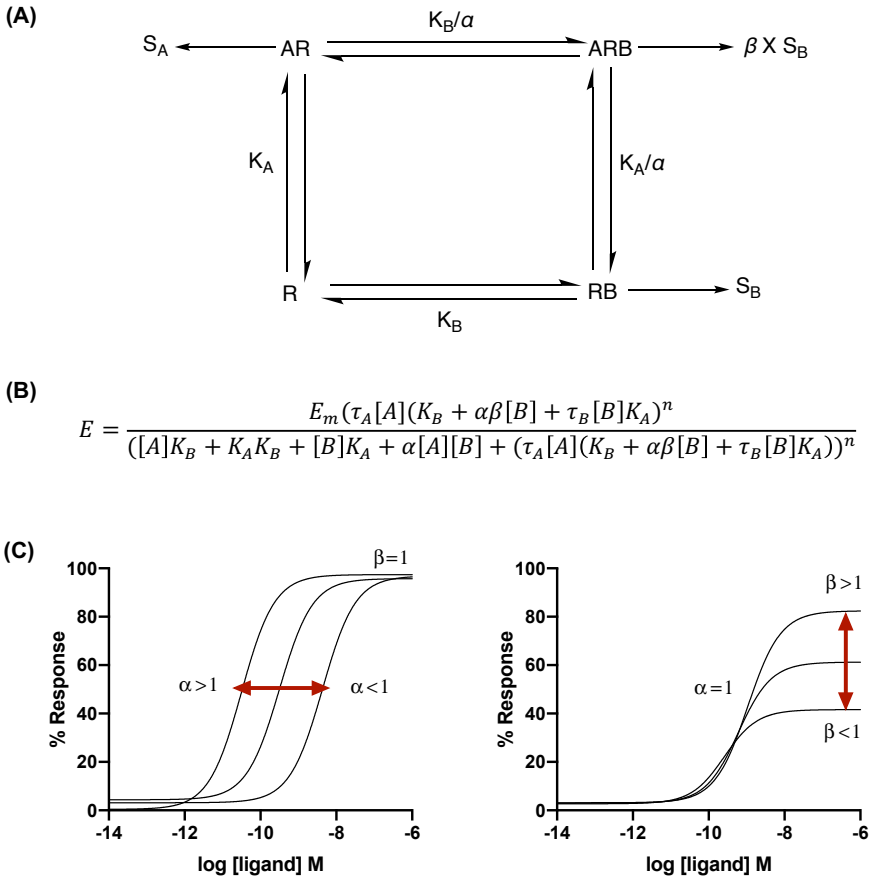

Figure 1.13: **Schematic diagram illustrating the operational model of agonism and allosterism.** (A) shows the operational model of agonism and allosterism while (B) shows the equation derived from (A). (C) shows the representative dose-response plots of how α and β are defined. Abbreviations: AR: orthosteric drug-receptor complex, RB: allosteric drug-receptor complex; ARB: the ternary complex; S_A: stimulus given by the orthosteric drug; S_B: stimulus given by the allosteric drug; τ_A and τ_B: the capacity of agonism exhibited by the orthosteric and allosteric ligands respectively; E_m: the maximal possible system response; n: the slope factor of the transducer function that links occupancy to response; α and β: the allosteric effect of the affinity and efficacy respectively.

attempt to develop small molecule GLP-1R agonists that can be potentially developed into oral T2DM drug treatments.

As previously discussed (section 1.5.6.1), GLP-1R possesses a larger ECD compared to other class A GPCRs, hence GLP-1R peptide ligands have more contacts with the ECD and parts of ECL [Jazayeri et al., 2017]. As the GLP-1R peptide ligands usually consist of 30-40 amino acids, it is difficult to construct small molecule ligands with sizes that are comparable to those of peptide ligands without compromising their drug-like properties [Willard and Sloop, 2012]. However, recent understanding towards GLP-1R agonism has been advanced thanks to the reports of full-length GLP-1R crystal structures that immensely facilitate drug design. Hence excitedly, GLP-1R small molecule agonists, TT-OAD2 [Zhao et al., 2020] and RGT1833 [Ma et al., 2020a] have been discovered very recently (their mechanisms of actions will be discussed later).

1.6.6 Existing GLP-1R small molecule PAMs, ago-PAMs and agonists

Alongside the search for potential small molecule agonists, efforts have also been made to design GLP-1R allosteric modulators. In fact, a few GLP-1R small molecule PAMs have been discovered prior to the spawning reports of GLP-1R full length structures (Fig. 1.14 and Table 1.2). The most studied compounds among all are compound 2 (developed by Novo Nordisk) [Knudsen et al., 2007] and BETP (developed by Eli Lilly) [Sloop et al., 2010], both of which give distinct signalling profiles [Lin and Wang, 2009, King et al., 2015]. However, none of them is successful in clinical trials due to various reasons, such as concerns of cytotoxicity [Coopman et al., 2010], lack of drug-like properties [Chen et al., 2007] and chemical instability in the presence of nucleophiles [Willard and Sloop, 2012] despite showing promising *in vitro* and *in vivo* insulinotropic actions. Hence, the search for GLP-1R small molecule PAMs is ongoing. The mechanisms of actions of compound 2, BETP, NNC0640, PF06372222, TT-OAD2, RGT1383 and LSN3160640 will be discussed in further details in next section.

1.6.6.1 Compound 2

Compound 2, together with BETP, are the most well-studied ago-PAMs [Koole et al., 2010, Coopman et al., 2010, Koole et al., 2011, Harikumar et al., 2012, Cheong et al., 2012, Li et al., 2012, Koole et al., 2015, Thompson and Kanamarlapudi, 2015, Thompson et al., 2016]. Compound 2 was originally discovered by Novo Nordisk in 2007 [Knudsen et al., 2007] and was shown to possess agonism at the GLP-1R, despite displaying bell-

shaped dose response curve at high concentrations. It was also reported in the original article that compound 2 was able to act as a PAM which enhanced GLP-1 affinity and cAMP accumulation response in Baby Hamster Kidney (BHK) cells expressing GLP-1R [Knudsen et al., 2007]. Compound 2 was also found to enhance insulin secretion in *ex vivo* isolated mouse islets as well as *in vivo* mouse models. Following the original report, extensive characterisation of this small molecule compound was performed by numerous research groups. They collectively showed that apart from GLP-1, compound 2 is also able to potentiate OXM, GLP-1(9-36)NH_2, GLP-1(1-37) and GLP-1(7-37) signalling responses, such as cAMP, iCa^{2+} mobilisation and phosphorylation of ERK1/2 using recombinant cell lines stably expressing GLP-1R [Coopman et al., 2010, Koole et al., 2010, Li et al., 2012]. However, further development of compound 2 as a T2DM drug treatment is limited by its cellular toxicity when used at high concentrations as well as its instability in the presence of nucleophiles [Coopman et al., 2010, Eng et al., 2013, Nolte et al., 2014, Bueno et al., 2016].

1.6.6.2 BETP

BETP, which is also called 'compound B', was discovered by Eli Lilly [Sloop et al., 2010]. It was originally reported to demonstrate micromolar agonism specifically at the GLP-1R as well as enhance GLP-1-mediated cAMP responses in Human Embryonic Kidney (HEK)-293 stably expressing human GLP-1R with cAMP responsive element (CRE) luciferase reporter [Sloop et al., 2010]. Furthermore, it was reported to potentiate insulin secretion in isolated mouse islets [Sloop et al., 2010]. Similar to Compound 2, extensive characterisation of BETP was also performed by various research groups [Wootten et al., 2012, Wootten et al., 2013a, Koole et al., 2015, Yin et al., 2016, Thompson et al., 2016], and the studies collectively suggest that BETP also potentiates the cAMP responses mediated by OXM and GLP-1(9-36)NH_2 [Willard et al., 2012b]. Yet, BETP has also been proven to be instable in the presence of nucleophiles [Eng et al., 2013, Nolte et al., 2014, Bueno et al., 2016], which also hindered its further development as a potential T2DM drug treatment.

1.6.6.3 NNC0640 and PF01672222

Limited functional data was reported for NNC0640 and PF01672222. However, both compounds were originally designed as GCGR antagonists but were later discovered to also possess NAM activity at the GLP-1R [Song et al., 2017, Wu et al., 2020].

1.6.6.4 TT-OAD2

TT-OAD2, which is part of the chemical series of the drug candidate TTP273 (which has completed phase IIa efficacy trial for T2DM), was developed by vTv Therapeutics [Zhao et al., 2020]. However, difficulties in identifying its optimal dosing were reported and therefore further studies were conducted to investigate its mechanisms of actions. Through conducting various functional assays, TT-OAD2 has been found to be a weak partial agonist for cAMP accumulation, iCa^{2+} mobilisation responses, phosphorylation of ERK1/2 and no detectable β-arrestin-1 recruitment, relative to the native GLP-1 peptide signalling. Furthermore, utilising split luciferase NanoBit G protein sensors, the authors showed that besides $G\alpha_s$ protein, $G\alpha_{i/o/z}$ subunits are also essential for its apparent cAMP signalling responses. Further utilisation of both the bioluminescence resonance energy transfer (BRET)-based G protein sensors and EPAC-biosensor demonstrated a slower kinetic in inducing conformation changes in recruiting $G\alpha_s$ protein displayed by TT-OAD2 in comparison to GLP-1. Overall, it shows that TT-OAD2 is a biased agonist that shows distinct activation kinetics in relative to the cognate endogenous ligand [Zhao et al., 2020].

Furthermore, co-applying TT-OAD2 with GLP-1 or OXM resulted in a dose-dependent reduction of the cAMP signalling responses of GLP-1 or OXM [Zhao et al., 2020]. This may provide a mechanistic explanation for its difficulties in determining the optimal dosage efficacy, as when TT-OAD2 is used at high concentration, the signalling responses of the endogenous agonists are reduced. In fact, it has been observed in clinical trials that TT-OAD2 is most effective when used at low dosage [Zhao et al., 2020].

1.6.6.5 RGT1383

Limited functional data regarding RGT1383 was reported by the authors [Ma et al., 2020a]. However according to the report, RGT1383 is a full agonist in mediating cAMP response and a partial agonist in β-arrestin-1 recruitment [Ma et al., 2020a].

1.6.6.6 LSN3160640

LSN3160630 has been shown to enhance both the potency and efficacy of GLP-1(9-36)NH_2-mediated cAMP responses, to an extent that GLP-1(9-36)NH_2 was potentiated to mediate full agonistic response in the presence of 1μM LSN3160630. In addition, LSN3160630 is able to enhance the binding of GLP-1(9-36)NH_2 to the GLP-1R by 70-fold

through radioligand displacement assay. Notably, the compound shows strong probe dependence towards GLP-1(9-36)NH_2 relative to GLP-1 and OXM [Bueno et al., 2020].

Furthermore, LSN3160630 is able to enhance GSIS in *ex vivo* isolated mouse islets and that the responses are glucose, ligand and GLP-1R-specific. Further intravenous glucose tolerance tests (ivGTTs) in Wistar rats showed that LSN3160630 illustrates dose-dependent insulinotropic effect in the presence of GLP-1(9-36)NH_2 [Bueno et al., 2020].

Table 1.2: **List of GLP-1R allosteric modulators, agonists or ago-PAMs published in literature.**

Compound	Form of allosterism	Probe dependence towards GLP-1R endogenous ligands	References
T-0632	NAM	N.D.	Tibaduiza et al., 2001
Compound 2	Ago-PAM	GLP-1, GLP-1(7-37), OXM, GLP-1(1-37), GLP-1(1-36), GLP-1(9-36)	Knudsen et al., 2007
Boc5	Agonist	N/A	Chen et al., 2007
Quercetin	PAM	GLP-1, Ex-4	Schann et al., 2009
BETP/Compound B	Ago-PAM	GLP-1, OXM, GLP-1(9-36)	Sloop et al., 2010
Catechin	NAM	GLP-1	Wootten et al., 2011
Compound 20	PAM (Weak antagonist of GCGR)	GLP-1	de Graaf et al., 2011
8e	Agonist	N/A	Zhang et al., 2014
VU0453379 (S-9b)	PAM	N.D.	Morris et al., 2014
*NNC0640	NAM	N.D.	Song et al., 2017
*PF06372222	NAM	N.D.	Song et al., 2017
C-1	Ago-PAM	GLP-1	Redij et al., 2019
Compound 19	PAM	GLP-1(9-36)	Méndez et al., 2020
*TT-OAD2	Agonist	N/A	Zhao et al., 2020
*RGT1383	Agonist	N/A	Ma et al., 2020
*LSN3160440	PAM	GLP-1(9-36)	Bueno et al., 2020

* indicate existing GLP-1R full length cryo-EM structures in complex with the small molecule compounds; N.D.: Not determined; N/A: Not applicable

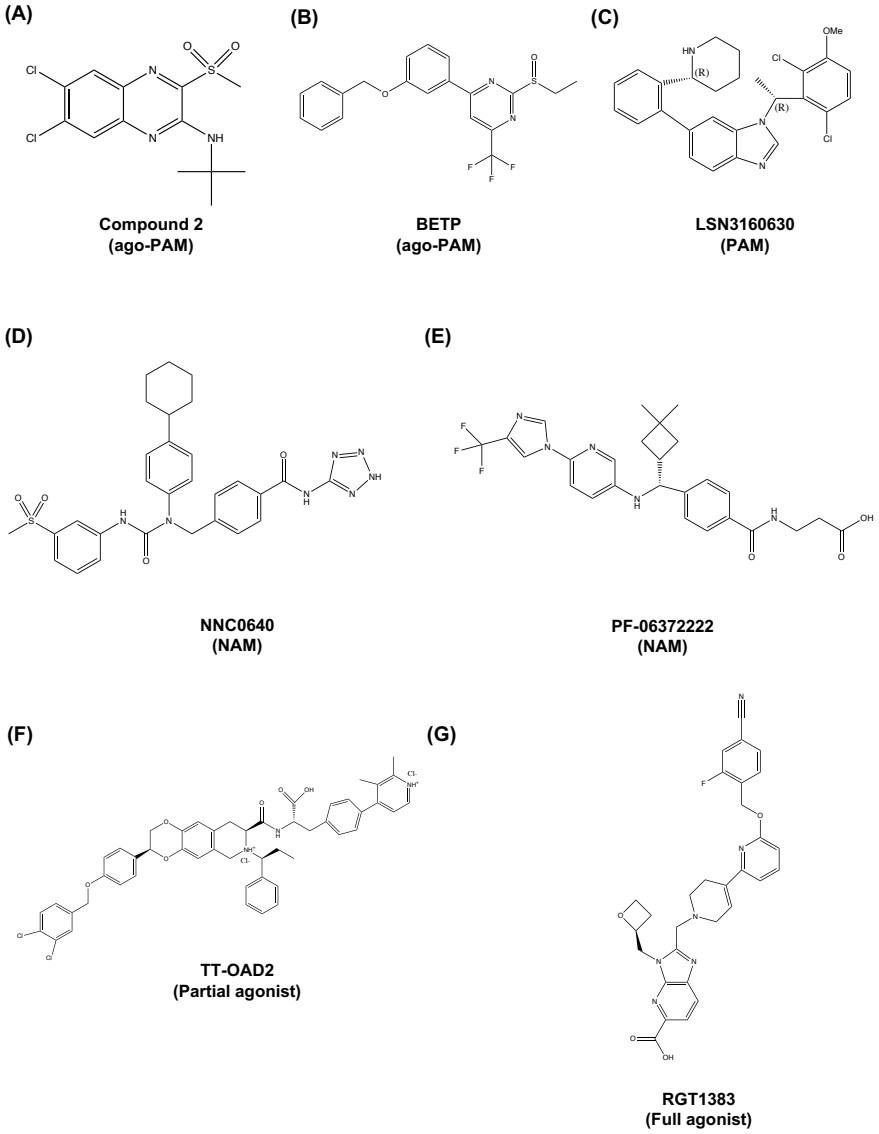

Figure 1.14: **Chemical structures of existing GLP-1R small molecule agonists and allosteric modulators.** The chemical structures of GLP-1R small molecule (A-B) ago-PAMs, (C) PAM, (D-E) NAMs, (F-G) agonists are shown in the above figures.

1.6.7 Proposed mechanisms of actions of GLP-1R small molecule agonism and allosterism

A number of cryo-EM full length structures of GLP-1R in complex with small molecule agonists [Zhao et al., 2020, Ma et al., 2020a], NAMs [Song et al., 2017] and PAM [Bueno et al., 2020] are reported which provide in-depth insights into the molecular understanding of GLP-1R allosterism. The following sections serve to discuss the existing possible binding modes of small molecule agonists and allosteric modulators at the GLP-1R.

1.6.7.1 Irreversible covalent linkage with the C347 residue at TM6

The crystal structures of GLP-1R binding to NAMs, NNC0640 and PF01672222, have been revealed recently [Song et al., 2017], which show that both NAMs bind to the binding pocket outside TM5-7 intracellularly. The authors further postulated that PAMs may also bind to the same binding pocket, but in between TM5-6. The authors further proposed a PAM binding model; they suggested that when ago-PAMs, such as compound 2, interacts with the GLP-1R, they induce conformational changes in the intracellular regions of TM5 and TM6 that results in a disruption of the intracellular ionic lock, opening up a cavity at the TM5 and TM6 to facilitate G protein binding [Song et al., 2017] (Fig. 1.16).

Apart from the interaction within the binding pockets, hydrophobicity and the interaction with $T^{6.44b}$, which is specific to the glucagon receptor family, may also play a role in determining the selectivity of small molecule allosteric modulators [Song et al., 2017]. In addition, residue Cysteine-(C)$347^{6.36b}$ is found to be important for the selectivity of small molecule allosteric modulators as it acts as the site of covalent interaction with the electrophilic groups of Compound 2 and BETP [Eng et al., 2013, Nolte et al., 2014, Bueno et al., 2016]. Compound 2 and BETP confer PAM activity on GLP-1R due to the formation of irreversible disulphide bond with the cysteine-347 residue on the ICL3 of the GLP-1R. Although C348 residue is also needed for the formation of the disulphide bond, only C347 has an effect on mediating allosteric modulation. However, drugs that form irreversible cross link is highly undesirable [Nolte et al., 2014], hence small molecule GLP-1R PAMs that act in a C347-independent mechanism have been prompted.

1.6.7.2 Molecule glue: a novel interaction between orthosteric and allosteric ligand

LSN3160640, which is a reported GLP-1R specific PAM that shows probe dependence towards GLP-1(9-36)NH_2 over GLP-1 and OXM, has been shown to mediate its positive cooperativity via the direct interaction with the orthosteric ligand [Bueno et al., 2020]. According to the cryo-EM structure which shows GLP-1R in complex with GLP-1, LSN3160640 and Gα_s subunit, the allosteric ligand binds at the higher end of the helical bundle, at the interface between TM1 and TM2 [Bueno et al., 2020] (Fig. 1.16). Unlike compound 2 and BETP, which covalently linked to the receptor for their mechanisms of action, intermolecular forces, such as van der Waals' forces, water-mediated hydrogen bonds and π-π stacking, at the residues of L142 (TM1), Y145 (TM1) and K202 (ECL1) at the receptor are essentials for the action of LSN3160640. Apart from receptor-PAM interactions, PAM-GLP-1 molecular interaction has also been identified, which shows that the molecule interacts via van der Waal's forces with the F12, V16 and L20 at the GLP-1 peptide [Bueno et al., 2020]. Interestingly, F12 and V16 residues at the GLP-1 peptide have not been shown to form contact with GLP-1R [Zhang et al., 2018] and that alanine scan also shows that the mutations of these two residues do not affect GLP-1 activity [Bueno et al., 2020]. Hence the authors were able to demonstrate that by bridging the contact between F12 and V16 of the GLP-1 peptide and TM1 and TM2 at the GLP-1R, LSN3160640 is able to enhance the affinity of the peptide to the receptor, thus offering a new mode of allosteric modulation.

More intriguingly, by aligning the amino acid sequences of GLP-1 and OXM, they identified a convergence of V16 at the GLP-1 to Y10 at OXM and that subsequent mutation to Y10V confers OXM a gain of function in potentiating the signal responses. These show that probe dependence can be controlled via direct mutation on the orthosteric ligand, thus providing a new mean in modulating the signal outcome [Bueno et al., 2020].

1.6.7.3 'Boomerang-like' receptor-compound interaction at the higher end of TM bundles

The partial agonist TT-OAD2 has been shown to bind high up in the helical bundles interacting with TM1, TM2, TM3 and ECL1 and ECL2 [Zhao et al., 2020] (Fig. 1.16). TT-OAD2 forms mainly hydrophobic interaction with the receptor, including a number of π-π stackings between the aromatic residues of the receptor and the phenolic regions of the compound. Interestingly, the compound forms a 'boomerang-like' orientation

within the binding site, with the 3,4-dichloro-benzyl moiety protruding beyond the receptor core through TM2 and TM3, interacting with W203 at the ECL1. A number of residues on the TM1, TM2 and TM3 have been identified, and mutagenesis studies further substantiated the importance of these key residues in mediating the cAMP responses, as reduction in cAMP signalling has been observed upon alanine mutations [Zhao et al., 2020].

Furthermore, the binding of TT-OAD2 shows limited overlapping with the binding of GLP-1 and ExP5. Apart from interacting with higher end of the TM1-3, the peptide-based agonists have been shown to engage deeply into the receptor core, interacting with TM5-7 [Zhang et al., 2017b, Liang et al., 2018b]. Furthermore, structural comparison combined with MD simulation suggest that there are only less than one third of common residues at the GLP-1R that interact with TT-OAD2, in comparison to its endogenous ligand GLP-1, further illustrating the unique mode of agonism conferred by TT-OAD2.

1.6.7.4 Additional interaction with TM7

Similar to TT-OAD2, the full agonist RGT1383 has also been shown to interact with residues at the higher end of TM1-3 bundles and ECL1 and ECL2 (Fig. 1.16). Yet, RGT1383 was also shown to interact with TM7 as well as the N-terminal ECD. Similarly, the use of mutagenesis studies has identified the key residues in mediating the agonistic cAMP signalling responses. In particular, W33 in the N-terminal ECD has been shown to be critical for mediating the full cAMP response agonism of RGT1383, which coincides with the interaction of TT-OAD2 and peptide 5 [Zhao et al., 2020, Liang et al., 2020a]. Compared to TT-OAD2, RGT1383 displays more extensive binding with residues at TM7, which induces inward displacements of the ECL3 and the extracellular ends of TM6 and TM7. Furthermore, in contrast to TT-OAD2, RGT1383 completely overlaps with the residues 10-20 at the GLP-1, and RGT1383 is much closer to TM6, which induces the unwinding of TM6, leading to subsequent GLP-1R activation via Gα_s binding [Ma et al., 2020a]. In addition, the authors attributed the biased signalling as observed at GLP-1, ExP5, peptide-5, TT-OAD2 and RGT1383 to the difference in inducing the conformation of the α-helix chain A at the N-terminal ECD, as well as binding at different orientations at the orthosteric binding pockets [Ma et al., 2020a]. The aforementioned allosteric and small molecule binding at the GLP-1R are summarised in Fig. 1.15.

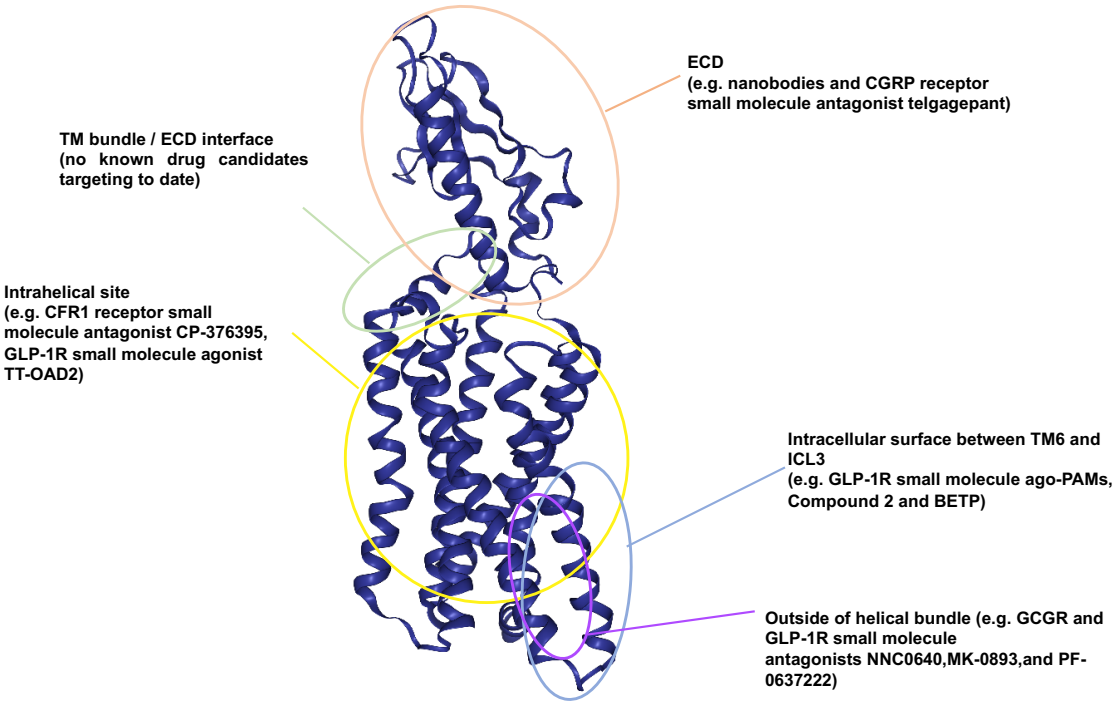

Figure 1.15: **Summary of reported small molecule agonist or allosteric modulator binding sites at the GLP-1R and other class B GPCRs.** Several binding sites have been postulated or proven for small molecule binding, which include: ECD, TM bundle/ECD interface, intrahelical site, intracellular surface between TM6 and ICL3 and outside of helical bundle.

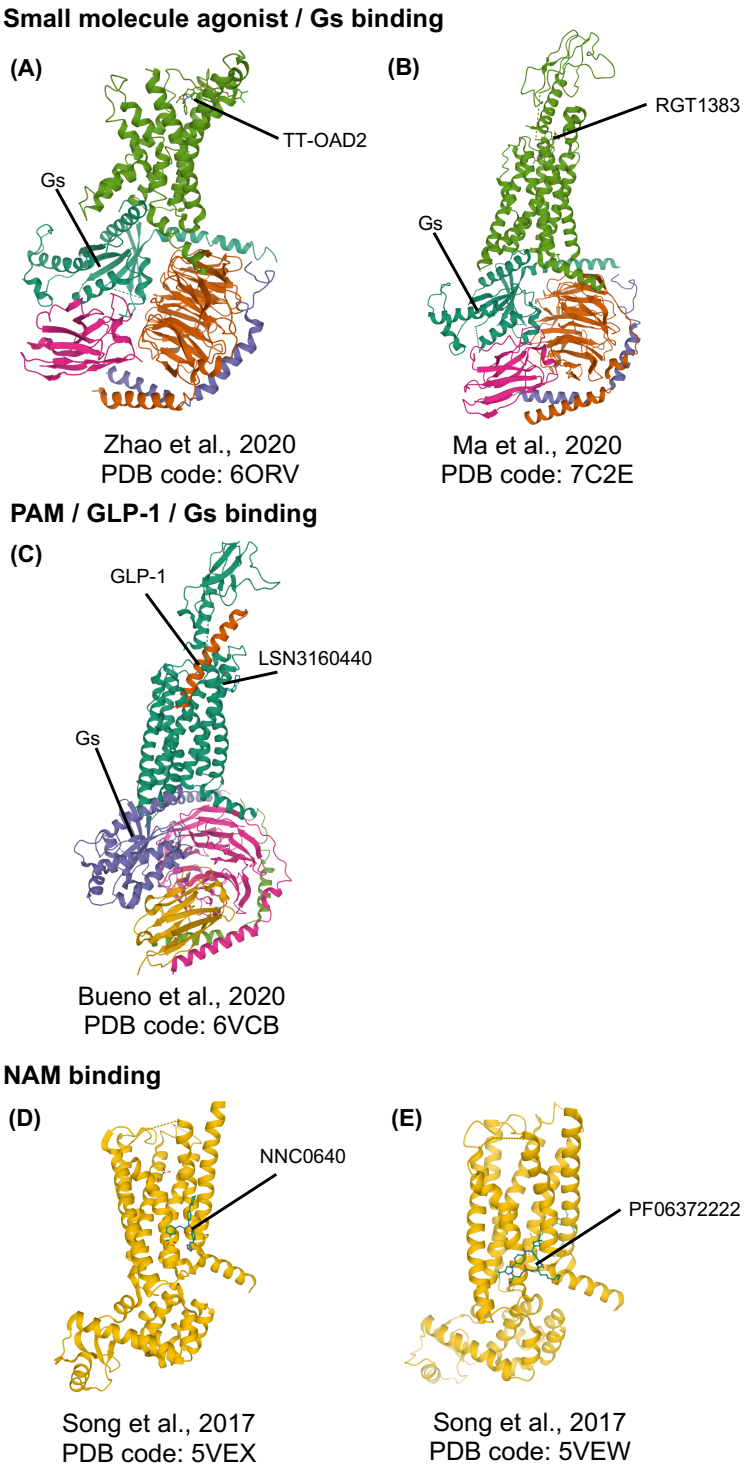

Figure 1.16: **Cryo-EM full length structures of GLP-1R in complex with NAMs, PAM and agonists.** (A) and (B) show the structures of GLP-1R in complex with TT-OAD2 and RGT1383 respectively; (C) shows the structure of GLP-1R in complex with LSN3160440 and Gα_s; (D) and (E) show the structures of GLP-1R in complex with NNC0640 and PF06372222 respectively.

1.7 Aims and objectives

Given the outstanding knowledge gaps in understanding glucagon secretion in pancreatic α cells, the main objective of this work is to unravel the intracellular signalling mechanisms of how GLP-1 inhibits glucagon secretion at the pancreatic α cells with the use of a range of pharmacological tools.

To achieve the objective of this work, I aim to:

- Evaluate the signalling responses (in terms of cAMP and iCa^{2+} mobilisation) of GLP-1R, GCGR and GIPR endogenous ligands using recombinant cell lines stably expressing receptors of interests and physiologically relevant α and β clonal models
- Investigate the cellular compositions of the α and β clonal cell models, especially their endogenous receptors and RAMPs expressions
- Apply receptor specific antagonists in order to decipher the individual receptor contribution towards the overall signalling in the α and β clonal cell models
- Investigate other factors (e.g. the presence of GPR119 and glucose culture conditions) that may affect intracellular signalling in rodent insulinoma and glucagonoma cell lines
- Optimise the use of the insulin and glucagon secretion assays, followed by characterising the insulin and glucagon secretion responses mediated by a range of glucagon-like peptides in rodent insulinoma and glucagonoma cell lines
- Apply receptor antagonists and pathway inhibitors to investigate the factors that are critical for GLP-1 mediated glucose homeostasis

Another objective of this work is to further characterise the pharmacological properties of the GLP-1R small molecule PAM, compound 249, discovered during my MPhil work, as well as to evaluate its potential to be further developed as a novel T2DM treatment. In order to do so, I aim to:

- Characterise the cAMP signalling, iCa^{2+} mobilisation and pERK1/2 response mediated by compound 249 using a range of functional assays, as well as to evaluate the effect of orthosteric ligand binding in the presence of compound 249 using BRET-based ligand binding assay

- Investigate the mechanism of actions of compound 249
- Perform structure-activity-relationship (SAR) studies using compound 249 as the lead compound
- Evaluate the extent of GSIS potentiation mediated by compound 249 in rat INS-1 832/3 cell line and *ex vivo* isolated mouse islets

Chapter 2

Methods and materials

2.1 Materials

2.1.1 Laboratory reagents

Unless otherwise specified, all laboratory reagents were purchased from Sigma-Aldrich (Dorset, U.K.).

2.1.2 Molecular biology reagents

DH5-α *Escherichia coli* (*E. coli*) competent cells were purchased from Stratagene (Santa Clara, U.S.) and were kept at -80°C before use. FuGENE® HD transfection reagent was purchased from Promega Corporation (Wisconsin, U.S.) and was stored at 4°C. Linear polyethylenimine (PEI) at 25,000g/mol molecular weight was purchased from Polysciences Inc. (Heidelberg, Germany) and was stored at -20°C upon reconstitution. QIAprep miniprep kit, QIAquick Gel Extraction kit, RNA Mini kit and QuantiTech Reverse Transcription kit were purchased from Qiagen (Hilden, Germany). Taq DNA polymerase with 10x standard Taq buffer, 10mM dNTP and 100 base-pair (bp) ladder were purchased from New England BioLabs (Massachusetts, U.S.). All forward and reverse primers used in reverse transcriptase-polymerase chain reaction (RT-PCR) and site-directed mutagenesis were synthesised by Sigma-Aldrich (Dorset, U.K.) and were stored at -20°C before use. Ampicillin was sourced from Sigma-Aldrich (Dorset, U.K.) and was made up to 100mg/ml in deionised water (dH_2O). It was stored at -20°C upon reconstitution.

2.1.3 Mammalian cell culture growth media

Dulbecco's Modified Eagle Medium: Nutrient Mixture F-12 (DMEM/F-12), Ham's F-12 Nutrient Mix with Glutamax™ and phenol red, Dulbecco's Modified Eagle Medium (DMEM), low glucose (1g/L) and high glucose (4.5g/L) solutions, Rosewell Park Memorial Institue (RPMI) 1640 media, RPMI 1640 (no glucose) media, Minimum Essential Medium (MEM), heat inactivated and non-heat inactivated fetal bovine serum (FBS), 1M HEPES solution, 100mM sodium pyruvate solution, MEM non-essential amino acids (100x) solution, antibiotic-antimycotic (100x) solution, penicillin-streptomycin (10,000U/ml) solutions, 0.05% Trypsin-EDTA with phenol red, cell dissociation buffer (Hank's based) and L-glutamine (200mM) solution were purchased from Gibco™ (Thermo-fisher Scientific, U.K.). All cell culture media were stored at 4°C and were warmed up to 37°C before use. The aminoglycoside antibiotic Geneticin (G418) was purchased from Sigma-Aldrich (Dorset, U.K.) and was stored at 4°C before use.

2.1.4 Peptide ligands

GLP-1, GLP-1(9-36)NH_2, GCG, Ex-4, Exendin(9-39) (Ex-9) and OXM were custom-synthesised by Generon (Slough, U.K.). GIP was purchased from Abcam (Cambridge, U.K.). All peptide ligands were made up to 1mM in dH_2O with 0.1% (w/v) bovine serum albumin (BSA). Peptide ligands were aliquoted and were stored at -20°C before assays. Once reconstituted, the peptide ligands were used within 3 months and were retested regularly to ensure consistent ligand potencies. All peptide ligands, apart from Ex-4 and Ex-9, were of human origins.

2.1.5 Pharmacological assay kits

LANCE® cAMP detection assay kit was purchased from PerkinElmer Life Sciences (Waltham, U.S.) and were stored at 4°C. Insulin ultra-sensitive assay kit and glucagon assay kit were purchased from Cisbio® (Codolet, France) and the antibody aliquots were stored at -80°C in dark after reconstitution. Fluo-4 AM calcium indicators supplemented with 2.5mM probenecid were purchased from Thermo Fisher Scientific (Waltham, U.S.) and were stored at -20°C in dark before assay. Homogenous Time-Resolved Fluorescence (HTRF) Tag-lite® GLP-1R fluorescent red agonist was purchased from Cisbio® (Codolet, France) and was stored at -80°C upon reconstitution. 384-well white Optiplates and white 96-well plates were purchased from PerkinElmer Life Sciences (Waltham, U.S.). All reagents from the assay kits were reconstituted according to the

manufacturers' recommendations.

2.1.6 Pharmacological activators and inhibitors

Forskolin was purchased from Cayman Chemical Company (Michigan, U.S.) and was made up to 10mM in DMSO. Phosphodiesterase (PDE) inhibitors namely rolipram, trequinsin and 3-isobutyl-1-methylxanthine (IBMX) were all purchased from Cayman Chemical Company (Michigan, U.S.). Rolipram, trequinsin and IBMX were made up to 25mM, 50mM and 1M in DMSO respectively. Ionomycin was purchased from Cayman Chemical Company (Michigan, U.S.) and was made up to 10mM in absolute ethanol. YM-254,890 was purchased from Alpha Laboratories (Eastleigh, U.K.), was made up to 100μM in DMSO and was stored at 4°C before use. Pertussis toxin (PTX) was purchased from Gibco™ (Thermo-fisher Scientific, U.K.) and was made up to 1μg/ml in dH_2O and kept at 4°C. PKA inhibitor, Rp-8-Br-cAMP, was purchased from Sigma-Aldrich (Dorset, U.K.) and was made up to 10mM in DMSO. GLP-1R peptide antagonist Ex-9 was purchased from Generon (Slough, U.K.) and was made up to 1mM in dH_2O with the addition of 0.1% (w/v) BSA. GCGR small molecule antagonist L-168,049 was purchased from Tocris Biosciences (Bristol, U.K.) and was made up to 10mM in DMSO. All compounds were stored at -20°C before assays unless otherwise stated.

2.1.7 Small molecule compounds

All drug candidates identified by ligand-based virtual screening (LBVS) (see section 2.2.5) were ordered via the commercial vendor 'MolPort' (https://www.molport.com) and were sourced from Enamine Ltd (Kiev, Ukraine). All small molecule compounds were made up to 10mM in dimethyl sulfoxide (DMSO) and were stored at -20°C before assay.

2.1.8 Laboratory buffer and media

2.1.8.1 Hank's buffered saline solution (HBSS) with or without Ca^{2+}

HBSS (without phenol red) with or without Ca^{2+} and Mg^{2+} solutions were purchased from Lonza (Basel, Switzerland) and were store at room temperature. Table 2.1 below outlines their compositions:

Table 2.1: **Compositions of HBSS with or without Ca^{2+} or Mg^{2+} solutions.**

Components	Concentration (g/L)	Molarity (mM)
Dextrose	1.000	5.551
KCL	0.400	5.366
KH_2PO_4	0.06	0.441
Na_2CO_3	0.350	4.166
NaCl	8.000	136.893
$Na_2HPO_4 \cdot 7H_2O$	0.09	0.336
$CaCl_2 \cdot 2H_2O$*	0.186	1.265
$MgSO_4 \cdot 7H_2O$*	0.2	0.811

* Indicates the presence in HBSS containing Ca^{2+} and Mg^{2+} solution only.

2.1.8.2 Phosphate buffered saline (PBS)

PBS was made by dissolving one PBS tablet into 200ml dH_2O and was then autoclaved for 15 minutes at 121°C for sterilization. A single tablet in 200 ml water yields 0.1M phosphate buffer, 0.0027M KCL and 0.137 M NaCl in the solution at a pH 7.4 at room temperature.

2.1.8.3 Krebs ringer buffer (KRB)

The formulation of KRB largely followed that described in [Naylor et al., 2016] for performing static incubation glucose-stimulated insulin secretion (GSIS) assays. The freshly reconstituted KRB was adjusted to pH 7.4 with 0.1M NaOH at room temperature and was made every two weeks. KRB was stored at 4°C before use. The compositions of the buffer are as follows (Table 2.2):

Table 2.2: **Compositions of KRB detailed in [Naylor et al., 2016]**

Components	Concentration (g/L)	Molarity (mM)
HEPES	4.766	20
KCL	0.298	4
KH_2PO_4	0.163	1.2
$NaHCO_3$	2.176	25.9
NaCl	5.756	98.5
$CaCl_2$	0.288	2.6
$MgSO_4$	0.144	1.2

2.1.8.4 Luria Broth (LB)

LB was made by dissolving 10g of the LB broth (Lennox) powder (Sigma-Aldrich, L3022) in 500ml dH_2O. The content was then autoclaved for sterilization. The compositions of LB broth are 10g/L tryptone, 5g/L yeast extract and 5g/L NaCl. Ampicillin was added in the LB broth at a final concentration of 100μg/ml once the solution was cooled down to room temperature.

LB agar plates were made using the same method as described above with the addition of 3% agar. After autoclaving, the content was cooled down in a 50°C water bath, followed by the addition of ampicillin at a final concentration of 100μg/ml. The solution was poured onto 90mm petri dishes in close proximity of a flame to ensure sterility. Plates were allowed to solidify at room temperature and were stored at 4°C until use.

2.1.8.5 NZY^+ broth

NZY^+ broth was made by dissolve 5g NZ amine, 2.5g yeast extract and 5g NaCl to 500ml dH_2O. The content was adjusted to pH 7.5 with NaOH before autoclaving. Once the content was cooled down to room temperature, the solution was aliquoted close to a flame to ensure sterility. 0.125μl each of sterilized-filtered 1M $MgCl_2$ and 1M $MgSO_4$ solution were added to the aliquoted NZY^+ broth prior to use.

2.1.8.6 40% glucose solution

40% (w/v) glucose solution was prepared by dissolve 40g of D-glucose powder into 60ml dH_2O to account for fluid displacement during autoclaving. Once the glucose solution was cooled down to room temperature after autoclaving, dH_2O was added to make up to 100ml 40% glucose solution. The glucose solution was stored at 4°C and were warmed up to 37°C with constant stirring before use.

2.1.8.7 Tris-Acetate-EDTA (TAE) electrophoresis buffer

50x concentrated TAE electrophoresis buffer was prepared by dissolving 242g Tris base and 18.61g disodium EDTA into 700ml dH_2O with constant stirring until components were well dissolved. 57.1ml glacial acetic acid was then added, followed by dH_2O to make up to final volume of 1L.

The concentrated TAE buffer was diluted to 1x with dH_2O before use in electrophoresis. The 1x TAE buffer thus contained 40mM Tris, 1mM EDTA and 20mM

acetate. The resultant pH of the TAE buffer used was pH 8.5 without adjustment.

2.2 Methods

2.2.1 Mammalian cell culture

2.2.1.1 Basis of cell culture subculturing

Cell lines were maintained using standard subculturing routines recommended by the American Type Culture Collection (ATCC). Mycoplasma infection was checked annually using an EZ-PCR mycoplasma kit from Biological Industries (Kibbutz Beit-Haemek, Israel). All mammalian cell cultures methods described below were performed in a sterile tissue culture hood with rigorous aseptic technique. All cell lines were propagated in a 37°C humidified incubator with 5% CO_2 and were maintained in either T25cm^2 or T75cm^2 rectangular canted neck cell culture flasks (Corning Life Science, New York, U.S.). Unless otherwise specified, cells from less than passage 15 were used in pharmacological assays.

2.2.1.2 Cell line origins and growth medium compositions

Chinese Hamster Ovary K1 (CHO-K1) cells were provided by Dr Ewan St. John Smith (Department of Pharmacology, University of Cambridge). CHO-K1 cells with low stable expression of GLP-1R, GCGR and GIPR were provided by Dr David Hornigold (AstraZeneca, Cambridge, U.K.). All CHO-K1 cell lines were cultured in Ham's F-12 Nutrient Mix with Glutamax™ and phenol red supplemented with 10% heat-inactivated FBS. Human Embryonic Kidney-293 (HEK293) cells were a gift from AstraZeneca (Cambridge, U.K.). HEK293T cells, HEK293S cells and COS-7 cells were given by Dr David Poyner (University of Aston, U.K.). All HEK293 cell lines and COS-7 cells were cultured in DMEM/F12 with glutaMAX™ supplemented with 10% heat-inactivated FBS. HEK293-calcitonin receptor knock-out (HEKΔCTR) cells were given by Drs. David Hornigold, Jacqueline Naylor and Alessandra Rossi (AstraZeneca, Cambridge, UK), and its use was described in [Bailey et al., 2019]. HEKΔCTR cells were cultured in MEM supplemented with 10% heat-inactivated FBS plus 1% non-essential amino acids and were used between passages 1 to 5. All growth medium contained 1% antibiotic antimycotic (100x) solution.

Rat insulinoma (INS-1 832/3) wild-type (WT) cell lines were given by Dr Jacqueline Naylor (AstraZeneca, Cambridge, U.K.). INS-1 832/3 GLP-1R knock-out (KO) and

GIPR KO cell lines were created by CRISPR/Cas9 knock-out technology detailed in [Naylor et al., 2016] and were also given by Dr Jacqueline Naylor. INS-1 832/3 cell lines were maintained in RPMI 1640 media supplemented with 5% heat-inactivated FBS, 10mM HEPES, 1mM sodium pyruvate, 50mM 2-mercaptoethanol, 100 U/ml penicillin and 100 mg/L streptomycin. Mouse MIN6-B1 cells [Lilla et al., 2003] were provided by Dr. Philippe Halban (University of Geneva, Switzerland) with permission from Dr. Jun-ichi Miyazaki, University of Osaka who produced the maternal MIN6 cell line. They were cultured in DMEM high glucose supplemented with 15% FBS, 71μM 2-mercaptoethanol, 2mM L-glutamine, 100 U/ml penicillin and 100 mg/L streptomycin. The MIN6-B1 cells were used from passage 25 to 30.

Mouse alpha TC1 clone 6 (αTC1.6) cells were purchased from the ATCC (Middlesex, U.K.). The ATCC recommends culturing αTC1.6 cells in DMEM, low glucose solution. However, a number of reports suggested that long-term culturing of αTC1.6 cells in high glucose media can enhance glucagon secretion [Diao et al., 2005, McGirr et al., 2005, Chuang et al., 2011, Asadi and Dhanvantari, 2019]. Therefore, αTC1.6 cells were cultured in DMEM containing 4.5g/L D-glucose supplemented with 10% non-heat inactivated FBS, 15mM HEPES, 0.1mM non-essential amino acids and 0.02% (w/v) BSA. Cells of early passages from 6 to 15 were used in performing secretion assays. Hamster InR1G9 cells [Takaki et al., 1986] were kindly given by Prof. Jacques Philippe (University of Geneva, Switzerland) and were maintained in RPMI 1640 media supplemented with 10% heat-inactivated FBS and 2mM L-glutamine.

2.2.1.3 Mammalian cell subculturing method

All solutions used in subculturing were warmed up to 37°C prior to use. Media were discarded and 0.05% Trypsin-EDTA with phenol red solution were added to the cells. The cells were incubated with the trypsin solution at 37°C for 5 to 10 minutes until the cells detached from the flasks. After the addition of fresh media to quench the action of trypsin, cell suspensions were transferred to 15ml centrifuge tubes and were spun at 1400 rpm for 4 minutes. The medium was removed upon centrifugation and the pellet was resuspended in fresh complete media. Appropriate aliquots of cell suspension were added to new culture vessels. Most cell lines used in the study were passaged every other day.

The subculturing method for the αTC1.6 cells largely followed the procedures outlined above; one of the differences was the use of cell dissociation buffer instead of trypsin solution to dislodge cells and the cell suspension was then centrifuged at 125

x g for 6 minutes. Since the αTC1.6 cells were slow growing cells, the cells were only subcultured once a week and their media were changed every two days.

2.2.1.4 Long-term cryostorage and cell recovery of mammalian cell lines

Upon harvesting cells which were fully confluent in T25cm^2 flasks, most cell lines were resuspended in freezing down media, which consisted of fresh complete media with the addition of 10% DMSO. For the αTC1.6 cell line, cells were resuspended in a different freezing down media which comprised of the complete media together with 5% DMSO and 40% non-heat inactivated FBS. All cell lines were then transferred to 1ml sterile cyrovial tubes (Grenier Bio-One, Kremsmünster, Austria) and were gradually frozen down from -80°C for 24 hours to -140°C ultra-low temperature freezer or liquid nitrogen tank for long term storage.

For cell recovery, cells were thawed in a 37°C water bath with constant agitation for 2 minutes. The cell suspensions were then transferred to 15ml centrifuge tubes with fresh media and were spun at 1400 rpm for 4 mins. The pellets were then resuspended with fresh media and were transferred to new culture vessels. Cells were allowed to recover in 37°C humidified incubator overnight.

2.2.1.5 Generation of stable cell lines

2.2.1.5.1 Viability curves generation to determine cell susceptibility to antibiotics

Cell viability curves were produced to determine the optimal concentration of G418 for the selection of cells that expressed the desired plasmid. To do so, untransfected HEK293S cells and HEKΔCTR cells were seeded onto 24 well-plates and were allowed to reach 90% confluence. A range of G418 concentrations, namely 0 (control), 200, 400, 600, 800 and 1000μg/ml were added onto each well. Cell viabilities from different wells receiving different treatments were determined every 2 days for a course of 10 days or until there were no viable cells left. The trypan blue staining method, of which the cells that were stained blue indicated cell death, was employed to differentiate viable cells from dead cells. So called 'kill curves' were determined by a plot of cell viabilities against different G418 concentrations (Fig. 2.1). The G418 concentration of 800μg/ml was chosen to be the optimal concentration for the exertion of selection pressure in both HEK293S cells and HEKΔCTR cells as it was the minimum concentration needed to ensure complete cell death in both cell lines after day 8 of treatment.

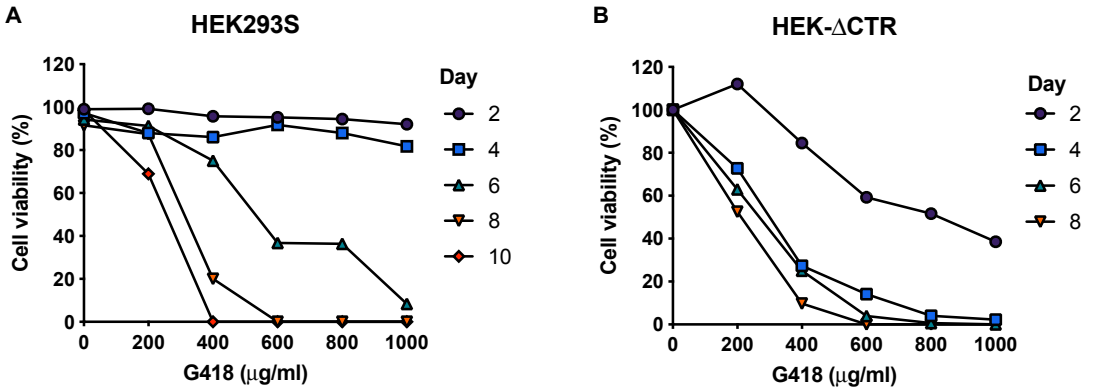

Figure 2.1: **Determination of the optimal G418 concentrations with the use of kill curves for the production of stable cell lines.** Kill curves were produced in (A) HEK293S and (B) HEKΔCTR cell lines in order to determine the optimal G418 concentration for effective selective pressure and 800μg/ml was chosen to be the optimal G418 concentrations needed in both cells lines to ensure complete cell death after day 8.

2.2.1.5.2 Generation of stable cell line Upon the determination of the optimal G418 concentration needed for maximal selective pressure, HEK293S cells stably expressing sigSNAP-GLP-1R-mCherry-Wildtype, HEK293S cells stably expressing sigSNAP-GLP-1R-mCherry-C347A and HEKΔCTR cells stably expressing GCGR were produced. To do so, cells were seeded onto a 24-well plate and were transfected with constructs of interests using FuGENE HD reagent (the transfection protocol is described in section 2.2.2.4). Cells were dislodged with the action of trypsin 48-hour post-transfection and were re-seeded onto a 6-well plate. Selection pressure was started by introducing G418 at 800μg/ml to the cells. Fresh G418 at 800μg/ml was replaced every 2 days for at least 14 days. Cell confluency higher than 25% were avoided in an attempt to ensure antibiotic efficiency as G418 works best when cells are actively dividing (according to the Toku-E protocol). Once a stable cell line was generated, lower concentration of G418 (200μg/ml) was applied to maintain long-term selection.

2.2.1.6 Mouse islet isolation

Mouse pancreas extractions at the 10-weeks old C57BL/6J mice were performed in accordance with the UK Animals (Scientific Procedures) Act 1986 by Dr Nikola Dolezalova (Department of Surgery, University of Cambridge) at the animal house located in the Cambridge Addenbrooke's Hospital site. Her protocol largely followed that detailed in [Li et al., 2009], during which 2.5ml ice-cold collagenase XI (1000 U/ml) were injected

into the bile duct, inflating the pancreas and its lobes. The pancreases were then carefully dissected and were placed on ice to prevent further collagenase digestion.

Mouse islet isolation was then proceeded at the Ladds laboratory. The pancreases were placed in a 37°C water bath for 13 minutes with shaking every 5 minutes. Once the tissues were dissolved into very fine particles, the collagenase digestions were terminated on ice and 25ml of ice-cold HBSS supplemented with 1mM $CaCl_2$ were added to the samples. The solutions were centrifuged at 300 x g for 1 minute at room temperature. The supernatants were discarded, and the pellets were washed by ice-cold HBSS twice before the addition of Histopaque solution (H8889, Sigma-Aldrich). RPMI serum-free solution were then carefully added to create density-gradient interfaces to separate islets from other digested debris. Once the sharp histopaque-RPMI interfaces were formed, the contents were centrifuged with brake-off for 15 minutes at 800 x g at room temperature. When the centrifugation was ended, the interfaces containing islets were removed and were transferred to complete RPMI media which consisted of 10% heat-inactivated FBS and 100 U/ml penicillin and 100 mg/L streptomycin for centrifugation in order to remove the residual Histopaque solution. The pellets were then resuspended in 10ml complete RPMI media. Viable islets, which showed clear borders and dense masses in the centre (Fig. 2.2), were handpicked with 200μl pipette tips under an inverted microscope. Islets were recovered overnight in a 90mm petri dish placed in a 37°C humidified incubator.

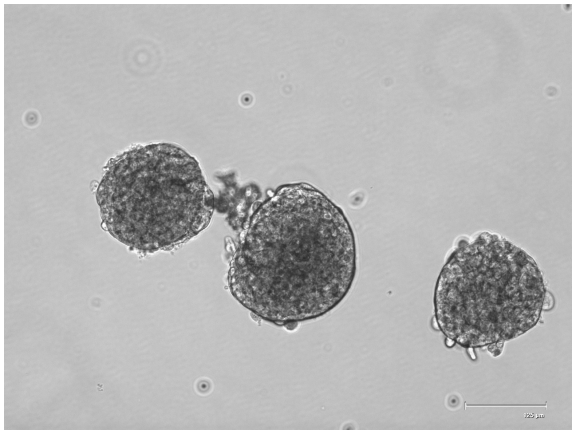

Figure 2.2: **Characteristics of viable islets.** Viable islets show dense masses in the centre as well as well-defined borders (scale bar shows 125μm).

2.2.2 Molecular biology technique

2.2.2.1 *Escherichia coli* transformations

E. coli DH5-α competent cells were used in amplifying plasmids of interests. Aliquots of 100μl *E. coli* were stored at -80°C and were allowed to be thawed on ice 30 minutes before use. Competent cells were transformed by the addition of 100-1000ng DNA on ice, followed by heat shock at 42°C for 30 seconds and lastly placed again on ice for 5 minutes. Cells were grown in LB with 100μg/ml ampicillin at 37°C overnight with constant shaking at 180rpm.

2.2.2.2 Plasmid amplifications and purifications

Plasmids were amplified using the E. coli transformation method described in the previous section 2.2.2.1. DNA was purified with the use of QIAprep mini prep kit (Qiagen) according to manufacturer's protocol, with DNA eluted and resuspended in 50°C dH_2O. The concentration and the purity of double stranded (ds)DNA were determined by NanoDrop Lite Spectrophotometer (Thermo Scientific, U.K.); samples with absorbance at 260nm and 280nm (A_{260}/A_{280}) ratio approximately equal to 1.8 was used in transfections. All purified constructs were stored at -20°C for long-term storage.

2.2.2.3 DNA expression constructs

Apart from the sigSNAP-GLP-1R-mCherry and Nluc-GLP-1R-WT constructs which were produced in Dr Graham Ladds' laboratory, all constructs were either gifted by our collaborators or obtained from cDNA.org and were summarised in Table 2.3.

Table 2.3: **Sources of the constructs used in various projects.**

Constructs	Prepared by/Sources from
sigSNAP-GLP-1R-mCherry	Cloned by Ashley Clark (Department of Pharmacology, University of Cambridge)
Nluc-GLP-1R-WT	Cloned by Abigail Pearce (Department of Pharmacology, University of Cambridge)
WT-GCGR	Ali Jazayeri (Heptares Therapeutics)
GLP2R in pRS306 vector	GSK
pcDNA3.1-CTR	cDNA.org
GHRH pcDNA3	GSK
CRF1 pcDNA3	GSK
CRF2 pcDNA3	GSK
pcDNA3.1-HA-CLR	cDNA.org
pcDNA3.1 FLAG-RAMP1	Wootten et al., 2013
pcDNA3.1 FLAG-RAMP2	Wootten et al., 2013
pcDNA3.1 FLAG-RAMP3	Wootten et al., 2013
pcDNA-GPR119	cDNA.org

2.2.2.4 Transfections

2.2.2.4.1 Transfections on 24-well plates Cells were seeded onto 24-well plates at a volume of 500μl and were allowed to reach 70% confluence prior to transfections. 500ng DNA constructs were transfected into the cells with the use of FuGENE® HD transfection reagent to ensure high transfection efficiency. Prior to transfections, constructs were diluted to 100ng/μl stock in dH_2O and were added to 18.5μl serum and antibiotic-free media. In accordance to the manufacturer's recommendations, 1.5μl of FuGENE® HD transfection reagent was lastly added at 1:3 DNA:FuGENE (w/v) ratio. The DNA-FuGENE complexes were incubated at room temperature for 15 minutes before being added drop-wise onto the cells. 48 hours transfections were allowed prior to assays.

2.2.2.4.2 Transfections on 6-well plates 1,000,000 cell/well were seeded on 6-well plates and were allowed to reach 70% confluence prior to transfections. PEI was used as the transfecting agent in 6-well plate format for economic purposes. DNA constructs were again diluted to 100ng/μl stock in dH_2O and a total of 1.5μg DNA constructs were transfected into the cells. A 1:6 DNA:PEI (w/v) ratio was adopted in this transfection protocol to enhance transfection efficiency. To do so, 15μl of diluted DNA constructs and 9μl of PEI were added separately to 150mM NaCl solutions which made up to final volumes of 50μl. The two mixtures were incubated at room temperature for 5 minutes before mixing together for a further incubation of 10 minutes. The resultant complex was added dropwise onto the well and were transfected for 48 hours prior to assays. Both transfection methods are summarised in Fig. 2.3.

2.2.2.5 RNA extractions

The work surface was being thoroughly cleaned with 70% ethanol followed by RNase AWAY™ surface decontaminant (ThermoFisher Scientific, U.K.) to eliminate RNase and DNA before RNA extraction. RNA were extracted from HEK293S and HEK293T, αTC1.6, INS-1 823/3 and MIN-6 B1 cells cultured to 80% confluence in T25cm^2 flasks using the RNeasy Mini Kit. For studies that aimed to determine the influence of different glucose concentrations on gene expressions, αTC1.6 and INS-1 823/3 cells were cultured in media containing various glucose concentrations for 72 hours before RNA extractions [Chuang et al., 2011].

The manufacturer's instructions were largely followed during the RNA extraction

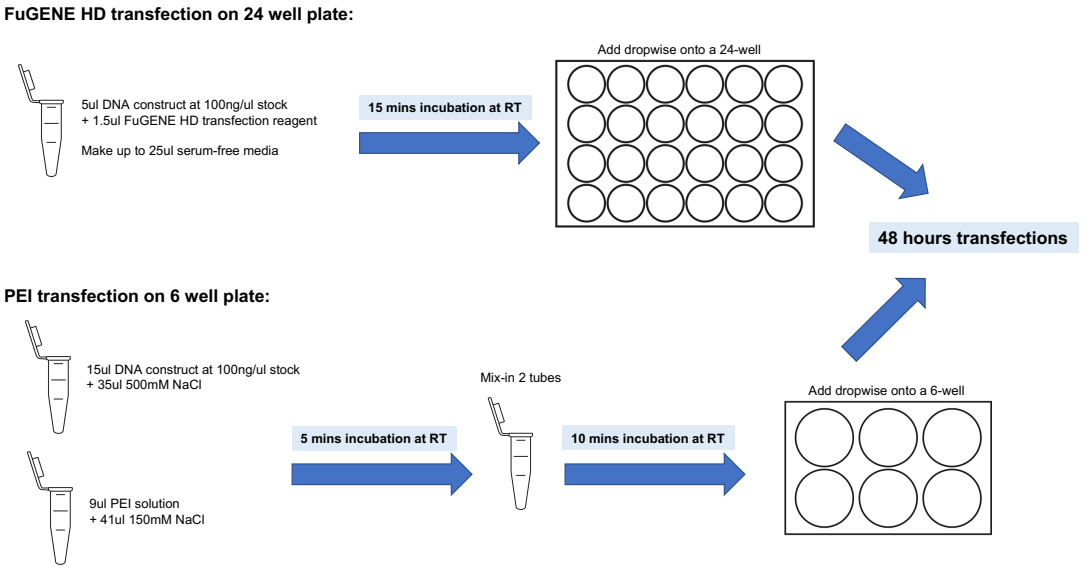

Figure 2.3: **Summary of two different transfection methods using FuGENE® HD transfection agent and PEI on a 24 well or a 6 well plate respectively.** For transfection in 24-well plate, a total of 500ng DNA constructs were transfected into the cells using 1:3 DNA:FuGENE (w/v) ratio as recommended by the manufacturer. As for transfection in 6-well plate, a total of 1.5μg DNA constructs were transfected into the cells using 1:6 DNA:PEI (w/v) ratio to further enhance transfection efficiency.

procedures. After cell harvesting, the cell pellets were resuspended in 350μl buffer RLT plus, which contains high composition of denaturing guanidine-isothiocyanate, and were homogenised by vortexing for 30s. 1 part of 70% ethanol (350μl) was added to the flow through, and was passed to RNeasy spin columns, spinning at 13,000rpm for 15 seconds. Buffers RW1 and RPE were added separately in later stages and the spin columns were spun for three additional times. Lastly, RNA was eluded with the addition of RNase-free water in 1.5ml micro-centrifuge tubes. The concentration and the purity of the RNA were determined by the NanoDrop Lite Spectrophotometer (Thermo Scientific, U.K.); samples with A_{260}/A_{280} ratio approximated to 1.9 to 2.1 was used in reverse transcriptase-polymerase chain reaction (RT-PCR). The RNA samples were stored at -80°C before further analysis.

2.2.2.6 Reverse transcriptase-polymerase chain reaction (RT-PCR)

2.2.2.6.1 gDNA elimination and cDNA synthesis After determining the RNA concentration and purity, complementary DNA (cDNA) was produced with the use of the QuantiTect Reverse Transcription kit (Qiagen) in accordance to the manufacturer's

recommendations. 1000ng template RNA was used in the reverse transcription as the kit was optimised to support cDNA synthesis up to 1000ng amount of RNA. After thawing the template RNA on ice, gDNA wipeout buffer was added together with the RNase-free water and were incubated for 2 mins at 42°C in order to eliminate contaminating genomic DNA (gDNA). Following gDNA elimination, reverse transcription was performed with the addition of Quantiscript Reverse Transcriptase, Quantiscript RT buffer and RT Primer Mix. Negative controls, which included the identical reaction components without the addition of the Quantiscript Reverse Transcriptase (-RT), were included in all RT-PCR performed so as to show presence of any contaminating gDNA. Incubation for 30 mins at 42°C was allowed in order to increase cDNA yield during the reverse transcription process. Upon incubation, the samples were incubated for 3 mins at 95°C to inactivate the Quantiscript Reverse Transcriptase.

2.2.2.6.2 Polymerase chain reaction (PCR) The samples from reverse transcription were placed on ice before proceeding to PCR amplification using Taq DNA polymerase according to the manufacturer's recommendations. 25μl for each PCR reaction was allowed and PCR reaction master mix, which included Taq DNA polymerase, 10mM dNTP, 10x Taq DNA polymerase buffer, template cDNA and nuclease-free water, was prepared on ice before aliquoting to sterile PCR tubes. 10μM each of forward and reverse primers of particular gene expressions were added lastly to the aliquoted PCR reaction master mix and were proceeded to thermocycling. The cycle parameters were described in Table 2.4 and the methods of designing primer sets targeting specific gene expressions are described next.

Table 2.4: **Cycle parameters for RT-PCR.**

Segment	Cycles	Temperature (°C)	Time (s)
1	1	95	30
2	42	95	30
		60	30
		68	20
3	1	68	300
Cool down to 4°C after thermocycling			

2.2.2.6.3 Design of primer sets The forward and reverse primers were designed with the use of NCBI Primer-BLAST online tool (https://www.ncbi.nlm.nih.gov/tools/primer-

blast/) upon searching for the succession numbers for specific gene expressions of designated species. Primer sets that spanned an exon-exon junction with a small predicted base pair product were selected in order to reduce the risk of false positives from off-target genes. The lists of the sets of primers used in RT-PCR were detailed in Table 2.5, 2.6 2.7 for cell lines of mus musculus, rat norvegicus and homo sapiens origins respectively.

Table 2.5: **Primer sets to determine GPCR, RAMPs and G proteins gene expression in cell lines of mus musculus origins.**

Gene	Forward primer sequence	Reverse primer sequence	Base pair	NCBI accession number
GAPDH	CCCTTAAGAGGGATGCTGCC	ACTGTGCCGTTGAATTTGCC	263	NM_001289726.1
Beta-actin	CACAGGCATTGTGATGGACT	CTTCTGCATCCTGTCAGCCAA	500	XM_030254057.1
GLP-1R	ACTCTCATCCCCCTTCTGGG	GGACACTTGAGGGGCTTCAT	254	NM_021332.2
GCGR	ATTGGCGATGACCTCAGTGTGA	GCAATAGTTGGCTATGATGCCG	105	XM_006532217.2
GIPR	CGGAGACAGACTCTGAGGGG	TCGTCAGGGACAGGGAGTAG	387	XM_011250615.1
RAMP 1	TGCTGAGGAGTTTATCGCAGG	GTAGAGGCCAAGGGCATCAG	105	NM_016894.3
RAMP 2	TGAGGACAGCCTTGTGTCAA	GGTCGCTGTAATGCCTGCTA	140	NM_019444.2
RAMP 3	GCTGCTTTGTGGTGAGTGTG	CCAGTAGCAGCCCATGATGT	205	NM_019511.3
GPR119	GGCAACTCCCTACTCAACCC	GGGAGAAGCTATCCCAAGGC	377	NM_181751.2
Gαs	GAGCTGGCCAACCCTGAGAA	CGATTTGCCAGCGAGGACTT	567	XM_006498779.4
Gαolf	AACTCACCGCCTGCTGCTTC	CAGGCCGCCACGTAAATGAT	588	XM_030250337.1
Gαi1	GGTGTGGGAGGGAGGAGTGA	GGCAGGTGCATCCAACCTCT	436	NM_010305.1
Gαi2	CGCCTTGAGCGCCTATGACT	GCAATCCTGCCAGGTCCACT	416	NM_008138.5
Gαi3	GAACCAGTGGGCTTGCTGCT	ATCCGAAAGCCGGATTGTGA	558	NM_010306.3
Gαo	ACCAGCCCACTGAGCAGGAC	GTTGGGTGAGCGGTTTTTGC	446	NM_010308.3
Gαt1	CAGCATCTGCTTCCCCGACT	TGGAATGGGGATCTGCTGGT	574	NM_008141.3
Gαt2	TGCTGGTGGAGGATGACGAA	TCACCAACAGGATGGGCTGA	480	NM_008141.3
Gαz	AAGCCGCGGTCTACATCCAA	GGCCAACTCAGGAAGGCAGA	546	NM_010311.4
Gαq	GCAGGGTGTGAACCGGAAAC	CGTTCGGCACAGTTTGCATC	469	NM_008139.6
Gα11	ACCGCATGGAGGAGAGCAAG	TCAGCTGCAGGATGGTGTCC	318	NM_010301.4
Gα14	CTCCTGCCTGGCTGTTCCAT	GCGCGCACAGTTCAAACAAC	590	NM_008137.4
Gα15	GCCTTCCGGCTGCTCATCTA	TCTCCTCCATGCGGTTCTCC	529	XM_006513234.4
Gα12	AGCGCCAGAAGTGGTTCCAG	AGCAGAGGGAGGGGCTGTCT	467	NM_010302.2
Gα13	ACCACCGCGATCAACACAGA	GGGCCGAGACTCCTCCCTAA	573	NM_010303.3

2.2.2.6.4 Visualising and confirming fidelity of RT-PCR products All products were resolved on 2% agarose gels made in 1x TAE buffer stained with 0.5 μg/ml ethidium bromide. Products were imaged using a G:Box iChemi gel documentation system (Syngene, Cambridge, UK). Densitometry was performed using Gene Tool analysis software (Syngene, Cambridge, UK). All results were normalised to the housekeeping genes, either glyceraldehyde 3-phosphate dehydrogenase (GAPDH) or β-actin. DNA fragments were also excised from the agarose gels with a clean scalpel. DNA were extracted from gels and were purified by using QIAquick Gel Extraction kit (Qiagen). After DNA purification, the samples were sent to the Department of Biochemistry, University of Cambridge for sequencing. The presence of gene expressions were con-

Table 2.6: **Primer sets to determine GPCR, RAMPs and G proteins gene expression in cell lines of rattus norvegicus origins.**

Gene	Forward primer sequence	Reverse primer sequence	Base pair	NCBI accession number
Beta-actin	CCGCGAGTACAACCTTCTTG	CAGTTGGTGACAATGCCGTG	297	NM_031144.3
GLP-1R	GGGCTCCTCTCGTATCAGGA	GTGAACAGCTTGACGAAGCG	512	NM_012728.1
GCGR	GGAGACATAGAAGGGGGACTCT	GCAGACCAGCTCAGTAGGTG	294	NM_172091.2
GIPR	AGGTGGTATTTGCTCCCGTG	AGGGGTCCCTTTACCTAGCA	331	XM_017588800.1
RAMP1	GATGTGAGGACAGGAACCAGA	TGGTCTTTCCCCAGTCACAC	355	XM_017596614.1
RAMP2	CTCCGGAGTCCCTGAATCAA	TCCAGTTGCACCAGTCCTTG	144	NM_031646.1
RAMP3	ACAAACATCGTGGGCTGCTA	CCACGGTCAACAAGACTGGA	166	NM_020100.2
Gαs	GCCTCGGCAACAGTAAGACC	TTGGTGGCCTTCTCACCATC	265	NM_019132.1
Gαolf	CCCACAGACCAGGACCTACT	TGGCCTCCAACGTCAAACAT	107	NM_001191836.2
Gαi1	GGATGATGCTCGCCAACTCT	TCATTCAGGTAGTACGCCGC	171	NM_013145.1
Gαi2	AGGGGCCAACAAGTATGACG	TAGGCAGGAGGCTCCCATC	231	XM_006243858.1
Gαi3	GGCGCTGGAGAATCTGGTAA	CACTCGTCCTCGGAATAGCC	80	NM_013106.1
Gαo	AACCGCTCACCCAACAAAGA	GGGGTCGTAGGTTAGACAGG	271	NM_017327.1
Gαt3	ATTAAACGTCTGTGGGGCGA	GCACGTCACTCCTTCAAAGC	282	NM_173139.1
Gαz	GTCATGCAAGTGTCACGGC	GTGGCCTCTCAGCACCTTAG	258	NM_013189.2
Gαq	CGGAGGATCAACGACGAGAT	TCATCAGAGTACCCCGACCC	155	NM_031036.1
Gα11	ATGGACACGCTCAAGATCCG	GGTCCACGTCCGTCAAGTAG	217	NM_031033.1
Gα12	CTCGAGGGTGCTTGTAGACG	AAACATCCCGTGCTTCTCGT	79	NM_031034.2
Gα13	CACGGAGACAAGTTGATGGC	ATGGATGCCTTTGGTGGGTC	270	NM_001013119.1
Gα14	AGCCTACGACACCCTACAGT	CGAGTCCTGAGTGCTTGTGT	225	NM_001013151.1

Table 2.7: **Primer sets to determine GPCRs, RAMPs, β-arrestins and RCP gene expressions in cell lines of homo sapiens origins.**

Gene	Forward primer sequence	Reverse primer sequence	Base pair	NCBI accession number	Reference
GAPDH	TGCACCACCAACTGCTTAGC	GGCATGGACTGTGGTCATGAG	87	NM_002046.7	-
GLP-1R	CTACGTGAGCATAGGCTGGG	ATGGGCAGCCGGATAATGAG	135	-	Ge et al., 2014
GCGR	CCAGTGTCACCACAACCTGA	AGGAATACTTGTCGAAGGTTCTGT	77	-	Zwermann et al., 2009
GIPR	ATGACTACCTCTCCGATCCTGC	AAGGACCCGTTACAGGCGA	194	NM_000164.4	-
RAMP 1	CTGCCAGGAGGCTAACTACG	GACCACGATGAAGGGGTAGA	298	-	Linscheid et al., 2005
RAMP 2	GGGGGACGGTGAAGAACTAT	GTTGGCAAAGTGGATCTGGT	227	-	Linscheid et al., 2005
RAMP 3	AACTTCTCCCGTTGCTGCT	GACGGGTATAACGATCAGCG	353	-	Linscheid et al., 2005
Beta-arretin 1	AAAGGGACCCGAGTGTTCAAG	CGTCACATAGACTCTCCGCT	159	-	Designed by Dr Kerry Barkan
Beta-arretin 2	TCCATGCTCCGTCACACTG	ACAGAAGGCTCGAATCTCAAAG	82	-	Designed by Dr Kerry Barkan
RCP	AGAGCAGCGTAAAGAAAGTGG	CTGACAATTTCAGGACTCTGGTG	129	-	Designed by Ashley Clark

firmed with the use of the NCBI primer-blast online tool which predicts the presences of specific gene expressions based on the comparison of the alignment of the nucleotide sequences of the DNA fragment and that of specific genes.

2.2.2.7 Methods for generating site-directed mutants in the GLP-1R

All primers used for single-site mutagenesis were designed using the online 'QuikChange Primer Design' online tool developed by Agilent Technologies (Santa Clara, U.S.) (available on https://www.agilent.com/store/primerDesignProgram.jsp). The oligonucleotide primer sets used in site-directed mutagenesis are summarised in Table 2.8. The QuikChange Lightening Site-directed Mutagenesis Kit (Agilent Technologies) was used to perform single-site mutagenesis. Manufacturer's instructions were largely followed in performing the mutagenesis. The reaction components were assembled according to the manufacturer's protocol (Table 2.9).

Since the plasmid length of pcDNA3.1 used to clone the sigSNAP-GLP-1R-mCherry-WT construct has a size of 5.248kb, 186 seconds/cycle at 68°C were allowed in part of the elongation step during thermocycling. The PCR cycle parameters were described in Table 2.10. Upon incubation of the PCR products in NZY^{+} buffer for one hour at 37°C at constant shaking at 180 rpm, the PCR products were then allowed to be grown on ampicillin-resistant bacterial agar plate overnight at 37°C. Colonies were hand-picked the next day and were grown in 5ml LB broth with 100μg/ml ampicillin overnight at 37°C with constant shaking at 180 rpm. The constructs were then purified as described in section 2.2.2.2 with the use of the Qiagen Mini-prep kit and the dsDNA content and purity were determined with a NanoDrop Lite Spectrophotometer. The samples were sent to the Department of Biochemistry at the University of Cambridge for sequencing. Point mutation at designated residues of the receptor of interest was confirmed by comparing the alignment of the sequencing results of the mutated receptor with that of the wildtype receptor via the online open-source MultAlin (http://multalin.toulouse.inra.fr/multalin/) and that no other unwanted mutations were introduced.

Table 2.8: **Oligonucleotides used in the site-directed mutagenesis to generate specific GLP-1R mutants.**

Target	Product	Oligonucleotide targeting sense strand of template	Oligonucleotide targeting anti-sense strand of template
TM6	C347A	5'-GTGGACTTGGCAAGTCTGgcTTTGATGTCTGTCTTGCAC-3'	5'-GTGCAAGACAGACATCAAAgcCAGACTTGCCAAGTCCAC-3'

Table 2.9: **Reaction components for SDM as recommended by the manufacturer.**

Reaction component	Volume or mass
10x reaction buffer	5μl
dsDNA template	100ng
Oligonucleotide targeting sense strand	100ng
Oligonucleotide targeting anti-sense strand	100ng
dNTP mix	1μl
QuikSolution reagent	1.5μl
ddH2O	To 50μl
QuikChange Lightning Enzyme	1μl

Table 2.10: **PCR cycle parameters used in the site-directed mutagenesis.**

Segment	Cycles	Temperature (°C)	Time (s)
1	1	95	120
2	18	95	20
		60	10
		68	186
3	1	68	300
Cool down to 4°C after thermocycling			

2.2.3 Pharmacological investigations and signalling assays

2.2.3.1 cAMP accumulation assay

2.2.3.1.1 Principle of cAMP accumulation assay LANCE® cAMP detection kit, which is a homologous time-resolved fluorescence resonance energy transfer (TR-FRET) based assay, was used to detect cAMP produced when GPCRs were stimulated with agonists. The principle of the assay is based on the competition of the binding sites on the cAMP-specific antibodies (Alexa Fluor-647) between the europium (Eu)-streptavidin chelated biotin-cAMP tracer and the cAMP produced. When the antibodies are bound to the Eu-chelated cAMP tracer, light pulse at 340nm excites the europium, which the energy emitted by the excited Eu-chelate tracer is then transferred to the Alexa Fluor-labelled antibody, emitting FRET signal at 665nm (Fig. 2.4). Therefore, the level of fluorescence emitted at 665nm decreases with the higher concentrations of cAMP produced, meaning the resulting fluorescence signals are inversely proportional to the cAMP concentrations in the assay.

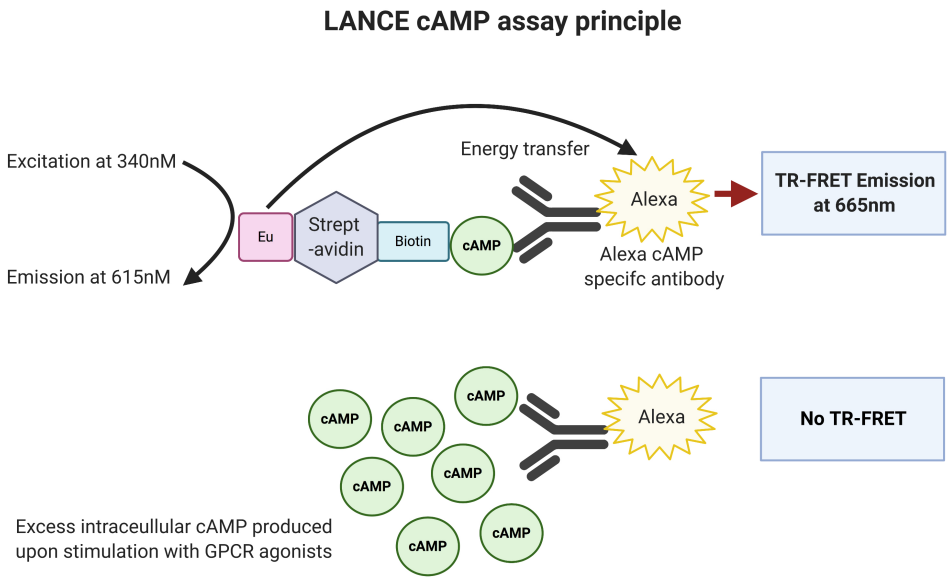

Figure 2.4: **Principle of LANCE® cAMP detection kit.** The assay is a TR-FRET based assay of which the Eu-chelated biotin-cAMP tracer competes with the cAMP produced for the binding site of the Alexa-Fluor 665 antibody. When the antibody is bound to the Eu-chelated cAMP tracer, light excitation at 340nm excites the europium, which the energy emitted by the excited Eu-chelated tracer is then transferred to the Alexa Fluor-labelled antibody, emitting FRET signal at 665nm. Therefore, the resulting fluorescence signals are inversely proportional to the cAMP produced by the stimulated GPCR.

2.2.3.1.2 Methods Stimulation buffer (SB) for the assay was made up of 20ml PBS containing 0.1% (w/v) BSA with or without the presence of PDE inhibitors, such as 0.5mM IBMX, 25μM rolipram or 25μM trequinsin, to prevent the breakdown of cAMP by PDEs. Ligands were serially diluted with SB in 96 well plates. For antagonist or allosteric modulator assay, a single concentration of the antagonist or compound was added to the serially diluted peptide ligands; the DMSO content was kept at 2% across all wells. Forskolin was also serially diluted in a range of 100μM to 10pM, which was used to normalise the data.

Cells were harvested and were washed in PBS, following resuspension in SB 30 minutes at room temperature before the start of assays. Upon cell counting with the haemocytometer, the volume of cells needed to make up to a designated cell number for the assay was determined and cells were seeded at 5μl/well onto the 384 white Optiplates. 5μl of ligands were added to the cells using a multichannel pipette and cells were stimulated with the ligands at room temperature under certain stimulation time. 10μl of detection buffer, which consisted of Eu-labelled streptavidin and biotin-cAMP diluted according to manufacturer's protocol, together with Triton-X were added to lyse the cells and to detect cAMP produced by incubating for an hour in the dark. cAMP accumulations were then measured with the Mithras LB 940 multimode microplate reader (Berthold Technologies, Germany), which filters were calibrated at 665nm emission and 340nm excitation and can be used directly for data analysis without quench correction (PerkinElmer, 2017). All data measured were normalised to the 100μM forskolin, which represents the maximum cAMP production that the cell system can produce.

2.2.3.2 Quantifying the release of calcium from intracellular compartments

80,000 cells/well were seeded onto the Costar® sterile black, clear bottomed, 96-well plates (Corning Life Science, New York, U.S.) coated with poly-L-lysine (PLL) solution. Cells were grown for 24 hours until fully confluent. Cells were washed once with Ca^{2+} containing HBSS before adding 40μl of 10μM Fluo-4/AM calcium dye containing 2.5mM probenecid to prevent dye leakage, followed by an hour of incubation in dark at room temperature. Cells were then washed twice with calcium containing HBSS before the addition of 100μl of Ca^{2+}-free HBSS supplemented with 0.1% (w/v) BSA.

Ligands were serially diluted in Ca^{2+}-free HBSS supplemented with 0.1% (w/v) BSA and were injected robotically onto the cell-containing black 96 well plate by BD pathway 855 high-content bioimager (BD Biosciences, Berkshire, U.K.) in a range

of 1μM to 1pM. Fluorescence were immediately detected upon ligand addition and images were captured every second for a duration of 80 seconds with an excitation and emission wavelength set to 494nm and 516nm respectively. Fiji (Image J) was used to compile all individual images captured into animations. The mean intensity of each individual animation with background fluorescence were corrected and were used to generate dose-response curves in GraphPad Prism 8.4. All data were normalised to 10μM ionomycin, which is an ionophore that raises the intracellular calcium level.

2.2.3.3 Measurement of ERK1/2 phosphorylation

ERK1/2 phosphorylation was measured with the use of Phospho-ERK1/2 (Thr202/Tyr4-04) kit (Cisbio, France). HEK293S stably expressing sigSNAP-GLP1R-mCherry-C347A and sigSNAP-GLP1R-mCherry-WT cells were serum starved overnight prior to assaying for ERK1/2 activation, in order to lower basal pERK1/2 levels and to gain a larger signalling window. The cells were harvested using trypsin as in cAMP assay and serum-free media was added. Cells were washed in Ca^{2+}-free HBSS before seeding at a cell density of 35,000 cells per well onto the 384 white Optiplates. The cells were pre-treated with compound 249 for 15 minutes before ligand stimulation for 5 minutes. Cells were then lysed for 30 minutes using lysis buffer made up according to manufacturer's protocol after ligand stimulation. A mixture of equal proportion of pERK1/2 d2 and pERK1/2 cryptate antibodies were added and incubated in the dark for 2 hours at room temperature. Plates were then read with the Mithras LB 940 multimode microplate reader (Berthold Technologies, Germany), which filters were calibrated at 665nm emission and 340nm excitation. ERK1/2 phosphorylation was then expressed as a ratio between the signals observed between 665nm and 620nm. A phorbol 12-myristate 13-acetate (PMA) dose-response curve was generated to determine the maximum ERK1/2 response given by the cells during assays.

2.2.3.4 Quantifying the affinity of ligand binding using fluorescent substrates

1,000,000 HEK 293T cells were seeded onto 6 well plates and cultured for 24 hours. Cells were then transiently transfected with NLuc-GLP-1R-WT with PEI (which method was described in section 2.2.2.4) and were grown overnight. Following harvesting, transfected cells were seeded at 50,000 cells/well onto white 96 well plates coated with PLL solution and were further cultured for 24 hours. After 48 hours transfection period, the media was removed and were washed with PBS prior to adding 80μl of modified

PBS containing with 0.49mM $MgCl_2 \cdot 6H_2O$, 0.9mM $CaCl_2 \cdot 2H_2O$ and 0.1% (w/v) BSA to each well. 10μl of Nano-Glo substrate (Promega Corporation), furimazine, which was diluted 100x in the modified PBS, was added to each well and the plate was incubated for 5 mins in the dark.

Upon incubation, 10μl of 400nM Tag-lite® GLP-1R red agonist (Cisbio® Codolet, France) was added to each well and emission was measured at 485nm and 530nm every 30 seconds for 25 minutes during which total binding was determined. Unlabeled, 'cold', GLP-1 or Ex-4 at 1μM was then injected into each well to displace all bound Tag-lite® GLP-1R red agonist, with emission measured every 30 seconds for a further 60 minutes, during which non-specific binding was determined. In both phases, vehicle was added alongside the ligands to act as a control which represented the background level of emission. The BRET signal was calculated by subtracting the 530 nm/485 nm emission ratio for vehicle treated cells from Tag-lite® GLP-1R red agonist treated cells.

2.2.3.5 Application of pharmacological inhibitors to probe downstream signaling events

Where appropriate, cells were pre-treated with 100nM YM-254,890, which is a $G\alpha_q/11$ inhibitor [Takasaki et al., 2004], for 30 minutes prior to assay. PTX at a final concentration of 200ng/ml was applied to cells 16 hours prior to assay, thereby ADP-ribosylated the $G\alpha_i$ protein, uncoupling receptor-mediated $G\alpha_i$-dependent cAMP inhibition [Pittman, 1979]. PKA inhibitor, Rp-8-Br-cAMP [Gjertsen et al., 1995], was applied to cells 15 mins prior to assay.

2.2.4 Insulin and glucagon secretion assays

2.2.4.1 Principle of glucose stimulated-insulin secretion (GSIS) assay

The principle of the Cisbio® insulin ultra-sensitive assay is based on the HTRF technology during which when insulin is present in the supernatant, the antibodies, europium cryptate (donor) and XL-665 (acceptor), will bind to insulin. When the antibodies are in close proximity, the excitation of the donor with a light source at wavelength 340nM triggers a FRET signal toward the acceptor, giving out fluorescence at 620nm and 665nm wavelength (Fig. 2.5). The signal intensity is thus proportional to the number of antibodies complex formed with insulin, hence directly proportional to the insulin concentration present in the supernatant.

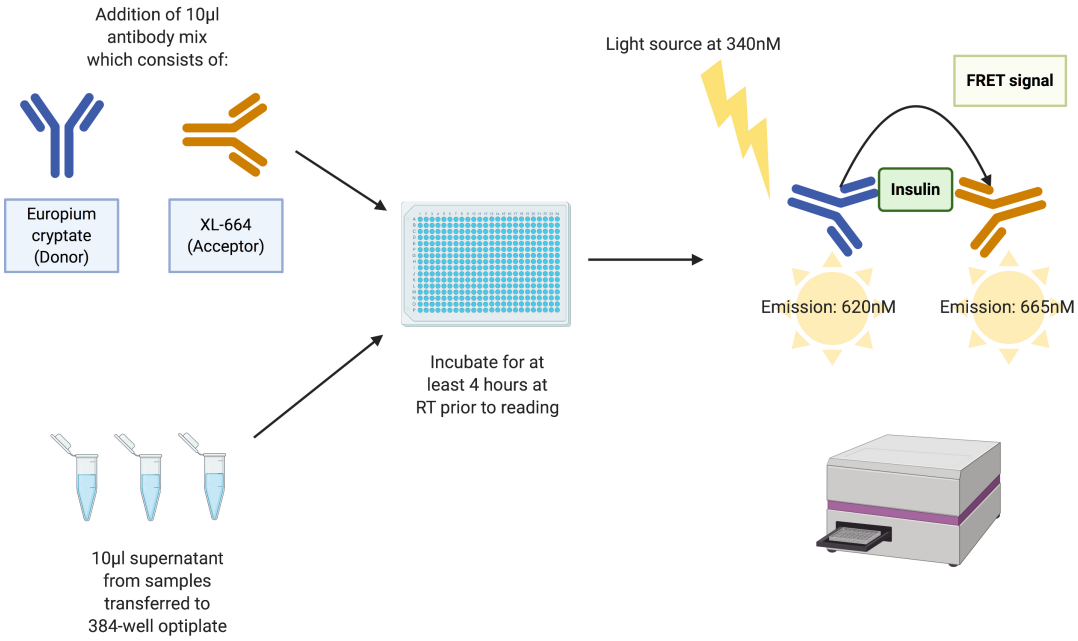

Figure 2.5: **Principle of the HTRF-based insulin ultra-sensitive assay.** When insulin is present in the supernatant, the antibodies, which consist of europium cryptate (donor) and XL-665 (acceptor), will bind to insulin. When the antibodies are in close proximity, the excitation of the donor with a light source at wavelength 340nM triggers a FRET signal toward the acceptor, giving out fluorescence at 620nm and 665nm wavelength. The signal intensity is thus proportional to the number of antibodies complex formed with insulin, hence directly proportional to the insulin concentration present in the supernatant.

2.2.4.2 GSIS assay in INS-1 832/3 cell lines

2.2.4.2.1 Methods 150,000 INS-1 832/3 cells/well were seeded onto clear bottom 96 well plates coated with PLL solution and were incubated overnight. On the day of assay, complete 11mM glucose RPMI media was replaced with complete 0mM glucose RPMI media for glucose starvation for 2 hours at 37°C humidified incubator [Yang et al., 2016]. The cells were then pre-incubated with 2.8mM glucose KRB supplemented with 0.1% (w/v) BSA for an hour at 37°C. Afterwards, the cells were washed twice with KRB, and were incubated further for an hour under different conditions, which were made up in 100μl KRB containing protease inhibitor aprotinin at 10μg/ml and DPP-IV enzyme inhibitor sitagliptin at 100nM to prevent the enzymatic breakdown of GLP-1 by the DPP-IV enzymes [Liu et al., 2014]. Supernatant was collected from each well after incubation and was spun at 5000rpm for 5 mins to remove any cell debris. Supernatants were transferred to fresh 500μl epperdorf tubes before being stored at -20°C until further analysis.

2.2.4.2.2 Acid-ethanol extraction to determine total insulin content in cells The acid-ethanol extraction steps were performed in an attempt to measure the total insulin content in cells. Once the supernatant was removed from the wells, the cells were washed with KRB once. 100μl of acid-ethanol mix, which was comprised of 0.18 M HCl in 96% ethanol (v/v), were added to the cells and were incubated at 4°C for 12 hours. Following 12 hours incubation, the cells were disrupted by vigorous pipetting. Supernatants were then centrifuged at 5,000 rpm for 5 mins to remove any cell debris. The supernatants were further diluted 1:100 in KRB before the addition of antibody mix.

2.2.4.2.3 Addition of antibody mix to quantify insulin concentrations On the day of analysis, the supernatants were thawed on ice and were diluted 1:25 in KRB before transferring 10μl onto the 384 well optiplate in duplicate. 10μl of XL-665 and anti-insulin antibody mix at 1:1 ratio was added using a multichannel pipette and 4-hour incubation in dark at room temperature was allowed. The results were measured with the Mithras LB 940 multimode microplate reader (Berthold Technologies, Germany), which filters were calibrated at 340nm excitation and 665nm and 620nm excitation.

2.2.4.2.4 Data analysis The ratio of the acceptor and donor emission signals were calculated for each individual well as follows:

$$Ratio = \frac{Signal\,665nm}{Signal\,620nm} \times 10^4 \tag{2.1}$$

The ΔF (%) which reflects the signal to background of the assay were calculated as below, of which $\text{Ratio}_{negative\,control}$ denotes the ratio given with only KRB present:

$$\Delta F(\%) = \frac{Ratio_{Sample} - Ratio_{Negative\,control}}{Ratio_{Negative\,control}} \times 100 \tag{2.2}$$

The insulin level (ng/ml) was then determined by interpolating the ΔF(%) of each sample against the standard curve produced according to the manufacturer's protocol.

2.2.4.3 Static incubation GSIS assay in isolated mouse islets

The GSIS assay in isolated mouse islets largely followed the protocol developed by our collaborators, Dr Reshma Ramracheya and Professor Patrik Rorsman (Oxford Centre for Diabetes, Endocrinology and Metabolism, University of Oxford, U.K.). Following overnight recovery after islets isolation, small to medium sized islets were hand-picked and size-matched under inverted microscope. Groups of 10 size-matched islets were transferred to 500μl epperdorf tubes containing 200μl of 0mM glucose RPMI. Supernatants were removed carefully without disturbing the pellets and were replaced with fresh 0mM RPMI, leaving in for 5 minutes so as to remove any excess 11mM glucose RPMI. The supernatants were again carefully removed, and 1mM glucose KRB were added into each tube. The islets were pre-incubated for an hour in the 37°C humidified incubator with 5% CO_2 before incubating with various conditions, including low glucose (1mM glucose) and high glucose (10mM), for a further hour. Afterwards, 250μl supernatants were removed and were transferred to fresh 500μl epperdorf tubes. The samples were kept at -80°C until further analysis.

Acid-ethanol steps were performed by adding 100μl of the acid-ethanol mix as described in section 2.2.4.2 into all tubes containing the remaining pellets. 10μl of aprotinin were added into each tube, followed by sonication for 15 seconds. The tubes were then stored at 4°C overnight before analysis.

The subsequent steps of the addition of antibody mix and data analysis largely follow that described in section 2.2.4.2. However, the supernatants from the samples were only diluted at 1:1 ratio before addition of the antibody mix.

2.2.4.4 Glucagon secretion assay

2.2.4.4.1 Principles The Cisbio® glucagon kit was employed to perform the glucagon secretion assay. The principle of the glucagon kit is largely similar to that of the Cisbio® insulin ultra-sensitive assay (Section 2.2.4.2); the only difference is the use of two different acceptor and donor antibodies, which are d2 and Terbium Cryptate antibodies respectively. The Cisbio® glucagon kit is highly specific for detecting glucagon produced by mouse species, with <0.07% specificity to oxyntomodulin, which is highly structurally similar to glucagon.

2.2.4.4.2 Methods 500,000 αTC1.6 cells/well were seeded onto fibronectin-coated 24 well plate and were cultured overnight at the 37°C humidified incubator with 5% CO_2. 2 hours before assay, fresh complete DMEM media containing 25mM glucose were replaced. The cells were then washed once with 25mM glucose KRB supplemented with 0.1% (w/v) BSA and were incubated with the same buffer at 37°C for an hour. Following the pre-incubation, the cells were washed twice with KRB, before further incubating for one hour under different conditions, which were made up in 5mM glucose KRB supplemented with 0.1% (w/v) BSA in the presence of 10μg/ml aprotinin and 100nM sitagliptin. Afterwards, supernatants were collected and transferred to fresh 500μl epperdorf tubes. The samples were stored at -80°C until further analysis. Acid-ethanol steps, the addition of antibody mix and data-analysis were performed according to what have been described in the previous section 2.2.4.2.

2.2.5 Compound screening

2.2.5.1 Ligand-based virtual screening

At the beginning of the project in 2016, full-length GLP-1R cryo-EM crystal structures were not available when the virtual screening for potential GLP-1R PAMs or agonists were performed. Hence, ligand-based virtual screening (LBVS) was adopted which facilitated the identifications of potential scaffolds based on existing GLP-1R ago-PAM structures, without the prerequisite requirement of the GLP-1R structural information. The methods described by Naylor and co-workers for their successful identification of NAADP chemical probes [Naylor et al., 2009] were largely followed to aid the identification of novel GLP-1R small molecule agonist scaffolds and the LBVS was conducted by Dr Taufiq Rahman (Department of Pharmacology, University of Cambridge). Virtual screening was conducted using Intel® Xeon® E3-1225v3 3.2GHz processor and 8.00GB

RAMs in Microsoft® Window 7 professional operating system (Seattle, U.S.A.).

2.2.5.2 Identifying baits for LBVS

Compound 2, BETP, compound 20, compound 8e, VU0453379 and a quinoxaline derivative were selected as baits for LBVS as they are well studied GLP-1R ago-PAMs. The 3D conformations of the query ligands were generated with OMEGA (OpenEye Scientific Software Inc., Santa Fe, New Mexico), which converted the 2D structures of the query ligands into 3D conformations using distance bounds method.

2.2.5.3 Selections of chemical libraries

ZINC (ZINC15, www.zinc.docking.org, Sterling and Irwin, 2015) and the GPCR library from Enamine Ltd (http://www.enamine.net) were used in LBVS which provided 3D molecular structures of commercially available small molecules. Both chemical libraries are free online databases which contains 35 million and 27,000 drug-like molecules for LBVS respectively. All the small molecules in these libraries have molecular weight between 250 to 500, log of partition coefficient between n-octanol and water (clogP) between 2 to 4, topological polar surface area (TPSA) less than 150$Å^2$, rotational bonds between 0 to 8 and hydrogen bond donors and acceptors of less than 4 and 10.

2.2.5.4 ROCS and EON programme

ROCS (v3.2.1.4., OpenEye Scientific Software Inc., Santa Fe, New Mexico) was used to compare the 3D structural similarities of the query ligands and the compounds listed in libraries. A cut-off shape Tanimoto score of 0.7 was set to identify the top 500 hits. The hits identified from ROCS were then output to the EON programme (v2.2.0.5., OpenEye Scientific Software Inc., Santa Fe, New Mexico), which calculated the electrostatic similarities between the query ligands and the top 500 hits. The electrostatic similarities were then quantified by the electrostatic combo score (ET_{combo}), representing the similarity of electrostatic fields between the query ligands and the top 500 hits [Jennings and Tennant, 2007]. A cut-off ET_{combo} score of 0.7 was also applied to further identify the top hits. The results obtained from both ROCS and EON programme were visualised with VIDA, which generated 3D coloured representations of conformations and electrostatic fields of the baits as well as the top 500 hits (v4.3.0.4., OpenEye Scientific Software Inc., Santa Fe, New Mexico). Potential test compounds

were then selected based on subjective judgement of the 3D structural and electrostatic field similarities between the query ligands and the top hits.

2.2.5.5 *In vitro* testing and validations

Potential compounds with the highest ET_{combo} scores as well as subjective prediction of the similarities of 3D conformations between the baits and the compounds were purchased from either ZINC or Enamine Ltd via the commercial vendor 'Molport'. As GLP-1R is predominantly $G\alpha_s$-coupled and the augmentation of cAMP production is instrumental to the enhancement of insulin secretion, cAMP accumulation assay serves as the preliminary screen for any viable candidates as GLP-1R small molecule agonists or allosteric modulators. The workflow of compound screening and subsequent identification of compound 249 as the potential GLP-1R PAM was outlined in Fig. 2.6.

2.2.5.6 Identification of compound 249 as the lead compound

Compound 11 was identified as a potential PAM on cAMP accumulation mediated by GLP-1(9-36)NH_2 and was reported in my MPhil thesis in 2016. The findings were also published in pA2 online as conference abstract [Yeung et al., 2016]. Compound 249, which is a close analogue of compound 11, was also identified as a potential GLP-1R PAM due to its potentiation effect on cAMP production mediated by OXM in the CHO-K1 cell line stably expressing GLP-1R. Thus, this PhD thesis mainly focuses on the further characterisation of the pharmacological properties of compound 249 and its analogues designed thereafter.

2.2.5.7 Design and *in vitro* screening of compound 249 analogues

Additional analogues, such as compound 248, 82 and 448, were designed manually based on the structure of compound 249 by Dr Taufiq Rahman (Department of Pharmacology, University of Cambridge). Other compound 249 analogues, namely compound 880, 297, 180, 607, 385, 106, 001, 246, 468, 646 and 518, were designed by Miss Kathleen Bowman (Department of Pharmacology, University of Cambridge) via LBVS which methods were the same as described above in this section using compound 249 as the bait. *In vitro* testing was also performed to validate analogues biological activities as described in section 2.2.5.5.

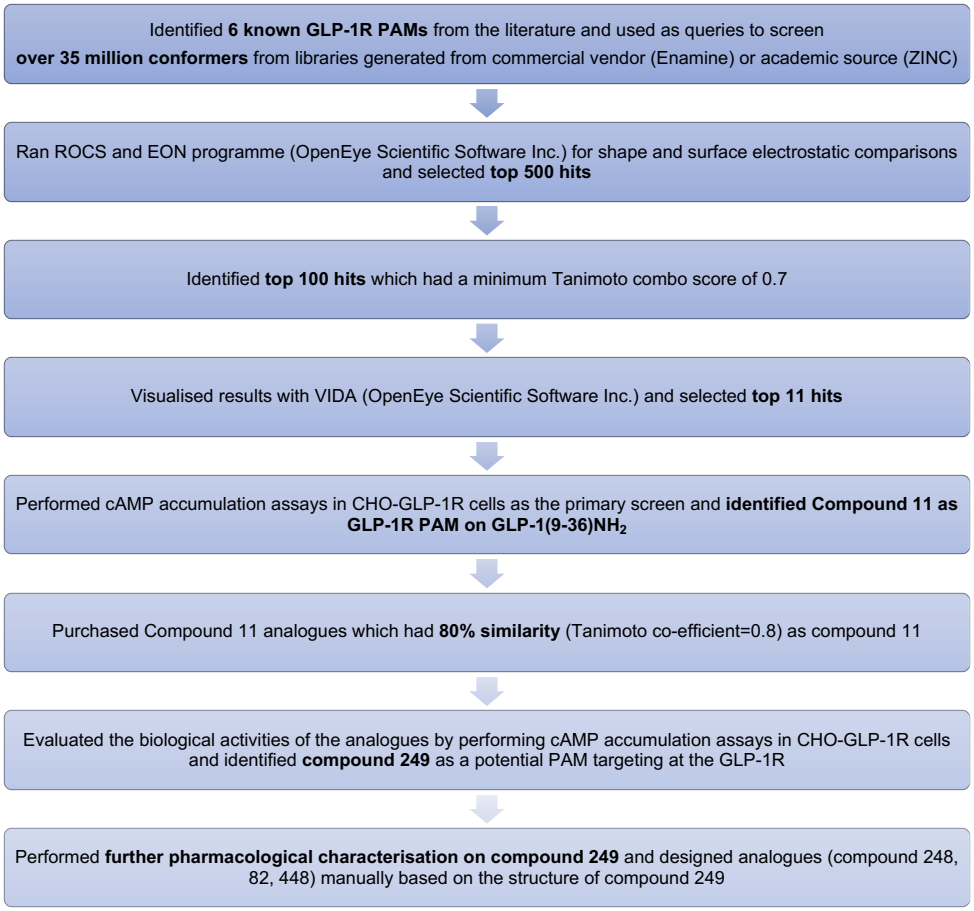

Figure 2.6: **Flowchart outlining the workflow of compound screening and subsequent identification of compound 249 as the potential GLP-1R PAM.** The above flowchart summarises how test compounds were identified with ligand-based virtual screening. Baits were chosen based on their known ago-PAM activities. ZINC and Enamine were used as the compound libraries for virtual screening. ROCS and EON programmes were run to compare the shape and surface electrostatic similarities, quantified by shape and electrostatic Tanimoto scores. The results obtained from ROCS and EON were visualised with VIDA and top hits were selected based on subjective judgement of the 3D shape and electrostatic field similarities. The top hits were purchased and their biological activities were validated with cAMP accumulation assay.

2.2.6 Data analysis

2.2.6.1 Dose-responses curve fitting

Data interpretation for the cAMP accumulation and intracellular calcium mobilisation assays were performed with the use of GraphPad Prism 8.4 (La Jolla, U.S.A.). Data were fitted to obtain concentration-response curves using the three parameters logistic equations with least square (ordinary) fit as the equation below:

$$Y = E_{\text{min}} + \frac{E_{\text{max}} - E_{\text{min}}}{1 + 10^{\log(\text{EC}_{50}) - x}} \tag{2.3}$$

where E_{max} and E_{min} are defined as the maximum and minimum responses of an agonist while EC_{50} is the concentration at which 50% of the maximal response is reached.

2.2.6.2 Operational model of agonism and allosterism

An operational model of agonism and allosterism was used to estimate the efficacy and cooperativity between the potential small molecule allosteric modulator and the peptide ligands [Leach et al., 2007, May et al., 2007]. Data were fitted into equation 2.4 as shown below:

$$E = \frac{E_{\text{m}}\left(\tau_A[A](K_B + \alpha\beta[B]) + \tau_B[B]K_A\right)^n}{([A]K_B + K_AK_B + [B]K_A + \alpha[A][B])^n + \left(\tau_A[A]\left(K_B + \alpha\beta[B]\right) + \tau_B[B]K_A\right)^n} \tag{2.4}$$

where E_m is the maximum response induced by an agonist, [A] and [B] are the concentrations of the orthosteric ligand and allosteric modulator respectively, K_A and K_B are the dissociation constants of the orthosteric ligand and the allosteric modulator respectively, EC_{50} is the concentration of the orthosteric ligand at which 50% of the response is achieved in the absence of the allosteric modulator, n is the transducer slope factor which links occupancy to response, α and β represent the allosteric effect on affinity and efficacy of the orthosteric ligand respectively, τ_A and τ_B represent the capacity of orthosteric and allosteric ligands to be agonists respectively, taking their intrinsic efficacies, the total density of the receptors and the efficiency of the stimulus-response coupling into account.

Equation 2.4 was fitted into GraphPad Prism 8.4 manually as in-built allosteric operational model is not available. The allosteric parameters were generated with the

help of Dr Graham Ladds (Department of Pharmacology, University of Cambridge).

2.2.6.3 Ligand binding association then dissociation model

For ligand binding association-dissociation experiments, data were fitted using the 'association then dissociation' model in GraphPad Prism 8.4 to obtain values for association rate (K_{on}), dissociation rate (K_{off}), dissociation constant (K_D) which is computed from K_{off}/K_{on}, and non-specific binding (NS).

2.2.7 Statistical analysis

All data were normalised to the average highest and lowest responses obtained when the cells were stimulated with forskolin at 100μM, ionomycin at 10μM or PMA at 100μM, and blank SB or HBSS without Ca^{2+}. The normalised values were plotted as a percentage of response against log concentrations of the test ligands. All the graphs represented were plotted $\pm$ S.E.M., with upper and lower error bars shown.

Student's (unpaired) t-tests with Welsh's correction or one-way ANOVA with post-hoc Dunnett's multiple comparisons were performed to analyse the statistical difference of the data set with the use of GraphPad Prism 8.4. Probability value (p) of less than 0.05 was considered to be statistically significant.

Chapter 3

Evaluation of the signalling responses of glucagon-like peptides

3.1 Introduction

As one of the main goals of the PhD project is to shed new light on how GLP-1(7-36)NH_2 (thereafter referred to as GLP-1) regulates glucagon secretion in pancreatic α cells, it is imperative that the signalling properties of GLP-1, in particular its facilitation on cAMP and intracellular calcium (iCa^{2+}) mobilisation responses which are critical for its glucagonostatic action, are thoroughly evaluated. Furthermore, given a few glucagon-like peptides, namely GCG, OXM, GIP and GLP-1(9-36)NH_2, also regulate glucagon secretion, the signalling properties of these peptide ligands were characterised in relative to GLP-1. Therefore, in this chapter the evaluation of cAMP responses mediated by GLP-1 and its structurally similar peptide ligands in recombinant hamster CHO-K1 and human HEK293 cell lines stably expressing GLP-1R, GIPR and GCGR will be first reported. iCa^{2+} mobilisation mediated by a selection of glucagon-like peptides were also quantified using the HEK293 recombinant cell systems. Following the establishment of the rank order of potency of these peptide agonists, the cAMP responses mediated by these glucagon-like peptides in physiologically relevant rodent pancreatic α and β cell lines, which are known to express endogenous incretin receptors, will be reported.

Secondly, as started in the introduction, many accessory proteins can influence the signalling of the glucagon-like receptors (see Section 1.5.7). Thus a detailed understanding of the molecular compositions, in particular the incretin receptors and RAMPs

expressions, in the recombinant and physiologically relevant cell lines which were frequently used in this project will be presented. To decipher the cellular compositions of these cell lines commonly used in understanding the signalling pathways of insulin or glucagon secretion, the evaluation of endogenous expressions of the receptors from the glucagon receptor family, G proteins as well as RAMPs using RT-PCR technique will be reported.

Lastly, having grasped a detailed understanding of the signalling properties and molecular compositions of the recombinant and immortalised α and β cell lines, the factors that modulate cAMP signalling mediated by these glucagon-like peptide ligands were investigated and the results of which will be reported in this chapter. Unfortunately, due to COVID-19 impact on experimental schedule, some of the results presented in this chapter are of preliminary nature only, and are noted accordingly. The quantitative measurement of cAMP accumulation, a technique which was frequently used throughout the project, will be first described to begin the chapter.

3.2 Characterisation of glucagon-like peptide ligands responses in recombinant cell systems

3.2.1 cAMP accumulation measurements

Given the importance of cAMP production in mediating insulin and glucagon secretion [Ahrén, 2009, Yang and Yang, 2016], the homologous TR-FRET based LANCE cAMP kit was employed to characterise the glucagon receptor family endogenous ligands cAMP accumulation responses upon receptor activation. As the Chinese Hamster Ovary (CHO-K1) cell line is an easy-to-culture cell line that can act as a robust system for evaluating secondary messenger responses for glucagon-like receptors [Wootten et al., 2012], CHO-K1 cell lines stably expressing GLP-1R, GCGR or GIPR (thereafter referred to as CHO-GLP-1R, CHO-GCGR or CHO-GIPR cells respectively) were used in functional assays in examining glucagon receptor family peptide agonist-mediated cAMP responses as well as characterising the pharmacological properties of small molecule allosteric modulators (see later in chapter 5).

Before performing the functional assays, forskolin, which is a direct adenylate adenylyl cyclase activator that facilitates the production of cAMP from the breakdown of ATP [Seamon et al., 1981], was applied to CHO-GLP-1R, CHO-GCGR, CHO-GIPR cells as well as untransfected CHO-K1 cells in an attempt to examine the potencies

(pEC_{50}) of forskolin-mediated cAMP responses of these cell lines, as the potency of forskolin varies among cell types [Hill et al., 2010]. Here the forskolin-mediated cAMP responses were established to be similar across various CHO-K1 cells stably expressing different receptors, validating the use of CHO-GLP-1R, CHO-GCGR, CHO-GIPR and CHO-K1 cells in subsequent cAMP functional assays (pEC_{50} values were 5.89 $\pm$ 0.06, 6.16 $\pm$ 0.06, 5.99 $\pm$ 0.07 and 6.09 $\pm$ 0.09 respectively) (Fig. 3.1 and Table 3.1). Furthermore, the forskolin concentration-response curves obtained were used to normalise the results generated from the functional assays, which facilitated the comparisons of the extent of cAMP production as well as accounted for daily cell variability. PDE inhibitors, such as 25μM rolipram, 0.5mM IBMX or 25μM trequinsin, were also added into the stimulation buffer to prevent the breakdown of cAMP [Hill et al., 2010]. Having validated the cell line as a system to evaluate the extent of cAMP production, the assessment of cAMP responses mediated by a range of glucagon-like peptide agonists on GLP-1R, GCGR and GIPR in the recombinant CHO-K1 cell systems were performed.

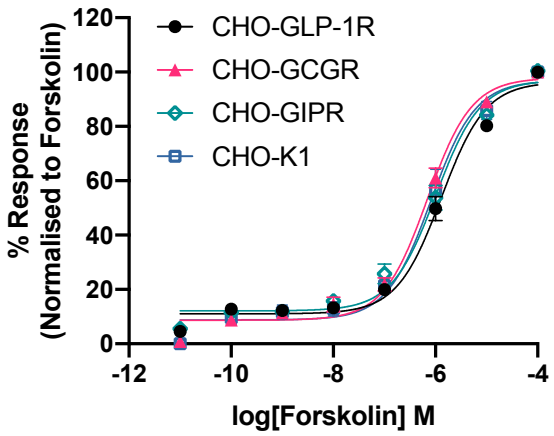

Figure 3.1: **Forskolin-activated cAMP accumulation responses in CHO-GLP-1R, CHO-GCGR, CHO-GIPR and CHO-K1 cells.** The above graph shows the concentration-response curves when CHO-GLP-1R, CHO-GCGR, CHO-GIPR and untransfected CHO-K1 cells were stimulated with forskolin, resulting in high cAMP responses. 1000 cells/well of CHO-GLP-1R, CHO-GCGR, CHO-GIPR or CHO-K1 cells in the presence of rolipram under 15-minute stimulation were used in the cAMP assays. All data were normalised to the forskolin concentration-response curve. All data were means of 6 independent experiments with duplicates $\pm$ S.E.M (upper error bars). Table 3.1 shows the pEC_{50} and E_{max} values of forskolin-induced cAMP accumulation responses in all CHO-K1 cell types.

Table 3.1: **cAMP potencies (pEC_{50}) and maximal responses (E_{max}) of forskolin when applied to CHO-K1 cells stably expressing GLP-1R, GCGR or GIPR and untransfected CHO-K1 cells.**

Cell line	pEC_{50} [a]	E_{max} [b]	Span	n
CHO-GLP-1R	5.89±0.06	96.38±2.00	85.45±2.22	12
CHO-GCGR	6.16±0.06	97.88±1.70	89.19±1.93	12
CHO-GIPR	5.99±0.07	97.03±2.33	84.88±2.59	12
CHO-K1	6.09±0.09	96.90±3.14	88.12±3.53	12

Values were generated when the data were fitted to the three-parameter logistic equation. Means ± S.E.M of n individual result sets were shown.
[a] Negative logarithm of agonist concentration when reaching half maximal response.
[b] % of maximal response observed when stimulated with ligands relative to forskolin.

3.2.2 Glucagon-like peptide ligand cAMP responses in CHO-K1 recombinant systems stably expressing GLP-1R, GCGR or GIPR

GLP-1R, GCGR and GIPR are known to be predominantly Gαs-coupled, promoting the activity of adenylyl cyclase upon receptor activation, leading to the production of cAMP [Wootten et al., 2013b, Graaf et al., 2016]. The increase in cAMP levels then further activate downstream pathways namely protein kinase A (PKA) and exchange protein directly activated by cAMP 2 (EPAC2), which are known to be instrumental to insulin release [Seino, 2012]. Given the importance of cAMP pathway activation, the extents of cAMP production mediated by different glucagon receptor family endogenous peptide agonists, namely GLP-1, GLP-1(9-36)NH_2, OXM, GCG and GIP, were next investigated. To determine the potencies and efficacies of various peptide ligands when acting on the GLP-1R, GCGR and GIPR, cAMP accumulation functional assays were performed. These endogenous peptide ligands were applied to CHO-GLP-1R, CHO-GCGR and CHO-GIPR cells and their extents of cAMP production in the presence of a PDE inhibitor rolipram were measured.

Concurred with the observations from other studies [Jorgensen et al., 2007, Willard and Sloop, 2012, Weston et al., 2015, Wootten et al., 2016a], GLP-1 was the most potent full agonist at the GLP-1R (pEC_{50}: 9.46 ± 0.05) while GCG was the most potent full agonist at the GCGR (pEC_{50}: 11.35 ± 0.09) (Fig. 3.2 and Table 3.2). Furthermore, GCG activated the GLP-1R (pEC_{50}: 8.32 ± 0.05), which was also reported recently [Chepurny et al., 2019]. The ability of GLP-1 activating the GCGR has been refuted by some reports [Runge et al., 2003, Jorgensen et al., 2007], yet here GLP-1 was shown to activate the GCGR and acted as a partial agonist (pEC_{50}: 7.21 ± 0.03), a finding which agreed with

the observations from Weston and colleagues [Weston et al., 2015], which they showed the partial agonism of GLP-1 at the GCGR using recombinant yeast strains expressing GCGR as well as HEK293 cells transiently transfected with GCGR. OXM acted as a dual full agonist at both GLP-1R and GCGR, resulting in a more potent cAMP response at the GCGR compared to the GLP-1R (pEC_{50} values of OXM were 9.20 $\pm$ 0.09 at the GCGR and 7.92 $\pm$ 0.06 at the GLP-1R), which agreed with the results reported by Pocai and colleagues [Pocai et al., 2009]. The highly abundant GLP-1 metabolite, GLP-1(9-36)NH_2, which was found to be a GLP-1R weak partial agonist here (pEC_{50}: 5.77 $\pm$ 0.22) as well as reported previously [Montrose-rafizadeh et al., 1997], also acted as a weak partial agonist at the GCGR (pEC_{50}: 6.44 $\pm$ 0.40), an observation that has not been reported in the literature. GIP acted as a potent full agonist only at the GIPR (pEC_{50}: 9.64 $\pm$ 0.11). It failed to activate GLP-1R and could only activate GCGR at high concentration. Furthermore, GLP-1, OXM, GCG and GLP-1(9-36)NH_2 did not activate GIPR, as also shown in other studies [Baggio and Drucker, 2007]. However, the receptor cell surface expressions were not determined in these CHO-K1 stable cell lines; the quantification of which will certainly facilitate a fairer comparison of the agonist responses among these GLP-1R, GIPR and GCGR stable cell lines. In essence, the rank order of potencies of various peptide ligands at GLP-1R, GCGR and GIPR evaluated at the CHO-K1 recombinant cell lines were as follows:

- For GLP-1R: GLP-1 > GCG > OXM > GIP > GLP-1(9-36)NH_2
- For GCGR: GCG > OXM > GLP-1 > GLP-1(9-36)NH_2 > GIP
- For GIPR: GIP (the rest of the ligands were not able to activate GIPR at concentrations < 1μM)

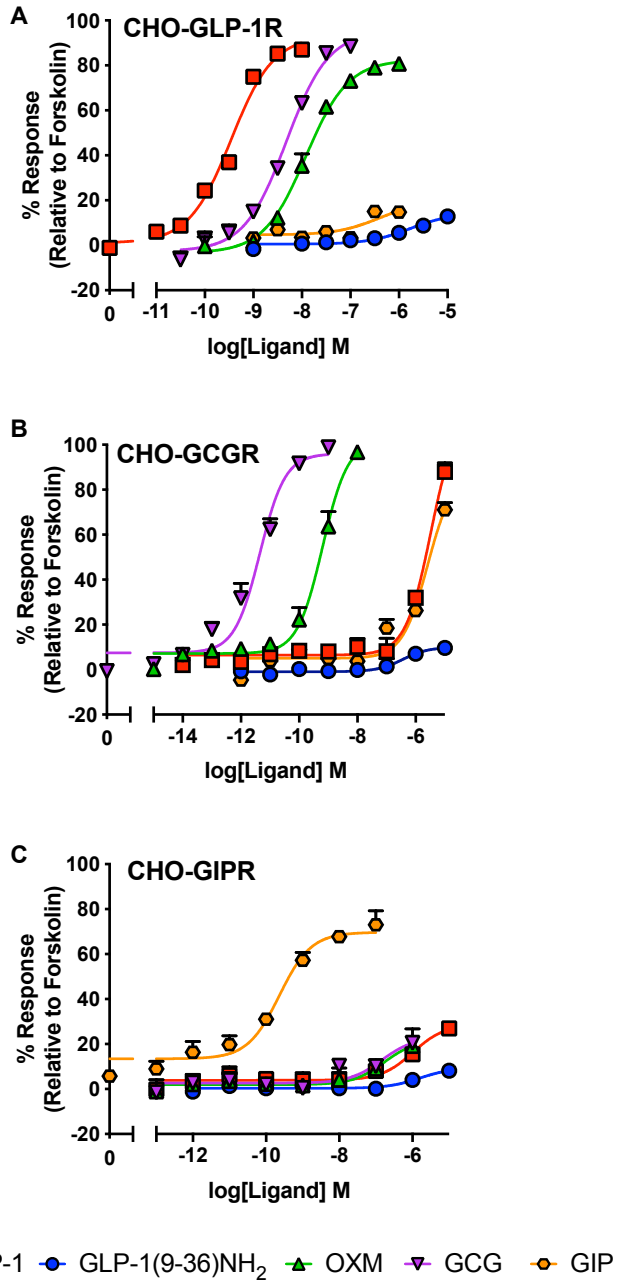

Figure 3.2: **Characterisation of glucagon receptor family endogenous ligands cAMP accumulation responses in CHO-K1 stably expressing GLP-1R, GCGR or GIPR cells.** Dose-response curves when (A) GLP-1R, (B) GCGR and (C) GIPR were stimulated with various glucagon receptor family endogenous ligands. 1000 CHO-GLP-1R, CHO-GCGR and CHO-GIPR cells/well were stimulated with ligands for 15 minutes in the presence of PDE inhibitor rolipram, except for measuring the ligand response of GLP-1(9-36)NH_2 during which 2000 cells/well were stimulated for 60 minutes. All data were normalised to the maximum cAMP response determined by 100μM forskolin stimulation. All data were means of 3 to 6 independent experimental results with duplicates $\pm$ S.E.M (upper error bars) and were fitted to the three-parameter logistic equation. Table 3.2 shows the pEC_{50} and E_{max} values of the individual ligand responses.

Table 3.2: **cAMP potencies (pEC_{50}) and maximal responses (E_{max}) of GLP-1R, GCGR and GIPR activation by their endogenous ligands in CHO-GLP-1R, CHO-GCGR and CHO-GIPR stable cell lines.**

Cell line	Ligand	pEC_{50} [a]	E_{max} [b]	Span	n
CHO-GLP-1R	GLP-1	9.46±0.05	93.14±1.95	92.09±2.18	10
	GLP-1(9-36)NH_2	5.77±0.22	14.42±2.06	13.93±2.00	10
	GCG	8.32±0.05	95.18±2.65	97.81±2.85	12
	OXM	7.92±0.06	82.53±1.88	85.97±2.56	6
	GIP	6.41±0.70	19.42±7.70	14.77±7.32	6
CHO-GCGR	GLP-1	7.21±0.30	76.8±23.85	108.2±10.36	6
	GLP-1(9-36)NH_2	6.44±0.40	9.965±2.13	10.89±2.22	6
	GCG	11.35±0.09	96.01±2.94	88.52±3.52	8
	OXM	9.20±0.09	101.8±4.36	94.64±4.47	10
	GIP	5.79±0.10	91.54±6.0	85.75±5.96	5
CHO-GIPR	GLP-1	5.99±0.34	28.76±5.7	24.86±5.70	6
	GLP-1(9-36)NH_2	5.80±0.33	9.41±1.60	9.07±1.63	6
	GCG	6.85±0.32	22.90±3.91	20.25±3.92	6
	OXM	6.76±0.43	22.11±5.22	20.19±5.24	6
	GIP	9.64±0.11	69.72±2.61	56.28±3.13	8

Values were generated when the data were fitted to the three-parameter logistic equation. Means ± S.E.M of n individual result sets were shown.

[a] Negative logarithm of agonist concentration when reaching half maximal response.

[b] % of maximal response observed when stimulated with ligands relative to forskolin.

3.2.3 Glucagon receptor family, RAMPs and β-arrestins mRNA expressions in HEK293S and HEK293T cell lines

After evaluating the extents of the cAMP responses of various endogenous glucagon-like peptide agonists in hamster CHO-K1 recombinant cell systems, the ligand responses in human embryonic kidney 293 (HEK293) recombinant cell lines were subsequently investigated. To begin with, the characterisation of the endogenous mRNA expressions of GLP-1R, GCGR and GIPR, together with RAMPs, β-arrestins and receptor component protein (RCP), were performed in order to fully evaluate the cellular background of the HEK293S and HEK293T cell lines. The mRNA expressions were measured by performing semi-quantitative RT-PCR and all expressions were relative to the house-keeping gene, glyceraldehyde-3-phosphate dehydrogenase (GAPDH). All RT-PCR performed included negative controls, which were identical reactions without the addition of reverse-transcriptase (rt-), to show the absence of contaminating gDNA.

Surprisingly, the HEK293S and HEK293T cell lines expressed low endogenous levels of GLP-1R, GCGR and GIPR, which were not shown in any published reports to date. The following results showed that the endogenous mRNA expressions of GLP-1R, GCGR, GIPR, RAMPs, β-arrestins and RCP were largely similar between HEK293S and HEK293T cell lines (Fig. 3.3). The endogenous expressions of GLP-1R, GCGR, and GIPR were very low, compared to GAPDH in both HEK293S and HEK293T cell lines. Among the three different RAMPs, RAMP1 showed the highest expressions in both cell lines, which were approximately 8-fold higher than that of the reference house-keeping gene, followed by RAMP2, which expressions were only one-fold higher than that of GAPDH, and a non-detectable level of RAMP3 in both cell lines. The RAMPs mRNA expression levels obtained were consistent with the RT-PCR results reported by Bailey and colleagues [Bailey et al., 2019], who also observed RAMP1 being the most abundant among the three RAMPs, followed by RAMP2 and a non-detectable level of RAMP3 in HEK293S and HEK293T cell lines; they also showed there was no major difference in terms of RAMPs expressions between the two HEK293 cell lines. The mRNA expressions of β-arrestins were also similar in both HEK293S and HEK293T cells, with β-arrestin 1 showing a higher expression, which was 3-fold higher than GAPDH, than β-arrestin 2. The results reported here were consistent with other studies that showed β-arrestin 1 was more abundant than β-arrestin 2 in HEK293 cells with the use of immunoblotting with β-arrestins specific antibodies [Ahn et al., 2004]. The expressions of RCP were of similar levels in both HEK293S and HEK293T cell lines (Fig.

3.3) and were nearly 3-fold higher than that of GAPDH. Following the characterisation of the molecular compositions of both HEK293S and HEK293T cell lines, HEK293 cell lines which stably express receptors of interest were then produced, in an attempt to further evaluate other signalling properties of the glucagon-like peptide ligands.

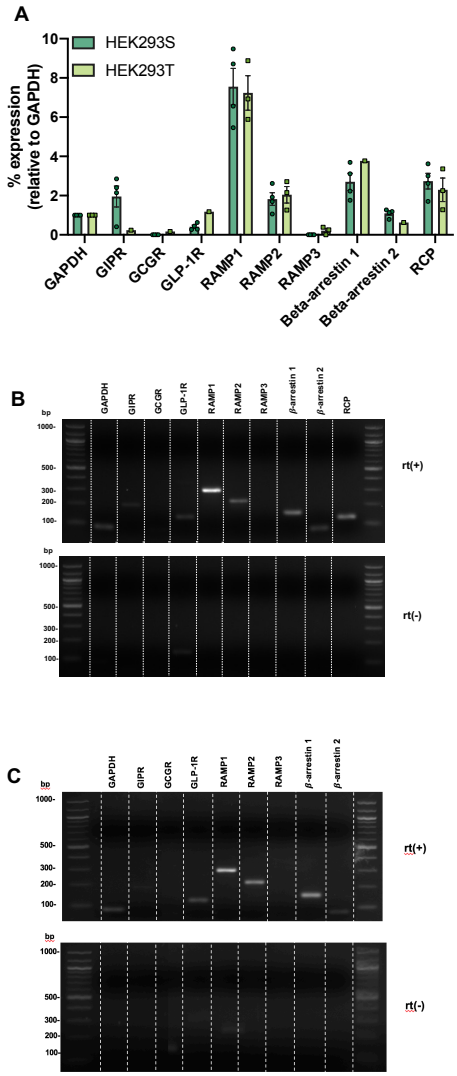

Figure 3.3: **Glucagon receptor family, RAMPs, β-arrestins and RCP expressions determined by RT-PCR in HEK293S and HEK293T cell lines.** (A) shows the comparison of expressions of GIPR, GCGR, GLP-1R, RAMPs, β-arrestins and RCP in HEK293S and HEK293T cell lines. All levels of gene expressions were normalised to the house-keeping gene GAPDH. Data were expressed as mean $\pm$ S.E.M. from 1 to 4 individual repeats. Only preliminary results for the receptors and β-arrestins expression studies in HEK293T cells were included due to COVID-19 obstruction of experimental schedule. (B) and (C) show the representative gel documentations in HEK293S and HEK293T cell lines respectively. Negative controls such as samples without the addition of reverse transcriptase (-RT) were also included in all experiments.

3.2.4 Production of HEK293S and HEK293-calcitonin receptor knock-out cell lines stably expressing GLP-1R and GCGR

GLP-1R and GCGR are known to share close structural resemblance and that these two receptors are also known to pleiotropically couple to different G proteins, such as the $G\alpha_q$ protein which is responsible for the downstream iCa^{2+} mobilisation [Montrose-rafizadeh et al., 1999, Wootten et al., 2012, Pabreja et al., 2014]. iCa^{2+} mobilisation is deemed to be an important signalling pathway which facilitates the exocytosis of insulin that are stored within the intracellular vesicles [Graaf et al., 2016]. Therefore, the iCa^{2+} signals upon receptor activation by GLP-1, GCG and OXM were quantified, given their prominent roles in modulating insulin and glucagon secretion as well as the cross-receptor sensitivity at GLP-1R and GCGR as discussed in section 3.2.2.

To do so, a HEK293S stably expressing GLP-1R cell line was produced with the use of the selection antibiotic G418 based on the previous evaluation of the molecular compositions of the two HEK293 cell lines as described in section 3.2.3. HEK293S cells were chosen in preference to HEK293T cells due to the fact that GLP-1R mRNA expression was seemingly lower in the HEK293S cells compared to that in the HEK293T cells. Although the GIPR endogenous expression was significantly higher in the HEK293S cell line compared to the HEK293T cell line, it was shown in section 3.2.2 that GIPR was not activated by any other glucagon-like peptides apart from its cognate ligand GIP. Therefore, there was less concern on cross-receptor sensitivity when a range of glucagon-like peptides were applied to the HEK293S stable cell line. More importantly, based on the previous experience in the Ladds' laboratory, the HEK293S cell line produces more potent iCa^{2+} responses compared to the HEK293T cell line, as Weston and colleagues showed that there was a difference in G proteins expressions among different HEK293 cell lines [Weston et al., 2016]. Based on the reasons stated above, a HEK293S-based stably expressing GLP-1R cell line (hereafter refer to as the HEK293S-GLP-1R-WT cell line) was produced to assist the quantification of iCa^{2+} release.

The GLP-1R construct, which was tagged with both N-terminal SNAP-tag preceded by a signal peptide, murine 5HT-3a, for efficient trafficking of the receptor to the cell surface and a C-terminal mCherry tag, was used to produce the stable GLP-1R cell line. This construct was cloned by Mr Ashley Clark (Department of Pharmacology, University of Cambridge) and the inclusion of these two components was used to investigate the mechanism of GLP-1R internalisation, which is out of the scope of this

thesis. Moreover, the mCherry-tagged construct allowed the verification of transfection efficiency as well as the monitoring of the expression of GLP-1R at different stages of the production of the stable cell line. The addition of the N-terminal SNAP-tag and the C-terminal mCherry tag at the GLP-1R did not affect GLP-1R G protein coupling and internalisation, as compared with the untagged GLP-1R construct.

A HEK293-calcitonin receptor knock-out (HEKΔCTR) stably expressing GCGR cell line was also created to allow the quantification of iCa^{2+} at the GCGR. The HEKΔCTR cell line was produced by Drs. David Hornigold, Jacqueline Naylor and Alessandra Rossi (AstraZeneca, Cambridge, U.K.), and was shown to exhibit very low levels of RAMPs expression [Bailey et al., 2019]. The HEKΔCTR cell line was employed to produce the GCGR stably expressing cell line in preference to the HEK293S cell line because RAMP2 was known to interact with GCGR, regulating its ligand binding and G protein selectivity [Weston et al., 2015, Cegla et al., 2017] and that the HEK293S cell line expressed RAMP2 (Fig. 3.3). The GCGR construct used to produce the stable cell line was given by Dr Ali Jazayeri (Heptares Therapeutics, Cambridge, U.K.). The GCGR stable cell line was also produced with the use of G418 as the selection antibiotic and was hereafter refer to as HEKΔCTR-GCGR cell line.

3.2.5 Establishing a system to quantify intracellular calcium mobilisation upon GLP-1R or GCGR activation

Following the production of two recombinant cell systems stably expressing GLP-1R and GCGR, the quantification of the extents of iCa^{2+} mobilisation at GLP-1R and GCGR upon ligand activation was next performed. HEK293S-GLP-1R-WT and HEKΔCTR-GCGR cell lines were seeded and plated on black 96 wells clear-bottom plates 24 hours prior to assay and the method for quantifying iCa^{2+} release was described previously in Section 2.2.3.2.

As anticipated, when 10μM ionomycin, which is a calcium ionophore [Liu and Hermann, 1978], was applied to both the HEK293S-GLP-1R-WT and HEKΔCTR-GCGR cell lines, potent iCa^{2+} mobilisation responses were observed, resulting in the brightest images captured compared to the rest of the other collated images. The traces of ionomycin were also deemed to have the highest peaks among all the individual traces relative to time in seconds (Fig. 3.4A-B and Fig. 3.5A-B). Applying Ca^{2+}-free HBSS blank solution to the cells, which also served as negative controls, did not mediate any calcium releases as also shown in Fig. 3.4A-B and 3.5A-B respectively.

Although not as potent as ionomycin, the activation of the GLP-1R and GCGR with their cognate ligands GLP-1 and GCG also mediated iCa^{2+} mobilisation. Furthermore, GLP-1 and GCG were able to activate GLP-1R and GCGR in a concentration-dependent manner, which were represented by the dose-dependent increase in resultant light intensity and were also clearly demonstrated by the concentration-dependent increase in the peak intensities of the individual traces (Fig. 3.4A-B and Fig. 3.5A-B). The peak values of these traces were then normalised to that of 10μM ionomycin and were used to construct the corresponding dose response curves (Fig. 3.4C and 3.5C). After the establishment of cell systems which allowed the quantitative measurements of iCa^{2+} mobilisation, the evaluation of the iCa^{2+} responses mediated GLP-1, GCG and OXM at both GLP-1R and GCGR was performed.

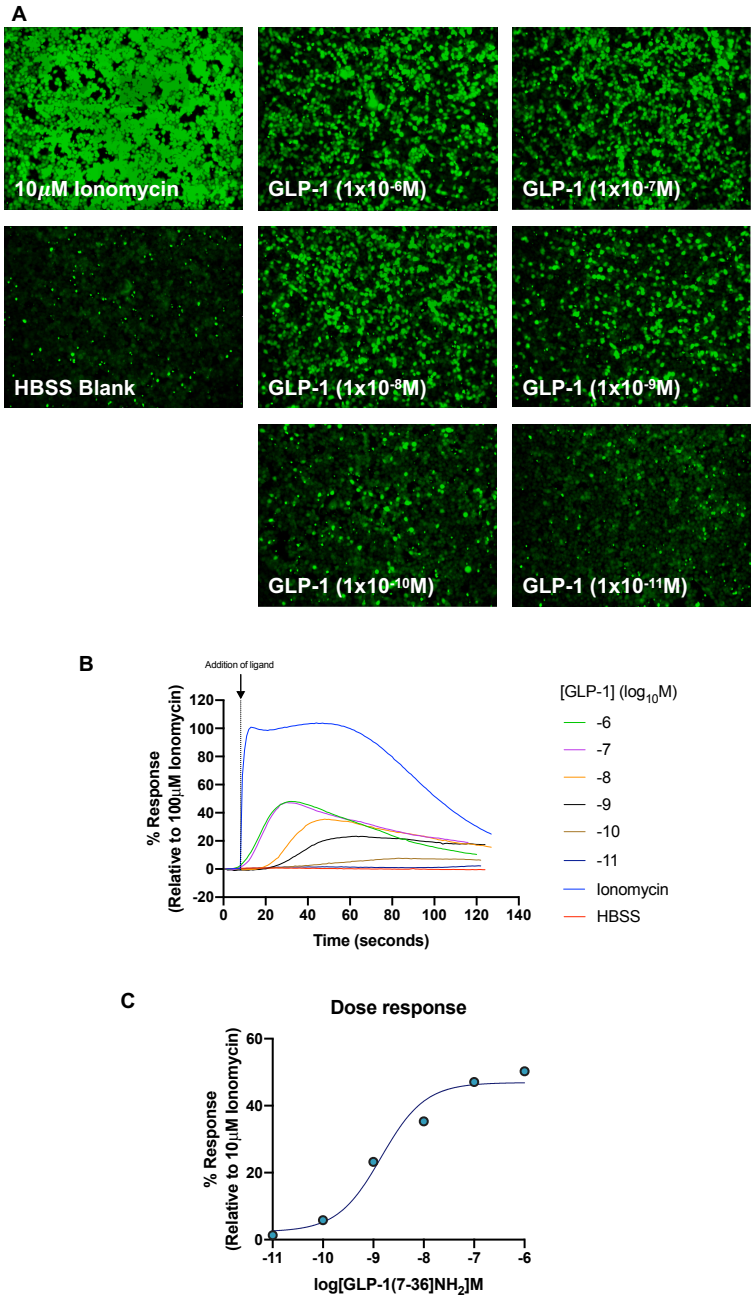

Figure 3.4: **Representative intracellular calcium release captured images to illustrate the process of calcium assay analysis in the HEK293S-GLP-1R-WT cell line.** (A) shows the photos captured at the peak of the intracellular calcium release when ligands were applied to the HEK293S cells stably expressing GLP-1R. Their mean peak intensities were measured by Image J and background fluorescence were then subtracted to obtain the mean peak intensity. (B) shows the background subtracted traces of a range of different GLP-1 concentrations normalised to 10μM ionomycin. The peaks of each normalised trace were then obtained and transformed into a dose response curve, which is shown in (C).

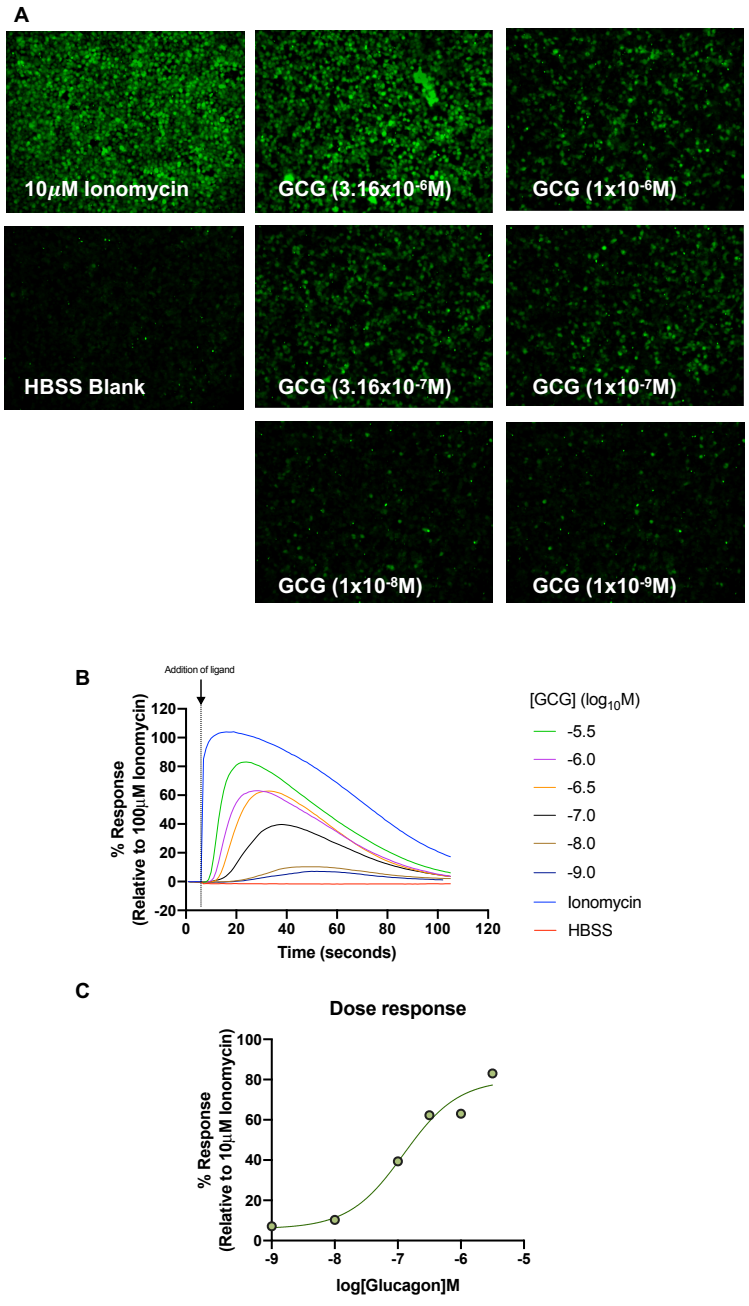

Figure 3.5: **Representative intracellular calcium release captured images to illustrate the process of calcium assay analysis in HEKΔCTR-GCGR cell line.** (A) shows the photos captured at the peak of the intracellular calcium release when ligands were applied to the HEK-calcitonin receptor knock-out cells stably expressing GCGR. Their mean peak intensities were measured by Image J and background fluorescence were then subtracted to obtain the mean peak intensity. (B) shows the background subtracted traces of a range of different GCG concentrations normalised to 10μM ionomycin. The peaks of each normalised trace were then obtained and transformed into a dose response curve, which is shown in (C).

3.2.6 cAMP and intracellular calcium release responses of glucagon-like peptide ligands in HEK293 recombinant cell lines

Following the validation of the two different human recombinant cell systems to quantify iCa^{2+} responses, GLP-1, OXM and GCG were applied to both HEK293S-GLP-1R-WT and HEKΔCTR-GCGR cells in an attempt to compare the extent of iCa^{2+} mobilisation mediated by these peptide agonists at GLP-1R and GCGR. The cAMP accumulation facilitated by these agonists at these two cell lines were also measured utilising the same TR-FRET cAMP accumulation assay employed in previous sections. However, since the HEK293S-GLP-1R-WT cell line was very responsive to cAMP production upon ligand stimulation, possibly due to a high expression of GLP-1R, PDE inhibitor was not included in the cAMP assay when this cell line was tested.

The following results showed that GLP-1, OXM and GCG not only induced cAMP production upon GLP-1R activation, as seen in the CHO-GLP-1R recombinant cell line (section 3.2.2), but also mediated iCa^{2+} mobilisation upon receptor activation (Fig. 3.6A, C, E and Table 3.3), which agreed with the observations from studies conducted in Flp-In-CHO cells stably expressing GLP-1R [Wootten et al., 2013a]. However, the order of cAMP response potency of ligands was different from the observation in the CHO-GLP-1R cells yet agreed with the findings in other studies utilising COS-7 stably expressing GLP-1R cell line [Jorgensen et al., 2007], with GLP-1 being the most potent (pEC_{50}: 12.05 $\pm$ 0.14), followed by OXM (pEC_{50}: 7.98 $\pm$ 0.06) and lastly GCG (pEC_{50}: 7.62 $\pm$ 0.04). This rank order potency discrepancy may be attributed to the differences in cellular background between hamster and human species. While for GCGR, the rank order of cAMP response potency concurred with that in CHO-GCGR recombinant cell line, with GCG being the most potent (pEC_{50}: 8.96 $\pm$ 0.06), followed by OXM (pEC_{50}: 7.26 $\pm$ 0.04) and GLP-1 (pEC_{50}: 5.32 $\pm$ 0.11) (Fig. 3.6B, D, F and Table 3.3). Similar to what was observed in the CHO-GCGR recombinant cell line and agreed with the observation by Weston and colleagues in HEK293 transiently transfected with GLP-1R cells [Weston et al., 2015], GLP-1 acted as a partial agonist at the GCGR. This rank order of potency at the GCGR again agreed with what was observed in the same study conducted by Jorgensen and colleagues [Jorgensen et al., 2007] in COS-7 stably expressing GCGR cell line.

In terms of the extent of iCa^{2+} mobilisation, all three peptide ligands were able to induce iCa^{2+} release at the GLP-1R, with GCG being the most potent (but partial) agonist in mediating iCa^{2+} mobilisation (pEC_{50}: 7.93 $\pm$ 0.14), closely followed by GLP-1

(pEC_{50}: 7.65 $\pm$ 0.29) and OXM (pEC_{50}: 7.10 $\pm$ 0.26). Likewise, potent GLP-1-mediated iCa^{2+} response was also reported by Li and colleagues utilising the HEK293 cells stably expressing GLP-1R [Li et al., 2012]. Other studies have also showed that GLP-1 was able to mediate a more potent iCa^{2+} response than OXM in FlpIn-CHO cells stably expressing GLP-1R [Koole et al., 2010]. However, there is no report on the GCG-mediated iCa^{2+} response at the GLP-1R to date. As at GCGR, only GCG and OXM were able to induce iCa^{2+} mobilisation at GCGR upon receptor activation, with GCG being the most potent ligand (pEC_{50}: 8.96 $\pm$ 0.26), followed by OXM (pEC_{50}: 6.95 $\pm$ 0.17); GLP-1 did not induce any iCa^{2+} signalling at the GCGR. The results obtained here differed from the report conducted by Cegla and colleagues [Cegla et al., 2017], which utilised CHO-K1 stably expressing GCGR cells to investigate the $G\alpha_q$ signalling pathway at the GCGR upon ligand activation. While Cegla and colleagues also showed potent iCa^{2+} responses mediated by GCG and OXM, they observed a linear correlation in terms of GLP-1-mediated iCa^{2+} response whereas here no calcium activation induced by GLP-1 was observed. The major difference may be attributed to the different techniques used in measuring iCa^{2+} release. Nonetheless, GCG and OXM were shown to be potent partial agonists for mediating iCa^{2+} release at the GCGR. However, the receptor cell surface expressions were not quantified in these HEK293-based stable cell lines and thus variations of GLP-1R and GCGR expressions in these two cell lines cannot be taken into account. In summary, the rank order of cAMP and iCa^{2+} responses potencies are as follow. The rank order of cAMP and iCa^{2+} responses potencies are summarised in Table 3.4.

cAMP:

- **GLP-1R:**: GLP-1 > OXM > GCG; **GCGR:** GCG > OXM > GLP-1

iCa^{2+} release:

- **GLP-1R:** GCG > GLP-1 > OXM; **GCGR:** GCG > OXM

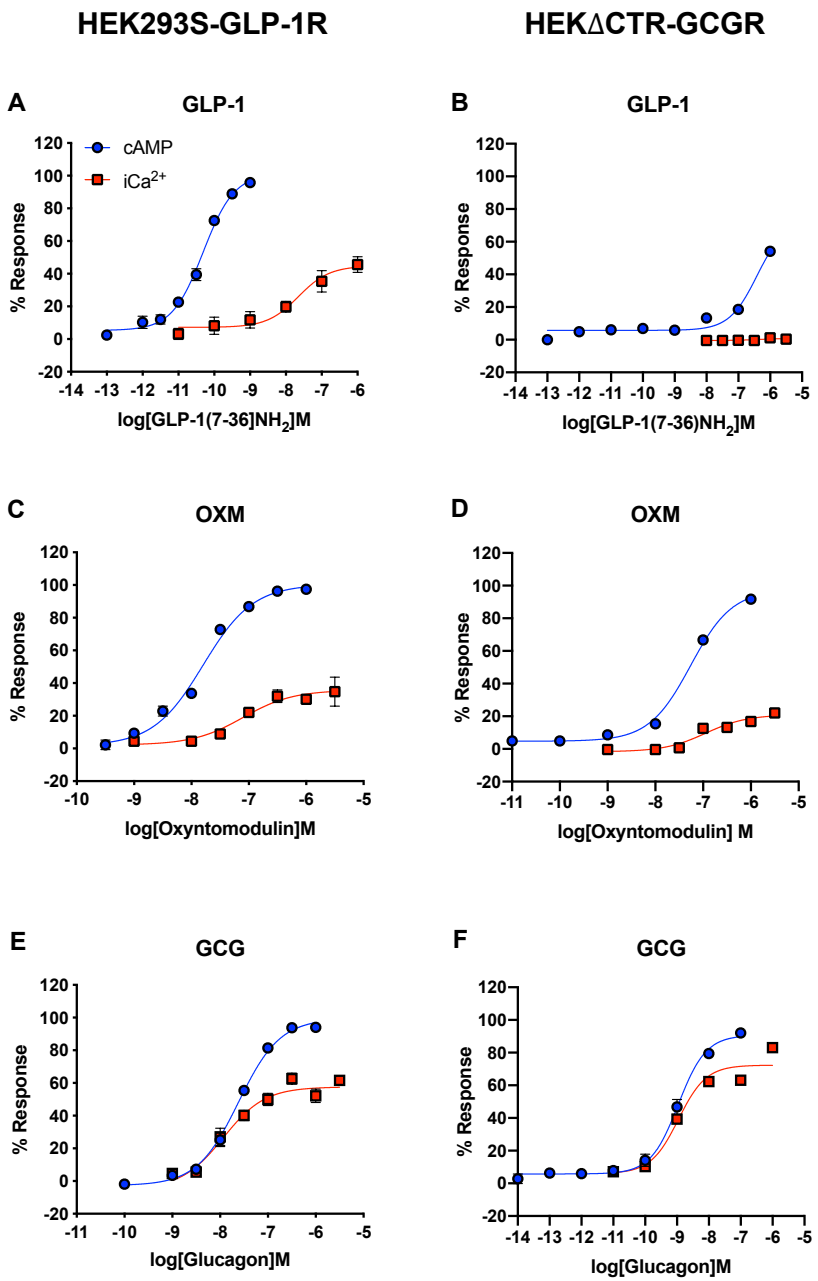

Figure 3.6: **Comparison of GLP-1R and GCGR endogenous agonists cAMP accumulation and intracellular calcium responses in HEK293S-GLP-1R and HEKΔCTR-GCGR cell lines.** The above figure shows the dose-response curves representing cAMP production and intracellular calcium mobilisation when HEK293S-GLP-1R cells (Fig. A, C and E) and HEKΔCTR-GCGR cells (Fig. B, D and F) were stimulated with GLP-1, OXM and GCG. 1000 HEK293S-GLP-1R-WT and HEKΔCTR-GCGR cells/well were stimulated with ligands for 15 minutes in the absence and presence of PDE inhibitor IBMX respectively. Dose-response curves for iCa^{2+} mobilisation were obtained as described in section 3.2.5. All data were normalised to the maximum cAMP production when stimulated with 100μM forskolin or maximum intracellular calcium response when stimulated with 10μM ionomycin. All data were means of 1 to 4 independent experiments with duplicate results $\pm$ S.E.M (upper and lower error bars). Table 3.3 shows the pEC_{50} and E_{max} values of ligand responses.

Table 3.3: **cAMP and intracellular calcium mobilisation potencies (pEC_{50}) and maximal responses (E_{max}) of GLP-1R and GCGR activation by their endogenous ligands.**

Receptor	Ligand	Pathway	pEC_{50} [a]	E_{max} [b]	Span	n
GLP-1R	GLP-1	cAMP	12.05±0.14	80.40±2.27	57.88±3.51	8
		iCa^{2+}	7.65±0.29****	44.80±4.54***	37.63±5.04***	4
	OXM	cAMP	7.98±0.06	117.7±4.23	115.0±4.18	8
		iCa^{2+}	7.10±0.26*	35.73±3.41*	$33.59±4.24^{ns}$	3
	GCG	cAMP	7.62±0.04	99.38±1.80	102.1±2.18	6
		iCa^{2+}	$7.93±0.14^{ns}$	57.60±2.49****	$62.04±5.21^{ns}$	5
GCGR	GLP-1	cAMP	5.32±0.11	56.46±7.08	66.80±7.20	6
		iCa^{2+}	6.38±1.06	0.85±0.87	1.41±0.83	2^{NB}
	OXM	cAMP	7.26±0.04	97.43±2.02	92.70±2.11	6
		iCa^{2+}	$6.95±0.17^{ns}$	20.98±1.68****	22.68±1.98****	3
	GCG	cAMP	8.96±0.06	90.70±2.20	84.94±2.45	6
		iCa^{2+}	8.96±0.26	72.35±5.37	66.37±8.26	2^{NB}

Values were generated when the data were fitted to the three-parameter logistic equation. Means ± S.E.M of n individual result sets were shown.
[a] Negative logarithm of agonist concentration when reaching half maximal response.
[b] % of maximal response observed when stimulated with ligands relative to forskolin or ionomycin.
[NB] Preliminary results are shown here only due to COVID-19 obstruction of experimental schedule.
Statistical significance compared between individual peptide ligand responses in cAMP response and intracellular calcium mobilisation at GLP-1R or GCGR were determined by Student's t-test with Welch's correction (*, p<0.05; ***, p<0.001; ****, p<0.0001; ns, non-statistically significant).

Table 3.4: **Summary of the rank order of cAMP potency in CHO-K1, HEK293S and HEKΔCTR recombinant cell lines stably expressing GLP-1R, GCGR and GIPR.**

Recombinant cell line	Receptor of stable expression	Rank order of potency of ligands in terms of cAMP potentiation (from high to low)
CHO-K1	GLP-1R	GLP-1 > GCG > OXM > GIP > GLP-1(9-36)NH_2
	GCGR	GCG > OXM > GLP-1 > GLP-1(9-36)NH_2 > GIP
	GIPR	GIP only
HEK293S	GLP-1R	GLP-1 > OXM > GCG
HEKΔCTR	GCGR	GCG > OXM > GLP-1

3.3 Characterisation of glucagon-like peptide cAMP responses in rodent immortalised α and β cell systems

Following the pharmacological characterisation of the extent of cAMP and iCa^{2+} signalling responses upon receptor activation induced by various glucagon-like peptide ligands in recombinant cell systems, the next goal was to translate the findings in the recombinant cell systems to the physiologically relevant cell models. To do so, two rodent glucagonoma cell lines, namely the mouse αTC1.6 cell line [Powers et al., 1990] and hamster InR1G9 cell line [Takaki et al., 1986], were used and two rodent insulinoma cell lines, which are the mouse MIN6-B1 cell line [Miyazaki et al., 1990] and rat INS-1 832/3 cell lines [Hohmeier et al., 2000], were also employed to mimic the individual α and β cell components in normal pancreatic islets. These rodent insulinoma and glucagonoma cell lines were widely used as surrogates for isolated mouse islets to elucidate the cellular signalling mechanism of insulin and glucagon secretion as they were responsive to glucose [McGirr et al., 2005, Cheng et al., 2012, Liu et al., 2018]. Furthermore, they were also known for endogenously expressing receptors from glucagon receptor family, which could facilitate the evaluation of the interplay among GLP-1R, GCGR and GIPR affecting insulin or glucagon secretion [Sonoda et al., 2008, Piro et al., 2014, Sancho et al., 2017]. However, it is of particular importance to note that these pancreatic α and β clonal cell lines contain a mixed population of pancreatic cell types, i.e. α, β and δ cells, yet these cell lines exhibit predominately insulin or glucagon-producing nature [Poitout et al., 1996, Nakashima et al., 2009]. In spite of the wide use of these rodent insulinoma and glucagonoma cell lines to investigate the cellular signalling of insulin and glucagon secretion, only limited reports documented the individual glucagon receptor family receptors and RAMPs expressions in these cell lines. Hence, a series of RT-PCR studies were performed in an attempt to elucidate a thorough understanding of the cellular background of these rodent immortalised pancreatic α and β cell systems, prior to further quantification of individual glucagon-like peptide cAMP responses.

3.3.1 GLP-1R, GCGR, GIPR and RAMPs expressions in mouse αTC1.6 and MIN6-B1 cell lines

Semi-quantitative RT-PCR experiments were performed in order to evaluate the cellular background of the pancreatic α cell line, αTC1.6 cells, and the β cell line, MIN6-B1

cells, which were both of mouse origin. All expressions were relative to that of the house-keeping gene, GAPDH, and identical reactions without the presence of reverse-transcriptase (rt-) were also included to act as negative controls to show the absence of contaminating genomic (g)DNA. Sets of oligonucleotide primers targeting specific mouse gene of interests were designed and were used in these RT-PCR experiments. In addition to quantifying the mRNA expressions of GLP-1R, GCGR and GIPR, the expression of the class A fatty-acid binding GPCR, GPR119, was also determined as GPR119 was postulated to play an important role in regulating insulin and glucagon secretion through modulating GLP-1R signalling response [Winzell and Ahrén, 2007, Flock et al., 2011, Cheng et al., 2015]. GPR119 was also shown to play a direct role in enhancing glucagon secretion [Li et al., 2018].

The following results suggested there was a stark difference in receptor expressions between the mouse α and β cell lines. GIPR was the highest expressing receptor among the glucagon receptor family in both cell lines (Fig. 3.7A), yet the expression of GIPR was higher in the αTC1.6 cell line compared to the MIN6-B1 cell line by 1.46-fold ($p < 0.05$). Despite the wide debate on the presence of GLP-1R on the pancreatic α cells [Moens et al., 1996, Heller et al., 1997, Tornehave et al., 2008, De Marinis et al., 2010], intriguingly a small but detectable level of GLP-1R expression was detected here in the αTC1.6 cells (Fig. 3.7A), a result that corroborated with other published reports which also showed the presence of GLP-1R on the pancreatic α cells utilising various techniques, such as confocal laser microscopes [Tornehave et al., 2008, Nakashima et al., 2018] and RT-PCR [Piro et al., 2014]. However, the GLP-1R expression level in the αTC1.6 cells was 3.15-fold lower than that in MIN6-B1 cells ($p < 0.0001$), which also concurred with other reports [Moens et al., 1996, Huising et al., 2010]. Moreover, the results here contrasted with the findings by Huising and colleagues, of which they showed GLP-1R was more abundant than GIPR in the MIN6-B1 cells using qPCR [Huising et al., 2010], yet here GIPR was shown to be more highly expressing than GLP-1R in the mouse β cell line. GCGR expression was nearly double of the expression of GLP-1R in the mouse αTC1.6, and it was the second highest receptor expression in the pancreatic α cell line (Fig. 3.7A).

Despite the wide use of αTC1.6 and MIN6-B1 cells to elucidate the molecular mechanism of glucagon receptor family signalling which was also known to be modulated by RAMPs, there were only limited studies on the characterisations of RAMPs expressions in these two cell lines. The results here showed that there were no statistically significant difference in the expression levels of RAMP1, RAMP2 and RAMP3 between

the αTC1.6 cell line and the MIN6-B1 cell line (Fig. 3.7A). Furthermore, contrary to what was observed in the HEK293 cell lines (Fig. 3.3), RAMP3 showed the highest expression in both mouse cell lines, followed by RAMP2 and non-existentvery low levels of RAMP1.

Interestingly, GPR119 was found to be highly expressing in the mouse α cell line compared to the β cell line and that the expression of GPR119 was seemingly higher or equal to that of GIPR in the α cell line (Fig. 3.7A). The observations reported here agreed with the report by Whalley and colleagues [Whalley et al., 2011] yet contrasted with that of Odori and colleagues [Odori et al., 2013], but the discrepancies might be explained by the difference in technique employed in quantifying the mRNA expressions of GPR119. Based on this interesting observation, further investigation into the interplay among GLP-1R, GCGR and GPR119 was performed and would be discussed in section 3.4.1.

To summarise, the order of expressions of GLP-1R, GCGR, GIPR and RAMPs in the α and β cell mouse models are shown below:

- α**TC1.6 cells:** GIPR > GCGR > GLP-1R
- **MIN6-B1:** GIPR > GLP-1R > GCGR
- RAMP3 > RAMP2 > RAMP1 in both cell lines

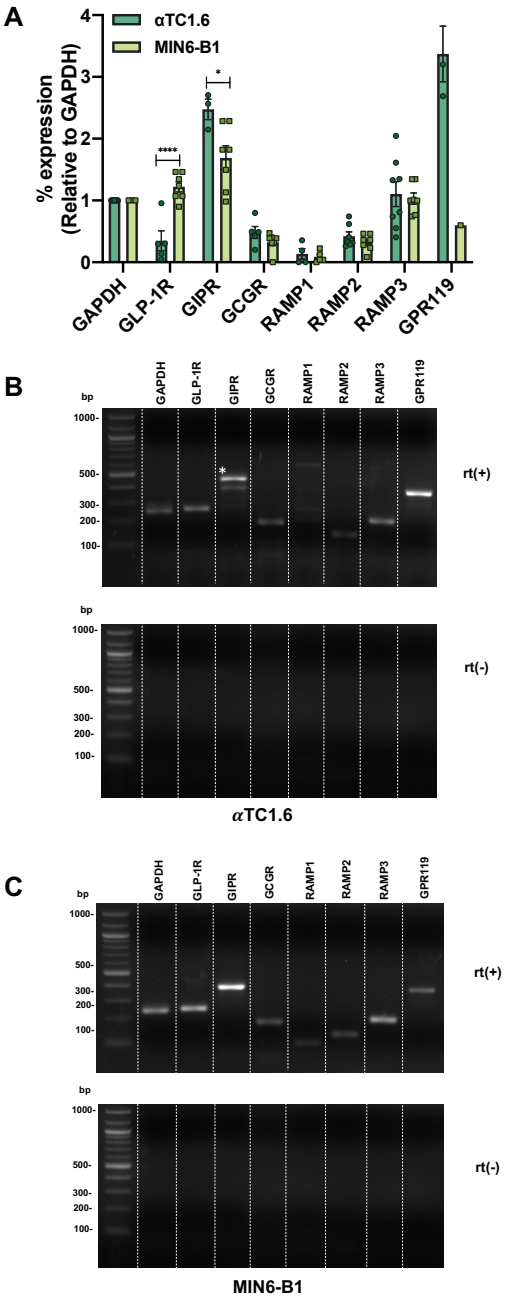

Figure 3.7: **Glucagon receptor family and RAMPs expressions determined by RT-PCR in mouse αTC1.6 and MIN6-B1 clonal cell lines.** (A) shows the comparison of GLP-1R, GIPR, GCGR, RAMPs and GPR119 gene expressions in αTC1.6 cells cultured in 5mM glucose (circle) and MIN6-B1 (square) cells. All mRNA expressions were relative to GAPDH. Data are expressed as mean $\pm$ S.E.M. from 1 to 8 individual repeats. Statistical significance compared between the expressions of individual receptors or RAMPs in αTC1.6 and MIN6-B1 cells were determined by Student's t-test with Welch's correction (*, $p<0.05$; ****, $p<0.0001$). (B) and (C) show the representative gel documentations of amplified GLP-1R, GIPR, GCGR, RAMPs and GPR119 genes in αTC1.6 and MIN6-B1 cells respectively. * indicates product with the correct band size. Negative controls such as samples without the addition of reverse transcriptase (rt-) were also included. n=1 for the determination of GPR119 expression in the MIN6-B1 cell line due to the restriction of COVID-19 lockdown.

3.3.2 Receptors and RAMPs expressions in rat INS-1 832/3 cell lines

After the characterisation of the glucagon receptor family and RAMPs expressions in the mouse α and β cell lines, the evaluation of mRNA expressions of incretin receptors and RAMPs was further extended to the rat β cell model, the INS-1 832/3 cell line, which was frequently used in the investigation of the insulin secretion cellular mechanism. RT-PCR was again performed and oligonucleotide primers which were designed to target gene of interests of rat species were used in the RT-PCR analysis. Identical reactions with the absence of reverse-transcriptase (rt-) and replacing cDNA with dH_2O were also included to act as negative controls to show the absence of contaminating gDNA.

In contrast to the RT-PCR results in the mouse β cell line, GLP-1R was found to be the highest expressing receptor, followed by GCGR and lastly GIPR (Fig. 3.8), suggesting the difference in receptor expressions was attributed to species variation. Furthermore, different to the observations in the MIN6-B1 cells (Fig. 3.7A), INS-1 832/3 cells expressed RAMP2 and RAMP3 at an equal level, and did not express RAMP1, as consistent with the findings in the MIN6-B1 cells. Having determined the differences in receptors and RAMPs expressions between the rodent α and β cell models, the G protein profiles of these cell systems were next determined.

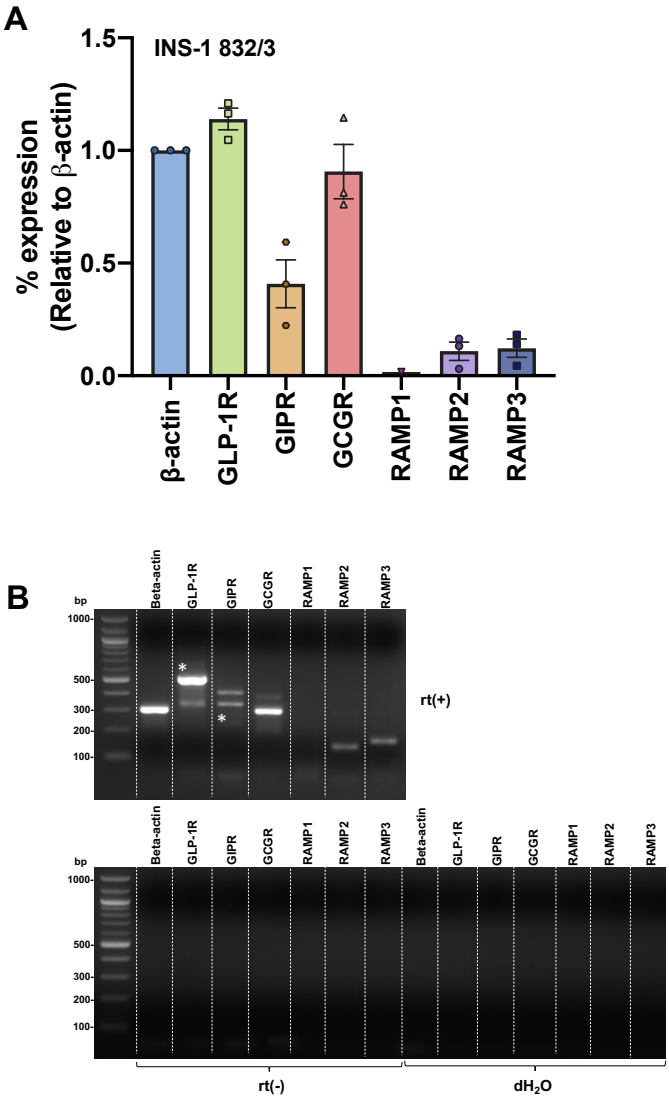

Figure 3.8: **Glucagon receptor family and RAMPs expressions determined by RT-PCR in rat clonal INS-1 832/3 cell lines.** (A) shows the comparison of GLP-1R, GIPR, GCGR and RAMPs gene expressions in rat INS-1 832/3 cell line. All expressions of genes of interests were relative to β-actin. Data are expressed as mean $\pm$ S.E.M. from 3 individual repeats. (B) shows the representative gel documentations of the same set of amplified genes in rat INS-1 832/3 cell line. Negative controls such as samples without the addition of reverse transcriptase (rt-) and without addition of cDNA with replacement of RNase-free water (dH_2O) were also included. * indicate products with the correct band sizes.

3.3.3 Characterising G protein expressions in mouse αTC1.6 and rat INS-1 832/3 cell lines

To elicit intracellular signalling, GPCRs couple with intracellular transducers such as heterotrimeric G proteins, which are formed by the Gα, Gβ and Gγ subunits. Gα subunits signal independently while the Gβ and Gγ subunits are heterodimers that function as a single unit. Furthermore, as GLP-1R and GCGR are well known to pleiotropically couple to different G proteins, namely Gα_i and Gα_q proteins [Montrose-rafizadeh et al., 1999, Wootten et al., 2012, Pabreja et al., 2014], it is of invaluable insight to evaluate the G protein compositions in the mouse glucagonoma and rat insulinoma cell models to predict the likelihood of GLP-1R and GCGR to pleiotropically couple to G proteins other than Gα_s protein.

To do so, RT-PCR experiments were again performed to decipher the G protein compositions in these two cell lines. However, some G protein, such as the Gα_{t1} and Gα_{t2} protein, cannot be determined in the INS-1 832/3 cell line due to a lack of suitable primers on the NCBI database. Likewise, Gα_{t3} and Gα_{13} were not determined in the α cell line because of the same technical reason. The G protein compositions in the αTC1.6 cell line were normalised to two different housekeeping genes, GAPDH and β-actin. β-actin was used in addition to GAPDH to normalise the RT-PCR results in an attempt to compare the G protein expressions fairly with the results obtained in INS-1 832/3 cells, which was normalised to β-actin. However, due to the lockdown, I was not able to produce further repeats to validate the results. Yet, similar profiles of G protein compositions were observed in both sets of data in the αTC1.6 cell line (Fig. 3.9A and C), albeit the use of different housekeeping genes.

Both α and β cell lines expressed high levels of Gα_s protein, verifying the ability of the GLP-1R, GCGR and GIPR to couple with the Gα_s protein, further activating adenylyl cyclase, facilitating the production of cAMP (Fig. 3.9). Interestingly, the Gα_i protein, which consists of Gα_{i1}, Gα_{i2} and Gα_{i3} subunits, were more abundant in the α cell line compared to that in the β cell line. Also, both cell lines expressed a high level of Gα_o, Gα_z and Gα_{11} proteins, yet the subtypes of Gα_o protein was not determined. Furthermore, both cell lines expressed G$\alpha_{q/11}$ protein, with the Gα_q subunit being more highly expressed in the α cell line. Moreover, Gα_{14} and Gα_{12} proteins were found to be highly present in α cell line, compared to that in the β cell line. Following the investigations of the incretin receptors, RAMPs and G protein expression profiles in the α and β cell lines, ligand-induced cAMP responses were subsequently determined.

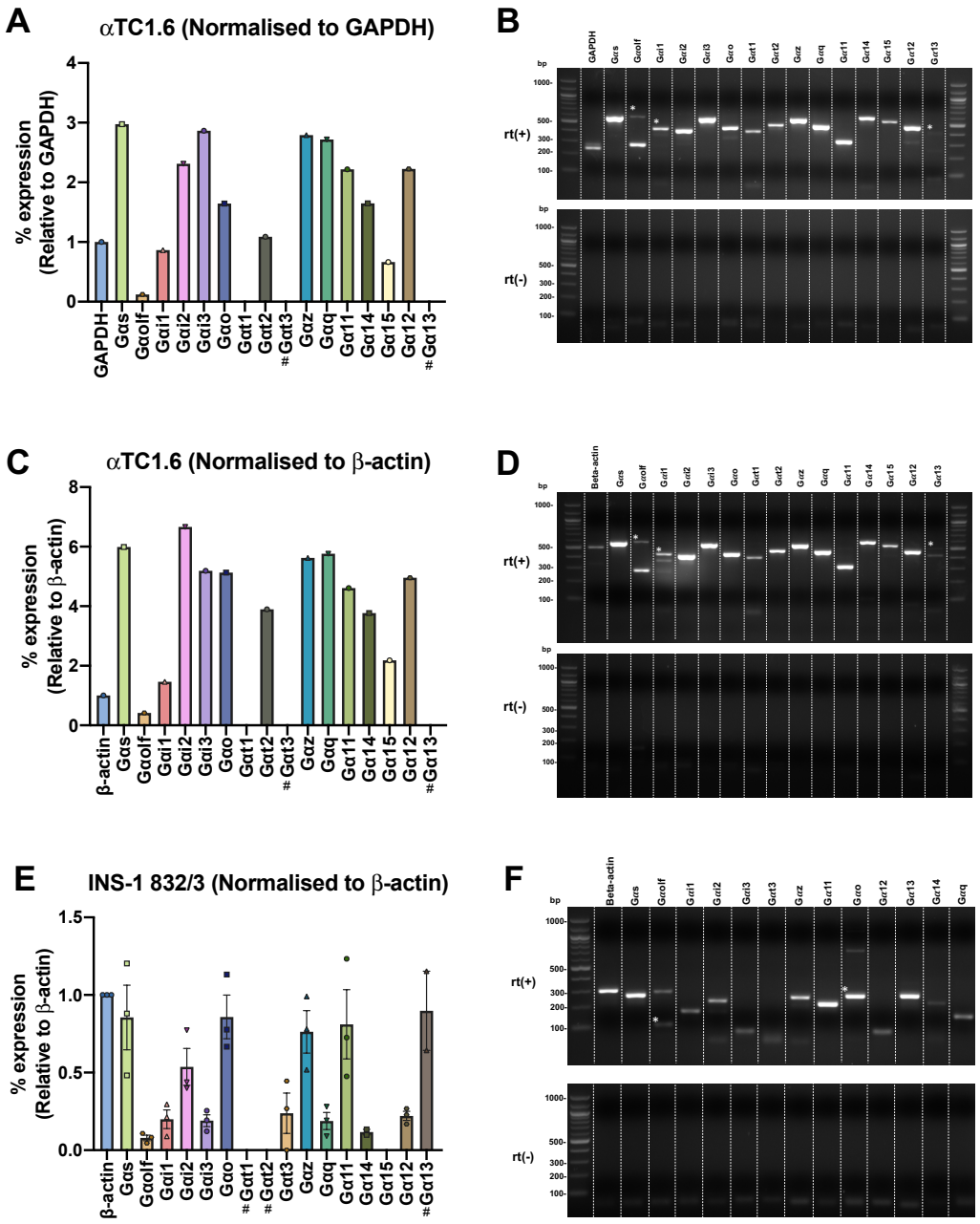

Figure 3.9: **G protein expressions determined by RT-PCR in αTC1.6 and INS-1 832/3 cell lines.** (A) and (C) show the G protein expressions in mouse αTC1.6 cell line cultured under low glucose (5mM) condition while (A) are relative to the expression of GAPDH and (C) are relative to β-actin. (E) shows the G protein expressions in rat INS-1 832/3 cell line under 11mM glucose condition respectively and the expressions of genes of interests are relative to β-actin. # denotes G proteins that are undeterminable because of the lack of specific primers. Data are expressed as mean $\pm$ S.E.M. from 1-3 individual repeats. Preliminary results of G protein expression profile of the αTC1.6 cells are presented here due to COVID-19 restriction. (B), (D) and (F) show the corresponding representative gel documentations of amplified G protein genes in mouse αTC1.6 and INS-1 832/3 cell lines. Negative controls (i.e. samples without the addition of reverse transcriptase, (-RT) were also shown). * indicate products with the correct band sizes.

3.3.4 Characterising glucagon-like peptide ligand cAMP responses in rodent insulinoma and glucagonoma cell models

Following the evaluation of the cellular background of various rodent pancreatic cell models, the cAMP responses mediated by a range of glucagon-like peptide agonists in the pancreatic α (via the use of mouse αTC1.6 and hamster InR1G9 cell lines) and β (via the use of mouse MIN6-B1 and rat INS-1 832/3 cell lines) cell models which expressed endogenous incretin receptors (see Section 3.3.1), except for the InR1G9 cell line, which did not express endogenous GLP-1R [Fehmann et al., 1999, Piro et al., 2014] were characterised. TR-FRET-based cAMP assays were again performed to determine the cAMP accumulation when these cell lines were stimulated with agonists of interest which were GLP-1, GLP-1(9-36)NH_2, OXM, GCG and GIP. IBMX, which is a pan-PDE inhibitor, was used in these assays to prevent the breakdown of cAMP.

Similar to the results observed in the recombinant cell models stably expressing GLP-1R, GCGR and GIPR, GLP-1, OXM and GCG showed potent cAMP responses in both rodent β cell lines (pEC_{50} values were 10.99 $\pm$ 0.19 for GLP-1, 8.27 $\pm$ 0.23 for OXM and 7.76 $\pm$ 0.11 for GCG in the MIN6-B1 cell line while pEC_{50} values 9.57 $\pm$ 0.17 for GLP-1, 7.02 $\pm$ 0.19 for OXM and 6.85 $\pm$ 0.16 for GCG in the INS-1 832/3 cell line) (Fig. 3.10A-B and Table 3.5); the agonist potencies agreed with the observed values in published reports [Naylor et al., 2016]. These observations could be attributed to the high expression of GLP-1R and GCGR in the β cell systems, as it has been shown in Fig. 3.7 and Fig. 3.8, as well as the highly abundant $G\alpha_s$ protein present in the rat INS-1 832/3 cell line (Fig. 3.9), as well as the fact that GCG can act at GLP-1R to mediate cAMP responses (Fig. 3.6). Furthermore, the potency of GLP-1 was expectedly lower in the rat β cell model compared to that in the mouse β cell model, as it has been shown that applying human GLP-1 agonist at the rat GLP-1R resulted in a less potent GLP-1 cAMP response, presumably due to the interspecies variation of the GLP-1R [Knudsen et al., 2012]. Hence, this finding could also explain the apparent decrease in GCG and OXM potencies in the rat β cell model compared to the mouse β cell line. GLP-1(9-36)NH_2 on the other hand did not appear to mediate any cAMP responses in the MIN6-B1 cell line yet it showed partial agonism on the INS-1 832/3 cell line (E_{max} values of GLP-1(9-36)NH_2 were 8.18 $\pm$ 4.58 and 27.27 $\pm$ 6.47 in the MIN6-B1 and INS-1 832/3 cell lines respectively) (Fig. 3.10A-B and Table 3.5).

GIP was the second most potent agonist in both rodent β cell lines (Fig. 3.10A-B and Table 3.5). Yet it was less efficacious in the MIN6-B1 cells compared to the INS-1 832/3

cells or the CHO-GIPR recombinant cell systems (E_{max} of GIP were 28.74 $\pm$ 6.95, 61.29 $\pm$ 6.57, 69.72 $\pm$ 2.61 in the systems expressing mouse, rat and human GIPR respectively). Furthermore, the potencies of GIP in human and mouse GIPR were largely similar yet the potency of GIP in rat GIPR was the lowest among the three species (pEC_{50} values of human GIP were 10.70 $\pm$ 0.77, 7.92 $\pm$ 0.16, 9.64 $\pm$ 0.11 when applied to in mouse, rat and human GIPRs respectively). Similarly, such discrepancies in potency and efficacy could again be explained by interspecies variation as here human GIP was applied to the mouse GIPR, which Sparre-Ulrich and colleagues also demonstrated an interspecies variation exist among the GIP/GIPR system [Sparre-Ulrich et al., 2016].

Contrary to the well characterised cAMP responses mediated by the glucagon-like peptides in the rodent insulinoma cell lines, only a few studies which evaluated the cAMP accumulation responses mediated by the incretin ligands in pancreatic α cell models have been published to date. Here in the mouse αTC1.6 cells, GLP-1 showed a concentration-dependent cAMP production, which concurred with the studies which showed an increment of concentration-dependent GLP-1-induced cAMP levels measured by ELISA analysis [Piro et al., 2014]. GLP-1 showed a weaker cAMP response compared to GIP, GCG and OXM, with GCG being the most potent ligand, followed by GIP and OXM (pEC_{50} values were 7.66 $\pm$ 0.34 for GCG, 7.54 $\pm$ 0.29 for GIP, 7.20 $\pm$ 0.51 for OXM and 6.85 $\pm$ 0.22 for GLP-1) (Fig. 3.10C and Table 3.6). In fact, similar observations that GIP being more stimulatory than GLP-1 were noted in other studies [Moens et al., 1996]. Furthermore, a weak cAMP response exerted by GLP-1(9-36)NH_2 was also detected (pEC_{50} of which was 5.77 $\pm$ 0.66) (Fig. 3.10C and Table 3.6), which suggested that the GLP-1 metabolite may also play a role in pancreatic α cells signalling.

Similarly, the hamster α cell line InR1G9 demonstrated a rank order of potency analogous to that of the mouse αTC1.6 cell line, yet GIP was shown to be the most potent endogenous ligand, followed by GLP-1, GCG, OXM and lastly GLP-1(9-36)NH_2 (pEC_{50} values were 7.59 $\pm$ 0.24 for GIP, 7.10 $\pm$ 0.31 for GLP-1, 7.03 $\pm$ 0.24 for GCG, 6.45 $\pm$ 0.33 for OXM and 6.30 $\pm$ 0.29 for GLP-1(9-36)NH_2) (Fig. 3.10D and Table 3.6). Interestingly, although several papers suggested there was no endogenous GLP-1R present in the InR1G9 cell line [Fehmann et al., 1994, Piro et al., 2014], GLP-1 and GLP-1(9-36)NH_2 were able to stimulate the hamster α cell model, producing cAMP responses. This observation thus poses further question of how GLP-1 and GLP-1(9-36)NH_2 mediate glucagonostatic actions in the absence of GLP-1R.

In essence, the rank order of agonist potencies in the β cell lines were largely similar

to those in the recombinant cell models (Table 3.7). More importantly, GLP-1 and GLP-1(9-36)NH_2 were able to produce cAMP responses through GCGR in the apparent absence of GLP-1R, as illustrated in the cAMP signalling observed in the hamster InR1G9 cell line. In the next section the factors that influence cAMP signalling in these physiologically relevant cell lines will be investigated.

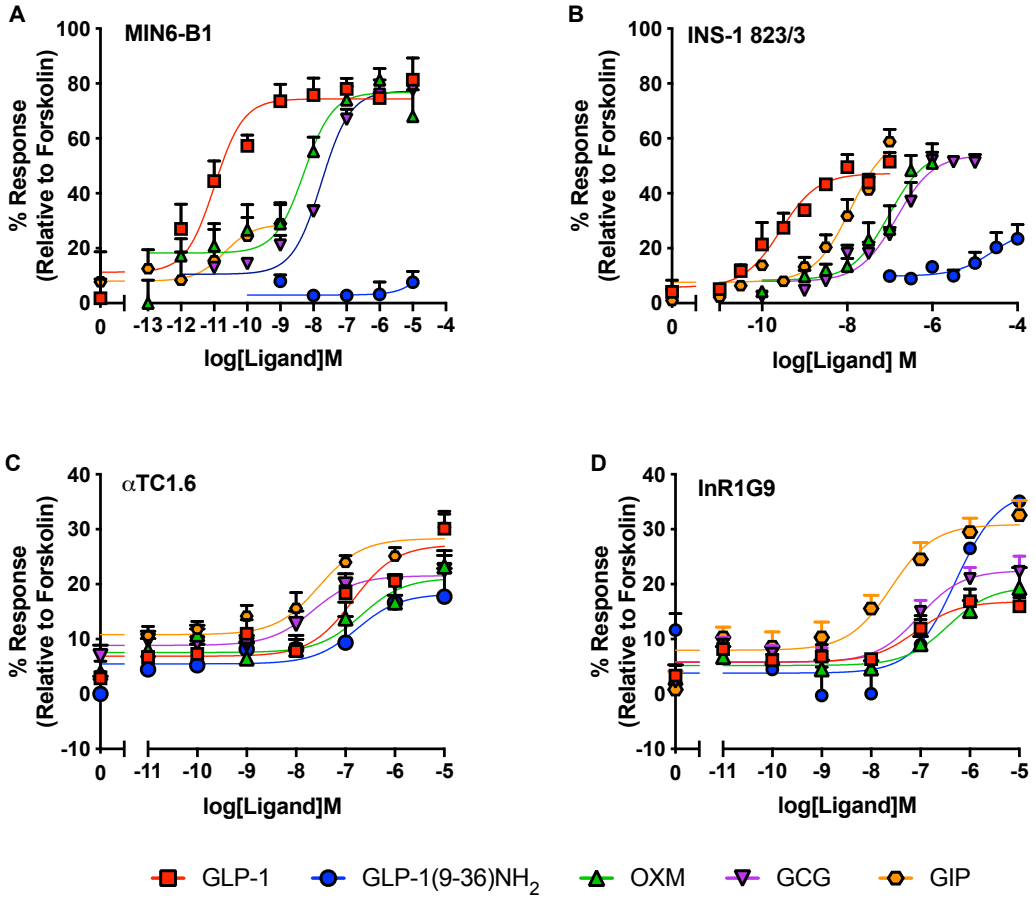

Figure 3.10: **Comparison of glucagon receptor family ligand responses in rodent cell lines endogenously expressing GLP-1R, GCGR and GIPR.** The above figure shows the cAMP production dose-response curves when β cell lines: (A) mouse MIN6-B1 and (B) rat INS-1 832/3 and α cell lines: (C) mouse αTC1.6 cultured in low glucose (5mM) and (D) hamster InR1G9 were stimulated with GLP-1, OXM, GCG, GIP and GLP-1(9-36)NH_2. 1000 MIN6-B1 and INS-1 832/3 cells/well and 4000 αTC1.6 and InR1G9 cells/well were stimulated with various ligands in the presence of PDE inhibitor IBMX. For measuring GLP-1(9-36)NH_2 ligand response, 2000 cells/well of MIN6-B1 and INS-1 832/3 cells were stimulated with the ligand for 60 mins. All data were normalised to the maximum cAMP production when stimulated with 100μM forskolin and were means of 1 to 7 independent experiments with duplicates $\pm$ S.E.M (upper error bars). Table 3.5 and 3.6 show the pEC_{50} and E_{max} values of ligand responses in α and β cell lines respectively.

Table 3.5: **cAMP accumulation potencies (pEC_{50}) and maximal responses (E_{max}) of GLP-1R, GIPR and GCGR endogenous ligands in MIN6-B1 and INS-1 832/3 cell lines.**

Cell line	Ligand	pEC_{50} [a]	E_{max} [b]	Span	n
MIN6-B1	GLP-1	10.99±0.19	74.38±2.77	63.19±6.99	4
	GLP-1(9-36)NH_2	6.31±1.81	8.18±4.58	5.317±5.56	2^{NB}
	OXM	8.27±0.23	76.76±2.54	58.48±3.09	4
	GCG	7.76±0.11	77.27±4.05	66.73±4.30	4
	GIP	10.70±0.77	28.74±6.95	20.70±7.44	2^{NB}
INS-1 832/3	GLP-1	9.57±0.17	47.24±2.58	41.56±3.67	4
	GLP-1(9-36)NH_2	4.60±0.49	27.27±6.47	17.42±6.14	2^{NB}
	OXM	7.02±0.19	55.92±5.13	47.53±5.11	4
	GCG	6.85±0.16	54.02±3.66	46.13±4.03	4
	GIP	7.92±0.16	61.29±6.57	53.66±6.44	4

Values were generated when the data were fitted to the three-parameter logistic equation. Means ± S.E.M of n individual result sets were shown.

[a] Negative logarithm of agonist concentration when reaching half maximal response.

[b] % of maximal response observed when stimulated with ligands relative to forskolin.

[NB] Preliminary results are shown here only due to COVID-19 obstruction of experimental schedule.

Table 3.6: **cAMP accumulation potencies (pEC_{50}) and maximal responses (E_{max}) of GLP-1R, GIPR and GCGR endogenous ligands in αTC1.6 and InR1G9 cell lines.**

Cell line	Ligand	pEC_{50} [a]	E_{max} [b]	Span	n
αTC1.6	GLP-1	6.85±0.22	27.18±1.56	20.30±1.81	12
	GLP-1(9-36)NH_2	5.77±0.66	18.23±3.47	12.74±3.67	6
	OXM	7.20±0.51	16.57±1.99	10.55±2.26	8
	GCG	7.66±0.34	21.55±1.46	12.69±1.80	14
	GIP	7.54±0.29	28.32±1.52	17.51±1.85	12
InR1G9	GLP-1	7.10±0.31^{ns}	16.82±0.31*	10.98±1.62^{ns}	12
	GLP-1(9-36)NH_2	6.30±0.29	37.03±0.29	33.22±4.97	2^{NB}
	OXM	6.45±0.33^{ns}	19.51±0.33^{ns}	14.32±2.23^{ns}	10
	GCG	7.03±0.24^{ns}	22.49±0.24^{ns}	16.72±1.82^{ns}	12
	GIP	7.59±0.24^{ns}	30.86±0.24^{ns}	22.88±2.27^{ns}	6

Values were generated when the data were fitted to the three-parameter logistic equation. Means ± S.E.M of n individual result sets were shown.
[a] Negative logarithm of agonist concentration when reaching half maximal response.
[b] % of maximal response observed when stimulated with ligands relative to forskolin.
[NB] Preliminary results are shown here only due to COVID-19 obstruction of experimental schedule.
Statistical significance compared between individual peptide ligand cAMP responses in αTC1.6 and InR1G9 cell lines were determined by Student's t-test with Welch's correction (ns, non-statistically significant).

Table 3.7: **Summary of the rank order of potency in the β cell lines, MIN6-B1 and INS-1 832/3 cell lines and the α cell lines, αTC1.6 and InR1G9 cell lines.**

Cell lineage	Cell line	Receptor expression order (From high to low)	RAMP expression order (From high to low)	Rank order of potency of ligands in terms of cAMP potentiation (from high to low)
β	MIN6-B1	GIPR > GLP-1R > GCGR	RAMP3 > RAMP2 > RAMP1	GLP-1 > GIP > OXM > GCG > GLP-1(9-36)NH_2
	INS-1 832/3	GLP-1R > GCGR > GIPR		
α	αTC1.6	GIPR > GCGR > GLP-1R		GCG > GIP > GLP-1 > OXM > GLP-1(9-36)NH_2
	InR1G9	-	-	GIP > GLP-1 > GCG > OXM > GLP-1(9-36)NH_2

3.4 Exploring the factors affecting cAMP signalling in pancreatic α cells

Following the evaluation of cAMP signalling responses mediated by glucagon-like peptide ligands in physiologically relevant rodent pancreatic clonal cell models, the factors that influence cAMP signalling were further explored. Four factors which were postulated to affect α cells signalling were investigated, which were 1) the interplay of GPR119 with GLP-1R and GCGR, 2) the cross-ligand-receptor sensitivity between GLP-1R and GCGR, 3) the influence of RAMPs at the GCGR and lastly 4) the glycaemic conditions in which the pancreatic models were cultured in. Validation assays were conducted alongside the pancreatic β cells model in order to highlight the contrasting difference between the α and β cells signalling when these factors were present. First the influence of GPR119 on GLP-1R and GCGR activation was considered.

3.4.1 Investigating the interplay of GLP-1R, GCGR and GPR119

The previous results showed that GPR119, which is a class A GPCR that has only been recently deorphansied [Overton et al., 2006], was highly expressed in the mouse αTC1.6 cells (Fig. 3.7). Given the recent evidence suggesting GPR119 played an important role in modulating insulin and glucagon secretion [Flock et al., 2011, Li et al., 2018], and that GPR119 agonists, namely the endocannabinoid-like lipids oleoylethanolamide (OEA) and 2-oleoylglycerol (2-OG), enhanced GLP-1 cAMP signalling in the mouse RINm5F β cell line [Cheng et al., 2015, Brown et al., 2018], it is of particular interest to see if the GPR119 agonists could also activate GLP-1R and GCGR, thereby contributing to the modulation of glucagon release. Furthermore, the extent of the close GLP-1 analogue, Ex-4, to act as a GCGR partial agonist, thereby contributing to the glucagonostatic action in the pancreatic α cells, was also evaluated.

Transient transfection was performed using of FuGENE HD transfection reagent to express human GPR119, GLP-1R and GCGR in the HEKΔCTR cells. 48-hour transfection was allowed prior to cAMP assays. Mock-transfected HEKΔCTR cells were also included to act as a negative control as the signalling at null-receptor background. In these series of experiments, both endogenous and synthetic small molecule agonists of GPR119, which were OEA [Overton et al., 2006] and AR231453 [Semple et al., 2008] respectively, were tested. HTRF-based cAMP accumulation assays were again performed in the presence of PDE inhibitor rolipram.

Here GLP-1, GCG and the two GPR119 agonists, OEA and AR231453, were able to activate their cognate receptors but not in mock-transfected HEKΔCTR cells, proving the successful transfections of GLP-1R, GCGR and GPR119 into the HEKΔCTR cells (Fig. 3.11 and Table 3.8). Notably, very high cAMP responses were induced by GLP-1 and its closely related full agonist, Ex-4, at the GLP-1R; their basal signals were massively increased despite the application of low agonist concentrations (i.e. below nanomolar range). It was due to the inclusion of a PDE inhibitor as well as the prolonged period of stimulation of 30 mins compared to 15 mins stimulation used in previous studies. However, the inclusion of a PDE inhibitor was required to enable a fair comparison of the signalling responses to other ligands. Similar to the cAMP responses in recombinant cell lines stably expressing GCGR, GCG was also able to act as a full agonist at the GCGR with a potent response (pEC_{50}: 9.06 $\pm$ 0.09). While OEA and AR231453 were able to activate GPR119, both agonists were less potent in here (pEC_{50} values were 5.64 $\pm$ 0.15 and 5.90 $\pm$ 0.31 respectively) compared to the published reports [Dale et al., 2015]. It may be attributed to the fact that HEKΔCTR cells which lack RAMPs expression [Bailey et al., 2019] were used in these series of experiments, as GPR119 has been shown to have a certain degree of interaction with RAMP2 (personal communication with Dr Matthew Harris), which may have contributed to the apparent difference in potencies in the GPR119 agonists.

Having determined the successful transfections of GLP-1R, GCGR and GPR119 in the HEKΔCTR cells, a range of GLP-1R, GCGR and GPR119 agonists, which were GLP-1, GLP-1(9-36)NH_2, GCG, Ex-4, AR231453 and OEA, were next applied onto the transiently transfected HEKΔCTR cells expressing different receptors. Again, GLP-1 and GCG partial agonisms were detected at the GCGR and GLP-1R respectively, as shown in Fig. 3.2 and 3.6. The GLP-1 metabolite, GLP-1(9-36)NH_2, was also able to act as a partial agonist at both GLP-1R and GCGR (pEC_{50} values were 6.01 $\pm$ 0.13 and 5.39 $\pm$ 0.16 at the GLP-1R and GCGR respectively) as shown previously in the CHO-K1 recombinant cell systems (Fig. 3.2). However, the efficacies of the GLP-1(9-36)NH_2 at both GLP-1R and GCGR were higher than that in CHO-K1 recombinant stable cell lines, presumably due to the human cell composition that the receptors were expressed in. Ex-4 did not activate the GCGR, as shown in the lack of difference between the potency and efficacy between the Ex-4 dose responses at the GCGR and the mock-transfected HEKΔCTR cells, illustrating Ex-4 was not an agonist at the GCGR. Importantly, here GPR119 agonists, when applied at the GLP-1R or GCGR, did not lead to receptor activation and vice versa, glucagon-like peptide agonists did not activate GPR119,

implying there was no cross-receptor sensitivity among GPR119, GLP-1R and GCGR ligands, despite the high expression of GPR119 at the α cells.

Having illustrated that GPR119 did not play a significant role in modulating cAMP signalling pathways at the GLP-1R and GCGR as widely postulated, the individual GLP-1R and GCGR contribution towards cAMP signalling in rodent pancreatic α and β cell models were to be deciphered.

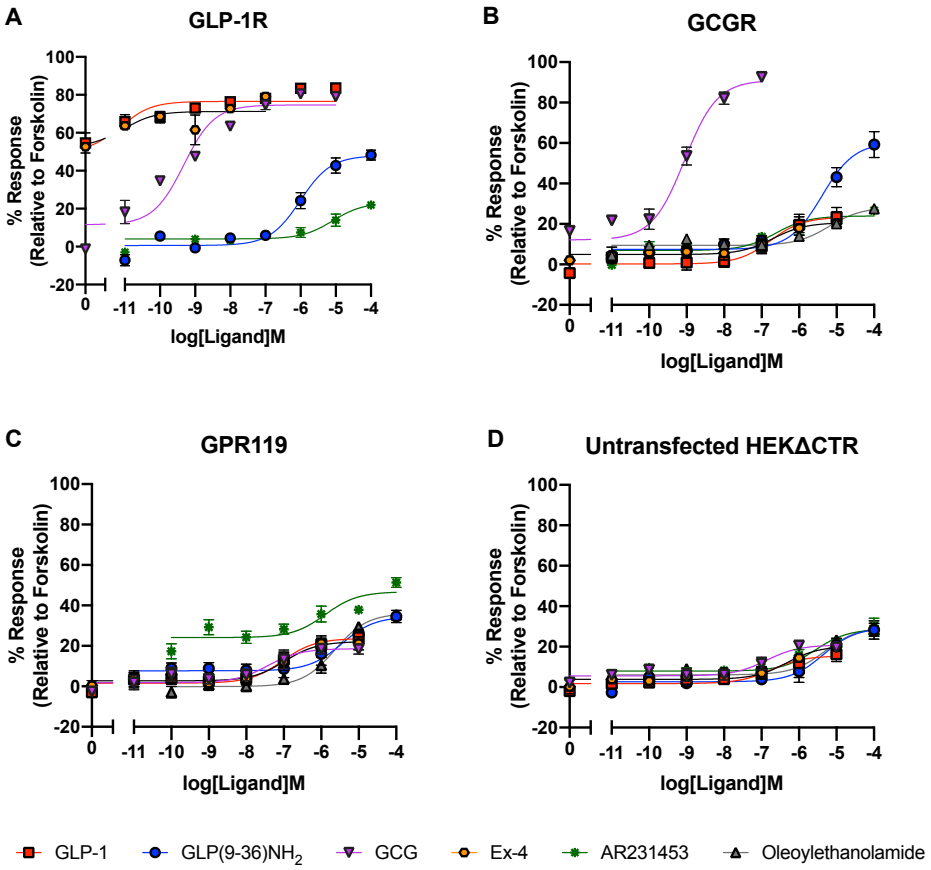

Figure 3.11: **GPR119, GLP-1R and GCGR are activated upon application of their cognate ligands only.** The above graphs demonstrate that (A) GLP-1R and (B) GCGR are not activated by the GPR119 agonists. The elevation of basal responses of both GLP-1 and Ex-4 were due to the inclusion of PDE inhibitor, IBMX, in the assay and that prolonged period of incubation were adopted. Similarly, the application of glucagon-like peptides do not result in cAMP responses on (C) GPR119. (D) Untransfected HEKΔCTR cells were used as a negative control for the null receptor background. 2000 cells/well of HEKΔCTR transiently transfected with GLP-1R, GCGR, GPR119 as well as pcDNA3.1 were used in the cAMP assays in the presence of rolipram. The cells were stimulated with ligands for 30 mins. Table 3.8 shows the pEC_{50} and E_{max} values of individual ligand responses. All data were normalised to the maximum cAMP production when stimulated with 100μM forskolin and were mean of at least 3 independent experiments with duplicates $\pm$ S.E.M (upper and lower error bars).

Table 3.8: **cAMP accumulation potencies (pEC_{50}) and maximal responses (E_{max}) of glucagon-like peptide ligands and GRP119 agonists at GLP-1R, GCGR and GPR119.**

Receptor	Ligand	pEC_{50} [a]	E_{max} [b]	Span	n
GLP-1R	**GLP-1**	11.13±0.25*	76.54±1.50****	27.62±3.80	8
	GLP-1(9-36)NH_2	6.01±0.13^{ns}	48.00±2.62*	47.40±2.90	8
	GCG	9.32±10.16***	74.68±2.52****	63.20±4.01	8
	Ex-4	11.05±0.68****	71.21±2.61****	19.15±6.00	8
	AR231453	5.09±0.28^{ns}	23.22±3.03^{ns}	19.16±3.10	8
	Oleoylethanolamide	-	-	-	-
GCGR	**GLP-1**	6.76±0.30^{ns}	23.38±3.43^{ns}	23.14±3.60	8
	GLP-1(9-36)NH_2	5.39±0.16^{ns}	60.32±4.09**	52.91±4.23	8
	GCG	9.06±0.09****	91.04±3.00****	79.00±3.38	8
	Ex-4	6.70±0.37^{ns}	20.66±2.49^{ns}	15.76±2.69	8
	AR231453	6.63±0.29^{ns}	23.97±1.73^{ns}	17.06±2.06	8
	Oleoylethanolamide	5.20±0.25^{ns}	28.21±2.67^{ns}	18.80±2.72	6
GPR119	**GLP-1**	7.03±0.27^{ns}	23.70±2.54^{ns}	22.12±2.85	8
	GLP-1(9-36)NH_2	5.45±0.30^{ns}	34.52±3.62^{ns}	26.82±3.77	8
	GCG	7.43±0.35^{ns}	18.61±1.98^{ns}	16.79±2.39	8
	Ex-4	6.98±0.31^{ns}	22.15±2.55^{ns}	19.42±2.87	8
	AR231453	5.90±0.31^{ns}	46.79±2.98**	22.67±3.38	8
	Oleoylethanolamide	5.64±0.15^{ns}	36.15±2.29^{ns}	36.27±2.47	6
Mock transfection	**GLP-1**	6.74±0.39	15.44±2.31^{ns}	13.68±2.49	8
	GLP-1(9-36)NH_2	5.35±0.22	29.42±2.79	26.76±2.88	8
	GCG	6.87±0.31	20.84±2.04	15.26±2.24	8
	Ex-4	6.32±0.30	20.33±2.48	16.50±2.55	8
	AR231453	5.57±0.31	28.70±2.85	20.75±2.99	8
	Oleoylethanolamide	5.30±0.36	29.68±3.66	23.60±3.77	6

Values were generated when the data were fitted to the three-parameter logistic equation. Means ± S.E.M of n individual result sets were shown.

[a] Negative logarithm of agonist concentration when reaching half maximal response.

[b] % of maximal response observed when stimulated with ligands relative to forskolin.

Statistical significance compared between individual peptide ligand cAMP responses in HEKΔCTR transiently transfected with GLP-1R, GCGR, GPR119 or pcDNA3.1 were determined by one-way ANOVA with post-hoc Dunnett's multiple comparisons (*, p<0.05; **, p<0.01; ***, p<0.001;****, p<0.0001, ns, non-statistically significant).

3.4.2 Characterising the effect of GLP-1R and GCGR antagonism on the signalling properties of GLP-1 and GCG

3.4.2.1 Applying GLP-1R and GCGR antagonists in recombinant cell lines stably expressing GLP-1R or GCGR

Having excluded the influence of GPR119 on the modulation of GLP-1R and GCGR effect towards glucagon secretion, the individual GLP-1R and GCGR contributions towards cAMP activation in the pancreatic α cells were to be dissected. To achieve this goal, GLP-1R specific peptide antagonist, Ex-9 [Raufman et al., 1992] and GCGR specific small molecule antagonist, L-168,049 [Cascieri et al., 1999] were utilised. Cells were first pre-treated with the antagonist under investigation 30 mins prior to agonist stimulation for 15 mins. The antagonist was not washed out and remained in the assay for the entire duration of the cAMP measurements.The PDE inhibitor, namely rolipram, was included in the cAMP assays to prevent the breakdown of cAMP produced. Before applying the antagonists into rodent pancreatic clonal cell lines, pharmacological characterisation of the GLP-1R and GCGR specific antagonists in CHO-GLP-1R and HEKΔCTR-GCGR recombinant cell lines were first performed and reported as follows.

As expected, Ex-9 exhibited potent antagonism on the GLP-1-mediated cAMP responses at the GLP-1R in a dose-dependent manner in CHO-GLP-1R cells (Fig. 3.12 and Table 3.9) (pEC_{50} value of GLP-1-mediated cAMP responses decreased from 9.46 $\pm$ 0.05 to 7.22 $\pm$ 0.05, 7.46 $\pm$ 0.11 and 7.87 $\pm$ 0.12 when 1x10^{-5}M, 1x10^{-6}M, and 1x10^{-7}M of Ex-9 were applied respectively, all $p < 0.0001$). Furthermore, Ex-9 also behaved as a competitive antagonist, as the efficacies of GLP-1 did not change in the presence of various concentrations of Ex-9, which conceded with the observation by Raufman and colleagues, who first reported on the discovery of Ex-9 as a GLP-1R antagonist [Raufman et al., 1992]. Also, stimulating the cells with Ex-9 alone did not result in any cAMP response at the GLP-1R, further illustrating its role as an antagonist.

Likewise, L-168,049 was able to reduce the potencies of the cAMP responses mediated by both cognate GCGR full agonists, GCG and OXM, in a dose-dependent manner at the HEKΔCTR-GCGR cells (the pEC_{50} values of GCG decreased from 8.96 $\pm$ 0.06 to 7.99 $\pm$ 0.06 and 8.31 $\pm$ 0.09 when 1x10^{-6}M and 1x10^{-7}M of L-168,049 were applied respectively, $p < 0.0001$ while the pEC_{50} values of OXM decreased from 7.26 $\pm$ 0.04 to 6.50 $\pm$ 0.08 and 6.58 $\pm$ 0.07 when 1x10^{-6}M and 1x10^{-7}M of L-168,049 were applied respectively, $p < 0.001$) (Fig. 3.13 and Table 3.10).

As previously established in Fig. 3.2 that GLP-1 and GLP-1(9-36)NH_2 act as GCGR

partial agonists, the extent of partial agonism of these two peptide agonists in the presence of GCGR antagonists were next measured, therefore further providing evidence for the binding of these two ligands at the GCGR. Here when L-168,049 was applied together with either GLP-1 or GLP-1(9-36)NH_2, there were reductions in efficacies of the cAMP responses mediated by GLP-1 (E_{max} of GLP-1 decreased from 56.46 $\pm$ 7.08 to 28.05 $\pm$ 2.42 when 1x10^{-6}M L-168,049 was applied, $p < 0.01$) (Fig. 3.13 and Table 3.10). More strikingly, the potency of GLP-1(9-36)NH_2-mediated cAMP response decreased from 5.36 $\pm$ 0.09 to 4.41 $\pm$ 0.16 ($p < 0.05$), further implying GLP-1(9-36)NH_2 was able to activate the GCGR by binding to the receptor and that the application of the GCGR antagonist competed with its binding site, thereby lowering the potency of GLP-1(9-36)NH_2. Furthermore, consistent with the results in Section 3.4.1, Ex-4, even though it is a close analogue of GLP-1, could not activate GCGR, and therefore, the application of L-168,049 did not influence Ex-4 action at the GCGR. Having characterised the extent of antagonism using GLP-1R and GCGR specific antagonists, the evaluation of GLP-1R and GCGR individual contributions towards cAMP signalling at the physiological rodent clonal cell models were performed next.

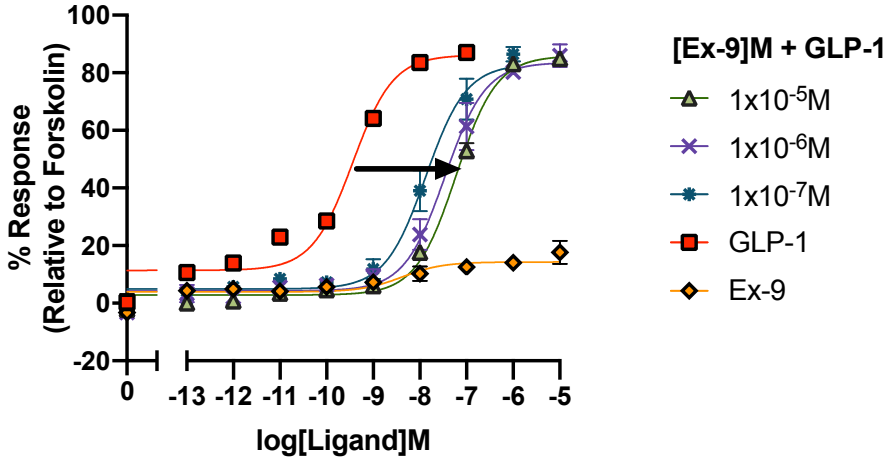

Figure 3.12: **Effect of GLP-1R peptide antagonist Ex-9 on cAMP accumulation responses mediated by GLP-1.** Ex-9 was pre-incubated with CHO-GLP-1R cells 30 mins before stimulated with GLP-1. Ex-9 was able to dose-dependently antagonise the cAMP responses mediated by GLP-1. 1000 cells/well were stimulated with ligands for 15 mins in the presence of rolipram before cAMP accumulation measurement. All data were normalised to the maximum cAMP production when stimulated with 100μM forskolin and were at least 2 independent experiments in duplicates with mean $\pm$ S.E.M (upper and lower error bars). Table 3.9 shows the pEC_{50} and E_{max} values of individual ligand responses.

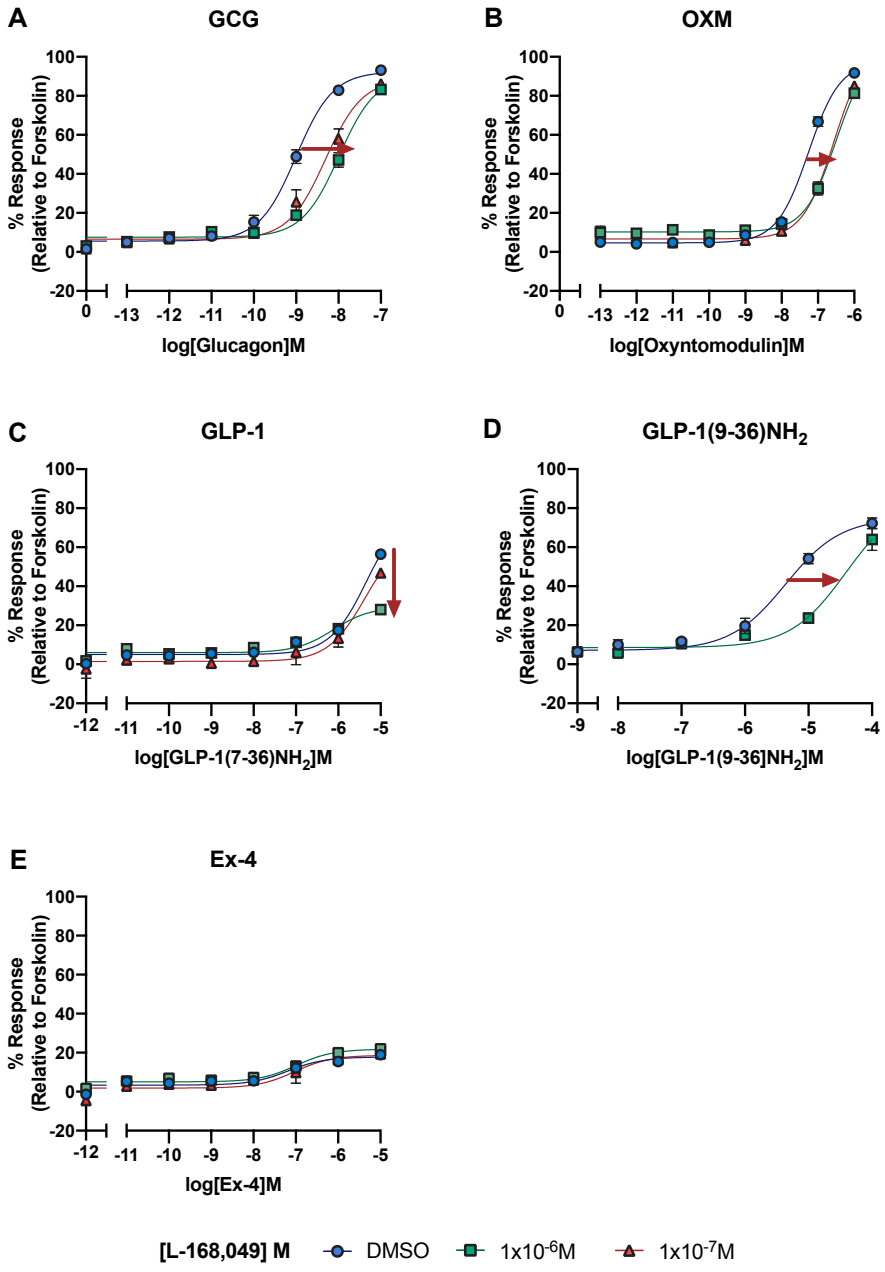

Figure 3.13: **Effect of GCGR small molecule antagonist L-168,049 in cAMP accumulation responses of GCG, OXM, GLP-1, GLP-1(9-36)NH_2 and Ex-4 at GCGR.** L-168,049 was pre-incubated with HEKΔCTR stably expressing GCGR cells 30 mins before stimulated with various glucagon-like peptide ligands. L-168,049 was able to antagonise the cAMP responses mediated by the known GCGR agonists GCG and OXM. The efficacies of GLP-1 and GLP-1(9-36)NH_2 were reduced respectively in the presence of the GCGR antagonist. Ex-4 was not able to mediate cAMP response at GCGR, indicating it is not an agonist of the receptor. 1000 cells per well were stimulated with ligands for 15 mins in the presence of rolipram before cAMP accumulation measurement. All data were normalised to the maximum cAMP production when stimulated with 100μM forskolin and were at least 3 to 7 independent experiments in duplicates with mean $\pm$ S.E.M (upper and lower error bars). Table 3.10 shows the pEC_{50} and E_{max} values of individual ligand responses.

Table 3.9: **cAMP accumulation potencies (pEC_{50}) and maximal responses (E_{max}) of GLP-1 cAMP responses in the presence of GLP-1R peptide antagonist Ex-9.**

Ligand	+ [Ex-9] (M)	pEC_{50} [a]	E_{max} [b]	Span	n
GLP-1	-	9.46±0.05	93.14±1.95	92.09±2.18	10
	$1x10^{-5}$	7.22±0.05	85.89±2.12	88.06±2.22	4
	$1x10^{-6}$	7.46±0.11	85.58±3.88	85.28±4.09	4
	$1x10^{-7}$	7.87±0.12	84.00±4.22	84.07±4.43	4
Ex-9	-	8.38±0.40	14.31±1.60	10.38±1.80	4

Values were generated when the data were fitted to the three-parameter logistic equation. Means ± S.E.M of n individual result sets were shown.

[a] Negative logarithm of agonist concentration when reaching half maximal response.

[b] % of maximal response observed when stimulated with ligands relative to forskolin.

Table 3.10: **cAMP accumulation potencies (pEC_{50}) and maximal responses (E_{max}) of various glucagon-like peptide cAMP responses in the presence of GCGR small molecule antagonist L-168,049.**

Ligand	+ [L-168,049] (M)	pEC_{50} [a]	E_{max} [b]	Span	n
GCG	-	8.96±0.06	92.40±1.89	86.83±2.10	14
	$1x10^{-6}$	7.99±0.06****	90.59±2.84	83.01±2.89	10
	$1x10^{-7}$	8.31±0.09****	88.46±3.81	81.93±3.93	10
OXM	-	7.26±0.04	97.41±1.93	92.75±1.98	6
	$1x10^{-6}$	6.50±0.08***	103.67±5.43	93.40±5.32	6
	$1x10^{-7}$	6.58±0.07***	106.68±5.07	100.00±4.98	6
GLP-1	-	5.32±0.11	56.46±7.08	75.72±6.93	10
	$1x10^{-6}$	6.12±0.19***	28.05±2.42**	23.34±2.48	10
	$1x10^{-7}$	5.37±0.24	46.85±12.15^{ns}	64.46±11.89	10
$GLP\text{-}1(9\text{-}36)NH_2$	-	5.36±0.09	74.93±3.08	33.00±1.82	10
	$1x10^{-6}$	4.41±0.16*	85.22±9.70^{ns}	20.76±3.07	6
Ex-4	-	7.19±0.22	17.76±1.17	14.38±1.33	10
	$1x10^{-6}$	6.99±0.19^{ns}	21.78±1.35	16.75±1.50	10
	$1x10^{-7}$	7.03±0.33^{ns}	18.64±2.29	16.78±2.56	10

Values were generated when the data were fitted to the three-parameter logistic equation. Means ± S.E.M of n individual result sets were shown.

[a] Negative logarithm of agonist concentration when reaching half maximal response.

[b] % of maximal response observed when stimulated with ligands relative to forskolin.

Statistical significance compared between individual peptide ligand cAMP accumulation responses in the presence of various concentrations of L-168,049 were determined by one-way ANOVA with post-hoc Dunnett's multiple comparisons (*,p<0.05; **, p<0.01; ***, p<0.001; ****, p<0.0001, ns, non-statistically significant)

3.4.2.2 Applying GLP-1R and GCGR antagonists in rat insulinoma cell line and hamster glucagonoma cell line

After the evaluation of the GCGR and GLP-1R antagonists in recombinant cell systems, Ex-9 and L-168,049 were next applied in the rat INS-1 832/3 cell line, in an attempt to decipher the individual cAMP agonism of GLP-1 and GCG at the GLP-1R and GCGR, which were expressed endogenously in the rat β cell line. Again, the same HTRF-based cAMP assays were used as performed in previous sections, with the INS-1 832/3 cells pre-treated with antagonists for 30 minutes before stimulating with agonists for 30 mins. A pan-PDE inhibitor, IBMX, was included to prevent the breakdown of cAMP produced.

Similar to the results in the recombinant cell systems, Ex-9 and L-168,049 did not have any antagonistic effect when applied on their own in the rat insulinoma cells. The results here concurred with the observations by Chepurny and colleagues that Ex-9 did not behave as an inverse agonist at the rat GLP-1R [Chepurny et al., 2019]. Expectedly, by stimulating INS-1 832/3 cells with Ex-9 together with GLP-1, Ex-9 blocked the agonism of GLP-1 at the GLP-1R, with its potency decreased from 8.68 $\pm$ 0.12 to 8.15 $\pm$ 0.29 in the presence of 1x10^{-7}M Ex-9, while the efficacy decreased from 48.62 $\pm$ 3.29 to 37.09 $\pm$ 5.22 (Fig. 3.14A and Table 3.11). Yet, GLP-1 agonism was not completely blocked by Ex-9, presumably due to the relatively low concentration of antagonist used in the assay. On the contrary to the apparent antagonism exhibited by Ex-9, incubating the insulinoma cells with L-168,049 did not affect GLP-1 signalling, which implied that GLP-1 mediates its cAMP response primarily through GLP-1R. The results here also corroborated with the findings by Chepurny and colleagues where they observed there was a lack of antagonism mediated by the GCGR specific peptide antagonist, des-His^{1}-Glu^{9}-Glucagon on GLP-1 signalling at the INS-1 832/3 cell line with the use of a real time FRET-based kinetic assays to measure cAMP production across time [Chepurny et al., 2019].

Interestingly, both Ex-9 and L-168,049 were able to antagonise GCG agonism at the rat insulinoma cell line (pEC_{50} value of GCG decreased from 7.32 $\pm$ 0.26 to 6.67 $\pm$ 0.33 in the presence of Ex-9 and to 7.12 $\pm$ 0.51 in the presence of L-168,049) (Fig. 3.14). However both antagonists when applied alone could not block the GCG-mediated cAMP responses completely, presumably due to the dual agonistic properties of GCG, of which compensatory cAMP activation can be mediated via the activation of either GLP-1R or GCGR that was not blocked by the antagonist, as well as the relatively low

concentration of antagonists applied to the cells. The results here also agreed with the observations by Chepurney and colleagues, which they also showed the residual action of GCG in the INS-1 832/3 cells when GCGR was blocked by des-His^{1}-Glu^{9}-Glucagon. They also showed further evidence that GCG agonism was completely eliminated when both des-His^{1}-Glu^{9}-Glucagon and Ex-9 were applied together in the presence of GCG [Chepurny et al., 2019].

Having evaluated the extent of GLP-1 and GCG agonism at the insulinoma cell line, GLP-1R and GCGR antagonists were then applied to the mouse and hamster glucagonoma cells in order to identify any potential difference in GLP-1R and GCGR signalling. Given that the signalling responses at the α cell lines were much weaker than that in the β cell line, it was proven to be technically challenging to characterise GLP-1 and GCG-mediated cAMP responses in the presence of antagonists (Fig. 3.14 and Table 3.11). Further optimisation in measuring cAMP responses upon co-stimulation with antagonists are therefore needed.

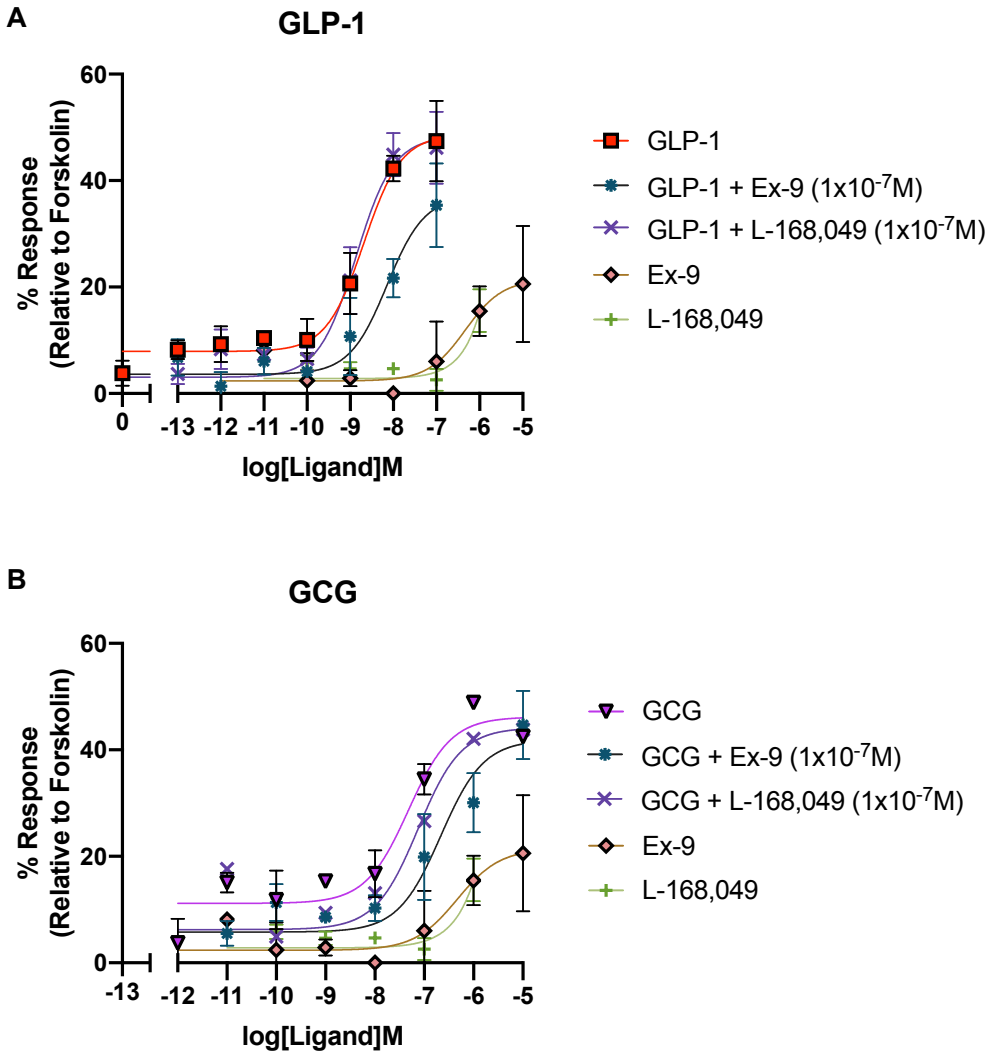

Figure 3.14: **Effect of GCGR small molecule antagonist L-168,049 and GLP-1R peptide antagonist Ex-9 on cAMP accumulation responses of GLP-1 and GCG in INS-1 832/3 cells.** L-168,049 and Ex-9 were pre-incubated respectively with INS-1 832/3 cells 30 mins before stimulating with GLP-1 and GCG. 1000 cells/well were stimulated with ligands for 30 mins in the presence of IBMX before cAMP accumulation measurement. All data were normalised to the maximum cAMP production when stimulated with 100μM forskolin and were means of one independent experiment in duplicates with $\pm$ S.E.M (upper and lower error bars).

Table 3.11: **cAMP accumulation potencies (pEC_{50}) and maximal responses (E_{max}) of GLP-1 and GCG in the presence of GLP-1R peptide antagonist Ex-9 and GCGR small molecule antagonist L-168,049 in INS-1 832/3 cell line.**

Ligand	+ Inhibitor (M)	pEC_{50} [a]	E_{max} [b]	Span	n
GLP-1	-	8.68±0.12	48.62±3.29	40.72±3.52	2^{NB}
	Ex-9 ($1x10^{-7}$M)	8.15±0.29	37.09±5.22	33.48±5.34	2^{NB}
	L-168,049 ($1x10^{-7}$M)	8.87±0.21	48.21±4.07	45.16±4.47	2^{NB}
GCG	-	7.32±0.26	46.19±4.33	35.02±4.59	2^{NB}
	Ex-9 ($1x10^{-7}$M)	6.67±0.33	41.88±5.26	36.10±5.61	2^{NB}
	L-168,049 ($1x10^{-7}$M)	7.12±0.51	44.18±7.89	37.93±8.70	2^{NB}
Ex-9	-	6.33±0.58	21.43±5.41	19.08±5.57	2^{NB}
L-168,049		3.37±1.34	18.67±2.42	18.32±2.48	2^{NB}

Values were generated when the data were fitted to the three-parameter logistic equation. Means ± S.E.M of n individual result sets were shown.
[a] Negative logarithm of agonist concentration when reaching half maximal response.
[b] % of maximal response observed when stimulated with ligands relative to forskolin.
[NB] Preliminary results are shown here only due to COVID-19 obstruction of experimental schedule.

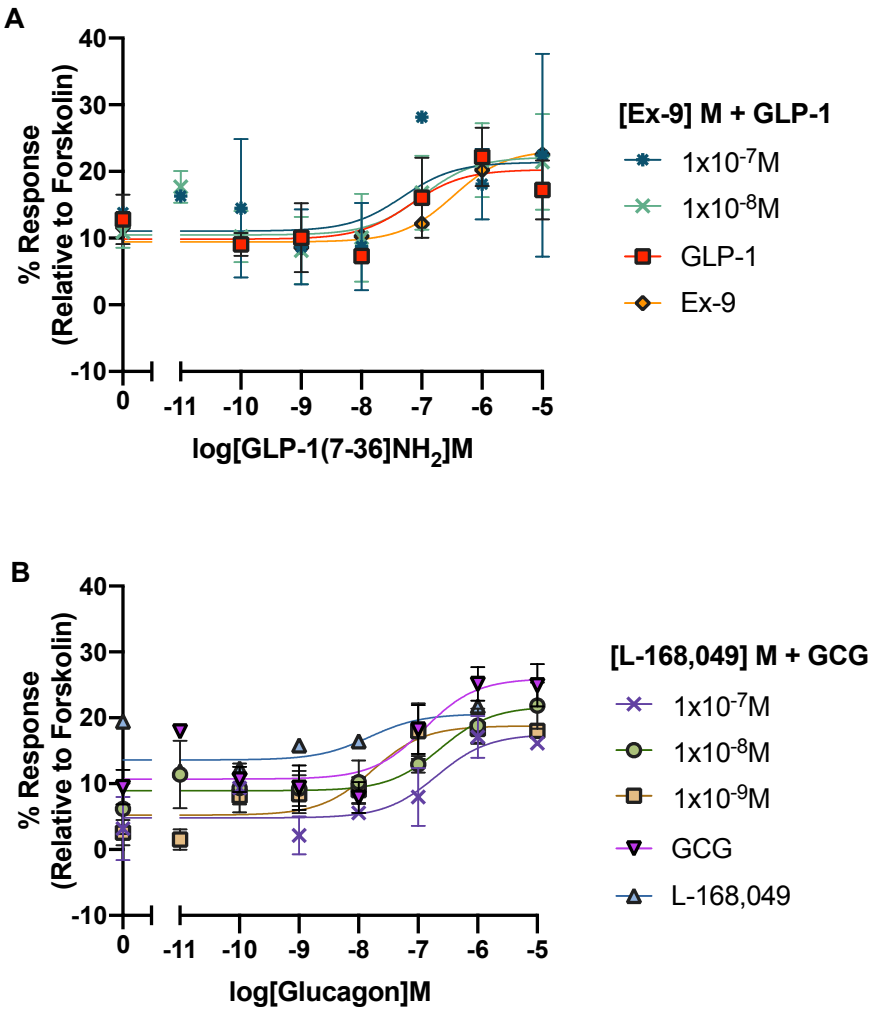

Figure 3.15: **Effect of GCGR small molecule antagonist L-168,049 and GLP-1R peptide antagonist Ex-9 in cAMP accumulation responses of GLP-1 and GCG in InR1G9 cells.** L-168,049 and Ex-9 were pre-incubated with InR1G9 cells 30 mins before stimulated with GLP-1 and GCG. 4000 cells per well were stimulated with ligands for 15 mins in the presence of IBMX before cAMP accumulation measurement. All data were normalised to the maximum cAMP production when stimulated with 100μM forskolin and were at least 2 independent experiments in duplicates with mean $\pm$ S.E.M (upper and lower error bars).

Table 3.12: **cAMP accumulation potencies (pEC_{50}) and maximal responses (E_{max}) of GLP-1 and GCG in the presence of GLP-1R peptide antagonist Ex-9 and GCGR small molecule antagonist L-168,049 in InR1G9 cell line.**

Ligand	Ex-9 or L-168,049 (M)	pEC_{50} [a]	E_{max} [b]	Span	n
GLP-1	-	7.18±0.86	20.23±3.53	10.43±4.24	4
	$1x10^{-7}$	7.32±2.08	21.37±5.92	10.31±7.35	4
	$1x10^{-8}$	6.70±0.95	22.15±4.15	11.68±4.74	4
Ex-9	-	6.48±1.03	23.19±6.13	13.77±6.67	4
GCG	-	6.90±0.38	25.98±2.48	15.27±2.74	6
	$1x10^{-7}$	6.69±0.51	17.53±2.80	12.73±3.06	4
	$1x10^{-8}$	6.63±0.56	21.73±3.19	12.80±3.33	4
	$1x10^{-9}$	7.77±0.37	18.78±1.85	13.56±2.21	4
L-168,049	-	7.81±1.34	20.60±5.22	6.99±5.49	4

Values were generated when the data were fitted to the three-parameter logistic equation. Means ± S.E.M of n individual result sets were shown.

[a] Negative logarithm of agonist concentration when reaching half maximal response.

[b] % of maximal response observed when stimulated with ligands relative to forskolin.

3.4.3 Characterising the effect of RAMP2 on the cAMP production of a range of glucagon-like peptide agonists

RAMPs have been shown to modulate various Class B GPCRs, but with a lesser degree with GLP-1R [McLatchie et al., 1998, Christopoulos et al., 2003, Wootten et al., 2013a, Hay et al., 2016]. In particular, RAMP2 has been shown to interact with the GCGR, enhancing the efficacies and altering the potencies of its agonists [Weston et al., 2015, Cegla et al., 2017]. Therefore, the role of RAMP2 on influencing GCGR endogenous agonist responses were examined in the HEKΔCTR cells, which lack the RAMPs expression [Bailey et al., 2019]. Equal ratio (1:1) of RAMP2 and GCGR constructs were co-transfected into the HEKΔCTR cells using FuGENE HD transfection reagent and 48-hour transfection were allowed prior to assays. Mock transfections were performed by substituting RAMP2 with the vector pcDNA3.1.

The forskolin-mediated cAMP accumulation was not affected by the expressions of RAMP2 in the cell systems, as shown in the identical forskolin-mediated cAMP response curves with or without the expression of RAMP2 (Fig. 3.16A). Also, there were no apparent alterations on the agonist responses of GLP-1, GCG, OXM and Ex-4 at the GCGR (Fig. 3.16B, C, E and F). The results here contrasted with that observed by Weston and colleagues, but it could be explained by the difference in the cell line employed in studying the RAMP2 effect, as HEK293T cell line was used in their study [Weston et al., 2015], and there was an endogenous expression level of RAMP2 in the HEK293T cell line as shown previously (Fig. 3.3). The results here also disagreed with the observations by Cegla and colleagues, which they have used CHO-K1 cell line to investigate the effect of RAMP2 on GCGR signalling and demonstrated a decrease in peptide cAMP responses in the presence of RAMP2 [Cegla et al., 2017]. The difference in results could be explained by the various methods used in measuring cAMP accumulation. The difference in terms of G proteins or RAMPs expression in CHO-K1 and HEKΔCTR recombinant cell systems may also explain such discrepancy. Intriguingly, an increase in the potency of GLP-1(9-36)NH_2-mediated cAMP responses was observed (Fig. 3.16), with its pEC_{50} value increased from 7.47 ± 0.41 to 9.12 ± 0.37 in the presence of RAMP2. Given RAMP2 was expressed in the pancreatic α and β cell models as shown in Fig. 3.7 and 3.8, it is likely that the expression of RAMP2 may enhance the cAMP signalling response of the highly abundant GLP-1 metabolite, thereby contributing to a great extent in the regulation of insulin and glucagon secretion.

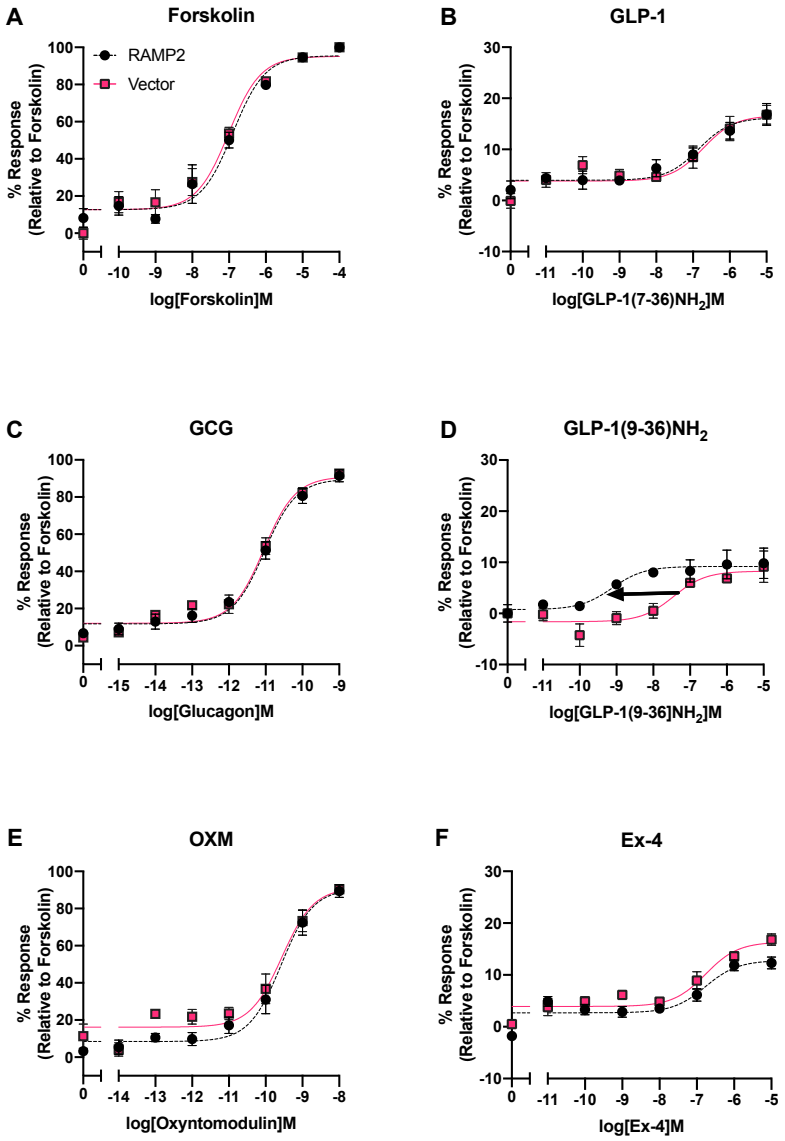

Figure 3.16: **Effect of RAMP2 on GCGR agonists cAMP signalling in HEKΔCTR transiently transfected with GCGR and RAMP2 or vector.** HEKΔCTR cells were transfected with GCGR and either RAMP2 or vector (pcDNA3.1) at 1:1 ratio with FuGENE HD transfection reagent for 48 hours on 24-well plate before the cAMP assays. 1000 transfected cells/well were stimulated with different ligands for 30 mins in the presence of rolipram, except for the measurement of cAMP response mediated by GLP-1(9-36)NH_2 of which 60 mins stimulation was allowed. All data were normalised to the maximum cAMP production when stimulated with 100μM forskolin and were means of 2 to 5 independent experiment in duplicates with $\pm$ S.E.M (upper and lower error bars).

Table 3.13: **cAMP accumulation potencies (pEC_{50}) and maximal responses (E_{max}) of various peptide agonists with or without the presence of RAMP2 at the GCGR.**

	Vector		RAMP2		
Ligand	**pEC_{50} [a]**	**E_{max} [b]**	**pEC_{50} [a]**	**E_{max} [b]**	**n**
Forskolin	7.00±0.12	95.49±2.95	6.89±0.11^{ns}	95.16±3.31^{ns}	6
GLP-1	6.84±0.26	16.63±1.64	6.72±0.30^{ns}	16.22±1.30^{ns}	10
GCG	11.05±0.09	91.04±3.00	11.03±0.09^{ns}	89.73±2.90^{ns}	8
GLP-1(9-36)NH_2	7.47±0.41	8.27±1.28	9.12±0.37	9.20±0.89	3
OXM	9.56±0.16	91.25±5.47	9.58±0.12^{ns}	90.69±4.53^{ns}	8
Ex-4	6.77±0.19	16.37±1.00	6.77±0.22^{ns}	12.80±0.96^{ns}	4

Values were generated when the data were fitted to the three-parameter logistic equation. Means ± S.E.M of n individual result sets were shown.

[a] Negative logarithm of agonist concentration when reaching half maximal response.

[b] % of maximal response observed when stimulated with ligands relative to forskolin.

Statistical significance compared between individual peptide ligand cAMP accumulation responses with or without the presence of RAMP2 were determined by Student's t-test with Welch's correction (ns, non-statistically significant).

3.4.4 GLP-1R, GCGR, GIPR and RAMPs expressions in rodent insulinoma and glucagonoma cell systems under high and low glucose conditions

After evaluating RAMPs influence on the glucagon-like peptide signalling, the influence of glucose culture conditions on the cAMP signalling pathways was explored since there has been reports showing glucagon receptor family expressions change with the glucose concentrations present in the culture conditions [Xu et al., 2007, Nakashima et al., 2018]. Furthermore, given the mouse αTC1.6 cell line was cultured in high glucose condition instead of the low glucose condition recommended by the ATCC, the effect of long-term glucose culture condition on the endogenous expressions of receptors from glucagon receptor family and RAMPs was evaluated.

In order to simulate low and high glucose culture conditions, the cells were incubated in different glucose conditions (5mM and 25mM glucose concentrations for the α cells and 2.8mM, 11mM and 16.7mM glucose concentrations for the β cells) for 72 hours in order to induce long term DNA expressions changes. Similar experimental approach was also adopted by Chuang and colleagues, which they investigated the effect of glucose conditions on the changes of gherlin receptor [Chuang et al., 2011]. Following 72 hours glucose incubation, RNA was extracted and RT-PCR studies were performed.

Here a downregulation of GIPR expression was observed when the α cells were cultured at 25mM glucose conditions (GIPR expression increased by 3.12-fold in 25mM glucose compared to that in 5mM glucose, $p < 0.01$) whereas there was no statistically significant changes in terms of the GLP-1R, GCGR and RAMPs expressions between the high and low glucose conditions (Fig. 3.17A). As for the INS-1 832/3 cells, no statistically significant changes in receptors and RAMPs expressions were observed among the hypo-, norm or hyperglycaemia conditions (Fig. 3.17B).

Interestingly, the results obtained here differed from what was observed in Xu and colleagues, which they noted a significant downregulation of GLP-1R and a slight degree of upregulation of GIPR when mouse islets were cultured in hyperglycaemic solutions (5-30mmol/L) for two days or in diabetic strain (db/db) mice [Xu et al., 2007]. Given that there is a mixture of different pancreatic cells in the mouse islets, crosstalk among different pancreatic cells might exist during the prolonged period of exposure to high glucose, while the strength of the experiments performed here clearly showed that the GIPR at the mouse α cells were particularly susceptible to changes in glucose conditions.

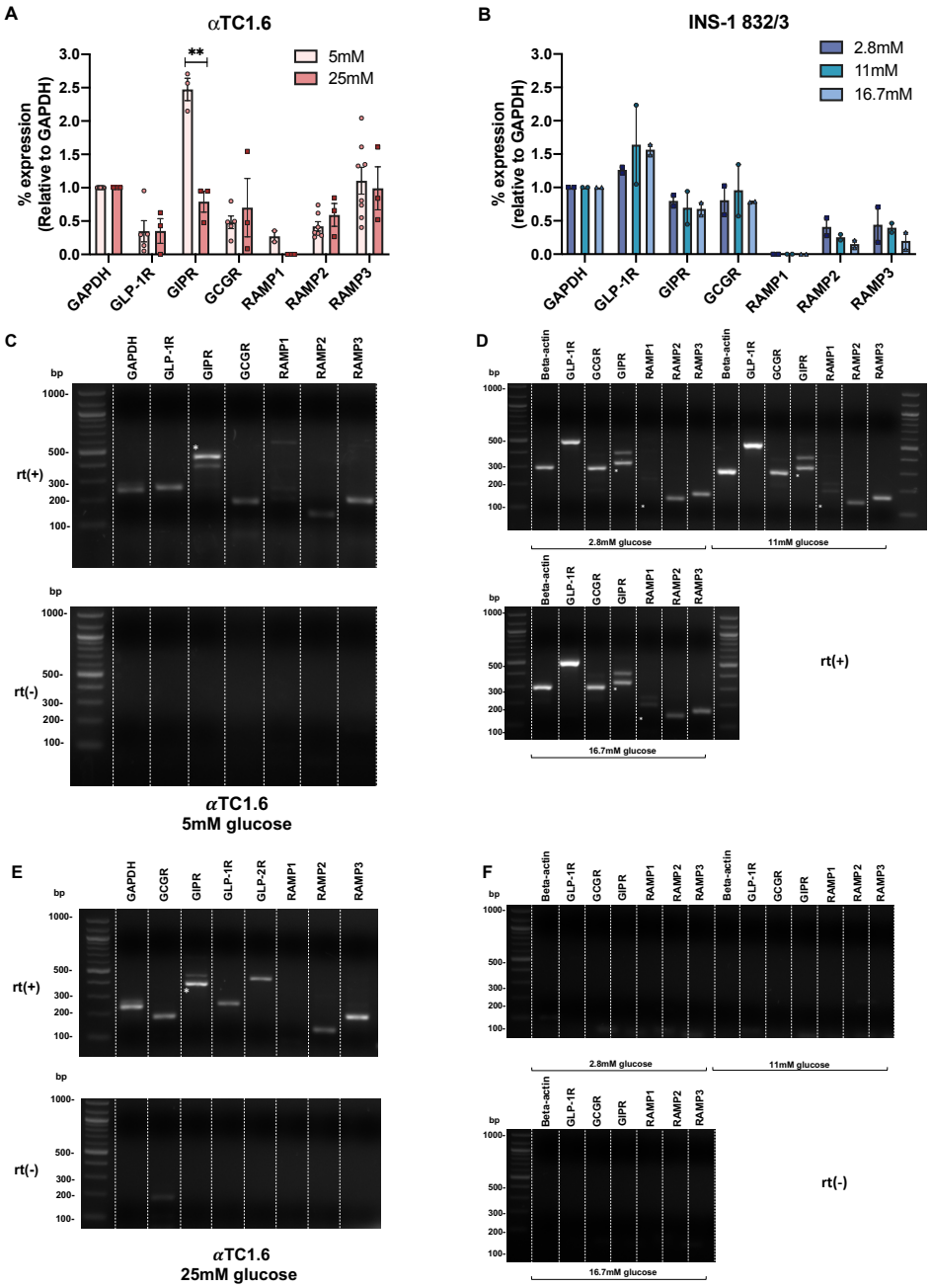

Figure 3.17: **Glucagon receptor family and RAMPs expressions determined by RT-PCR in αTC1.6 and INS-1 832/3 cell lines under different glucose conditions cultured in 72 hours.** The above figure shows the GLP-1R, GCGR, GIPR and RAMPs expressions in (A) mouse αTC1.6 cell line cultured under different glucose conditions (5mM and 25mM) and (B) rat INS-1 832/3 cell lines under 2.8mM, 11mM and 16.7mM glucose conditions respectively. (C), (D) and (E) show the representative gel images of the RT-PCR results of αTC1.6 and INS-1 832/3 cell lines cultured under high and low glucose respectively while (F) shows the rt(-) treatment of the cDNA of INS-1 832/3 cells cultured at different glucose conditions. All expressions of genes of interests are relative to GAPDH. Data are expressed as mean $\pm$ S.E.M. from 2 to 7 individual repeats. Statistical significance compared between the expressions of individual receptors or RAMPs in αTC1.6 and INS-1 832/3 cells were determined by Student's t-test with Welch's correction (**, $p < 0.01$). The asterisk (*) on the gel images indicate the correct band size for gene of interest.

3.4.5 cAMP responses of glucagon-like peptides in rodent insulinoma and glucagonoma cell systems under high and low glucose conditions

Following the findings that there was a change in GIPR expression in hyperglycaemic conditions in the pancreatic α cells, the effect of high and low glucose on the incretin cAMP signalling in the glucagonoma cell line was subsequently evaluated. The HTRF-based cAMP assay was again utilised to determine the extent of cAMP production. Similarly, cells were cultured in the two different glucose conditions for 72 hours prior to assays.

As shown in the above section that there were no changes in the expressions of GLP-1R and GCGR in different glucose conditions, the potencies and efficacies of the cognate peptide agonists of GLP-1R and GCGR, GLP-1 and GCG, did not alter. Interestingly, the potency of the GLP-1 metabolite, GLP-1(9-36)NH_2 decreased from 5.77 $\pm$ 0.66 to 5.28 $\pm$ 0.28 ($p < 0.05$) while its efficacy increased from 18.23 $\pm$ 3.47 to 41.69 $\pm$ 3.83 ($p < 0.01$) when cultured under high glucose condition. Given that the GIPR expression was downregulated under hyperglycaemic condition, it was not surprising the cAMP potency mediated by GIP decreased from 7.54 $\pm$ 0.29 to 6.00 $\pm$ 0.22 ($p < 0.01$) under 25mM glucose condition. Yet the efficacy of GIP increased from 28.32 $\pm$ 1.52 to 36.65 $\pm$ 4.67 ($p < 0.001$) in the presence of high glucose (Fig 3.18 and Table 3.14). Here under different glucose conditions, the cAMP production mediated by GIP and GLP-1(9-36)NH_2 changes according to the glucose concentrations and the difference in potencies and efficacies under high and low glucose conditions are further summarised in Fig. 3.19. The significance of the findings will be discussed in the following sections.

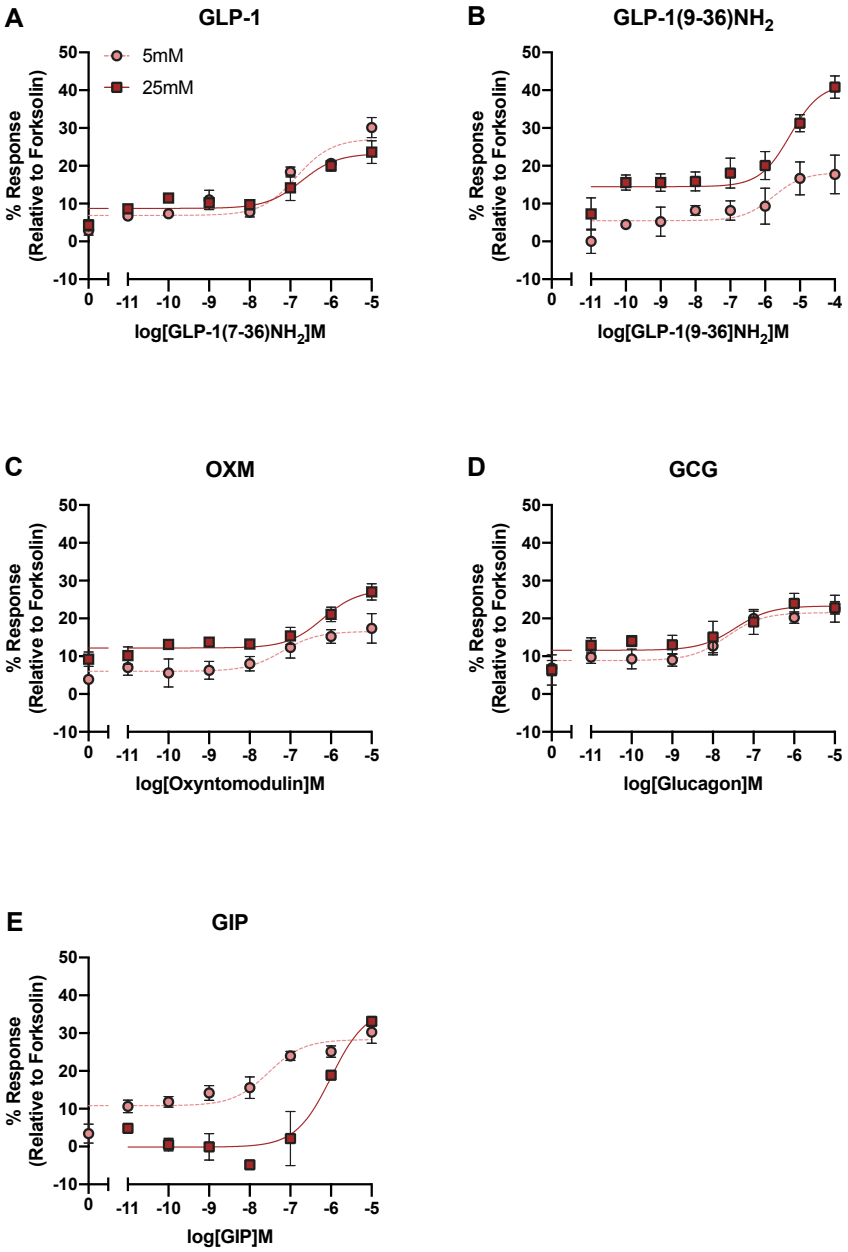

Figure 3.18: **Dose-response curves showing cAMP accumulation responses when αTC1.6 cells cultured in low and high glucose conditions were stimulated with different glucagon receptor family ligands.** The above figure shows the cAMP production dose-response curves when αTC1.6 cells, which were cultured in low and high glucose conditions (5mM and 25mM respectively) were stimulated with (A) GLP-1, (B) GLP-1(9-36)NH_2, (C) OXM, (D) GCG and (E) GIP. 4000 αTC1.6 cells/well cultured in 5mM and 25mM glucose conditions were stimulated with various ligands in the presence of PDE inhibitor IBMX. All data were normalised to the maximum cAMP production when stimulated with 100μM forskolin and were means of 2 to 7 independent experiments with mean $\pm$ S.E.M (upper and lower error bars). Table 3.14 shows the pEC_{50} and E_{max} values of ligand responses.

Table 3.14: **cAMP accumulation potencies (pEC_{50}) and maximal responses (E_{max}) of glucagon receptor family endogenous ligands in αTC1.6 cells cultured under low (5mM) and high (25mM) glucose concentrations.**

Glucose concentration	Ligand	pEC_{50} [a]	E_{max} [b]	Span	n
5mM	GLP-1	6.85±0.22	27.18±1.56	20.30±1.81	12
	GLP-1(9-36)NH_2	5.77±0.66	18.23±3.47	12.74±3.67	6
	OXM	7.20±0.51	16.57±1.99	10.55±2.26	8
	GCG	7.66±0.34	21.55±1.46	12.69±1.80	14
	GIP	7.54±0.29	28.32±1.52	17.51±1.85	12
25mM	GLP-1	6.72±0.31^{ns}	23.26±1.95^{ns}	14.52±2.13^{ns}	4
	GLP-1(9-36)NH_2	5.28±0.28*	41.69±3.83**	27.20±3.93^{ns}	4
	OXM	6.20±0.26^{ns}	27.67±2.12^{ns}	15.48±2.20^{ns}	4
	GCG	7.45±0.51^{ns}	23.30±2.13^{ns}	11.72±2.47^{ns}	4
	GIP	6.00±0.22**	36.65±4.67***	36.79±4.76^{ns}	5

Values were generated when the data were fitted to the three-parameter logistic equation. Means ± S.E.M of n individual result sets were shown.

[a] Negative logarithm of agonist concentration when reaching half maximal response.

[b] % of maximal response observed when stimulated with ligands relative to forskolin.

Statistical significance compared between individual peptide ligand cAMP accumulation responses under low and high glucose conditions were determined by Student's t-test with Welch's correction (*, p<0.05; **, p<0.01; ***, p<0.001; ns, non-statistically significant).

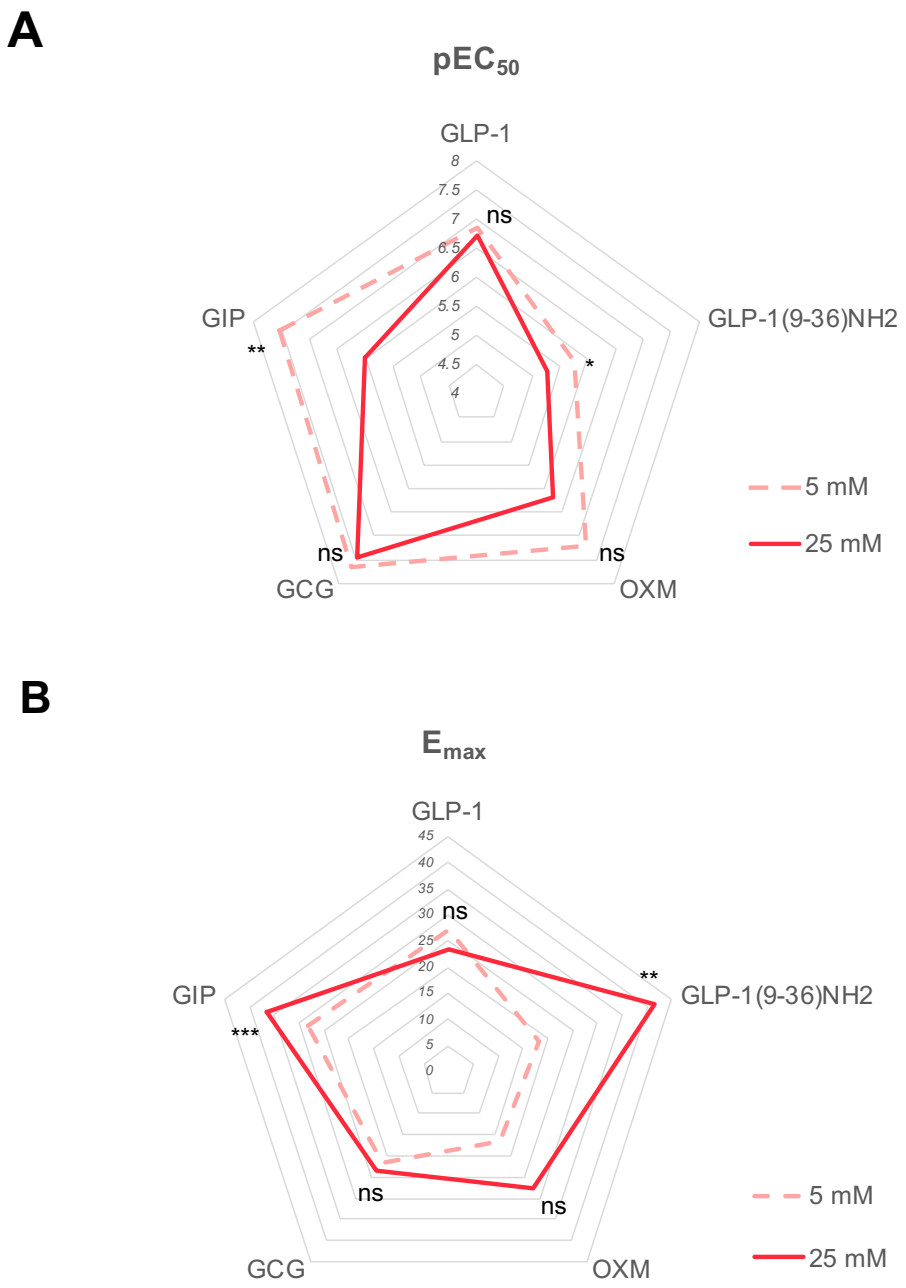

Figure 3.19: **Representative radar plots summarising the difference in potencies and efficacies of glucagon receptor family ligand cAMP responses in αTC1.6 cells cultured under low and high glucose conditions.** The above radar plots describe the difference in cAMP responses (A) potencies and (B) efficacies when αTC1.6 cells, which were cultured in low and high glucose conditions (5mM and 25mM respectively), were stimulated with GLP-1, GLP-1(9-36)NH_2, OXM, GCG and GIP. Table 3.14 shows the pEC_{50} and E_{max} values of ligand responses. Statistical significance compared between individual peptide ligand cAMP accumulation responses in low and high glucose concentration culture conditions were determined by Student's t-test with Welch's correction (*, p<0.05; **, p<0.01, ***, p<0.001; ns, non-statistically significant).

3.5 Discussion

GLP-1 has been known to possess both insulinotropic and glucagonostatic properties [Drucker, 2018]. However, compared to its well-studied GSIS mechanism of action, its glucagon inhibitory action is still unclear. Furthermore, apart from GLP-1, a range of glucagon-like peptides, namely OXM, GCG, GIP and GLP-1(9-36)NH_2, have also been known to regulate glucagon secretion and/or facilitate GSIS [Sandoval and D'Alessio, 2015]. Therefore, to understand how GLP-1 regulates glucagon secretion, robust *in vitro* testing systems, the recombinant hamster and human cell systems stably expressing glucagon-like receptors and rodent clonal α and β cell lines, were established. Moreover, there has been ongoing debates on the expression of GLP-1R on pancreatic α cells [Moens et al., 1996, Heller et al., 1997, Tornehave et al., 2008, De Marinis et al., 2010, Ramracheya et al., 2018, Zhang et al., 2019]. By using semi-quantitative RT-PCR, the glucagon-like receptors expressions, as well as RAMPs, which have been known to interact with some of the glucagon-like receptors, were determined. Lastly, the factors that may influence glucagon-like peptide signalling, such as the influence of GPR119, glucagon-like receptor antagonisms, RAMPs interaction and long-term glucose culture conditions, were investigated in an attempt to further understand the extent of glucagon-like peptide signalling in physiologically relevant settings. The significance of the findings will be discussed as follows.

3.5.1 Glucagon-like peptide ligand crosstalk at GLP-1R and GCGR

There were reports suggesting cross-receptor activation among the glucagon-like peptides [Wootten et al., 2013a, Graaf et al., 2016, Chepurny et al., 2019]. Hence, the experimental approach of evaluating the cAMP responses of GLP-1, OXM, GCG, GLP-1(9-36)NH_2 and GIP in both CHO-K1 and HEK293 recombinant cell lines stably expressing GLP-1R, GCGR and GIPR (Fig. 3.2 and 3.6) confers distinct advantage of being able to evaluate the individual intrinsic agonism of each glucagon-like peptides on the receptors. GIP was found to be a full agonist at GIPR only (Fig. 3.2) and did not share cross-receptor reactivity with GLP-1R and GCGR. On the other hand, concurred with other published reports [Pocai, 2012, Chepurny et al., 2019], GLP-1, OXM and GCG can activate both GLP-1R and GCGR albeit at varying potencies and efficacies. Intriguingly, the physiologically abundant GLP-1 metabolite, GLP-1(9-36)NH_2, is a weak partial agonist of not only GLP-1R, but also of GCGR (Fig. 3.2), an observation which has not been noted to date. More importantly, these five endogenous agonists

also mediate cAMP responses in the physiologically relevant rodent insulinoma and glucagonoma cell lines, despite their differences in terms of potency rank order (Fig. 3.10 and Table 3.7). Further applications of specific GLP-1R and GCGR antagonists, Ex-9 and L-168,049, blocked the cAMP signalling mediated by these peptide agonists in CHO-GLP-1R cells (Fig. 3.12), HEKΔCTR-GCGR (Fig. 3.13) as well as in rat INS-1 832/3 cells (Fig. 3.14), therefore providing evidence of their dual agonisms at both GLP-1R and GCGR. These ligand-receptor crosstalk then pose an interesting question if GLP-1 and GLP-1(9-36)NH_2 mediate their glucagonostatic actions also via GCGR, given the low expression of GLP-1R detected in the αTC1.6 cells (Fig. 3.7), as well as reported by other studies [De Marinis et al., 2010, Piro et al., 2014, Ramracheya et al., 2018, Nakashima et al., 2018, Zhang et al., 2019]. This observation warranted further experimental validations, which will be reported in the next chapter.

However, there are several limitations to the studies on investigating ligand crosstalk reported in this chapter. Firstly, due to time constraints, the changes of cAMP responses over time stimulated by these peptide agonists were not investigated, which may shed new light on how internalisation and desensitisation of GLP-1R, GCGR and GIPR affect physiological cAMP production. Secondly, a caveat using pancreatic clonal cell systems in the current studies is the mixed origins of islets cell types present in the pancreatic α and β clonal cell lines. Hence primary α and β cells isolated from mouse islets may serve as a better experimental approach in examining ligand responses in pure populations of α and β cells. Lastly, intracellular calcium responses in pancreatic α and β clonal cell lines were not examined due to technological limitations. The examination of which may offer an important insight into how incretins regulate insulin secretion via modifying iCa^{2+} release in both α and β cells.

3.5.2 GPR119 does not affect cAMP signalling of GLP-1R and GCGR

GPR119, which can also stimulate glucagon secretion upon activation, was found to be highly expressing in the mouse α cell line compared to the β cell line and that the expression of GPR119 was seemingly higher or equal to that of GIPR in the α cell line (Fig. 3.7A); the observations here agreed with other published report [Whalley et al., 2011]. However, based on the findings using cAMP functional assaying technique, during which GLP-1R, GCGR and GPR119 agonists were applied to HEKΔCTR transiently expressing GLP-1R, GCGR or GPR119, no ligand-receptor crosstalk was observed (Fig. 3.11). Therefore, the notion of GPR119 influencing GLP-1-mediated glucagon secretion via modulating GLP-1-mediated cAMP signalling is ruled out.

3.5.3 Implications of the differences in receptors, RAMPs and G protein expressions in rodent immortalised α and β cell models

3.5.3.1 Differences in terms of glucagon-like receptor expressions

The mRNA expressions of incretin receptors were examined in the rodent clonal pancreatic α and β cell lines (Fig. 3.7 and 3.8), in order to explain the differences of the signalling responses of glucagon-like peptides observed in these physiologically relevant cell lines. GLP-1R was found to express at a very low level in the αTC1.6 cells, which significance was discussed above. As for GCGR and GIPR, the results reported here (Fig. 3.7 and 3.8) also differed from the report by Huising and colleagues, of which they showed the isolated β cells from mouse islets did not express any GCGR while the isolated α cells expressed abundant GCGR [Huising et al., 2010]. Yet the results here agreed with the report by Ma and colleagues, which demonstrated the presence of GCGR in both fluorescence-activated cell sorting (FACS) purified rat α and β cells with the use of RT-PCR [Ma et al., 2005]. Therefore, the semi-quantitative RT-PCR results here reflect the importance on the evaluation of the cellular background of the cell lines to be used as well as the selection of cell systems to evaluate glucagon-like peptides signalling responses, as there are considerable differences in terms of receptor expressions between immortalised cell lines and *ex vivo* primary cells. However, one caveat of using semi-quantitative RT-PCR in these sets of experiments, as well as the subsequent experiments on determining the influence of glucose on receptor expressions, is that it only provides a glimpse towards whether certain mRNA of interest is present or absent, and thus does not represent a true quantitative measure of gene expression. In order to accurately quantify receptor RNA or DNA expression, qPCR (quantitative real-time polymerase chain reaction) should be used and may serve as a piece of important future work.

The influence of high and low glucose under long term (72 hours) conditions on receptor expressions was also elucidated (Fig. 3.17) and an upregulation of GIPR expression under hypoglycaemic condition was noted in the αTC1.6 cells, while the expressions of GLP-1R, GCGR and RAMPs remained unchanged. In contrast to the observations in the α cells, the receptors and RAMPs expressions were not affected by the changes in glucose conditions in the β cells. Accordingly, the cAMP responses of GIP in the α cells were also more potent under hypoglycaemic condition (Fig. 3.18 and 3.19). This observation agrees with the stimulatory action of GIP on glucagon secretion, as under hypoglycaemia, glucose homeostasis can be maintained through augmenting

glucagon secretion, thereby promoting liver glycogenolysis and gluconeogenesis [Holst, 2007]. Such observations may also imply that the pancreatic α cells experience constant tonic inhibition of glucagon secretion [Zhang et al., 2019] via the regulation of GLP-1R and GCGR, as their expressions remain unchanged regardless of the differences in glucose culture conditions. Alternatively, such *in vitro* observations may also explain why T2DM patients experience chronic high blood glucose level due to a reduction of GIPR expression, which leads to less pronounced glucagon-stimulatory actions in promoting glucose homeostasis. However, further studies, such as short-term changes in glucose conditions, are needed to further understand the changes of glucagon-like receptor expressions.

3.5.3.2 Differences in terms of RAMPs expressions

RAMPs have been demonstrated to play a role in modulating Class B GPCRs physiological activities [McLatchie et al., 1998, Wootten et al., 2013a, Weston et al., 2015, Hay et al., 2016, Routledge et al., 2017, Cegla et al., 2017] and indeed RAMP2 has been shown to enhance the potencies of GLP-1(9-36)NH_2 selectively (Fig. 3.16). Yet their expressions in the pancreatic α cells was scarcely reported. Here the RAMPs mRNA expression in the αTC1.6 cell line, together with MIN6-B1 cell line to act as a comparison, were determined (Fig. 3.7 and 3.8). The observation, which RAMP3 was highly present in both α and β cell lines (Fig. 3.7), concurred with the report by our collaborators, of which they employed RNAscope technique and demonstrated the same trend of RAMPs expressions in mouse islets. The observation also agreed with Lilla and colleagues, whose team confirmed the presence of the mRNA expression of RAMP2 using Affymetrix microarrays technique [Lilla et al., 2003]. However, they did not investigate further into the presence of RAMP1 and RAMP3, hence comparisons cannot be drawn. The observation here also contrasted with the investigation conducted by Martínez and colleagues [Martínez et al., 2000]. In their studies, they performed RT-PCR followed by Southern blot on two pancreatic β cell lines, which were the mouse CRL 2055 and hamster CRL 1777 cell lines. They showed the presence of RAMP1 and RAMP3 in the CRL 2055 cell line whereas only a high abundant expression of RAMP3 was present in the CRL 1777 cell line. McLatchie and colleagues also reported the presence of all three RAMPs in human pancreatic tissues using northern blots, yet concluding RAMP1 being the most abundant among all three RAMPs, followed by RAMP3 and lastly RAMP2 [McLatchie et al., 1998]. All these varying results yet again emphasise the fact that the expressions of RAMPs were cell-line and species dependent [Hay et al., 2016]. Hence,

careful considerations in evaluating ligand responses are needed.

3.5.3.3 Differences in terms of G protein expressions

Apart from predominantly coupling to the $G\alpha_s$ subunit to mediate cAMP responses, GLP-1R and GCGR have been shown to also pleiotropically couple to $G\alpha_i$ and $G\alpha_q$ subunits [Montrose-rafizadeh et al., 1997, Wootten et al., 2012, Pabreja et al., 2014], inhibiting cAMP responses and mediating downstream iCa^{2+} responses (Fig. 3.6) respectively [Seino, 2012]. Therefore, the G protein subunit profile was established in the rodent insulinoma and glucagonoma cell line, in order to evaluate if GLP-1R and GCGR can also pleiotropically coupled to various G proteins in the physiologically relevant cell lines (Fig. 3.9).

The findings in Fig. 3.9 agreed with the studies conducted by Gasa and colleagues [Gasa et al., 1999], which they also showed the expression of $G\alpha_{q/11}$ protein in INS-1 832/3 cell line using immunoblotting technique. Studies by Montrose-rafizadeh and colleagues who looked into the G protein composition in the rat RIN1046-38 pancreatic β cell line with endogenous expression of GLP-1R also demonstrated high levels of $G\alpha_s$, $G\alpha_q$, followed by $G\alpha_{i1}$, $G\alpha_{i2}$ and a relatively low level of $G\alpha_{i3}$ [Montrose-rafizadeh et al., 1999], which contrasted with the findings in the INS-1 832/3 cell line (Fig. 3.9). Yet, the results collectively illustrate the expressions of $G\alpha_s$, $G\alpha_q$ and $G\alpha_i$ subunits, validating the notion that insulin secretion can be regulated through GLP-1R and GCGR pleiotropically coupled to various G proteins.

In contrast to the well-characterised G protein profile in insulinoma cell lines, there is no reported literature on the G protein compositions of the frequently used α cell models to date. Hence the RT-PCR studies on the G protein composition on the α cell model provided an interesting insight into the difference of the G protein compositions between the α and β cell models, which high levels of $G\alpha_s$ subunit and higher levels of $G\alpha_i$ and $G\alpha_q$ subunits compared to the INS-1 832/3 cell line in the αTC1.6 cell lines have been highlighted (Fig. 3.9). This observation poses another interesting question if the glucagon secretion is predominantly $G\alpha_i$ and $G\alpha_q$-mediated via the action of GLP-1R and GCGR. The importance of which will be further explored in the next chapter.

3.6 Chapter summary

The findings of the chapter are concluded as follows:

- GLP-1 and GCG are the most potent full agonists at the GLP-1R and GCGR respectively, which are consistently shown in the CHO-K1 and HEK293 recombinant cell systems. Yet GCG is also a full agonist at the GLP-1R, despite being less potent than GLP-1 while GLP-1 acts as a partial agonist at the GCGR. Both GLP-1 and GCG are not able to activate GIPR. The GLP-1 metabolite, GLP-1(9-36)NH_2 is a weak partial agonist at both GLP-1R and GCGR.
- GLP-1 together with GIP are the most potent agonists at the physiologically relevant pancreatic β cell models, while GIP and GCG are the most potent agonists at the pancreatic α cell models.
- RAMP1 is the most abundantly expressing in the HEK293-based recombinant cell systems while RAMP3 is the most abundantly expressing in both the pancreatic α and β cell models, suggesting caution must be made when translating cAMP responses into the more physiologically relevant settings.
- GPR119 agonists do not activate GLP-1R and GCGR and likewise GLP-1R and GCGR agonists do not activate GPR119
- The presence of RAMP2 at the GCGR enhances the potency of GLP-1(9-36)NH_2 only but not other GCGR ligands
- The GIPR expression was downregulated under hyperclycemic condition and the cAMP signalling of GIP and GLP-1(9-36)NH_2 changes under hyperglycaemic conditions.

Chapter 4

Quantitative measurements of insulin and glucagon secretion

4.1 Introduction

Following the characterisation of the intracellular cAMP signalling mediated by various glucagon-like peptides at the physiologically relevant rodent pancreatic α and β clonal cell systems, the insulin and glucagon secretion upon stimulation with these glucagon-like peptides in the same rodent pancreatic cell lines were quantitatively measured. The quantitative measurements of insulin and glucagon secretion in clonal cell systems are relatively new assaying technique at the Ladds' laboratory, therefore the assay protocol of the Cisbio® ultra-sensitive insulin kit and glucagon kit was first optimised, which preliminary results were available in Appendix A.1. After assay optimisation, quantitative measurements of the levels of insulin and glucagon secretion potentiated by a range of glucagon-like peptides were proceeded. Given our collaborators, the research group led by Dr Reshma Ramracheya and Prof. Patrik Rorsman (Oxford Centre for Diabetes, Endocrinology and Metabolism, University of Oxford), illustrated that GLP-1 and GLP-1(9-36)NH_2 mediate their glucagonostatic actions in the pancreatic α cells via promiscuous receptor activation and that the glucagonostatic actions of these two peptide ligands may or may not be $G\alpha_i$-dependent [Guida et al., 2020], the postulated phenomenon was then further investigated through the applications of receptor-specific antagonists, as well as a range of pharmacological activator and inhibitors in the mouse αTC1.6 glucagonoma cell line. The same pharmacological activator and inhibitors were also applied in the rat insulinoma INS-1 832/3 cell line,

as well as utilising GLP-1R or GIPR CRISPR/Cas9 knockout (KO) INS-1 832/3 cell lines [Naylor et al., 2016], in order to aid the comparison of the molecular mechanisms that regulate insulin and glucagon secretion in the α and β cells. Unfortunately, due to COVID-19 impact on experimental schedule, some of the results presented in this chapter are of preliminary nature only, and are noted accordingly. Furthermore, one caveat which may affect the validity of the results shown in this chapter is the lack of measurement of total insulin/glucagon content in samples; yet subsequent re-analysis of the total insulin/glucagon cell contents were not possible due to the deterioration of samples. Firstly, the assay principle of both the insulin and glucagon secretion assays will be described as follows.

4.2 Assay principle of the Cisbio® ultra-sensitive insulin and glucagon kit

As described in section 2.2.4.1, the principle of the Cisbio® ultra-sensitive insulin kit (thereafter referred to as insulin secretion assay) is based on the TR-HTRF technology, during which when insulin is present in the supernatant, the donor and acceptor antibodies, which are Europium Cryptate and XL-665 respectively, bind to insulin. When the antibodies are in close proximity, the excitation of the donor with a light source at wavelength 340nM triggers a FRET signal toward the acceptor, giving out fluorescence at 620nm and 665nm wavelength. The signal intensity is thus proportional to the number of antibodies complex formed with insulin, hence directly proportional to the insulin concentration present in the supernatant. Likewise, the Cisbio® glucagon kit (thereafter referred to as glucagon secretion assay) employs the same technology, but the only difference is the use of two different acceptor and donor antibodies, which are d2 and Terbium Cryptate respectively. The Cisbio® insulin assay is intended for quantitative measurement of insulin in pancreatic β cell or islets supernatants, and is compatible with human, mouse, rat, porcine and bovine species. The Cisbio® glucagon kit is only intended for the measurement of glucagon in cell or tissue supernatant and is also highly specific for detecting glucagon produced by human, mouse and rat species, with <0.07% specificity to OXM, which is highly structurally similar to GCG.

The Cisbio® TR-HTRF insulin and glucagon assays were introduced to the commercial market only in 2016. However, given the relative ease of use of these kits and the high sensitivity and specificity in detecting insulin and glucagon in the samples compared to the traditional enzyme-linked immunosorbent assay (ELISA) and

radioimmunoassay (RIA) approaches, the Cisbio® TR-HTRF insulin and glucagon assays have been widely used in other published reports on the measurement of insulin and glucagon secretions in both rodent clonal systems and *ex vivo* mouse islets [Kim et al., 2017, Yau et al., 2019, Yau et al., 2020].

4.3 Measuring ligand responses in insulin and glucagon secretion

After optimising the assay protocol to aid the quantitative measurement of insulin or glucagon levels in the test samples (Appendix A.1), the glucose-responsiveness in the rat insulinoma cell line and the mouse glucagonoma cell line were next evaluated. It is of particular interest to deduce if the GSIS relationship, as established in other reports in rat insulinoma cell line [Yang et al., 2016] as well as in isolated mouse islets [Shigeto et al., 2015], can be observed.

4.3.1 Glucose-dependent insulin and glucagon secretion

The well documented GSIS in the INS-1 832/3 cell lines was first explored. To do so, all of the optimisations as mentioned above were included: the INS-1 832/3 cells were pre-incubated at 0mM RPMI for three hours prior to incubating the cells at KRB supplemented with 2.8mM glucose for an hour. After an hour of pre-incubation, the cells were challenged with glucose at different concentrations, which were (in mM) 1, 2.8, 5, 10, 16.7 and 25 for a further hour before the collection of supernatant on ice.

The following results showed the expected GSIS relationship displayed at the INS-1 832/3 cells, whereby the higher the glucose concentrations, the higher the level of insulin released at the rat insulinoma cells (Fig. 4.1A and C). However, the insulin level measured seemed to have reached the maximum detection limit of the insulin secretion assay, which a higher level of insulin was not detected above 10mM glucose application. More importantly, there was a statistically significant difference between the 2.8mM and 16.7mM glucose conditions (3.88-fold difference, $p < 0.01$), which were the reference glucose points that were commonly reported in many papers which utilised the rat β cells to investigate the mechanism of insulin secretion. Therefore, these two glucose concentrations were also selected to represent the high and low glucose conditions for subsequent insulin secretion assays.

In contrast to GSIS, a totally opposite trend was observed in the mouse glucagonoma

cell line, where the higher the glucose concentrations applied to the αTC1.6 cell line, the more the glucagon secretion inhibitory effect observed, which also concurred with other studies conducted in the mouse α clonal cells [Diao et al., 2005, McGirr et al., 2005]. Furthermore, 1mM and 5mM glucose seemed to result in the most potent glucagon secretion stimulation in the pancreatic α cells, which also agreed with the reports that utilised the mouse αTC1.6 cell line to investigate the glucagon secretion mechanism [Piro et al., 2014]. However, a paradoxical increase in glucagon secretion was observed when 25mM glucose was applied to the mouse α cells, which concurred with the observation in the hamster InR1G9 α cell line [Salehi et al., 2006]. The mechanism of the paradoxical increase in glucagon secretion at high glucose level is yet to be explained. However it was not due to glucotoxicity given that the αTC1.6 cells were able to mediate cAMP signalling responses (Fig. 3.18 and 3.19) under long-term culture at 25mM glucose. Given that the most potent stimulatory and inhibitory effects on glucagon release in the mouse αTC1.6 cells were observed when 5mM and 16.7mM glucose were used, these two glucose concentrations were subsequently used as the representative low and high glucose concentrations respectively in the following glucagon secretion assays.

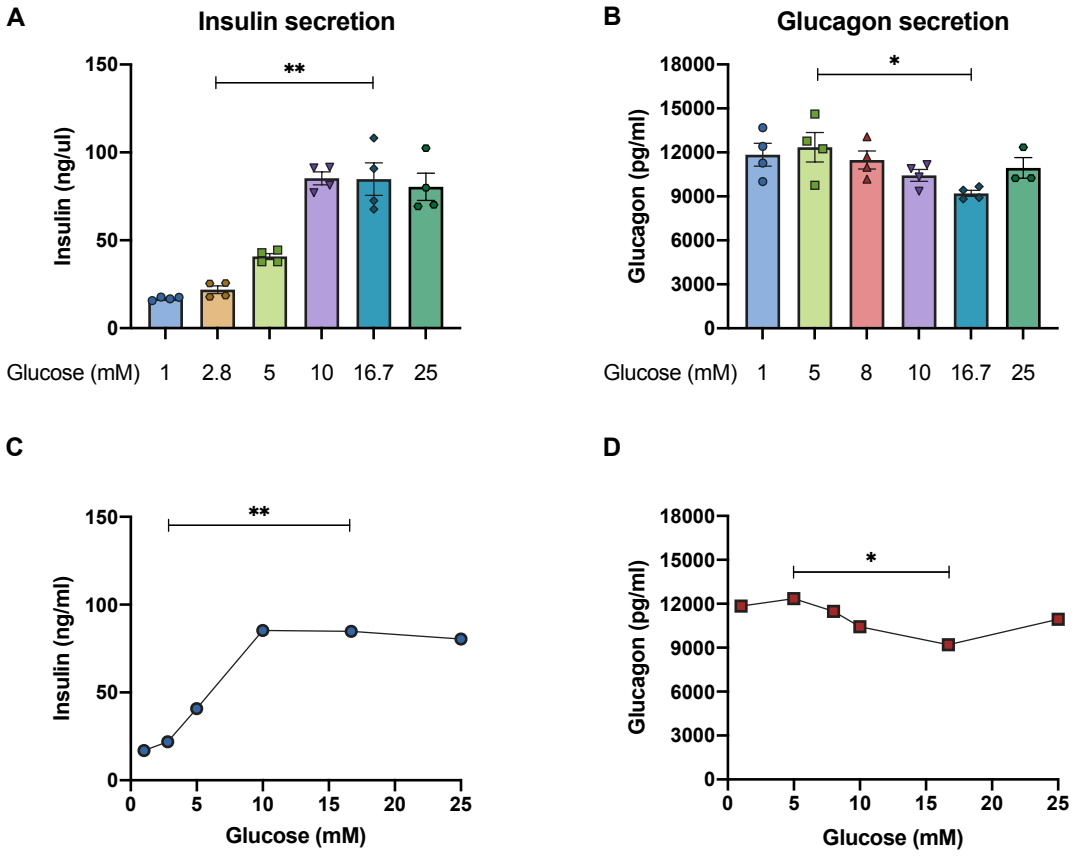

Figure 4.1: **Glucose-dependent insulin and glucagon secretions.** (A) shows the glucose-stimulated insulin secretion in the rat INS-1 832/3 WT cell line. (B) shows the glucose-regulated glucagon secretion in mouse αTC1.6 cell line. Mean $\pm$ S.E.M. insulin and glucagon secretion data (reported as interpolated insulin and glucagon levels) in 4 independent experiments with quadruplicates are shown in the above scatter plots. Statistical significance compared between low glucose and high glucose conditions in INS-1 832/3 WT cells (2.8mM vs 16.7mM) and αTC1.6 (5mM vs 16.7mM) cells were determined by Student's t-test with Welch's correction (*, $p < 0.05$; **, $p < 0.01$).

4.3.2 Glucagon-like peptides concentration-dependent effect on glucagon secretion

Prior to investigating the effects of the glucagon-like peptides on glucagon secretion, the optimal concentration of GLP-1 or GLP-1(9-36)NH_2 to be used in the following glucagon secretion assays were to be deduced, as it has been shown by our collaborators that GLP-1 and GLP-1(9-36)NH_2 did not exhibit dose-dependent inhibition and that they exerted their maximal inhibitions at picomolar range rather than at nanomolar range (0.1 to 100nM). In order to select the optimal GLP-1 and GLP-1(9-36)NH_2 doses in the glucagon secretion assays, similar to the previous approach in measuring glucagon secretion, the mouse α cells were pre-incubated in high glucose containing KRB for an hour, then GLP-1 and GLP-1(9-36)NH_2 were applied at three different concentrations, which were 10000pM, 100pM and 1pM respectively; an hour stimulation in the presence of low glucose was allowed. The supernatants were again collected, and the glucagon content were measured. The results obtained here were normalised to the mean glucagon secretion at 5mM glucose, which stimulated the highest extent of glucagon secretion, so as to faciliate the monitoring of the extent of inhibitory effect mediated by GLP-1 and GLP-1(9-36)NH_2 against the maximal glucagon stimulation.

Consistent with the observations in Fig. 4.1, a small but significant decrease in glucagon secretion in the presence of high glucose compared to the low glucose stimulation was resulted (8.9% decrease, $p < 0.01$), proving the functionality of the α cells (Fig. 4.2). Similar to the observation by our collaborators, concentration-dependent glucagonostatic actions mediated by the two peptide ligands were not observed, as when high concentration (10000pM) of GLP-1 or GLP-1(9-36)NH_2 was applied, less glucagonostatic effect was resulted. Yet when these two ligands were applied at 100pM, maximal glucagonostatic effects were achieved, resulting in 17.5% ($p < 0.001$) and 25.6% ($p < 0.001$) decrease in glucagon secretion due to GLP-1 and GLP-1(9-36)NH_2 respectively relative to low glucose stimulation alone (Fig. 4.2). However, when an even lower GLP-1 or GLP-1(9-36)NH_2 concentration was applied (1pM), glucagon secretion were slightly stimulated, illustrating a non-concentration dependent relationship between the concentrations of ligands and the glucagonostatic effect.

Provided that 100pM GLP-1 and GLP-1(9-36)NH_2 mediated the most potent glucagonostatic actions, these two concentrations were used in the subsequent glucagon secretion assays. The effects of insulin or glucagon secretion mediated by other glucagon-like peptide ligands were next characterised in the α and β clonal cell systems.

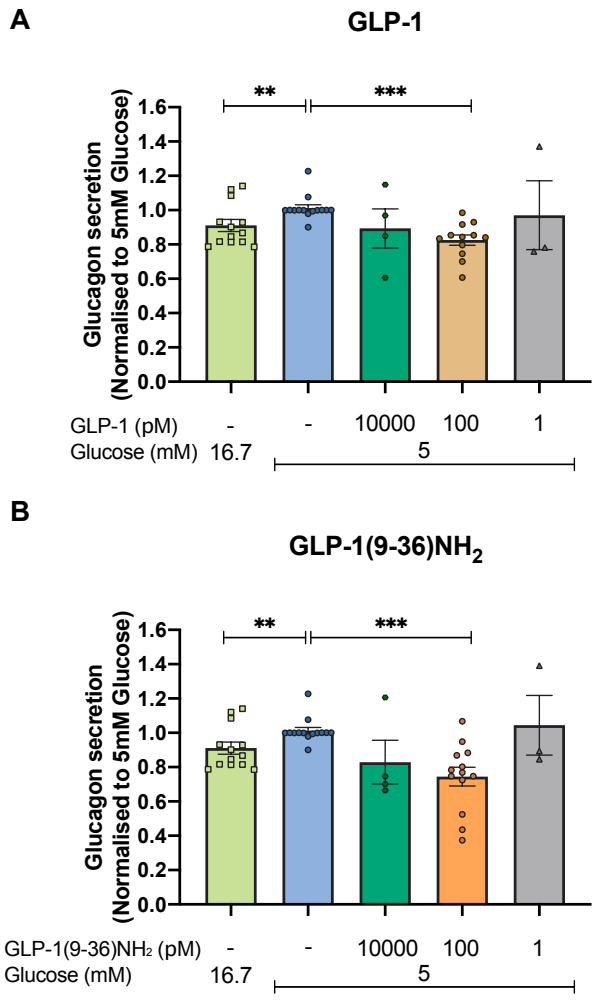

Figure 4.2: **Inhibition of glucagon secretion mediated by GLP-1 and GLP-1(9-36)NH_2 are not concentration-dependent in αTC1.6 cells.** (A) and (B) show the glucagon secretion inhibitory effect exerted by GLP-1 and GLP-1(9-36)NH_2 respectively. Mean $\pm$ S.E.M. glucagon secretion data (responses normalised to glucagon secretion responses at 5mM) in 3 to 13 independent experiments with quadruplicates are shown in the above scatter plots. Statistical significance compared among responses with peptide ligands and 5mM glucose were determined by non-parametric Kruskal-Wallis test and are indicated by asterisks above the bars (**, $p<0.01$; ***, $p < 0.01$)

4.3.3 Glucagon-like peptide ligand responses in α and β clonal cell systems

After deducing that picomolar ranges of GLP-1 and GLP-1(9-36)NH_2 were sufficient to stimulate the most potent glucagonostatic effect in the mouse α cells, insulin and glucagon secretion responses upon stimulation with other glucagon-like peptides were next evaluated. Following the optimised insulin secretion assay protocol, the INS-1 832/3 cells were first glucose-starved for three hours prior to pre-incubating the cells in KRB containing 2.8mM glucose. The β cells were then stimulated with a range of ligands, namely GLP-1, GLP-1(9-36)NH_2, OXM, GIP and GCG, either at 10nM or 1μM, for an hour; the application of peptide ligands at 10nM was in line with other studies which investigated the effect of GLP-1 on insulin secretion [Naylor et al., 2016]. The supernatants from each stimulation condition were then collected and the insulin level present in the supernatant were determined. Likewise, the mouse αTC1.6 cells were pre-incubated in KRB containing 16.7mM glucose for an hour yet without prior glucose-starving step. They were then stimulated with a range of ligands for an hour, following supernatant collection and determination of glucagon levels. The effect of OXM on glucagon secretion was not investigated as GCG and OXM share a close structural homology.

4.3.3.1 Ligand responses in inducing insulin secretion

Similar to the observation in Fig. 4.1, in the presence of high glucose, insulin secretion was enhanced by 480% ($p < 0.05$) compared to that at low glucose condition (Fig. 4.3A), validating the functionality of the rat insulinoma cells in responding to glucose stimulation. When GLP-1 at 10nM was applied to the rat β cells, GSIS was further enhanced by 483% compared to when stimulated with high glucose alone (Fig. 4.3A), which concurred with the observations of a lot of published literature that GLP-1 acts as an incretin hormone [Naylor et al., 2016] via the GLP-1R to mediate its insulinotropic action, given their high expression in the rat β cells as established previously (Fig. 3.8). Another important incretin hormone, GIP, was also able to further augment GSIS by 231% compared to the presence of high glucose alone (Fig. 4.3A), yet its extent in enhancing GSIS was less prominent than GLP-1. This prominent GSIS effect potentiated by GIP by activating the GIPR present in the rat β cells (Fig. 3.8) also corroborated with the published reports which investigated the GIP augmentation of GSIS in the rat β cells [Naylor et al., 2016]. OXM, when applied at 1μM, also mediated augmentation of GSIS by 458% (Fig. 4.3A) when compared to high glucose alone.

The results here agreed with the observations by Maida and colleagues, where they also observed a dose-dependent GSIS augmentation facilitated by OXM [Maida et al., 2008]. Interestingly, GLP-1(9-36)NH_2 did not appear to enhance GSIS despite high concentration (at 1μM) was applied, suggesting it was not insulinotropic (Fig. 4.3A). The observation again concurred with the studies by Bueno and colleagues as well as by our collaborators, where they showed there was a lack of augmentation when GLP-1(9-36)NH_2 were applied to the isolated mouse islets at high glucose condition [Bueno et al., 2020]. Furthermore, GCG, which should expectedly facilitate GSIS as reported previously [Svendsen et al., 2018, Lee and Jun, 2018] given its role in mediating glucose homeostasis, did not further enhance GSIS (Fig. 4.3A). However, a relatively low concentration was applied in these set of experiments therefore a prominent enhancement might not be observed. Yet due to the current lockdown, I was not able to perform insulin secretion experiments to test a higher concentration of GCG.

4.3.3.2 Ligand responses in inducing glucagon secretion

In terms of glucagon secretion in the mouse glucagonoma cell line, the presence of low glucose was able to stimulate a small yet statistically significant increase by 9.9% ($p < 0.01$) in glucagon secretion compared to high glucose condition (Fig. 4.3B), validating the functionality of the mouse glucagonoma cells in response to the changes of glucose stimulations. Given the sensitivity of the glucagon measurement in the pancreatic α cells compared to that in the pancreatic β cells, this small change in glucagon secretion in contrast to the large fold of increase in insulin secretion was considered to be significant, analogous to other published reports which conducted the measurement of glucagon secretion in the mouse α clonal cell systems [Diao et al., 2005, McGirr et al., 2005] and our collaborators in isolated mouse islets. Concurred with other published observations conducted in either isolated human or mouse islets [De Marinis et al., 2010, Ramracheya et al., 2018] and as previously shown in Fig. 4.2, GLP-1 and GLP-1(9-36)NH_2, despite their concentrations at picomolar range, were able to inhibit glucagon secretion by 18.5% ($p < 0.01$) and 26.8% ($p < 0.001$) (Fig. 4.3B). Also, GLP-1 exerted a glucagonostatic effect comparable to that mediated by the presence of 16.7mM glucose alone, and that GLP-1(9-36)NH_2 was able to induce a more prominent glucagonostatic effect than that at 16.7mM glucose inhibition of glucagon secretion, an observation also noted by our collaborators. Corroborated with other published reports, GIP at 10pM facilitated glucagon secretion by 18.0% compared to the sole presence of 5mM glucose (Fig. 4.3B). This glucagon-stimulatory effect mediated by GIP was also demonstrated in

the isolated mouse islets [De Marinis et al., 2010].

To sum up, the extent of the potentiation of GSIS mediated by a range of glucagon-like peptide ligands was illustrated in the rat insulinoma cells. Opposing actions of GLP-1, GLP-1(9-36)NH_2 and GIP on glucagon secretion were also demonstrated in the mouse glucagonoma cell lines. In the next section, the factors that may influence the insulin and glucagon secretion will be presented.

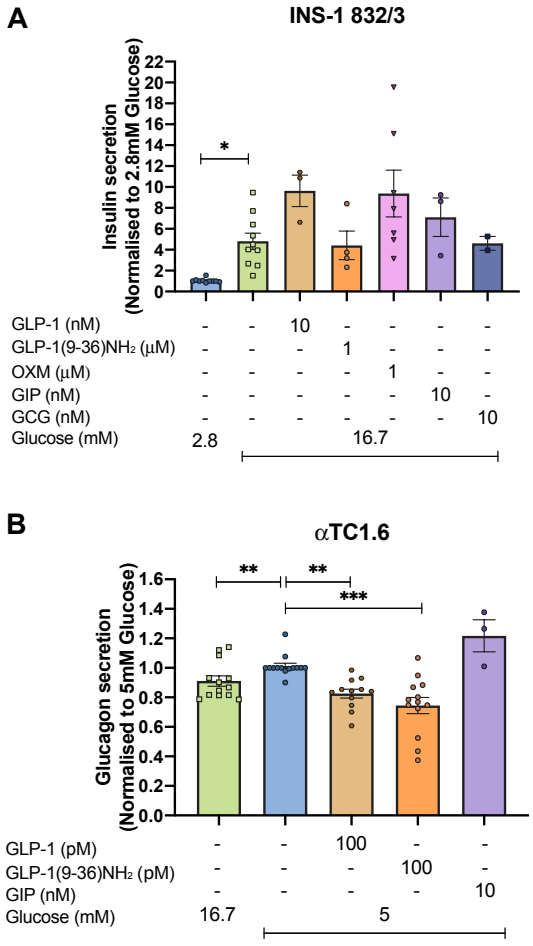

Figure 4.3: **Glucagon receptor family peptide ligands effect on GSIS or glucagon secretion in INS-1 832/3 and αTC1.6 cells.** (A) shows the enhancement of GSIS facilitated by 10nM GLP-1, 1μM GLP-1(9-36)NH_2, 1μM OXM, 10nM GIP and 10nM GCG in high glucose condition (16.7mM). (B) shows the glucagon secretion inhibitory effect exerted by 100pM GLP-1 and 100pM GLP-1(9-36)NH_2 whereas 10nM GIP stimulates glucagon secretion at low glucose condition (5mM glucose). Mean $\pm$ S.E.M. insulin and glucagon secretion data (responses normalised to the GSIS and glucagon secretion responses at 2.8mM and 5mM respectively) in 2 to 13 independent experiments with quadruplicates are shown in the above scatter plots. Statistical significance compared among responses with the mean of 2.8mM or 5mM glucose in insulin or glucagon secretion assays respectively were determined by non-parametric Kruskal-Wallis test and are indicated by asterisks above the bars (*, p<0.05; **, p<0.01; ***, p<0.001)

4.4 Receptor antagonism on insulin and glucagon secretion

4.4.1 GLP-1R or GIPR-knockout effect on insulin secretion

Following the evaluation of individual ligand potentiation on GSIS in the rat β clonal cells, the individual receptor contributions, in particular GLP-1R and GIPR, towards the augmentation of GSIS were next determined, so as to serve as a useful comparison to the individual receptor contributions to the α cell model. To do so, the GLP-1R and GIPR CRISPR/Cas9 knockout INS-1 832/3 cell lines (thereafter referred to as INS-1 GLP-1R KO or INS-1 GIPR KO cell line) [Naylor et al., 2016] were used which were kindly shared by our collaborators, Dr Jacqueline Naylor and Dr David Hornigold at AstraZeneca, U.K, to aid the investigations as there was currently a lack of suitable antagonist for GIPR. There were no morphological discrepancies among the wildtype, GLP-1R and GIPR KO INS-1 832/3 cell lines. The receptors KO rat β cell lines were also cultured in the same media as the wildtype INS-1 832/3 cell line. Insulin secretion assays were again performed as previously described and the results were normalised to the insulin secretion level at 2.8mM glucose in each individual cell line.

The following results showed that all three different cell lines, namely the INS-1 832/3 wildtype, GIPR KO and GLP-1R KO cell lines were able to mediate GSIS in the presence of high glucose, with the extent of GSIS mediated in the wildtype cell line the highest, followed by the GIPR KO cell line and lastly the GLP-1R KO cell line (the potentiation of GSIS were by 480% ($p < 0.0001$), 309% ($p < 0.05$) and 287% respectively) (Fig. 4.4). After showing that the GIPR KO and GLP-1R KO cell lines were able to respond to glucose stimulation despite the lack of either GIPR or GLP-1R, these three different cell lines were then stimulated with a range of glucagon-like peptides at high glucose conditions. Concurred with the previous results (Fig. 4.3A), when 10nM GLP-1 was applied to the wildtype cell line, GSIS was potentiated by 213% compared to the high glucose condition ($p < 0.05$). Similarly, GLP-1 was able to potentiate GSIS in the GIPR KO cell line by 415% compared to the high glucose condition ($p < 0.01$); yet, the larger increment of GSIS at the GIPR KO cell line may be due to the apparent smaller GSIS induced at high glucose setting. GLP-1 was not able to further facilitate GSIS in the GLP-1R KO cell line, implying that GLP-1 required the presence of GLP-1R to mediate its insulinotropic action, and that GIPR and GCGR did not play a role in mediating GLP-1-potentiated GSIS in the rat β cells. Similarly, 10nM Ex-4, which is a close analogue of GLP-1, potentiated GSIS in the wildtype by 152% and in the GIPR

KO cell line by 489%, yet it was not able to augment GSIS in the GLP-1R KO cell line, further illustrating GLP-1R was essential for the insulinotropic action of Ex-4.

On the other hand, GIP at 10nM was able to facilitate GSIS in the wildtype setting, resulting in a 231% increase in insulin secretion compared to when 16.7mM glucose was applied (Fig. 4.4). GIP was also able to augment GSIS in the GLP-1R KO cell line, with its potentiation significantly higher than the stimulation in the wildtype cell line, illustrating GIP did not require GLP-1R in mediating its insulinotropic action. Yet it was not able to enhance GSIS in the GIPR KO cell line, highlighting GIPR was essential for GIP-mediated potentiated GSIS. The observations here concurred with the published report by our collaborators, where they observed the lack of potentiation in GSIS in the absence of GIPR KO when GIP were applied [Naylor et al., 2016]. The results here also further validated the absence of GIPR and GLP-1R in the KO cell lines.

As previously shown in Fig. 4.3A, GLP-1(9-36)NH_2, even when applied at high concentration (1μM), did not potentiate insulin secretion; the GLP-1 metabolite also did not have any augmentative effect in the GIPR KO and GLP-1R KO cell line (Fig. 4.4). OXM, when applied at 1μM, was able to enhance GSIS in the wildtype rat β cells by 458% compared to the high glucose alone ($p < 0.05$), as established in Fig. 4.3A. OXM also increased GSIS by 359% in the GIPR KO cell line, which suggested the OXM insulinotropic action was not mediated via GIPR. Interestingly, when OXM was applied to the GLP-1R KO cell line, a small but statistically significant enhancement of GSIS was observed (increase by 188%, compared to high glucose alone, $p < 0.01$). It is plausible that OXM mediated its insulinotropic action through GCGR as OXM was known to be a dual agonist of both GLP-1R and GCGR [Pocai et al., 2009]. It was previously demonstrated in the cAMP functional assays utilising CHO-GLP-1R and CHO-GCGR cells that OXM was capable of inducing potent cAMP responses at these two structurally homologous receptors (Fig. 3.2) as well as the antagonist assays which showed the action of OXM being partially blocked by the antagonisms of GCGR (Fig. 3.13).

Due to the outbreak of COVID-19, I was not able to include the evaluation of the extent of GCG on the potentiation of insulin secretion in the three different INS-1 cell lines. However, the results of which would serve as a valuable insight for the whole picture of how different incretin hormones initiate their insulinotropic actions. Following the characterisation of individual receptor contribution towards the potentiation of GSIS in the rat β cells, the input of GLP-1R and GCGR on the pancreatic α cells was next explored.

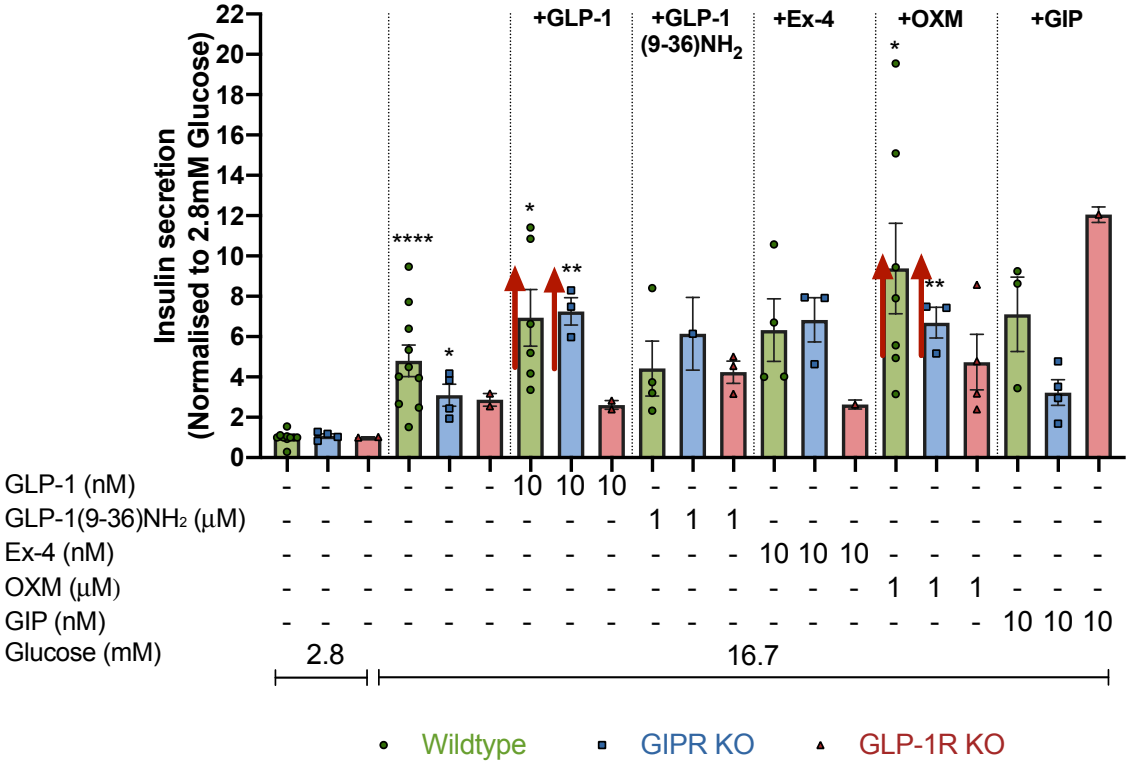

Figure 4.4: **The effects of GLP-1R KO or GIPR KO on glucagon-like peptide ligands facilitation of GSIS in INS-1 832/3 cell lines.** Mean ± S.E.M. insulin secretion data (responses normalised to the insulin secretion response at 2.8mM) in 1-10 independent experiments with quadruplicates are shown in the above scatter plots. Only preliminary results for some of the experiments conducted in the GLP-1R KO cell line are presented due to COVID-19 obstruction of experimental schedule. Statistical significance compared among peptide ligand responses in three different INS-1 832/3 cell lines were determined by non-parametric Kruskal-Wallis test and are indicated by asterisks above the bars (*, $p<0.05$; **, $p<0.01$; ****, $p<0.0001$).

4.4.2 GLP-1R or GCGR antagonism on glucagon secretion

After evaluating the extent of insulin secretion in the GLP-1R KO or GIPR KO rat β cells and proving the importance of GLP-1R in mediating the insulinotropic action by GLP-1, it is of particular interest to deduce the individual receptor contribution towards glucagon secretion in the mouse α cells. However, GLP-1R CRISPR/Cas9 KO mouse αTC1.6 cell line was not readily available and that conducting glucagon secretion in the InR1G9 cells, which lack endogenously expressed GLP-1R, was proven to be technologically challenging due to their weaker glucagon secretion response [Powers et al., 1990]. Furthermore, it has been noted by our collaborators that GCGR ablation in mouse was not experimentally feasible as it led to marked α-cell hyperplasia as well as failure to respond to elevated glucose. Therefore, GLP-1R specific peptide antagonist, Ex-9, and GCGR specific small molecule antagonist, L-168,049, were utilised to aid the following investigations. Here the mouse α cells were pre-incubated in high glucose (16.7mM) containing KRB for an hour, followed by pre-incubation of receptor specific antagonists (1μM Ex-9, 1μM L-168,049 or a combination of both) for 30 mins, and lastly incubated with GLP-1 or GLP-1(9-36)NH_2 in the presence of the antagonists for an hour; the DMSO content were equal across all conditions. The glucagon levels were then quantitatively measured. The concentrations of antagonists applied here aligned with the doses commonly used in the investigation of the effect of receptor antagonism on glucagon secretion [De Marinis et al., 2010, Ramracheya et al., 2018, Guida et al., 2020].

The following preliminary results showed that glucagon secretion was promoted in the presence of low glucose by 14.8% compared to the presence of high glucose, again validating the functionality of the mouse α cells in responding to glucose stimulation (Fig. 4.5). Furthermore, the presence of 1μM Ex-9 or 1μM L-168,049 alone did not affect glucagon secretion in the presence of 5mM glucose, illustrating these two antagonists did not interfere with glucagon secretion in the mouse α cells, which also agreed with the observations by our collaborators who applied L-168,049 or Ex-9 in isolated mouse islets [De Marinis et al., 2010, Guida et al., 2020]. Similar to the previous observations in Fig. 4.2B, 100pM GLP-1 or GLP-1(9-36)NH_2 suppressed glucagon secretion in low glucose condition by 13.2% or 18.9% respectively, reversing the glucagon secretion level to the same level as at 16.7mM glucose (Fig. 4.5). However, when 1μM Ex-9 was applied together with GLP-1 or GLP-1(9-36)NH_2, the GLP-1 or GLP-1(9-36)NH_2-mediated glucagon inhibition was reversed, resulting in a higher glucagon level that

was on par or higher than that due to the 5mM glucose stimulation, suggesting GLP-1R was essential for their glucagonostatic actions (Fig. 4.5).

On the other hand, when 1μM L-168,049 was applied together with GLP-1 or GLP-1(9-36)NH_2, similar reversal actions of the inhibition of glucagon secretion were observed. It also implied that GCGR was essential for mediating the glucagon inhibition in the α cells (Fig. 4.5). Interestingly, when 1μM Ex-9 and 1μM L-168,049 were both co-stimulated with either GLP-1 or GLP-1(9-36)NH_2, reversal effect were once again observed, which resulted in an even greater glucagon secretion increase by 36.1% and 50.0% compared to when GLP-1 and GLP-1(9-36)NH_2 alone (Fig. 4.5). The significance of this finding will be further discussed in later section.

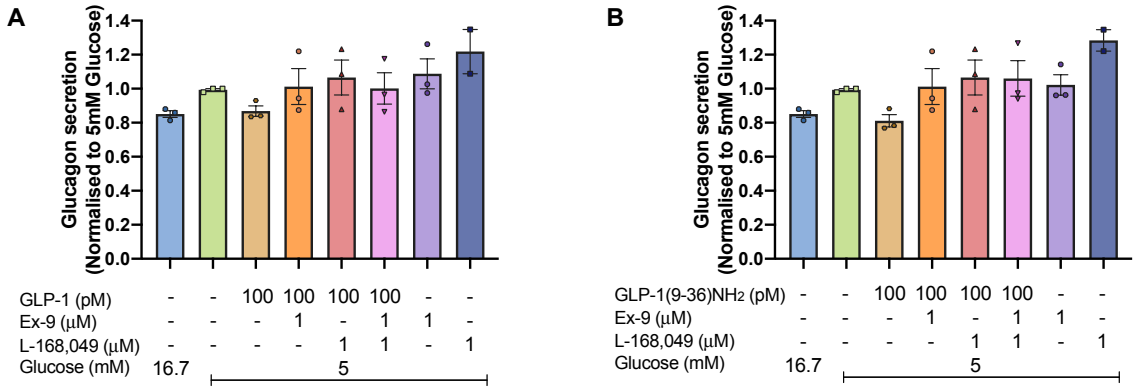

Figure 4.5: **The extent of glucose-dependent glucagon secretion mediated by GLP-1 and GLP-1(9-36)NH_2 in the presence of GLP-1R and GCGR antagonists, Ex-9 and L-168,049, in mouse αTC1.6 cells.** The above figures show the extent of glucagon secretion when the αTC1.6 cells were pre-treated with GLP-1R and GCGR antagonists, Ex-9 and/or L-168,049 respectively, 30 minutes before co-stimulating with (A) GLP-1 and (B) GLP-1(9-36)NH_2 at low glucose condition (5mM glucose) for an hour. Mean $\pm$ S.E.M. glucagon secretion data (responses normalised to the glucagon secretion response at 5mM) in at least 2 independent experiments with quadruplicates were shown in the above scatter plots. Statistical significance compared with or without GLP-1R and GCGR antagonists in the presence of GLP-1 or GLP-1(9-36)NH_2 were determined by non-parametric Kruskal-Wallis test and are all non-statistically significant.

4.5 Pharmacological inhibition of the effect of insulin or glucagon secretion

After determining the individual receptor contributions towards insulin and glucagon secretion in rat insulinoma and mouse glucagonoma cells, the application of various pharmacological inhibitors to further dissect the importance of individual signal transduction pathway in mediating insulin and glucagon secretion was next attempted. However, due to the outbreak of COVID-19, I was not able to complete the thorough evaluation of individual intracellular signal transduction pathway mediated by each individual glucagon-like peptide. Therefore, preliminary findings on the effect of pharmacological blockage only on GLP-1-mediated GSIS were reported.

As consistent with the findings presented in previous chapter, together with many other published studies, GLP-1R is capable of not only couple to $G\alpha_s$ proteins, but also the possibility of activating $G\alpha_i$ proteins, therefore promoting or inhibiting adenylyl cyclase to increase or reduce the production of cAMP. It was also shown that GLP-1R can also activate the $G\alpha_{q/11}$ protein (Fig. 3.6), further activating the PLC/DAG/IP_3 pathway to facilitate iCa^{2+} release, mediating insulin exocytosis process [Shigeto et al., 2015]. Furthermore, when the intracellular cAMP level is increased, PKA pathway is activated, therefore enhancing the activity of the K_{ATP} channel, mediating insulin secretion via membrane depolarization. The importance of EPAC1/2 signalling pathway in mediating GLP-1 potentiated GSIS was acknowledged. However, due to the time constraints, I was not able to perform the investigations towards the EPAC signalling pathway on GLP-1 potentiated GSIS. Therefore, in order to deduce individual pathway contribution towards GLP-1-potentiated GSIS, forskolin (direct adenylyl cyclase activator) [Seamon et al., 1981], pertussis toxin (PTX) (irreversible $G\alpha_i$ protein ADP-ribosylator) [Katada and Ui, 1982], YM-254,890 (selective $G\alpha_{q/11}$ inhibitor) [Takasaki et al., 2004] as well as 8-Br-Rp-cAMP (PKA-inhibitor) [Gjertsen et al., 1995] were applied into the rat insulinoma cells, in an attempt to understand the blockage of specific downstream signalling pathway on the effect of GSIS. Given that the α and β clonal cell lines were only incubated with these pathway inhibitors for a short period of time (i.e two hours), their effects on cell viability and proliferation were assumed to be minimal [Vivot et al., 2016]. Unfortunately, the effect of PTX on α and β clonal cell proliferation has not yet been investigated. However, there were studies suggesting blocking $G\alpha_{i/o}$ signalling increased β cell mass in mice [Berger et al., 2015]. Hence it was assumed that the α and β clonal cells were viable for insulin and glucagon secretion

assays despite having received overnight PTX treatment.

4.5.1 Effects on insulin secretion

In order to demonstrate that the activation of Gα_s pathway would lead to an increase in insulin secretion in rat β cells, forskolin, which is a direct adenylyl cyclase activator, thereby promoting the production of intracellular cAMP levels, was applied to the rat β cells. Here three different concentrations of forskolin (1μM, 0.01μM and 0.0001μM) were applied in order to deduce if concentration-dependent effect exists in the cAMP activation pathway on insulin secretion. The extent of forskolin potentiated GSIS was then compared with that mediated by GLP-1 at 10nM.

Similar to previous observations (Fig. 4.1), insulin secretion was further enhanced in the presence of high glucose by 615%, proving the functionality of the rat insulinoma cells (Fig. 4.6A). Furthermore, the addition of 10nM GLP-1 further potentiated the GSIS at high glucose by 169%, agreeing with the previous observations (Fig. 4.3 and 4.4). Notably, forskolin induced a dose-dependent increase of GSIS, whereby the higher the forskolin concentrations applied, the greater the potentiation of GSIS was (262% and 165% increases in GSIS when 1μM and 0.01μM forskolin were applied), further illustrating the importance of the activation of Gα_s pathway in mediating insulin secretion (Fig. 4.6A). Also, similar level of potentiation of insulin secretion between 10nM GLP-1 and the low concentration of 0.01μM forskolin was noted, further illustrating GLP-1 did not require a high level of Gα_s activation to promote potent potentiation of insulin secretion.

On the other hand, the activation of Gα_i pathway influences the ultimate cAMP production level as the activation of Gα_i pathway leads to an inhibition of the adenylyl cyclase, therefore resulting in a lower level of cAMP production. To investigate the influence of Gα_i pathway on insulin secretion, the INS-1 832/3 wildtype cells were pre-treated with 200ng/μl PTX 16 hours prior to assays. PTX works by irreversibly ADP-ribosylating the Gα_i protein, thereby uncoupling receptor-mediated Gα_i-dependent cAMP inhibition [Katada and Ui, 1982]. The rat insulinoma cells were then stimulated with GLP-1 at 10nM for one hour and insulin level was determined. Interestingly, the PTX-pre-treated rat β cells did not show any statistically significant insulin secretion changes compared to that with 10nM GLP-1 (Fig. 4.6B). However, an experimental flaw, which was the lack of positive control of the PTX effect in the presence of high glucose precluded the authenticity of such observation. Hence the results here were only of preliminary nature.

The effect of PKA pathway inhibition on the potentiation of GSIS mediated by GLP-1 was next investigated. Upon pre-treating the rat β cells with the PKA inhibitor, 0.1mM 8-Rp-Br-cAMP for 30 mins prior to one hour co-stimulation with 10nM GLP-1, no changes in GSIS in the presence of high glucose was observed, which concurred with the observations from other published papers which showed that the application of PKA inhibitor (myr-PKI) alone in high glucose condition in mouse islets did not affect GSIS [Shigeto et al., 2015]. The potentiation of GSIS mediated by GLP-1 in the presence of PKA inhibition (245%, when compared to high glucose alone) was higher compared to that with GLP-1 stimulation only (by 158%, when compared to high glucose alone) (Fig. 4.6C), which did not concur with the notion that PKA inhibition would lead to the partial inhibition of GSIS mediated by GLP-1 as supported by other published reports [Shigeto et al., 2015, Khajavi et al., 2018]. However, it is plausible that alternative EPAC1/2 pathway was further potentiated, therefore compensating the blockage of PKA pathway.

Lastly, the effect of $G\alpha_q$ pathway blockage on the effect of GSIS was investigated. The rat β cells were pre-treated with 0.1μM YM-254,890 30 mins prior to co-stimulating with 10nM GLP-1 for an hour. Here when the rat β cells were pre-treated with the $G\alpha_{q/11}$ inhibitor, GSIS in the presence of high glucose was decreased by 225% (Fig. 4.6D). When the rat β cells were stimulated with 10nM GLP-1 in the presence of the $G\alpha_{q/11}$ inhibitor, no changes in the insulin secretion were observed, yet this may be attributed to the mixed population of resultant extent of insulin secretion and can be improved by performing more experimental repeats. Given that GLP-1R is known to be capable of activating $G\alpha_q$ protein and that $G\alpha_q$ and especially $G\alpha_{11}$ proteins were highly expressed in the INS-1 832/3 cells (Fig. 3.9), it was expected to see that the insulin secretion in β cells would be decreased considering the intracellular iCa^{2+} release pathway is instrumental to insulin secretion [Seino, 2012].

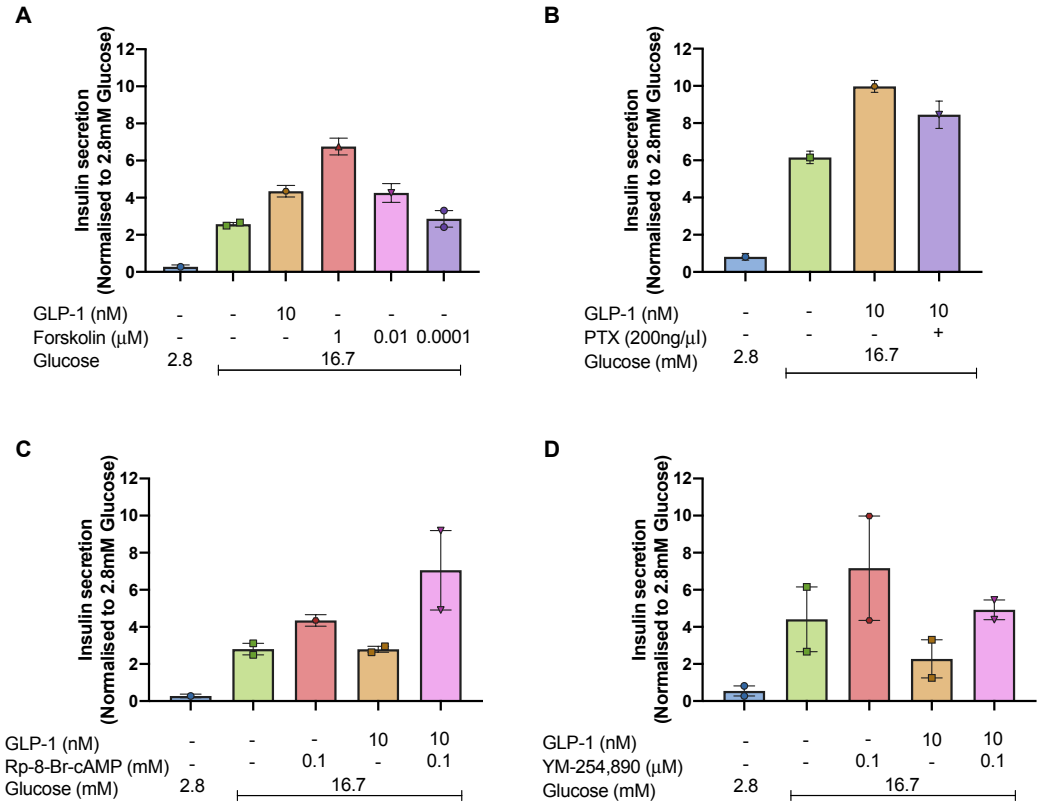

Figure 4.6: **The extent of GSIS enhanced by GLP-1 in the presence of pharmacological pathway inhibitors PTX, YM-254,890 and Rp-8-Br-cAMP and adenylyl cyclase activator forskolin in INS-1 832/3 WT cells.** (A) shows the facilitation of GSIS when the rat insulinoma cells were stimulated at different concentrations of the adenylyl cyclase activator, forskolin, at 1μM, 10nM and 0.1nM. (B) shows the extent of GSIS when INS-1 832/3 WT cells were pre-treated with PTX for 16 hours prior to assay. (C) shows the enhancement of GSIS when cells were pre-treated with the PKA inhibitor, Rp-8-Br-cAMP at 0.1μM, 30 minutes, before co-stimulating with GLP-1 at high glucose condition. (D) shows the inhibition of GSIS when the rat β cells were pre-treated with the G$\alpha_{q/11}$ inhibitor 0.1μM YM-254,890 30 minutes before stimulating with high glucose and/or GLP-1. Mean $\pm$ S.E.M. insulin secretion data (responses normalised to the insulin secretion response at 2.8mM) in an independent experiments with quadruplicates are shown in the above scatter plots.

4.5.2 Effects on glucagon secretion

Similar to the previous experimental approach in dissecting the individual pathway contributions to the potentiation of GSIS mediated by GLP-1 in the rat β cells, pathway inhibitors, namely PTX and YM-254,890, were also applied to the mouse αTC1.6 cells, in an attempt to provide preliminary insights towards the mechanisms of how glucagon secretion is affected by the blockage of Gα_i and Gα_q signalling pathway.

The mouse α cells were pre-treated with 200ng/μl PTX for 16 hours prior to being stimulated with 100pM GLP-1 or GLP-1(9-36)NH_2. Similar to the previous observations, the stimulation of the mouse α cells with either GLP-1 or GLP-1(9-36)NH_2 led to the suppression of GCG secretion by 7.88% and 13.8% respectively (Fig. 4.7A). However, by inhibiting the Gα_i protein, the glucagon secretion inhibitory effect mediated by both GLP-1 or GLP-1(9-36)NH_2 was reversed; glucagon secretion mediated by GLP-1 and GLP-1(9-36)NH_2 after PTX pre-treatment were enhanced to a level that were similar to that by the 5mM glucose stimuli (Fig. 4.7A). Yet, an important control of pre-treating the α cells with PTX at 5mM glucose was missing in this set of experiment, therefore precluding the validity of the results.

Likewise, the mouse α clonal cells were also pre-treated with the G$\alpha_{q/11}$ inhibitor, YM-254,890 at 0.1μM, for 30 mins prior to co-stimulating with GLP-1 and GLP-1(9-36)NH_2 for an hour. Notably, when YM-254,890 was applied in the presence of low glucose only, it did not affect the basal glucagon secretion level (Fig. 4.7B), which differed from the observations in the rat insulinoma cells, wherein the application of YM-254,890 in the presence of high glucose would reduce the basal insulin secretion (Fig. 4.6D). Similarly, GLP-1 and GLP-1(9-36)NH_2 demonstrated glucagonostatic effect in the presence of low glucose stimulation, by suppressing glucagon secretion by 20.2% and 36.8% when compared to the low glucose stimulation alone, proving the functionality of the mouse αTC1.6 cells (Fig. 4.7B). Yet, when either GLP-1 or GLP-1(9-36)NH_2 was applied in the presence of YM-254,890, the inhibitory effect mediated by GLP-1 or GLP-1(9-36)NH_2 was reversed, with the glucagon secretion level reverted back to the level which was similar to the 5mM glucose stimulation (for the case of GLP-1) or to a much greater extent than the 5mM glucose stimulation alone (for the case of GLP-1(9-36)NH_2) (Fig. 4.7B). These series of experiments implied the importance of Gα_q activation in regulating glucagon secretion in the α cells, which will be discussed in later section.

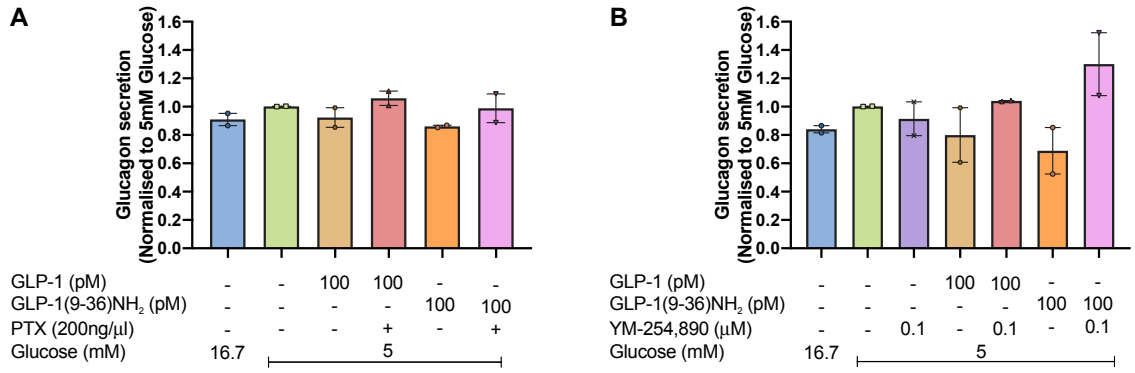

Figure 4.7: **The extent of glucagon secretion mediated by GLP-1 and GLP-1(9-36)NH_2 in the presence of pharmacological inhibitors PTX and YM-254,890 in αTC1.6 cells.** (A) shows the extent of glucagon secretion when αTC1.6 cells were pre-incubated overnight with PTX, irreversibly uncoupling receptor-mediated $G\alpha_i$-dependent cAMP inhibition. (B) shows the extent of glucagon secretion when the cells were pre-treated with the $G\alpha_{q/11}$ protein inhibitor 0.1μM YM-254,890 30 minutes before applying peptide ligands. Mean $\pm$ S.E.M. glucagon secretion data (responses normalised to the glucagon secretion response at 5mM) in 2 independent experiments with quadruplicates are shown in the above scatter plots. Results of 2 independent experiments are shown here due to COVID-19 obstruction of experimental schedule.

4.6 Discussion

In this chapter, the insulin and glucagon secretion assaying technique, which are relatively novel to the Ladds' laboratory, were optimised and were subsequently utilised to facilitate the investigations towards how GLP-1, and other glucagon-like peptides, promote GSIS. The glucagonostatic actions of GLP-1 and its metabolite were also of particular focus in this chapter. With the newly established technique, GLP-1R and GCGR-specific antagonists and pharmacological inhibitors were employed to investigate the importance of individual receptor contribution and downstream signalling on insulin and glucagon secretion. The significance of the findings will be discussed as follows.

4.6.1 Glucagon secretion is regulated by a tight balance of cAMP production

GLP-1 has been shown to induce a dose-dependent augmentation of GSIS in isolated mouse islets, presumably attributable to the increment of cAMP production upon receptor activation via the $G\alpha_s$ pathway [Shigeto et al., 2015]. Yet in the pancreatic α cells, a reverse trend was observed: a high concentration of GLP-1 (10000pM) led to a stimulation of glucagon secretion (Fig. 4.2), while at the optimally low concentration (i.e. 100pM), maximal inhibition was observed; the glucagonostatic effect was once again revered when an even lower GLP-1 concentration (1pM) was applied. Although a smaller decrement of GLP-1 concentrations should have been used in this set of experiment, here with the use of three concentrations that spanned across 1pM to 10000pM, the lack of dose-dependency of GLP-1 suppression of glucagon secretion was observed. Similar findings were also noted by our collaborators using isolated mouse islets [Guida et al., 2020]. This observation suggests a lack of dose-dependent relationship of GLP-1 inhibition of glucagon secretion, unlike the concentration-dependent effect of GLP-1 on insulin secretion. Interestingly, the application of a range of forskolin (0.1-10000nM) to the mouse islets also mimicked the non-linear relationship observed in the relationship between GLP-1 concentrations and glucagon secretion [De Marinis et al., 2010]. The authors attributed the phenomenon to the sensitivity of the α cells towards cAMP activation, that a high level of cAMP production would in turn stimulate the release of glucagon secretion, activating the type II PKA and EPAC pathway. On the other hand, only a small range of intracellular cAMP level is needed to activate the type I PKA pathway, which is responsible for the inhibition of glucagon release [De Marinis

et al., 2010], thereby explaining why GLP-1 and GLP-1(9-36)NH_2 at picomolar range appear to be more glucagonostatic than when applied at nanomolar range (Fig. 4.2). Furthermore, other studies have shown that although Ca^{2+} is an important player in inducing exocytosis of glucagon containing vesicles, it only plays a permissive role in mediating exocytosis as the magnitude of exocytosis is predominantly regulated by cAMP [Tengholm and Gylfe, 2017, Yu et al., 2019]. Also, total plasma GLP-1 levels range between 10-50 pM of which only less than 20% is attributed to GLP-1 [Holst, 2007], which coincides with the extremely low concentration needed to inhibit glucagon secretion (Fig. 4.2). Therefore, it is postulated that glucagon secretion may be under strong tonic inhibition by low picomolar range circulating GLP-1 or GLP-1(9-36)NH_2 [Guida et al., 2020]. This tonic inhibition may be mediated by the GLP-1 activation of the extremely low level of GLP-1R, producing a much lower level of cAMP, yet sufficient for the inhibitory action of glucagon secretion.

Contrary to GLP-1, GIP stimulates glucagon secretion (Fig. 4.3). Given that the GIPR had a higher expression of 5-fold difference compared to that of GLP-1R in the mouse αTC1.6 cells (Fig. 3.7) and it was previously shown in Fig. 3.2 that GIP selectively activated GIPR, the glucagon-stimulatory effect observed was likely to be attributed to the GIPR. As previously discussed, only a small range of intracellular cAMP production is needed to suppress glucagon secretion [De Marinis et al., 2010]. Therefore, the apparent GIP stimulatory effect glucagon secretion can be explained by the fact that GIP activates the highly abundant $G\alpha_s$-coupled GIPR in the mouse α cells, thereby produces a higher level of cAMP, leading to the stimulation of glucagon secretion. In fact, the higher level of cAMP produced by GIP compared to that of GLP-1 in the mouse glucagonoma has been shown in Fig. 3.10 (pEC_{50} of GIP and GLP-1 were 7.54 $\pm$ 0.29 and 6.85 $\pm$ 0.22 respectively). It again suggests the importance of maintaining the tight cAMP production balance in the regulation of glucagon secretion, as a slight deviation of cAMP levels leads to differences in the physiological outcome.

4.6.2 Direct involvement of GLP-1R and GCGR in inhibiting glucagon secretion

GLP-1 requires GLP-1R to mediate its insulinotropic action, which was demonstrated in Fig. 4.4, as GLP-1 could not further enhance GSIS in the INS-1 GLP-1R KO cell line. The results here also agreed with the observation by our collaborators who created the CRISPR-KO cell lines [Naylor et al., 2016] as well as agreeing with Shigeto and colleagues who utilised both isolated human and mouse islets with the application

of GLP-1R specific antagonist, Ex-9, and showed that antagonism of GLP-1R did not lead to GLP-1-potentiated GSIS [Shigeto et al., 2015]. The results also concurred with the previous observation in Fig. 3.14, whereby the extent of cAMP accumulation mediated by GLP-1 in the presence of the GCGR specific antagonist, L-168,049, was not affected in the INS-1 832/3 WT cells, suggesting GCGR was not critical in mediating GLP-1-potentiated GSIS.

Similar to its insulinotropic action via GLP-1R, GLP-1, as well as its metabolite GLP-1(9-36)NH_2, required GLP-1R to mediate their glucagonostatic action, as the presence of the specific GLP-1R antagonist reversed their glucagonostatic actions (Fig. 4.5). The results here agreed with the previous reports by our collaborators where they also applied 1μM Ex-9 together with GLP-1 in the isolated mouse and human islets and observed a reversal in GLP-1 inhibitory effect on the glucagon secretion [De Marinis et al., 2010, Ramracheya et al., 2018]. Interestingly, the results here showed that GLP-1(9-36)NH_2 also required GLP-1R to mediate its glucagon-inhibitory action, which were different from that observed by our collaborators. In their studies, they applied GLP-1(9-36)NH_2 to the isolated GLP-1R-knock out mouse islets and showed that GLP-1(9-36)NH_2 was still able to inhibit glucagon secretion despite the lack of GLP-1R [Guida et al., 2020]. However, they acknowledged the fact that genetically knockout mice might not be sufficient in evaluating the influence of receptor antagonism on glucagon secretion. They suggested that it would be more appropriate to both apply antagonists and genetically knockout receptors of interest in order to deduce the true effect of individual receptor contribution on glucagon secretion [Guida et al., 2020]. Nonetheless, there is a universal agreement that the low expression level of GLP-1R in the pancreatic α cells are directly involved in mediating GLP-1 glucagonostatic action.

Interestingly, GLP-1, together with its metabolite, can also mediate their glucagonostatic actions via GCGR (Fig. 4.5). The findings here also corroborated with the results from our collaborators, which they demonstrated that both GLP-1 and GLP-1(9-36)NH_2 could no longer mediate their glucagonostatic actions in the presence of L-168,049 mediated GCGR antagonism [Guida et al., 2020] as well as other studies using des-His^1-Glu^9-Glucagon [Ma et al., 2005]. In fact, according to the results shown in Fig. 3.2, GLP-1 and GLP-1(9-36)NH_2 mediated their partial agonism at the GCGR, resulting in cAMP production despite at very low potencies. Furthermore, coupled with RAMP2, GLP-1(9-36)NH_2 potency was enhanced by more than 10-fold (Fig. 3.16). Yet the physiological significance of RAMP2 on GLP-1(9-36)NH_2 suppression of glucagon secretion was not explored and will be served as an important piece of future work.

Also, both GLP-1 and GLP-1(9-36)NH_2 agonistic action in enhancing cAMP production can be blocked by L-168,049 (Fig. 3.13), substantiating the notion that both GLP-1 and GLP-1(9-36)NH_2 may act through GCGR in the mouse α cells to mediate their glucagonostatic action.

More intriguingly, the antagonism of both receptors led to an even greater increase in glucagon secretion (Fig. 4.5), further suggesting the co-presence of these two receptors was crucial for the inhibitory actions of both GLP-1 and GLP-1(9-36)NH_2, presumably via the tight control of cAMP levels upon receptor activation as discussed previously. The above findings pose further question if crosstalk exists between GLP-1R and GCGR in the pancreatic α cells [Roed et al., 2015]. According to the studies which co-expressed GLP-1R and GCGR in recombinant cell systems, the authors suggested that the GLP-1R and GCGR co-expression did not affect cAMP signalling, but only reduced iCa^{2+} release and pERK1/2 signals at the GLP-1R [Roed et al., 2015]. Given that iCa^{2+} release also plays a role, despite a permissive one, in the regulation of glucagon secretion (Fig. 4.7; which will be discussed below), it may be possible that the crosstalk between GLP-1R and GCGR which regulates the iCa^{2+} release may be crucial to the GLP-1 and GLP-1(9-36)NH_2 glucagonostatic action. However, more studies, such as applying specific inhibitors that target Ca^{2+} signalling, are needed to investigate such hypothesis.

4.6.3 $G\alpha_q$ and $G\alpha_i$ subunits: key players of GLP-1 glucagonostatic action?

While the blockage of $G\alpha_i$ activation in the rat β clonal cell system did not appear to have any influence on insulin secretion (Fig. 4.6), the inhibition of $G\alpha_i$ activation was found to reverse the glucagonostatic actions mediated by GLP-1 and GLP-1(9-36)NH_2 (Fig. 4.7). In fact, our collaborators have also shown similar observations, however they noted that only the GLP-1(9-36)NH_2-mediated glucagon inhibitory effect was sensitive to the $G\alpha_i$ inhibition while the GLP-1 suppression on glucagon secretion was not affected in the mouse isolated islets [Guida et al., 2020]. Yet, the utilisation of a pure population of mouse clonal α cell systems here confers distinct advantage in observing specific effect on a particular pancreatic cell forms, as opposed to using isolated mouse islets, as a mixed population of pancreatic cell components are present in the isolated mouse islets. Therefore, the findings here may reflect the true $G\alpha_i$-inhibited effect on the GLP-1 and GLP-1(9-36)NH_2 glucagonostatic effect. Furthermore, given the role of $G\alpha_i$ in inhibiting adenylyl cyclase, thereby reducing the level of intracellular cAMP produced, the results here also imply that the $G\alpha_i$ signalling pathway are critical for the tight regulation of intracellular cAMP level; a slight disturbance of the system may

lead to the stimulation of glucagon secretion.

Intriguingly, the blockage of $G\alpha_q$ pathway with the use of YM-254,890 reversed the glucagonostatic action of GLP-1 and to an even greater extent for GLP-1(9-36)NH_2 (Fig. 4.7), which contrasted with a recent study utilising the human pseudoislets systems expressing the designer receptors exclusively activated by designer drugs (DREADDs) hM4Di or hM3Dq to investigate $G\alpha_i$ and $G\alpha_q$ signalling on insulin and glucagon secretion [Walker et al., 2020]. In their studies, the authors showed that the $G\alpha_q$ activation robustly stimulated glucagon secretion under low glucose condition, in contrast to the inconclusive stimulatory or inhibitory effect on GSIS [Walker et al., 2020]. However, given the fact that GIPR has been shown to pleiotropically couple to $G\alpha_q$, it may suggest GIPR may stimulate glucagon secretion via $G\alpha_q$ activation, and indeed GIPR has been shown to pleiotropically couple to $G\alpha_q$ [Harris et al., 2017]. While the contrasting glucagon secretion inhibitory action mediated by GLP-1 and GLP-1(9-36)NH_2 may be due to the outcome of $G\alpha_s$ and $G\alpha_i$ activation. However, more studies are needed to explore such linkage between the two pathways in mediating glucagon secretion.

Given the time constraints, I was not able to further investigate the role of PKA activation on the GLP-1(9-36)NH_2-mediated glucagonostatic action. It would be of significant interest to investigate the role of PKA activation in glucagon secretion as our collaborators suggested a differential impact of PKA activation on GLP-1 and GLP-1(9-36)NH_2 inhibition of the glucagon secretion in isolated mouse islets [De Marinis et al., 2010, Ramracheya et al., 2018, Guida et al., 2020].

4.7 Chapter summary

In this chapter, the optimisation of the insulin and glucagon secretion assays was first described. They served as invaluable tools towards the understanding insulin and glucagon secretion molecular mechanism as well as for compound screening, which will be described in the next chapter. Key aspects that are crucial to the regulation of insulin and glucagon secretion are highlighted as follows:

- Insulin secretion is glucose-dependent. On the other hand, glucagon secretion is inversely correlated to the glucose level, during which the lower the glucose applied, the higher the glucagon secretion is. However, paradoxical glucagon secretion exists at very high glucose level (i.e. above 25mM), which also agreed with other published reports.
- A range of glucagon-like peptides, namely GLP-1, OXM, Ex-4, GCG and GIP are able to potentiate GSIS in the rat β cells. GLP-1(9-36)NH_2 is the exception.
- In terms of glucagon secretion, GLP-1 and GLP-1(9-36)NH_2 at picomolar range mediate potent glucagon secretion inhibitory effect in the mouse α cells compared to when nanomolar concentration of peptide ligands are applied. On the other hand, GIP potentiates glucagon secretion in the mouse α cells.
- GLP-1 and Ex-4 require GLP-1R activation to mediate the potentiation of GSIS, as both peptide ligands do not potentiate GSIS in GLP-1R KO INS-1 cell line. Likewise, GIP requires GIPR to augment GSIS. OXM requires both GLP-1R and GCGR to potentiate GSIS.
- GLP-1 and GLP-1(9-36)NH_2 require both the GLP-1R and GCGR to mediate their glucagonostatic actions in the mouse α cells, as the blockage of either one of the receptors with the use of antagonists reverses their suppressive actions on glucagon secretion.
- 0.01μM forskolin potentiates GSIS as a similar level to 10nM GLP-1 in the rat β cells. PTX, YM-254,890 and PKA inhibitor does not influence the insulin secretion in β cells, however further studies are needed.
- PTX and YM-254,890 inhibitions lead to the reversal action of GLP-1 and GLP-1(9-36)NH_2 in the mouse α cells, illustrating the importance of these two pathways in regulating glucagon secretion in the α cells.

Chapter 5

Identification and characterisation of GLP-1R small molecule positive allosteric modulators

5.1 Introduction

GLP-1-based therapies, such as the injectable-based exenatide (Ex-4) and liraglutide, as well as the newly developed orally-administered semaglutide [Thethi et al., 2020], have been increasingly used as T2DM treatments in recent years due to their clinically proven efficacy in reducing blood glucose level as well as the reported beneficial weight loss effect in obese T2DM patients [Drucker, 2018]. However, given that most of these extortionate GLP-1-based drug treatments are injection-based, patient compliance is significantly hindered [Defronzo et al., 2015]. Also, immense costs are incurred in producing peptide-based drugs, therefore prompting the need to develop small molecule drugs. Furthermore, despite their proven clinical efficacy, side effects, such as pancreatitis, nausea and vomiting, are intolerable to certain patient groups, urging the need to improve existing GLP-1-based treatments [Harris and McCarty, 2015]. Therefore, alternative GLP-1-targeted T2DM treatments are prompted, leading to the search for small molecule agonists or positive allosteric modulators (PAM) that target GLP-1 cognate receptor, GLP-1R, in an attempt to not only potentially improve the clinical tolerance profile of the existing GLP-1-based T2DM treatments, but also reduce the cost of the peptide-based therapies.

A series of novel quinoxaline-based GLP-1R small molecule PAMs which enhance

GLP-1(9-36)NH_2-mediated cAMP responses were identified during my MPhil project, supervised by Dr Graham Ladds [Yeung et al., 2016]. Compound 249, in particular, potentiates OXM-mediated cAMP responses in CHO-GLP-1R cells (Appendix B.1). OXM, as shown in Fig. 3.2 and 3.6, is a dual full agonist at both GLP-1R and GCGR; it is proposed to be a novel drug target for both obesity and T2DM treatments [Holst et al., 2018]. Given the distinct potentiation of the OXM-mediated cAMP responses demonstrated by compound 249, further pharmacological validations of this small molecule were conducted using the HEK293S-GLP-1R-WT cell line as part of my PhD work. Following the validation of the pharmacological properties of compound 249, its potential augmentation of GSIS were tested in the rat clonal pancreatic β cell line as well as in *ex vivo* isolated mouse islets, using the insulin secretion assaying technique established in Section A.1.

Furthermore, given the unique profile of compound 249, a series of compound 249-derived analogues were designed by our collaborator, Dr Taufiq Rahman (Department of Pharmacology, University of Cambridge), in order to further explore the structure-activity-relationship (SAR) among compound 249, as the lead pharmacophore, and its analogues. A further series of analogues were also identified via ligand-based virtual screening using compound 249 as the bait by Miss Kathleen Bowman (Department of Pharmacology, University of Cambridge); the biological screenings of which will also be presented in this chapter. Apart from the compound 249 analogues, another series of compounds, which were based on the reported central nervous system penetrant GLP-1R PAM, VU0453379 (also known as S-9b) [Morris et al., 2014], as well as another series which were designed to mimic the structure of GLP-1, were also designed by Dr Taufiq Rahman. Given their lack of intrinsic GLP-1R agonism and allosterism, the results of which will not be reported but are available in the Appendix B.2 and B.3. Unfortunately, due to COVID-19 obstruction of experimental schedule, some of the results presented in this chapter are of preliminary nature only, and are noted accordingly. First, the screening of compound 249 in various class B GPCRs will be discussed.

5.2 Class B GPCR screening

5.2.1 Screening of compound 249 agonism against other Class B GPCRs

It was established in my MPhil work that compound 249 does not possess intrinsic GLP-1R agonism. However, its intrinsic agonism on other structurally related class B GPCRs has not been investigated. Hence to deduce if compound 249 activates other class B GPCRs, plasmids encoding GLP-1R, glucagon-like peptide 2 receptor (GLP-2R), calcitonin receptor (CTR), growth-hormone-releasing hormone receptor (GHRHR), corticotropin-releasing hormone receptor 1 (CRF1) and corticotropin-releasing hormone receptor 2 (CRF2) were transfected into HEK293S cells at a 1:1 receptor-to-vector ratio; the transfection of calcitonin-like receptor (CLR) and RAMP1 at a 1:1 ratio were included. The determination of compound 249 agonism at GCGR and GIPR was not included in this screen but will be discussed in later section (Section 5.5). HEK293S cells transiently transfected with vector were used as null receptor background for the identification of agonistic activity.

Similar to the previous approach in examining the cAMP signalling properties of GLP-1R endogenous peptide agonists (Section 3.2.2) and given the fact that GLP-1R is predominantly Gα_s-coupled, cAMP functional assays were used again as the preliminary biological screens for potential agonism. BETP, which is a known GLP-1R ago-PAM [Sloop et al., 2010], was included to act as a positive control to demonstrate GLP-1R activation. HEK293S cells transiently transfected with different receptors of interests were exposed to a range of compound 249 and BETP (from 100μM to 10pM) for 15 mins in the presence of the PDE inhibitor, rolipram, before the measurement of cAMP accumulation.

Concurred with the previous observation in the CHO-GLP-1R cell line, compound 249 did not demonstrate GLP-1R agonism, nor did it activate other class B GPCRs (Fig. 5.1). The slight increase in cAMP activation at high concentration was due to the autofluorescence of the compound when high concentration (i.e. at 100μM) was added, as the cAMP functional assay was TR-FRET based. In contrast to compound 249, BETP exhibited weak GLP-1R agonism (pEC_{50} being 5.62 $\pm$ 0.26), corroborating with other published papers [Sloop et al., 2010]. The agonistic activity of BETP is GLP-1R specific, as it did not activate other class B GPCRs (Fig. 5.1). Having concluded that compound 249 did not activate GLP-1R and that the reference compound, BETP, exhibited GLP-1R agonism, the potential allosterism of compound 249 on other class B GPCRs was next

determined.

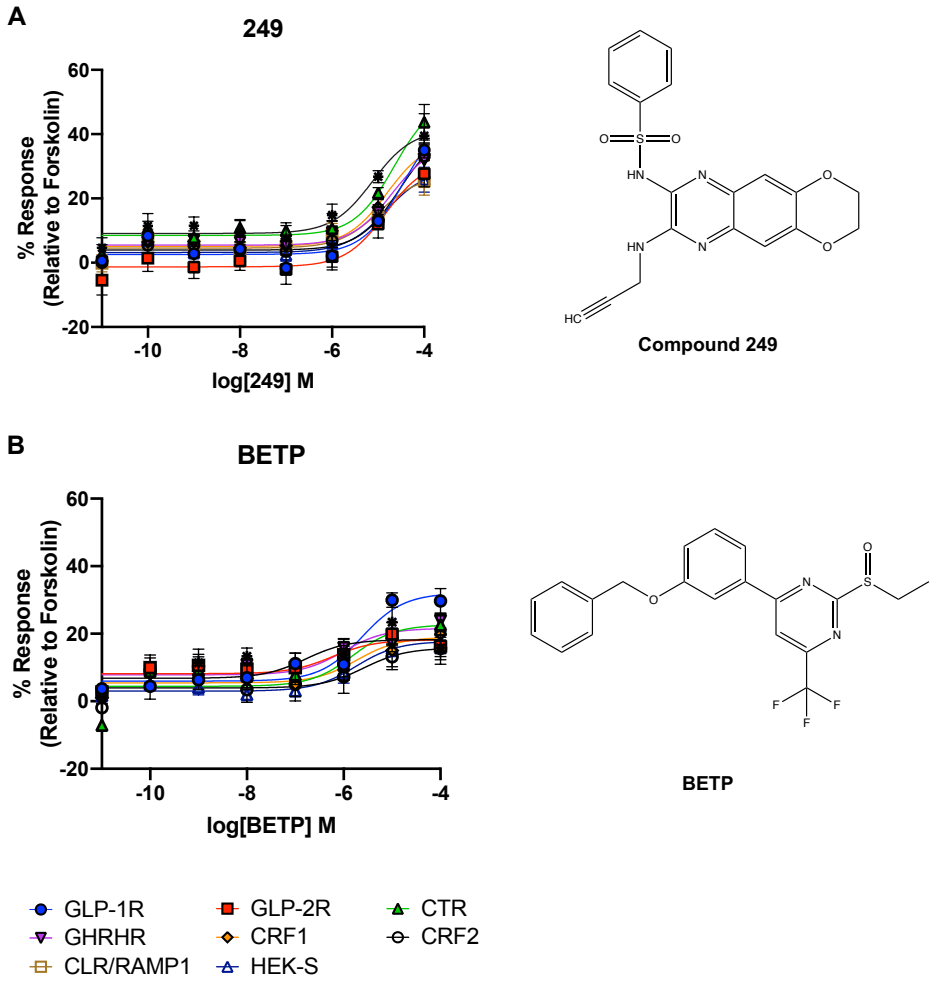

Figure 5.1: **Compound 249 Class B GPCR agonism screening.** (A) Compound 249 was screened against other class B GPCRs in order to determine if it has any agonistic activities towards GLP-1R, GLP-2R, GHRH, CRF1, CRF2, CTR, and CLR/RAMP1 complex. (B) BETP was also screened against the class B GPCRs. 1000 cells/well HEK293S transiently transfected with receptors or/and RAMP1 of interest were stimulated with compound 249 or BETP for 15 minutes in the presence of PDE inhibitor rolipram. All data were normalised to the maximum cAMP response determined by 100μM forskolin stimulation. All data are means of 3 independent experimental with duplicates results $\pm$ S.E.M (upper error bars) and were fitted to the three-parameter logistic equation.

5.2.2 Screening of compound 249 allosteric effect on other Class B GPCRs

Following the conclusion of compound 249 lack of intrinsic agonism at class B GPCRs, compound 249 allosterism on cognate endogenous ligands of different secretin-like receptors were examined. To do so, HEK293S cells which transiently expressed class B GPCRs of interests were stimulated with their respective cognate agonists, which were, OXM for GLP-1R, glucagon-like peptide-2 (GLP-2) for GLP-2R, growth-hormone-release hormone (GHRH) for GHRHR, corticotropin-releasing hormone (CRF) for both CRF1 and CRF2, calcitonin (CT) for CTR, and lastly calcitonin gene-related peptide (CGRP), adrenomedullin (AM) and adrenomedullin 2 (AM2) for CLR/RAMP1 complex in the presence of a fixed concentration (at 10^{-5}M) of compound 249 or BETP for 15 mins prior to cAMP measurement. Again, the determination of compound 249 allosterism on GCGR and GIPR will be presented in later section (Section 5.5).

Compound 249 demonstrated potentiation of OXM-mediated cAMP responses at the GLP-1R (pEC_{50} value increased from 8.01 $\pm$ 0.13 to 8.57 $\pm$ 0.10, $p < 0.01$) (Fig. 5.2 and Table 5.1). Moreover, compound 249 did not modulate the potencies or efficacies of other cognate agonists of class B GPCRs. Intriguingly, the preliminary results here showed that BETP, which is GLP-1R-specific ago-PAM [Sloop et al., 2010], reduced the potency of GLP-2 at the GLP-2R (pEC_{50} value decreased from 9.71 $\pm$ 0.23 to 9.29 $\pm$ 0.13) and potentiated GHRH potency at the GHRHR (pEC_{50} value increased from 8.14 $\pm$ 0.18 to 9.27 $\pm$ 0.32) (Fig. 5.2 and Table 5.1). Based on the GLP-1R-specific cAMP potentiation demonstrated by compound 249, further pharmacological characterisation was performed to validate its potential to be further developed as a novel T2DM treatment.

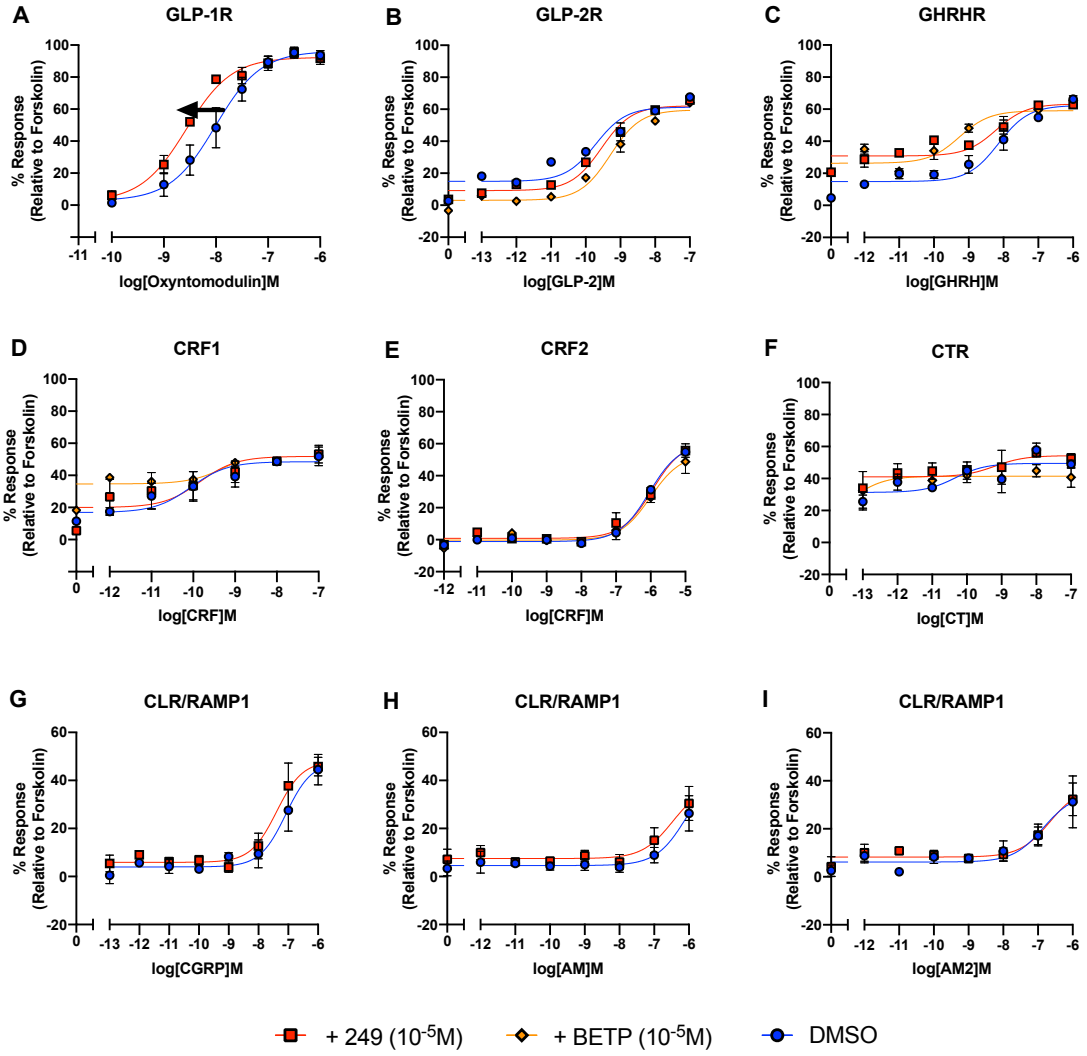

Figure 5.2: **Compound 249 class B GPCRs allosteric modulation screening.** Compound 249 was screened against other class B GPCRs in order to determine if it has any allosteric modulation activities towards other class B GPCR other than GLP-1R. Compound 249 was screened against (A) OXM/GLP-1R, (B) GLP-2/GLP-2R, (C) GHRH/GHRHR, (D) CRF/CRF1, (E) CRF/CRF2, (F) CT/CTR, CLR/RAMP in the presence of (G) CGRP, (H) AM and (I) AM2. 1000 cells/well of HEK293S transiently transfected with receptors of interest and/or RAMP1 were stimulated with their cognate ligands for 15 minutes in the presence of PDE inhibitor rolipram. All data were normalised to the maximum cAMP response determined by 100μM forskolin stimulation. All data are means of 1 to 3 independent experimental results with duplicates $\pm$ S.E.M (upper error bars) and were fitted to the three-parameter logistic equation. Table 5.1 shows the pEC_{50} and E_{max} values of the individual ligand responses.

Table 5.1: **cAMP accumulation potencies (pEC_{50}) and maximal responses (E_{max}) of compound 249 class B GPCRs allosteric modulation screening in HEK239S transiently transfected with receptors of interest.**

Receptor	Cognate ligands	Compound (at 10^{-5}M)	pEC_{50} [a]	E_{max} [b]	Span	n
GLP-1R	OXM	DMSO	8.01±0.13	96.24±4.26	93.51±6.10	4
		249	8.57±0.10	92.36±2.18	90.00±4.52	4
		BETP	-	-	-	-
GLP-2R	GLP-2	DMSO	9.71±0.23	61.33±3.67	46.40±4.43	6
		249	9.55±0.13^{ns}	62.17±2.35^{ns}	53.01±2.76	6
		BETP	9.29±0.13	59.59±2.68	56.50±3.06	2^{NB}
GHRHR	GHRH	DMSO	8.14±0.18	62.34±3.38	47.51±3.81	6
		249	8.21±0.28^{ns}	63.26±3.57^{ns}	32.45±4.05	6
		BETP	9.27±0.32	59.05±3.23	32.76±4.21	2^{NB}
CRF1	CRF	DMSO	10.05±0.31	48.54±3.03	31.65±4.17	6
		249	9.84±0.44^{ns}	51.86±4.38^{ns}	31.87±5.96	6
		BETP	9.21±3.16	56.30±5.24	21.38±62.05	2^{NB}
CRF2		DMSO	6.04±0.05	60.06±1.69	61.23±1.72	6
		249	5.95±0.14^{ns}	61.48±4.94^{ns}	60.61±5.01	6
		BETP	6.01±0.16	53.44±4.91	53.69±4.99	2^{NB}
CTR	CT	DMSO	10.33±0.63	49.51±3.33	18.19±4.81	6
		249	9.20±0.79^{ns}	54.31±4.02^{ns}	13.23±4.70	6
		BETP	13.17±5.40	41.40±2.52	22.38±166.19	2^{NB}
CLR/RAMP1	CGRP	DMSO	7.08±0.25	47.72±6.04	43.73±6.20	6
		249	7.39±0.21^{ns}	48.07±3.94^{ns}	42.18±4.09	6
		BETP	-	-	-	-
	AM	DMSO	6.07±0.84	44.78±37.06	40.21±36.63	4
		249	6.47±0.61	38.17±12.50	30.69±12.27	4
		BETP	-	-	-	-
	AM2	DMSO	6.85±0.35	34.57±6.71	28.40±6.73	4
		249	6.65±0.37	37.66±7.23	29.42±7.15	4
		BETP	-	-	-	-

Values were generated when the data were fitted to the three-parameter logistic equation. Means ± S.E.M of n individual result sets were shown.

[a] Negative logarithm of agonist concentration when reaching half maximal response.

[b] % of maximal response observed when stimulated with ligands relative to forskolin.

[NB] Preliminary results are shown here only due to COVID-19 obstruction of experimental schedule.

Statistical significance compared cAMP accumulation ligand responses between cognate ligand in the presence of DMSO and in the presence of compound 249 or BETP were determined by Student's t-test with Welch's correction or one-way ANOVA with Bonferroni's correction (**, $p < 0.01$; ns, non-statistically significant).

5.3 Pharmacological characterisation of compound 249 allosterism at GLP-1R

Previously, the potentiation of cAMP response mediated by compound 249 was established to be GLP-1R-selective. In this section, pharmacological characterisation of compound 249 was performed in an attempt to deduce its potential modulation of other downstream signalling pathways, such as iCa^{2+} release and phosphorylation of ERK1/2 (pERK1/2). HEK293S-GLP-1R-WT cell line, as established in Section 3.2.6 to be a useful system in investigating iCa^{2+} signalling, was used again as its use is also validated by other research groups to be a robust system for identifying small molecule agonists or PAMs [Wootten et al., 2012, Bueno et al., 2020]. But first, the comparison of the extent of intrinsic agonism exhibited by compound 249, and the two well-studied ago-PAMs [Knudsen et al., 2007, Sloop et al., 2010], compound 2 and BETP will be reiterated for completeness.

5.3.1 Compound 249 lacks intrinsic agonism at the GLP-1R

Compound 2 and BETP were used frequently in this project to act as reference compounds to compare the pharmacological action with compound 249. To establish a comparison of the extent of agonism among compound 249, compound 2 and BETP, these compounds were applied to HEK293-GLP-1R-WT cells at a range of concentrations (from 100μM to 10pM). Concurred with the results shown previously in Fig. 5.1, compound 249 did not activate GLP-1R (Fig. 5.3). Corroborated with the published reports, compound 2 and BETP were partial agonists at the GLP-1R (their pEC_{50} values being 5.57 $\pm$ 0.08 and 5.63 $\pm$ 0.22 respectively) [Knudsen et al., 2007, Sloop et al., 2010], with Compound 2 being more efficacious than BETP.

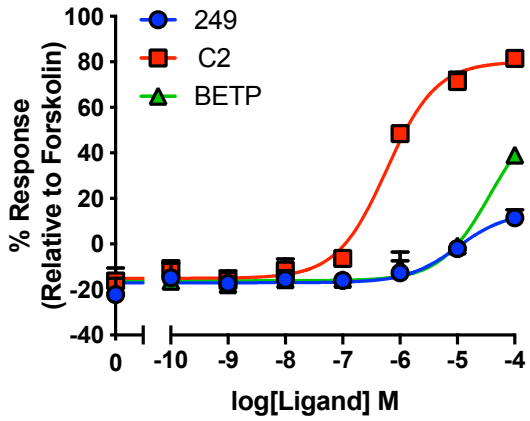

Figure 5.3: **Compound 249 does not exhibit agonism in HEK293S-GLP-1R-WT cells.** 1000 cells/well of HEK293S-GLP-1R-WT cells were stimulated with compound 249, Compound 2 and BETP at a range from 100μM to 10pM for 8 minutes without the presence of PDE inhibitors to measure cAMP accumulation. All data were normalised to the maximum cAMP response determined by 100μM forskolin stimulation and were means of duplicate from 3 independent experiments $\pm$ S.E.M (upper error bars).

5.3.2 Compound 249 positive allosteric modulation of GLP-1R peptide agonists

Following the observations that compound 249 did not activate GLP-1R and that it showed preferential potentiation of OXM-mediated cAMP accumulation response in the CHO-GLP-1R cell line, the findings were further validated in the HEK293S-GLP-1R-WT cell line. To do so, cAMP functional assays were performed during which various fixed concentrations of compound 249 were added to the GLP-1R endogenous agonists, namely GLP-1, OXM and GCG. Compound 2 and BETP were again assayed alongside compound 249 to act as comparisons of the allosteric activity of compound 249.

Concurred with the findings in the CHO-GLP-1R cell line (Appendix B.1), compound 249 demonstrated robust concentration-dependent augmentation of OXM-mediated cAMP responses only, which it enhanced the potency of OXM by 4.47-fold (pEC_{50} values increased from 7.98 $\pm$ 0.06 to 8.69 $\pm$ 0.08, $p < 0.001$) when compound 249 at 10μM was applied (Fig. 5.4 and Table 5.2). Compared to compound 2 which enhanced the basal activities of OXM due to its potent intrinsic GLP-1R agonism as seen in Fig. 5.3 (E_{min} increased from 2.62 $\pm$ 1.84 to 81.88 $\pm$ 1.50, $p < 0.0001$), compound 249 did not affect the basal activity of OXM (Fig. 5.4 and Table 5.2), as it did not activate GLP-1R (Fig. 5.3). Furthermore, compound 249 only marginally enhanced cAMP responses mediated by GLP-1 and GCG, while compound 2 and BETP were able to significantly facilitate all three agonists-mediated cAMP responses (Fig. 5.4 and Table 5.2), as also shown by other published papers [Koole et al., 2010, Wootten et al., 2013a].

As explained in Section 1.6.4, the operational model of allosterism is commonly used to aid the classification of the mode of actions of allosteric modulators, which can be a PAM, a negative allosteric modulator (NAM) or a neutral allosteric ligand (NAL), depending on the quantified outcome represented by $\log\alpha\beta$. To elucidate compound 249 mode of allosterism, the operational model of allosterism was applied in order to obtain the allosteric parameters, which is a product of affinity (α) and efficacy (β), which quantify the extent of cooperativity. Here a positive $\log\alpha\beta$ value of 1.02 was resulted, which confirmed the action of compound 249 as a PAM on the OXM-mediated cAMP response (other allosteric parameters were detailed in Table 5.4). After the examination of the compound 249 positive allosterism of cAMP responses, the effect of compound 249 on $G\alpha_i$-inhibition of cAMP responses was next investigated.

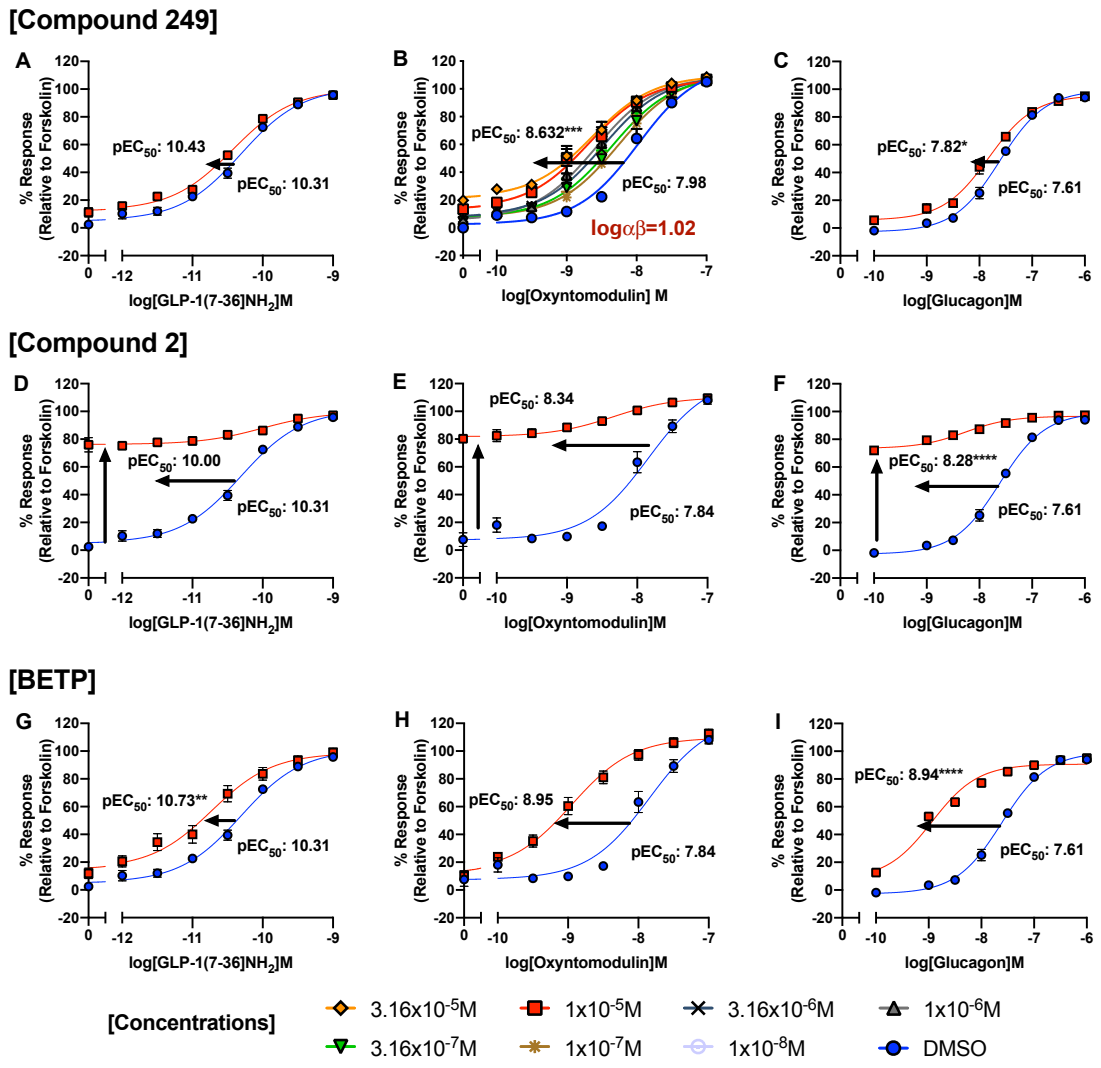

Figure 5.4: **Compound 249 only displays prominent positive allosteric modulation on OXM-mediated cAMP accumulation response in HEK293S-GLP-1R-WT cells.** Panel A-C show that compound 249 exhibits a prominent positive allosteric potentiation only in OXM-mediated cAMP response but not in GLP-1- or GCG-mediated cAMP responses. Panel D to F show the positive allosteric modulation mediated by compound 2 at GLP-1, OXM and GCG while Panel G to I show the same PAM activity mediated by BETP. 500 HEK293S-GLP-1R-WT cells/well under 8-minute co-stimulation with peptide ligands without the use of PDE inhibitor were used in the cAMP assays. All data were normalised to the maximum cAMP response determined by 100μM forskolin stimulation. All data are means from at least 3 independent experiments with duplicates $\pm$ S.E.M (upper error bars). Statistical significance compared with GLP-1, OXM or GCG (*, $p < 0.05$; **, $p < 0.01$; ***, $p < 0.001$, ****, $p < 0.0001$) for compound 249, compound 2 and BETP were determined by one-way ANOVA with post-hoc Dunnett's multiple comparisons.

Table 5.2: **Compound 249 exhibits a positive allosteric modulation specifically on OXM-mediated cAMP response in HEK293S-GLP-1R-WT cell line.**

Ligand	Compound	Conc.	pEC_{50} [a]	E_{max} [b]	E_{min} [c]	Span	n
GLP-1	DMSO	-	10.31±0.05	101.28±2.44	5.29±1.63	95.99±2.62	8
	249	1x10^{-5}M	10.43±0.05^{ns}	99.92±1.92	12.57±1.42	87.35±2.12	8
	Compound 2	1x10^{-5}M	10.00±0.18^{ns}	99.59±2.33	76.28±1.33****	23.31±2.36	8
	BETP	1x10^{-5}M	10.73±0.11**	98.71±3.57	15.54±3.41	83.17±4.41	8
OXM	DMSO	-	7.98±0.06	117.7±4.2	2.62±1.84	115.0±4.18	8
	249	1x10^{-5}M	8.69±0.08***	107.1±3.0	14.06±2.76	93.05±3.64	8
	Compound 2	1x10^{-5}M	8.34±0.16^{ns}	110.2±2.1	81.88±1.50****	28.37±2.27	6
	BETP	1x10^{-5}M	8.95±0.08****	109.7±2.7	13.11±3.18	96.64±3.78	6
GCG	DMSO	-	7.61±0.04	99.38±1.80	2.75±1.67	102.13±2.18	6
	249	1x10^{-5}M	7.82±0.06*	95.74±1.95	5.67±2.19	90.07±2.62	6
	Compound 2	1x10^{-5}M	8.28±0.14****	96.70±1.08	73.44±1.67****	23.26±1.82	4
	BETP	1x10^{-5}M	8.94±0.06****	90.75±1.24	7.76±3.20	82.99±3.25	6

Values were generated when the data were fitted to the three-parameter logistic equation. Means ± S.E.M of n individual result sets were shown.

[a] Negative logarithm of agonist concentration when reaching half maximal response.

[b] % of maximal response observed when stimulated with ligands relative to forskolin.

[c] % of minimal response observed when stimulated with ligands relative to forskolin.

Statistical significance compared with GLP-1, OXM or GCG (*, $p < 0.05$; **, $p < 0.01$; ***, $p < 0.001$, ****, $p < 0.0001$; ns, non-statistically significant) for compound 249, compound 2 and BETP were determined by one-way ANOVA with post-hoc Dunnett's multiple comparisons.

5.3.3 Compound 249 negative allosteric modulation of Gα_i-inhibition cAMP responses

As stated previously (section 1.5.2) that both Gα_s and Gα_i subunits activation contribute to the overall intracellular cAMP production and that GLP-1R is known to pleiotropically couple to different G proteins, including the Gα_i subunit [Weston et al., 2014], compound 249 influence on the Gα_i-inhibition of cAMP response was examined in the HEK293S-GLP-1R-WT cell line. To do so, the cells were pre-treated with 200ng/μl pertussis toxin (PTX) or vehicle 16 hours prior to assaying, the total cAMP accumulation upon agonist stimulation were then measured.

Consistent with previously established results (Fig. 5.4), compound 249 was able to enhance OXM-mediated cAMP responses by 4.47-fold (pEC_{50} values increased from 7.98 $\pm$ 0.06 to 8.69 $\pm$ 0.08, $p < 0.001$) in the vehicle pre-treated cells. Yet in cells receiving PTX-pre-treatment, the potency of OXM decreased from 7.98 $\pm$ 0.06 to 7.75 $\pm$ 0.07 (Fig. 5.5). More importantly, the potentiation of OXM-mediated cAMP response mediated by compound 249 occurred to a lesser degree by 2.09-fold compared to the cells without PTX-pre-treatment, implying compound 249 exhibited negative allosteric modulation of the Gα_i subunit, thereby resulting in a greater increment in total cAMP responses observed in the untreated cells. Following the investigation of compound 249 modulation of cAMP responses mediated via both Gα_s and Gα_i subunits, its potential allosteric effects on iCa^{2+} signalling were then explored.

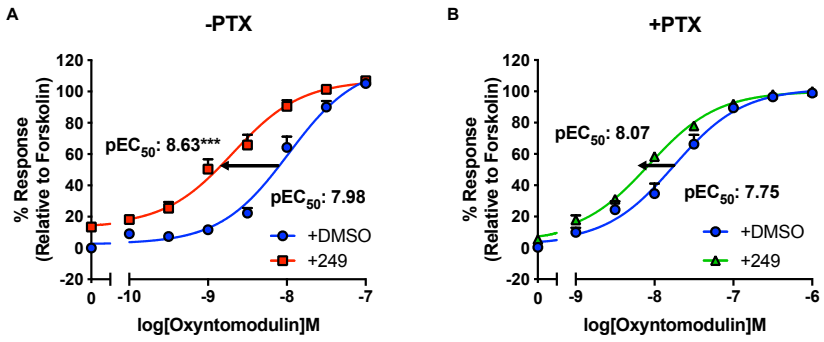

Figure 5.5: **Compound 249 allosteric modulation of OXM-mediated cAMP response is Gα_i-dependent in HEK293S-GLP-1R-WT cells.** HEK293S-GLP-1R-WT cells were pre-treated without (A) or with (B) pretreatment of 200ng/μl PTX 16 hours prior to cAMP assays. 500 HEK293S-GLP-1R-WT cells/well under 8-minute co-stimulation with peptide ligands in the absence of PDE inhibitor were used in the cAMP assays. All data were normalised to the maximum cAMP response determined by 100μM forskolin stimulation. All data are means from at least 3 independent experiments with duplicates $\pm$ S.E.M (upper error bars). Statistical significance compared with OXM and DMSO in both with or without PTX treatment conditions (***, $p < 0.001$) were determined by one-way ANOVA with post-hoc Dunnett's multiple comparisons.

5.3.4 Compound 249 negative allosteric modulation of iCa^{2+} release

GLP-1R has been shown to be able to activate the $G\alpha_q$ pathway, which is responsible for the mediation of downstream iCa^{2+} release, hence facilitating insulin secretion in pancreatic β cells [Xu and Xie, 2009, Shigeto et al., 2015]. Thus, following the evaluation of compound 249 effect on the overall cAMP response, its ability to modulate iCa^{2+} signalling was determined. To quantify iCa^{2+} mobilisation, HEK293S-GLP-1R-WT cells were pre-treated with fixed concentrations of compound 249 (at $1x10^{-4}$M, $3.16x10^{-5}$M and $1x10^{-5}$M) or DMSO which acted as control, prior to co-stimulation with GLP-1, OXM or GCG, also in the presence of the compound. iCa^{2+} release were then quantified with the use of the BD pathway 855 high-content bioimager, as described in section 3.2.6. As OXM has a relatively weak iCa^{2+} mobilisation [Wootten et al., 2016b], high concentration of OXM (i.e. at $3.16x10^{-5}$M) was applied in the assays.

Contrary to its apparent positive allosteric modulation on the OXM-mediated cAMP response (Fig. 5.4), compound 249 exhibited significant concentration-dependent inhibition on both GLP-1 and OXM-mediated iCa^{2+} responses, reducing the potencies of the iCa^{2+} responses of GLP-1 and OXM by 4.37-fold and 7.94-fold respectively (pEC_{50} value of GLP-1-mediated iCa^{2+} response decreased from 7.65 $\pm$ 0.29 to 7.04 $\pm$ 0.21, $p < 0.01$; pEC_{50} of OXM-mediated iCa^{2+} response decreased from 7.07 $\pm$ 0.27 to 6.17 $\pm$ 0.32, $p < 0.05$). Notably, the potency of GCG-mediated iCa^{2+} response was not affected, yet an apparent decrease in efficacy was observed (E_{max} decreased from 63.57 $\pm$ 1.89 to 43.69 $\pm$ 2.28) (Fig. 5.6 and Table 5.3).

The operational model of allosterism was then applied to quantify the cooperativity of compound 249 on modulating the iCa^{2+} signalling pathway. Through fitting the results into the mathematical model, negative cooperativity on GLP-1 and OXM-induced iCa^{2+} release indicated by negative $\log\alpha\beta$ values of -0.852 and -1.84 were obtained respectively. These results affirmed the role of compound 249 as a NAM in iCa^{2+} mobilisation mediated by GLP-1 and OXM specifically. The detailed report of the allosteric parameters of compound 249 negative allosteric modulation on OXM-mediated iCa^{2+} release is further outlined in Table 5.4.

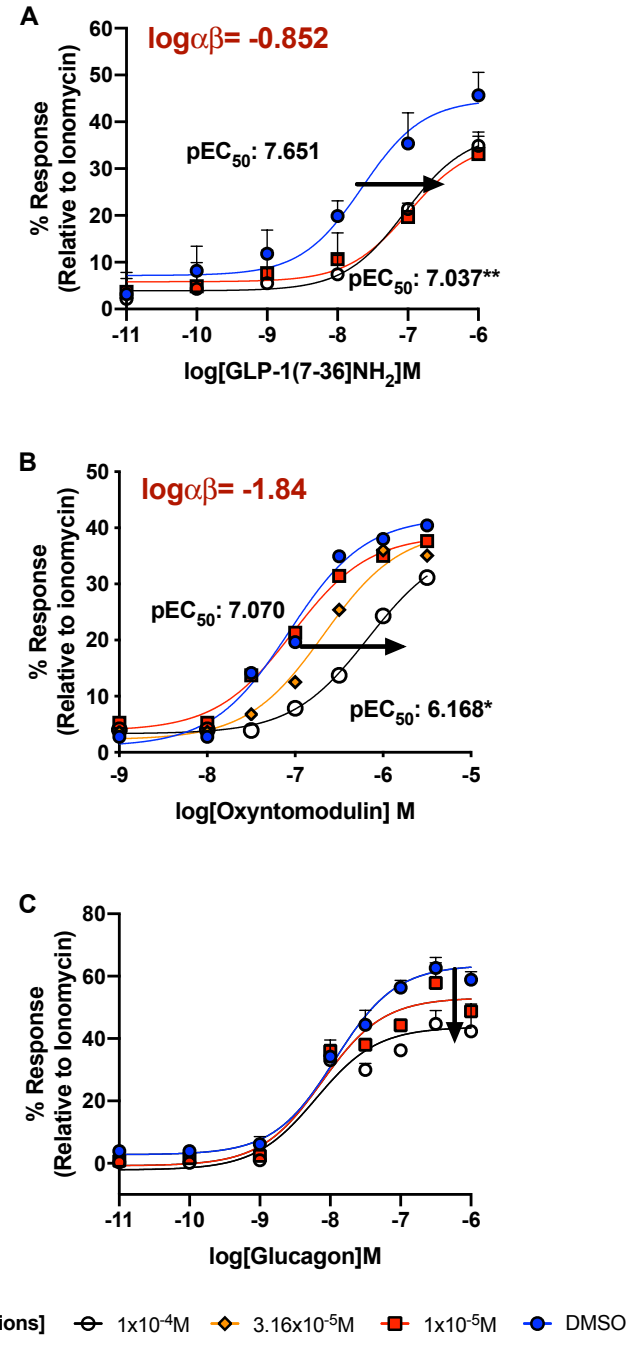

Figure 5.6: **Compound 249 exhibits concentration-dependent negative allosteric modulation on GLP-1, OXM and GCG-mediated intracellular calcium responses in HEK293S-GLP-1R-WT cells.** Compound 249 demonstrates negative allosteric modulation in (A) GLP-1, (B) OXM and (C) GCG mediated iCa^{2+} responses. 80,000 cells/well of HEK293S-GLP-1R-WT cells were seeded onto black-96 well plate overnight and the cells were pre-treated with compound 249 for 15 mins prior to the measurement of intracellular calcium mobilisation. All data were normalised to the 10μM ionomycin concentration-response curve. All data are means from at least 3 independent experiments with duplicates $\pm$ S.E.M (upper error bars). Table 5.3 show the pEC_{50} and E_{max} values of GLP-1, OXM and GCG-mediated iCa^{2+} responses in the presence of various concentrations of compound 249. Statistical significance compared with GLP-1, OXM or GCG (*, $p < 0.05$; **, $p < 0.01$) with or without compound 249 at various concentrations were determined by one-way ANOVA with post-hoc Dunnett's multiple comparisons.

Table 5.3: **Compound 249 exhibits a concentration-dependent negative allosteric modulation on GLP-1, OXM and GCG-mediated intracellular calcium responses in HEK293S-GLP-1R-WT cell line.**

Ligand	[Cmpd 249]M	pEC_{50} [a]	E_{max} [b]	Span	n
GLP-1	DMSO	7.65±0.29	44.80±4.54	37.63±5.03	4
	$1x10^{-4}$M	7.04±0.21**	37.68±3.95	33.58±4.06	3
	$3.16x10^{-5}$M	-	-	-	-
	$1x10^{-5}$M	6.99±0.34**	35.65±5.82	29.82±5.97	3
OXM	DMSO	7.07±0.27	41.89±4.48	40.86±5.39	5
	$1x10^{-4}$M	6.17±0.32*	37.44±7.75	34.12±7.39	5
	$3.16x10^{-5}$M	6.68±0.12	39.68±2.34	37.42±2.45	5
	$1x10^{-5}$M	7.03±0.20	38.68±3.59	34.87±3.92	5
GCG	DMSO	7.93±0.09	63.57±1.89	60.81±2.51	3
	1x10-4M	8.20±0.17	43.69±2.28	45.81±3.21	3
	$3.16x10^{-5}$M	-	-	-	3
	$1x10^{-5}$M	8.12±0.14	53.09±2.42	53.90±3.07	3

Values were generated when the data were fitted to the three-parameter logistic equation. Means ± S.E.M of n individual result sets were shown.

[a] Negative logarithm of agonist concentration when reaching half maximal response.

[b] % of maximal response observed when stimulated with ligands relative to ionomycin.

Statistical significance compared with GLP-1, OXM or GCG (*, $p < 0.05$; **, $p < 0.01$; ns, non-statistically significant) in the presence of various concentrations of compound 249 were determined by one-way ANOVA with post-hoc Dunnett's multiple comparisons.

5.3.5 Compound 249 lacks allosteric modulation on pERK1/2 activation

Penultimately, the effect of compound 249 on modulating the pERK1/2 pathway was evaluated with the use of Cisbio® Phospho-ERK1/2 (Thr202/Tyr404) kit (see Section 2.2.3.3 for methods). To do so, HEK293S-GLP-1R-WT cells were serum-starved overnight and were pre-treated with fixed concentrations of compound 249 or DMSO for 15 mins prior to agonist stimulation for 5 mins in the presence of compounds. The results obtained were then normalised to 100μM phorbol 12-myristate 13-acetate (PMA) response.

Compound 249 did not affect OXM-mediated pERK1/2 response (Fig. 5.7), suggesting the activation of pERK1/2 induced by OXM may not be Gα_q-linked [Lei et al., 2018] given its inhibition of OXM-mediated iCa^{2+} release. A positive log$\alpha\beta$ value of 0.323, yet less than 1, was obtained through the application of the operational model of allosterism, indicating compound 249 was a NAL of the OXM-mediated pERK1/2 pathway. Details of the allosteric parameters can be found in Table 5.4.

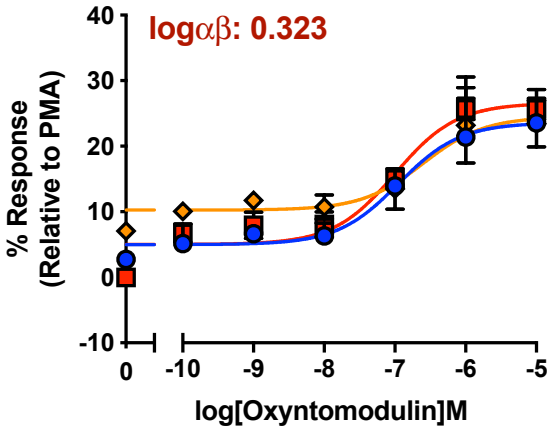

Figure 5.7: **Compound 249 does not affect pERK1/2 response in HEK293-GLP-1R-WT cells.** Compound 249 does not induce potentiation or inhibition of OXM-mediated pERK1/2 signalling. 35,000 cells/well of HEK293-GLP-1R-WT cells were used in the pERK1/2 assays. All data were normalised to the 100μM PMA and were means of 3 independent results with duplicates ± S.E.M.

5.3.6 Compound 249 does not affect GLP-1 orthosteric binding

Lastly, compound 249 orthosteric ligand binding at GLP-1R was evaluated. To do so, bioluminescence resonance energy transfer (BRET)-based ligand binding assay was employed (see Section 2.2.3.4 for methods), during which HEK293T cells were transiently transfected with the Nluc-tagged GLP-1R construct 48 hours prior to assaying. HEK293T cells transiently expressing Nluc-tagged GLP-1R were incubated with the Nano-Glo substrate, furimazine, prior to the addition of Tag-lite® GLP-1R red agonist (which is Ex-4 based) in the presence of a fixed concentration of compound 249 at 10μM or DMSO. Once total binding was reached, dissociation phase was initiated by injecting 1μM of 'cold' GLP-1 to dissociate the binding complex.

In the absence of compound 249, the association (K_{on}) and dissociation (K_{off}) constants were 7.02x10^{-7}M^{-1}min^{-1} and 0.017min^{-1} respectively, resulting in the equilibrium dissociation constant (K_D) of 2.49x10^{-10}M. Similarly in the presence of compound 249, GLP-1 binding affinity to the GLP-1R was not affected, as the K_{on} and K_{off} constants remained largely unchanged, resulting in values of 6.74x10^{-7}M^{-1}min^{-1} and 0.117min^{-1} respectively, and a K_D value of 1.26x10^{-10}M. It further illustrated that compound 249 did not affect GLP-1 binding and that it did not compete with GLP-1 for the orthosteric binding site at the GLP-1R (Fig. 5.8). However, binding experiments in the presence of OXM was not performed due to time contraints and will remain as an important piece of future work.

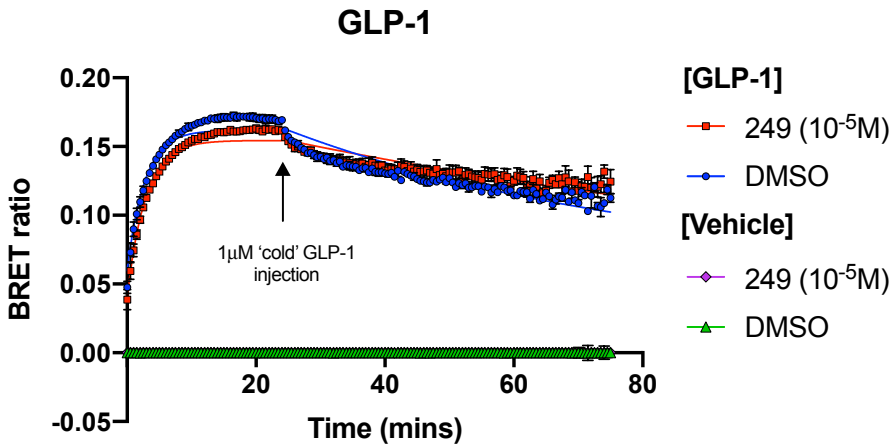

Figure 5.8: **Compound 249 does not affect ligand binding at the GLP-1R.** HEK293T cells were transiently transfected with Nluc-GLP-1R constructs prior to the ligand binding assay. Cells were incubated with Nano-Glo substrate, furimazine, prior to the addition of Tag-lite® GLP-1R red agoinst and emission was measured at 485nm and 530nm every 30 seconds for 25 minutes during which total binding was determined. Unlabeled, 'cold', GLP-1 at 1μM was then injected into each well to displace all bound Tag-lite® GLP-1R red agonist, with emission measured every 30 seconds for a further 60 minutes, during which non-specific binding was determined. Vehicle was added alongside the ligands to act as a control which represented the background level of emission. The BRET signal was calculated by subtracting the 530 nm/485 nm emission ratio for vehicle treated cells from Tag-lite® GLP-1R red agonist treated cells. Data were fitted using the 'association then dissociation' model in GraphPad Prism 8.4 and the above results were means of 3 independent results with duplicates $\pm$ S.E.M.

5.3.7 Summary of compound 249 allosteric modulation at the GLP-1R

Compound 249 does not influence GLP-1R agonist binding nor does it affect pERK1/2 activation. More importantly, compound 249 is a PAM of OXM-mediated cAMP responses, without imposing any allosteric effects on the other two GLP-1R agonists, GLP-1 and GCG (Fig. 5.4). It is a NAM on $G\alpha_i$-inhibited cAMP responses, as the inhibition of $G\alpha_i$ subunit resulted in a smaller extent of the potentiation of OXM-mediated overall cAMP response (Fig. 5.5). It is also a NAM on GLP-1 and OXM-induced iCa^{2+} mobilisation and a NAL on OXM-mediated pERK1/2 pathway. Table 5.4 summarises the allosteric parameters that describe the allosteric effect of compound 249 on the affinity and efficacy of the orthosteric agonists. Fig. 5.9 concludes the allosteric modulation of compound 249 in pathways such as cAMP responses, iCa^{2+} release and pERK1/2 mediated by all three GLP-1R endogenous agonists.

Table 5.4: **Allosteric modulation parameters, α and β, of compound 249 actions of OXM-mediated cAMP accumulation, intracellular calcium responses and phosphorylation of ERK1/2 in HEK293S-GLP-1R-WT cells.**

GLP-1R	Signalling pathway	α[a]	β[b]	$\alpha\beta$[c]	log$\alpha\beta$	R^2 [d]
Wildtype	cAMP	4.800	2.189	10.50	1.02	0.9661
	iCa^{2+}	0.01343	1.076	0.0145	-1.84	0.8627
	pERK1/2	2.672	0.7891	2.108	0.323	0.8629

[a] represents the cooperativity determined by the operational model of agonism and allosterism.
[b] represents the scaling factor determined by the operational model of agonism and allosterism.
[c] represents the combinatorial values of both cooperativity and scaling factors. A positive log$\alpha\beta$ value > 1 denotes positive allosteric modulation; a negative log$\alpha\beta$ value < 1 denotes negative allosteric modulation; and a log$\alpha\beta$ value between 0 and 1 indicates the nature of neutral allosteric ligand.
[d] denotes the goodness of fit of the data set to the operational model of agonism and allosterism.

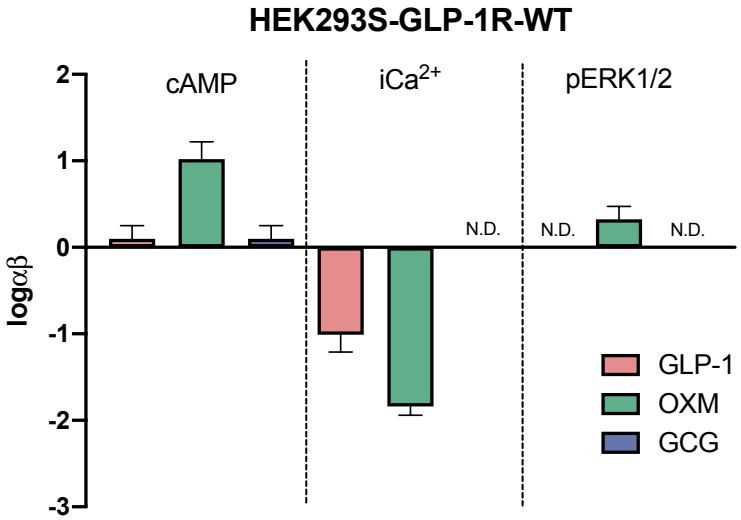

Figure 5.9: **Bar chart summarising compound 249 allosterism.** The above bar chart summarises compound 249 allosteric actions in terms of log$\alpha\beta$ values on GLP-1, OXM and GCG-mediated GLP-1R signalling pathways. The log$\alpha\beta$ values of iCa^{2+} mobilisation mediated by GCG, phosphorylation of ERK1/2 mediated by GLP-1 and GCG in the presence of compound 249 were not determined and are indicated by N.D.

5.4 Exploration of compound 249 pharmacological mechanism of action

Following the pharmacological characterisation of compound 249, the mechanism of action of compound 249 was then explored. The cysteine-347 (C347) residue on the lower end of TM6 of the GLP-1R is postulated to be responsible for the ago-PAM actions of compound 2 and BETP, and many other potential GLP-1R small molecule PAMs [Eng et al., 2013, Nolte et al., 2014, Bueno et al., 2016, Song et al., 2017]. These two GLP-1R ago-PAMs mediate their actions by forming irreversible disulphide cross-links with the cysteine residue, which is a property that is highly undesirable in drug development due to potential toxicity [Eng et al., 2013]. Therefore, GLP-1R-C347A functional assays have been proposed to facilitate the screening of GLP-1R small molecule PAMs that do not form irreversible disulphide conjugate with the cysteine residue [Bueno et al., 2016]. Hence, a C347-alanine (C347A) point mutation GLP-1R construct was created with the use of QuikChange® Lightning Site Directed Mutagenesis kit (for methods see Section 2.2.2.7). The point mutation was confirmed by aligning the C347A sequencing results with that of wildtype GLP-1R. Stable cell lines expressing the desired DNA constructs were produced in HEK293S cells due to their ease of transfection. The details of the production of the stable cell lines were outlined in Section 2.2.1.5.2.

5.4.1 Compound 2 and BETP activate GLP-1R via the C347A residue

As noted above, the C347 residue of GLP-1R is critical for the ago-PAM actions of compound 2 and BETP. To validate the notion and to determine if the point mutation was introduced at the desired location, a range of concentrations of compound 2 and BETP (100μM to 10pM) were applied to both HEK293S cell lines stably expressing GLP-1R-C347A (thereafter referred to as HEK293S-GLP-1R-C347A) and HEK293S-GLP-1R-WT cells. Their subsequent cAMP responses were determined with the use of cAMP functional assays as described previously. However, due to the high GLP-1R expression in these two stable cell lines, PDE inhibitor was not included as a result of the high level of cAMP produced. Compound 249 was also applied so as to determine the effect of C347A on its intrinsic GLP-1R agonism. Forskolin was used to normalise the results generated in these two stable cell lines.

The following results illustrated that the efficacy of compound 2 was abolished in HEK293S-GLP-1R-C347A cells (E_{max} values decreased from 80.15 $\pm$ 3.01 to 17.92 $\pm$

1.82, $p < 0.05$, Fig. 5.10 and Table 5.5). Not only did the result confirm the desired site-directed mutagenesis at the 347 position, but it also verified the observations that C347 is essential for the ago-PAM activity. The results also affirmed the use of these two stable cell lines as a system for the investigation of the mechanisms of actions of GLP-1R PAMs.

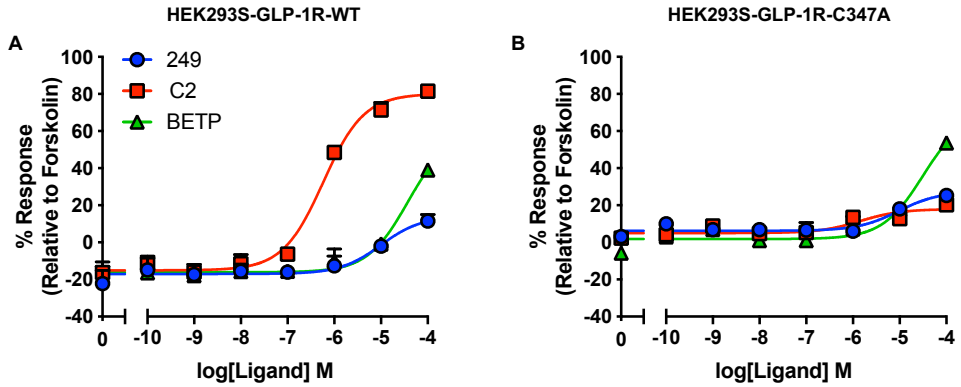

Figure 5.10: **Intrinsic agonism of compound 2 and BETP are abolished in HEK293S-GLP-1R-C347A cells.** 1000 cells/well of HEK293S stably expressing sigSNAP-GLP-1R-mCherry with (A) wildtype or (B) C347A point mutation were stimulated with different concentrations of compound 249, Compound 2 and BETP for 8 minutes without the presence of PDE inhibitors to measure cAMP accumulation. All data were normalised to the maximum cAMP response determined by 100μM forskolin stimulation and were means of duplicate from 2 independent experiments with duplicates ± S.E.M (upper error bars).

Table 5.5: **GLP-1R activation mediated by compound 249, C2 and BETP in HEK293S-GLP-1R-WT and HEK293S-GLP-1R-C347A cells.**

GLP-1R	Compound	pEC_{50} [a]	E_{max} [b]	Span	n
WT	Cmpd 249	5.00±0.31	14.10±5.69	31.13±5.79	4
	Cmpd 2	6.23±0.08	80.15±3.01	95.22±3.41	4
	BETP	4.43±0.16	59.72±9.39	75.82±9.19	4
C347A	Cmpd 249	5.85±0.41	27.38±3.03	21.13±3.09	4
	Cmpd 2	5.85±0.41	17.92±1.82	12.92±1.97	4
	BETP	4.50±0.20	69.88±9.70	68.10±9.51	4

Values were generated when the data were fitted to the three-parameter logistic equation. Means ± S.E.M of n individual result sets were shown.

[a] Negative logarithm of agonist concentration when reaching half maximal response

[b] % of maximal response observed when stimulated with ligands relative to forskolin

5.4.2 Compound 249 exhibits PAM activity in a GLP-1R cysteine-347-independent manner

Following the validation of cell systems for investigating compound 249 actions in the absence of the C347 residue, cAMP functional assays were next performed as described previously in both HEK293S-GLP-1R-WT and HEK293S-GLP-1R-C347A cell lines. Similarly, PDE inhibitor was not included due to the high level of receptor expression in these two stable cell lines.

HEK293S-GLP-1R-C347A cell line showed a robust potent OXM-mediated cAMP response comparable to that of HEK293S-GLP-1R-WT cell line (Fig. 5.11). More importantly, compound 249 potentiated the OXM-mediated cAMP response by nearly 10-fold in a concentration-dependent manner in the HEK293S-GLP-1R-C347A cells, a potentiation that has also been demonstrated in the HEK293S-GLP-1R-WT cells (pEC_{50} values increased from 8.20 $\pm$ 0.06 to 8.93 $\pm$ 0.09 in HEK293S-GLP-1R-C347A cells, $p < 0.001$, while pEC_{50} values increased from 7.98 $\pm$ 0.06 to 8.69 $\pm$ 0.08 in HEK293S-GLP-1R-WT cells, $p < 0.001$) (Fig. 5.11 A-B, Fig. 5.12 and Table 5.6). Further applications of the results to the operational model of allosterism resulted in positive cooperativity $\log\alpha\beta$ values of 1.02 and 1.14 in both GLP-1R-WT and C347A settings respectively, confirming compound 249 positive allosteric modulation regardless of the absence of C347 residue (Table 5.7). Compared to compound 2 and BETP, which PAM activities on OXM-mediated cAMP responses were completely abolished in the absence of C347 residue, as also shown in other studies in CHO-K1 cells expressing GLP-1R-C347A [Nolte et al., 2014] (Fig. 5.11 C-F and Table 5.6), compound 249 works in a C347-independent mechanism, which provides further evidence in support of the recent discovery of alternative small molecule agonist binding site at the GLP-1R [Zhao et al., 2020, Bueno et al., 2020]; the significance of the findings here will be further discussed in section 5.8.3.

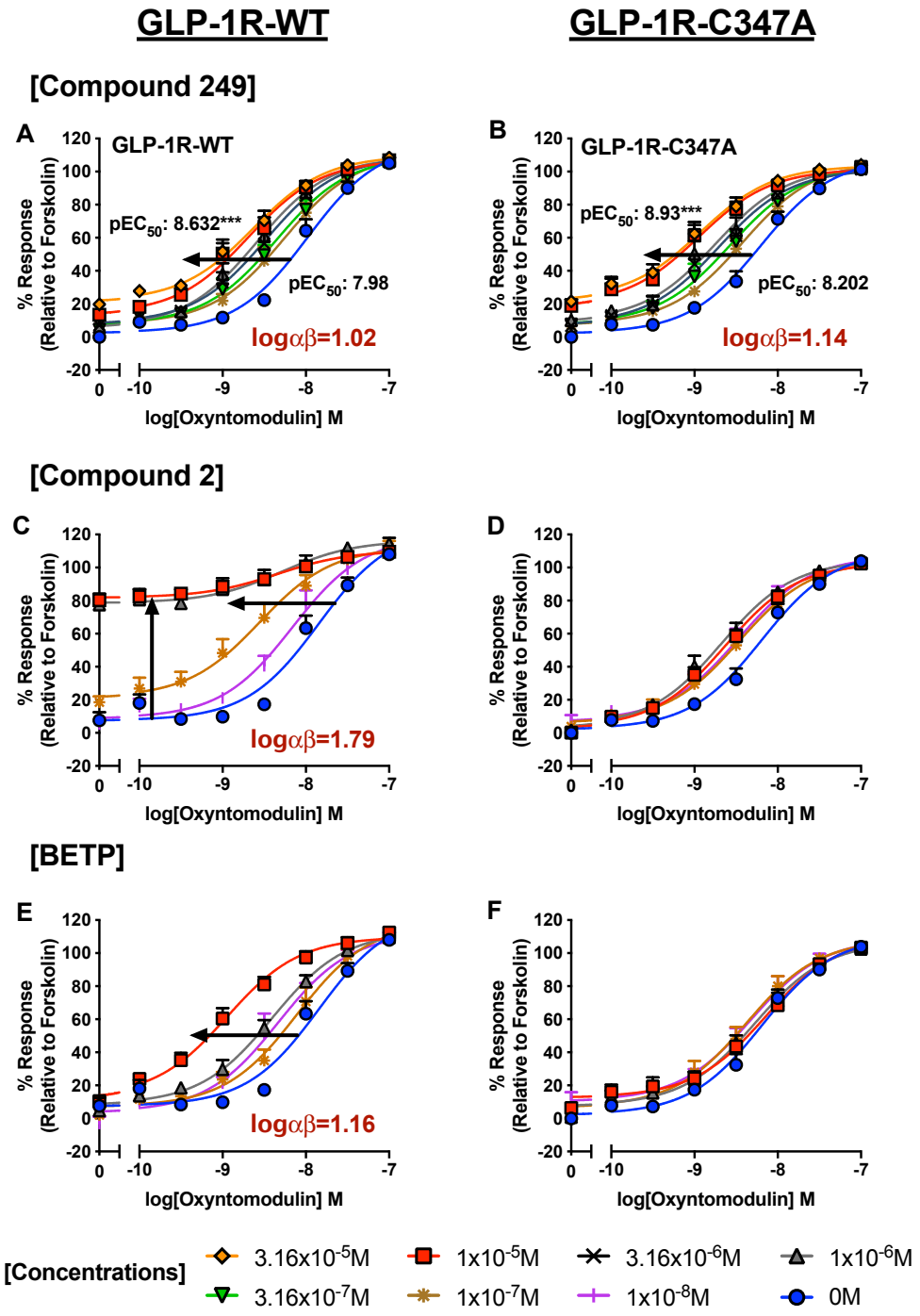

Figure 5.11: **Compound 249 allosteric modulation of OXM-mediated cAMP accumulation at the GLP-1R is C347 residue independent.** 1000 cells/well of HEK293S-GLP-1R-WT (A, C and E) or HEK293S-GLP-1R-C347A (B, D and F) cells were co-stimulated with different concentrations of 249, compound 2 and BETP OXM for 8 minutes without the presence of PDE inhibitors to measure cAMP accumulation. All data were normalised to the maximum cAMP response determined by 100μM forskolin stimulation and were means of at least 3 independent experiments with duplicates $\pm$ S.E.M (upper error bars). Statistical significance compared with OXM (***, $p < 0.001$) for compound 249, compound 2 and BETP were determined by one-way ANOVA with post-hoc Dunnett's multiple comparisons.

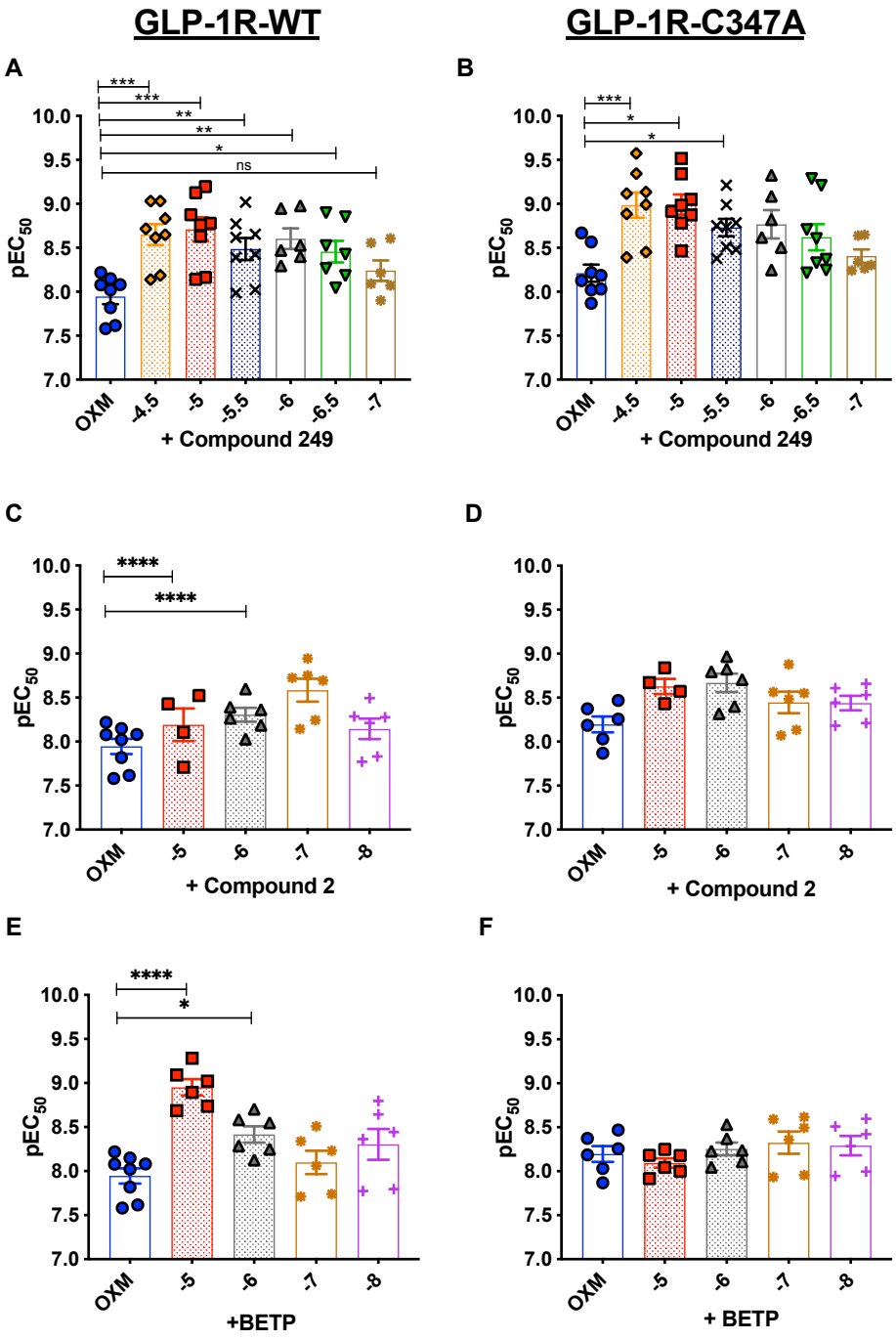

Figure 5.12: **Scatter plots illustrating compound 249 allosteric modulation of OXM-mediated cAMP accumulation is GLP-1R C347 residue independent.** 1000 cells/well of HEK293S stably expressing SigSNAP-GLP-1R-mCherry wildtype (A, C and E) or C347A (B, D and F) cells were co-stimulated with different concentrations of 249, compound 2 and BETP OXM for 8 minutes without the presence of PDE inhibitors to measure cAMP accumulation. All data were normalised to the maximum cAMP response determined by 100μM forskolin stimulation and were means of at least 3 independent experiments with duplicates $\pm$ S.E.M (upper error bars). Statistical significance compared with OXM (*, $p < 0.05$; **, $p < 0.01$; ***, $p < 0.001$; ****, $p < 0.0001$; ns, non-statistically significant) for compound 249, compound 2 and BETP were determined by one-way ANOVA with post-hoc Dunnett's multiple comparisons.

Table 5.6: **Concentration-dependent allosteric modulations of OXM-mediated cAMP accumulation potentiated by compound 249 in HEK293S-GLP-1R-WT or GLP-1R-C347A cells.**

GLP-1R	Cmpd	Conc.	pEC_{50} [a]	E_{max} [b]	E_{min} [c]	Span	n
WT	DMSO	-	7.98±0.06	117.7±4.2	2.62±1.84	115.0±4.18	8
	Compound 249	3.16x10^{-5}M	8.63±0.07***	109.6±2.6	21.77±2.31	87.84±3.14	8
		1x10^{-5}M	8.69±0.08***	107.1±3.0	14.06±2.76	93.05±3.64	8
		3.16x10^{-6}M	8.48±0.07**	109.3±3.2	8.37±2.45	100.9±3.63	8
		1x10^{-6}M	8.59±0.06**	109.0±2.8	6.30±2.34	102.7±3.26	6
		3.16x10^{-7}M	8.35±0.07*	109.5±3.6	7.76±2.42	101.7±3.91	8
		1x10^{-7}M	8.26^{ns}±0.08	111.1±4.0	7.91±2.41	103.2±4.20	6
	Compound 2	1x10^{-5}M	8.34±0.16^{ns}	110.2±2.1	81.88±1.50	28.37±2.27	6
		1x10^{-6}M	8.29±0.27^{ns}	116.4±5.2	78.70±3.40	37.66±5.59	4
		1x10^{-7}M	8.55±0.12***	112.5±4.9	21.59±4.01	90.88±5.69	6
		1x10^{-8}M	8.16±0.09^{ns}	119.1±5.2	8.95±2.81	110.1±5.35	6
	BETP	1x10^{-5}M	8.95±0.08****	109.7±2.7	13.11±3.18	96.64±3.78	6
		1x10^{-6}M	8.40±0.06*	113.1±3.2	8.70±2.23	104.4±3.49	6
		1x10^{-7}M	8.11±0.09^{ns}	118.5±5.6	7.34±2.83	111.2±5.66	6
		1x10^{-8}M	8.33±0.1^{ns}	112.1±5.6	4.04±3.97	108.0±6.04	6
C347A	DMSO	-	8.20±0.06	108.2±3.3	2.39±1.84	105.8±3.37	8
	Compound 249	3.16x10^{-5}M	8.93±0.09***	103.6±2.7	22.96±3.16	80.65±2.77	8
		1x10^{-5}M	8.95±0.09***	101.6±2.8	19.37±3.38	82.21±3.98	8
		3.16x10^{-6}M	8.70±0.07*	101.4±2.5	7.77±2.41	93.67±3.15	8
		1x10^{-6}M	8.75^{ns}±0.09	102.9±3.5	9.82±3.44	93.12±4.42	7
		3.16x10^{-7}M	8.57^{ns}±0.08	103.3±3.3	8.21±2.69	95.09±3.78	8
		1x10^{-7}M	8.43^{ns}±0.06	106.1±2.8	7.76±2.04	98.38±3.14	6
	Compound 2	1x10^{-5}M	8.62±0.05^{ns}	102.8±2.2	3.20±1.90****	99.64±2.58	6
		1x10^{-6}M	8.67±0.06^{ns}	104.5±2.8	3.85±2.49****	100.6±3.33	4
		1x10^{-7}M	8.46±0.09^{ns}	104.3±3.8	6.69±3.05****	97.61±4.35	6
		1x10^{-8}M	8.47±0.08^{ns}	107.0±3.7	7.35±2.86****	99.66±4.14	6
	BETP	1x10^{-5}M	8.15±0.08^{ns}	110.2±4.1	12.87±2.42	97.36±4.24	6
		1x10^{-6}M	8.28±0.08^{ns}	107.0±3.7	7.80±2.48	99.23±3.98	6
		1x10^{-7}M	8.38±0.08^{ns}	108.3±3.9	7.15±2.82	101.1±4.27	6
		1x10^{-8}M	8.32±0.08^{ns}	108.9±3.9	10.72±2.64	98.23±4.14	6

Values were generated when the data were fitted to the three-parameter logistic equation. Means ± S.E.M of n individual result sets were shown.

[a] Negative logarithm of agonist concentration when reaching half maximal response

[b] % of maximal response observed when stimulated with ligands relative to forskolin

[c] % of minimal response observed when stimulated with ligands relative to forskolin.

Statistical significance compared with OXM (*, $p < 0.05$; **, $p < 0.01$; ***, $p < 0.001$, ****, $p < 0.0001$; ns, non-statistically significant) for compound 249, compound 2 and BETP were determined by one-way ANOVA with post-hoc Dunnett's multiple comparisons.

Table 5.7: **Allosteric modulation parameters, α and β, of compound 249, compound 2 and BETP allosteric modulation of OXM-mediated cAMP responses at both HEK293S-GLP-1R-WT and HEK293S-GLP-1R-C347A cell lines.**

GLP-1R	Compound	α [a]	β [b]	$\alpha\beta$ [c]	log$\alpha\beta$	R^2 [d]
Wildtype	Cmpd 249	4.800	2.189	10.50	1.02	0.9661
	Cmpd 2	5.904	10.37	61.22	1.79	0.9018
	BETP	25.92	0.5582	14.47	1.16	0.9197
C347A	Cmpd 249	35.73	0.3908	13.96	1.14	0.9691
	Cmpd 2			N.D.		
	BETP					

[a] represents the cooperativity determined by the operational model of agonism and allosterism.
[b] represents the scaling factor determined by the operational model of agonism and allosterism.
[c] represents the combinatorial values of both cooperativity and scaling factors. A positive log$\alpha\beta$ value > 1 denotes positive allosteric modulation.
[d] denotes the goodness of fit of the data set to the operational model of agonism and allosterism.

5.4.3 Compound 249 allosteric effect on intracellular calcium mobilisation in the absence of C347

Having elucidated the C347-independent mechanism of action of compound 249 on potentiating OXM-mediated cAMP responses, the effect of C347 mutation on iCa^{2+} mobilisation was investigated. To do so, iCa^{2+} mobilisation was determined in both HEK293S-GLP-1R-WT and HEK293S-GLP-1R-C347A cell lines, which methods closely followed those utilised in Section 5.3.4. Similar to its negative allosteric modulation on OXM-mediated iCa^{2+} response in the wildtype setting, compound 249 also exhibited negative allosteric modulation in OXM-mediated iCa^{2+} response in the absence of C347, of which it retained its reduction of potency of OXM-mediated iCa^{2+} mobilisation by nearly 10-fold (pEC_{50} value of OXM in GLP-1R-C347A setting reduced from 7.15 $\pm$ 0.16 to 6.46 $\pm$ 0.21, $p < 0.05$) (Fig. 5.13 and Table 5.8). The results were again fitted into the operational model of allosterism which showed negative cooperativity $\log\alpha\beta$ values of 1.92, further suggesting compound 249 role as a NAM on OXM-mediated iCa^{2+} mobilisation in a C347-independent manner (Table 5.8).

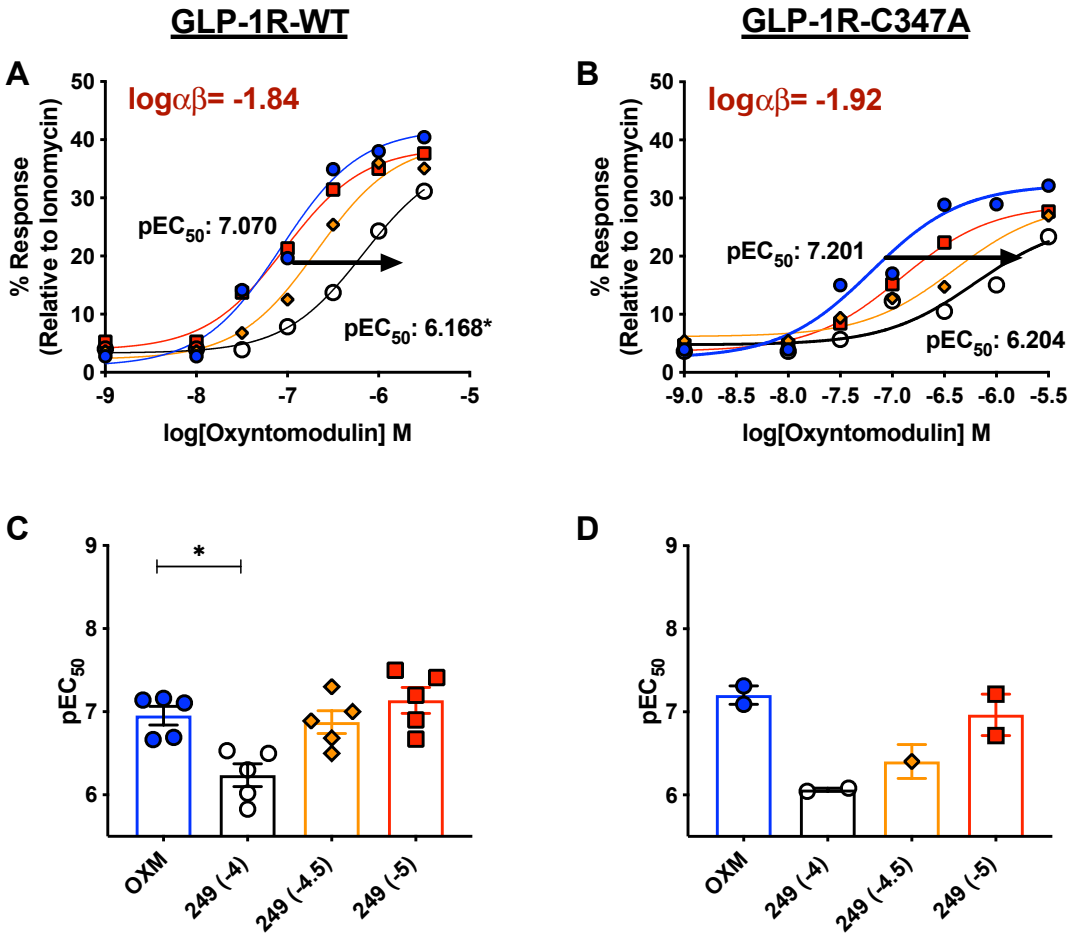

Figure 5.13: **Compound 249 shows negative allosteric modulation on OXM-mediated intracellular calcium mobilisation in HEK293S-GLP-1R-WT and HEK293S-GLP-1R-C347A cells.** Intracellular calcium mobilisation was measured with the methods of pre-treatment of compound 249 for 15 mins prior to the addition of OXM without washing of compounds. Graphs (A) and (B) show that compound 249 inhibits intracellular calcium mobilisation in a concentration-dependent manner in both HEK293S cells stably expressing GLP-1R-WT and GLP-1R-C347A respectively. (C) and (D) show the scatter plots of the results from (A) and (B). 80,000 cells/well of HEK293S-GLP-1R-WT or HEK293S-GLP-1R-C347A cells were seeded onto black-96 well plate overnight prior to the measurement of intracellular calcium mobilisation by the pre-treatment of compound 249 with OXM. All data were normalised to the 10μM ionomycin concentration-response curve. All data are means from at least 2 independent experiments $\pm$ S.E.M (upper error bars). Statistical significance compared with OXM (*, $p < 0.05$) for compound 249 at different concentrations was determined by one-way ANOVA with post-hoc Dunnett's multiple comparisons.

Table 5.8: **Concentration-dependent negative allosteric modulations of OXM-mediated iCa^{2+} mobilisation potentiated by compound 249 in HEK293S-GLP-1R-WT or HEK293S-GLP-1R-C347A cell lines.**

GLP-1R	Conc.	pEC_{50} [a]	E_{max} [b]	Span	n
WT	DMSO	7.07±0.27	41.89±4.48	40.86±5.39	5
	1x10^{-4}M	6.17±0.32*	37.44±7.75	34.12±7.39	5
	3.16x10^{-5}M	6.68±0.12	39.68±2.34	37.42±2.45	5
	1x10^{-5}M	7.03±0.20	38.68±3.59	34.87±3.92	5
C347A	DMSO	7.15±0.16	32.64±2.03	27.62 ± 2.38	2
	1x10^{-4}M	6.46±0.21	22.47±2.29	18.77 ± 2.28	2
	3.16x10^{-5}M	6.98±0.36	28.92±3.38	20.58 ± 4.06	1
	1x10^{-5}M	7.00±0.22	32.93±3.44	28.00 ± 3.69	2

Values were generated when the data were fitted to the three-parameter logistic equation. Means ± S.E.M of n individual result sets were shown.

[a] Negative logarithm of agonist concentration when reaching half maximal response

[b] % of maximal response observed when stimulated with ligands relative to ionomycin

Statistical significance compared with OXM (*, $p < 0.05$) for compound 249 at different concentrations was determined by one-way ANOVA with post-hoc Dunnett's multiple comparisons.

5.4.4 Effect on ERK1/2 phosphorylation

Lastly, the effect of the introduction of C347A mutation to the GLP-1R on OXM-mediated pERK1/2 signalling was investigated. Using the same approach in measuring pERK1/2 signalling in the HEK293S-GLP-1R-WT cells, compound 249 did not exert any allosteric effect in the HEK293S-GLP-1R-C347A cell line (Fig. 5.14 and Table 5.9). However, the results could not be fitted into the operational model of allosterism due to its weak effect on pERK1/2 activation in the GLP-1R-C347A setting. Yet, it was concluded that compound 249 is a NAL in both HEK293S-GLP-1R-WT and HEK293S-GLP-1R-C347A cell lines given these collective observations.

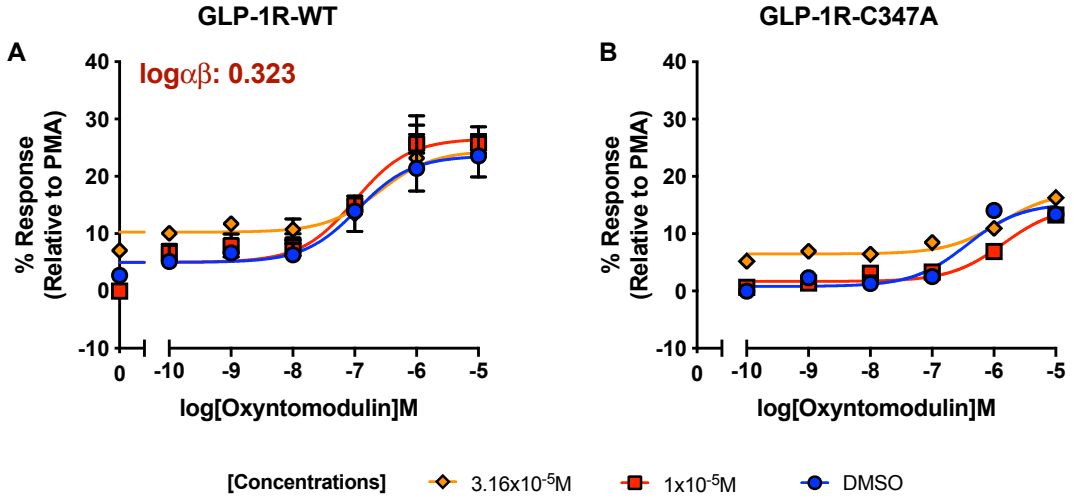

Figure 5.14: **Compound 249 acts as a neutral allosteric ligand of pERK1/2 in HEK293S-GLP-1R-WT and HEK293S-GLP-1R-C347A cells.** Compound 249 does not induce potentiation or inhibition of OXM-mediated pERK1/2 signalling in both HEK293S-GLP-1R-WT and HEK293S-GLP-1R-C347A cell lines. 35,000 cells/well of HEK293 cells stably expressing wildtype or C347A-mutated GLP-1R were used in the ERK1/2 assays. All data were normalised to 100μM PMA and were means of duplicates of at least one independent experiment $\pm$ S.E.M (upper error bars).

Table 5.9: **Compound 249 acts as a neutral allosteric ligand of OXM-mediated ERK1/2 phosphorylation in both HEK293S-GLP-1R-WT and HEK293S-GLP-1R-C347A cells.**

GLP-1R	Conc.	pEC_{50} [a]	E_{max} [b]	Span	n
WT	DMSO	6.94±0.51	23.58±3.24	18.60±3.73	4
	$3.16x10^{-5}$M	6.60±0.20	24.50±2.58	14.24±2.82	4
	$1x10^{-5}$M	7.00±0.21	26.58±1.85	21.57±2.12	4
C347A	DMSO	6.44±0.26	15.30±1.96	14.50±2.00	2[NB]
	$3.16x10^{-5}$M	5.89±0.19	17.40±1.22	10.93±1.24	2[NB]
	$1x10^{-5}$M	5.85±0.14	14.87±1.12	13.21±1.14	2[NB]

Values were generated when the data were fitted to the three-parameter logistic equation. Means ± S.E.M of n individual result sets were shown.
[a] Negative logarithm of agonist concentration when reaching half maximal response
[b] % of maximal response observed when stimulated with ligands relative to PMA
[NB] Preliminary results are shown here only due to COVID-19 obstruction of experimental schedule.

5.4.5 Summary of compound 249 C347-independent allosteric modulation

To conclude, compound 249 demonstrated analogous allosteric modulation in the GLP-1R-C347A setting when compared to the wildtype GLP-1R. Table 5.10 summarises the allosteric parameters for each signalling pathway. The bar charts (Fig. 5.15) also depict compound 249 unique mode of allosteric action in both GLP-1R-WT and GLP-1R-C347A settings.

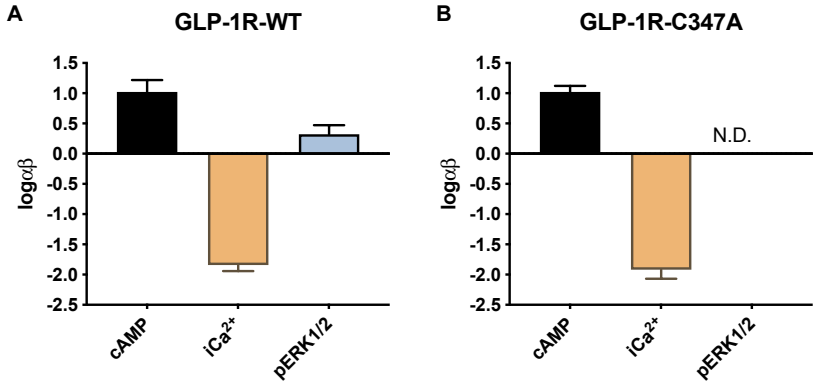

Figure 5.15: **Bar charts summarising compound 249 allosterism in both HEK293S-GLP-1R-WT and HEK293S-GLP-1R-C347A cells.** The above bar charts summarise compound 249 allosteric actions on OXM-mediated GLP-1R signalling pathways. It is concluded that compound 249 is a PAM on cAMP accumulation, a NAM on iCa^{2+} mobilisation and a NAL on pERK1/2 pathway. N.D. indicates not determined.

Table 5.10: **Allosteric modulation parameters, α and β, of compound 249 allosterism of OXM-mediated cAMP accumulation, iCa^{2+} mobilisation and pERK1/2 activation in both HEK293S-GLP-1R-WT or HEK293S-GLP-1R-C347A cells.**

GLP-1R	Signalling pathway	α[a]	β[b]	$\alpha\beta$[c]	log$\alpha\beta$	R^2[d]
Wildtype	cAMP	4.800	2.189	10.50	1.02	0.9661
	iCa^{2+}	0.01343	1.076	0.0145	-1.84	0.8627
	pERK1/2	2.672	0.7891	2.108	0.323	0.8629
C347A	cAMP	35.73	0.3908	13.96	1.14	0.9691
	iCa^{2+}	0.01164	1.042	0.0121	-1.92	0.8563
	pERK1/2	N.D.				

[a] represents the cooperativity determined by the operational model of agonism and allosterism.
[b] represents the scaling factor determined by the the operational model of agonism and allosterism.
[c] represents the combinatorial values of both cooperativity and scaling factors. A positive log$\alpha\beta$ value > 1 and <1 denote positive and negative allosteric modulation respectively.
[d] denotes the goodness of fit of the data set to the operational model of agonism and allosterism.

5.5 Compound 249 allosteric modulation on GCGR and GIPR

5.5.1 Compound 249 does not activate GCGR and GIPR

Given the close structural homology among the glucagon-like receptor family, compound 249 ability to activate GCGR and GIPR was investigated. CHO-GCGR and CHO-GIPR cells, which illustrated robust agonistic responses upon receptor activation in Section 3.2.2, were utilised to facilitate the screening. A range of concentration of compound 249 (from 100μM to 10pM) were applied to CHO-GCGR and CHO-GIPR cells, wherein 15 minutes ligand stimulation was allowed in the presence of the PDE inhibitor, rolipram. CHO-GLP-1R cells were included to act as a comparison to the results in CHO-GCGR and CHO-GIPR cells. Untransfected CHO-K1 cells were used as a null receptor background.

Similar to the observations in the closely related GLP-1R, compound 249 also did not activate either GCGR or GIPR (Fig. 5.16 and Table 5.11). Again, the apparent increase in cAMP production when compound 249 at 100μM was applied was due to autofluorescence. Having concluded that compound 249 lacked intrinsic agonism in both GIPR and GCGR, its potential allosterism at both GCGR and GIPR were subsequently investigated.

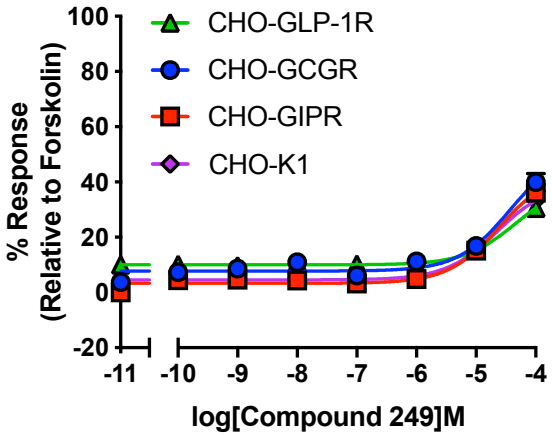

Figure 5.16: **Compound 249 does not activate GLP-1R, GCGR and GIPR.** Compound 249 fails to activate cAMP accumulation responses at the GLP-1R, GCGR and GIPR. 1000 CHO-GLP-1R, CHO-GCGR, CHO-GIPR and CHO-K1 cells/well under 15-minute stimulation in the presence of rolipram were used in the cAMP assays. All data were normalised to the maximum cAMP response determined by 100μM forskolin stimulation. All data were means of 2 independent experiments with duplicates $\pm$ S.E.M (upper error bars). Table 5.11 shows the pEC_{50} and E_{max} values of ligand responses.

Table 5.11: **Compound 249 does not activate GLP-1R, GCGR and GIPR.**

Cell line	pEC_{50} [a]	E_{max} [b]	Span	n
CHO-GLP-1R	4.33±0.31	40.26±8.83	43.92±7.46	4
CHO-GCGR	4.44±0.24	51.66±7.61	40.90±5.28	4
CHO-GIPR	4.61±0.23	44.21 5.42	30.24±8.69	4
CHO-K1	4.64±0.12	39.88±3.25	35.31±3.25	4

Values were generated when the data were fitted to the three-parameter logistic equation. Means ± S.E.M of n individual result sets were shown.
[a] Negative logarithm of agonist concentration when reaching half maximal response
[b] % of maximal response observed when stimulated with ligands relative to forskolin

5.5.2 Compound 249 is not a GIPR allosteric modulator

In order to determine if compound 249 exhibited any allosteric modulation at the GIPR, cAMP functional assay was performed, which CHO-GIPR cells were co-stimulated with a range of GIPR cognate ligand, GIP, and a fixed concentration of compound 249 (at 10μM) for 15 minutes in the presence of PDE inhibitor rolipram. Here compound 249 did not significantly potentiate GIP-mediated cAMP responses (Fig. 5.17 and Table 5.12). Therefore, it was concluded that compound 249 did not allosterically modulate GIPR.

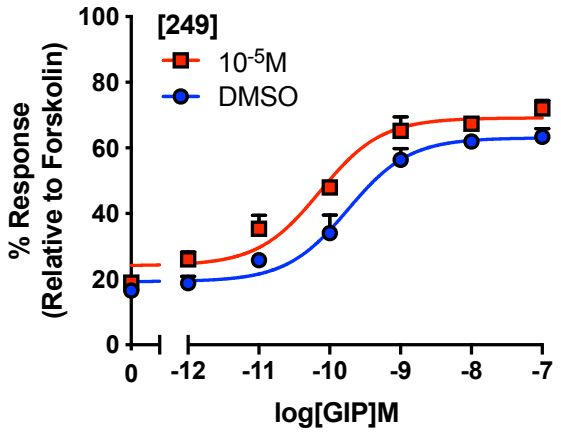

Figure 5.17: **Compound 249 does not exhibit allosteric modulation on GIP-mediated cAMP accumulation response in CHO-GIPR cells.** 1000 CHO-GIPR cells/well under 15-minute co-stimulation with GIP in the presence of rolipram were used in the cAMP assays. All data were normalised to the maximum cAMP response determined by 100μM forskolin stimulation. All data are means from at least 2 independent experiments ± S.E.M (upper error bars).

Table 5.12: **Compound 249 does not exhibit allosteric modulation in GIP-mediated cAMP accumulation response in CHO-GIPR cells.**

Compound	Conc.	pEC_{50} [a]	E_{max} [b]	E_{min} [c]	Span	n
DMSO	-	9.64±0.11	69.72±2.61	19.28±1.69	56.28±3.13	8
249	10^{-5}M	9.84±0.15^{ns}	69.24±2.17	24.15±2.28	44.99±3.01	4

Values were generated when the data were fitted to the three-parameter logistic equation. Means ± S.E.M of n individual result sets were shown.
[a] Negative logarithm of agonist concentration when reaching half maximal response
[b] % of maximal response observed when stimulated with ligands relative to forskolin
[c] % of minimal response observed when stimulated with ligands relative to forskolin.
Statistical significance compared with GIP (ns, non-statistically significant) for compound 249 was determined by Student's t-test with Welch's correction.

5.5.3 Characterisation of compound 249 allosteric modulation at the GCGR

Given the structural resemblance between GLP-1R and GCGR and that OXM could activate both receptors, it is of particular interest to determine if compound 249 can also allosterically modulate OXM-mediated cAMP responses at the GCGR. Therefore, cAMP functional assays were performed in CHO-GCGR cells. Compound 2 and BETP, albeit their GLP-1R specificity [Koole et al., 2010, Willard et al., 2012a], were also assayed to compare with compound 249 potential allosteric actions at the GCGR.

The following results illustrated that compound 249 enhanced the potency of OXM-mediated cAMP response at the GCGR by more than 17-fold in a concentration-dependent manner (pEC_{50} value increased from 9.19 ± 0.11 to 10.24 ± 0.09 when compound 249 at 10μM was applied, $p < 0.0001$) (Fig. 5.18, Fig. 5.19 and Table 5.13). The data were further applied into the operational model of allosterism and a positive $\log\alpha\beta$ value of 1.48 was resulted, indicating positive allosteric modulation (Table 5.15). Similar to the observation at GLP-1R (Fig. 5.4), compound 249 only potentiated GCG-mediated cAMP response at the GCGR at a high concentration (i.e. at 3.16x10^{-5}M), even though OXM and GCG are closely related [Pocai et al., 2009] (Fig. 5.18, Fig. 5.19 and Table 5.14). Collectively, these findings suggested compound 249 acted as a GLP-1R and GCGR small molecule PAM that selectively potentiated OXM-mediated cAMP production when tested in the CHO-GCGR cell system. Given its unique properties at both structurally related receptors, other signalling properties of compound 249 at the GCGR were further explored.

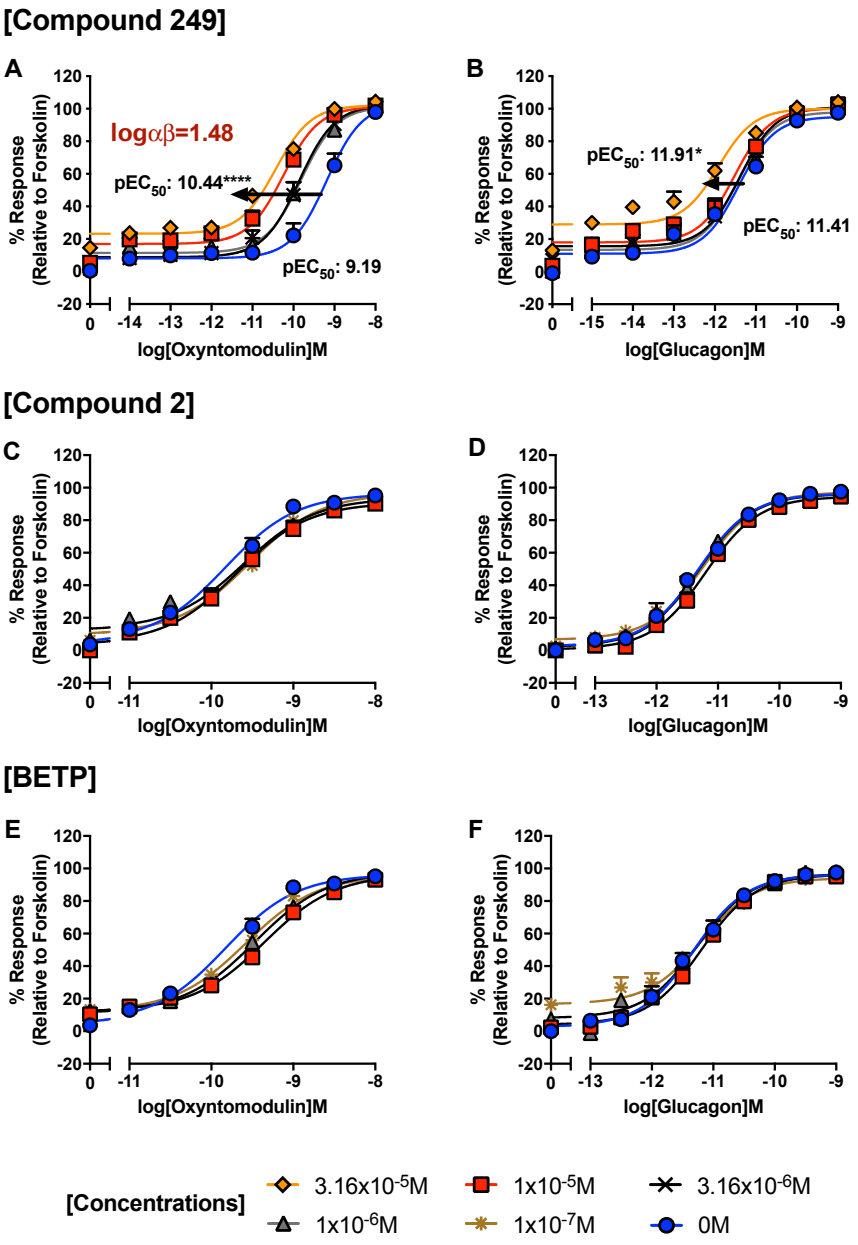

Figure 5.18: **Compound 249 induces a concentration-dependent positive allosteric modulation on OXM-mediated cAMP accumulation response in CHO-GCGR cells.** Compound 249 potentiates a concentration-dependent OXM-mediated cAMP accumulation response at GCGR as shown in (A) and (B). Compound 2 (C and D) and BETP (E and F) do not have any allosteric effect on OXM and GCG-mediated cAMP responses. 1000 CHO-GCGR cells/well under 15-minute co-stimulation with OXM or GCG in the presence of rolipram were used in the cAMP assays. All data were normalised to the maximum cAMP response determined by 100μM forskolin stimulation. All data are means of duplicate from at least one independent experiment with duplicates $\pm$ S.E.M (upper error bars). Statistical significance compared with OXM (*, $p < 0.05$; ****, $p < 0.0001$) for compound 249 was determined by one-way ANOVA with post-hoc Dunnett's multiple comparisons.

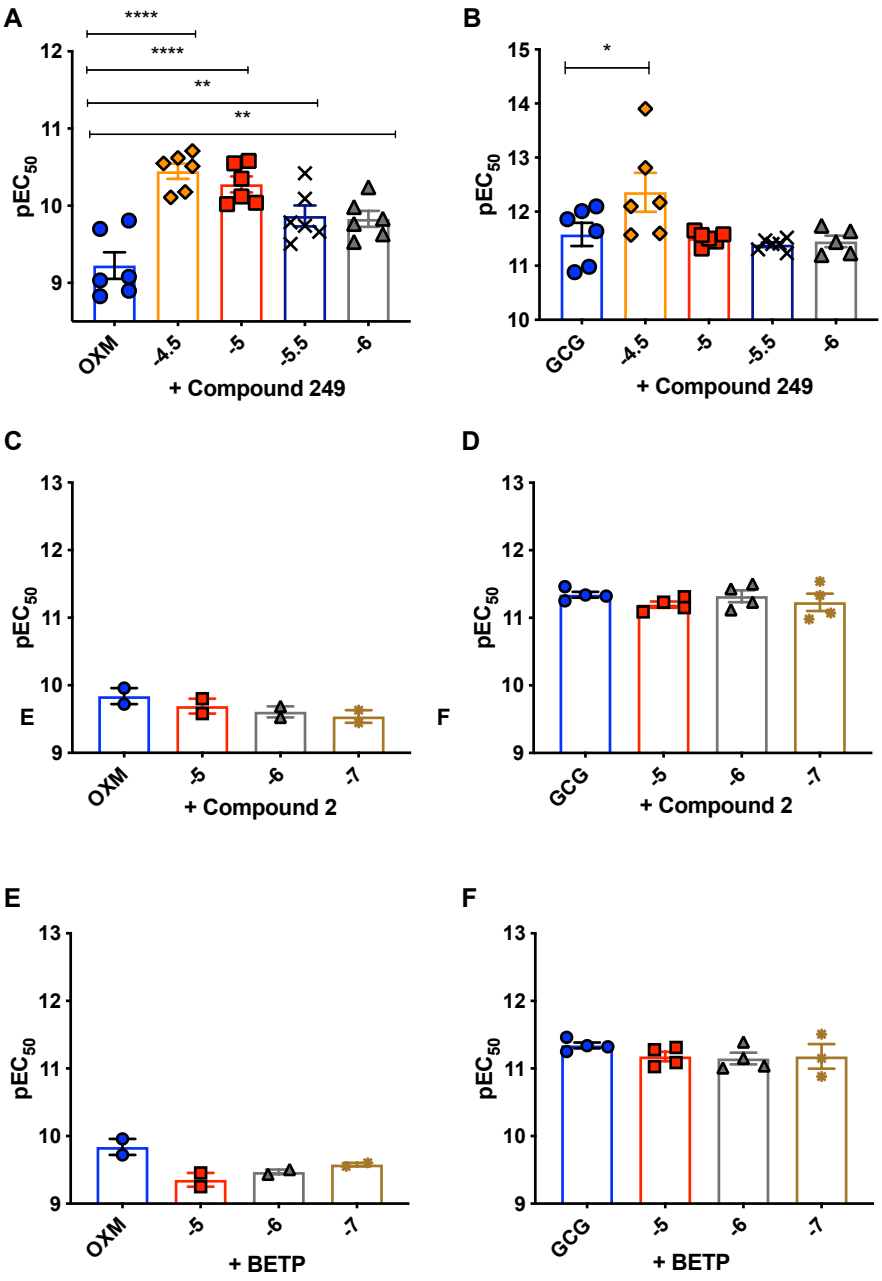

Figure 5.19: **Scatter plots illustrating compound 249 induces a concentration-dependent positive allosteric modulation on OXM-mediated cAMP accumulation response in CHO-GCGR cells.** Compound 249 potentiates a concentration-dependent OXM-mediated cAMP accumulation response at GCGR as shown in A. Compound 2 (C and D) and BETP (E and F) do not have any allosteric effect on OXM and GCG-mediated cAMP responses. 1000 CHO-GCGR cells/well under 15-minute co-stimulation with OXM or GCG in the presence of rolipram were used in the cAMP assays. All data were normalised to the maximum cAMP response determined by 100μM forskolin stimulation. All data are means of duplicates from at least one independent experiment $\pm$ S.E.M (upper error bars). Statistical significance compared with OXM (*, $p < 0.05$; **, $p < 0.01$; ****, $p < 0.0001$) for compound 249 was determined by one-way ANOVA with post-hoc Dunnett's multiple comparisons.

Table 5.13: **Concentration-dependent allosteric modulations of OXM-mediated cAMP accumulation potentiated by compound 249, Compound 2 and BETP in CHO-GCGR cells.**

Ligand	Compound	Concentration	pEC_{50} [a]	E_{max} [b]	E_{min} [c]	Span	n
OXM	DMSO	-	9.19±0.11	103.46±5.41	8.09±1.90	95.37±5.55	6
	Compound 249	3.16x10^{-5}M	10.44±0.08****	102.18±2.37	23.25±1.60	78.93±2.74	6
		1x10^{-5}M	10.24±0.09****	101.28±2.77	16.95±1.73	84.33±3.14	6
		3.16x10^{-6}M	9.86±0.08**	102.38±3.27	8.84±1.76	93.53±3.59	6
		1x10^{-6}M	9.81±0.10**	101.34±4.02	11.45±2.11	89.89±4.38	6
	Compound 2	1x10^{-5}M	9.69±0.07	90.85±2.39	4.41±2.21	86.44±2.91	2^{NB}
		1x10^{-6}M	9.60±0.08	93.64±2.89	13.13±2.50	80.52±3.40	2^{NB}
		1x10^{-7}M	9.54±0.10	96.63±3.68	10.39±3.60	86.24±4.55	2^{NB}
	BETP	1x10^{-5}M	9.35±0.05	96.62±2.04	12.56±1.36	84.06±2.20	2^{NB}
		1x10^{-6}M	9.47±0.02	97.93±1.10	11.70±0.82	86.23±1.23	2^{NB}
		1x10^{-7}M	9.58±0.06	95.95±2.31	12.19±1.93	83.75±2.69	2^{NB}

Values were generated when the data were fitted to the three-parameter logistic equation. Means ± S.E.M of n individual result sets were shown.

[a] Negative logarithm of agonist concentration when reaching half maximal response

[b] % of maximal response observed when stimulated with ligands relative to forskolin

[c] % of minimal response observed when stimulated with ligands relative to forskolin.

[NB] Preliminary results are shown here only due to COVID-19 obstruction of experimental schedule.

Statistical significance compared with OXM (**, $p < 0.01$; ****, $p < 0.0001$) for compound 249 was determined by one-way ANOVA with post-hoc Dunnett's multiple comparisons.

Table 5.14: **Concentration-dependent allosteric modulations of GCG-mediated cAMP accumulation potentiated by Compound 2 and BETP but not compound 249 in CHO-GCGR cells.**

Ligand	Compound	Concentration	pEC_{50} [a]	E_{max} [b]	E_{min} [c]	Span	n
GCG	DMSO	-	11.41±0.13	95.14±2.83	11.01±2.56	84.13±4.41	6
	Compound 249	3.16x10^{-5}M	11.91±0.12*	100.08±2.67	28.99±2.24	71.09±3.38	6
		1x10^{-5}M	11.51±0.08	100.32±2.34	17.98±1.64	82.35±2.73	6
		3.16x10^{-6}M	11.39±0.10	100.99±3.07	15.59±2.04	85.40±3.53	6
		1x10^{-6}M	11.43±0.12	98.00±3.49	13.41±2.36	84.59±4.03	6
	Compound 2	1x10^{-5}M	11.20±0.05	94.49±1.75	0.81±1.73	93.69±2.24	4
		1x10^{-6}M	11.32±0.06	96.11±2.13	2.42±2.53	93.70±3.03	4
		1x10^{-7}M	11.23±0.06	97.28±2.25	6.77±2.14	90.51±2.82	4
	BETP	1x10^{-5}M	11.19±0.05	96.32±1.71	24.25±1.76	92.07±2.20	4
		1x10^{-6}M	11.26±0.08	96.66±2.70	8.32±3.25	88.34±3.81	4
		1x10^{-7}M	11.19±0.10	94.13±3.40	16.86±3.09	77.27±4.10	3

Values were generated when the data were fitted to the three-parameter logistic equation. Means ± S.E.M of n individual result sets were shown.

[a] Negative logarithm of agonist concentration when reaching half maximal response

[b] % of maximal response observed when stimulated with ligands relative to forskolin

[c] % of minimal response observed when stimulated with ligands relative to forskolin.

Statistical significance compared with GCG (*, $p < 0.05$) for compound 249, Compound 2 and BETP was determined by one-way ANOVA with post-hoc Dunnett's multiple comparisons.

Table 5.15: **Allosteric modulation parameters, α and β, of compound 249 actions of OXM-mediated cAMP accumulation in CHO-GCGR cells.**

Cell line	Ligand	α[a]	β[b]	$\alpha\beta$[c]	log$\alpha\beta$	R^2[d]
CHO-GCGR	OXM	14.24	2.124	30.25	1.48	0.9145
	GCG	3.278	0.001986	2.00	0.30	0.9256

[a] represents the cooperativity determined by the operational model of agonism and allosterism.
[b] represents the scaling factor determined by the operational model of agonism and allosterism.
[c] represents the combinatorial values of both cooperativity and scaling factors. A positive log$\alpha\beta$ value > 1 and a log$\alpha\beta$ value between 0 and 1 denote positive allosteric modulation and neutral allosteric ligand respectively.
[d] denotes the goodness of fit of the data set to the operational model of agonism and allosterism.

5.5.4 Compound 249 allosteric modulation at HEKΔCTR recombinant cell line

Having discovered the allosteric modulation of OXM-mediated cAMP responses in the CHO-GCGR cell line, the allosteric effect of compound 249 was further validated in the HEKΔCTR-GCGR cell line. The use of this cell line in measuring robust cAMP and iCa^{2+} signalling responses mediated by GCGR peptide agonists were described in section 3.2.6.

5.5.4.1 Compound 249 is not a PAM on cAMP signalling at the GCGR

To determine compound 249 allosterism at the GCGR, a range of concentrations of OXM and GCG were applied to the HEKΔCTR-GCGR cells together with fixed concentrations of compound 249 for 15 mins in the presence of PDE inhibitor rolipram. Interestingly, unlike the observations in the CHO-GCGR cell line (Fig. 5.18), compound 249 did not significantly potentiate OXM-mediated cAMP production (Fig. 5.20), presumably due to the innate cellular composition difference between cell lines of rodent and human species. Further application of the operational model of allosterism resulted in a positive, yet less than 1, log$\alpha\beta$ value of 0.7355, indicating its effect as a NAL. Consistent with the observation in CHO-GCGR cell line, compound 249 did not potentiate cAMP responses mediated by GCG (Fig. 5.20). Compound 249 was also found to marginally potentiate the cAMP response of GCG, however such augmentation was not statistically significant. In spite of the conclusion that compound 249 did not allosterically modulate cAMP responses in the HEKΔCTR-GCGR cells, compound 249 allosteric actions in iCa^{2+} signalling at the GCGR were still evaluated.

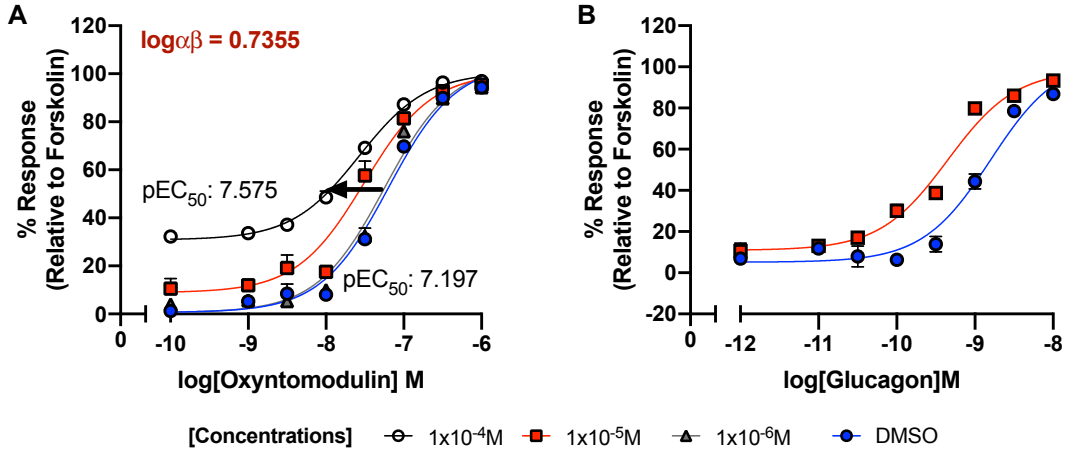

Figure 5.20: **Compound 249 does not exhibit a concentration-dependent positive allosteric modulation on OXM-mediated cAMP accumulation response in HEKΔCTR-GCGR cells.** (A) Compound 249 does not potentiate a concentration-dependent OXM-mediated cAMP accumulation response at GCGR as in HEKΔCTR-GCGR cells, nor in the (B) GCG-mediated cAMP response. 1000 HEKΔCTR-GCGR cells/well under 15-minute co-stimulation with OXM or GCG in the presence of rolipram were used in the cAMP assays. All data were normalised to the maximum cAMP response determined by 100μM forskolin stimulation. All data are means of duplicates from at least one independent experiment ± S.E.M (upper error bars).

Table 5.16: **Compound 249 does not exhibit a concentration-dependent positive allosteric modulation on OXM-mediated cAMP accumulation responses in HEKΔCTR-GCGR cells.**

Ligand	[249] M	pEC_{50} [a]	E_{max} [b]	Span	n
OXM	DMSO	7.20±0.06	104.47±3.38	103.83±3.50	4
	1x10^{-4}M	7.58±0.04^{ns}	100.63±1.15	69.78±1.33	4
	1x10^{-5}M	7.51±0.08	100.53±3.26	91.67±3.71	4
	1x10^{-6}M	7.25±0.08	104.07±4.10	103.47±4.29	4
GCG	DMSO	8.80±0.11	104.48±7.11	99.36±6.91	2^{NB}
	1x10^{-5}M	9.35±0.08	98.56±3.58	87.67±3.85	2^{NB}

Values were generated when the data were fitted to the three-parameter logistic equation. Means ± S.E.M of n individual result sets were shown.

[a] Negative logarithm of agonist concentration when reaching half maximal response

[b] % of maximal response observed when stimulated with ligands relative to forskolin

[NB] Preliminary results are shown here only due to COVID-19 obstruction of experimental schedule.

Statistical significance compared with OXM (ns, non-statistically significant) in the presence of various concentrations of compound 249 was determined by one-way ANOVA with post-hoc Dunnett's multiple comparisons.

5.5.4.2 Compound 249 is a NAM on iCa^{2+} signalling at GCGR

Similar to the approach in Section 5.3.4, the HEKΔCTR-GCGR cells were pre-incubated with fixed concentrations of compound 249, prior to co-stimulating with the GCGR agonists, OXM and GCG. In the presence of compound 249, the OXM-mediated iCa^{2+} release was reduced by nearly 5-fold in a dose-dependent manner, yet the reduction was non-statistically significant (pEC$_{50}$ value decreased from 7.07 $\pm$ 0.18 to 6.40 $\pm$ 0.21) (Fig. 5.21 and Table 5.17). The log$\alpha\beta$ value generated through the operational model of allosterism resulted in a negative value of -0.8599, further implicating its role as a NAM. Similar to the observation at the GLP-1R, compound 249 did not affect the iCa^{2+} release mediated by GCG, further illustrating the probe dependence of compound 249 actions towards OXM mediated signalling responses at both GLP-1R and GCGR.

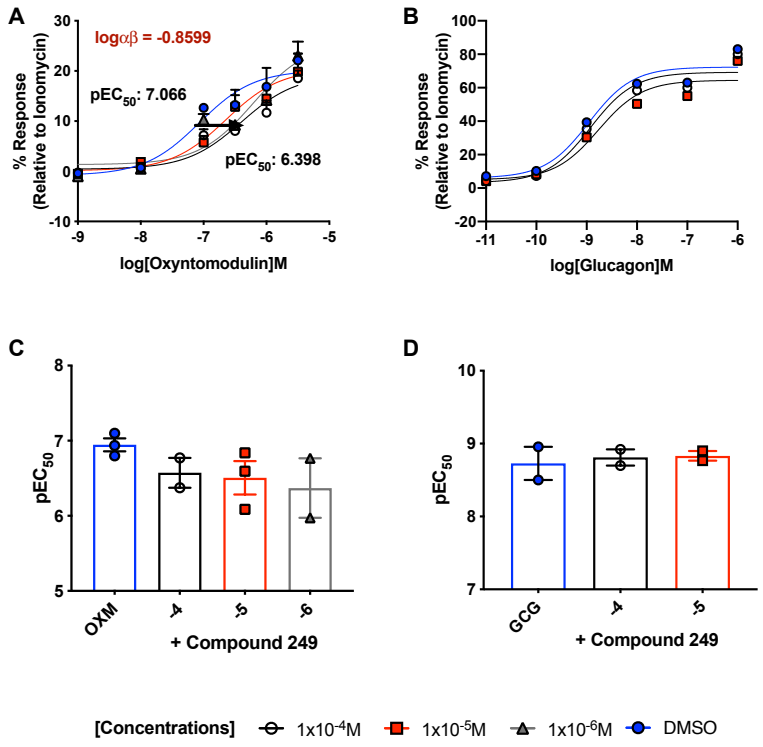

Figure 5.21: **Compound 249 shows negative allosteric modulation on OXM-mediated intracellular calcium mobilisation in HEKΔCTR-GCGR cells.** (A) shows that compound 249 inhibits OXM-mediated iCa^{2+} mobilisation in a concentration-dependent manner in HEKΔCTR-GCGR cells while not in GCG-mediated iCa^{2+} response. (C) and (D) show the scatter plots of the results in HEKΔCTR-GCGR acting at OXM and GCG respectively. 80,000 cells/well of HEKΔCTR-GCGR cells were seeded onto black-96 well plate overnight prior to the measurement of intracellular calcium mobilisation by the pre-treatment of compound 249 for 15 mins before the addition of OXM or GCG without washing off the compound. All data were normalised to the 10μM ionomycin concentration-response curve. All data are means from at least 2 independent experiments with duplicates $\pm$ S.E.M (upper error bars).

Table 5.17: **Compound 249 shows negative allosteric modulation on OXM-mediated intracellular calcium mobilisation in GCGR.**

Ligand	Concentration	pEC_{50} [a]	E_{max} [b]	Span	n
OXM	DMSO	7.07±0.18	20.18±1.50	21.00±1.91	3
	1x10^{-4}M	6.40±0.21^{ns}	19.23±2.43	18.81±2.42	2
	1x10^{-5}M	6.65±0.28^{ns}	20.41±2.95	20.30±3.22	3
	1x10^{-6}M	6.21±0.26^{ns}	25.87±4.12	24.54±4.01	2
GCG	DMSO	8.96±0.26	72.35±5.37	66.36±8.26	2
	1x10^{-4}M	8.92±0.26^{ns}	69.23±5.44	65.98±8.28	2
	1x10^{-5}M	8.77±0.33^{ns}	64.47±6.18	59.43±8.93	2

Values were generated when the data were fitted to the three-parameter logistic equation. Means ± S.E.M of n individual result sets were shown.

[a] Negative logarithm of agonist concentration when reaching half maximal response

[b] % of maximal response observed when stimulated with ligands relative to ionomycin

Statistical significance compared with OXM and (ns, non-statistically significant) in the presence of various concentrations of compound 249 were determined by one-way ANOVA with post-hoc Dunnett's multiple comparisons.

5.5.5 Summary of compound 249 allosteric action at the GCGR

In summary, compound 249 acts as a PAM on OXM-mediated cAMP response in CHO-GCGR cell line but not in the HEKΔCTR-GCGR cell line, highlighting the importance of considering the cellular composition difference between the rodent and human recombinant cell systems when evaluating GCGR allosteric modulators. Similar to its action at the GLP-1R, compound 249 acts as a NAM on OXM-mediated iCa^{2+} response but has no influence on GCG-mediated iCa^{2+} response. The summary of allosteric modulation of compound 249 at the GCGR in terms of $\log\alpha\beta$ is shown in Fig. 5.22.

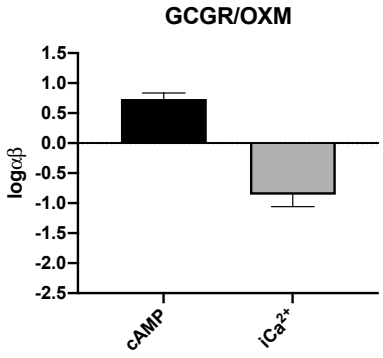

Figure 5.22: **Bar chart summarising compound 249 allosterism in the HEKΔCTR-GCGR cells.** The above bar chart summarises compound 249 allosteric actions on OXM-mediated GCGR signalling pathways. It is concluded that compound 249 is a NAL on cAMP accumulation and a NAM on iCa^{2+} mobilisation in relation to the OXM-mediated signalling pathway.

5.6 Evaluation of compound 249 allosterism in rodent insulinoma cell line

5.6.1 cAMP accumulation in INS-1 832/3 cell lines

As discovered previously, compound 249 is a PAM on OXM-mediated cAMP response in both CHO-GLP-1R (Appendix B.1) and HEK293S-GLP-1R-WT (Fig. 5.4) cell lines. To translate the results to a more physiologically relevant setting, compound 249 was then tested in the rat INS-1 832/3 wildtype cell line, which endogenously co-expresses both rat GLP-1R and GCGR which are functionally similar to those of human GLP-1R and GCGR [Knudsen et al., 2012]. The contribution of GIPR and GLP-1R to the allosteric modulation of compound 249 was also determined with the use of the INS-1 832/3 GIPR-KO and GLP-1R-KO knock-out cell lines [Naylor et al., 2016]. Similar cAMP functional assays as in those performed in the HEK293S-GLP-1R-WT cells in the presence of PDE inhibitor, trequinsin, were conducted.

Here compound 249 induced nearly 10-fold increase in the potency of OXM-mediated cAMP response (pEC_{50} values increased from 7.12 $\pm$ 0.14 to 7.74 $\pm$ 0.07, $p < 0.01$, (Fig. 5.23 and Table 5.18) in the INS-1 832/3 wildtype cell line. These data sets were further fitted into the operational model of allosterism, of which a positive $\log\alpha\beta$ of 0.991 was obtained (Table 5.19), indicating compound 249 positive allosteric modulation in the rat insulinoma system. Likewise compound 249 also exhibited potentiation of OXM-mediated cAMP response in the INS-1 GIPR-KO cell system (pEC_{50} values increased from 7.62 $\pm$ 0.08 to 8.11 $\pm$ 0.13, $p < 0.001$), further illustrating compound 249 did not require GIPR to mediate its allosteric action (Fig. 5.23 and Table 5.18). A positive $\log\alpha\beta$ of 0.963 also illustrated compound 249 role as a PAM in the INS-1 GIPR-KO cell line (Table 5.19). More importantly, compound 249 did not potentiate cAMP responses in the INS-1 GLP-1R-KO cell line (Fig. 5.23 and Table 5.18), despite the fact that it was determined previously in CHO-GCGR cell line that compound 249 potentiated OXM-mediated cAMP response (Fig. 5.23). Yet the results here in INS-1 GLP-1R-KO cell line aligned with the results obtained in the HEKΔCTR-GCGR cell line, which showed the compound only exhibited minimal cAMP response potentiation (Fig. 5.20). Following the characterisation of the potentiation of cAMP response mediated by compound 249, compound 249 ability to facilitate GSIS was subsequently determined.

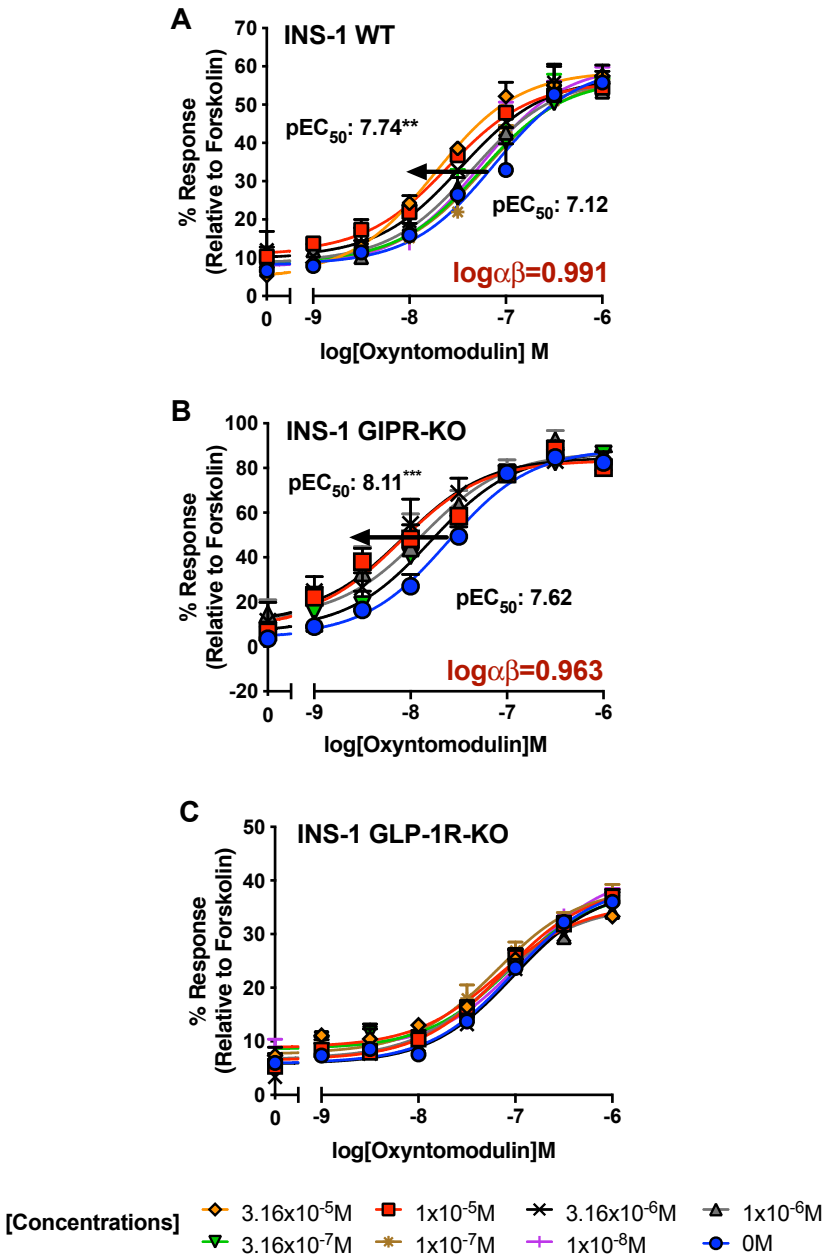

Figure 5.23: **Compound 249 induces a concentration-dependent positive allosteric modulation on OXM-mediated cAMP accumulation responses at the INS-1 832/3 WT and GIPR-KO cell line but not the GLP-1R-KO cell line.** Compound 249 shows OXM-mediated cAMP potentiation in both INS-1 832/3 WT and INS-1 GIPR-KO cells. Compound 249 has no allosteric modulation activity without the presence of GLP-1R. 2000 INS-1 WT, GIPR-KO or GLP-1R-KO cells/well under 15-minute co-stimulation with OXM in the presence of trequinsin were used in the cAMP assays. All data were normalised to the maximum cAMP response determined by 100μM forskolin stimulation. All data are means from at least 2 independent experiments with duplicates $\pm$ S.E.M (upper error bars). Table 5.18 show the pEC_{50} and E_{max} values of OXM-mediated cAMP accumulation responses in the presence of various concentrations of compound 249. Statistical significance compared with OXM (**, $p < 0.01$; ***, $p < 0.001$) for different concentrations of compound 249 was determined by one-way ANOVA with post-hoc Dunnett's multiple comparisons.

Table 5.18: **Compound 249 induces a concentration-dependent positive allosteric modulation on OXM-mediated cAMP accumulation responses at the INS-1 832/3 WT and GIPR-KO cell line but not the GLP-1R-KO cell line.**

INS-1 cell line	[Compound 249]M	pEC_{50} [a]	E_{max} [b]	Span	n
Wildtype	DMSO	7.12±0.14	60.32±4.16	52.11±4.14	5
	3.16x10^{-5}M	7.74±0.07**	58.79±1.59^{ns}	53.46±1.98	4
	1x10^{-5}M	7.60±0.08**	56.04±1.62^{ns}	55.85±1.84	6
	3.16x10^{-6}M	7.47±0.12*	57.08±2.72^{ns}	46.98±3.01	4
	1x10^{-6}M	7.35±0.12^{ns}	57.15±2.95^{ns}	48.30±3.18	6
	3.16x10^{-7}M	7.26±0.08^{ns}	56.80±1.79^{ns}	48.02±1.92	6
	1x10^{-7}M	7.23±0.10^{ns}	57.42±2.23^{ns}	48.51±2.28	6
	1x10^{-8}M	7.26±0.11^{ns}	60.43±2.94^{ns}	52.49±3.07	6
GIPR-KO	DMSO	7.62±0.08	88.74±2.67	84.05±3.22	6
	1x10^{-5}M	8.11±0.13***	83.44±3.52^{ns}	72.71±5.09	6
	3.16x10^{-6}M	8.08±0.17***	84.66±4.13^{ns}	71.94±6.08	6
	1x10^{-6}M	7.88±0.18**	87.00±5.26^{ns}	72.36±6.96	6
	3.16x10^{-7}M	7.79±0.11^{ns}	87.17±3.42^{ns}	79.62±4.38	6
GLP-1R-KO	DMSO	7.02±0.07	39.46±1.34	33.51±1.35	6
	3.16x10^{-5}M	7.18±0.09^{ns}	35.62±1.27^{ns}	26.72±1.33	6
	1x10^{-5}M	7.13±0.08^{ns}	38.79±1.46^{ns}	32.21±1.49	6
	3.16x10^{-6}M	7.01±0.08^{ns}	38.79±1.68^{ns}	32.95±1.69	6
	1x10^{-6}M	7.21±0.08^{ns}	35.29±1.19^{ns}	28.51±1.25	6
	3.16x10^{-7}M	7.06±0.11^{ns}	38.04±1.91^{ns}	29.44±1.97	6
	1x10^{-7}M	7.20±0.10^{ns}	38.68±1.61^{ns}	30.95±1.66	6
	1x10^{-8}M	6.92±0.09^{ns}	41.54±1.67^{ns}	32.76±1.63	6

Values were generated when the data were fitted to the three-parameter logistic equation. Means ± S.E.M of n individual result sets were shown.

[a] Negative logarithm of agonist concentration when reaching half maximal response.

[b] % of maximal response observed when stimulated with ligands relative to forskolin.

Statistical significance compared with OXM (*, $p < 0.05$; **, $p < 0.01$; ***, $p < 0.001$, ns, non-statistically significant) for different concentrations of compound 249 was determined by one-way ANOVA with post-hoc Dunnett's multiple comparisons.

Table 5.19: **Allosteric modulation parameters, α and β, of compound 249 actions of OXM-mediated cAMP responses in INS-1 832/3 WT and INS-1 GIPR-KO cells.**

Cell line	α [a]	β [b]	$\alpha\beta$ [c]	log$\alpha\beta$	R^2 [d]
INS-1 Wildtype	8.136	1.204	9.796	0.991	0.8948
INS-1 GIPR-KO	8.194	1.12	9.177	0.963	0.8561

[a] represents the cooperativity determined by the operational model of agonism and allosterism.
[b] represents the scaling factors determined by the operational model of agonism and allosterism.
[c] represents the combinatorial values of both cooperativity and scaling factors. A positive log$\alpha\beta$ value > 1 denotes positive allosteric modulation respectively.
[d] denotes the goodness of fit of the data set to the operational model of agonism and allosterism.

5.6.2 Investigation of compound 249 facilitation of insulin secretion

5.6.2.1 Insulin secretion in low and high glucose settings

The ability of compound 249 on mediating GSIS in the absence of GLP-1R endogenous agonists was first investigated. To do so, compound 249 at a fixed concentration (10μM) was tested in both low (2.8mM) and high (16.7mM) glucose conditions, in order to determine if any potentiation of insulin secretion by compound 249 was glucose-dependent, as well as to examine if the test compound would interfere with the TR-FRET-based insulin secretion assay. BETP (at 10μM) was also included in the assays to act as a comparison for the effect of compound 249 on GSIS. Apart from the INS-1 832/3 WT cell line, the INS-1 GIPR-KO and INS-1 GLP-1R-KO cell lines were also included in the assays in order to explore if the compound's effect on GSIS is GLP-1R-specific. The measurement of insulin secretion in the rat clonal pancreatic β cell lines has been validated in Section A.1, and the secretion assaying methods were described in Section 2.2.4.2. The DMSO content were kept constant across all conditions. However, one caveat for the insulin secretion results reported in the following sections is that the overall insulin content were not measured due to the deterioration of samples and COVID-19 obstruction of experimental schedule. Therefore, the following insulin secretion results are of preliminary nature only.

Corroborated with the observations in Fig. 4.4, the INS-1 832/3 WT, GIPR-KO and GLP-1R-KO cell lines responded to the high glucose challenge by significantly enhancing insulin secretion (Fig. 5.24), proving the functionality of the rat β cell lines in responding to glucose stimuli. Furthermore, compound 249 did not facilitate GSIS in the presence of high glucose stimuli in all three INS-1 WT, GIPR-KO and GLP-1R-KO cell lines, which further substantiated the observation that compound 249 did not

possess intrinsic agonism to mediate GSIS (Fig. 5.1 and 5.16). In contrary to compound 249, the ago-PAM BETP facilitated GSIS in the INS-1 832/3 WT cell line by 2.17-fold, the INS-1 GIPR-KO cell line by 1.75-fold and interestingly also in INS-1 GLP-1R-KO cell line by 2.07-fold, which contrasted with some reports suggesting its GLP-1R-specific action [Sloop et al., 2010] (Fig. 5.24). Notably, compound 249 and BETP did not enhance insulin secretion in low glucose condition, suggesting both compounds did not interfere with the TR-FRET-based assay, and the insulin potentiation effects were purely glucose-dependent. Having deduced compound 249 did not facilitate GSIS in the presence of glucose alone, its abilities to promote GSIS in the presence of GLP-1R endogenous agonists were then explored.

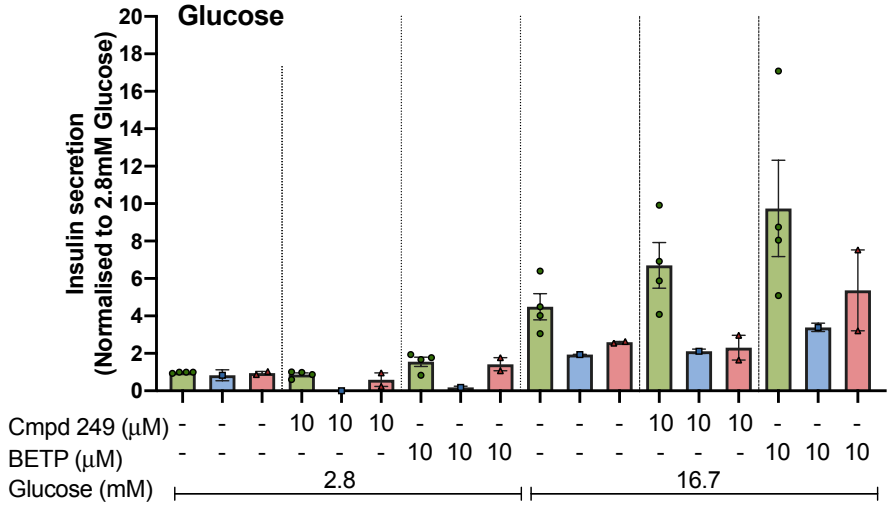

Figure 5.24: **Compound 249 does not affect GSIS in INS-1 832/3 WT, GIPR-KO and GLP-1R-KO cells when co-applied with high glucose.** Compound 249 does not facilitate GSIS while BETP enhances GSIS in the presence of 16.7mM glucose in INS-1 832/3 WT, GLP-1R-KO and GIPR-KO cell lines. Mean ± S.E.M. insulin secretion data (responses normalised to the GSIS secretion responses at 2.8mM respectively) in 1 to 4 independent experiments with quadruplicates are shown in the above scatter plots. Preliminary results are shown here due to COVID-19 obstruction of experimental schedule.

5.6.2.2 Compound 249 selectively potentiates GLP-1 and OXM-mediated GSIS

After concluding that compound 249 did not facilitate GSIS in the presence of glucose stimuli alone, its abilities to augment GSIS in the presence of GLP-1R endogenous and synthetic agonists, namely GLP-1, OXM, GLP-1(9-36)NH_2 and Ex-4, were then investigated. Again, the INS-1 GIPR-KO and GLP-1R-KO cell lines, together with the INS-1 832/3 WT cell line, were used in order to determine if the potentiation of GSIS was receptor-specific. To do so, following an hour of low glucose pre-incubation,

the INS-1 832/3 cells were incubated for an hour with a fixed concentration (10μM) of compound 249, BETP or DMSO as vehicle in the presence of GLP-1R agonists. Supernatants were then collected, and insulin levels were then measured.

Statistically significant difference in terms of insulin secretion between low and high glucose conditions in all rat β cell lines were observed, proving the responsiveness of the rat insulinoma cell lines to high glucose stimulation. Furthermore, 10nM GLP-1, 1μM OXM and 10nM Ex-4 further stimulated GSIS in both INS-1 832/3 WT and INS-1 GIPR-KO cell lines, implying the functional presence of the GLP-1R, as well as concurring with the results in Fig. 4.4. As shown previously in Fig. 4.4, GLP-1 and Ex-4 did not enhance GSIS in the INS-1 GLP-1R-KO cell line, implying the absence of GLP-1R in the GLP-1R-KO cell line. The presence of 1μM GLP-1(9-36)NH_2 also did not promote GSIS in all three INS-1 832/3 cell lines, corroborating with the notion that GLP-1(9-36)NH_2 is not insulinotropic.

The following results suggested that compound 249 potentiated the effect of GLP-1-mediated GSIS in both INS-1 832/3 WT cell line (by 1.25-fold; $p < 0.05$) and GIPR-KO (by 1.14-fold; $p < 0.01$) (Fig. 5.25A). However, no facilitation of GSIS mediated by compound 249 was observed in the INS-1 GLP-1R-KO cell line, further implying compound 249 facilitation of GLP-1-mediated GSIS is GLP-1R specific. Indeed, the cAMP functional assays conducted in the INS-1 GLP-1R-KO cell line also suggested compound 249 mediates its PAM action in the absence of GLP-1R (Fig. 5.23). In contrary to compound 249, BETP did not promote GLP-1-mediated GSIS, which corroborated with other studies suggesting its selectivity towards GLP-1(9-36)NH_2 and OXM-biased allosteric modulation [Koole et al., 2012, Bueno et al., 2020]. In fact, the same preferential potentiation exhibited by BETP were also observed here, which BETP promoted OXM-mediated GSIS in the INS-1 GIPR-KO cell line by 1.60-fold ($p < 0.01$) (Fig. 5.25B) and GLP-1(9-36)NH_2-mediated GSIS in INS-1 832/3 WT cell lines by 1.76-fold ($p < 0.05$) (Fig. 5.25D).

In spite of a lesser degree of potentiation compared to BETP, compound 249 facilitated OXM-mediated GSIS in the INS-1 GIPR-KO cell line (by 1.33-fold; $p < 0.01$), while having no statistically significant enhancement of GSIS in both INS-1 832/3 WT and INS-1 GLP-1R-KO cell lines (Fig. 5.25B). Although Ex-4 shares close homology with GLP-1, compound 249 did not significantly facilitate Ex-4-mediated GSIS in all three INS-1 cell lines (Fig. 5.25C), suggesting compound 249 preferential allosteric action on GLP-1. Compound 249 also did not enhance GLP-1(9-36)NH_2-mediated GSIS in all three rat insulinoma cell lines (Fig. 5.25D). Collectively, the results suggested that

compound 249 selectively facilitated both GLP-1 and OXM-promoted GSIS, and that the facilitation required the presence of functional GLP-1R.

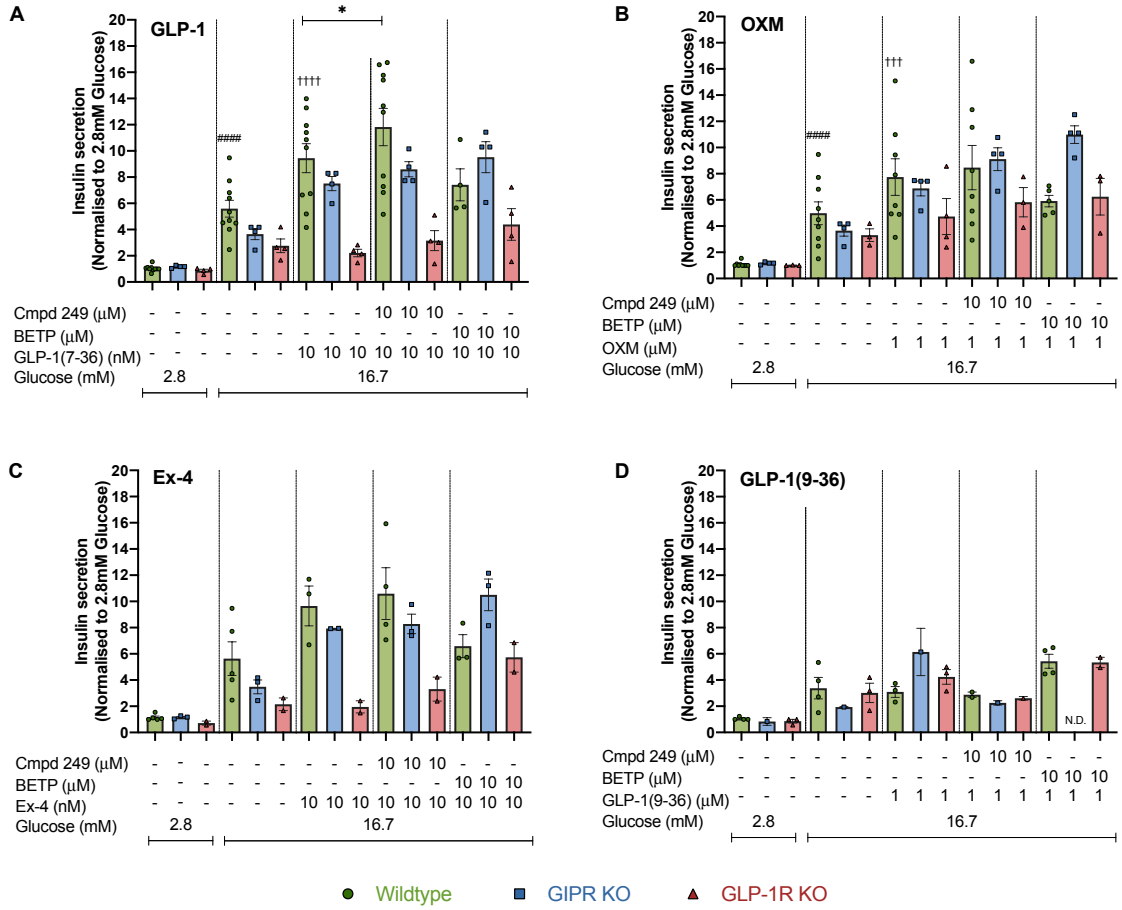

Figure 5.25: **Compound 249 facilitates GSIS mediated by GLP-1 and OXM in INS-1 832/3 WT and GIPR-KO cells.** Compound 249 further facilitates GSIS mediated by (A) GLP-1 and (B) OXM in the presence of 16.7mM glucose in INS-1 823/3 WT and GIPR-KO cell lines. Compound 249 has minimal GSIS facilitation mediated by (C) Ex-4 and (D) GLP-1(9-36)NH_2. Mean ± S.E.M. insulin secretion data (responses normalised to the GSIS secretion responses at 2.8mM respectively) in 1 to 10 independent experiments with quadruplicates are shown in the above scatter plots. Statistical significance compared between responses at 2.8mM and 16.7mM glucose among the three different INS-1 cell lines are determined by Student's t-test with Welch's correction and are indicated by hash above the bars (####, $p<0.0001$). Statistical significance compared among the peptide ligand influence on GSIS in INS-1 WT, GIPR KO and GLP-1R KO were determined by one-way ANOVA with Bonferroni's corrections compared with the mean of the WT group and are indicated by obelisk above the bars (+++, $p<0.001$, ++++, $p<0.0001$, ns, non-statistically significant). Statistical significance compared between responses with or without the presence of peptide ligands at 16.7mM glucose in insulin secretion assays respectively are determined by Student's t-test with Welch's correction and are indicated by asterisks above the bars (*, $p<0.05$). Some of the preliminary results (n=1) are shown here due to COVID-19 obstruction of experimental schedule.

5.6.2.3 Compound 249 potentiates GLP-1 and OXM-mediated GSIS in a concentration-dependent manner

Following the observations of compound 249 facilitation of GLP-1 and OXM-mediated GSIS, the compound's concentration-dependent potentiation effect was then tested. Here a range of concentrations of compound 249 (from 100μM to 0.1μM) were stimulated in the presence of either GLP-1 or OXM in the INS-1 832/3 WT cell lines for an hour and the extent of insulin secretion was then measured. The DMSO content were kept constant across all concentrations.

Differences in insulin secretion between high and low glucose stimulation were again observed, proving the functionality of the INS-1 832/3 WT to high glucose stimuli. The presence of 10nM GLP-1 and 1μM OXM further enhanced GSIS, which concurred with the results in Fig. 5.25 and also implied the responsiveness of the clonal pancreatic β cells to incretin stimulation. Here, a concentration-dependent potentiation effect of GLP-1-mediated GSIS mediated by compound 249 was observed, with a 1.62-fold increase ($p < 0.01$) when compound 249 at 100μM was applied, followed by a 1.22-fold increase ($p < 0.05$) when compound 249 at 10μM was added (Fig. 5.26). Similarly, a concentration-dependent OXM-mediated GSIS facilitative effect mediated by compound 249 was also observed, with a 2.16-fold increase ($p < 0.0001$) was observed when compound 249 at 100μM was added, followed a 1.49-fold increase ($p < 0.001$) induced by compound 249 at 10μM (Fig. 5.26). These results further illustrated compound 249 facilitation of GLP-1 and OXM-mediated GSIS.

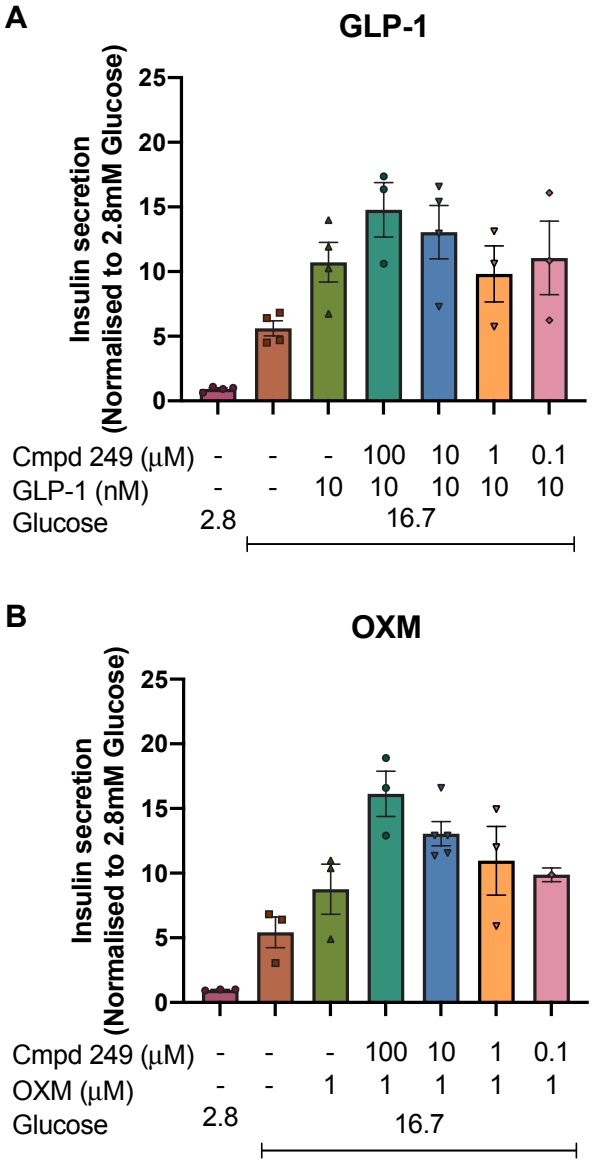

Figure 5.26: **Compound 249 concentration-dependent facilitation of GSIS mediated by GLP-1 and OXM in INS-1 832/3 WT cells.** Panel A and B show the concentration-dependent effect of compound 249 on GSIS mediated by GLP-1 and OXM in the presence of 16.7mM glucose in INS-1 832/3 WT cell lines. Mean ± S.E.M. insulin secretion data (responses normalised to the GSIS secretion responses at 2.8mM respectively) in at least 1 to 5 independent experiments with quadruplicates are shown in the above scatter plots.

5.6.2.4 Compound 249 potentiates OXM-mediated GSIS in isolated mouse islets

After demonstrating the ability of compound 249 to promote OXM-mediated GSIS in rat insulinoma cell line, more physiologically relevant primary cells, namely the isolated mouse pancreatic islets (kindly provided by Dr Nikola Dolezalova of the Department of Surgery, University of Cambridge), were used to further validate the compound 249 facilitation of GSIS. Similar to the approach in measuring insulin secretion in the rat insulinoma cell line, following low glucose pre-incubation, the mouse islets were incubated with 10μM compound 249, BETP or vehicle for an hour. Insulin levels in each condition were then measured as described in section 2.2.4.2.

In spite of a non-statistically significant increase in the insulin secretion level between low and high glucose, the isolated mouse islets were still able to respond to the stimuli of 1μM OXM, illustrating the functionality of the mouse islets in responding to agonist stimulation. Strikingly, there was a significant increment in GSIS by nearly 2-fold when 10μM compound 249 was co-applied with OXM to the mouse islets; the reference compound BETP was also able to enhance OXM-mediated GSIS to a similar extent (Fig. 5.27). These preliminary results further substantiated compound 249 ability to enhance OXM-mediated GSIS in both *in vitro* and *ex vivo* settings. The implication of which will be discussed in the section 5.8.

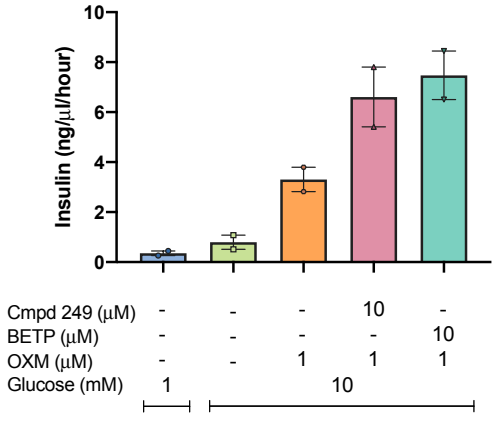

Figure 5.27: **Compound 249 further facilitates GSIS mediated by OXM in isolated mouse islets.** Compound 249 further facilitates GSIS mediated by OXM in the presence of 10mM glucose in isolated mouse islets. Insulin secretion is reported as ng/μl per hour in 2 independent experiments with 6-replicates and are shown in the above scatter plots.

5.7 Screening of compound 249-derived analogues

To further explore the structure-activity-relationship (SAR) of the quinoxaline-based scaffold of compound 249, three analogues which shared 80% structure similarity as the parent compound 249 were designed by Dr Taufiq Rahman (Department of Pharmacology, University of Cambridge) (Fig. 5.28 A-C) by structure modification of the compound 249. The alkyne group present in compound 249 was retained in analogue 248 but it was now positioned in a cis-conformation. The alkyne group was removed in compound 82 and was substituted by a saturated C-C bond at the amino position; as for compound 448, an alkene group was introduced to investigate the effect of different electrostatic density on the allosteric modulation. Both compound 82 and 448 now contained dioxane rings.

Furthermore, 11 analogues were selected based on the results of ligand-based virtual screening using compound 249 as a bait performed by Miss Kathleen Bowman (Department of Pharmacology, University of Cambridge). These compounds namely compound 880, 297, 180, 607, 385, 106, 001, 246, 646, 468 and 518 (Fig. 5.28 D-N), were chosen as they were the highest-ranking candidates based on the similarities of 3D steric conformation and electrostaticity of compound 249.

The biological screening approach for these analogues were the same as the identification of compound 249, which cAMP accumulation assays were primarily used as the default screening assay. Interesting candidates were then further characterised for their iCa^{2+} release properties. The intrinsic agonisms of these compound 249-derived analogues were first investigated, followed by the SAR studies of compound 249 and the three other closely-derived analogues in the following section.

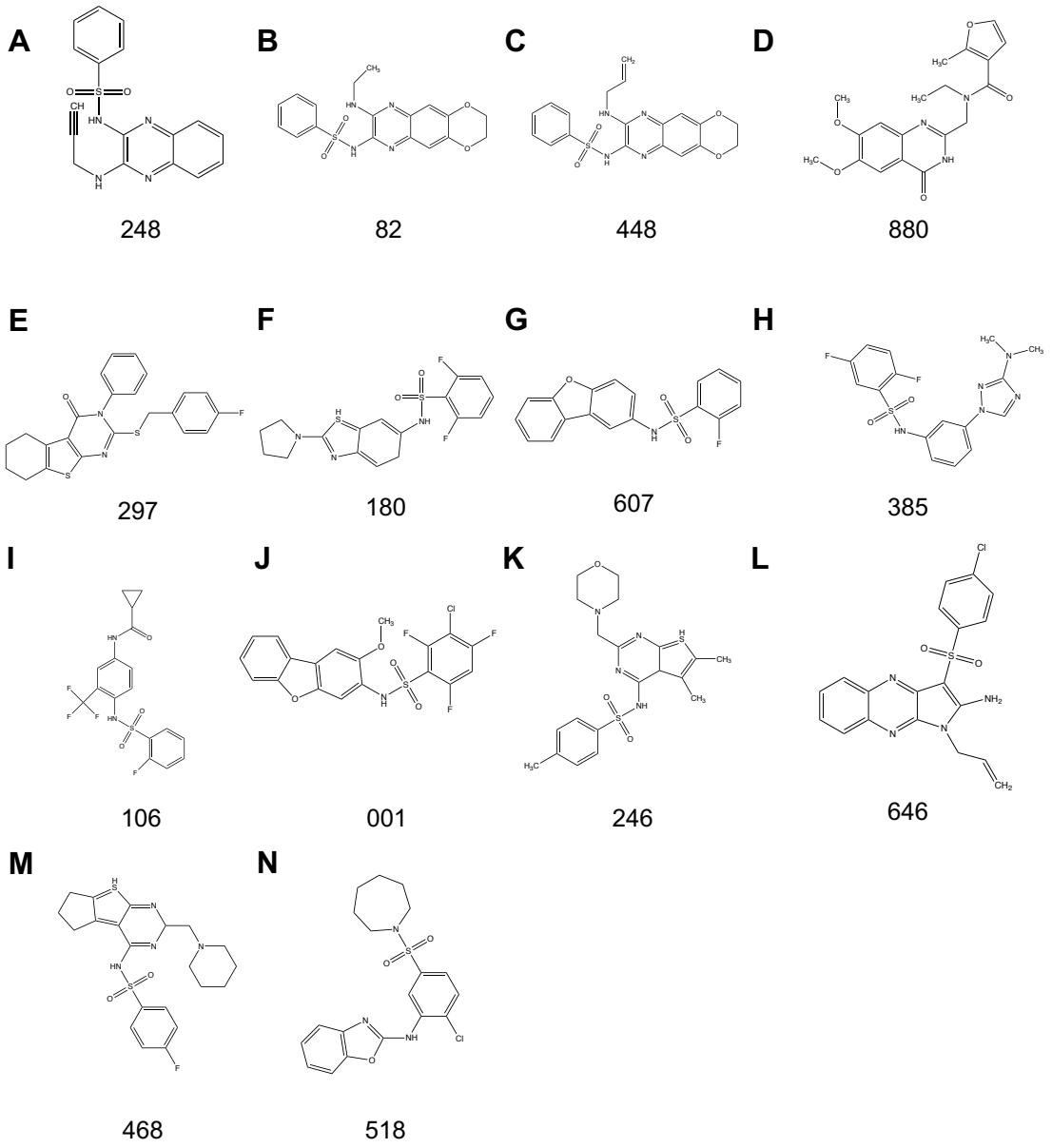

Figure 5.28: **Structures of analogues of compound 249.** Panel A to C show the 2D structures of the analogues of compound 249 which share a close structural homology to compound 249 (Fig. 5.1). These molecules are designed based on 80% structural similarity as the parent compound 249. Different C-bonds are introduced in the compound 249 analogues, with analogue 248 retaining the alkyne group from compound 249 but in a different conformation. A saturated C-C bond is introduced in analogue 82 while an alkene group is introduced in analogue 448. Panel D to N show the 2D structures of the analogues of compound 249 which are based on the structures of compound 249 using virtual screening conducted by Miss Kathleen Bowmen.

5.7.1 Compound 249 analogues lack GLP-1R and GCGR intrinsic agonism

Similar to the determination of compound 249 intrinsic agonism at the GLP-1R, the same cAMP functional assays were performed in CHO-GLP-1R and CHO-GCGR cells in order to determine if the analogues demonstrated any intrinsic GLP-1R and GCGR agonism. Compound 249 analogues at a range of concentrations (100μM to 10pM) were applied to CHO-GLP-1R and/or CHO-GCGR cells. Untransfected CHO-K1 cells, which acted as a null receptor background, were also stimulated with compound 249 analogues. Here all compound 249 analogues lacked GLP-1R intrinsic agonism (Fig. 5.29). Furthermore, compound 248, 82 and 448 also lacked GCGR intrinsic agonism (Fig. 5.29), and their apparent slight activation of cAMP responses when compounds at 100μM were applied were due to autofluorescence. Having concluded these small molecules were not GLP-1R and/or GCGR agonists, the SAR studies of compound 249 were reported.

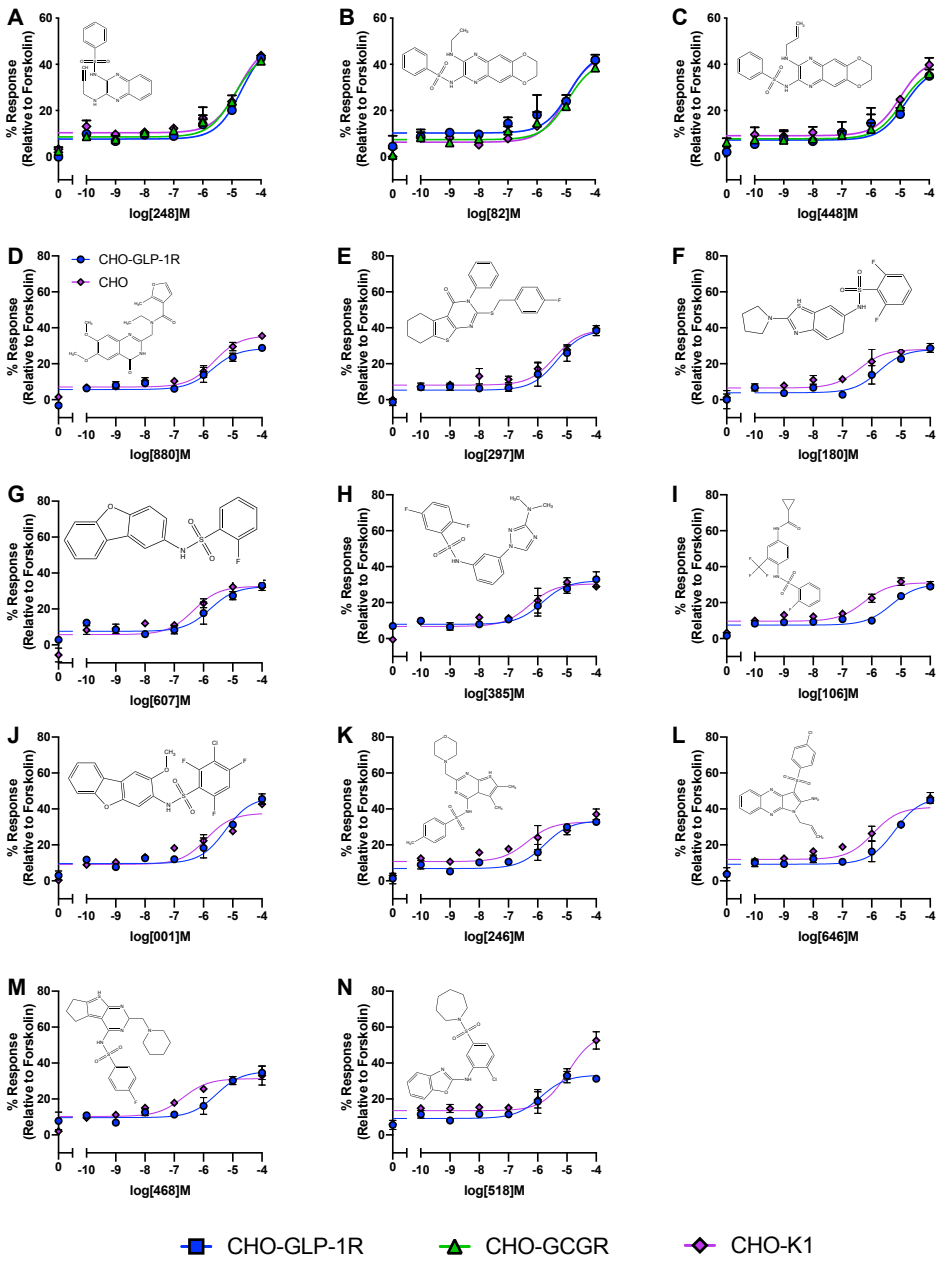

Figure 5.29: **Analogues of compound 249 do not activate GLP-1R and GCGR.** Analogues of compound 249 fail to activate cAMP accumulation responses at the GLP-1R and GCGR. 1000 CHO-GLP-1R, CHO-GCGR and CHO-K1 cells/well under 15-minute stimulation in the presence of rolipram were used in the cAMP assays. All data are normalised to the maximum cAMP response determined by 100μM forskolin stimulation. All data are means of 2 independent experiments with duplicates $\pm$ S.E.M (upper error bars).

5.7.2 Structure-activity-relationship studies on compound 249 analogues

5.7.2.1 Compound 248, 82, 448 allosteric modulation on cAMP responses

An initial screening of the allosterism of the compound 249 analogues was conducted in the CHO-GLP-1R cells using the same cAMP functional assaying technique. Given that none of the analogues exhibited any allosteric modulation of OXM and GCG-mediated cAMP responses, the results are not shown here but are available in Appendix B.4.

The HEK293S-GLP-1R-WT cell line was again used to validate if these compounds were NALs on OXM or GCG-mediated cAMP responses in the human-origin cell line. Similar to the observations in CHO-GLP-1R cell line, compound 248, 82 and 448 were classified as NALs via the application of operational model of allosterism, despite showing slight degree of inhibition of OXM-mediated cAMP responses (Fig. 5.30, Fig. 5.31 and Table 5.20). Likewise, the three analogues were also NALs of GCG-mediated cAMP responses, albeit showing slight potentiation when very high concentration (at 100μM) was applied (Fig. 5.30, Fig. 5.31 and Table 5.20). These results illustrated that the trans-conformation of the alkyne group of compound 249 may be critical for its allosterism on cAMP responses. Following the conclusion that these three analogues were NALs on cAMP responses at the GLP-1R, their ability to modulate iCa^{2+} responses were next examined.

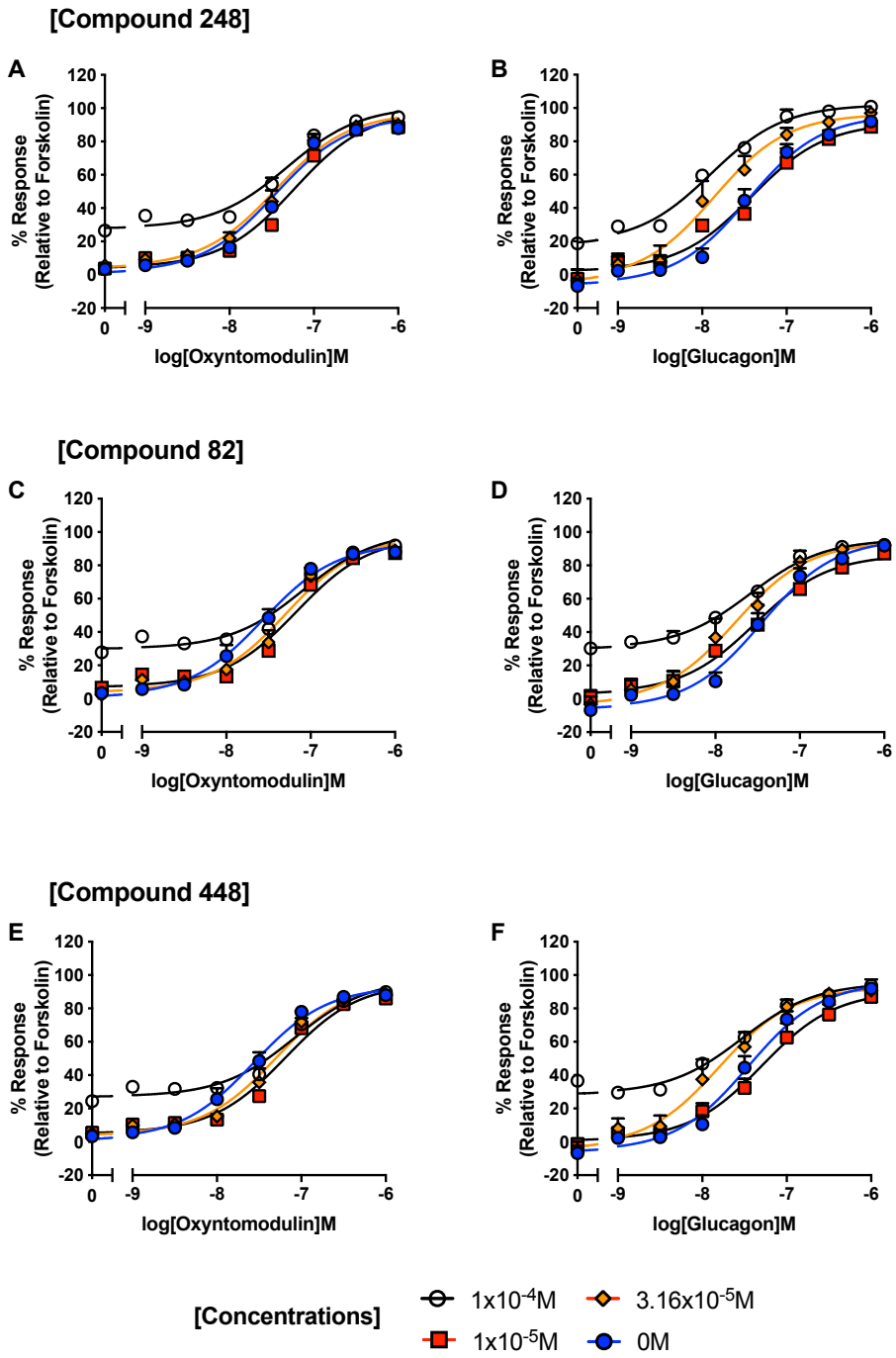

Figure 5.30: **Analogues of compound 249 do not allosterically modulate GLP-1R and GCGR.** Analogues of compound 249 are not allosteric modulators at the GLP-1R and GCGR. 500 HEK293S-GLP-1R-WT cells/well under 8-minute stimulation in the absence of PDE inhibitor were used in the cAMP assays. All data were normalised to the maximum cAMP response determined by 100μM forskolin stimulation. All data were means of 1 to 4 independent experiments with duplicates $\pm$ S.E.M (upper error bars).

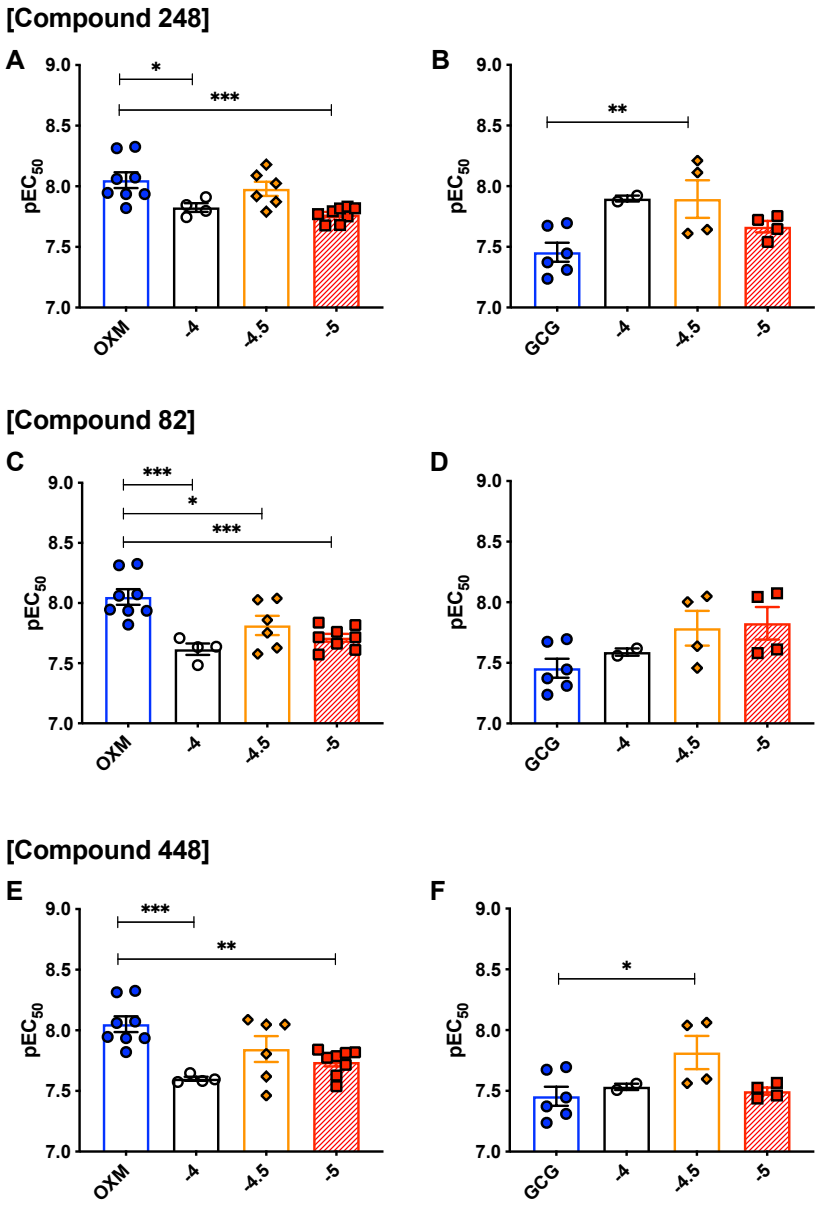

Figure 5.31: **Scatter plots illustrating compound 249 analogues do not induce allosteric modulation on OXM or GCG-mediated cAMP accumulation in HEK293S-GLP-1R-WT cells.** Panel A, C and E show that compound 248, 82 and 448 do not potentiate OXM-mediated cAMP accumulation even when high concentration at 10^{-4}M is applied to the HEK293S-GLP-1R-WT cells. Similarly, panels B, D, and F show that these analogues are not allosteric modulators on GCG-mediated cAMP accumulation. 500 HEK293S-GLP-1R-WT cells/well under 8-minute co-stimulation with peptide ligands in the absence of PDE inhibitor were used in the cAMP assays. All data were normalised to the maximum cAMP response determined by 100μM forskolin stimulation. All data are means from 1 to 4 independent experiments with duplicates $\pm$ S.E.M (upper error bars). Statistical significance compared with OXM or GCG (*, $p < 0.05$; **, $p < 0.01$; ***; $p < 0.001$) in the presence of different concentrations of compound 248, 82 and 448 was determined by one-way ANOVA with post-hoc Dunnett's multiple comparisons.

Table 5.20: **Allosteric modulations of OXM and GCG-mediated cAMP responses by analogues of compound 249 in HEK293S-GLP-1R-WT cells.**

Ligand	Compound	Concentrations	pEC_{50} [a]	E_{max} [b]	Span	n
OXM	DMSO	-	7.98±0.06	117.7±4.23	115.0±4.18	8
	248	$1x10^{-4}$M	7.83±0.09*	98.93±2.37	69.73±3.08	4
		$3.16x10^{-5}$M	7.98±0.08	94.85±2.40	89.98±3.39	6
		$1x10^{-5}$M	7.77±0.05***	94.92±1.94	90.02±2.47	8
	82	$1x10^{-4}$M	7.62±0.08***	97.03±2.26	65.91±2.67	4
		$3.16x10^{-5}$M	7.81±0.09*	94.63±3.00	88.73±2.87	6
		$1x10^{-5}$M	7.70±0.06***	93.67±2.09	85.96±2.59	8
	448	$1x10^{-4}$M	7.60±0.08***	94.60±2.29	66.24±2.69	4
		$3.16x10^{-5}$M	7.83±0.10	93.39±3.20	88.90±4.42	6
		$1x10^{-5}$M	7.73±0.07**	91.93±2.36	86.46±2.93	8
GCG	DMSO	-	7.62±0.04	99.38±1.80	102.1±2.18	6
	248	$1x10^{-4}$M	7.90±0.07	102.08±2.16	83.29±2.91	2^{NB}
		$3.16x10^{-5}$M	7.86±0.12**	96.55±4.48	100.03±5.99	4
		$1x10^{-5}$M	7.41±0.12	91.25±4.89	88.66±5.36	6
	82	$1x10^{-4}$M	7.59±0.07	95.72±2.03	65.38±2.38	2^{NB}
		$3.16x10^{-5}$M	7.76±0.11	94.24±4.24	96.61±5.34	4
		$1x10^{-5}$M	7.53±0.16	86.47±6.30	83.10±6.92	6
	448	$1x10^{-4}$M	7.53±0.08	95.37±2.19	66.57±2.58	2^{NB}
		$3.16x10^{-5}$M	7.80±0.12*	92.65±4.63	95.96±5.94	4
		$1x10^{-5}$M	7.29±0.11	90.50±4.72	89.47±4.99	6

Values were generated when the data were fitted to the three-parameter logistic equation. Means ± S.E.M of n individual result sets were shown.

[a] Negative logarithm of agonist concentration when reaching half maximal response.

[b] % of maximal response observed when stimulated with ligands relative to forskolin.

[NB] Preliminary results are shown here only due to COVID-19 obstruction of experimental schedule.

Statistical significance compared with OXM or GCG (*, $p < 0.05$; **, $p < 0.01$; ***, $p < 0.001$) in the presence of different concentrations of compound 248, 82 and 448 was determined by one-way ANOVA with post-hoc Dunnett's multiple comparisons.

5.7.2.2 Allosteric modulation of the compound 249 analogues on iCa^{2+} release

After concluding that these analogues were NALs of cAMP responses, their effect on iCa^{2+} mobilisation were subsequently evaluated. Same as previous approach (section 5.3.4), HEK293S-GLP-1R-WT cells were pre-treated with a range of fixed concentrations of compound 249 analogues prior to stimulation with GLP-1, OXM or GCG in the presence of the analogues.

Here the preliminary results suggested that all three compound 249 analogues reduced the efficacies of GLP-1-induced iCa^{2+} responses (E_{max} of GLP-1 reduced from 77.24 $\pm$ 8.89 to 29.75 $\pm$ 3.46, 47.23 $\pm$ 7.59 and 7.90 $\pm$ 0.93 by compound 248, 82 and 448, all at 1x10^{-4}M respectively) (Fig. 5.32 and Table 5.21). Intriguingly, among the three compound 249 analogues, only compound 248 illustrated concentration-dependent negative allosteric modulation on OXM-mediated iCa^{2+} release (pEC_{50} reduced from 6.90 $\pm$ 0.14 to 6.14 $\pm$ 0.24, non-statistically significant, when 1x10^{-5}M of compound 248 was applied). Further application of the operational model of allosterism into the data set resulted in a negative log$\alpha\beta$ value of -1.371, further illustrating that compound 248 is a NAM on OXM-mediated iCa^{2+} release at the GLP-1R. Compound 82 and 448 on the other hand did not influence OXM-mediated iCa^{2+} release, and further application of the operational model of allosterism resulted in log$\alpha\beta$ values of 0.439 and 0.594, which suggested both were NALs of OXM-mediated iCa^{2+} release at the GLP-1R.

Contrary to being a NAL of OXM-mediated iCa^{2+} release, compound 448 potentiated GCG-mediated iCa^{2+} responses in a concentration-dependent manner (Fig. 5.32 and Table 5.21) (pEC_{50} value increased from 5.82 $\pm$ 0.29 to 6.80 $\pm$ 0.33, non-statistically significant, at 1x10^{-4}M respectively). A positive log$\alpha\beta$ value of 2.65 was obtained when the results were applied to the operational model of allosterism, further illustrating its role as a PAM in GCG-mediated iCa^{2+} response. Unlike compound 448, compound 248 and 82 did not affect GCG-mediated iCa^{2+} response. The above results illustrated how subtle changes in the compound 249 scaffold can lead to opposing cAMP and iCa^{2+} release signalling responses.

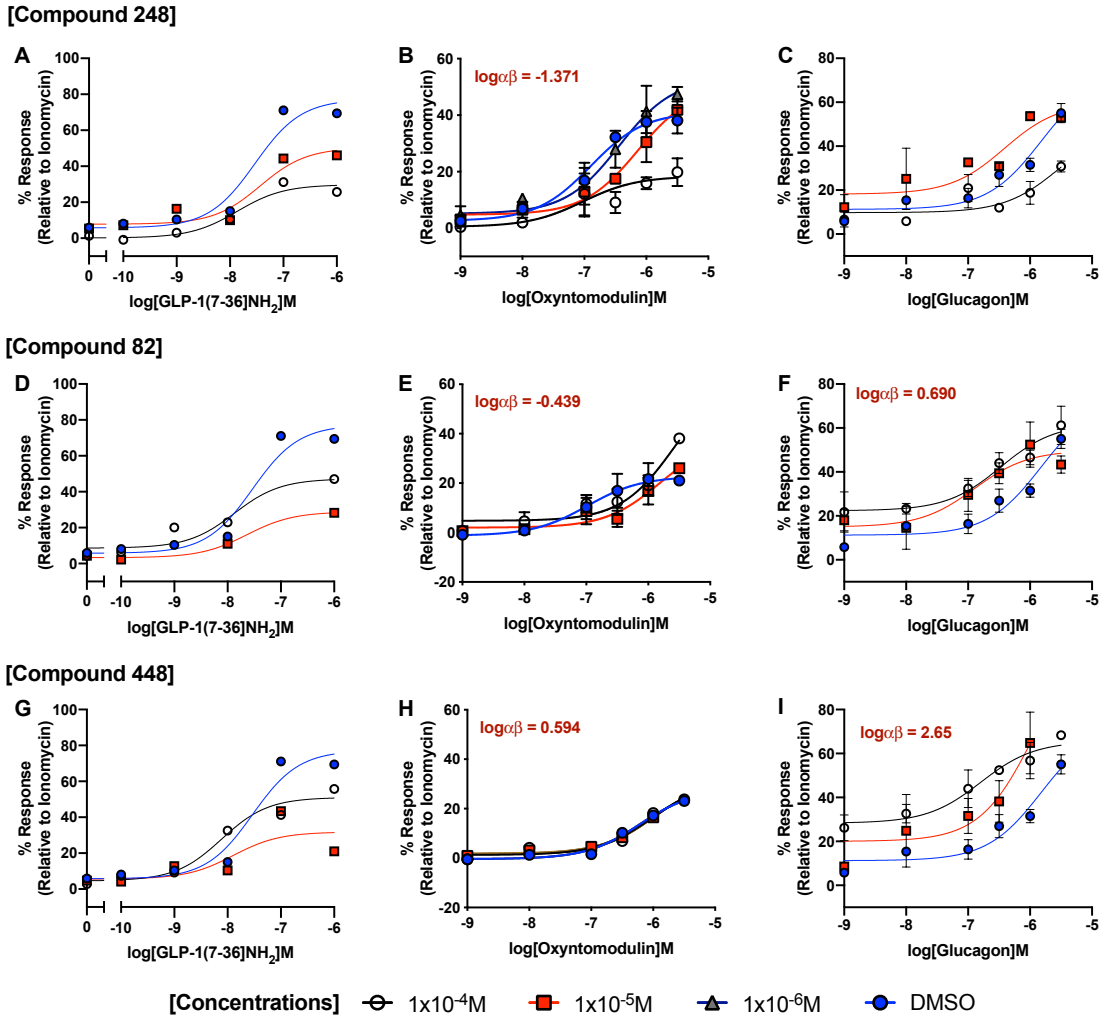

Figure 5.32: **Analogues of compound 249 act as positive or negative allosteric modulators at GLP-1, OXM or GCG-mediated iCa^{2+} release in HEK293S-GLP-1R-WT cells.** Panel A, D and G show that compound 248, 82 and 448 act as NAMs in GLP-1-mediated intracellular calcium release. Panel B, E and H show that compound compound 248 is a NAM on OXM-mediated intracellular calcium release. Panel C, F and I show that compound 448 has a potent positive allosteric modulation at the GCG-mediated intracellular calcium release. 80,000 cells/well of HEK293S-GLP-1R-WT cells were seeded onto black-96 well plate overnight prior to the measurement of intracellular calcium mobilisation. Cells were pre-treated with compounds prior to stimulation with peptide ligands. All data were normalised to the 10μM ionomycin concentration-response curve. All data are means from 1 to 3 independent experiments $\pm$ S.E.M (upper error bars).

Table 5.21: **Allosteric modulations of GLP-1, OXM or GCG-mediated iCa^{2+} mobilisation by analogues of compound 249 in HEK293S-GLP-1R-WT cells.**

Ligand	Compound	Concentrations	pEC_{50} [a]	E_{max} [b]	Span	n
GLP-1	248	DMSO	7.53±0.29	77.24±8.89	71.50±9.59	1[NB]
		1x10^{-4}M	7.87±0.28	29.75±3.46	29.60±4.04	1[NB]
		1x10^{-5}M	7.45±0.40	50.31±7.68	42.51±8.15	1[NB]
	82	DMSO	7.53±0.29	77.24±8.89	71.50±9.59	1[NB]
		1x10^{-4}M	7.88±0.40	47.23±7.59	38.60±8.72	1[NB]
		1x10^{-5}M	7.64±0.15	28.85±1.66	25.57±1.96	1[NB]
	448	DMSO	7.53±0.29	77.24±8.89	71.50±9.59	1[NB]
		1x10^{-4}M	8.11±0.23	7.90±0.93	46.46±5.12	1[NB]
		1x10^{-5}M	7.90±0.93	31.79±9.93	26.17±11.68	1[NB]
OXM	248	DMSO	6.90±0.14	41.19±2.52	38.58±2.90	3
		1x10^{-4}M	7.02±0.37[ns]	18.37±2.81[ns]	17.88±3.47	3
		1x10^{-5}M	6.14±0.24[ns]	49.91±8.13[ns]	45.14±7.85	3
		1x10^{-6}M	6.44±0.26[ns]	53.10±7.44[ns]	47.94±7.63	3
	82	DMSO	6.90±0.14	41.19±2.52	38.58±2.90	3
		1x10^{-4}M	5.57±0.44[ns]	64.75±33.78[ns]	59.99±32.99	3
		1x10^{-5}M	5.82±0.44[ns]	37.62±16.72[ns]	35.61±16.14	3
	448	DMSO	6.21±0.14	27.89±2.69	28.24±2.61	3
		1x10^{-4}M	6.02±0.30	31.34±7.19	30.04±7.01	1[NB]
		1x10^{-5}M	5.93±0.30	33.52±12.37	31.65±12.08	1[NB]
GCG	248	DMSO	5.82±0.29	73.36±17.91	62.11±17.14	3
		1x10^{-4}M	5.55±0.78[ns]	49.07±36.77[ns]	39.29±35.74	3
		1x10^{-5}M	6.41±0.41[ns]	59.76±10.06[ns]	41.58±10.35	3
	82	DMSO	5.82±0.29	73.36±17.91	62.11±17.14	3
		1x10^{-4}M	6.48±0.32[ns]	61.99±7.38[ns]	39.64±7.61	3
		1x10^{-5}M	6.90±0.40[ns]	49.84±6.28[ns]	34.89±7.52	3
	448	DMSO	5.82±0.29	73.36±17.91	62.11±17.14	3
		1x10^{-4}M	6.80±0.33[ns]	65.56±6.28[ns]	37.26±6.94	3
		1x10^{-5}M	6.26±0.33[ns]	72.52±20.33[ns]	63.58±19.43	3

Values were generated when the data were fitted to the three-parameter logistic equation. Means ± S.E.M of n individual result sets were shown.

[a] Negative logarithm of agonist concentration when reaching half maximal response.

[b] % of maximal response observed when stimulated with ligands relative to ionomycin.

[NB] Preliminary results are shown here only due to COVID-19 obstruction of experimental schedule.

Statistical significance compared with GLP-1, OXM and GCG (ns, non-statistically significant) in the presence of different concentrations of compound 248, 82 and 448 were determined by one-way ANOVA with post-hoc Dunnett's multiple comparisons.

5.7.2.3 Summary of compound 248, 82 and 448 allosteric modulation

Compound 248, 82 and 448 demonstrate distinct allosteric modulation profile compared to their parent compound 249. In terms of the allosterism on the cAMP signalling, all analogues were NALs while compound 249 was the only PAM on OXM-mediated cAMP responses. In terms of agonist-induced iCa^{2+} mobilisation, only compound 249 and compound 248 were NAMs on OXM-mediated iCa^{2+} release while compound 82 and 448 were NALs in such pathway. Interestingly, among the four compounds, only compound 448 was able to enhance GCG-mediated iCa^{2+} signalling responses (Fig. 5.33). These results illustrated an interesting SAR studies which explored the probe dependence effect of compound 249 scaffold. The significance of the findings will be discussed in later Discussion section.

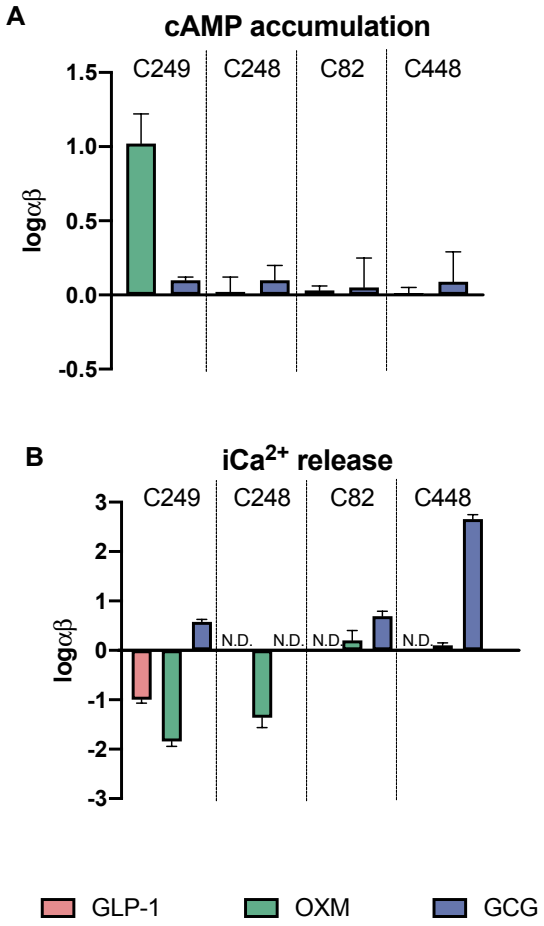

Figure 5.33: **Bar charts summarising compound 249 analogues allosterism in HEK293S-GLP-1R-WT cells.** The above bar charts summarise compound 249 analogues allosteric actions on GLP-1, OXM and GCG-mediated (A) cAMP accumulation and (B) iCa^{2+} release. N.D.: not determined.

5.7.3 Screening of other compound 249 based analogues

5.7.3.1 Allosteric modulation on cAMP accumulation

Following the SAR studies of the three closely related analogues of compound 249, the potential allosteric activities of the other 11 compounds, which were identified through ligand-based virtual screening, were examined. Again, cAMP functional assays were employed and fixed concentrations (at 100μM and 10μM) of analogues were applied in the presence of a range of GLP-1 or OXM to the CHO-GLP-1R cells. The extents of cAMP accumulation were then measured.

Among the 11 small molecule candidates, only compound 607 demonstrated the most significant extent of inhibition of both GLP-1 and OXM-mediated cAMP responses among all small molecule candidates (Fig. 5.34 and Fig. 5.35) when high concentration (i.e. at 100μM) was applied (pEC_{50} value of GLP-1 reduced from 9.46 $\pm$ 0.05 to 9.03 $\pm$ 0.06, $p < 0.001$ and pEC_{50} value of OXM decreased from 7.92 $\pm$ 0.06 to 6.93 $\pm$ 0.08, $p < 0.0001$). Other compounds induced marginal yet statistically significant changes in the potencies of both GLP-1 and OXM-mediated cAMP responses (Fig. 5.36). Given compound 607 potent inhibitory action of GLP-1 and OXM-mediated cAMP responses, further investigation on its effect on iCa^{2+} release was performed.

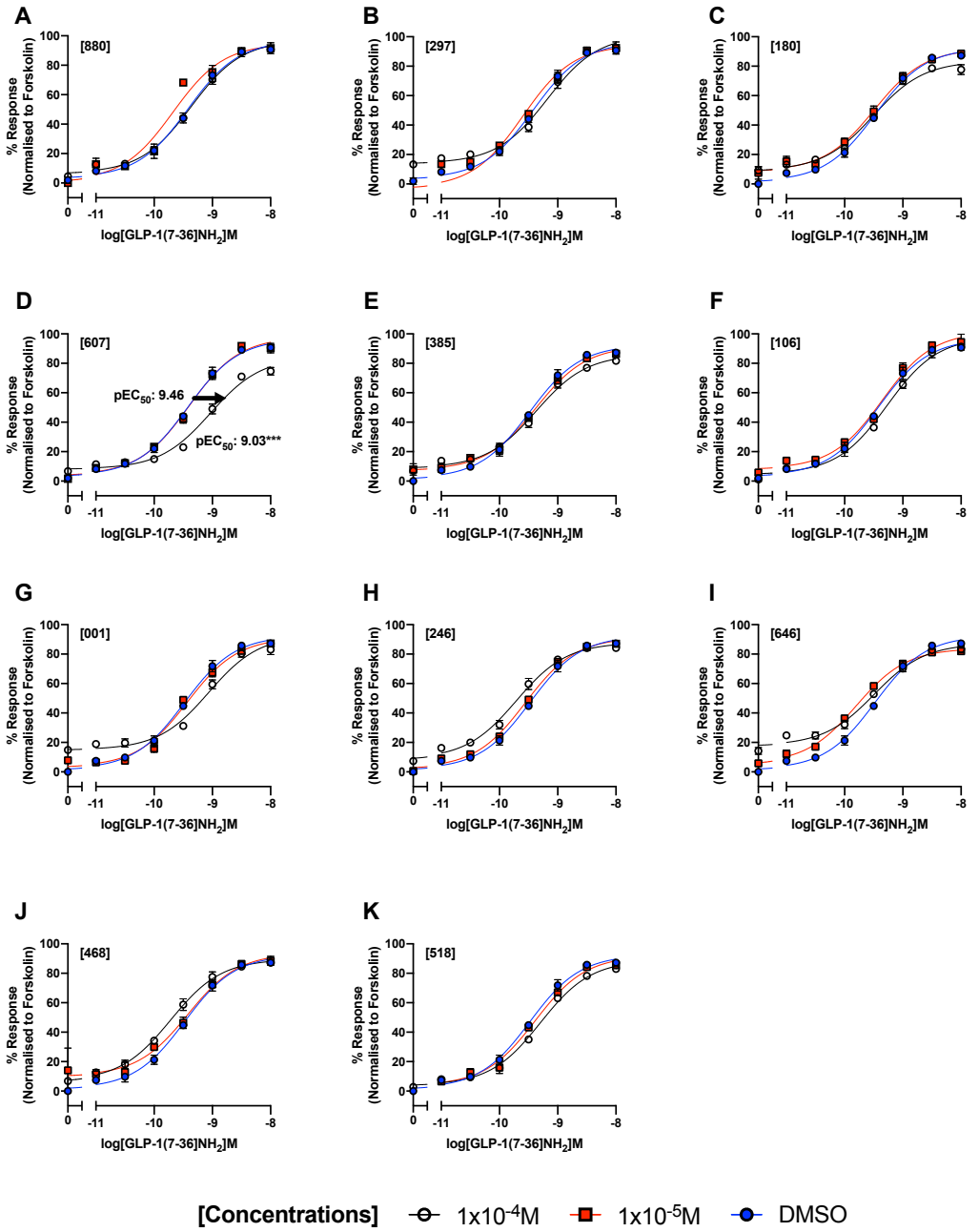

Figure 5.34: **Only analogue 607 demonstrates negative allosteric modulation on GLP-1-mediated cAMP accumulation in CHO-GLP-1R cells.** Panel A to K show that the analogues of compound 249 do not potentiate GLP-1-mediated cAMP accumulation even when high concentration at 10^{-4}M were applied to the CHO-GLP-1R cells, except for panel D where analogue 607 demonstrates negative allosterism. 500 CHO-GLP-1R cells/well under 15-minute co-stimulation with peptide ligands in the presence of rolipram were used in the cAMP assays. All data were normalised to the maximum cAMP response determined by 100μM forskolin stimulation. All data are means from at least 2 independent experiments with duplicates $\pm$ S.E.M (upper error bars). Statistical significance compared with GLP-1 (***, $p < 0.001$) in the presence of different concentrations of compound 607 were determined by one-way ANOVA with post-hoc Dunnett's multiple comparisons.

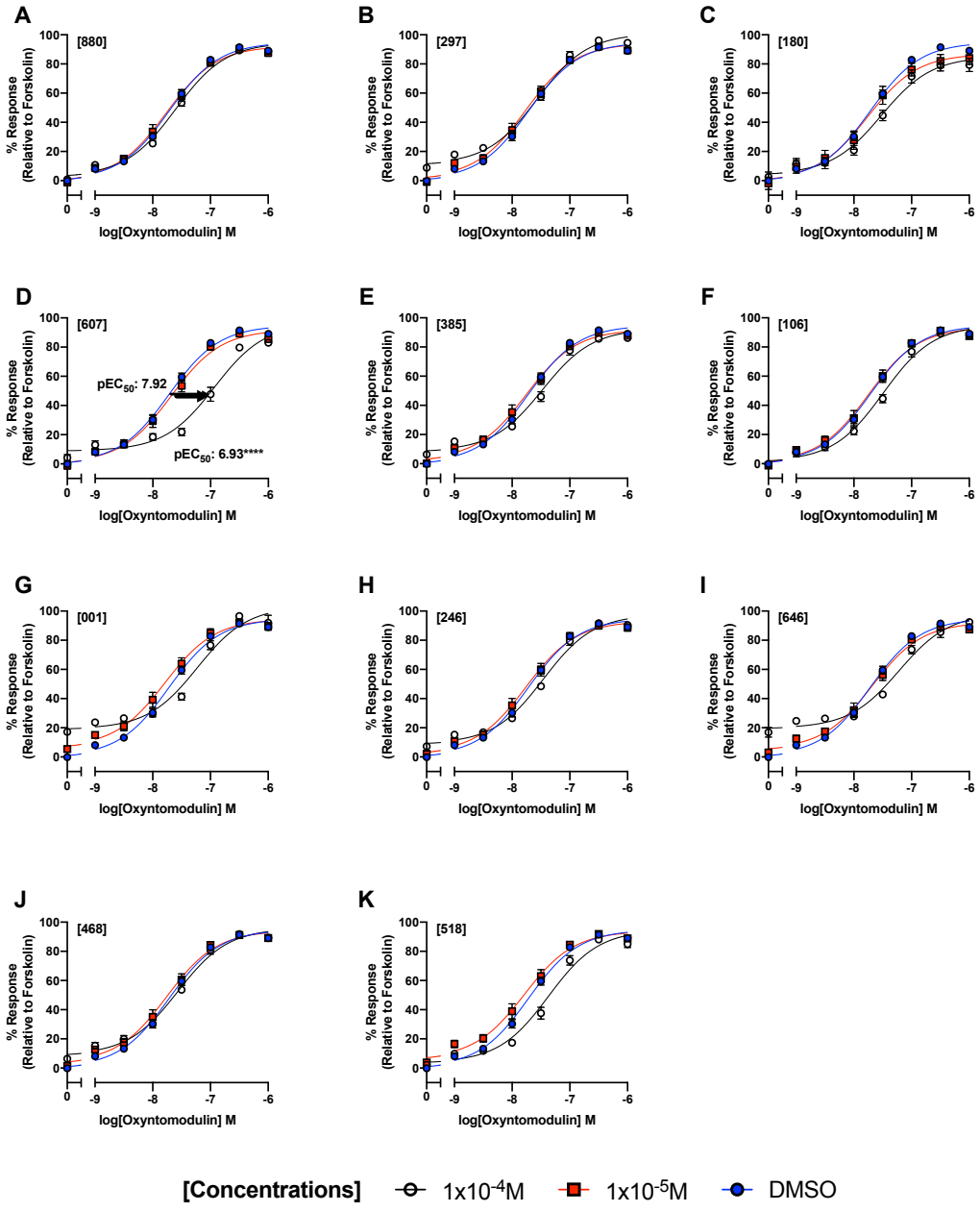

Figure 5.35: **Only analogue 607 demonstrates negative allosteric modulation on OXM-mediated cAMP accumulation in CHO-GLP-1R cells.** Panel A to K show that the analogues of compound 249 do not potentiate OXM-mediated cAMP accumulation even when high concentration at 10^{-4}M were applied to the CHO-GLP-1R cells, except for panel D where analogue 607 demonstrates negative allosterism. 500 CHO-GLP-1R cells/well under 15-minute co-stimulation with peptide ligands in the presence of rolipram were used in the cAMP assays. All data were normalised to the maximum cAMP response determined by 10μM forskolin stimulation. All data are means from at least 3 independent experiments with duplicates $\pm$ S.E.M (upper error bars). Statistical significance compared with OXM (****, $p < 0.0001$) in the presence of different concentrations of compound 607 were determined by one-way ANOVA with post-hoc Dunnett's multiple comparisons.

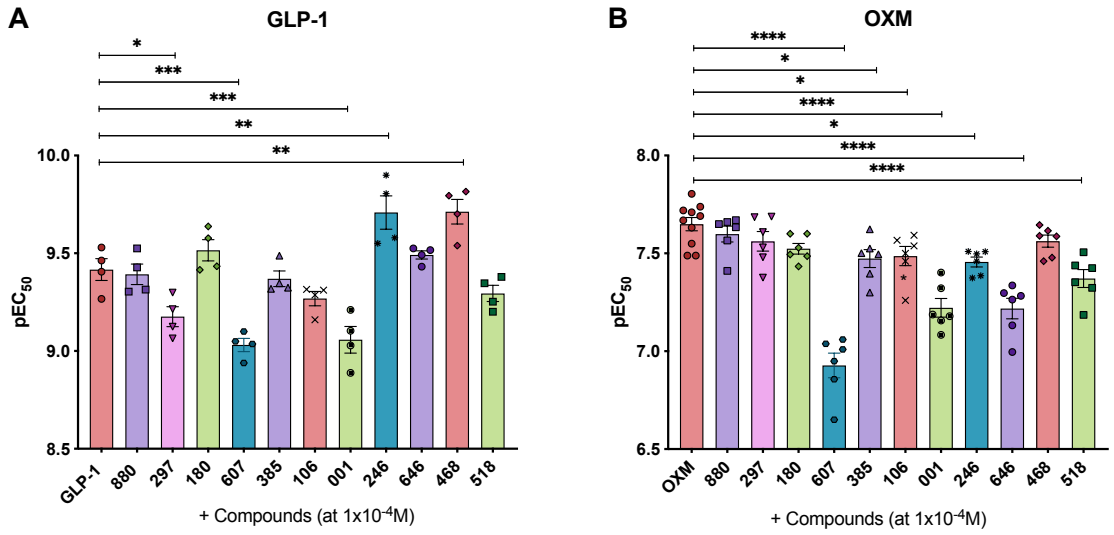

Figure 5.36: **Scatter plots summarising the allosteric modulation of analogues of compound 249 on GLP-1 and OXM-mediated cAMP accumulation in CHO-GLP-1R cells.** 500 cells/well of CHO-GLP-1R cells were co-stimulated with fixed concentrations of analogues at 10^{-4}M in the presence of GLP-1 or OXM for 15 minutes with the presence of rolipram to measure cAMP accumulation. All data were normalised to the maximum cAMP response determined by 100μM forskolin stimulation and were means of at least 3 independent experiments with duplicates $\pm$ S.E.M (upper error bars). Statistical significance compared with GLP-1 or (*, $p < 0.05$; **, $p < 0.01$; ***, $p < 0.001$; ****, $p < 0.0001$) in the presence of compound 607 were determined by one-way ANOVA with post-hoc Dunnett's multiple comparisons.

5.7.3.2 Analogue 607 allosteric modulation on iCa^{2+} release

Following the identification of compound 607 as a NAM in cAMP responses, its effect on iCa^{2+} release was investigated. To do so, HEK293S-GLP-1R-WT cells were pre-treated with compound 607 at 100μM prior to OXM stimulation in the presence of compound 607. Compound 607 reduced OXM-mediated iCa^{2+} response (pEC_{50} of OXM decreased from 7.10 $\pm$ 0.26 to 6.55 $\pm$ 0.18) (Fig. 5.37). The efficacy of the iCa^{2+} responses was also reduced (E_{max} decreased from 35.73 $\pm$ 3.41 to 21.91 $\pm$ 1.83), yet the reduction was non-statistically significant. Overall, compound 607 exhibited negative alosteric modulation of cAMP and iCa^{2+} responses at the GLP-1R. However, due to its inhibitory effect on both cAMP responses and iCa^{2+} release at the GLP-1R, as well as its ability to reduce insulin secretion in the INS-1 832/3 WT cell line (data not shown, but available in Appendix B.5 and B.13), it was apparent that compound 607 was not an appropriate drug candidate to be further developed as a T2DM treatment. However, it may serve as a useful tool for structural biology studies of the GLP-1R. The implications of the SAR studies will be discussed in the following section.

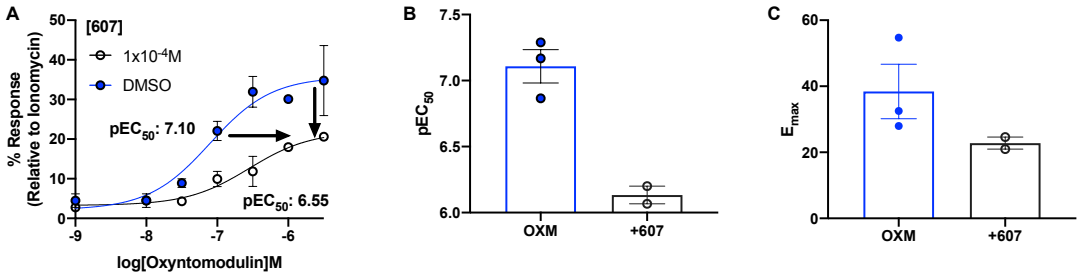

Figure 5.37: **Analogue 607 shows negative allosterism of OXM-mediated iCa^{2+} release in HEK293S-GLP-1R-WT cells.** (A) Compound 607 at 100μM shows inhibition on OXM-mediated intracellular calcium release. (B) and (C) show the scatter plots representing the changes in potencies and efficacies of the OXM-mediated iCa^{2+} responses. 80,000 cells/well of HEK293S-GLP-1R-WT cells were seeded onto black-96 well plate overnight prior to the measurement of intracellular calcium mobilisation. Cells were pre-treated with compound 607 prior to stimulation with OXM. All data were normalised to the 10μM ionomycin concentration-response curve. All data are means from at least 2 independent experiments $\pm$ S.E.M (upper error bars).

5.8 Discussion

The search for GLP-1R small molecule agonists or PAMs to act as novel GLP-1R-targeted T2DM therapies has been prompted for many years and it was only until the recent decades that there was a surge of reports of GLP-1R small molecule ago-PAMs or PAMs [Tibaduiza et al., 2001, Knudsen et al., 2007, Chen et al., 2007, Koole et al., 2010, Sloop et al., 2010, Graaf et al., 2011, Zhang et al., 2014, Redij et al., 2019, Méndez et al., 2020, Zhao et al., 2020, Bueno et al., 2020]. Despite showing promising potentiation of insulin secretion in *in vitro* and *in vivo* rodent studies, many of the reported GLP-1R PAMs or agonists were discovered to either display cell toxicity when used at high concentration [Knudsen et al., 2007], or violate the Lipinski's rule of five [Chen et al., 2007] that further hindered their drug development. Therefore, the pursuit of a feasible GLP-1R small molecule agonist or PAM is still ongoing.

Compound 249 was identified as a GLP-1R PAM during my MPhil project in 2017. To evaluate the feasibility of compound 249 to be further developed as a novel T2DM therapy, pharmacological characterisation, through utilising various functional assays, of the compound were performed as part of my PhD work and was summarised in Fig. 5.9. The significance of the findings will be discussed as follows.

5.8.1 Compound 249 displays a unique probe dependence profile

Compound 249 shows a distinct probe dependence profile, which it exhibits positive allosteric modulation with OXM-mediated cAMP response, negative allosteric modulation with GLP-1 and OXM-mediated iCa^{2+} mobilisation, and neutral cooperativity with OXM-mediated pERK1/2 (Fig. 5.9). Compared to the two well-studied GLP-1R ago-PAMs, compound 2 and BETP, compound 249 illustrated a completely different probe dependence profile in a way that it selectively potentiates OXM-mediated cAMP response vs GLP-1 or GCG-mediated cAMP responses, unlike BETP potentiation on both GLP-1(9-36)NH_2 and OXM-mediated cAMP responses [Sloop et al., 2010, Willard and Sloop, 2012] and compound 2 enhancement on all GLP-1R agonists-mediated cAMP responses [Coopman et al., 2010, Koole et al., 2010, Li et al., 2012]. These differences in probe dependence illustrate the advantage of designing drugs that selectively enhance certain signalling pathway mediated by specific agonists, while silencing the other, thereby reducing any possible side effects [Wootten et al., 2016a]. The unique probe dependence profile of compound 249 may also serve as a useful experimental tool in understanding the conformation of GLP-1R that facilitates such probe dependence

towards OXM.

5.8.2 Use of kinetic assays to investigate compound 249 distinct allosteric effect on G protein dissociation

Apart from utilising end-point signal transduction functional assays to characterise the pharmacological properties of compound 249, the NanoLuc® Binary Technology (NanoBiT) was used to investigate the kinetic aspect of allosteric modulation of compound 249 on G protein dissociation (the principle of which is explained in Appendix B.7). The NanoBiT G protein dissociation assays were performed by Dr Matthew Harris (Department of Pharmacology, University of Cambridge) in collaboration with Prof. Patrick Sexton (Monash Institute of Pharmaceutical Science).

In these experiments, the allosteric modulation of compound 249 on certain subsets of G protein dissociation, namely $G\alpha_s$, $G\alpha_{i1}$, $G\alpha_{i2}$, $G\alpha_{i3}$ and $G\alpha_q$ subunits, were tested. Coincided with the role of compound 249 as a NAM on iCa^{2+} release in Fig. 5.6, compound 249 caused a significant reduction in the dissociation of $G\alpha_q$ (Appendix B.7), consistent with the iCa^{2+} mobilisation experiment. Furthermore, the dissociation of $G\alpha_{i2}$ subunit was also shown to be significantly inhibited (by 10-fold, $p < 0.01$) in the presence of compound 249 (Appendix B.7). This finding suggested the possibility of compound 249 marginal potentiation of GLP-1-mediated cAMP response (Fig. 5.4) may be as a result of the delay in dissociating the G_{i2} subunit, thereby reducing the inhibition of cAMP production, leading to a slightly overall increase in cAMP responses, while having no apparent effect on the $G\alpha_s$, $G\alpha_{i1}$ and $G\alpha_{i3}$ subunits. However, further experiments, such as testing the influence of compound 249 on GLP-1-mediated cAMP responses in the presence of PTX (so far the PTX experiments were only conducted in OXM-mediated cAMP accumulation studies), are needed to support such hypothesis. However, given the less potent full agonism of OXM at the GLP-1R, the results from the NanoBiT G protein dissociation assay depicted a less prominent influence of compound 249 on G protein dissociation (Appendix B.7). Nonetheless, the NanoBiT G protein dissociation assay serves as a useful mechanistic tool in defining the compound 249 allosterism.

5.8.3 Compound 249 predicted binding mode at the GLP-1R

As discussed in the Introduction (section 1.6.7), the design of small molecule drug candidates that target class B GPCRs has been proven to be technically challenging

due to the fact that class B GPCRs possess larger N-terminus extracellular domains (ECDs) compared to the class A GPCRs [Willard and Sloop, 2012, Jazayeri et al., 2017, Hilger et al., 2020]. However, the understanding towards class B GPCR activation and allosterism have been advanced in the past 5 years thanks to the availability of numerous full-length high-resolution crystal structures determined by cryo-electron microscopy (EM) of class B GPCRs, in particular the GLP-1R and GCGR crystal structures [Song et al., 2017, Jazayeri et al., 2017, Zhang et al., 2017a, Zhang et al., 2017b, Zhang et al., 2018, Chang et al., 2020, Bueno et al., 2020, Zhao et al., 2020, Ma et al., 2020a, Hilger et al., 2020, Qiao et al., 2020]. These full-length GLP-1R crystal structures interacting with different GLP-1R cognate peptides, small molecule agonists [Zhao et al., 2020, Ma et al., 2020a], allosteric modulators [Song et al., 2017, Bueno et al., 2020] or Gαs subunit [Zhang et al., 2017a, Liang et al., 2018b] facilitate the structure-based virtual screening for new drug candidates, as well as the *in silico* docking of compound 249 in order to predict where it is bound to at the GLP-1R.

An allosteric binding pocket has been identified at the GLP-1R [Song et al., 2017]. The two GLP-1R NAMs, PF-06372222 and NNC0640, have been shown to bind to the allosteric pocket situated outside transmembrane (TM) 5 to 7, near the intracellular half of GLP-1R [Song et al., 2017]. According to the studies by Song and colleagues, it is predicted that compound 2 mediates its allosteric effect by binding to the same allosteric pocket [Song et al., 2017] and indeed other studies have shown that both compound 2 and BETP modulate the GLP-1R via covalent modification with the C347 residue [Nolte et al., 2014, Bueno et al., 2016]. Intriguingly, compound 249, as shown in Fig. 5.11, is able to potentiate OXM-mediated cAMP response in the absence of C347 residue, implying its action is C347-independent and that it may bind to an alternative allosteric pocket within the GLP-1R or it may mediate its action via alternative allosteric action.

In fact, recent papers by Zhao and colleagues [Zhao et al., 2020] and Ma and colleagues [Ma et al., 2020a] demonstrated that alternative allosteric target sites exist within the GLP-1R. Using a novel small molecule GLP-1R partial agonist, TT-OAD2, the authors resolved the full length GLP-1R cryo-EM structure with the binding of TT-OAD2 (Fig. 1.16). They show that the compound binds to the top part of the helical bundle, interacting hydrophobically with residues within TM1, TM2, TM3, extracellular loop (ECL) 1 and ECL2, with TM2/ECL1 and ECL2 being the major driver for its agonism [Zhao et al., 2020]. Furthermore, another novel small molecule GLP-1R full agonist, RGT1383, was also reported [Ma et al., 2020a]. The cryo-EM studies showed

that RGT1383 interacted with residues on TM1, TM2, TM3, TM7 and ECL1 and 2 as well as ECD. Notably, the compound almost completely overlapped with the position where residues 10-20 of GLP-1 occupied, which may confer its intrinsic agonism. Interestingly, both research groups suggest the importance of the W33 residue in the ECD to play a critical role in mediating binding of both peptide and non-peptide GLP-1 agonists [Zhao et al., 2020, Ma et al., 2020a].

Moreover, based on the *in silico* docking studies performed by Dr Taufiq Rahman (Department of Pharmacology, University of Cambridge), via docking compound 249 into the modified full length cryo-EM GLP-1R structures bound to peptide 5 [Jazayeri et al., 2017] and GLP-1/Gαs complex [Zhang et al., 2017b], three potential binding sites of compound 249 at the GLP-1R were suggested (Appendix B.8). Compound 249 was predicted to bind to the ECD and ECL1 (model 1), ECL2 (model 2) and TM3 and 4 core (model 3). The recent discovery of novel binding pockets targeted by the small molecule agonists TT-OAD2 and RGT1383 support the possibility that compound 249 may also bind to the top part of the helical bundle. However, due to time constraints, I was not able to perform mutagenesis studies to validate the binding mode of compound 249. It will serve as an important future work in order to fully decipher how compound 249 allosterically modulates GLP-1R.

Intriguingly, the recent paper by Bueno and colleagues [Bueno et al., 2020], suggested a new mode of GLP-1R allosteric modulation via the direct interaction of the small molecule with the orthosteric ligand at the ECD. They discovered a small molecule PAM, LSN3160440, which shows strong probe dependence towards GLP-1(9-36)NH_2, potentiates the binding and cAMP responses of GLP-1(9-36)NH_2 by simultaneously interacting with the receptor interface between TM1 and TM2, as well as the orthosteric ligand (Fig. 1.16). They demonstrated that LSN3160440 is the first-in-class so-called 'molecular glue' as it mediates its PAM action via stabilising the protein-protein-interaction through van der Waals' interaction between the residues of F12, V16 and L20 on the orthosteric GLP-1 ligand and L384 and L388 both on TM7 of the GLP-1R [Bueno et al., 2020]. Given the prediction of compound 249 binding close to the ECD in model 1, there is also a possibility that compound 249 may serve as a 'molecular glue' by enhancing the binding of OXM to the receptor via the modification of the Y10 residue on OXM, which is an equivalent of the V16 residue of the GLP-1 ligand. Therefore, further structure-based *in silico* docking incorporating the orthosteric ligand should be conducted in order to include such possibilities, as such class of unusual allosteric modulation may serve as a novel mean of receptor modulation.

Furthermore, it has been shown that OXM binds to the GLP-1R differently compared to GLP-1 and Ex-4 [Wootten et al., 2016b, Lei et al., 2018]. For example, OXM has been shown to interact more with ECL1 to mediate its cAMP response compared to the involvement of ECL2 for GLP-1 and Ex-4, and that certain mutagenesis of the residues on ECL2 eliminate cAMP responses of GLP-1 and Ex-4 but not OXM [Wootten et al., 2016b]. It has been shown that OXM displays shallower orientation into the GLP-1R binding groove due to the fact that it bears an uncharged Gln residue, which is equivalent to the positively charged Glu-9 on the GLP-1 that is responsible for the deep entry of GLP-1 into the transmembrane domain [Lei et al., 2018]. Furthermore, pERK1/2 activation was mainly contributed to ECL3/TM7, with very little involvement at the ECL2 [Wootten et al., 2016b]. Therefore, based on the current predicted docking models, it is possible that compound 249 may interact with the residues that lies within the ECL1/ECL2 interface which are important for OXM signal transduction, therefore potentiating cAMP responses and inhibiting iCa^{2+} mobilisation. More interestingly, given the close resemblance of GCG and OXM (i.e. OXM is a seven amino acid residue extended form of GCG) [Pocai, 2012], it was anticipated that compound 249 would also mediate its allosteric modulation on GCG, yet the notion was rejected experimentally (Fig. 5.4). Hence, it may suggest that the activation of GLP-1R mediated by GCG may be different from the mechanism initiated by OXM, yet such structural insight is still lacking to date, and would warrant detailed studies, due to the importance of GCG in modulating glucose homeostasis.

5.8.4 SAR studies to explore the importance of compound 249 functional groups

Given the distinct pharmacological activity of compound 249, SAR studies were conducted to further explore the importance of the trans-alkyne side chain of compound 249 in mediating its allosterism (Section 5.7.2). Strikingly, the reposition of the trans-alkene side chain to a cis-conformation (compound 248), an alkane group (compound 82) or an alkene group (compound 448) eliminated the positive cooperativity of OXM-mediated cAMP accumulation (Fig. 5.30), implying the importance of the trans-alkyne side chain in conferring the positive cooperativity of OXM-mediated cAMP response, possibly due to the steric hindrance with essential electronegativity, promoting a conformation that is conducive to cAMP response potentiation.

Intriguingly, compound 249 and compound 248, both possess the alkyne side chain, displayed negative cooperativity towards OXM-mediated iCa^{2+} release while

the replacement of such functional group with an alkene group, together with the introduction of the dioxane group on the quinoxaline ring, induced positive cooperativity on GCG-mediated iCa^{2+} mobilisation, as demonstrated by compound 448 (Fig. 5.32). Hence, such SAR studies suggest that the modulation of GCG-mediated iCa^{2+} release may be regulated by a change in electron-density.

Given the structural similarity between compound 249 and compound 2, which were both quinoxaline-based compounds, the introduction of alternative functional groups led to drastic changes in probe dependence profiles and converted compound 249 into a pure PAM. Therefore, further investigation on the quinoxaline scaffold should be performed in order to facilitate the design of small molecules pharmacological tool in understanding the biased signalling and probe dependence at the GLP-1R.

5.8.5 Compound 249 serves as further evidence on the importance of cAMP activation in mediating insulin secretion

Besides the promotion of cAMP production, the augmentation of iCa^{2+} release has been widely attributed to the release of insulin at the pancreatic β cells [Seino, 2012]. In spite of the inhibition of GLP-1 and OXM-mediated iCa^{2+} release (Fig. 5.6), compound 249 was able to promote GSIS facilitated by OXM in *in vitro* insulin secretion assays as well as in *ex vivo* isolated mouse islets (Fig. 5.25 and 5.27). The observations further substantiate the postulation that the extent of promoting cAMP responses is more crucial in enhancing insulin secretion [Gylfe, 2016]. Furthermore, despite the fact that compound 249 can only marginally potentiate GLP-1-mediated cAMP response (Fig. 5.4), given the importance of enhancing cAMP responses in facilitating GSIS, such slight degree of potentiation is sufficient to induce potentiation of GLP-1-mediated GSIS, as illustrated in Fig. 5.25. Overall, the potentiation of GLP-1 and OXM-mediated GSIS facilitated by compound 249 illustrates the importance of targeting cAMP signalling pathway in relative to iCa^{2+} release.

5.9 Chapter summary

The findings of the chapter are concluded as follows:

- Compound 249 exhibits unique pharmacological activity as it acts as a PAM on the OXM-mediated cAMP response, a NAM on GLP-1 and OXM-mediated iCa^{2+} mobilisation, and a NAL at the pERK1/2 pathway (Fig. 5.9).
- It does not require the presence of the cysteine 347 residue to mediate its allosteric modulation activity (Fig. 5.15).
- Compound 249 illustrates potentiation effect on GLP-1 and OXM-mediated GSIS in a dose-dependent manner in rat INS-1 832/3 wildtype and INS-1 GIPR-KO cell lines, yet it shows a lack of effect on the INS-1 GLP-1R-KO cell line, further implying the importance of GLP-1R on mediating the action of compound 249 (Fig. 5.23 and 5.25).
- Preliminary results on *ex vivo* isolated mouse islets show that compound 249 is able to augment GSIS mediated by OXM, further proving the feasibility of compound 249 to be further developed as a potential T2DM drug treatment targeting the action of OXM (Fig. 5.27).
- SAR studies show that the alkyne moiety on compound 249 may be essential for its unique probe dependence on OXM signalling pathway, as analogues 248, 82 and 448, despite their close structural relationships, do not demonstrate similar signalling profiles as compound 249 (Fig. 5.30 and 5.32).
- Among the drug candidates selected based on ligand-based virtual screening, only compound 607 illustrates NAM activity on both the cAMP responses and iCa^{2+} mobilisation mediated by GLP-1 and OXM, which may serve as a tool in understanding the structural conformation of GLP-1R (Fig. 5.36).

Chapter 6

General discussion and future work

Glucose homeostasis has been well established to be regulated via the actions of insulin, which is secreted from the pancreatic β cells, and glucagon, which is secreted from the pancreatic α cells [Unger et al., 1963]. Apart from insulin and glucagon, incretin hormones, in particular GLP-1 and GIP, have been shown to influence glucose homeostasis via their 'incretin effect' at the pancreatic β cells, which leads to higher insulin secretion upon gastric feeding compared to intravenous glucose administration [Elrick et al., 1964, Seino et al., 2010]. However, contrasting actions, i.e. GLP-1 inhibits while GIP stimulates glucagon secretion, have been noted. Unlike the relatively well understood mechanisms of incretin regulation of GSIS in the pancreatic β cells, the mechanisms that explain the opposing actions of GLP-1 and GIP are lacking, prompting the need for elucidating the highly physiologically relevant mechanism. Therefore, this work serves to determine the molecular mechanisms of how GLP-1 mediates its glucagonostatic action.

6.1 Proposed mechanisms of GLP-1 regulation of glucagon secretion

The central research question of this work is to understand how GLP-1 directly inhibits glucagon secretion in the pancreatic α cells. Therefore, different aspects of how GLP-1 interplays with other factors that modulate glucagon secretion are considered and will be discussed in the following sections.

6.1.1 Crosstalk of GLP-1R and GCGR activation

Individual receptor activation by GLP-1 and a range of glucagon-like peptides, namely OXM, GCG, GIP and especially the highly abundant GLP-1 metabolite GLP-1(9-36)NH_2, were evaluated in CHO-K1 recombinant cell lines stably expressing their canonical receptors: GLP-1R, GCGR and GIPR. Their extent of stimulating cAMP responses, which are one of the most important secondary messengers in relaying downstream signalling cascades ultimately leading to glucagon secretion, were evaluated. From these series of cAMP functional assays, it was discovered that GLP-1R and GCGR can be activated by the same pool of ligands, namely GLP-1, OXM, GCG and surprisingly GLP-1(9-36)NH_2, albeit at varying potencies, and that GIP can only specifically activate GIPR (Fig. 3.2). Further antagonist studies also confirmed that these peptide agonists activate GCGR, as their cAMP responses are blocked in the presence of the GCGR specific small molecule antagonist, L-168,049 (Fig. 3.13). The conclusion that GLP-1(9-36)NH_2 acts not only through GLP-1R, but also GCGR, substantiates the GLP-1(9-36)NH_2 'dual receptor theory' [Tomas-Falco and Habener, 2010, Guglielmi and Sbraccia, 2017]: rather than activating a completely unidentified receptor, GLP-1(9-36)NH_2 activates a promiscuous receptor, GCGR. In addition, GCGR has been shown to interact with RAMP2, an accessory protein, which modulates the signal transduction and receptor trafficking of GCGR [Weston et al., 2015, Cegla et al., 2017]. Indeed, the potency of cAMP responses of GLP-1(9-36)NH_2 has been found to be greatly enhanced in the presence of RAMP2 using HEK293-based stably expressing GCGR cell line with a null RAMP-background (Fig. 3.16). These results imply that RAMPs may also play a physiological role in modulating glucagon secretion via augmenting GLP-1(9-36)NH_2 cAMP responses. Using rodent clonal α and β cell lines, the extent of cAMP responses mediated by the glucagon-like peptides were also determined (Fig. 3.10). GIP and GCG were found to be the most potent peptide agonists in the α cell lines, followed by GLP-1 and OXM and lastly GLP-1(9-36)NH_2. These findings posed further question if GLP-1, and other glucagon-like peptides, in particular its highly abundant metabolite which physiological function is yet to be fully understood, regulate glucagon secretion via non-canonical receptors and therefore the incretin receptor expressions were examined in mouse clonal α and β cell models.

6.1.2 Expressions of GLP-1R in pancreatic α cells

The expressions of GLP-1R in pancreatic α cells have been long speculated [Moens et al., 1996, Kedees et al., 2009, Tornehave et al., 2008] and the reason for a lack of definitive conclusion for GLP-1R expression is a lack of a highly sensitive GLP-1R antibody that deters investigation using high-resolution microscopy techniques [Ramracheya et al., 2018]. In fact, a lot of recent studies, which used varying experimental techniques such as real-time RT-PCR and confocal laser scanning microscopy, have demonstrated the expressions of GLP-1R in mouse clonal α cells as well as in more physiologically relevant settings such as the rodent islets [Piro et al., 2014, Nakashima et al., 2018, Ramracheya et al., 2018, Zhang et al., 2019], albeit at a very low expression in comparison to its presence in the β and δ cells. In fact, in this work the mRNA levels of GLP-1R has also been detected in mouse αTC1.6 cell line with the use of semi-quantitative RT-PCR technique (Fig. 3.7). The relative expressions of GLP-1R in the α and β cells were also in line with other studies [Ramracheya et al., 2018, Zhang et al., 2019], which showed that there was a higher expression of GLP-1R in the β cells compared to the α cells. Furthermore, GLP-1R expression was found to be unaltered in long-term low and high glucose conditions (Fig. 3.17). In addition, among the incretin receptors, GIPR has been shown to be the most highly present receptor in the mouse clonal α cells, followed by equally low expression levels of GLP-1R and GCGR according to the qRT-PCR studies (Fig. 3.7). Aligning with the observations from the cAMP functional assays which illustrate crosstalk between GLP-1R and GCGR, the notion of whether glucagon secretion is regulated through the crosstalk of the low expressions of GLP-1R and GCGR is postulated.

Furthermore, the expression of GPR119, which is a class A GPCR that has been shown to regulate the cAMP signalling of GLP-1R [Cheng et al., 2015, Brown et al., 2018], was also evaluated in the mouse clonal α and β cell lines. Despite its relatively high expression in the mouse clonal α cells, based on the conclusion from the functional cAMP studies that showed GPR119 endogenous and synthetic agonists did not activate GLP-1R and GCGR and vice versa, glucagon-like peptides did not activate GPR119 (Fig. 3.11), the speculation that glucagon-like peptides mediate glucagon secretion via the highly expressed GPR119 was dismissed. Given the close structural homology between GLP-1R and GCGR, the influence of GCGR on GLP-1 regulated glucagon secretion was further investigated.

6.1.3 Deciphering the crosstalk of GLP-1R and GCGR using glucagon secretion studies

Following the optimisation of the insulin and glucagon secretion assaying technique which is relatively new to our laboratory (Fig. A.2 and A.3), the extent of glucagon secretion mediated by GLP-1 and GLP-1(9-36)NH_2 were examined (the glucagon-stimulatory action of OXM was not investigated due to its close structural similarity with GCG). Consistent with the findings from our collaborators [Guida et al., 2020], optimal inhibition of glucagon secretion by GLP-1 and GLP-1(9-36)NH_2 was achieved at sub-picomolar concentration (i.e. at 100pM), whereas glucagon secretion was not suppressed if the concentrations applied deviated from this optimal concentration (i.e. at 100nM and 1pM), illustrating glucagon inhibition is tightly controlled by specific amount of agonist stimulation at the pancreatic α cells (Fig. 4.2) and further substantiated the postulation of the tonic inhibition of glucagon secretion by the low circulating GLP-1 and GLP-1(9-36)NH_2 [Guida et al., 2020].

Following the deduction of the optimal concentrations of GLP-1 and GLP-1(9-36)NH_2 to be used in subsequent glucagon secretion assays, antagonist studies, with the use of GLP-1R and GCGR specific antagonists, Ex-9 and L-168,049 respectively, were conducted to further envisage the physiological outcome of blocking one receptor to another. Intriguingly, the blocking of either GLP-1R or GCGR reversed the glucagonostatic actions of both GLP-1 and GLP-1(9-36)NH_2 at low glucose condition (Fig. 4.5). The application of both receptor antagonists further enhanced glucagon secretion, and that this effect was not an artifact effect of the antagonists as applying the antagonists alone did not influence glucagon secretion (Fig. 4.5). These results implicate that both GLP-1R and GCGR are critical in mediating the glucagonostatic action of not only GLP-1, but also GLP-1(9-36)NH_2. This glucagon secretion antagonist study also sheds new light on a physiologically relevant role of the GLP-1(9-36)NH_2 in inhibiting *in vitro* glucagon secretion that has not been described in literature.

6.1.4 Influence of G protein activation on GLP-1 and GLP-1(9-36)NH_2 regulated glucagon secretion

GLP-1R and GCGR are known to pleiotropically couple to not only $G\alpha_s$ subunit predominantly, but also $G\alpha_i$ and $G\alpha_q$ proteins; the latter two G protein subunits are linked to the inhibition of the adenylyl cyclase activity, leading to a reduction of intracellular cAMP levels, as well as the activation of the PLC/iCa^{2+} pathway which is responsible for a range of physiological events respectively. Therefore, the influence of $G\alpha_i$ and $G\alpha_q$ activation on glucagon secretion was also examined. To examine the $G\alpha_q$ activation, as measurable by iCa^{2+} mobilisation, the iCa^{2+} responses upon GLP-1R and GCGR activation by GLP-1, OXM and GCG were determined in HEK293S-GLP-1R and HEKΔCTR-GCGR stable cell lines (Fig. 3.6); the iCa^{2+} mobilisation induced by GLP-1(9-36)NH_2 was not investigated due to its very weak calcium signalling response. Here, it was established OXM and GCG were able to mediate partial agonisms on iCa^{2+} responses at both receptors, while GLP-1 can only mediate iCa^{2+} release at GLP-1R (Fig. 3.6). However, the relevant influence of $G\alpha_i$ activation on iCa^{2+} responses at both receptors was not investigated, but study has shown that the iCa^{2+} release is regulated via both $G\alpha_q$ and $G\alpha_i$ pathway at the GCGR [Xu and Xie, 2009]. In addition, according to the qRT-PCR studies, the mouse αTC1.6 cell line expresses high levels of $G\alpha_s$, and $G\alpha_{i2}$, $G\alpha_{i3}$ and $G\alpha_{q/11}$ subunits (Fig. 3.9). These all point to the question if $G\alpha_i$ and $G\alpha_q$ coupling are essential for glucagon secretion. Therefore, $G\alpha_i$ irreversible inhibitor, PTX, and $G\alpha_{q/11}$ inhibitor, YM-254,890, were applied to the mouse αTC1.6 cells and the physiological effect of $G\alpha_i$ and $G\alpha_q$ blockage on glucagon secretion were explored. Here, blocking of $G\alpha_i$-coupling with PTX led to a reversal of actions of both GLP-1 and GLP-1(9-36)NH_2 mediated glucagonostatic action (Fig. 4.7), which is in contrast to the observations by our collaborators which they show the glucagonostatic action of GLP-1 is $G\alpha_i$-independent while that of GLP-1(9-36)NH_2 is $G\alpha_i$-dependent in isolated mouse islets [Guida et al., 2020]. Furthermore, the inhibition of $G\alpha_q$ also leads to a reversal of both ligands' glucagonostatic action, further implying the importance of subsequent downstream intracellular calcium mobilisation in regulating glucagon secretion (Fig. 4.7). However, due to time constraints, the influence of downstream PKA signalling was not investigated, and remains an essential future work as our collaborators have shown that the glucagon secretion inhibitory effect mediated by GLP-1 is partially PKA-dependent, while that of GLP-1(9-36)NH_2 is PKA-independent [Guida et al., 2020].

6.1.5 Working model of how GLP-1 regulates glucagon secretion in pancreatic α cells

In this work, signal transduction functional assays, semi-quantitative RT-PCR studies and glucagon secretion assays have been frequently employed in an attempt to explore how GLP-1 regulates glucagon secretion in pancreatic α cells. Surprisingly, GLP-1 has been found to mediate its glucagonostatic action not only via its canonical receptor, GLP-1R, but also via the promiscuous activation of GCGR. In addition, GLP-1(9-36)NH_2 is also shown to potently inhibit glucagon secretion via the actions of both GLP-1R and GCGR, an observation that has not been noted to date. Based on all the observations as discussed above as well as the findings by our collaborators [De Marinis et al., 2010, Ramracheya et al., 2018, Guida et al., 2020], a working model of the mechanisms of GLP-1 regulation of glucagon secretion is proposed (Fig. 6.1).

DPP-IV enzymes are ubiquitously present in the pancreatic α cells, metabolising GLP-1 to GLP-1(9-36)NH_2 within 1-2 minutes [Eng et al., 2014]. GLP-1(9-36)NH_2 is a partial agonist at both GLP-1R and GCGR. Therefore, GLP-1 and the widely abundant GLP-1(9-36)NH_2 bind to the low expressing GLP-1R and GCGR, which are predominantly Gα_s-coupled. Upon receptor activation, the activity of adenylyl cyclase is facilitated, thereby catalysing the conversion of ATP to cAMP. Furthermore, the extent of cAMP production mediated by GLP-1(9-36)NH_2 is facilitated by the GCGR:RAMP2 interaction, thereby enhancing the overall cAMP response potency. However, the overall intracellular cAMP level is tightly controlled not only by Gα_s activation, but also by the Gα_i subunit. As GLP-1R and GCGR can pleiotropically couple to both Gα_s and Gα_i subunits, Gα_i activation upon receptor activation also play a role in maintaining the tight cAMP level essential for the glucagon inhibitory effect, as established by our collaborators [De Marinis et al., 2010].

The low level of cAMP produced upon receptor activation by GLP-1 and GLP-1(9-36)NH_2 thus activates the type I PKA, which has been shown to require less intracellular cAMP level for its activation compared to the type II PKA [De Marinis et al., 2010, Yang and Yang, 2016]. As suggested by our collaborators, the activation of type I PKA leads to a closure of the P/Q-type Ca^{2+} channel via protein phosphorylation, which ultimately results in the inhibition of glucagon secretion through inhibiting exocytosis of glucagon-containing vesicles (Fig. 6.1)

On the other hand, the predominantly Gα_s-coupled GIPR is highly expressed in the pancreatic α cells. Hence, GIP can activate the highly dense GIPR to give a higher

intracellular cAMP level compared to the low intracellular cAMP responses upon GLP-1R activation. The type I PKA is activated, which also inhibits the P/Q-type Ca^{2+} channel, resulting in an inhibition of exocytosis. However, the inhibition of exocytosis is overcome by the high level of cAMP production, which also activates the type II PKA that requires a higher level of cAMP level for its activation. The activation of the type II PKA thus leads to a direct promotion of glucagon secretion. The high intracellular cAMP level also leads to the activation of EPAC2, which further triggers an opening of the L-type Ca^{2+} channel, thereby enhancing an influx of iCa^{2+}, ultimately leading to glucagon secretion through exocytosis [De Marinis et al., 2010]. These differences in the types of PKA activated due to the innate varying level of cAMP produced may have contributed to the apparent glucagon secretion stimulatory and inhibitory effect mediated by GLP-1, GLP-1(9-36)NH_2 and GIP.

In addition, $G\alpha_q$ activation was also shown to be critical for the glucagonostatic action of GLP-1 and its metabolite as a blockage of which leads to a reversal of glucagonostatic action (Fig. 4.7). However the precise mechanism of how the regulation of iCa^{2+} level leads to inhibition of glucagon secretion is not further investigated in this work. The mechanism of which will be instrumental to advance the understanding of GLP-1 and GLP-1(9-36)NH_2 mediated glucagonostatic action and will serve as an important piece of future work.

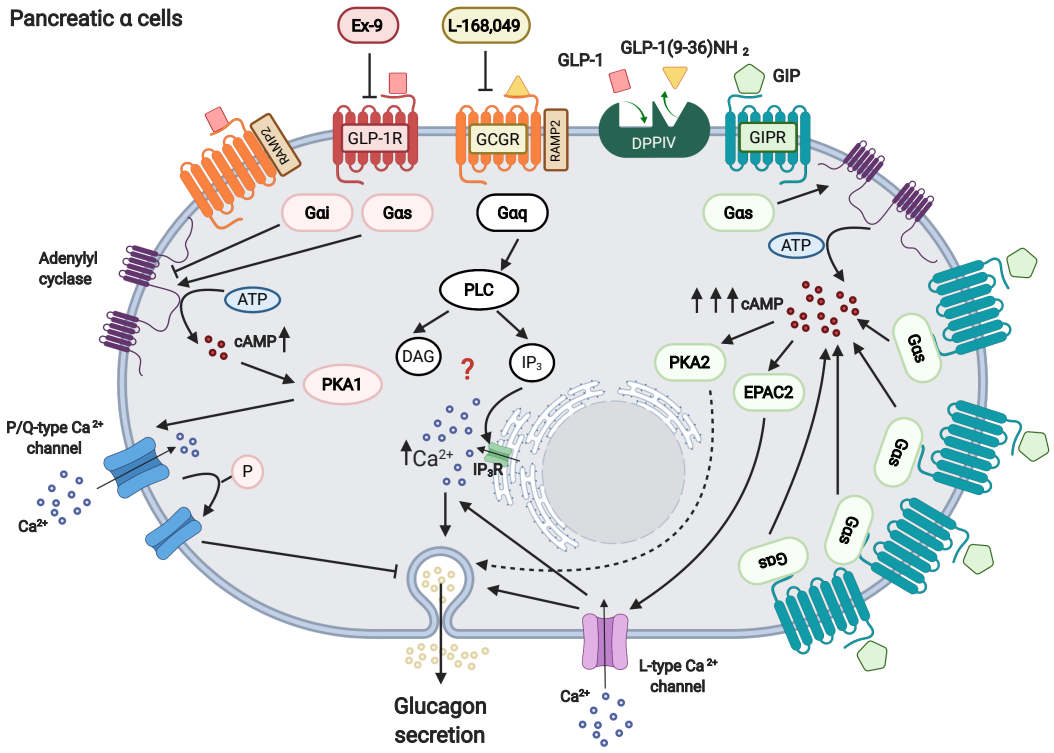

Figure 6.1: **Schematic diagram proposing the mechanisms of actions of how GLP-1 and GLP-1(9-36)NH_2 regulate glucagon secretion in pancreatic α cells.** The glucagonostatic actions of GLP-1 and GLP-1(9-36)NH_2 are proposed as follow: 1) GLP-1 and GLP-1(9-36)NH_2 act directly on the low expressing GLP-1R and GCGR, which are predominantly Gα_s-coupled. 2) The activation of the receptors lead to the activation of the Gα_s-pathway, whereby the activity of adenylyl cyclase is facilitated, leading to the conversion of ATP to cAMP. 3) The low level of intracellular cAMP produced is just sufficient to activate the type I PKA, which leads to a closure of the P/Q-type Ca^{2+} channel via protein phosphorylation. 4) The closure of the P/Q-type Ca^{2+} channel inhibits exocytosis, therefore inhibiting glucagon secretion. The glucagon-stimulatory action of GIP is proposed as follow: 1) Compared to GLP-1R, GIPR is highly present. Therefore, a higher level of intracellular cAMP is produced upon GIPR activation. 2) This high cAMP level produced not only triggered the activation of the type I PKA, but also the type II PKA which requires a higher level of cAMP for its activation. The activation of type II PKA directly leads to enhancing exocytosis of glucagon-containing vesicles. 3) This high level of cAMP produced also activates EPAC2, which facilitates the opening of the L-type Ca^{2+} channel, thereby enhancing the influx of Ca^{2+} into the cytoplasm, ultimately enhancing iCa^{2+} level. 4) This augmentation of iCa^{2+} level then leads to exocytosis, resulting in glucagon secretion. Diagram created by BioRender.com.

6.2 Differences between GLP-1 regulated insulin and glucagon secretion

As the mechanisms of how GLP-1 and GIP regulate GSIS have been thoroughly elucidated by other research groups [Seino et al., 2010, Cho et al., 2014] and is summarised in Fig. 6.2, the major differences between the molecular mechanisms of GLP-1 mediated insulin and glucagon secretion in the pancreatic β and α cells will be highlighted in this section.

6.2.1 GLP-1R densities differences

Firstly, the contrasting GLP-1 actions on insulin and glucagon secretion can be attributed to the GLP-1R densities on both α and β cells. Compared to pancreatic α cells, GLP-1R is highly present in the pancreatic β cells, as deduced by the qRT-PCR studies in the rodent clonal pancreatic cell lines (Fig. 3.7 and Fig. 3.8). This stark contrast in GLP-1R expression therefore leads to a higher intracellular level of cAMP produced in the pancreatic β cells compared to the α cells upon receptor activation by GLP-1, thereby leading to the activation of both PKA (presumably via the type II PKA) and EPAC2, resulting in a series of downstream signalling effect, ultimately augmenting insulin secretion. This cAMP effect on insulin secretion can be further emulated with the use of forskolin, which is a direct adenylyl cyclase activator, as the higher the forskolin concentration applied, the higher the insulin secretion observed, as shown in the insulin secretion studies in the INS-1 832/3 cell line (Fig. 4.6).

6.2.2 GLP-1R: the sole mediator of GSIS

As discussed above, GLP-1 has been shown to be a dual agonist at both GLP-1R and GCGR (Fig. 3.2). Despite the antagonist studies demonstrated that both GLP-1R and GCGR contributed to the overall cAMP responses when the INS-1 832/3 cells were stimulated with GLP-1 in the presence of GLP-1R and GCGR specific antagonists (Fig. 3.14), GLP-1R has been shown to be the sole mediator of the augmentation of GSIS, as GLP-1 failed to stimulate GSIS in the INS-1 832/3 GLP-1R KO cell line (Fig. 4.4). This observation is unlike the proposed glucagon secretion mechanism observed in the pancreatic α cells, whereby GLP-1 requires both GLP-1R and GCGR to achieve the fine balance of intracellular cAMP levels that is essential for its inhibitory action.

6.2.3 GLP-1(9-36)NH_2 does not play a role in GSIS

Furthermore, GLP-1(9-36)NH_2 does not possess insulinotropic action in the pancreatic β cells, which contrasts with the published reports on *in vivo* studies [Elahi et al., 2008], yet concurred with the observations from our collaborators in the isolated mouse islets [Guida et al., 2020]. The molecular mechanisms of such evidential difference are unknown. However, it may be attributable to the potent cAMP responses upon GLP-1R activation by GLP-1, which masks the weak partial agonism cAMP responses of the GLP-1 metabolite.

6.2.4 Less involvement of Gα_i and Gα_q activation in GLP-1 regulated GSIS

In addition, compared to the stark reversal of the glucagon secretion inhibitory effect upon the application of both Gα_i inhibitor (PTX) and G$\alpha_{q/11}$ inhibitor (YM-254,890) (Fig. 4.7), the blockages of both Gα_i and G$\alpha_{q/11}$-coupling had less significant effect on insulin secretion (Fig. 4.6). This may suggest, and further affirm, the notion that cAMP activation is the most critical signalling pathway, and that Ca^{2+} plays a more permissive role in GLP-1 regulated GSIS [Tengholm and Gylfe, 2017]. However, further studies, such as through the application of Gα_s selective inhibitor, such as cholera toxin (CTX), is needed to confirm such hypothesis.

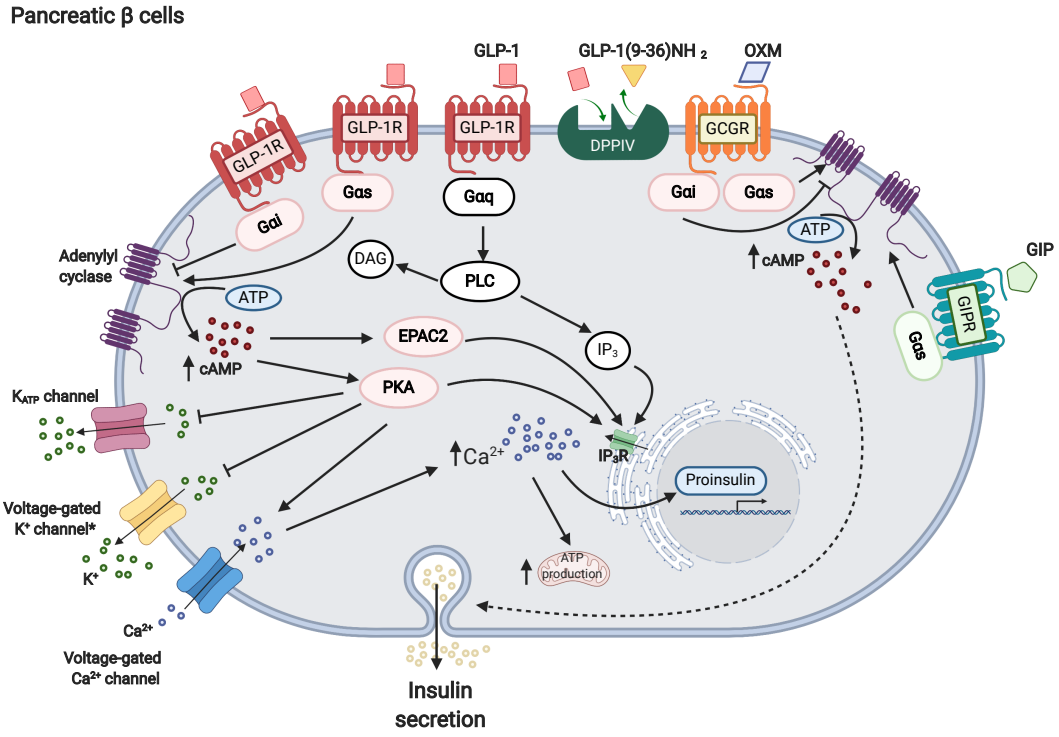

Figure 6.2: **Schematic diagram proposing the mechanisms of actions of how GLP-1 and other glucagon-like peptides promote insulin secretion in pancreatic β cells.** The above diagram illustrates how incretins, such as GLP-1 and GIP, regulate GSIS. 1) Upon GLP-1 and GIP binding to their canonical receptors, GLP-1R and GIPR, the Gα_s subunits are activated, which facilitate the adenylyl cyclase activity, leading to increases in intracellular cAMP levels. 2) The increase in cAMP production results in the activation of PKA and EPAC2. 3) The PKA-dependent pathway leads to the inhibition of the K_{ATP} channel, thereby resulting in membrane depolarisation. 4) Furthermore, PKA, together with PKC, inhibit the voltage-gated K^+ channel, which repolarises the membrane potential via the efflux of K^+. 5) This delays repolarization, leading to an increase in iCa^{2+} via the voltage-gated Ca^{2+} channel. 6) EPAC2 together with PKA enhance the release of Ca^{2+} from intracellular stores through Ca^{2+}-induced Ca^{2+} release in the endoplasmic reticulum (ER) through the action of IP_3R. 7) These collective enhancements of iCa^{2+} level promote the exocytosis of the insulin-containing granules, therefore enhancing GSIS in the β cells. 8) Furthermore, both PKA and EPAC2 have been shown to have direct effect on the exocytosis of insulin-containing vesicles and are not depicted in the diagram. Diagram created by BioRender.com.

6.3 Pharmacological regulation of GLP-1-mediated insulin secretion

Another focus of this thesis is to identify viable pharmacological means to regulate GLP-1-mediated glucose homeostasis, given the gravity of the economic and social burden of T2DM at individual and social levels [International Diabetes Federation, 2019]. Incretin-based drug treatments for T2DM have been developed in the past few decades and are proven to be highly effective in reducing long term blood glucose level as well as inducing weight loss effect on T2DM patients who are often overweight or obese [Oh and Olefsky, 2016]. However, their uses have been limited by their side effects, from mild gastrointestinal disturbances, to potentially fatal pancreatitis [Meier, 2012]. Furthermore, they are peptide-based drugs, hence incurring high production cost [Hansen et al., 2020]. Despite the arrival of the latest FDA-approved oral semaglutide T2DM treatment, the production cost involved in producing peptide-based drug treatments and the healthcare cost of using these incretin-based treatments on regular basis are still extortionate [Hansen et al., 2020]. Therefore, alternative incretin-based oral therapies have been prompted, in a hope to improve current T2DM treatments.

GLP-1R small molecule agonists have been prompted as substitutes for the peptide-based incretin treatments. However, the development of such agonists has been historically hindered by the structural feature of GLP-1R, which is a large ECD compared to the other classes of GPCRs [Jazayeri et al., 2017, Graaf et al., 2016]. This large and highly flexible ECD warrants a great challenge for the design of GLP-1R small molecule agonist, as the identification of potential small molecule binding pockets is next to impossible. In addition, it is highly difficult to design small molecules that mimic the extensive interactions with the ECD. Therefore, alternative option, which is the development of allosteric modulators, is pursued.

Developing allosteric modulators have been proven to be an easier option due to the fact that multiple allosteric sites exist within the receptor [Kenakin, 2012, Thal et al., 2018]. Furthermore, there are immense advantages for developing allosteric modulators, which have been discussed in section 1.6.1. Hence, the identification of a viable small molecule GLP-1R PAM, that has the potential of being further developed as a new form of incretin-based T2DM treatment, has been the main focus of the other part of this thesis. Through *in silico* virtual screening and biological validations, compound 249 was identified to be a promising drug candidate among all of the other tested compounds.

6.3.1 Compound 249 displays unique pharmacological properties

Compound 249 is a distinct small molecule as it acts as a PAM on OXM-mediated cAMP responses selectively, a NAM on GLP-1 and OXM-mediated iCa^{2+} responses, and a NAL on OXM-mediated pERK1/2 responses (Fig. 5.9). Furthermore, compound 249 does not influence binding of GLP-1 at the GLP-1R (Fig. 5.8), although its effect on OXM binding has not yet been investigated and will be an important piece of future work. These results obtained through the use of a range of functional assays imply that compound 249 displays a unique pharmacological profile that is completely different from other reported GLP-1R small molecule PAMs [Knudsen et al., 2007, Schann et al., 2008, Sloop et al., 2010, Graaf et al., 2011, Redij et al., 2019, Méndez et al., 2020]. More intriguingly, the results from the functional assays which quantify the end-point measurement of secondary messengers align with the results from the mechanistic G protein dissociation studies, and revealed that compound 249 is a NAM on $G\alpha_{i2}$ pathway (appendix B.7). However, so far, the canonical signalling pathways (i.e. cAMP and iCa^{2+}) which has been known to implicate insulin secretion were investigated in this work. The influence of compound 249 on non-canonical signalling pathways are yet to be explored and may serve as an important piece of future work.

6.3.2 Compound 249 selectively enhances GLP-1 and OXM-mediated GSIS

Compound 249 enhances insulin secretion in a glucose, peptide ligand, GLP-1R-dependent manner using the INS-1 832/3 wildtype, GLP-1R and GIPR CRISPR-Cas9 knock-out cell lines [Naylor et al., 2016] (Fig. 5.24 and 5.25). In essence, compound 249 only potentiates GSIS in the presence of GLP-1 and OXM, but not GSIS mediated by the close GLP-1 analogue, Ex-4, and the GLP-1 metabolite, GLP-1(9-36)NH_2. Preliminary results also suggest compound 249 potentiates OXM-mediated GSIS in isolated mouse islets (Fig. 5.27), further substantiating the positive influence of compound 249 in enhancing insulin secretion at a physiological level. In addition, the unique pharmacological profile of compound 249, that it is a PAM in cAMP signalling pathway and a NAM in iCa^{2+}, poses an interesting question if the activation of cAMP plays a more critical role in mediating GSIS, while Ca^{2+} plays a relatively permissive role [Tengholm and Gylfe, 2017]. However, further experimental validations through quantifying iCa^{2+} release with or without the presence of compound 249 in physiological relevant systems, i.e. rodent β clonal cells or isolated mouse islets, are needed to confirm such hypothesis. Furthermore, the influence of compound 249 on glucagon secretion is yet

to be examined, and will be an important piece of future work in order to fully evaluate its overall regulation of glucose homeostasis.

6.3.3 Where does compound 249 bind at the GLP-1R?

The ultimate question of where compound 249 binds at the GLP-1R remain unvalidated due to time constraint, despite it has been shown that compound 249 does not require the C347 residue (Fig. 5.11 and 5.15), which has been thought to be critical for the PAM action of compound 2 and BETP [Song et al., 2017], for its pharmacological action. Given that multiple allosteric and small molecule agonist sites have been discovered at the GLP-1R (Fig. 1.15), numerous possible binding mode of compound 249 arise. Thanks to the docking results performed by Dr Taufiq Rahman (Department of Pharmacology, University of Cambridge), three main binding mode of compound 249 are suggested: which is via the ECD and ECL1 (model 1), ECL2 (model 2) and via the TM3 and TM4 core (model 3) (Appendix B.8). Therefore, future studies will involve performing mutagenesis studies to identify the allosteric pocket which compound 249 binds to and the key interacting amino acid residues.

6.4 Future work

6.4.1 Do RAMPs play any physiological role in regulating insulin and glucagon secretion?

One of the outstanding questions in this work is to evaluate the physiological impact of RAMPs on regulating insulin and glucagon secretion. RAMPs have been shown to interact with a range of Class B GPCRs, many of which are responsible for the regulation of glucose homeostasis [Hay et al., 2016]. Specifically, GCGR has been shown to interact with RAMP2 to significantly enhance GLP-1(9-36)NH_2 cAMP response (Fig. 3.16) [Weston et al., 2015, Cegla et al., 2017]. GIPR has been shown to interact with all three RAMPs, modulating its signal transduction and receptor trafficking properties [Harris et al., 2017]. Amylin, which is a glucoregulatory hormone that has also been developed as a T2DM treatment (pramlinitide), activates the amylin receptors, which are formed on the basis of interaction of CTR and RAMPs [Bower and Hay, 2016]. In spite of the reports using global and conditional RAMP knock-down mouse which illustrated the knock-down of individual RAMPs linked to a range of disorders, such as diverticular disease [Pauza et al., 2019], excessive fluid accumulation associated

with lymphatic insufficiency [Kadmiel et al., 2017], primary open-angle glaucoma [Gong et al., 2019] and nondiabetic obesity [Kim et al., 2015], none of the reports have explored any potential *in vitro* and *in vivo* effect on glucose homeostasis. Therefore, the implications of genetically knock-down of RAMPs on glucose homeostasis remain unaddressed and suggest a need to investigate such implications in *in vitro* and *in vivo* settings.

6.4.2 Use of genetically encoded indicators to examine how the dynamics of cAMP and Ca^{2+} signalling regulate insulin and glucagon secretion

The initiations of insulin and glucagon secretion via cAMP production and iCa^{2+} release have been known to be real-time events, which both processes occur within milliseconds [Gromada et al., 2007]. In this work, the extent of cAMP production was only quantified in terms of total accumulation within a designated time period in both recombinant and pancreatic clonal cell lines. The advantage of such approach facilitated the pharmacological characterisation of the potencies and efficacies of agonists in different cell models. However such experimental approach may not account for the spatial-compartmentalisation aspect of signalling [Tengholm and Gylfe, 2017]. Therefore, in order to fully understand the influence of cAMP dynamics on insulin and glucagon secretion in the pancreatic α and β cells, the use of genetically modified sensors, such as the EPAC-sensors [Patel and Gold, 2015], e.g. T-Epac-VV [Klarenbeek et al., 2011], EPAC-SH189 [Klarenbeek et al., 2015] or EPAC2-camps [Nikolaev et al., 2004], should be included as future work. These FRET-based biosensors confer distinct advantages in allowing time-lapse monitoring of downstream cAMP signalling in isolated α and β cells from mouse islets [Capozzi et al., 2019], intact *ex vivo* mouse islets [Denwood et al., 2019, Capozzi et al., 2019] and *in vivo* mouse models [Kim et al., 2008]. Unfortunately, iCa^{2+} release was not quantified in the pancreatic α and β clonal cell lines due to time constraints. Given the reported equal importance of both cAMP and Ca^{2+} in regulating insulin and glucagon secretion, the investigation of iCa^{2+} mobilisation in pancreatic α and β cells warrants further future work. Thanks to the recent development of the genetically encoded protein Ca^{2+} single fluorophore indicators [Mank and Griesbeck, 2008], such as G-CaMPs [Nakai et al., 2001], iCa^{2+} release can be monitored in real-time via fluorescent microscopy technique. In fact, these Ca^{2+} sensors have already been widely used to aid the investigation of the Ca^{2+} dynamics in human EndoC-βH1 beta clonal cell line [Cardenas-Diaz et al., 2020], *ex vivo* islets [Dadi et al., 2015, Adriaenssens et al., 2016, Hamilton et al., 2018] and in *in*

vivo mouse models in a non-invasive manner [Hasan et al., 2004, Ji et al., 2004, Heim et al., 2007]. The aforementioned genetically encoded protein sensors all illustrate their potential as useful tools in opening up a whole new avenue for understanding the cAMP and Ca^{2+} signalling dynamic in the regulation of insulin and glucagon secretion.

6.4.3 Use of pseudoislets for prospective insulin and glucagon secretion studies

A lot of this work utilised rodent clonal α and β cell lines grown adhesively in monolayers to investigate the signal transduction, as well as insulin and glucagon secretion stimulatory responses of glucagon-like peptides. This approach confers distinct advantages of being able to evaluate glucagon-like peptide responses at a single cell population, allowing efficient testing. However, the islets of Langerhans are known to be composed of a mixture of β, α and δ cells [Cabrera et al., 2006, Kelly et al., 2011, Brereton et al., 2015, Da Silva Xavier, 2018], and gap junctional coupling and paracrine signalling between endocrine cells are essential for its glucoregulatory function [Meda et al., 1991]. Hence the results obtained from monolayer of a single cell population may be difficult to be translated across to the more physiologically relevant systems i.e. isolated mouse islets, thus explaining some of the apparent discrepancies between the results in this work and those by our collaborators. Yet, obtaining rodent, and to a more challenging extent human isolated islets are labour-intensive processes and primary islets are difficult for experimental manipulation [Walker et al., 2020]. Therefore, alternative approach has been prompted which involves the formation of pseudoislets [Hauge-Evans et al., 1999].

Pseudoislets can be made through allowing pancreatic clonal cell lines [Hauge-Evans et al., 1999, Brereton et al., 2007, Guo-Parke et al., 2012, Chowdhury et al., 2013, Teraoku and Lenzen, 2017, Tsonkova et al., 2018] or single cells from isolated mouse or human islets [Lorza-Gil et al., 2019, Walker et al., 2020] to reaggregate on non-adhesive cell culture dishes with constant low-speed spinning in the presence of a rich supplement of nutrient and growth factor media. Once these single cells are allowed to reaggregate after a week, cell clusters are formed which mimic the size and morphology of primary islets [Lorza-Gil et al., 2019, Walker et al., 2020]. More importantly, the insulin and glucagon secretion responses of pseudoislets upon glucose and incretins stimulation have been shown to be robustly higher than those of monolayers of clonal cell lines, plausibly due to the availability of cell-to-cell interaction within the pseudoislet environment [Hauge-Evans et al., 1999, Kelly et al., 2011, Chowdhury et al.,

2013]. In addition, compared to using primary islets, the pseudoislets systems are more amenable to genetic modification, thereby facilitating intracellular signalling studies at a mechanistic level. One of the prime examples is the recent study of the effect of $G\alpha_i$ and $G\alpha_q$ signalling pathways on insulin and glucagon secretion using human pseudoislets, which express the designer receptors exclusively activated by designer drugs (DREADDs) hM4Di or hM3Dq [Walker et al., 2020]. The use of pseudoislets has been indeed viewed to be a useful tool and has been used routinely in academic [Hauge-Evans et al., 1999, Brereton et al., 2007, Guo-Parke et al., 2012, Chowdhury et al., 2013, Teraoku and Lenzen, 2017] and industrial settings [Tsonkova et al., 2018]. Therefore, the pseudoislet system may be an invaluable tool for the future studies on the relationship between $G\alpha_q$ activation and GLP-1 or GLP-1(9-36)NH_2 mediated glucagonostatic action.

6.4.4 Future design of GLP-1R allosteric modulator guided by structure-based virtual screening

The recent spawning reports of GLP-1R full-length crystals structures in complex with small molecule agonists [Zhao et al., 2020, Ma et al., 2020a], NAMs [Song et al., 2017] and PAM [Bueno et al., 2020] have undoubtedly advanced the future design of GLP-1R small molecule agonists or allosteric modulators. In fact, GLP-1R specific PAM, C-1 [Redij et al., 2019], has been identified utilising structure-based virtual screening approach, through identifying the potential allosteric site using the full-length GLP-1R structure in complex with GLP-1 and $G\alpha_s$ subunit [Zhang et al., 2017a]. This example suggests an exciting avenue for future fruitful search of GLP-1R small molecule agonists and PAMs aided by the advanced knowledge of the GLP-1R structure.

6.5 Concluding remarks

Two main objectives were explored in this thesis: 1) to investigate how GLP-1 regulates glucose homeostasis in the pancreatic β and α cells; 2) to discover novel pharmacological mean to regulate GLP-1-mediated glucose homeostasis. The first objective was achieved via mechanistically evaluate the signalling responses, primarily the key secondary messengers, cAMP and Ca^{2+}, mediated by the glucagon-like peptides at the GLP-1R, GCGR and GIPR. The mRNA expressions of incretin receptors, as well as the accessory proteins RAMPs, were also deduced in order to facilitate the translation of the evaluation of signalling responses in recombinant cell backgrounds to the more physiologically

relevant pancreatic clonal cell lines. Following the mechanistic evaluation of signalling responses, the physiological impact of incretins on insulin and glucagon secretion were evaluated, using the newly optimised insulin and glucagon secretion assaying technique. GLP-1R and GCGR specific antagonists as well as a range of pharmacological pathway inhibitors were further applied to probe the effect of receptor or signalling pathway blockage on insulin and glucagon secretion. From these series of experiments, it was concluded that glucagon secretion is regulated by both GLP-1 and GLP-1(9-36)NH_2 via the direct interaction of the low expressing GLP-1R and GCGR at the pancreatic α cells.

The second goal of this work is to identify novel means to pharmacologically regulate GLP-1-mediated glucose homeostasis. Following ligand-based virtual screening and biological validation through the use of cAMP accumulation assays, compound 249 was identified as one of the interesting drug compounds that was GLP-1R-specific and was a PAM of OXM-mediated cAMP signalling. Further pharmacological characterisation also showed that it was OXM-selective, and that it acted as a NAM in GLP-1 and OXM-mediated iCa^{2+} release. More intriguingly, with the use of HEK293S stably expressing GLP-1R-C347A cell line, compound 249 was discovered to function via a C347-independent manner, which implied that it may bind at an alternative allosteric site. With the use of subsequent SAR studies which involved the design of multiple compound 249 analogues, it was discovered that the trans-alkyne moiety on compound 249 was conducive to its apparent unique pharmacological profile. More importantly, with the use of the insulin secretion assaying technique, compound 249 was found to robustly enhance the OXM and GLP-1-mediated GSIS in INS-1 832/3 cell line in a glucose, peptide and GLP-1R-specific manner. Further *ex vivo* insulin secretion assay conducted in isolated mouse islets also confirmed its augmentation of OXM-mediated GSIS. These collective results affirmed the potential future development of compound 249 as a T2DM treatment as well as an invaluable experimental tool to explore OXM-biased signalling at the GLP-1R.

Bibliography

[Adriaenssens et al., 2016] Adriaenssens, A. E., Svendsen, B., Lam, B. Y. H., Yeo, G. S. H., Holst, J. J., Reimann, F., and Gribble, F. M. (2016). Transcriptomic profiling of pancreatic alpha, beta and delta cell populations identifies delta cells as a principal target for ghrelin in mouse islets. *Diabetologia*, 59(10):2156–2165.

[Ahn et al., 2004] Ahn, S., Wei, H., Garrison, T. R., and Lefkowitz, R. J. (2004). Reciprocal regulation of angiotensin receptor-activated extracellular signal-regulated kinases by β-arrestins 1 and 2. *Journal of Biological Chemistry*, 279(9):7807–7811.

[Ahrén, 2009] Ahrén, B. (2009). Islet G protein-coupled receptors as potential targets for treatment of type 2 diabetes. *Nat Rev Drug Discov*, 8(5):369–385.

[Alexander et al., 2019] Alexander, S. P. H., Christopoulos, A., Davenport, A. P., Kelly, E., Mathie, A., Peters, J. A., Veale, E. L., Armstrong, J. F., Faccenda, E., Harding, S. D., Pawson, A. J., Sharman, J. L., Southan, C., and Davies, J. A. (2019). THE CONCISE GUIDE TO PHARMACOLOGY 2019/20: G protein-coupled receptors. *British journal of pharmacology*, 176(Suppl 1):S21–S141.

[Almahariq et al., 2014] Almahariq, M., Mei, F. C., and Cheng, X. (2014). Cyclic AMP sensor EPAC proteins and energy homeostasis. *Trends in Endocrinology and Metabolism*, 25(2):60–71.

[Aroda et al., 2012] Aroda, V. R., Henry, R. R., Han, J., Huang, W., DeYoung, M. B., Darsow, T., and Hoogwerf, B. J. (2012). Efficacy of GLP-1 receptor agonists and DPP-4 inhibitors: meta-analysis and systematic review. *Clinical Therapeutics*, 34(6):1247–1258.e22.

[Asadi and Dhanvantari, 2019] Asadi, F. and Dhanvantari, S. (2019). Plasticity in the glucagon interactome reveals novel proteins that regulate glucagon secretion in α-TC1-6 cells. *Frontiers in Endocrinology*, 9(January):1–15.

[Baggio and Drucker, 2007] Baggio, L. L. and Drucker, D. J. (2007). Biology of Incretins: GLP-1 and GIP. *Gastroenterology*, 132(6):2131–2157.

[Bailey, 2015] Bailey, C. J. (2015). The current drug treatment landscape for diabetes and perspectives for the future. *Clinical Pharmacology and Therapeutics*, 98(2):170–184.

[Bailey et al., 2019] Bailey, S., Harris, M., Barkan, K., Winfield, I., Harper, M. T., Simms, J., Ladds, G., Wheatley, M., and Poyner, D. (2019). Interactions between RAMP2 and CRF receptors: The effect of receptor subtypes, splice variants and cell context. *Biochimica et Biophysica Acta - Biomembranes*, 1861(5):997–1003.

[Ban et al., 2010] Ban, K., Kim, K.-h., Cho, C.-k., Sauve, M., Diamandis, E. P., Backx, P. H., Drucker, D. J., and Husain, M. (2010). Glucagon-Like Peptide (GLP)-1(9-36)amide-mediated cytoprotection is blocked by exendin(9-39) yet does not require the known GLP-1 receptor. *Endocrinology*, 151(4):1520–1531.

[Berger et al., 2015] Berger, M., Scheel, D. W., Macias, H., Miyatsuka, T., Kim, H., Hoang, P., Ku, G. M., Honig, G., Liou, A., Tang, Y., Regard, J. B., Sharifnia, P., Yu, L., Wang, J., Coughlin, S. R., Conklin, B. R., Deneris, E. S., Tecott, L. H., and German, M. S. (2015). Gαi/o-coupled receptor signaling restricts pancreatic β-cell expansion. *Proceedings of the National Academy of Sciences*, 112(9):2888–2893.

[Bower and Hay, 2016] Bower, R. L. and Hay, D. L. (2016). Amylin structure-function relationships and receptor pharmacology: implications for amylin mimetic drug development. *British journal of pharmacology*, 173(12):1883–1898.

[Brereton et al., 2007] Brereton, H., Carvell, M., Persaud, S., and Jones, P. (2007). Islet α-cells do not influence insulin secretion from β-cells through cell-cell contact. *Endocrine*, 31(1):61–65.

[Brereton et al., 2015] Brereton, M. F., Vergari, E., Zhang, Q., and Clark, A. (2015). Alpha-, Delta- and PP-cells: Are they the architectural cornerstones of islet structure and co-ordination? *The journal of histochemistry and cytochemistry : official journal of the Histochemistry Society*, 63(8):575–91.

[Briant et al., 2016] Briant, L., Salehi, A., Vergari, E., Zhang, Q., and Rorsman, P. (2016). Glucagon secretion from pancreatic α-cells. *Upsala Journal of Medical Sciences*, 121(2):113–119.

[Briant et al., 2017] Briant, L. J. B., Zhang, Q., Vergari, E., Kellard, J. A., Rodriguez, B., Ashcroft, F. M., and Rorsman, P. (2017). Functional identification of islet cell types by electrophysiological fingerprinting. *Journal of The Royal Society Interface*, 14(128):20160999.

[Brown et al., 2018] Brown, J. D., McAnally, D., Ayala, J. E., Burmeister, M. A., Morfa, C., Smith, L., and Ayala, J. E. (2018). Oleoylethanolamide modulates glucagon-like peptide-1 receptor agonist signaling and enhances exendin-4-mediated weight loss in obese mice. *American Journal of Physiology-Regulatory, Integrative and Comparative Physiology*, 315(4):R595–R608.

[Bueno et al., 2016] Bueno, A. B., Showalter, A. D., Wainscott, D. B., Stutsman, C., Marín, A., Ficorilli, J., Cabrera, O., Willard, F. S., and Sloop, K. W. (2016). Positive allosteric modulation of the glucagon-like peptide-1 receptor by diverse electrophiles. *Journal of Biological Chemistry*, 291(20):10700–10715.

[Bueno et al., 2020] Bueno, A. B., Sun, B., Willard, F. S., Feng, D., Ho, J. D., Wainscott, D. B., Showalter, A. D., Vieth, M., Chen, Q., Stutsman, C., Chau, B., Ficorilli, J., Agejas, F. J., Cumming, G. R., Jiménez, A., Rojo, I., Kobilka, T. S., Kobilka, B. K., and Sloop, K. W. (2020). Structural insights into probe-dependent positive allosterism of the GLP-1 receptor. *Nat Chem Biol*, 16:1105–1110.

[Cabrera et al., 2006] Cabrera, O., Berman, D. M., Kenyon, N. S., Ricordi, C., Berggren, P.-O., and Caicedo, A. (2006). The unique cytoarchitecture of human pancreatic islets has implications for islet cell function. *Proceedings of the National Academy of Sciences of the United States of America*, 103(7):2334–9.

[Cabrera-Vera et al., 2003] Cabrera-Vera, T. M., Vanhauwe, J., Thomas, T. O., Medkova, M., Preininger, A., Mazzoni, M. R., and Hamm, H. E. (2003). Insights into G Protein structure, function, and regulation. *Endocrine Reviews*, 24(6):765–781.

[Campbell and Smrcka, 2018] Campbell, A. P. and Smrcka, A. V. (2018). Targeting G protein-coupled receptor signalling by blocking G proteins. *Nat Rev Drug Discov*, 17(11):789–803.

[Campbell and Drucker, 2013] Campbell, J. E. and Drucker, D. J. (2013). Pharmacology, physiology, and mechanisms of incretin hormone action. *Cell Metabolism*, 17(6):819–837.

[Campbell and Drucker, 2015] Campbell, J. E. and Drucker, D. J. (2015). Islet α cells and glucagon - critical regulators of energy homeostasis. *Nature Reviews Endocrinology*, 11(6):329–338.

[Capozzi et al., 2018] Capozzi, M. E., DiMarchi, R. D., Tschöp, M. H., Finan, B., and Campbell, J. E. (2018). Targeting the Incretin/Glucagon system with triagonists to treat diabetes. *Endocrine Reviews*, 39(5):719–738.

[Capozzi et al., 2019] Capozzi, M. E., Svendsen, B., Encisco, S. E., Lewandowski, S. L., Martin, M. D., Lin, H., Jaffe, J. L., Coch, R. W., Haldeman, J. M., MacDonald, P. E., Merrins, M. J., D'Alessio, D. A., and Campbell, J. E. (2019). β-cell tone is defined by proglucagon peptides through cyclic AMP signaling. *JCI Insight*.

[Carbone et al., 2019] Carbone, S. E., Veldhuis, N. A., Gondin, A. B., and Poole, D. P. (2019). G protein-coupled receptor trafficking and signaling: New insights into the enteric nervous system. *American Journal of Physiology - Gastrointestinal and Liver Physiology*, 316(4):G446–G452.

[Cardenas-Diaz et al., 2020] Cardenas-Diaz, F. L., Leavens, K. F., Kishore, S., Osorio-Quintero, C., Chen, Y.-J., Stanger, B. Z., Wang, P., French, D., and Gadue, P. (2020). A dual reporter EndoC-βH1 human β-cell line for efficient quantification of calcium flux and insulin secretion. *Endocrinology*, 161(2).

[Cascieri et al., 1999] Cascieri, M. A., Koch, G. E., Ber, E., Sadowski, S. J., Louizides, D., De Laszlo, S. E., Hacker, C., Hagmann, W. K., MacCoss, M., Chicchi, G. G., and Vicario, P. P. (1999). Characterization of a novel, non-peptidyl antagonist of the human glucagon receptor. *Journal of Biological Chemistry*, 274(13):8694–8697.

[Cegla et al., 2017] Cegla, J., Jones, B. J., Gardiner, J. V., Hodson, D. J., Marjot, T., McGlone, E. R., Tan, T. M., and Bloom, S. R. (2017). RAMP2 influences glucagon receptor pharmacology via trafficking and signaling. *Endocrinology*, 158(8):2680–2693.

[Chalmers and Behan, 2002] Chalmers, D. T. and Behan, D. P. (2002). The use of constitutively active GPCRs in drug discovery and functional genomics. *Nature reviews. Drug discovery*, 1(8):599–608.

[Chang et al., 2020] Chang, R., Zhang, X., Qiao, A., Dai, A., Belousoff, M. J., Tan, Q., Shao, L., Zhong, L., Lin, G., Liang, Y.-L., Ma, L., Han, S., Yang, D., Danev, R., Wang, M.-w., Wootten, D., Wu, B., and Sexton, P. M. (2020). Cryo-electron microscopy structure of the glucagon receptor with a dual-agonist peptide. *Journal of Biological Chemistry*, 15:1–26.

[Chen et al., 2007] Chen, D., Liao, J., Li, N., Zhou, C., Liu, Q., Wang, G., Zhang, R., Zhang, S., and Lin, L. (2007). A nonpeptidic agonist of glucagon-like peptide 1 receptors with efficacy in diabetic db/db mice. *PNAS*, 104(3):943–948.

[Cheng et al., 2012] Cheng, K., De lghingaro Augusto, V., Nolan, C. J., Turner, N., Hallahan, N., Andrikopoulos, S., and Gunton, J. E. (2012). High passage MIN6 cells have impaired insulin secretion with impaired glucose and lipid oxidation. *PLoS ONE*, 7(7).

[Cheng et al., 2015] Cheng, Y. H., Ho, M. S., Huang, W. T., Chou, Y. T., and King, K. (2015). Modulation of glucagon-like peptide-1 (GLP-1) potency by endocannabinoid-like lipids represents a novel mode of regulating GLP-1 receptor signaling. *Journal of Biological Chemistry*, 290(23):14302–14313.

[Cheong et al., 2012] Cheong, Y. H., Kim, M. K., Son, M. H., and Kaang, B. K. (2012). Two small molecule agonists of glucagon-like peptide-1 receptor modulate the receptor activation response differently. *Biochemical and Biophysical Research Communications*, 417:558–563.

[Chepurny et al., 2019] Chepurny, O. G., Matsoukas, M. T., Liapakis, G., Leech, C. A., Milliken, B. T., Doyle, R. P., and Holz, G. G. (2019). Nonconventional glucagon and GLP-1 receptor agonist and antagonist interplay at the GLP-1 receptor revealed in high-throughput FRET assays for cAMP. *Journal of Biological Chemistry*, 294(10):3514–3531.

[Cho et al., 2014] Cho, Y. M., Fujita, Y., and Kieffer, T. J. (2014). Glucagon-like peptide-1: glucose homeostasis and beyond. *Annual Review of Physiology*, 76(1):535–559.

[Chowdhury et al., 2013] Chowdhury, A., Satagopam, V. P., Manukyan, L., Artemenko, K. A., Fung, Y. M. E., Schneider, R., Bergquist, J., and Bergsten, P. (2013). Signaling in insulin-secreting MIN6 pseudoislets and monolayer cells. *Journal of Proteome Research*, 12(12):5954–5962.

[Christopoulos, 2002] Christopoulos, A. (2002). Allosteric binding sites on cell-surface receptors: novel targets for drug discovery. *Nature Reviews Drug Discovery*, 1(March):198–210.

[Christopoulos, 2014] Christopoulos, A. (2014). Advances in G protein-coupled receptor allostery: from function to structure. *Molecular Pharmacology*, 86(November):463–478.

[Christopoulos et al., 2003] Christopoulos, A., Christopoulos, G., Morfis, M., Udawela, M., Laburthe, M., Couvineau, A., Kuwasako, K., Tilakaratne, N., and Sexton, P. M. (2003). Novel receptor partners and function of receptor activity-modifying proteins. *Journal of Biological Chemistry*, 278(5):3293–3297.

[Chu et al., 2008] Chu, Z. L., Carroll, C., Alfonso, J., Gutierrez, V., He, H., Lucman, A., Pedraza, M., Mondala, H., Gao, H., Bagnol, D., Chen, R., Jones, R. M., Behan, D. P., and Leonard, J. (2008). A role for intestinal endocrine cell-expressed G protein-coupled receptor 119 in glycemic control by enhancing glucagon-like peptide-1 and glucose-dependent insulinotropic peptide release. *Endocrinology*, 149(5):2038–2047.

[Chuang et al., 2011] Chuang, J.-C., Sakata, I., Kohno, D., Perello, M., Osborne-Lawrence, S., Repa, J. J., and Zigman, J. M. (2011). Ghrelin directly stimulates glucagon secretion from pancreatic α-cells. *Molecular Endocrinology*, 25(9):1600–1611.

[Coopman et al., 2010] Coopman, K., Huang, Y., Johnston, N., Bradley, S. J., Wilkinson, G. F., and Willars, G. B. (2010). Comparative effects of the endogenous agonist glucagon-like allosteric agent 'Compound 2' at the GLP-1 receptor. *The Journal of pharmacology and experimental therapeutics*, 334(3):795–808.

[Couvineau and Laburthe, 2012] Couvineau, A. and Laburthe, M. (2012). The family B1 GPCR: structural aspects and interaction with accessory proteins. *Current Drug Targets*, 13(1):103–115.

[Da Silva Xavier, 2018] Da Silva Xavier, G. (2018). The cells of the islets of Langerhans. *Journal of Clinical Medicine*, 7(3):54.

[Dadi et al., 2015] Dadi, P. K., Luo, B., Vierra, N. C., and Jacobson, D. A. (2015). TASK-1 potassium channels limit pancreatic α-cell calcium influx and glucagon secretion. *Molecular endocrinology (Baltimore, Md.)*, 29(5):777–787.

[Dale et al., 2015] Dale, I., Brown, A. J., Bussey, C. E., Hothersall, J. D., Scott, J. S., and Rawlins, P. (2015). Sustained wash-resistant receptor activation responses of GPR119 agonists. *European Journal of Pharmacology*, 762:430–442.

[Day et al., 2012] Day, J. W., Gelfanov, V., Smiley, D., Carrington, P. E., Eiermann, G., Chicchi, G., Erion, M. D., Gidda, J., Thornberry, N. A., Tscho, M. H., Marsh, D. J., Sinharoy, R., Dimarchi, R., and Pocai, A. (2012). Optimization of co-agonism at GLP-1 and glucagon receptors to safely maximize weight reduction in DIO-rodents. *Peptide Science*, 98(5):443–450.

[De Heer et al., 2008] De Heer, J., Rasmussen, C., Coy, D. H., and Holst, J. J. (2008). Glucagon-like peptide-1, but not glucose-dependent insulinotropic peptide, inhibits glucagon secretion via somatostatin (receptor subtype 2) in the perfused rat pancreas. *Diabetologia*, 51(12):2263–2270.

[De Marinis et al., 2010] De Marinis, Y. Z., Salehi, A., Ward, C. E., Zhang, Q., Abdulkader, F., Bengtsson, M., Braha, O., Braun, M., Ramracheya, R., Amisten, S., Habib, A. M., Moritoh, Y., Zhang, E., Reimann, F., Rosengren, A., Shibasaki, T., Gribble, F., Renström, E., Seino, S., Eliasson, L., and Rorsman, P. (2010). GLP-1 inhibits and adrenaline stimulates glucagon release by differential modulation of N-and L-type Ca2+ channel-dependent exocytosis. *Cell Metabolism*, 11(6):543–553.

[Deacon, 2004] Deacon, C. F. (2004). Circulation and degradation of GIP and GLP-1. *Hormone and Metabolic Research*, 36(11-12):761–765.

[Deacon, 2019] Deacon, C. F. (2019). Physiology and pharmacology of DPP-4 in glucose homeostasis and the treatment of Type 2 Diabetes. *Frontiers in Endocrinology*, 10(February):10:80.

[Defronzo, 2009] Defronzo, R. A. (2009). From the triumvirate to the ominous octet: a new paradigm for the treatment of type 2 diabetes mellitus. *Diabetes*, 58:773–795.

[DeFronzo et al., 2013] DeFronzo, R. A., Eldor, R., and Abdul-Ghani, M. (2013). Pathophysiologic approach to therapy in patients with newly diagnosed type 2 diabetes. *Diabetes Care*, 36(Supp 2):S127–S138.

[Defronzo et al., 2015] Defronzo, R. A., Ferrannini, E., Groop, L., Henry, R. R., Herman, W. H., Holst, J. J., Hu, F. B., Kahn, C. R., Raz, I., Shulman, G. I., Simonson, D. C., Testa, M. A., and Weiss, R. (2015). Type 2 diabetes mellitus. *Nature Reviews Disease Primers*, 1(July):1–23.

[Denwood et al., 2019] Denwood, G., Tarasov, A., Salehi, A., Vergari, E., Ramracheya, R., Takahashi, H., Nikolaev, V. O., Seino, S., Gribble, F., Reimann, F., Rorsman, P., and Zhang, Q. (2019). Glucose stimulates somatostatin secretion in pancreatic δ-cells by cAMP-dependent intracellular Ca2+ release. *Journal of General Physiology*, 151(9).

[Diao et al., 2005] Diao, J., Asghar, Z., Chan, C. B., and Wheeler, M. B. (2005). Glucose-regulated glucagon secretion requires insulin receptor expression in pancreatic α-cells. *Journal of Biological Chemistry*, 280(39):33487–33496.

[Dickerson, 2013] Dickerson, I. M. (2013). Role of CGRP-receptor component protein (RCP) in CLR/RAMP function. *Current protein & peptide science*, 14(5):407–415.

[Ding et al., 1997] Ding, W.-g., Renstrom, E., Rorsman, P., Buschard, K., and Gromada, J. (1997). Glucagon-like peptide I and glucose-dependent insulinotropic polypeptide stimulate Ca2+-induced secretion in rat α-cells by a protein kinase A-mediated mechanism. *Diabetes*, 46:792–800.

[Dong et al., 2017] Dong, Y., Betancourt, A., Belfort, M., and Yallampalli, C. (2017). Targeting adrenomedullin to improve lipid homeostasis in diabetic pregnancies. *The Journal of Clinical Endocrinology & Metabolism*, 102(9):3425–3436.

[Drucker, 2018] Drucker, D. J. (2018). Mechanisms of action and therapeutic application of glucagon-like peptide-1. *Cell Metabolism*, 27(4):740–756.

[Drucker and Nauck, 2006] Drucker, D. J. and Nauck, M. A. (2006). The incretin system: glucagon-like peptide-1 receptor agonists and dipeptidyl peptidase-4 inhibitors in type 2 diabetes. *Lancet*, 368(9548):1696–1705.

[Dunning et al., 2005] Dunning, B. E., Foley, J. E., and Ahrén, B. (2005). Alpha cell function in health and disease: Influence of glucagon-like peptide-1. *Diabetologia*, 48(9):1700–1713.

[Elahi et al., 2008] Elahi, D., Egan, J. M., Shannon, R. P., Meneilly, G. S., Khatri, A., Habener, J. F., and Andersen, D. K. (2008). GLP-1 (9-36) amide, cleavage product of GLP-1 (7-36) amide, is a glucoregulatory peptide. *Obesity*, 16(7):1501–1509.

[Elrick et al., 1964] Elrick, H., Stimmler, L., Hlad Jr, C., and Arai, Y. (1964). Plasma insulin response to oral and intravenous glucose administration. *Journal of Clinical Investigation*, 24:1076–1082.

[Eng et al., 2014] Eng, C., Kramer, C., Zinman, B., and Retnakaran, R. (2014). Glucagon-like peptide-1 receptor agonist and basal insulin combination treatment for the management of type 2 diabetes: a systematic review and meta-analysis. *Lancet*, 384(9961):2228–2234.

[Eng et al., 2013] Eng, H., Sharma, R., Mcdonald, T. S., Edmonds, D. J., Fortin, J.-P., Li, X., Stevens, B. D., Griffith, D. A., Limberakis, C., Nolte, W. M., Price, D. A., Jackson, M., and Kalgutkar, A. S. (2013). Demonstration of the innate electrophilicity of 4-(3-(BETP), a small-molecule positive allosteric modulator of the glucagon-like peptide-1 receptor. *Drug Metabolism and Disposition*, (August):1470–1479.

[Eng et al., 1992] Eng, J., Kleinman, W. A., Singh, L., Singh, G., and Raufman, J. P. (1992). Isolation and characterization of exendin-4, an exendin-3 analogue, from Heloderma suspectum venom. *Journal of Biological Chemistry*, 267(11):7402–7405.

[Farino et al., 2016] Farino, Z. J., Morgenstern, T. J., Vallaghe, J., Gregor, N., Donthamsetti, P., Harris, P. E., Pierre, N., Freyberg, R., Charrier-Savournin, F., Javitch, J. A., and Freyberg, Z. (2016). Development of a rapid insulin assay by homogenous time-resolved fluorescence. *PLoS ONE*, 11(2):1–17.

[Fava et al., 2016] Fava, G. E., Dong, E. W., and Wu, H. (2016). Intra-islet glucagon-like peptide 1. *Journal of Diabetes and its Complications*, 30(8):1651–1658.

[Fehmann et al., 1999] Fehmann, H., Janssen, M., and Göke, B. (1999). Interaction of glucagon-like peptide-I (GLP-I) and galanin in insulin (beta TC-1)- and somatostatin (RIN T3)-secreting cells and evidence that both peptides have no receptors on glucagon (INR1G9)-secreting cells. *Acta Diabetol*, 32(3):176–81.

[Fehmann et al., 1994] Fehmann, H., Jiang, J., Schweinfurth, J., Wheeler, M. B., Boyd, A., and Göke, B. (1994). Stable expression of the rat GLP-I receptor in CHO Cells: activation and binding. *Peptides*, 15(3):453–456.

[Feinstein et al., 2013] Feinstein, T. N., Yui, N., Webber, M. J., Wehbi, V. L., Stevenson, H. P., King, J. D. J., Hallows, K. R., Brown, D., Bouley, R., and Vilardaga, J.-P. (2013). Noncanonical control of vasopressin receptor type 2 signaling by retromer and arrestin. *The Journal of biological chemistry*, 288(39):27849–27860.

[Ferrandon et al., 2009] Ferrandon, S., Feinstein, T. N., Castro, M., Wang, B., Bouley, R., Potts, J. T., Gardella, T. J., and Vilardaga, J.-P. (2009). Sustained cyclic AMP production by parathyroid hormone receptor endocytosis. *Nature chemical biology*, 5(10):734–742.

[Fletcher et al., 2018] Fletcher, M. M., Halls, M. L., Zhao, P., Clydesdale, L., Christopoulos, A., Sexton, P. M., and Wootten, D. (2018). Glucagon-like peptide-1 receptor internalisation controls spatiotemporal signalling mediated by biased agonists. *Biochemical Pharmacology*, 156(July):406–419.

[Flock et al., 2011] Flock, G., Holland, D., Seino, Y., and Drucker, D. J. (2011). GPR119 regulates murine glucose homeostasis through incretin receptor-dependent and independent mechanisms. *Endocrinology*, 152(2):374–383.

[Gabe et al., 2019] Gabe, M. B. N., van der Velden, W. J., Smit, F. X., Gasbjerg, L. S., and Rosenkilde, M. M. (2019). Molecular interactions of full-length and truncated GIP peptides with the GIP receptor - A comprehensive review. *Peptides*, 125(November 2019):170224.

[Galsgaard et al., 2019] Galsgaard, K. D., Pedersen, J., Knop, F. K., Holst, J. J., and Albrechtsen, N. J. (2019). Glucagon receptor signaling and lipid metabolism. *Frontiers in Physiology*, 10(APR):1–11.

[Garelja et al., 2020] Garelja, M. L., Au, M., Brimble, M. A., Gingell, J. J., Hendrikse, E. R., Lovell, A., Prodan, N., Sexton, P. M., Siow, A., Walker, C. S., Watkins, H. A., Williams, G. M., Wootten, D., Yang, S. H., Harris, P. W. R., and Hay, D. L. (2020). Molecular mechanisms of class B GPCR activation: insights from adrenomedullin receptors. *ACS pharmacology & translational science*, 3(2):246–262.

[Gasa et al., 1999] Gasa, R., Trinh, K. Y., Yu, K., Wilkie, T. M., and Newgard, C. B. (1999). Overexpression of G(11α) and isoforms of phospholipase C in islet β- cells reveals a lack of correlation between inositol phosphate accumulation and insulin secretion. *Diabetes*, 48(5):1035–1044.

[Ghanim et al., 2020] Ghanim, H., Batra, M., Green, K., Abuaysheh, S., Hejna, J., Makdissi, A., Borowski, R., Kuhadiya, N. D., Chaudhuri, A., and Dandona, P. (2020). Liraglutide treatment in overweight and obese patients with type 1 diabetes: A 26-week randomized controlled trial; mechanisms of weight loss. *Diabetes, obesity & metabolism*, 22(10):1742–1752.

[Gjertsen et al., 1995] Gjertsen, B. T., Mellgren, G., Otten, A., Maronde, E., Genieser, H. G., Jastorff, B., Vintermyr, O. K., McKnight, G. S., and Døskeland, S. O. (1995). Novel (Rp)-cAMPS analogs as tools for inhibition of cAMP-kinase in cell culture. *Journal of Biological Chemistry*, 270(35):20599–20607.

[Goldsmith and Dhanasekaran, 2007] Goldsmith, Z. G. and Dhanasekaran, D. N. (2007). G Protein regulation of MAPK networks. *Oncogene*, 26(22):3122–3142.

[Gong et al., 2019] Gong, B., Zhang, H., Huang, L., Chen, Y., Shi, Y., Tam, P. O.-S., Zhu, X., Huang, Y., Lei, B., Sundaresan, P., Li, X., Jiang, L., Yang, J., Lin, Y., Lu, F., Chen, L., Li, Y., Leung, C. K.-S., Guo, X., Zhang, S., Huang, G., Wu, Y., Zhou, T., Shuai, P., Tham, C. C.-Y., Weisschuh, N., Krishnadas, S. R., Mardin, C., Reis, A., Yang, J., Zhang, L., Zhou, Y., Wang, Z., Qu, C., Shaw, P. X., Pang, C.-P., Sun, X., Zhu, W., Li, D. Y., Pasutto, F., and Yang, Z. (2019). Mutant RAMP2 causes primary open-angle glaucoma via the CRLR-cAMP axis. *Genetics in medicine : official journal of the American College of Medical Genetics*, 21(10):2345–2354.

[Graaf et al., 2016] Graaf, C. D., Donnelly, D., Wootten, D., Lau, J., Sexton, P. M., Miller, L. J., Ahn, J.-m., and Liao, J. (2016). Glucagon-like peptide-1 and its class B G protein-coupled receptors: a long march to therapeutic successes. *Pharmacological Reviews*, 68:954–1013.

[Graaf et al., 2011] Graaf, C. D., Rein, C., Piwnica, D., Giordanetto, F., and Rognan, D. (2011). Structure-based discovery of allosteric modulators of two related class B G-protein-coupled receptors. *ChemMedChem*, 6:2159–2169.

[Graaf et al., 2017] Graaf, C. D., Song, G., Cao, C., Zhao, Q., and Wang, M.-w. (2017). Extending the structural view of class B GPCRs. *Trends in Biochemical Sciences*, 42(12):946–960.

[Greenwell et al., 2020] Greenwell, A. A., Chahade, J. J., and Ussher, J. R. (2020). Cardiovascular biology of the GIP receptor. *Peptides*, 125(October 2019):170228.

[Grill, 2020] Grill, H. J. (2020). A role for GLP-1 in treating hyperphagia and obesity. *Endocrinology*, 161(8).

[Gromada et al., 2018] Gromada, J., Chabosseau, P., and Rutter, G. A. (2018). The α-cell in diabetes mellitus. *Nature Reviews Endocrinology*.

[Gromada et al., 2007] Gromada, J., Franklin, I., and Wollheim, C. B. (2007). α-Cells of the endocrine pancreas: 35 years of research but the enigma remains. *Endocrine Reviews*, 28(1):84–116.

[Grøndahl et al., 2017] Grøndahl, M. F., Keating, D. J., Vilsbøll, T., and Knop, F. K. (2017). Current therapies that modify glucagon secretion: what is the therapeutic effect of such modifications? *Current Diabetes Reports*, 17(128).

[Guglielmi and Sbraccia, 2017] Guglielmi, V. and Sbraccia, P. (2017). GLP-1 receptor independent pathways: emerging beneficial effects of GLP-1 breakdown products. *Eating and Weight Disorders*, 22(2):231–230.

[Guida et al., 2020] Guida, C., Miranda, C., Asterholm, I. W., Basco, D., Benrick, A., Chanclon, B., Chibalina, M. V., Harris, M., Kellard, J., Mcculloch, L. J., Real, J., Rorsman, N. J. G., Yeung, H. Y., Reimann, F., Shigeto, M., Clark, A., Thorens, B., Rorsman, P., Ladds, G., and Ramracheya, R. (2020). GLP-1(9-36) mediates the glucagonostatic effect of GLP-1 by promiscuous activation of the glucagon receptor. *Biorxiv.org*, 1.

[Guo-Parke et al., 2012] Guo-Parke, H., McCluskey, J. T., Kelly, C., Hamid, M., McClenaghan, N. H., and Flatt, P. R. (2012). Configuration of electrofusion-derived human insulin-secreting cell line as pseudoislets enhances functionality and therapeutic utility. *Journal of Endocrinology*, 214(3):257–265.

[Gurevich and Gurevich, 2019] Gurevich, V. V. and Gurevich, E. V. (2019). GPCR signaling regulation: The role of GRKs and arrestins. *Frontiers in Pharmacology*, 10(FEB):1–11.

[Gylfe, 2016] Gylfe, E. (2016). Glucose control of glucagon secretion-'There's a brand-new gimmick every year'. *Upsala Journal of Medical Sciences*, 121(2):120–132.

[Hamilton et al., 2018] Hamilton, A., Zhang, Q., Salehi, A., Willems, M., Knudsen, J. G., Ringgaard, A. K., Chapman, C. E., Gonzalez-Alvarez, A., Surdo, N. C., Zaccolo, M., Basco, D., Johnson, P. R. V., Ramracheya, R., Rutter, G. A., Galione, A., Rorsman, P., and Tarasov, A. I. (2018). Adrenaline stimulates glucagon secretion by Tpc2-dependent Ca2+ mobilization from acidic stores in pancreatic α-cells. *Diabetes*.

[Hancock, 2010] Hancock, J. (2010). Detection of extracellular signals: the role of receptors. In *Cell Signalling*, chapter 5, pages 78–102. Oxford University Press, Oxford, 3ed. edition.

[Hansen et al., 2020] Hansen, B. B., Nuhoho, S., Ali, S. N., Dang-Tan, T., Valentine, W. J., Malkin, S. J. P., and Hunt, B. (2020). Oral semaglutide versus injectable glucagon-like peptide-1 receptor agonists: a cost of control analysis. *Journal of medical economics*, 23(6):650–658.

[Harikumar et al., 2012] Harikumar, K. G., Wootten, D., Pinon, D. I., Koole, C., Ball, A. M., Furness, S. G. B., Graham, B., Dong, M., Christopoulos, A., Miller, L. J., and Sexton, P. M. (2012). Glucagon-like peptide-1 receptor dimerization differentially regulates agonist signaling but does not affect small molecule allostery. *Proceedings of the National Academy of Sciences*, 109(45):18607–18612.

[Harris and McCarty, 2015] Harris, K. and McCarty, D. (2015). Efficacy and tolerability of glucagon-like peptide-1 receptor agonists in patients with type 2 diabetes mellitus. *Therapeutic Advanced Endocrinology and Metabolism*, 6(1):3–18.

[Harris et al., 2017] Harris, M., Winfield, I., Harper, M., and Ladds, G. (2017). Characterising glucose-dependent insulinotropic polypeptide receptor signalling. In *Proceedings of the British Pharmacological Society*.

[Hasan et al., 2004] Hasan, M. T., Friedrich, R. W., Euler, T., Larkum, M. E., Giese, G., Both, M., Duebel, J., Waters, J., Bujard, H., Griesbeck, O., Tsien, R. Y., Nagai, T., Miyawaki, A., and Denk, W. (2004). Functional fluorescent Ca2+ indicator proteins in transgenic mice under TET control. *PLoS biology*, 2(6):e163.

[Hauge-Evans et al., 1999] Hauge-Evans, A. C., Squires, P. E., Persaud, S. J., and Jones, P. M. (1999). Pancreatic β-cell-to-β-cell interactions are required for integrated responses to nutrient stimuli: Enhanced Ca2+ and insulin secretory responses of MIN6 pseudoislets. *Diabetes*, 48(7):1402–1408.

[Hay et al., 2016] Hay, D. L., Walker, C. S., Gingell, J. J., Ladds, G., Reynolds, C. A., and Poyner, D. R. (2016). Receptor activity-modifying proteins; multifunctional G protein-coupled receptor accessory proteins. *Biochemical Society Transactions*, 44:568–573.

[Heim et al., 2007] Heim, N., Garaschuk, O., Friedrich, M. W., Mank, M., Milos, R. I., Kovalchuk, Y., Konnerth, A., and Griesbeck, O. (2007). Improved calcium imaging in transgenic mice expressing a troponin C-based biosensor. *Nature methods*, 4(2):127–129.

[Heller et al., 1997] Heller, R., Kieffer, T., and Habener, J. (1997). Insulinotropic glucagon-like peptide I receptor expression in glucagon-producing α-cells of the rat endocrine pancreas. *Diabetes*, 46(5):785–791.

[Heppner and Perez-Tilve, 2015] Heppner, K. M. and Perez-Tilve, D. (2015). GLP-1 based therapeutics: Simultaneously combating T2DM and obesity. *Frontiers in Neuroscience*, 9(MAR):1–11.

[Hilger et al., 2020] Hilger, D., Kumar, K. K., Hu, H., Pedersen, M. F., O'Brien, E. S., Giehm, L., Jennings, C., Eskici, G., Inoue, A., Lerch, M., Matthiesen, J. M., Skiniotis, G., and Kobilka, B. K. (2020). Structural insights into differences in G protein activation by family A and family B GPCRs. *Science*, 369(6503).

[Hilger et al., 2018] Hilger, D., Masureel, M., and Kobilka, B. K. (2018). Structure and dynamics of GPCR signaling complexes. *Nature structural & molecular biology*, 25(1):4–12.

[Hill et al., 2010] Hill, S. J., Williams, C., and May, L. T. (2010). Insights into GPCR pharmacology from the measurement of changes in intracellular cyclic AMP; advantages and pitfalls of differing methodologies. *British Journal of Pharmacology*, 161(August 2009):1266–1275.

[Hoare, 2005] Hoare, S. R. J. (2005). Mechanisms of peptide and nonpeptide ligand binding to Class B G protein-coupled receptors. *Drug Discovery Today*, 10(6):417–427.

[Hohmeier et al., 2000] Hohmeier, H. E., Mulder, H., Chen, G., Henkel-Rieger, R., Prentki, M., and Newgard, C. B. (2000). Isolation of INS-1-derived cell lines with robust ATP-sensitive K+ channel-dependent and -independent glucose-stimulated insulin secretion. *Diabetes*, 49(3):424–430.

[Hollenstein et al., 2014] Hollenstein, K., De Graaf, C., Bortolato, A., Wang, M. W., Marshall, F. H., and Stevens, R. C. (2014). Insights into the structure of class B GPCRs. *Trends in Pharmacological Sciences*, 35(1):12–22.

[Holst et al., 2011a] Holst, J., Christensen, M., Lund, A., De Heer, J., Svendsen, B., Kielgast, U., and Knop, F. K. (2011a). Regulation of glucagon secretion by incretins. *Diabetes, Obesity and Metabolism*, 13(SUPPL. 1):89–94.

[Holst, 2006] Holst, J. J. (2006). Glucagon-like peptide-1: From extract to agent. The Claude Bernard Lecture, 2005. *Diabetologia*, 49(2):253–260.

[Holst, 2007] Holst, J. J. (2007). The physiology of glucagon-like peptide 1. *Physiological Review*, 87:1409–1439.

[Holst et al., 2018] Holst, J. J., Albrechtsen, N. J., Gabe, M. B. N., and Rosenkilde, M. M. (2018). Oxyntomodulin: Actions and role in diabetes. *Peptides*, 100(August 2017):48–53.

[Holst et al., 2011b] Holst, J. J., Knop, F. K., Vilsbøll, T., Krarup, T., and Madsbad, S. (2011b). Loss of incretin effect is a specific, important, and early characteristic of Type 2 Diabetes. *Diabetes Care*, 34(Supp 2):S251–257.

[Honigberg et al., 2020] Honigberg, M. C., Chang, L.-S., McGuire, D. K., Plutzky, J., Aroda, V. R., and Vaduganathan, M. (2020). Use of glucagon-like peptide-1 receptor agonists in patients With type 2 diabetes and cardiovascular disease: a review. *JAMA cardiology*, June.

[Hothersall et al., 2016] Hothersall, J. D., Brown, A. J., Dale, I., and Rawlins, P. (2016). Can residence time offer a useful strategy to target agonist drugs for sustained GPCR responses? *Drug Discovery Today*, 21(1):90–96.

[Huising et al., 2010] Huising, M. O., Van Der Meulen, T., Vaughan, J. M., Matsumotoa, M., Donaldson, C. J., Park, H., Billestrup, N., and Vale, W. W. (2010). CRFR1 is expressed on pancreatic β cells, promotes β cell proliferation, and potentiates insulin secretion in a glucose-dependent manner. *Proceedings of the National Academy of Sciences of the United States of America*, 107(2):912–917.

[International Diabetes Federation, 2019] International Diabetes Federation (2019). *IDF Diabetes Atlas, 9th edn.* Brussels, Belgium.

[Ionescu-Tirgoviste et al., 2015] Ionescu-Tirgoviste, C., Gagniuc, P. A., Gubceac, E., Mardare, L., Popescu, I., Dima, S., and Militaru, M. (2015). A 3D map of the islet routes throughout the healthy human pancreas. *Scientific reports*, 5:14634.

[Islam, 2019] Islam, M. S. (2019). *Calcium Signaling*. Springer.

[Janssen et al., 2013] Janssen, P., Rotondo, A., Mulé, F., and Tack, J. (2013). Review article: A comparison of glucagon-like peptides 1 and 2. *Alimentary Pharmacology and Therapeutics*, 37(1):18–36.

[Jazayeri et al., 2017] Jazayeri, A., Rappas, M., Brown, A. J. H., Kean, J., Errey, J. C., Robertson, N. J., Fiez-Vandal, C., Andrews, S. P., Congreve, M., Bortolato, A., Mason, J. S., Baig, A. H., Teobald, I., Doré, A. S., Weir, M., Cooke, R. M., and Marshall, F. H. (2017). Crystal structure of the GLP-1 receptor bound to a peptide agonist. *Nature*, 546(7657):254–258.

[Jennings and Tennant, 2007] Jennings, A. and Tennant, M. (2007). Selection of molecules based on shape and electrostatic similarity: Proof of concept of 'electroforms'. *Journal of Chemical Information and Modeling*, 47(5):1829–1838.

[Ji et al., 2004] Ji, G., Feldman, M. E., Deng, K.-Y., Greene, K. S., Wilson, J., Lee, J. C., Johnston, R. C., Rishniw, M., Tallini, Y., Zhang, J., Wier, W. G., Blaustein, M. P., Xin, H.-B., Nakai, J., and Kotlikoff, M. I. (2004). Ca2+-sensing transgenic mice: postsynaptic signaling in smooth muscle. *The Journal of biological chemistry*, 279(20):21461–21468.

[Johansson et al., 1989] Johansson, H., Gylfe, E., and Hellman, B. (1989). Cyclic AMP raises cytoplasmic calcium in pancreatic alpha 2-cells by mobilizing calcium incorporated in response to glucose. *Cell calcium*, 10(4):205–211.

[Johnson et al., 2011] Johnson, P. R. V., Takeuchi, K., Hazama, M., Yashiro, H., Rorsman, P., and Tsujihata, Y. (2011). The effects of TAK-875, a selective G protein-coupled receptor 40/free fatty acid 1 agonist, on insulin and glucagon secretion in isolated rat and human islets. *Journal of Pharmacology and Experimental Therapeutics*, 340(2):483–489.

[Jones et al., 2018] Jones, B., Buenaventura, T., Kanda, N., Chabosseau, P., Owen, B. M., Scott, R., Goldin, R., Angkathunyakul, N., Jr, I. R. C., Bosco, D., Johnson, P. R., Piemonti, L., Marchetti, P., Shapiro, A. M. J., Cochran, B. J., Hanyaloglu, A. C., Inoue, A., Tan, T., Rutter, G. A., Tomas, A., and Bloom, S. R. (2018). Targeting GLP-1 receptor trafficking to improve agonist efficacy. *Nature Communications*, 9(1602).

[Jorgensen et al., 2007] Jorgensen, R., Kubale, V., Vrecl, M., Schwartz, T. W., and Elling, C. E. (2007). Oxyntomodulin differentially affects glucagon-like peptide-1 receptor beta-arrestin recruitment and signaling through Galpha-s. *The Journal of pharmacology and experimental therapeutics*, 322(1):148–154.

[Kadmiel et al., 2017] Kadmiel, M., Matson, B. C., Espenschied, S. T., Lenhart, P. M., and Caron, K. M. (2017). Loss of receptor activity-modifying protein 2 in mice causes placental dysfunction and alters PTH1R regulation. *PloS one*, 12(7):e0181597.

[Kamato et al., 2015] Kamato, D., Thach, L., Bernard, R., Chan, V., Zheng, W., Kaur, H., Brimble, M., Osman, N., and Little, P. J. (2015). Structure, function, pharmacology, and therapeutic potential of the G protein, Gα/q11. *Frontiers in Cardiovascular Medicine*, 2:14.

[Karageorgos et al., 2018] Karageorgos, V., Venihaki, M., Sakellaris, S., Pardalos, M., Kontakis, G., Matsoukas, M.-T., Gravanis, A., Margioris, A., and Liapakis, G. (2018). Current understanding of the structure and function of family B GPCRs to design novel drugs. *Hormones*, 17(1):45–59.

[Katada and Ui, 1982] Katada, T. and Ui, M. (1982). ADP ribosylation of the specific membrane protein of C6 cells by islet-activating protein associated with modification of adenylate cyclase activity. *Journal of Biological Chemistry*, 257(12):7210–7216.

[Kedees et al., 2009] Kedees, M. H., Grigoryan, M., Guz, Y., and Teitelman, G. (2009). Differential expression of glucagon and glucagon-like peptide 1 receptors in mouse pancreatic alpha and beta cells in two models of alpha cell hyperplasia. *Molecular and Cellular Endocrinology*, 311(1-2):69–76.

[Kelly et al., 2011] Kelly, C., McClenaghan, N. H., and Flatt, P. R. (2011). Role of islet structure and cellular interactions in the control of insulin secretion. *Islets*, 3(2):41–47.

[Kenakin and Christopoulos, 2013] Kenakin, T. and Christopoulos, A. (2013). Signalling bias in new drug discovery: detection, quantification and therapeutic impact. *Nature reviews. Drug discovery*, 12(March 2013):205–16.

[Kenakin and Miller, 2010] Kenakin, T. and Miller, L. J. (2010). Seven transmembrane receptors as shapeshifting proteins: the impact of allosteric modulation and functional selectivity on new drug discovery. *Pharmacological reviews*, 62(2):265–304.

[Kenakin, 2012] Kenakin, T. P. (2012). Biased signalling and allosteric machines: New vistas and challenges for drug discovery. *British Journal of Pharmacology*, 165(6):1659–1669.

[Khajavi et al., 2018] Khajavi, N., Finan, B., Kluth, O., Müller, T. D., Mergler, S., Schulz, A., Kleinau, G., Scheerer, P., Schürmann, A., Gudermann, T., Tschöp, M. H., Krude, H., DiMarchi, R. D., and Biebermann, H. (2018). An incretin-based tri-agonist promotes superior insulin secretion from murine pancreatic islets via PLC activation. *Cellular Signalling*, 51(May):13–22.

[Khan et al., 2020] Khan, R., Tomas, A., and Rutter, G. A. (2020). Effects on pancreatic beta and other islet cells of the glucose-dependent insulinotropic polypeptide. *Peptides*, 125(August 2019):170201.

[Kim et al., 2017] Kim, J., Okamoto, H., Huang, Z. J., Anguiano, G., Chen, S., Liu, Q., Cavino, K., Xin, Y., Na, E., Hamid, R., Lee, J., Zambrowicz, B., Unger, R., Murphy, A. J., Xu, Y., Yancopoulos, G. D., hong Li, W., and Gromada, J. (2017). Amino acid transporter Slc38a5 controls glucagon receptor inhibition-induced pancreatic α cell hyperplasia in mice. *Cell Metabolism*, 25(6):1348–1361.e8.

[Kim et al., 2008] Kim, J. W., Roberts, C. D., Berg, S. A., Caicedo, A., Roper, S. D., and Chaudhari, N. (2008). Imaging cyclic AMP changes in pancreatic islets of transgenic reporter mice. *PLOS ONE*, 3(5):e2127.

[Kim et al., 2015] Kim, S. M., Lee, E. J., Jung, H. S., Han, N., Kim, Y. J., Kim, T. K., Kim, T. N., Kwon, M. J., Lee, S. H., Park, J. H., Rhee, B. D., and Kim, M.-K. (2015). Co-culture of αTC-6 Cells and βTC-1 Cells: morphology and function. *Endocrinology and Metabolism*, 30(1):92.

[King et al., 2015] King, K., Lin, N. P., Cheng, Y. H., Chen, G. H., and Chein, R. J. (2015). Isolation of positive modulator of glucagon-like peptide-1 signaling from trigonella foenum-graecum (Fenugreek) seed. *Journal of Biological Chemistry*, 290(43):26235–26248.

[Klarenbeek et al., 2015] Klarenbeek, J., Goedhart, J., van Batenburg, A., Groenewald, D., and Jalink, K. (2015). Fourth-generation epac-based FRET sensors for cAMP feature exceptional brightness, photostability and dynamic range: characterization of dedicated sensors for FLIM, for ratiometry and with high affinity. *PloS one*, 10(4):e0122513.

[Klarenbeek et al., 2011] Klarenbeek, J. B., Goedhart, J., Hink, M. A., Gadella, T. W. J., and Jalink, K. (2011). A mTurquoise-based cAMP sensor for both FLIM and ratiometric read-out has improved dynamic range. *PloS one*, 6(4):e19170.

[Knop et al., 2007] Knop, F. K., Vilsbøll, T., Højberg, P. V., Larsen, S., Madsbad, S., Vølund, A., Holst, J. J., and Krarup, T. (2007). Reduced incretin effect in type 2 diabetes: cause or consequence of the diabetic state? *Diabetes*, 56(8):1951–1959.

[Knudsen et al., 2012] Knudsen, L. B., Hastrup, S., Rye, C., Schjellerup, B., and Fleckner, J. (2012). Functional importance of GLP-1 receptor species and expression levels in cell lines. *Regulatory Peptides*, 175:21–29.

[Knudsen et al., 2007] Knudsen, L. B., Kiel, D., Teng, M., Behrens, C., Bhumralkar, D., Kodra, J. T., Holst, J. J., Jeppesen, C. B., Johnson, M. D., de Jong, J. C., Jorgensen, A. S., Kercher, T., Kostrowicki, J., Madsen, P., Olesen, P. H., Petersen, J. S., Poulsen, F., Sidelmann, U. G., Sturis, J., Truesdale, L., May, J., and Lau, J. (2007). Small-molecule agonists for the glucagon-like peptide 1 receptor. *Proceedings of the National Academy of Sciences of the United States of America*, 104(3):937–942.

[Koole et al., 2013] Koole, C., Pabreja, K., Savage, E. E., Wootten, D., Furness, S. G. B., Miller, L. J., Christopoulos, A., and Sexton, P. M. (2013). Recent advances in understanding GLP-1R (glucagon-like peptide-1 receptor) function. *Biochemical Society Transactions*, 41:172–179.

[Koole et al., 2012] Koole, C., Wootten, D., Simms, J., Miller, L. J., Christopoulos, A., and Sexton, P. M. (2012). Second extracellular loop of human glucagon-like peptide-1 receptor (GLP-1R) has a critical role in GLP-1 peptide binding and receptor activation. *Journal of Biological Chemistry*, 287(6):3642–3658.

[Koole et al., 2015] Koole, C., Wootten, D., Simms, J., Miller, L. J., Christopoulos, A., and Sexton, P. M. (2015). Differential impact of amino acid substitutions on critical residues of the human glucagon-like peptide-1 receptor involved in peptide activity and small-molecule allosterys. *J Pharmacol Exp Ther*, 353:52–63.

[Koole et al., 2011] Koole, C., Wootten, D., Simms, J., Valant, C., Miller, L. J., Christopoulos, A., and Sexton, P. M. (2011). Polymorphism and ligand dependent changes in human glucagon-like peptide-1 receptor (GLP-1R) function: allosteric rescue of loss of function mutation. *Molecular Pharmacology*, 80(3):486–497.

[Koole et al., 2010] Koole, C., Wootten, D., Simms, J., Valant, C., Sridhar, R., Woodman, O. L., Miller, L. J., Summers, R. J., Christopoulos, A., and Sexton, P. M. (2010). Allosteric ligands of the glucagon-like peptide 1 receptor (GLP-1R) differentially modulate endogenous and exogenous peptide responses in a pathway-selective manner: implications for drug screening. *Molecular pharmacology*, 78(3):456–65.

[Kosinski et al., 2012] Kosinski, J. R., Hubert, J., Carrington, P. E., Chicchi, G. G., Mu., J., Miller, C., Cao, J., Bianchi., E., Pessi, A., Sinharoy, R., Marsh, D. J., and Pocai, A. (2012). The glucagon receptor is involved in mediating the body weight-lowering effects of oxyntomodulin. *Obesity*, 20(8):1566–1571.

[Kozasa et al., 2011] Kozasa, T., Hajicek, N., Chow, C. R., and Suzuki, N. (2011). Signalling mechanisms of RhoGTPase regulation by the heterotrimeric G proteins G12 and G13. *Journal of Biochemistry*, 150(4):357–369.

[Krumm and Roth, 2020] Krumm, B. and Roth, B. L. (2020). A structural understanding of class B GPCR selectivity and activation revealed. *Structure*, 28(3):277–279.

[Kuna et al., 2013] Kuna, R. S., Girada, S. B., Asalla, S., Vallentyne, J., Maddika, S., Patterson, J. T., Smiley, D. L., DiMarchi, R. D., and Mitra, P. (2013). Glucagon-like peptide-1 receptor-mediated endosomal cAMP generation promotes glucose-stimulated insulin secretion in pancreatic β-cells. *American Journal of Physiology - Endocrinology and Metabolism*, 305(2):161–170.

[Kuszak et al., 2010] Kuszak, A. J., Yao, X. J., Rasmussen, S. G. F., Kobilka, B. K., and Sunahara, R. K. (2010). *Functional studies of isolated GPCR-G protein complexes in the membrane bilayer of lipoprotein particles*, pages 32–52. Cambridge University Press.

[Lane et al., 2017] Lane, J. R., May, L. T., Parton, R. G., Sexton, P. M., and Christopoulos, A. (2017). A kinetic view of GPCR allostery and biased agonism. *Nature Chemical Biology*, 13(9):929–937.

[Leach et al., 2007] Leach, K., Sexton, P. M., and Christopoulos, A. (2007). Allosteric GPCR modulators: taking advantage of permissive receptor pharmacology. *Trends in Pharmacological Sciences*, 28(8):382–389.

[Lee et al., 2011] Lee, Y., Wang, M.-y., Du, X. Q., Charron, M. J., and Unger, R. H. (2011). Glucagon receptor knockout prevents insulin-deficient type 1 diabetes in mice. *Diabetes*, 60:391–397.

[Lee and Jun, 2018] Lee, Y.-S. and Jun, H.-S. (2018). Glucagon-like peptide-1 receptor agonist and glucagon increase glucose-stimulated insulin secretion in beta cells via distinct adenylyl cyclases. *International Journal of Medical Sciences*, 15(6):603–609.

[Lei et al., 2018] Lei, S., Clydesdale, L., Dai, A., Cai, X., Feng, Y., Yang, D., Liang, Y.-L., Koole, C., Zhao, P., Coudrat, T., Christopoulos, A., Wang, M.-W., Wootten, D., and Sexton, P. M. (2018). Two distinct domains of the glucagon-like peptide-1 receptor control peptide-mediated biased agonism. *Journal of Biological Chemistry*, 293(3):9370–9387.

[Li et al., 2009] Li, D. S., Yuan, Y. H., Tu, H. J., Liang, Q. L., and Dail, L. J. (2009). A protocol for islet isolation from mouse pancreas. *Nature Protocols*, 4(11):1649–1652.

[Li et al., 2017] Li, J., Zheng, J., Wang, S., Lau, H. K., Fathi, A., and Wang, Q. (2017). Cardiovascular Benefits of Native GLP-1 and its Metabolites: An Indicator for GLP-1-Therapy Strategies. *Frontiers in Physiology*, 8(January):1–13.

[Li et al., 2012] Li, N., Lu, J., and Willars, G. B. (2012). Allosteric modulation of the activity of the glucagon-like peptide-1 (GLP-1) metabolite GLP-1(9-36)amide at the GLP-1 receptor. *PLoS ONE*, 7(10):e47936.

[Li et al., 2018] Li, N. X., Brown, S., Kowalski, T., Wu, M., Yang, L., Dai, G., Petrov, A., Ding, Y., Dlugos, T., Wood, H. B., Wang, L., Erion, M., Sherwin, R., and Kelley, D. E. (2018). GPR119 agonism increases glucagon secretion during insulin-induced hypoglycemia. *Diabetes*, 67(7):1401–1413.

[Liang et al., 2020a] Liang, Y.-L., Belousoff, M. J., Fletcher, M. M., Zhang, X., Khoshouei, M., Deganutti, G., Koole, C., Furness, S. G. B., Miller, L. J., Hay, D. L., Christopoulos, A., Reynolds, C. A., Danev, R., Wootten, D., and Sexton, P. M. (2020a). Structure and dynamics of adrenomedullin receptors AM1 and AM2 reveal key mechanisms in the control of receptor phenotype by receptor activity-modifying proteins. *ACS Pharmacology & Translational Science*, 3(2):263–284.

[Liang et al., 2020b] Liang, Y.-L., Belousoff, M. J., Zhao, P., Koole, C., Fletcher, M. M., Truong, T. T., Julita, V., Christopoulos, G., Xu, H. E., Zhang, Y., Khoshouei, M., Christopoulos, A., Danev, R., Sexton, P. M., and Wootten, D. (2020b). Toward a Structural Understanding of Class B GPCR Peptide Binding and Activation. *Molecular cell*, 77(3):656–668.e5.

[Liang et al., 2018a] Liang, Y.-L., Khoshouei, M., Deganutti, G., Glukhova, A., Koole, C., Peat, T. S., Radjainia, M., Plitzko, J. M., Baumeister, W., Miller, L. J., Hay, D. L., Christopoulos, A., Reynolds, C. A., Wootten, D., and Sexton, P. M. (2018a). Cryo-EM structure of the active, Gs-protein complexed, human CGRP receptor. *Nature*, 561(7724):492–497.

[Liang et al., 2018b] Liang, Y. L., Khoshouei, M., Glukhova, A., Furness, S. G., Zhao, P., Clydesdale, L., Koole, C., Truong, T. T., Thal, D. M., Lei, S., Radjainia, M., Danev, R., Baumeister, W., Wang, M. W., Miller, L. J., Christopoulos, A., Sexton, P. M., and Wootten, D. (2018b). Phase-plate cryo-EM structure of a biased agonist bound human GLP-1 receptor-Gs complex. *Nature*, 555(7694):121–125.

[Liang et al., 2017] Liang, Y.-L., Khoshouei, M., Radjainia, M., Zhang, Y., Glukhova, A., Tarrasch, J., Thal, D. M., Furness, S. G. B., Christopoulos, G., Coudrat, T., Danev, R., Baumeister, W., Miller, L. J., Christopoulos, A., Kobilka, B. K., Wootten, D., Skiniotis, G., and Sexton, P. M. (2017). Phase-plate cryo-EM structure of a class B GPCR-G-protein complex. *Nature*, 546(7656):118–123.

[Lilla et al., 2003] Lilla, V., Webb, G., Rickenbach, K., Maturana, A., Steiner, D. F., Halban, P. A., and Irminger, J. C. (2003). Differential gene expression in well-regulated and dysregulated pancreatic beta-cell (MIN6) sublines. *Endocrinology*, 144(4):1368–1379.

[Lin and Wang, 2009] Lin, F. and Wang, R. (2009). Molecular modeling of the three-dimensional structure of GLP-1R and its interactions with several agonists. *Journal of Molecular Modeling*, 15:53–65.

[Liu and Hermann, 1978] Liu, C.-m. and Hermann, T. E. (1978). Characterization of ionomycin as a calcium ionophore. *Journal of Biological Chemistry*, 253(17):5892–5894.

[Liu et al., 2014] Liu, L., Omar, B., Marchetti, P., and Ahrén, B. (2014). Dipeptidyl peptidase-4 (DPP-4): Localization and activity in human and rodent islets. *Biochemical and Biophysical Research Communications*, 453(3):398–404.

[Liu et al., 2018] Liu, P., Song, J., Liu, H., Yan, F., He, T., Wang, L., Shen, H., Hou, X., and Chen, L. (2018). Insulin regulates glucagon-like peptide-1 secretion by pancreatic alpha cells. *Endocrine*, 62(2):394–403.

[Lorza-Gil et al., 2019] Lorza-Gil, E., Gerst, F., Oquendo, M. B., Deschl, U., Häring, H. U., Beilmann, M., and Ullrich, S. (2019). Glucose, adrenaline and palmitate antagonistically regulate insulin and glucagon secretion in human pseudoislets. *Scientific Reports*, 9(1):1–11.

[Lund et al., 2011] Lund, A., Vilsboll, T., Bagger, J. I., Holst, J. J., and Knop, F. K. (2011). The separate and combined impact of the intestinal hormones, GIP, GLP-1, and GLP-2, on glucagon secretion in type 2 diabetes. *Am J Physiol Endocrinol Metab*, 300(6):E1038–46.

[Ma et al., 2020a] Ma, H., Huang, W., Wang, X., Zhao, L., Jiang, Y., Liu, F., Guo, W., Sun, X., Zhong, W., Yuan, D., and Xu, H. E. (2020a). Structural insights into the activation of GLP-1R by a small molecule agonist. *Cell Research*, 1:5–7.

[Ma et al., 2020b] Ma, S., Shen, Q., Zhao, L.-H., Mao, C., Zhou, X. E., Shen, D.-D., de Waal, P. W., Bi, P., Li, C., Jiang, Y., Wang, M.-W., Sexton, P. M., Wootten, D., Melcher, K., Zhang, Y., and Xu, H. E. (2020b). Molecular basis for hormone recognition and activation of corticotropin-releasing factor receptors. *Molecular cell*, 77(3):669–680.e4.

[Ma et al., 2005] Ma, X., Zhang, Y., Gromada, J., Sewing, S., Berggren, P.-O., Buschard, K., Salehi, A., Vikman, J., Rorsman, P., and Eliasson, L. (2005). Glucagon stimulates exocytosis in mouse and rat pancreatic α-cells by binding to glucagon receptors. *Molecular Endocrinology*, 19(1):198–212.

[Maida et al., 2008] Maida, A., Lovshin, J. A., Baggio, L. L., and Drucker, D. J. (2008). The glucagon-like peptide-1 receptor agonist oxyntomodulin enhances β-cell function but does not inhibit gastric emptying in mice. *Endocrinology*, 149(11):5670–5678.

[Mank and Griesbeck, 2008] Mank, M. and Griesbeck, O. (2008). Genetically Encoded Calcium Indicators. *Chemical Reviews*, 108(5):1550–1564.

[Martínez et al., 2000] Martínez, A., Kapas, S., Miller, M., Ward, Y., and Cuttitta, F. (2000). Coexpression of receptors for adrenomedullin, calcitonin gene-related peptide, and amylin in pancreatic beta-cells. *Endocrinology*, 141(1):406–411.

[May et al., 2007] May, L. T., Leach, K., Sexton, P. M., and Christopoulos, A. (2007). Allosteric modulation of G protein-coupled receptors. *Ann Rev Pharmacol Toxicol*, 47:1–51.

[McClendon et al., 2014] McClendon, C. L., Kornev, A. P., Gilson, M. K., and Taylor, S. S. (2014). Dynamic architecture of a protein kinase. *Proceedings of the National Academy of Sciences*, 111(43):E4623–E4631.

[McGirr et al., 2005] McGirr, R., Ejbick, C. E., Carter, D. E., Andrews, J. D., Nie, Y., Friedman, T. C., and Dhanvantari, S. (2005). Glucose dependence of the regulated secretory pathway in αTC1-6 cells. *Endocrinology*, 146(10):4514–4523.

[McLatchie et al., 1998] McLatchie, L. M., Fraser, N. J., Main, M. J., Wise, A., Brown, J., Thompson, N., Solari, R., Lee, M. G., and Foord, S. M. (1998). RAMPS regulate the transport and ligand specificity of the calcitonin- receptor-like receptor. *Nature*, 393(6683):333–339.

[Meda et al., 1991] Meda, P., Chanson, M., Pepper, M., Giordano, E., Bosco, D., Traub, O., Willecke, K., el Aoumari, A., Gros, D., and Beyer, E. C. (1991). In vivo modulation of connexin 43 gene expression and junctional coupling of pancreatic β-cells. *Experimental cell research*, 192(2):469–480.

[Meier, 2012] Meier, J. J. (2012). GLP-1 receptor agonists for individualized treatment of type 2 diabetes mellitus. *Nature Reviews Endocrinology*, 8(12):728–742.

[Meier and Nauck, 2010] Meier, J. J. and Nauck, M. A. (2010). Is the diminished incretin effect in type 2 diabetes just an epi-phenomenon of impaired β-cell function? *Diabetes*, 59(5):1117–1125.

[Méndez et al., 2020] Méndez, M., Matter, H., Defossa, E., Kurz, M., Lebreton, S., Li, Z., Lohmann, M., Löhn, M., Mors, H., Podeschwa, M., Rackelmann, N., Riedel, J., Safar, P., Thorpe, D. S., Schäfer, M., Weitz, D., and Breitschopf, K. (2020). Design, synthesis, and pharmacological evaluation of potent positive allosteric modulators of the glucagon-like peptide-1 receptor (GLP-1R). *Journal of Medicinal Chemistry*, 63(5):2292–2307.

[Miller et al., 2000] Miller, K. G., Emerson, M. D., McManus, J. R., and Rand, J. B. (2000). RIC-8 (Synembryn): A novel conserved protein that is required for G(q)α signaling in the C. elegans nervous system. *Neuron*, 27(2):289–299.

[Milligan and Kostenis, 2006] Milligan, G. and Kostenis, E. (2006). Heterotrimeric G-proteins: a short history. *British Journal of Pharmacology*, 147(SUPPL. 1):S46–55.

[Miyazaki et al., 1990] Miyazaki, J., Araki, K., Yamato, E., Ikegami, H., Asano, T., Shibasaki, Y., Oka, Y., and Yamamura, K. (1990). Establishment of a pancreatic β cell line that retains glucose-inducible insulin secretion: special reference to expression of glucose transporter isoforms. *Endocrinology*, 127(1):126–132.

[Moens et al., 1996] Moens, K., Heimberg, H., Flamez, D., Huypens, P., Quartier, E., Ling, Z., Pipeleers, D., Gremlich, S., Thorens, B., and Schuit, F. (1996). Expression and functional activity of glucagon, glucagon-like peptide I, and glucose-dependent insulinotropic peptide receptors in rat pancreatic islet cells. *Diabetes*, (12):257–261.

[Montrose-rafizadeh et al., 1999] Montrose-rafizadeh, C., Avdonin, P., Garant, M. J., Rodgers, B. D., Kole, S., Yang, H., Levine, M. A., Schwindinger, W., and Bernier, M. (1999). Pancreatic glucagon-like peptide-1 receptor couples to multiple G proteins and activates mitogen-activated protein kinase pathways in chinese hamster ovary cells. *Endocrinology*, 140(3):1132–1140.

[Montrose-rafizadeh et al., 1997] Montrose-rafizadeh, C., Yang, H., Rodgers, B. D., Beday, A., Pritchette, L. A., and Eng, J. (1997). High potency antagonists of the pancreatic glucagon-like peptide-1 receptor. *The Journal of Biological Chemistry*, 272(34):21201–21206.

[Morris et al., 2014] Morris, L. C., Days, E. L., Maxine, T., Mi, D., Lindsley, C. W., Weaver, D., Niswender, K. D., Turney, M., Mi, D., Lindsley, C. W., Weaver, C. D., and Niswender, K. D. (2014). A duplexed high-throughput screen to identify allosteric modulators of the glucagon-like peptide 1 and glucagon receptors. *Journal of Biomolecular Screening 2014,*, 19(6):847–858.

[Müller et al., 2017] Müller, T. D., Finan, B., Clemmensen, C., DiMarchi, R. D., and Tschöp, M. H. (2017). The new biology and pharmacology of glucagon. *Physiological Reviews*, 97(2):721–766.

[Müller et al., 1973] Müller, W. A., Faloona, G. R., and Unger, R. H. (1973). Hyperglucagonemia in diabetic ketoacidosis. Its prevalence and significance. *The American journal of medicine*, 54(1):52–57.

[Murray, 2008] Murray, A. J. (2008). Pharmacological PKA inhibition: All may not be what it seems. *Science Signaling*, 1(22):1–7.

[Nakai et al., 2001] Nakai, J., Ohkura, M., and Imoto, K. (2001). A high signal-to-noise Ca2+ probe composed of a single green fluorescent protein. *Nature Biotechnology*, 19(2):137–141.

[Nakane et al., 2015] Nakane, A., Gotoh, Y., Ichihara, J., and Nagata, H. (2015). New screening strategy and analysis for identification of allosteric modulators for glucagon-like peptide-1 receptor using GLP-1 (9-36) amide. *Analytical Biochemistry*, 491:23–30.

[Nakashima et al., 2009] Nakashima, K., Kanda, Y., Hirokawa, Y., Kawasaki, F., Matsuki, M., and Kaku, K. (2009). MIN6 Is not a pure beta cell line but a mixed cell line with other pancreatic endocrine hormones. *Endocrine Journal*, 56(1):45–53.

[Nakashima et al., 2018] Nakashima, K., Kaneto, H., Shimoda, M., Kimura, T., and Kaku, K. (2018). Pancreatic alpha cells in diabetic rats express active GLP-1 receptor: Endosomal co-localization of GLP-1/GLP-1R complex functioning through intra-islet paracrine mechanism. *Scientific Reports*, 8(1):1–14.

[Naylor et al., 2009] Naylor, E., Arredouani, A., Vasudevan, S. R., Lewis, A. M., Parkesh, R., Mizote, A., Rosen, D., Thomas, J. M., Izumi, M., Ganesan, A., Galione, A., and Churchill, G. C. (2009). Identification of a chemical probe for NAADP by virtual screening. *Nat Chem Biol*, 5(4):220–226.

[Naylor et al., 2016] Naylor, J., Suckow, A. T., Seth, A., Baker, D. J., Sermadiras, I., Ravn, P., Howes, R., Li, J., Snaith, M. R., Coghlan, M. P., and Hornigold, D. C. (2016). Use of CRISPR/Cas9-engineered INS-1 pancreatic β cells to define the pharmacology of dual GIPR/GLP-1R agonists. *Biochemical Journal*, 473(18):2881–2891.

[Nikolaev et al., 2004] Nikolaev, V. O., Bünemann, M., Hein, L., Hannawacker, A., and Lohse, M. J. (2004). Novel single chain cAMP sensors for receptor-induced signal propagation. *Journal of Biological Chemistry*, 279(36):37215–37218.

[Nolte et al., 2014] Nolte, W. M., Fortin, J.-P., Stevens, B. D., Aspnes, G. E., Griffith, D. A., Hoth, L. R., Ruggeri, R. B., Mathiowetz, A. M., Limberakis, C., Hepworth, D., and Carpino, P. A. (2014). A potentiator of orthosteric ligand activity at GLP-1R acts via covalent modification. *Nature Chemical Biology*, 10(8):629–631.

[Northup et al., 1980] Northup, J. K., Sternweis, P. C., Smigel, M. D., Schleifer, L. S., Ross, E. M., and Gilman, A. G. (1980). Purification of the regulatory component of adenylate cyclase. *Proceedings of the National Academy of Sciences of the United States of America*, 77(11):6516–6520.

[Odori et al., 2013] Odori, S., Hosoda, K., Tomita, T., Fujikura, J., Kusakabe, T., Kawaguchi, Y., Doi, R., Takaori, K., Ebihara, K., Sakai, Y., Uemoto, S., and Nakao, K. (2013). GPR119 expression in normal human tissues and islet cell tumors: Evidence for its islet-gastrointestinal distribution, expression in pancreatic beta and alpha cells, and involvement in islet function. *Metabolism: Clinical and Experimental*, 62(1):70–78.

[Oh and Olefsky, 2016] Oh, D. Y. and Olefsky, J. M. (2016). G protein-coupled receptors as targets for anti-diabetic therapeutics. *Nature Reviews Drug Discovery*, 15(3):161–172.

[Ørgaard and Holst, 2017] Ørgaard, A. and Holst, J. J. (2017). The role of somatostatin in GLP-1-induced inhibition of glucagon secretion in mice. *Diabetologia*, 60(9):1731–1739.

[Orskov et al., 1988] Orskov, C., Holst, J. J., and Nielsen, O. V. (1988). Effect of truncated glucagon-like peptide-1 [proglucagon-(78-107) amide] on endocrine secretion from pig pancreas, antrum, and nonantral stomach. *Endocrinology*, 123(4):2009–2013.

[Overton et al., 2006] Overton, H. A., Babbs, A. J., Doel, S. M., Fyfe, M. C., Gardner, L. S., Griffin, G., Jackson, H. C., Procter, M. J., Rasamison, C. M., Tang-Christensen, M., Widdowson, P. S., Williams, G. M., and Reynet, C. (2006). Deorphanization of a G protein-coupled receptor for oleoylethanolamide and its use in the discovery of small-molecule hypophagic agents. *Cell Metabolism*, 3(3):167–175.

[Owens et al., 2017] Owens, D. R., Monnier, L., and Barnett, A. H. (2017). Future challenges and therapeutic opportunities in type 2 diabetes: Changing the paradigm of current therapy. *Diabetes, Obesity and Metabolism*, (April):1–14.

[Pabreja et al., 2014] Pabreja, K., Mohd, M. A., Koole, C., Wootten, D., and Furness, S. G. (2014). Molecular mechanisms underlying physiological and receptor pleiotropic effects mediated by GLP-1R activation. *British Journal of Pharmacology*, 171(5):1114–1128.

[Parthier et al., 2009] Parthier, C., Reedtz-Runge, S., Rudolph, R., and Stubbs, M. T. (2009). Passing the baton in class B GPCRs: peptide hormone activation via helix induction? *Trends in Biochemical Sciences*, 34(6):303–310.

[Patel and Gold, 2015] Patel, N. and Gold, M. G. (2015). The genetically encoded tool set for investigating cAMP: more than the sum of its parts. *Frontiers in Pharmacology*, 6:164.

[Patil et al., 2020] Patil, M., Deshmukh, N. J., Patel, M., and Sangle, G. V. (2020). Glucagon-based therapy: Past, present and future. *Peptides*, 127(October 2019):170296.

[Patriti et al., 2007] Patriti, A., Aisa, M. C., Annetti, C., Sidoni, A., Galli, F., Ferri, I., Gullà, N., and Donini, A. (2007). How the hindgut can cure type 2 diabetes. Ileal transposition improves glucose metabolism and beta-cell function in Goto-kakizaki rats through an enhanced Proglucagon gene expression and L-cell number. *Surgery*, 142(1):74–85.

[Pauza et al., 2019] Pauza, A. G., Rysevaite-Kyguoliene, K., Malinauskas, M., Lukosiene, J. I., Alaburda, P., Stankevicius, E., Kupcinskas, J., Saladzinskas, Z., Tamelis, A., and Pauziene, N. (2019). Alterations in enteric calcitonin gene-related peptide in patients with colonic diverticular disease: CGRP in diverticular disease. *Autonomic neuroscience : basic & clinical*, 216:63–71.

[Pavlos and Friedman, 2017] Pavlos, N. J. and Friedman, P. A. (2017). GPCR signaling and trafficking: the long and short of it. *Trends in Endocrinology and Metabolism*, 28(3):213–226.

[Peddibhotla et al., 2019] Peddibhotla, S., Hegde, V., Akheruzzaman, M., and Dhurandhar, N. V. (2019). E4orf1 protein reduces the need for endogenous insulin. *Nutrition and Diabetes*, 9(17):1–9.

[Piro et al., 2014] Piro, S., Mascali, L. G., Urbano, F., Filippello, A., Malaguarnera, R., Calanna, S., Rabuazzo, A. M., and Purrello, F. (2014). Chronic exposure to GLP-1 increases GLP-1 synthesis and release in a pancreatic alpha cell Line (α-TC1): evidence of a direct effect of GLP-1 on pancreatic alpha cells. *PLoS One*, 9(2):e90093.

[Pittman, 1979] Pittman, M. (1979). Pertussis toxin: The cause of the harmful effects and prolonged immunity of whooping cough. A hypothesis. *Reviews of Infectious Diseases*, 1(3):401–412.

[Pocai, 2012] Pocai, A. (2012). Unraveling oxyntomodulin, GLP1's enigmatic brother. *Journal of Endocrinology*, 215(3):335–346.

[Pocai et al., 2009] Pocai, A., Carrington, P. E., Adams, J. R., Wright, M., Eiermann, G., Zhu, L., Du, X., Petrov, A., Lassman, M. E., Jiang, G., Liu, F., Miller, C., Tota, L. M., Zhou, G., Zhang, X., Sountis, M. M., Santoprete, A., Capito, E., Chicchi, G. G., Thornberry, N., Bianchi, E., Pessi, A., Marsh, D. J., and Sinharoy, R. (2009). Glucagon-like peptide 1/glucagon receptor dual agonism reverses obesity in mice. *Diabetes*, 58(October):2258–2266.

[Poitout et al., 1996] Poitout, V., Olson, L., and Robertson, R. (1996). Insulin-secreting cell lines: classification, characteristics and potential applications. *Diabetes & metabolism*, 22 1:7–14.

[Powers et al., 1990] Powers, A., Efrat, S., Mojsov, S., Spector, D., Habener, J. F., and Hanahan, D. (1990). Proglucagon processing similar to normal islets in pancreatic alpha-like cell line derived from transgenic mouse tumor. *Diabetes*, 39:406–414.

[Prado et al., 2002] Prado, M. A., Evans-Bain, B., and Dickerson, I. M. (2002). Receptor component protein (RCP): a member of a multi-protein complex required for G-protein-coupled signal transduction. *Biochemical Society transactions*, 30(4):460–464.

[Putney and Tomita, 2012] Putney, J. W. and Tomita, T. (2012). Phospholipase C signaling and calcium influx. *Advances in biological regulation*, 52(1):152–164.

[Qiao et al., 2020] Qiao, A., Han, S., Li, X., Li, Z., Zhao, P., Dai, A., Chang, R., Tai, L., Tan, Q., Chu, X., Thorsen, T. S., Reedtz-runge, S., Yang, D., Wang, M.-w., Sexton, P. M., Wootten, D., Sun, F., Zhao, Q., and Wu, B. (2020). Structural basis of Gs and Gi recognition by the human glucagon receptor. *Science*, 1352(March):1346–1352.

[Rajagopal and Shenoy, 2018] Rajagopal, S. and Shenoy, S. K. (2018). GPCR desensitisation: acute and prolonged phases. *Cell Signal*, 41:9–16.

[Ramracheya et al., 2018] Ramracheya, R., Chapman, C., Chibalina, M., Dou, H., Miranda, C., González, A., Moritoh, Y., Shigeto, M., Zhang, Q., Braun, M., Clark, A., Johnson, P. R., Rorsman, P., and Briant, L. J. B. (2018). GLP-1 suppresses glucagon secretion in human pancreatic alpha-cells by inhibition of P/Q-type Ca2+ channels. *Physiological Reports*, 6(17):e13852.

[Raufman et al., 1992] Raufman, J., Singh, L., Singh, G., and Eng, J. (1992). Truncated glucagon-like peptide-1 GLP-1(7-36)NH2 interacts with exendin receptors on dispersed chief cells from guinea pig stomach. *Journal of Biological Chemistry*, 267(30):21432–21437.

[Ravassa et al., 2017] Ravassa, S., Zudaire, A., and Diez, J. (2017). Glucagon-like peptide 1 and cardiac cell survival. *Endocrinology Nutrition*, 59(9):561–569.

[Redij et al., 2019] Redij, T., Ma, J., Li, Z., Hua, X., and Li, Z. (2019). Discovery of a potential positive allosteric modulator of glucagon-like peptide 1 receptor through virtual screening and experimental study. *Journal of Computer-Aided Molecular Design*, 33(11):973–981.

[Retamal et al., 2019] Retamal, J. S., Ramírez-García, P. D., Shenoy, P. A., Poole, D. P., and Veldhuis, N. A. (2019). Internalized GPCRs as potential therapeutic targets for the management of pain. *Frontiers in molecular neuroscience*, 12:273.

[Richards et al., 2014] Richards, P., Parker, H. E., Adriaenssens, A. E., Hodgson, J. M., Cork, S. C., Trapp, S., Gribble, F. M., and Reimann, F. (2014). Identification and characterization of GLP-1 receptor-expressing cells using a new transgenic mouse model. *Diabetes*, 63(4):1224–1233.

[Roed et al., 2015] Roed, S. N., No, A. C., Wismann, P., Iversen, H., Bräuner-Osborne, H., Knudsen, S. M., and Waldhoer, M. (2015). Functional consequences of glucagon-like peptide-1 receptor cross-talk and trafficking. *Journal of Biological Chemistry*, 290(2):1233–1243.

[Roed et al., 2014] Roed, S. N., Wismann, P., Underwood, C. R., Kulahin, N., Iversen, H., Cappelen, K. A., Schäffer, L., Lehtonen, J., Hecksher-Soerensen, J., Secher, A., Mathiesen, J. M., Bräuner-Osborne, H., Whistler, J. L., Knudsen, S. M., and Waldhoer, M. (2014). Real-time trafficking and signaling of the glucagon-like peptide-1 receptor. *Molecular and Cellular Endocrinology*, 382(2):938–949.

[Rosenstock et al., 2020] Rosenstock, J., Nino, A., Soffer, J., Erskine, L., Acusta, A., Dole, J., Carr, M. C., Mallory, J., and Home, P. (2020). Impact of a weekly glucagon-like peptide 1 receptor agonist, albiglutide, on glycemic control and on reducing prandial insulin use in type 2 diabetes inadequately controlled on multiple insulin therapy: a randomized trial. *Diabetes care*, 43(10):2509–2518.

[Routledge et al., 2017] Routledge, S. J., Ladds, G., and Poyner, D. R. (2017). The effects of RAMPs upon cell signalling. *Molecular and Cellular Endocrinology*, 449:12–20.

[Routledge et al., 2020] Routledge, S. J., Simms, J., Clark, A., Yeung, H. Y., Wigglesworth, M. J., Dickerson, I. M., Kitchen, P., Ladds, G., and Poyner, D. R. (2020). Receptor component protein, an endogenous allosteric modulator of family B G protein coupled receptors. *Biochimica et Biophysica Acta - Biomembranes*, 1862(3):183174.

[Runge et al., 2003] Runge, S., Wulff, B. S., Madsen, K., Bräuner-Osborne, H., and Knudsen, L. B. (2003). Different domains of the glucagon and glucagon-like peptide-1 receptors provide the critical determinants of ligand selectivity. *British journal of pharmacology*, 138(5):787–794.

[Salehi et al., 2006] Salehi, A., Vieira, E., and Gylfe, E. (2006). Paradoxical stimulation of glucagon secretion by high glucose concentrations. *Diabetes*, 55(8):2318–2323.

[Sancho et al., 2017] Sancho, V., Daniele, G., Lucchesi, D., Lupi, R., Ciccarone, A., Penno, G., Bianchi, C., Dardano, A., Miccoli, R., and Del Prato, S. (2017). Metabolic regulation of GLP-1 and PC1/3 in pancreatic α-cell line. *PLoS ONE*, 12(11):1–12.

[Sandoval and D'Alessio, 2015] Sandoval, D. A. and D'Alessio, D. A. (2015). Physiology of proglucagon peptides: role of glucagon and GLP-1 in health and disease. *Physiological reviews*, 95(2):513–548.

[Sato et al., 2006] Sato, M., Blumer, J. B., Simon, V., and Lanier, S. M. (2006). Accessory proteins for G proteins: Partners in Signaling. *Annual Review of Pharmacology and Toxicology*, 46(1):151–187.

[Schann et al., 2008] Schann, S., Mayer, S., Frauli, M., Franchet, C., and Neuville, P. (2008). Sounds of silence: Innovative approach for identification of novel GPCR-modulator chemical entities. In *238th ACS National Meeting, Washington, DC*, Washington.

[Schmidt et al., 2020] Schmidt, M., Cattani-Cavalieri, I., Nuñez, F. J., and Ostrom, R. S. (2020). Phosphodiesterase isoforms and cAMP compartments in the development of new therapies for obstructive pulmonary diseases. *Current opinion in pharmacology*, 51:34–42.

[Seamon et al., 1981] Seamon, K. B., Padgett, W., and Daly, J. W. (1981). Forskolin: unique diterpene activator of adenlyate cyclase in membranes and in intact cells. *Proceedings of the National Academy of Sciences*, 78(6):3363–3367.

[Seino, 2012] Seino, S. (2012). Cell signalling in insulin secretion: The molecular targets of ATP, cAMP and sulfonylurea. *Diabetologia*, 55(8):2096–2108.

[Seino et al., 2010] Seino, Y., Fukushima, M., and Yabe, D. (2010). GIP and GLP-1, the two incretin hormones: Similarities and differences. *Journal of Diabetes Investigation*, 1(1-2):8–23.

[Semple et al., 2008] Semple, G., Fioravanti, B., Pereira, G., Calderon, I., Uy, J., Choi, K., Xiong, Y., Ren, A., Morgan, M., Dave, V., Thomsen, W., Unett, D. J., Xing, C., Bossie, S., Carroll, C., Chu, Z. L., Grottick, A. J., Hauser, E. K., Leonard, J., and Jones, R. M. (2008). Discovery of the first potent and orally efficacious agonist of the orphan G-protein coupled receptor 119. *Journal of Medicinal Chemistry*, 51(17):5172–5175.

[Serafin et al., 2020] Serafin, D. S., Harris, N. R., Nielsen, N. R., Mackie, D. I., and Caron, K. M. (2020). Dawn of a New RAMPage. *Trends in Pharmacological Sciences*, 41(4):249–265.

[Sharma et al., 2013] Sharma, R., Mcdonald, T. S., Eng, H., Limberakis, C., Stevens, B. D., Patel, S., and Kalgutkar, A. S. (2013). In vitro metabolism of the glucagon-like peptide-1 (GLP-1)- derived metabolites GLP-1 (9-36) amide and GLP-1 (28-36) amide in mouse and human hepatocytes. *Drug Metabolism and Disposition*, 41:2148–2157.

[Shigeto et al., 2015] Shigeto, M., Ramracheya, R., Tarasov, A. I., Cha, C. Y., Chibalina, M. V., Hastoy, B., Philippaert, K., Reinbothe, T., Rorsman, N., Salehi, A., Sones, W. R., Vergari, E., Weston, C., Gorelik, J., Katsura, M., Nikolaev, V. O., Vennekens, R., Zaccolo, M., Galione, A., Johnson, P. R., Kaku, K., Ladds, G., and Rorsman, P. (2015). GLP-1 stimulates insulin secretion by PKC-dependent TRPM4 and TRPM5 activation. *Journal of Clinical Investigation*, 125(12):4714–4728.

[Sloop et al., 2010] Sloop, K. W., Willard, F. S., Brenner, M. B., Ficorilli, J., Valasek, K., Showalter, A. D., Farb, T. B., Cao, J. X. C., Cox, A. L., Michael, M. D., Maria, S., Sanfeliciano, G., Tebbe, M. J., and Coghlan, M. J. (2010). Novel small molecule glucagon-like peptide-1 receptor agonist stimulates insulin secretion in rodents and from human islets. *Diabetes*, 59(December):3099–3107.

[Smits et al., 2016] Smits, M. M., Bunck, M. C., Diamant, M., Corner, A., Eliasson, B., Heine, R. J., Smith, U., Yki-j, H., and Raalte, H. V. (2016). Effect of 3 Years of treatment with exenatide on postprandial glucagon levels. *Diabetes Care*, 39(March):42–43.

[Smrcka, 2008] Smrcka, A. V. (2008). G protein $\beta\gamma$ subunits: Central mediators of G protein-coupled receptor signaling. *Cell Mol Life Sci*, 65(14):2191–2214.

[Song et al., 2017] Song, G., Yang, D., Wang, Y., Graaf, C. D., Zhou, Q., Jiang, S., Liu, K., Cai, X., Dai, A., Lin, G., Liu, D., Wu, F., Wu, Y., Zhao, S., Ye, L., Han, G. W., Lau, J., Wu, B., Hanson, M. A., Liu, Z.-J., Wang, M.-W., and Stevens, R. C. (2017). Human GLP-1 receptor transmembrane domain structure in complex with allosteric modulators. *Nature*, 546(7657):312–315.

[Sonoda et al., 2008] Sonoda, N., Imamura, T., Yoshizaki, T., Babendure, J. L., Lu, J.-c., and Olefsky, J. M. (2008). Beta-Arrestin-1 mediates glucagon-like peptide-1 signaling to insulin secretion in cultured pancreatic beta cells. *Proceedings of the National Academy of Sciences of the United States of America*, 105(18):6614–9.

[Spain et al., 2016] Spain, C. V., Wright, J. J., Hahn, R. M., Wivel, A., and Martin, A. A. (2016). Self-reported barriers to adherence and persistence to treatment with injectable medications for type 2 diabetes. *Clinical Therapeutics*, 38(7):1653–1664.e1.

[Sparre-Ulrich et al., 2016] Sparre-Ulrich, A. H., Hansen, L. S., Svendsen, B., Christensen, M., Knop, F. K., Hartmann, B., Holst, J. J., and Rosenkilde, M. M. (2016). Species-specific action of (Pro3)GIP - A full agonist at human GIP receptors, but a partial agonist and competitive antagonist at rat and mouse GIP receptors. *British Journal of Pharmacology*, 173(1):27–38.

[Sriram and Insel, 2018] Sriram, K. and Insel, P. A. (2018). G protein-coupled receptors as targets for approved drugs: How many targets and how many drugs? *Molecular Pharmacology*, 93(4):251–258.

[Stevenson et al., 1987] Stevenson, R. W., Williams, P. E., and Cherrington, A. D. (1987). Role of glucagon suppression on gluconeogenesis during insulin treatment of the conscious diabetic dog. *Diabetologia*, 30(10):782–790.

[Stratakis and Cho-Chung, 2002] Stratakis, C. A. and Cho-Chung, Y. S. (2002). Protein kinase A and human disease. *Trends in Endocrinology & Metabolism*, 13(2):50–52.

[Suga et al., 2019] Suga, T., Kikuchi, O., Kobayashi, M., Matsui, S., Yokota-Hashimoto, H., Wada, E., Kohno, D., Sasaki, T., Takeuchi, K., Kakizaki, S., Yamada, M., and Kitamura, T. (2019). SGLT1 in pancreatic α cells regulates glucagon secretion in mice, possibly explaining the distinct effects of SGLT2 inhibitors on plasma glucagon levels. *Molecular Metabolism*, 19(October 2018):1–12.

[Svendsen et al., 2018] Svendsen, B., Larsen, O., Gabe, M. B. N., Christiansen, C. B., Rosenkilde, M. M., Drucker, D. J., and Holst, J. J. (2018). Insulin secretion depends on intra-islet glucagon signaling. *Cell Reports*, 25(5):1127–1134.e2.

[Syrovatkina et al., 2016] Syrovatkina, V., Alegre, K. O., Dey, R., and Huang, X. Y. (2016). Regulation, signaling and physiological functions of G-proteins. *Journal of Molecular Biology*, 428(19):3850–3868.

[Tahrani et al., 2016] Tahrani, A. A., Barnett, A. H., and Bailey, C. J. (2016). Pharmacology and therapeutic implications of current drugs for type 2 diabetes mellitus. *Nature Reviews Endocrinology*, 12(10):566–592.

[Takaki et al., 1986] Takaki, R., Ono, J., Nakamura, M., Yokogawa, Y., Kumae, S., Hiraoka, T., Yamaguchi, K., Hamaguchi, K., and Uchida, S. (1986). Isolation of glucagon-secreting cell lines by cloning insulinoma cells. *In vitro ceullular & developmental biology*, 22(3):120–126.

[Takasaki et al., 2004] Takasaki, J., Saito, T., Taniguchi, M., Kawasaki, T., Moritani, Y., Hayashi, K., and Kobori, M. (2004). A novel Gαq/11-selective inhibitor. *Journal of Biological Chemistry*, 279(46):47438–47445.

[Tengholm, 2012] Tengholm, A. (2012). Cyclic AMP dynamics in the pancreatic beta-cell. *Upsala Journal of Medical Sciences*, 117(August):355–369.

[Tengholm and Gylfe, 2017] Tengholm, A. and Gylfe, E. (2017). cAMP signalling in insulin and glucagon secretion. *Diabetes, Obesity and Metabolism*, 19(March):42–53.

[Teraoku and Lenzen, 2017] Teraoku, H. and Lenzen, S. (2017). Dynamics of insulin secretion from EndoC-βH1 β-Cell pseudoislets in response to glucose and other nutrient and nonnutrient secretagogues. *Journal of Diabetes Research*, 2017.

[Thal et al., 2018] Thal, D. M., Glukhova, A., Sexton, P. M., and Christopoulos, A. (2018). Structural insights into G-protein-coupled receptor allostery. *Nature*, 559(7712):45–53.

[Thethi et al., 2020] Thethi, T. K., Pratley, R., and Meier, J. J. (2020). Efficacy, safety and cardiovascular outcomes of once-daily oral semaglutide in patients with type 2 diabetes: The PIONEER programme. *Diabetes, Obesity and Metabolism*, 22(8):1263–1277.

[Thomas et al., 2015] Thomas, M. C., Cooper, M. E., and Zimmet, P. (2015). Changing epidemiology of type 2 diabetes mellitus and associated chronic kidney disease. *Nature Reviews Nephrology*, 12(2):73–81.

[Thompson and Kanamarlapudi, 2015] Thompson, A. and Kanamarlapudi, V. (2015). Agonist-induced internalisation of the glucagon-like peptide-1 receptor is mediated by the Galpha-q pathway. *Biochemical Pharmacology*, 93(1):72–84.

[Thompson et al., 2016] Thompson, A., Stephens, J. W., Bain, S. C., and Kanamarlapudi, V. (2016). Molecular characterisation of small molecule agonists effect on the human glucagon like peptide-1 receptor internalisation. *PLoS ONE*, 11(4):1–22.

[Tibaduiza et al., 2001] Tibaduiza, E. C., Chen, C., and Beinborn, M. (2001). A small molecule ligand of the glucagon-like peptide 1 receptor targets its amino-terminal hormone binding domain. *Journal of Biological Chemistry*, 276(41):37787–37803.

[Tomas-Falco and Habener, 2010] Tomas-Falco, E. and Habener, J. F. (2010). Insulin-like actions of glucagon-like peptide-1: a dual receptor hypothesis. *Trends in Endocrinology and Metabolism*, 21(2):59–67.

[Tornehave et al., 2008] Tornehave, D., Kristensen, P., Rømer, J., Knudsen, L. B., and Heller, R. S. (2008). Expression of the GLP-1 receptor in mouse, rat, and human pancreas. *Journal of Histochemistry & Cytochemistry*, 56(9):841–851.

[Trott and Olson, 2010] Trott, O. and Olson, A. J. (2010). AutoDock Vina: improving the speed and accuracy of docking with a new scoring function, efficient optimization, and multithreading. *Journal of computational chemistry*, 31(2):455–461.

[Tsonkova et al., 2018] Tsonkova, V. G., Sand, F. W., Wolf, X. A., Grunnet, L. G., Kirstine Ringgaard, A., Ingvorsen, C., Winkel, L., Kalisz, M., Dalgaard, K., Bruun, C., Fels, J. J., Helgstrand, C., Hastrup, S., Öberg, F. K., Vernet, E., Sandrini, M. P. B., Shaw, A. C., Jessen, C., Grønborg, M., Hald, J., Willenbrock, H., Madsen, D., Wernersson, R., Hansson, L., Jensen, J. N., Plesner, A., Alanentalo, T., Petersen, M. B. K., Grapin-Botton, A., Honoré, C., Ahnfelt-Rønne, J., Hecksher-Sørensen, J., Ravassard, P., Madsen, O. D., Rescan, C., and Frogne, T. (2018). The EndoC-βH1 cell line is a valid model of human beta cells and applicable for screenings to identify novel drug target candidates. *Molecular Metabolism*, 8(December 2017):144–157.

[Unger et al., 1963] Unger, R., Eisentraut, A., and Madison, L. (1963). The effects of total starvation upon the levels of circulating glucagon and insulin in man. *Journal of Clinical Investigation*, 42(7):1031–1039.

[Unger and Cherrington, 2012] Unger, R. H. and Cherrington, A. D. (2012). Glucagonocentric restructuring of diabetes: a pathophysiologic and therapeutic makeover. *The Journal of Clinical Investigation*, 122(1):4–12.

[Verspohl, 2009] Verspohl, E. J. (2009). Novel therapeutics for type 2 diabetes: Incretin hormone mimetics (glucagon-like peptide-1 receptor agonists) and dipeptidyl peptidase-4 inhibitors. *Pharmacology and Therapeutics*, 124(1):113–138.

[Vivot et al., 2016] Vivot, K., Moullé, V. S., Zarrouki, B., Tremblay, C., Mancini, A. D., Maachi, H., Ghislain, J., and Poitout, V. (2016). The regulator of G-protein signaling RGS16 promotes insulin secretion and β-cell proliferation in rodent and human islets. *Molecular Metabolism*, 5(10):988–996.

[von Mering and Minkowski, 1889] von Mering, J. and Minkowski, O. (1889). Diabetes mellitus nach Pankreasextirpation. *Centralblatt für klinische Medicin*, 10:393–394.

[Walker et al., 2011] Walker, J. N., Ramracheya, R., Zhang, Q., Johnson, P. R. V., Braun, M., and Rorsman, P. (2011). Regulation of glucagon secretion by glucose: paracrine, intrinsic or both? *Diabetes, Obesity and Metabolism*, 13(Suppl. 1):95–105.

[Walker et al., 2020] Walker, J. T., Haliyur, R., Nelson, H. A., Ishahak, M., Poffenberger, G., Aramandla, R., Reihsmann, C., Luchsinger, J. R., Saunders, D. C., Wang, P., Garcia-Ocana, A., Bottino, R., Agarwal, A., Powers, A. C., and Brissova, M. (2020). Integrated human pseudoislet system and microfluidic platform demonstrates differences in GPCR signaling in islet cells. *JCI Insight*, (12):1–15.

[Werry et al., 2005] Werry, T. D., Sexton, P. M., and Christopoulos, A. (2005). 'Ins and outs' of seven-transmembrane receptor signalling to ERK. *Trends in Endocrinology and Metabolism*, 16(1):26–33.

[Weston et al., 2015] Weston, C., Lu, J., Li, N., Barkan, K., Richards, G. O., Roberts, D. J., Skerry, T. M., Poyner, D., Pardamwar, M., Reynolds, C. A., Dowell, S. J., Willars, G. B., and Ladds, G. (2015). Modulation of glucagon receptor pharmacology by receptor activity-modifying protein-2 (RAMP2). *Journal of Biological Chemistry*, 290(38):23009–23022.

[Weston et al., 2014] Weston, C., Poyner, D., Patel, V., Dowell, S., and Ladds, G. (2014). Investigating G protein signalling bias at the glucagon-like peptide-1 receptor in yeast. *British Journal of Pharmacology*, 171(15):3651–3665.

[Weston et al., 2016] Weston, C., Winfield, I., Harris, M., Hodgson, R., Shah, A., Dowell, S. J., Mobarec, J. C., Woodcock, D. A., Reynolds, C. A., Poyner, D. R., Watkins, H. A., and Ladds, G. (2016). Receptor activity modifying protein-directed G protein signaling specificity for the calcitonin gene-related peptide family of receptors. *Journal of Biological Chemistry*, (291):21925–21944.

[Wewer Albrechtsen et al., 2016] Wewer Albrechtsen, N. J., Kuhre, R. E., Pedersen, J., Knop, F. K., and Holst, J. J. (2016). The biology of glucagon and the consequences of hyperglucagonemia. *Biomarkers in Medicine*, 10(11):1141–1151.

[Whalley et al., 2011] Whalley, N. M., Pritchard, L. E., Smith, D. M., and White, A. (2011). Processing of proglucagon to GLP-1 in pancreatic α-cells: is this a paracrine mechanism enabling GLP-1 to act on β-cells? *Journal of Endocrinology*, 211(1):99–106.

[Willard et al., 2012a] Willard, F. S., Bueno, A. B., and Sloop, K. W. (2012a). Small molecule drug discovery at the glucagon-like peptide-1 receptor. *Experimental Diabetes Research*, 2012:1–9.

[Willard and Sloop, 2012] Willard, F. S. and Sloop, K. W. (2012). Physiology and emerging biochemistry of the glucagon-like peptide-1 receptor. *Experimental Diabetes Research*, 2012:1–12.

[Willard et al., 2012b] Willard, F. S., Wootten, D., Showalter, A. D., Savage, E. E., Ficorilli, J., Farb, T. B., Bokvist, K., Alsina-fernandez, J., Furness, S. G. B., Christopoulos, A., Sexton, P. M., and Sloop, K. W. (2012b). Small molecule allosteric modulation of the glucagon-like peptide-1 receptor enhances the insulinotropic effect of oxyntomodulin. *Molecular Pharmacology*, 82(6):1066–1073.

[Winzell and Ahrén, 2007] Winzell, M. S. and Ahrén, B. (2007). G-protein-coupled receptors and islet function-implications for treatment of type 2 diabetes. *Pharmacology & Therapeutics*, 116(3):437–448.

[Wolfe and Trejo, 2007] Wolfe, B. L. and Trejo, J. A. (2007). Clathrin-dependent mechanisms of G protein-coupled receptor endocytosis. *Traffic*, 8(5):462–470.

[Wootten et al., 2018] Wootten, D., Christopoulos, A., Marti-Solano, M., Babu, M. M., and Sexton, P. M. (2018). Mechanisms of signalling and biased agonism in G protein-coupled receptors. *Nature Reviews Molecular Cell Biology*, 19(10):638–653.

[Wootten et al., 2013a] Wootten, D., Christopoulos, A., and Sexton, P. M. (2013a). Emerging paradigms in GPCR allostery: implications for drug discovery. *Nature reviews. Drug discovery*, 12(8):630–44.

[Wootten and Miller, 2020] Wootten, D. and Miller, L. J. (2020). Structural basis for allosteric modulation of class B G protein-coupled receptors. *Annual Review of Pharmacology and Toxicology*, 60(1):89–107.

[Wootten et al., 2016a] Wootten, D., Miller, L. J., Koole, C., Christopoulos, A., and Sexton, P. M. (2016a). Allostery and biased agonism at class B G protein-coupled receptors. *Chemical reviews*, 117:111–138.

[Wootten et al., 2016b] Wootten, D., Reynolds, C. A., Smith, K. J., Mobarec, J. C., Furness, S. G. B., Miller, L. J., Christopoulos, A., and Sexton, P. M. (2016b). Key interactions by conserved polar amino acids located at the transmembrane helical

boundaries in Class B GPCRs modulate activation, effector specificity and biased signalling in the glucagon-like peptide-1 receptor. *Biochemical Pharmacology*, 118:68–87.

[Wootten et al., 2016c] Wootten, D., Reynolds, C. A., Smith, K. J., Mobarec, J. C., Koole, C., Savage, E. E., Pabreja, K., Simms, J., Sridhar, R., Furness, S. G. B., Liu, M., Thompson, P. E., Miller, L. J., Christopoulos, A., and Sexton, P. M. (2016c). The extracellular surface of the GLP-1 receptor is a molecular trigger for biased agonism. *Cell*, 165(7):1632–1643.

[Wootten et al., 2012] Wootten, D., Savage, E. E., Valant, C., May, L. T., Sloop, K. W., Ficorilli, J., Showalter, A. D., Willard, F. S., Christopoulos, A., and Sexton, P. M. (2012). Allosteric modulation of endogenous metabolites as an avenue for drug discovery. *Molecular Pharmacology*, 82(2):281–290.

[Wootten et al., 2013b] Wootten, D., Savage, E. E., Willard, F. S., Bueno, A. B., Sloop, K. W., Christopoulos, A., and Sexton, P. M. (2013b). Differential activation and modulation of the glucagon-like peptide-1 receptor by small molecule ligands. *Molecular Pharmacology*, 83(4):822–834.

[Wu et al., 2020] Wu, F., Yang, L., Hang, K., Laursen, M., Wu, L., Han, G. W., Ren, Q., Roed, N. K., Lin, G., Hanson, M. A., Jiang, H., Wang, M. W., Reedtz-Runge, S., Song, G., and Stevens, R. C. (2020). Full-length human GLP-1 receptor structure without orthosteric ligands. *Nature Communications*, 11(1):1–10.

[Wynne et al., 2010] Wynne, K., Field, B., and Bloom, S. (2010). The mechanism of action for oxyntomodulin in the regulation of obesity. *Current Opinion in Investigational Drugs*, 11(10):1151–1157.

[Xu et al., 2007] Xu, G., Kaneto, H., Laybutt, D. R., Duvivier-kali, V. F., Trivedi, N., Suzuma, K., King, G. L., Weir, G. C., and Bonner-weir, S. (2007). Downregulation of GLP-1 and GIP receptor expression by hyperglycemia. *Diabetes*, 56(June):1551–1558.

[Xu and Xie, 2009] Xu, Y. and Xie, X. (2009). Glucagon receptor mediates calcium signaling by coupling to Gαq/11 and Gαi/o in HEK293 cells. *Journal of Receptors and Signal Transduction*, 29(6):318–25.

[Yang and Yang, 2016] Yang, H. and Yang, L. (2016). Targeting cAMP/PKA pathway for glycemic control and type 2 diabetes therapy. *Journal of Molecular Endocrinology*, 57(2):R93–R108.

[Yang et al., 2016] Yang, S. Y., Lee, J. J., Lee, J. H., Lee, K., Oh, S. H., Lim, Y. M., Lee, M. S., and Lee, K. J. (2016). Secretagogin affects insulin secretion in pancreatic β-cells by regulating actin dynamics and focal adhesion. *Biochemical Journal*, 473(12):1791–1803.

[Yau et al., 2019] Yau, B., Blood, Z., An, Y., Su, Z., and Kebede, M. A. (2019). Type 2 diabetes-associated single nucleotide polymorphism in Sorcs1 gene results in alternative processing of the Sorcs1 protein in INS1 β-cells. *Scientific Reports*, 9(1):1–11.

[Yau et al., 2020] Yau, B., Hays, L., Liang, C., Laybutt, D. R., Thomas, H. E., Gunton, J. E., Williams, L., Hawthorne, W. J., Thorn, P., Rhodes, C. J., and Kebede, M. A. (2020). A fluorescent timer reporter enables sorting of insulin secretory granules by age. *Journal of Biological Chemistry*, 295(27):8901–8911.

[Yeung et al., 2016] Yeung, H. Y., Barkan, K., Rahman, T., and Ladds, G. (2016). Identification and characterisation of a novel series of quinoxaline-based small molecules as GLP-1R allosteric modulators. In *Proceedings of the British Pharmacological Society*, volume 18.

[Yin et al., 2016] Yin, Y., Zhou, X. E., Hou, L., Zhao, L.-h., Liu, B., Wang, G., Jiang, Y., Melcher, K., and Xu, H. E. (2016). An intrinsic agonist mechanism for activation of glucagon-like peptide-1 receptor by its extracellular domain. *Cell Discovery*, 2:16042.

[Yu et al., 2019] Yu, Q., Shuai, H., Ahooghalandari, P., Gylfe, E., and Tengholm, A. (2019). Glucose controls glucagon secretion by directly modulating cAMP in alpha cells. *Diabetologia*, 62(7):1212–1224.

[Zhang et al., 2020] Zhang, H., Nielsen, A. L., and Strømgaard, K. (2020). Recent achievements in developing selective G(q) inhibitors. *Medicinal research reviews*, 40(1):135–157.

[Zhang et al., 2017a] Zhang, H., Qiao, A., Yang, D., Yang, L., Dai, A., de Graaf, C., Reedtz-Runge, S., Dharmarajan, V., Zhang, H., Han, G. W., Grant, T. D., Sierra, R. G., Weierstall, U., Nelson, G., Liu, W., Wu, Y., Ma, L., Cai, X., Lin, G., Wu, X., Geng, Z., Dong, Y., Song, G., Griffin, P. R., Lau, J., Cherezov, V., Yang, H., Hanson, M. A., Stevens, R. C., Zhao, Q., Jiang, H., Wang, M.-W., and Wu, B. (2017a). Structure of the full-length glucagon class B G-protein-coupled receptor. *Nature*, 546(7657):259–264.

[Zhang et al., 2018] Zhang, H., Qiao, A., Yang, L., Van Eps, N., Frederiksen, K. S., Yang, D., Dai, A., Cai, X., Zhang, H., Yi, C., Cao, C., He, L., Yang, H., Lau, J., Ernst, O. P., Hanson, M. A., Stevens, R. C., Wang, M. W., Reedtz-Runge, S., Jiang, H., Zhao, Q., and Wu, B. (2018). Structure of the glucagon receptor in complex with a glucagon analogue. *Nature*, 553(7686):106–110.

[Zhang et al., 2015] Zhang, H., Sturchler, E., Zhu, J., Nieto, A., Cistrone, P. A., Xie, J., He, L., Yea, K., Jones, T., Turn, R., Di Stefano, P. S., Griffin, P. R., Dawson, P. E., McDonald, P. H., and Lerner, R. A. (2015). Autocrine selection of a GLP-1R G-protein biased agonist with potent antidiabetic effects. *Nature Communications*, 6(May):1–13.

[Zhang et al., 2019] Zhang, Y., Parajuli, K. R., Fava, G. E., Gupta, R., Xu, W., Nguyen, L. U., Zakaria, A. F., Fonseca, V. A., Wang, H., Mauvais-Jarvis, F., Sloop, K. W., and Wu, H. (2019). GLP-1 receptor in pancreatic α cells regulates glucagon secretion in a glucose-dependent bidirectional manner. *Diabetes*, 68:34–44.

[Zhang et al., 2014] Zhang, Y., Shen, L., Cheon, H., Xu, Y., and Jeong, J. (2014). Synthesis and biological evaluation of glucagon-like peptide-1 receptor agonists. *Archives of Pharmacal Research*, 37:588–599.

[Zhang et al., 2017b] Zhang, Y., Sun, B., Feng, D., Hu, H., Chu, M., Qu, Q., Tarrasch, J. T., Li, S., Sun Kobilka, T., Kobilka, B. K., and Skiniotis, G. (2017b). Cryo-EM structure of the activated GLP-1 receptor in complex with a G protein. *Nature*, 546:248–253.

[Zhao et al., 2020] Zhao, P., Liang, Y. L., Belousoff, M. J., Deganutti, G., Fletcher, M. M., Willard, F. S., Bell, M. G., Christe, M. E., Sloop, K. W., Inoue, A., Truong, T. T., Clydesdale, L., Furness, S. G., Christopoulos, A., Wang, M. W., Miller, L. J., Reynolds, C. A., Danev, R., Sexton, P. M., and Wootten, D. (2020). Activation of the GLP-1 receptor by a non-peptidic agonist. *Nature*, 577(7790):432–436.

[Zheng et al., 2018] Zheng, Y., Ley, S. H., and Hu, F. B. (2018). Global aetiology and epidemiology of type 2 diabetes mellitus and its complications. *Nature Reviews Endocrinology*, 14(2):88–98.

Appendix A

A.1 Optimisation of the Cisbio® insulin and glucagon assays

The optimisation of the insulin assay has been reported by Farino and colleagues [Farino et al., 2016]. In their report, they suggested various approaches that would lead to much higher HTRF final readings, which were to allow the antibodies to be incubated overnight at room temperature, as well as to maintain the pH of the diluent at 7.4. Therefore, their recommendations were incorporated into the assay protocol, while further optimising other experimental factors. Prior to optimising the protocol, the standard curves were first established to aid the interpolation of insulin and glucagon concentrations in test samples.

A.1.1 Establishing standard curves for the interpolation of insulin or glucagon concentrations

To establish the standard curves for the interpolation of insulin and glucagon concentrations in test samples, the manufacturer's instruction was followed and a range of concentrations of insulin (0.03 to 8 ng/ml) and glucagon (15.6 to 2000 pg/ml) were prepared using the insulin or glucagon stock of known concentrations provided with the kits. To dilute the insulin and glucagon stock, the Krebs Ringer Buffer (KRB; for formulation see Table 2.1.8.3) supplemented with 20mM HEPES and 0.1% (w/v) BSA at pH 7.4 in the absence of glucose was used as diluent instead of diluent #5 (formulation undisclosed by the manufacturer) provided with the kit. The reason for diluting the stock in KRB was due to the fact that KRB would be used throughout the pre-incubation and stimulation period, and that the supernatant, which was consisted of the insulin or glucagon secreted by the insulinoma and glucagonoma cells, would also be contained in the KRB diluent. After the preparation of a range of diluted insulin and glucagon concentrations according to the manufacturer's protocol, the diluted stocks were added

onto the 384-optiplate, followed by the addition of the antibodies mix at 1:1 ratio. The plate was sealed and incubated overnight at room temperature before being measured with the Mithras LB 940 multimode microplate reader, which filters were calibrated at 340nm excitation and 665nm and 620nm excitation.

After the measurement of the HTRF acceptor and donor emission signals for each well, the ratio of the acceptor over donor emission signals was calculated (Eq. 2.1) and subsequently the ΔF(%) (Eq. 2.2) was obtained, which reflected the signal to background of the assay as well as accounted for the day-to-day variability of the cells. The ΔF(%) was calculated by the subtraction of the ratio of the standards by the ratio of the negative control (which was represented by the blank well which contained diluent only), over the ratio of the negative control. Having obtained the ΔF(%) of each standard concentration, the standard curves were obtained by plots of ΔF(%) against the range of insulin or glucagon concentrations (Fig. A.1). The standard curves were fitted into the hyperbola model with the use of GraphPad Prism 8.3.4.

The standard curve of the insulin assay obtained after curve fitting resembled an exponential correlation between the ΔF(%) and the insulin concentrations, which agreed with the suggestion from the manufacturer. Similarly, the standard curve of the glucagon assay concurred with what has been suggested by the manufacturer, which was a linear relationship between the ΔF(%) and the glucagon concentrations. After establishing the standard curves to aid the quantitative measurements of insulin or glucagon levels in the test samples, the insulin and glucagon secretion protocols were further optimised.

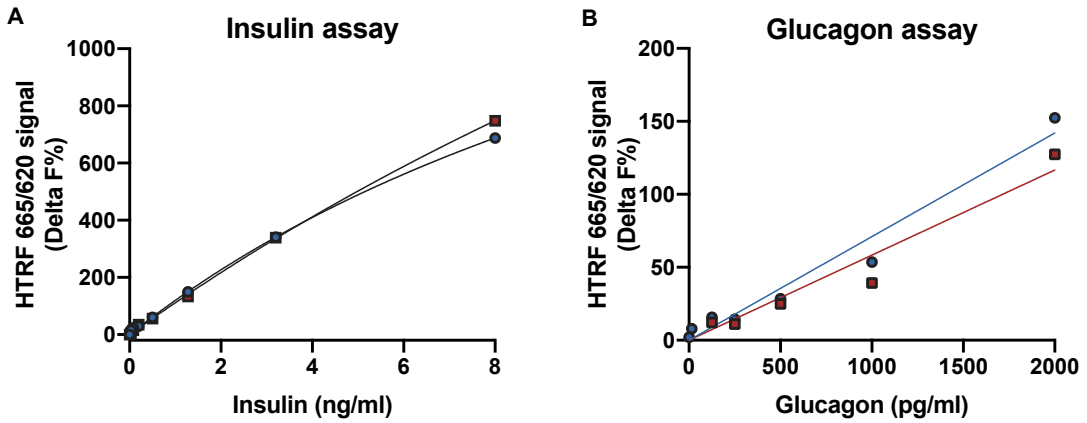

Figure A.1: **Standard curves for the interpolation of insulin and glucagon secretion levels in test samples.** (A) shows the standard curve used to interpolate the insulin concentration (ng/ml) in samples using the Cisbio® ultra-sensitive insulin kit whereas (B) shows the standard curve used to interpolate the glucagon concentration (pg/ml) in samples using the Cisbio® glucagon kit. ΔF(%) was first determined according to the equations 2.1 and 2.2 stated in section 2.2.4.2.4. ΔF(%) calculated were then plotted against a range of known insulin and glucagon concentrations in accordance to the manufacturer's protocols. KRB without any supplement of glucose were used as diluents in determining both standard curves. The graphs were fitted using the hyperbola function in GraphPad Prism 8.3.4 as recommended by the manufacturer.

A.1.2 Addition of the protease inhibitor aprotinin

Following the establishment of the standard curves for the interpolation of insulin or glucagon levels in test samples, the assay protocols were further optimised. In the subsequent optimisation of the insulin secretion assays, the rat INS-1 832/3 cells were solely utilised as the surrogate β cell model given the faster cell growth rate and the relative ease in culturing compared to the mouse MIN6-B1 cell line. The mouse αTC1.6 cell line will be used in the following glucagon secretion assays as the surrogate α cell model as this mouse α cell line was reported to be able to secrete a higher level of glucagon upon glucose stimulation compared to the hamster InR1G9 cell line [Powers et al., 1990].

Notably, a lot of published insulin secretion assay protocol included aprotinin [Patriti et al., 2007], which is a protease inhibitor, in their incubation buffer in order to avoid the breakdown of insulin or glucagon produced during the stimulation period. Therefore, the notion of adding aprotinin in the KRB was tested to deduce if it would indeed enhance the insulin measurement. 2.8mM and 16.7mM glucose concentrations were assigned to represent low and high glucose conditions respectively, as these two concentrations were widely used in other published reports utilising the INS-1 832/3 cell line to measure insulin secretion and that 16.7mM glucose has been shown to stimulate a strong GSIS response [Naylor et al., 2016]. An hour of low or high glucose stimulation period was allowed, which complied with other published protocols [Naylor et al., 2016]. Furthermore, the interpolated insulin level was normalised to the basal insulin level of the INS-1 832/3 cells when stimulated with low glucose, so as to facilitate simpler means in describing the changes in insulin levels between the basal insulin level and other high glucose containing conditions.

A marginal difference between the low and high glucose stimulation was observed in the absence of the protease inhibitor (Fig. A.2A), suggesting there might be a significant breakdown of insulin during the stimulation period with high glucose. However, in the presence of aprotinin in the stimulation buffer, a larger difference between the low and high glucose was resulted ($p < 0.05$), which implied the insulin secreted was prevented from the protease degradation by aprotinin. Furthermore, there was a stark difference when aprotinin was included in the stimulation buffer which contained 100nM GLP-1 compared to that without aprotinin (1.49-fold difference) (Fig. A.2A), illustrating the advantage of adding aprotinin into the stimulating buffer in aiding the final detectable insulin level.

A.1.3 Introducing glucose-starvation prior to high glucose challenge

Furthermore, as the rat INS-1 832/3 cells were incubated in 11mM glucose-containing RPMI media, a lot of published protocols suggested pre-incubating the INS-1 832/3 cells with low glucose buffer at least an hour prior to challenging with high glucose, so as to perform the so-called 'glucose-starvation' stage in the INS-1 832/3 cells, in an attempt to introduce a greater stimulation in insulin secretion [Maida et al., 2008, Lee and Jun, 2018, Peddibhotla et al., 2019]. Furthermore, the glucose starvation step was also found to be able to synchronise the cells across treatment, which ultimately reduced cell-to-cell variability in insulin secretion [Peddibhotla et al., 2019].

To test this phenomenon, the rat β cells were first incubated in glucose-absent RPMI media for 3 hours at 37°C humidified incubator with 5% CO_2, in order to increase cell viability after long period of low glucose incubation, prior to further pre-incubation with 2.8mM glucose containing KRB. INS-1 832/3 cells which were incubated in normal RPMI containing 11mM glucose were used as a control; aprotinin was not included in the stimulation buffer in order to observe the influence of low glucose pre-incubation on subsequent insulin secretion.

A stark difference was observed between the low glucose and high glucose stimulation in the glucose-starved INS-1 832/3 cells (1.24-fold increase), compared to the non-glucose-starved rat β cells (Fig. A.2B). In spite of the more statistically significant potentiation of GSIS mediated by GLP-1 under normal 11mM pre-incubation, insulinoma cells pre-incubated at 11mM glucose failed to respond to high glucose challenge, therefore their functionality responding to glucose challenge was questioned. Hence, to enhance the functionality of the insulinoma cells responding to glucose stimuli, 0mM glucose pre-incubation was adopted in the subsequent insulin assay protocol. Given the similarity between the working principles of the insulin and glucagon assays, these optimisations were also introduced into the glucagon secretion assay protocol. However, as the mouse αTC1.6 cells were cultured long-term in 25mM-glucose containing media, and that the presence of high glucose was needed to maintain its basal glucagon secretion, additional glucose-starving step was not performed in the αTC1.6 cells.

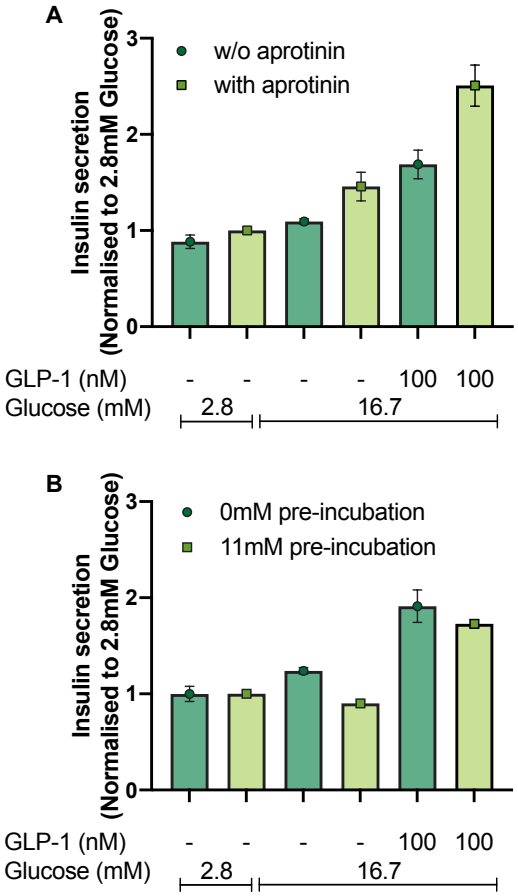

Figure A.2: **The optimisation of the Cisbio® ultra-sensitive insulin secretion kit.** (A) shows the insulin levels are higher in samples with the addition of protease inhibitor aprotinin compared to those without (w/o) aprotinin. (B) shows that pre-incubating INS-1 832/3 cells with 0mM glucose RPMI media 3 hours before assays leads to a prominent difference in insulin levels between low glucose and high glucose stimulation. These optimisations are adopted thereafter in the insulin secretion assay protocol, as well as the glucagon secretion assay, given the similarity between the principles of the Cisbio® ultra-sensitive insulin secretion and the glucagon secretion assays. Mean $\pm$ S.E.M. insulin secretion data (responses normalised to the GSIS responses at 2.8mM glucose) in an independent experiment with quadruplicates are shown in the above scatter plots.

A.1.4 Inclusion of DPP-IV enzyme inhibitor in the stimulation buffer

Following the elucidation of the beneficial effect of including protease inhibitor in the stimulation buffer and the implementation of glucose starvation on GSIS, the effect of the addition of DPP-IV inhibitor into the stimulation buffer on insulin secretion was investigated. GLP-1 and GIP are known to be metabolised rapidly by the endogenous DPP-IV enzymes, resulting in the widely abundant N-terminally truncated GLP-1(9-36)NH_2 and GIP(3-42) metabolites [Deacon, 2004, Deacon, 2019]. To circumvent these breakdown, DPP-IV inhibitors are developed which prevent the rapid breakdown of GLP-1 and GIP, thereby acting as a T2DM therapeutic treatment. Furthermore, the INS-1 832/3 cells have been shown to possess a high level of DPP-IV activity [Liu et al., 2014]. Therefore, it is of particular interest to test if the inclusion of a DPP-IV inhibitor in the stimulation buffer could further improve insulin measurements in the INS-1 832/3 cells. Sitagliptin at 100nM [Liu et al., 2014], which is one of the DPP-IV inhibitors that is widely used in T2DM treatment, was added to the stimulation buffer. The rat β cells were stimulated with GLP-1 at 100nM with or without sitagliptin and the insulin levels were measured.

Again, a prominent difference in insulin secretion was observed when GLP-1 at 100nM was applied to the rat β cells (1.54-fold increase; Fig. A.3). The introduction of 100nM sitagliptin together with 100nM GLP-1 resulted in a nearly doubling in GSIS when compared to the application of GLP-1 alone, suggesting the protective effect of the DPP-IV inhibitor prevented GLP-1 from being broken down by the DPP-IV enzymes expressed in the INS-1 832/3 cells and that the insulin level measurement in the presence of sitagliptin represented the true effect of the potentiation of GSIS mediated by GLP-1. Moreover, the application of sitagliptin alone did not enhance GSIS, implying sitagliptin did not stimulate insulin secretion on its own. Furthermore, it also suggested that the augmentation in insulin secretion observed previously in the presence of sitagliptin was mainly due to GLP-1 stimulation in the presence of high glucose. The results here concurred with the studies by Liu and colleagues, which they also showed an enhanced insulin secretion mediated by GLP-1 in the presence of 100nM vildagliptin, which is a DPP-IV inhibitor that is currently in clinically use [Liu et al., 2014]. Knowing that the addition of DPP-IV inhibitor in the stimulation buffer further enhanced insulin secretion in INS-1 832/3 cells as well as allowed the detection of the true effect of GLP-1-facilitated GSIS, 100nM sitagliptin was thereafter included in the KRB stimulation buffer.

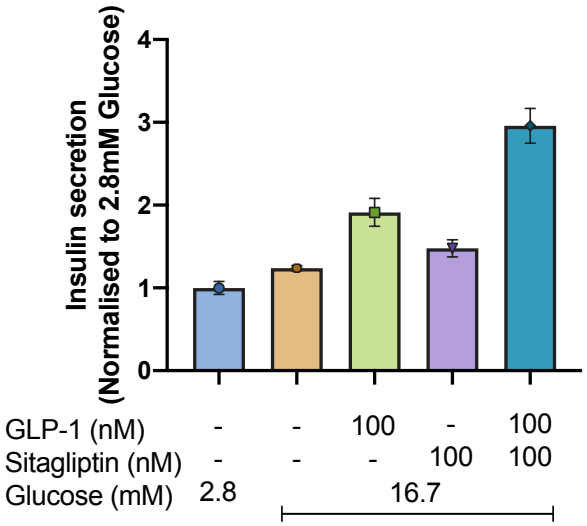

Figure A.3: **The presence of the DPP-IV inhibitor sitagliptin further enhances GLP-1 mediated GSIS in INS-1 832/3 WT cells.** The insulin levels measured are higher when INS-1 832/3 WT cells are stimulated with GLP-1 in the presence of 100nM sitagliptin than that without sitagliptin. The presence of sitagliptin alone does not enhance GSIS. Mean $\pm$ S.E.M. insulin secretion data (responses normalised to the GSIS responses at 2.8mM glucose) in an independent experiment with quadruplicates are shown in the above scatter plots.

Appendix B

B.1 Compound 249 enhances OXM-mediated cAMP response in CHO-GLP-1R cells

The following results (Fig. B.1 and B.2) were originally reported in my MPhil thesis. cAMP functional assays were conducted during which the CHO-GLP-1R cells were co-stimulated with both compound 249 at fixed concentrations together with a range of concentrations of GLP-1, OXM or GCG in the presence of the PDE inhibitor rolipram for 15 mins. Compound 249 displayed enhancement of the OXM-mediated cAMP response (pEC_{50} values increased from 7.92 $\pm$ 0.06 to 8.71 $\pm$ 0.07, $p < 0.0001$) (Fig. B.1, B.2, Table B.2). Further application of the operational model of allosterism resulted in a positive cooperativity value ($\log\alpha\beta$) of 1.04, implying the positive allosteric modulation exhibited by compound 249. Compound 249 did not potentiation GLP-1 nor GCG-mediated cAMP responses, compared to the robust augmentation of cAMP responses mediated across all peptide agonists exhibited by compound 2 and BETP (Fig. B.1, B.2, Table B.1 and B.3).

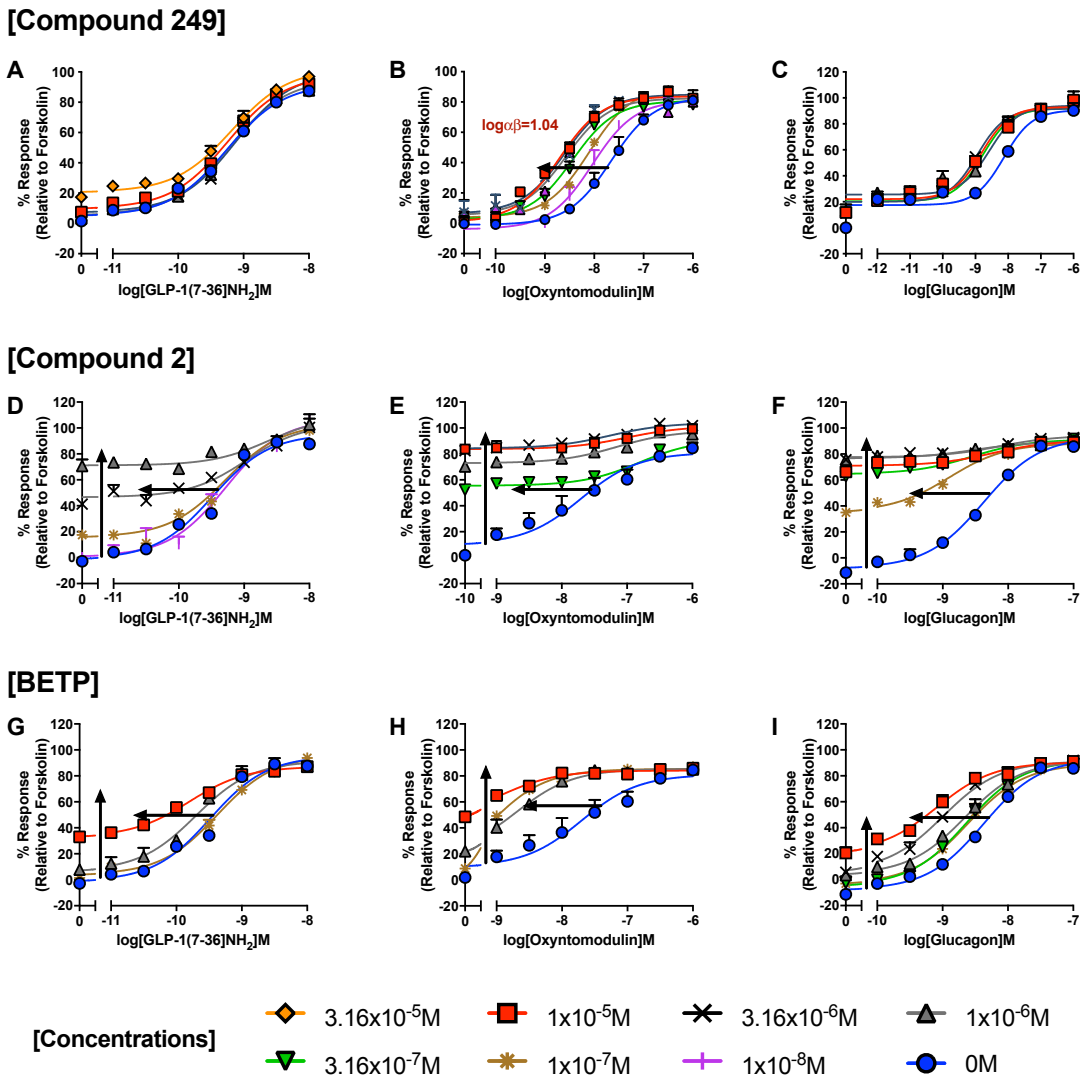

Figure B.1: **Compound 249 only induces a concentration-dependent positive allosteric modulation on OXM-mediated cAMP accumulation response in CHO-GLP-1R cells.** Compound 249 (A to C) only exhibits a concentration-dependent positive allosteric modulation on OXM-mediated cAMP accumulation response, as shown in panel B. Compound 2 (D to F) and BETP (G to I) are able to mediate positive allosteric modulation on GLP-1, OXM and GCG-mediated cAMP accumulation respectively. 500 CHO-GLP-1R cells/well under 15-minute co-stimulation with peptide ligands in the presence of rolipram were used in the cAMP assays. All data were normalised to the maximum cAMP response determined by 100μM forskolin stimulation. All data are means from 2 to 5 independent experiments with duplicates $\pm$ S.E.M (upper error bars).

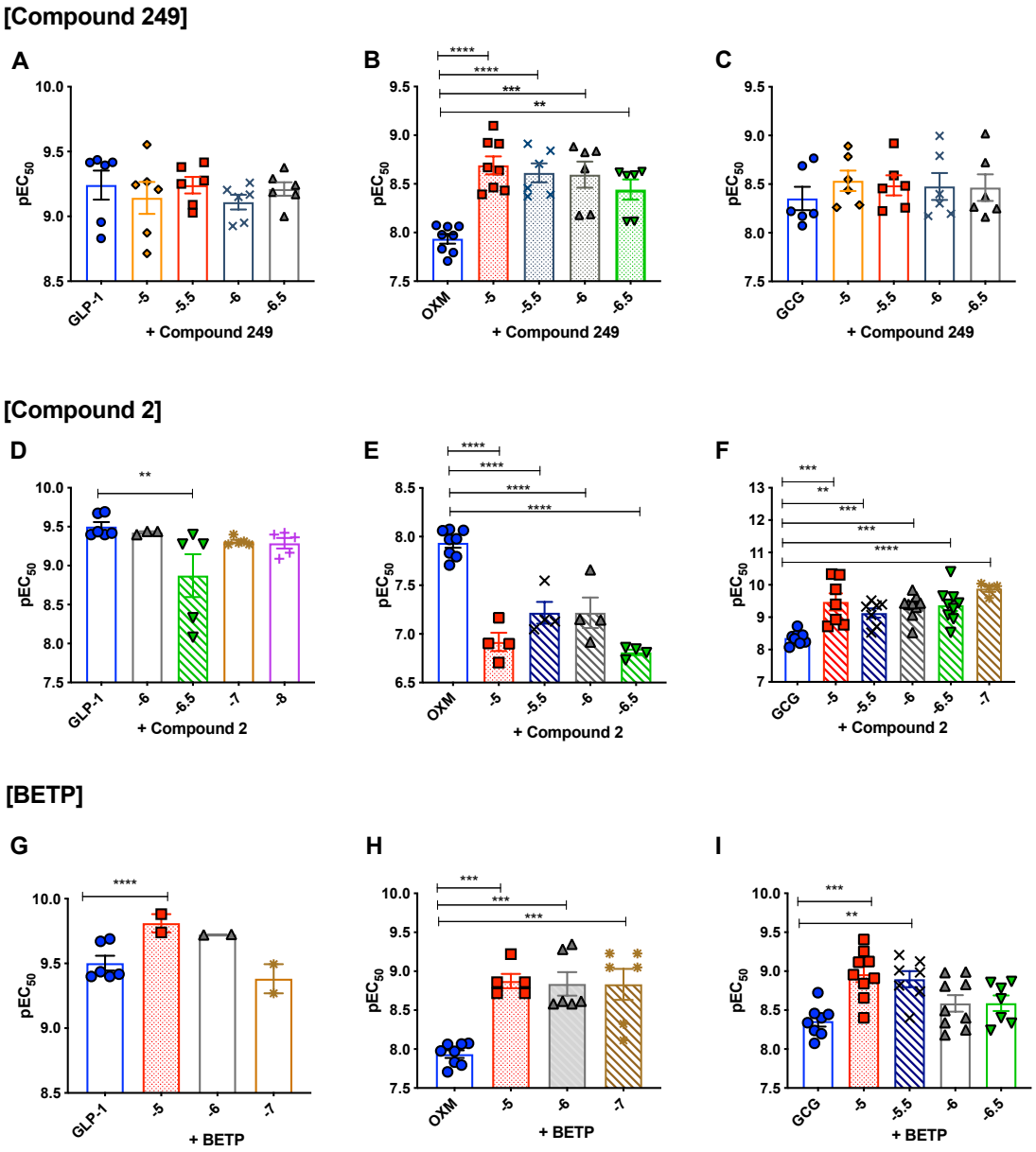

Figure B.2: **Scatter plots illustrating compound 249 only induces a concentration-dependent positive allosteric modulation on OXM-mediated cAMP accumulation response in CHO-GLP-1R cells.** Compound 249 only exhibits a concentration-dependent positive allosteric modulation on OXM-mediated cAMP accumulation response (A to C). Panel D to I showed the allosteric modulation of compound 2 and BETP on GLP-1, OXM and GCG-mediated cAMP accumulation. 500 CHO-GLP-1R cells/well under 15-minute co-stimulation with peptide ligands in the presence of rolipram were used in the cAMP assays. All data were normalised to the maximum cAMP response determined by 100μM forskolin stimulation. All data are means from 2 to 5 independent experiments with duplicates $\pm$ S.E.M (upper error bars). Statistical significance compared with GLP-1(7-36)NH_2, OXM and GCG (*, $p < 0.05$; **, $p < 0.01$; ***, $p < 0.001$; ****, $p < 0.0001$) for compound 249, Compound 2 and BETP was determined by one-way ANOVA with post-hoc Dunnett's multiple comparisons.

Appendix B.

Table B.1: **Concentration-dependent allosteric modulation of GLP-1(7-36)NH_2-mediated cAMP accumulation potentiated by Compound 2 and BETP but not compound 249 in CHO-GLP-1R cells.**

Ligand	Compound	Concentration	pEC_{50} [a]	E_{max} [b]	E_{min} [c]	Span	n
GLP-1	DMSO	-	9.46±0.05	93.14±1.95	1.06±1.44	87.21±3.99	10
	Compound 249	**3.16x10^{-5}M**	9.18±0.07	102.10±2.81	20.72±1.5	81.42±2.83	6
		1x10^{-5}M	9.24±0.04	98.01±1.92	9.86±1.1	88.14±1.97	6
		3.16x10^{-6}M	9.12±0.05	100.32±2.73	7.41±1.4	92.94±2.76	6
		1x10^{-6}M	9.22±0.05	95.31±2.12	5.65±1.2	89.65±2.23	6
	Compound 2	**1x10^{-6}M**	10.1±0.6**	109.1±4.9	72.2±2.9*	37.89±7.99	4
		3.16x10^{-7}M	9.68±0.3*	103.4±5.7	50.0±3.5^{ns}	56.77±5.35	4
		1x10^{-7}M	9.67±0.1*	103.3±3.1	19.9±2.5*	87.40±2.60	4
		1x10^{-8}M	9.75±0.2*	107.1±6.3	5.26±4.9^{ns}	106.14±7.51	4
	BETP	**1x10^{-5}M**	9.81±0.06*	87.2±1.29	33.04±1.3****	54.12±1.70	4
		1x10^{-6}M	9.71±0.09^{ns}	91.5±3.0	6.81±2.8^{ns}	84.73±3.68	4
		1x10^{-7}M	9.38±0.06^{ns}	95.9±2.7	3.86±1.8^{ns}	92.05±2.88	4

Values were generated when the data were fitted to the three-parameter logistic equation. Means ± S.E.M of n individual result sets were shown.

[a] Negative logarithm of agonist concentration when reaching half maximal response.

[b] % of maximal response observed when stimulated with ligands relative to forskolin.

[c] % of minimal response observed when stimulated with ligands relative to forskolin.

Statistical significance compared with GLP-1(7-36)NH_2 (*, $p < 0.05$; **, $p < 0.01$; ***, $p < 0.001$; ****, $p < 0.0001$ ns, non-statistically significant) for compound 249, Compound 2 and BETP was determined by one-way ANOVA with post-hoc Dunnett's multiple comparisons.

B.1. Compound 249 enhances OXM-mediated cAMP response in CHO-GLP-1R cells

Table B.2: **Concentration-dependent allosteric modulation of OXM-mediated cAMP accumulation potentiated by Compound 2 and BETP but not compound 249 in CHO-GLP-1R cells.**

Ligand	Compound	Concentration	pEC_{50} [a]	E_{max} [b]	E_{min} [c]	Span	n
OXM	DMSO	-	7.92±0.06	82.53±1.88	10.30±1.65	85.83±2.40	10
	Compound 249	**1x10^{-5}M**	8.71±0.07****	83.79±2.08	1.63±2.68	82.17±3.18	8
		3.16x10^{-6}M	8.60±0.10****	84.97±2.65	6.84±3.13	78.14±3.80	6
		1x10^{-6}M	8.57±0.12**	82.49±3.63	5.65±3.80	76.85±4.89	6
		3.16x10^{-7}M	8.44±0.08**	80.79±2.28	2.86±2.83	77.94±3.36	6
	Compound 2	**1x10^{-5}M**	7.88±0.097^{ns}	101.4±3.9	83.8±2.2****	17.66±3.98	4
		3.16x10^{-6}M	7.00±0.40^{ns}	104.0±2.5	84.4±1.6****	19.64±2.67	4
		1x10^{-6}M	7.26±0.3^{ns}	97.9±2.4	72.9±1.3****	24.99±2.49	4
		3.16x10^{-7}M	6.81±0.4^{ns}	91.18±2.6	55.52±0.89****	35.66±2.57	4
	BETP	**1x10^{-5}M**	7.95±0.1^{ns}	84.14±0.9	45.71±2.6****	38.43±2.65	6
		1x10^{-6}M	7.70±0.07^{ns}	85.48±1.3	18.51±2.8^{ns}	66.97±2.90	6
		1x10^{-7}M	7.13±0.06^{ns}	85.47±1.0	1.43±3.5^{ns}	86.89±3.47	6

Values were generated when the data were fitted to the three-parameter logistic equation. Means ± S.E.M of n individual result sets were shown.

[a] Negative logarithm of agonist concentration when reaching half maximal response.

[b] % of maximal response observed when stimulated with ligands relative to forskolin.

[c] % of minimal response observed when stimulated with ligands relative to forskolin.

Statistical significance compared with OXM (*, $p < 0.05$; **, $p < 0.01$; ***, $p < 0.001$; ****, $p < 0.0001$ ns, non-statistically significant) for compound 249, Compound 2 and BETP was determined by one-way ANOVA with post-hoc Dunnett's multiple comparisons.

Table B.3: **Concentration-dependent allosteric modulation of GCG-mediated cAMP accumulation potentiated by Compound 2 and BETP but not compound 249 in CHO-GLP-1R cells.**

Ligand	Compound	Concentration	pEC_{50} [a]	E_{max} [b]	E_{min} [c]	Span	n
GCG	DMSO	-	8.32±0.05	95.18±2.65	5.96±1.7	87.69±2.82	8
	Compound 249	**3.16x10^{-5}M**	8.56±0.06	98.83±1.7	21.26±1.8	79.34±2.45	6
		1x10^{-5}M	8.52±0.07	93.25±2.2	13.01±2.4	81.74±3.23	6
		3.16x10^{-6}M	8.50±0.06	91.87±2.0	9.04±2.0	84.71±2.86	6
		1x10^{-6}M	8.49±0.06	90.61±1.8	7.50±1.9	85.42±2.59	6
	Compound 2	**1x10^{-5}M**	8.43±0.30^{ns}	90.47±3.1	71.02±1.8****	19.45±3.44	6
		3.16x10^{-6}M	8.23±0.27^{ns}	94.28±2.4	77.63±1.3****	19.45±3.22	6
		1x10^{-6}M	8.13±0.32^{ns}	89.51±1.9	76.75±1.4****	12.76±2.09	6
		3.16x10^{-7}M	8.53±0.20^{ns}	91.27±2.4	64.75±2.1****	26.51±2.84	6
		1x10^{-7}M	8.56±0.13^{ns}	88.35±2.6	35.57±2.9****	52.79±3.57	4
	BETP	**1x10^{-5}M**	9.15±0.12***	90.18±3.1	16.63±4.4****	69.70±3.85	6
		3.16x10^{-6}M	8.99±0.08**	91.35±2.5	6.44±3.1**	84.90±3.58	6
		1x10^{-6}M	8.73±0.08^{ns}	90.70±3.1	-1.18±3.0^{ns}	88.02±3.36	6
		3.16x10^{-7}M	8.63±0.07^{ns}	92.25±2.7	-4.64±2.3^{ns}	96.89±3.24	6
		1x10^{-7}M	8.81±0.07^{ns}	89.75±2.8	-11.77±2.9^{ns}	92.48±4.18	4

Values were generated when the data were fitted to the three-parameter logistic equation. Means ± S.E.M of n individual result sets were shown.

[a] Negative logarithm of agonist concentration when reaching half maximal response.

[b] % of maximal response observed when stimulated with ligands relative to forskolin.

[c] % of minimal response observed when stimulated with ligands relative to forskolin.

Statistical significance compared with GCG (*, $p < 0.05$; **, $p < 0.01$; ***, $p < 0.001$; ****, $p < 0.0001$ ns, non-statistically significant) for compound 249, Compound 2 and BETP was determined by one-way ANOVA with post-hoc Dunnett's multiple comparisons.

B.2 Screening results of VU0453379-derived small molecules

VU0453379 is a selective GLP-1R PAM which is penetrable to the central nervous system (CNS) [Morris et al., 2014]. Given its uniqueness in being a CNS penetrant, which can be potentially used as novel treatment for Parkinson's disease as GLP-1 has been shown to be able to improve cognitive function [Drucker, 2018], a series of VU0453379-derived analogues were designed (Fig. B.3) by our collaborator, Dr Taufiq Rahman (Department of Pharmacology, University of Cambridge). However, none of these 26 analogues appeared to have intrinsic agonism towards GLP-1R (Fig. B.4). Furthermore, they did not illustrate potentiation towards GLP-1 (Fig. B.5 and B.6) nor its close homologue, Ex-4 (Fig. B.7) mediated cAMP responses. Therefore, further pharmacological validation of this set of analogues was not pursued.

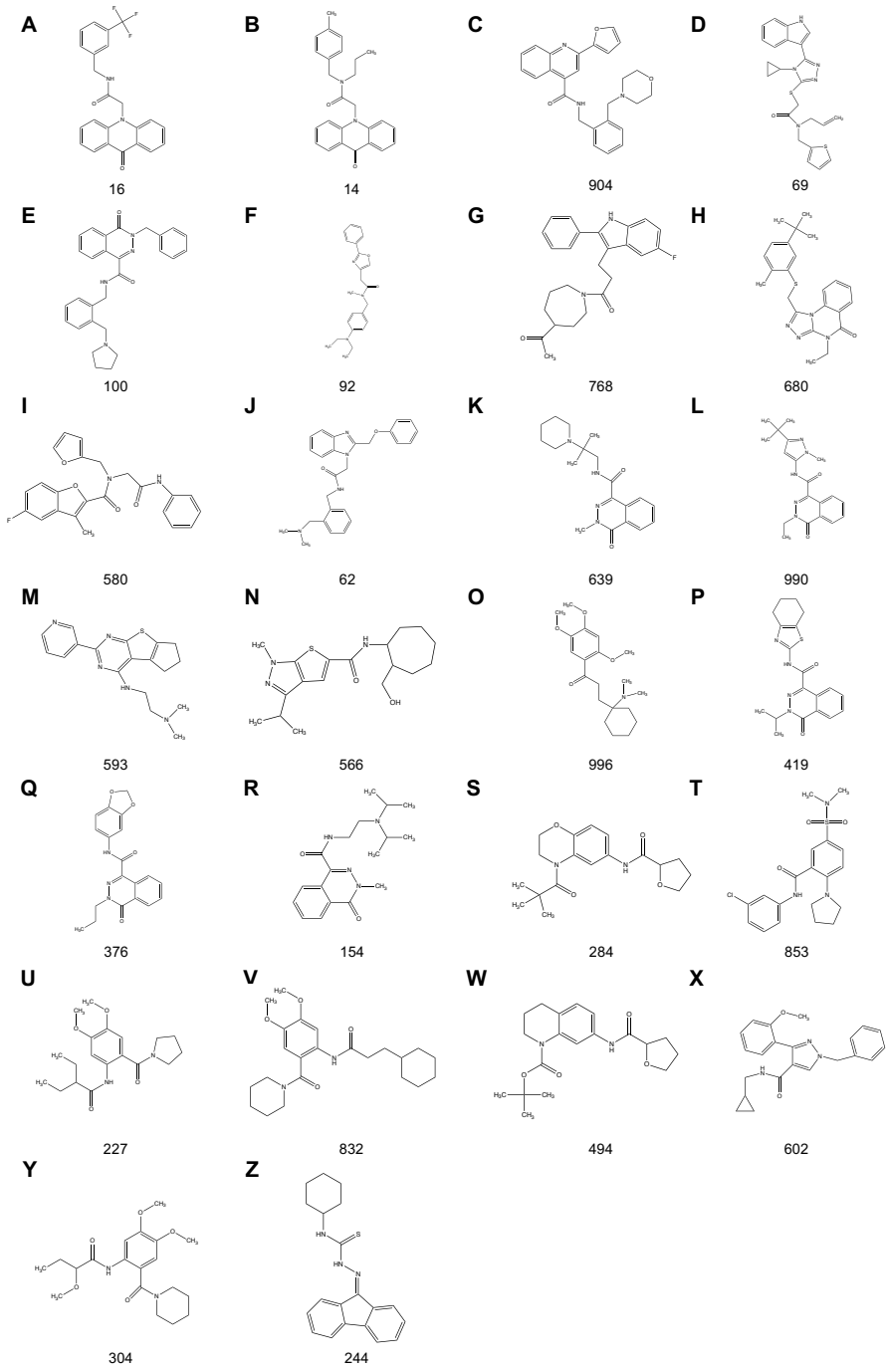

Figure B.3: **Structures of VU0453379-based small molecules.** Panel A to Z show the 2D structures of small molecule candidates based on the structures of the GLP-1R PAM VU0453379 [Morris et al., 2014]. These small molecules were designed by Dr. Taufiq Rahman using ligand-based virtual screening approach.

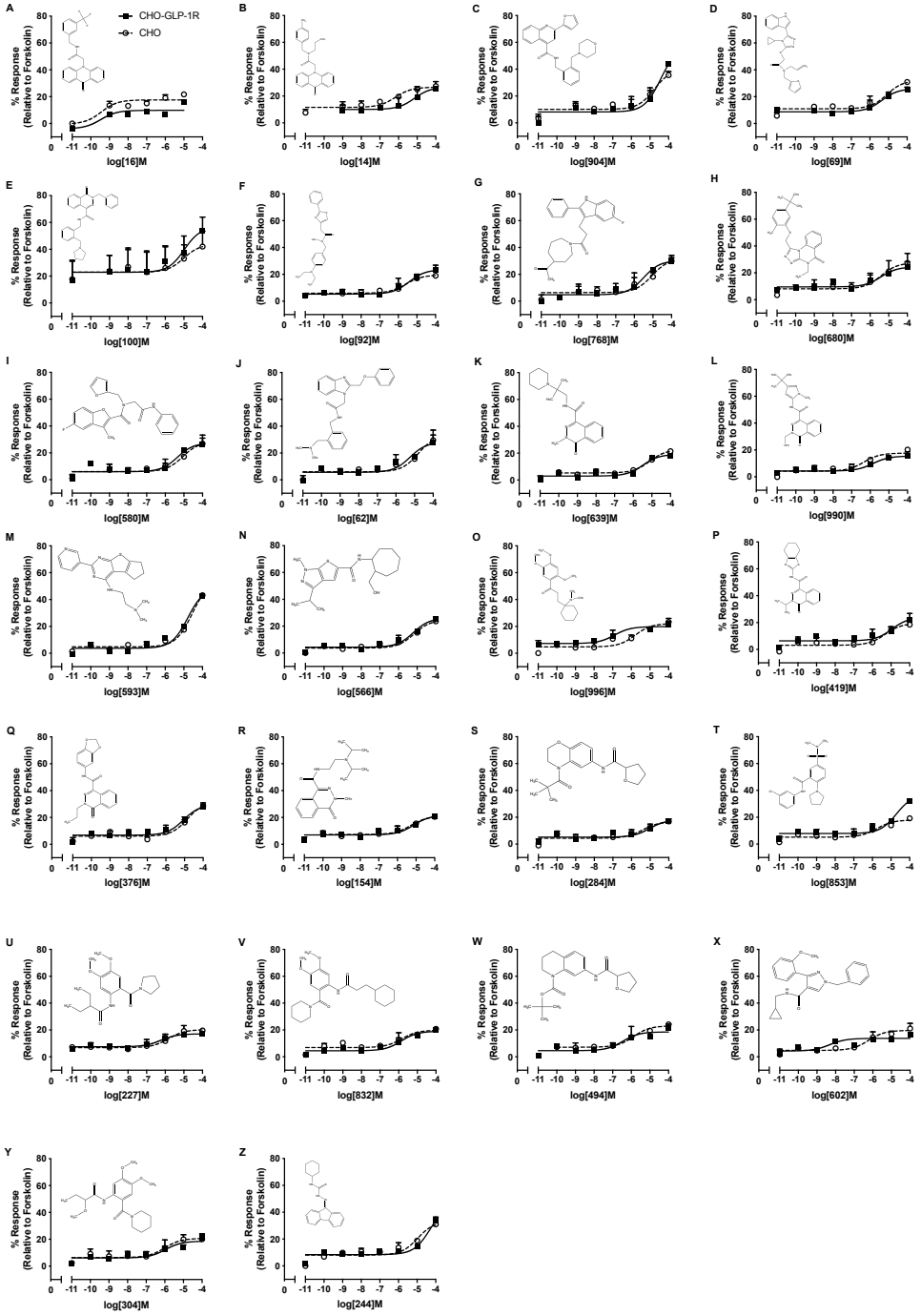

Figure B.4: **Compound agonistic activity screening of VU-0453379 analogues in CHO-GLP-1R cells.** Panel A to Z show that the VU-0453379-based small molecules do not demonstrate GLP-1R agonism in CHO-GLP-1R cells. 500 CHO-GLP-1R cells/well under 15-minute stimulation with the VU-0453379 analogues in the presence of rolipram were used in the cAMP assays. All data were normalised to the maximum cAMP response determined by 100μM forskolin stimulation. All data are means from at least 3 independent experiments with duplicates $\pm$ S.E.M (upper error bars).

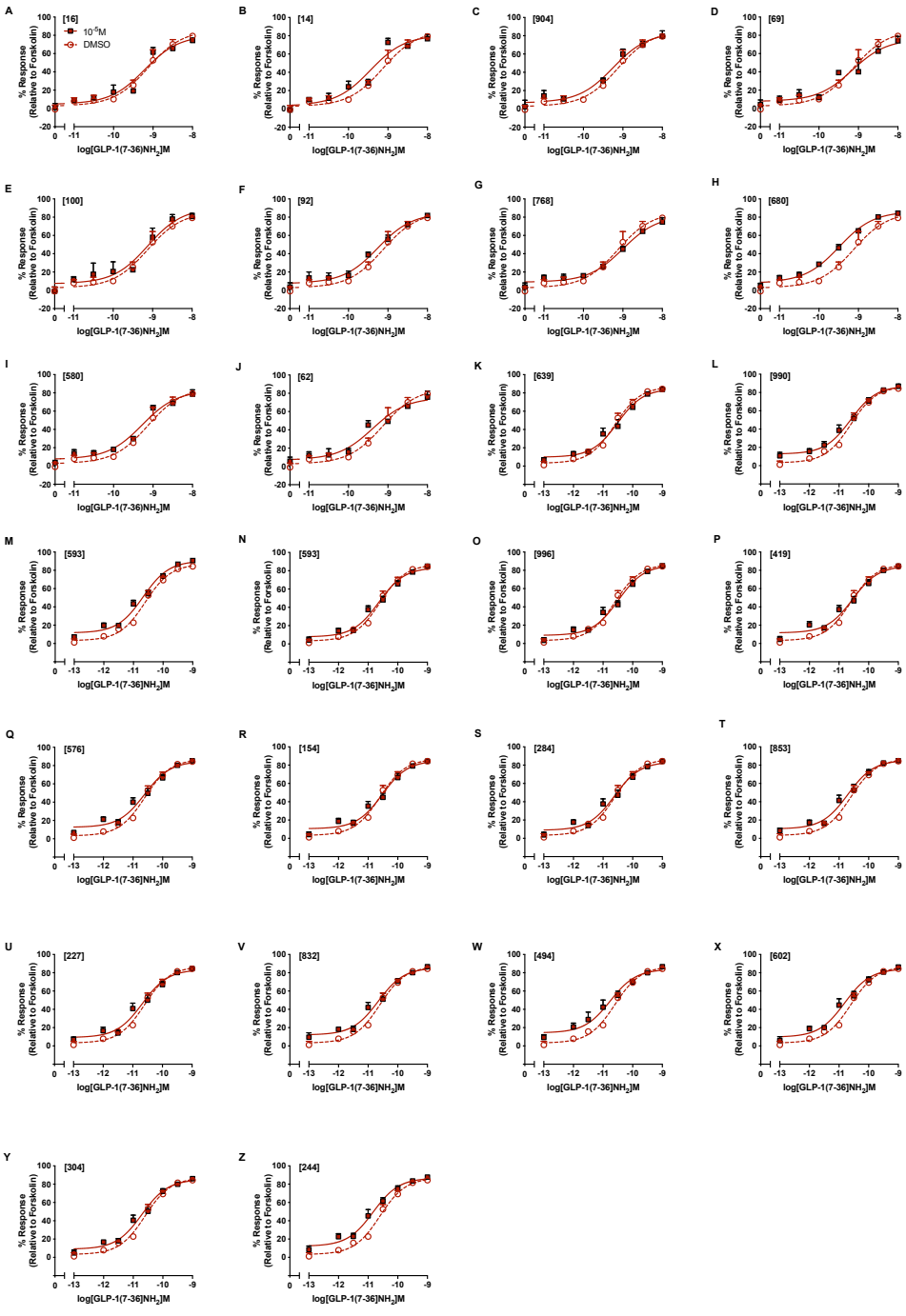

Figure B.5: **Compound allosteric activity screening of VU-0453379 analogues in CHO-GLP-1R cells.** Panel A to Z show that these small molecule compounds based on the structure of VU-0453379 do not exhibit allosteric of GLP-1-mediated allosteric effect in CHO-GLP-1R cells. 500 CHO-GLP-1R cells/well under 15-minute co-stimulation with peptide ligands in the presence of rolipram were used in the cAMP assays. All data were normalised to the maximum cAMP response determined by 100μM forskolin stimulation. All data are means from at least 3 independent experiments with duplicates $\pm$ S.E.M (upper error bars).

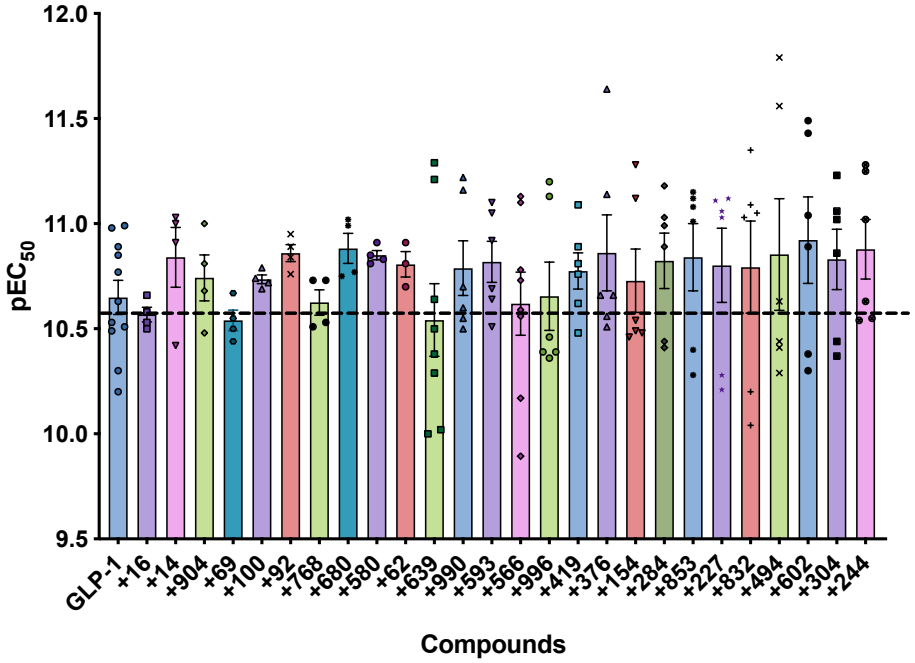

Figure B.6: **Scatter plot summarising compound allosteric activity screening of VU-0453379 analogues in CHO-GLP-1R cells.** The above scatter plot shows that these small molecule compounds based on the structure of VU-0453379 do not exhibit GLP-1-mediated allosteric effect in CHO-GLP-1R cells. 500 CHO-GLP-1R cells/well under 15-minute co-stimulation with GLP-1 in the presence of rolipram were used in the cAMP assays. All data were normalised to the maximum cAMP response determined by 100μM forskolin stimulation. All data are means from at least 3 independent experiments with duplicates $\pm$ S.E.M (upper error bars).

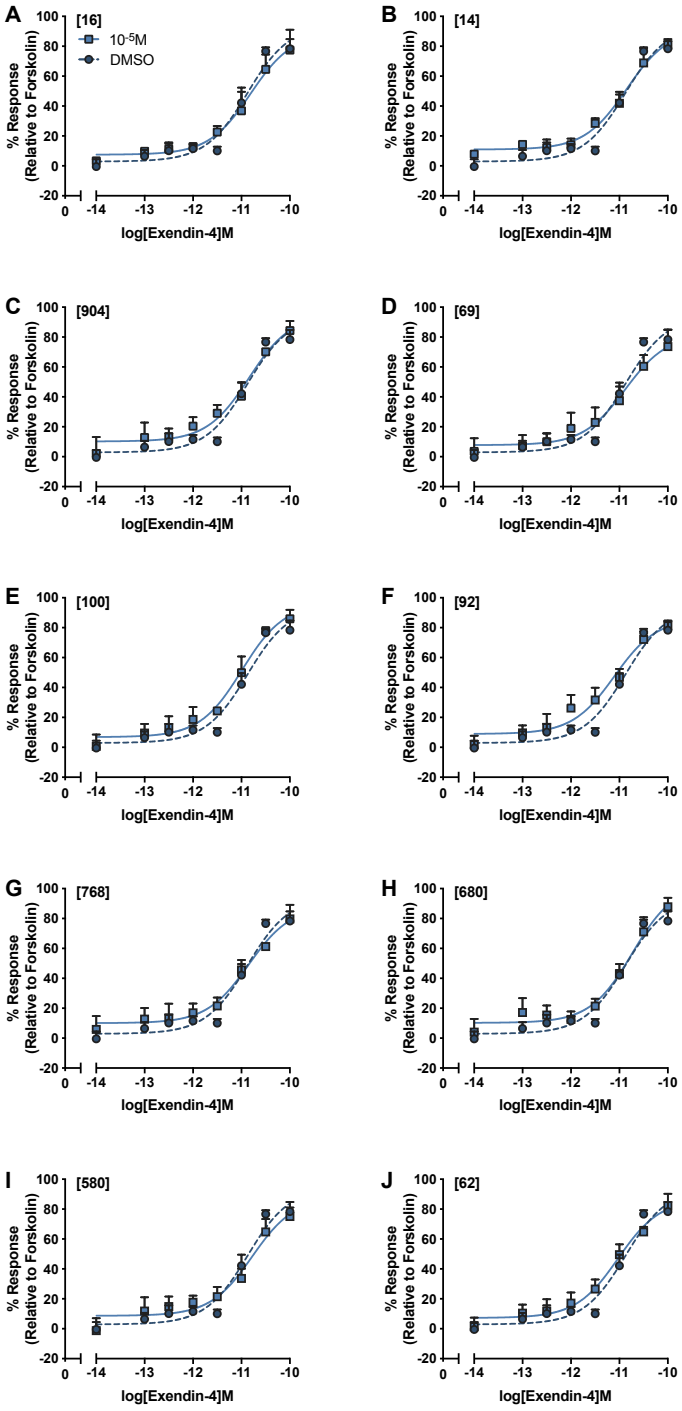

Figure B.7: **Compound allosteric activity screening of VU-0453379 analogues in CHO-GLP-1R cells.** Panel A to J show that these small molecule compounds based on the structure of VU-0453379 do not exhibit allosteric of Ex-4-mediated allosteric effect in CHO-GLP-1R cells. 500 CHO-GLP-1R cells/well under 15-minute co-stimulation with Ex-4 in the presence of rolipram were used in the cAMP assays. All data were normalised to the maximum cAMP response determined by 100μM forskolin stimulation. All data are means from at least 3 independent experiments with duplicates $\pm$ S.E.M (upper error bars).

B.3 Screening results of GLP-1-based small molecules

In an attempt to identify small molecule GLP-1R agonists that can be developed as novel T2DM treatment, a set of compounds were designed to mimic the points of interaction of GLP-1 at the ECD of GLP-1R (Fig. B.8). These compounds were identified with structure-based virtual screening and were conducted by Dr Taufiq Rahman (Department of Pharmacology, University of Cambridge).

The compounds were tested using the cAMP accumulation assay in both CHO-GLP-1R and untransfected CHO-K1 cells in an attempt to identify any intrinsic agonism at the GLP-1R. Both cell lines were stimulated with fixed concentrations of compounds (all at the highest concentrations 100μM) in the presence of PDE inhibitor rolipram for 15 mins. Most of the compounds reported here did not demonstrate intrinsic GLP-1R agonism (Fig. B.9). Furthermore, compound 141 demonstrated potential cell toxicity as it induced a significant decrease in cAMP production in both CHO-GLP-1R and untransfected CHO-K1 cell lines.

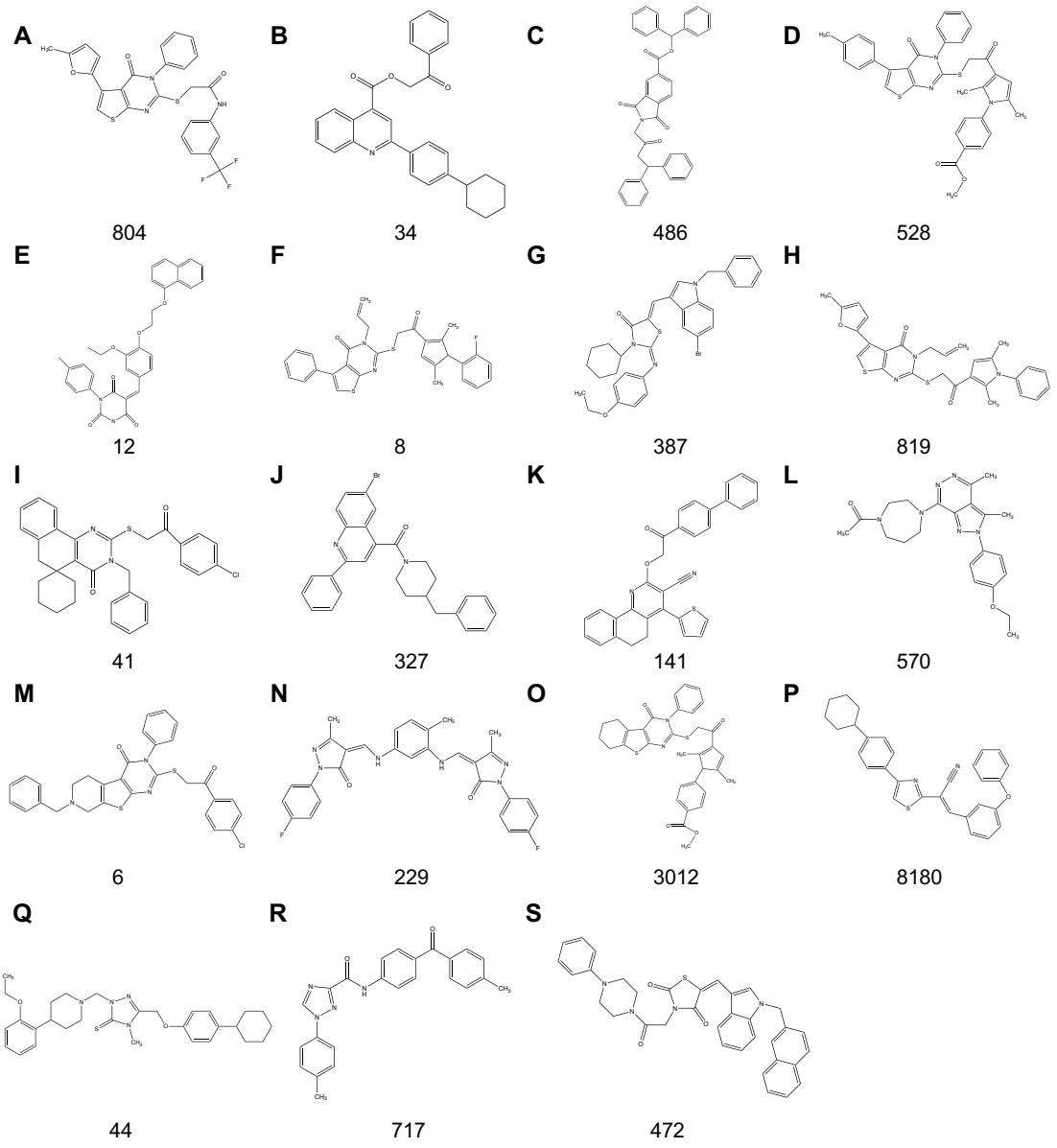

Figure B.8: **Structures of potential GLP-1R agonist small molecule compounds.** Panel A to S show the 2D structures of small molecule candidates that are designed to mimic the contact point of GLP-1 to the ECD. These small molecules were designed by Dr. Taufiq Rahman using virtual screening approach.

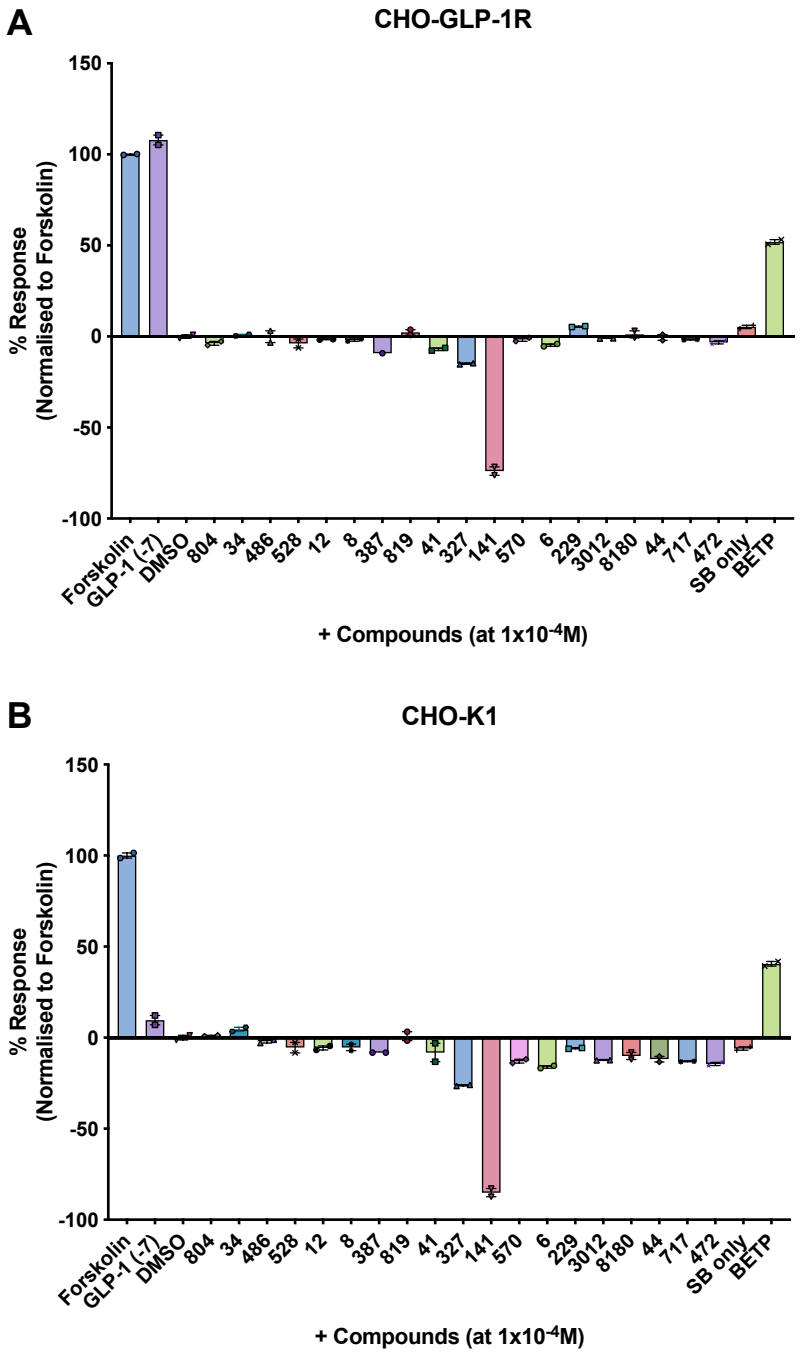

Figure B.9: **Scatter plot summarising compound agonistic activity point screening in CHO-GLP-1R and untransfected CHO-K1 cells.** The above scatter plots representing point screening in (A) CHO-GLP-1R cells and (B) CHO-K1 cells. It shows that most of the drug candidates do not exhibit GLP-1R agonism. 500 CHO-GLP-1R or CHO-K1 cells/well under 15-minute co-stimulation with peptide ligands in the presence of rolipram were used in the cAMP assays. All data were normalised to the maximum cAMP response determined by 100μM forskolin stimulation. All data are means from one independent experiments with duplicates $\pm$ S.E.M (upper error bars).

B.4 Determination of allosteric modulation of compound 249 analogues

The same cAMP functional assays for identifying potential GLP-1R and GCGR allosteric modulators were performed in the CHO-GLP-1R and CHO-GCGR cells. The cells were co-stimulated with fixed concentrations of analogues and a range of concentrations of OXM and GCG. Intriguingly, unlike compound 249, all three compound 249 analogues did not show any allosteric activities on OXM-mediated cAMP responses at GLP-1R (Fig. B.10 and B.11). Yet, similar to compound 249, the three analogues also did not potentiate GCG-mediated cAMP responses.

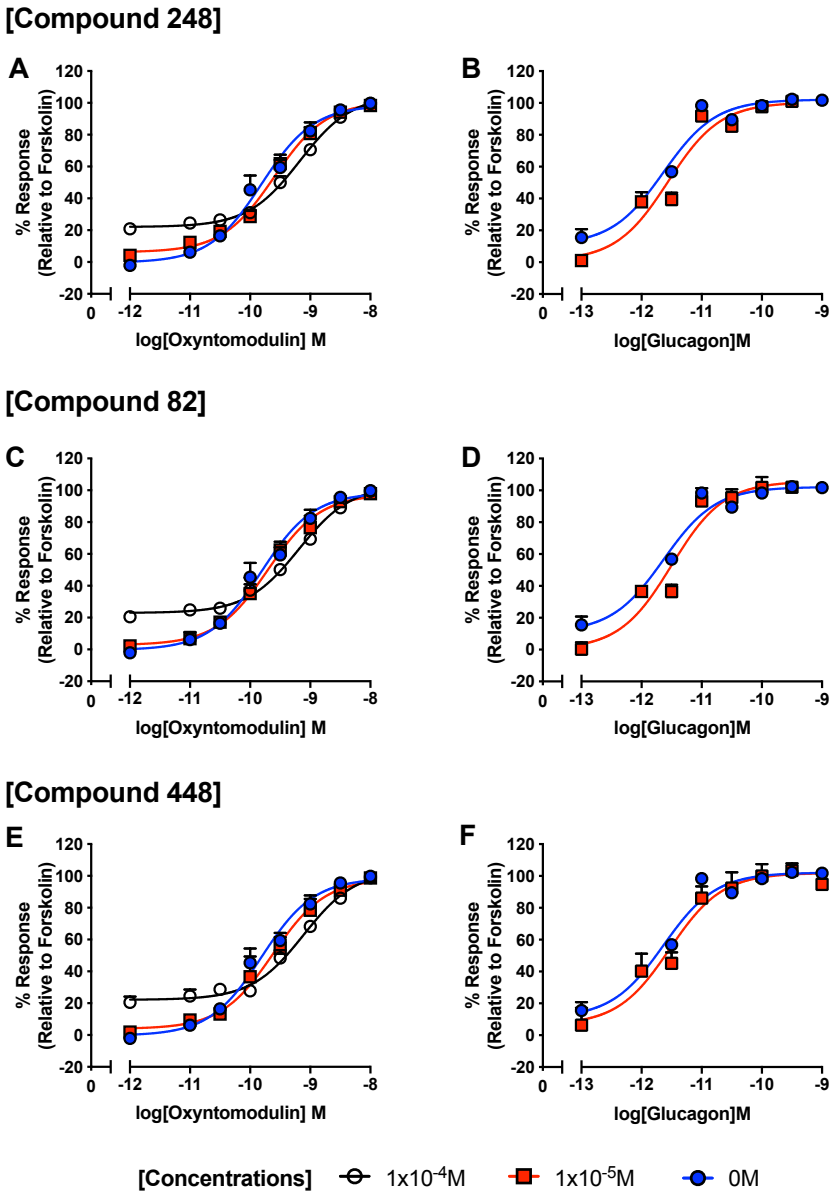

Figure B.10: **Analogues of compound 249 do not induce allosteric modulation on OXM or GCG-mediated cAMP accumulation in CHO-GLP-1R cells.** Panel A, C and E show that compound 248, 82 and 448 do not potentiate OXM-mediated cAMP accumulation even when high concentration at 10^{-4}M was applied to the CHO-GLP-1R cells. Similarly, panels B, D, and F show that these analogues are not allosteric modulators on GCG-mediated cAMP accumulation. 500 CHO-GLP-1R cells/well under 15-minute co-stimulation with peptide ligands in the presence of rolipram were used in the cAMP assays. All data were normalised to the maximum cAMP response determined by 100μM forskolin stimulation. All data are means from at least 2 independent experiments with duplicates $\pm$ S.E.M (upper error bars).

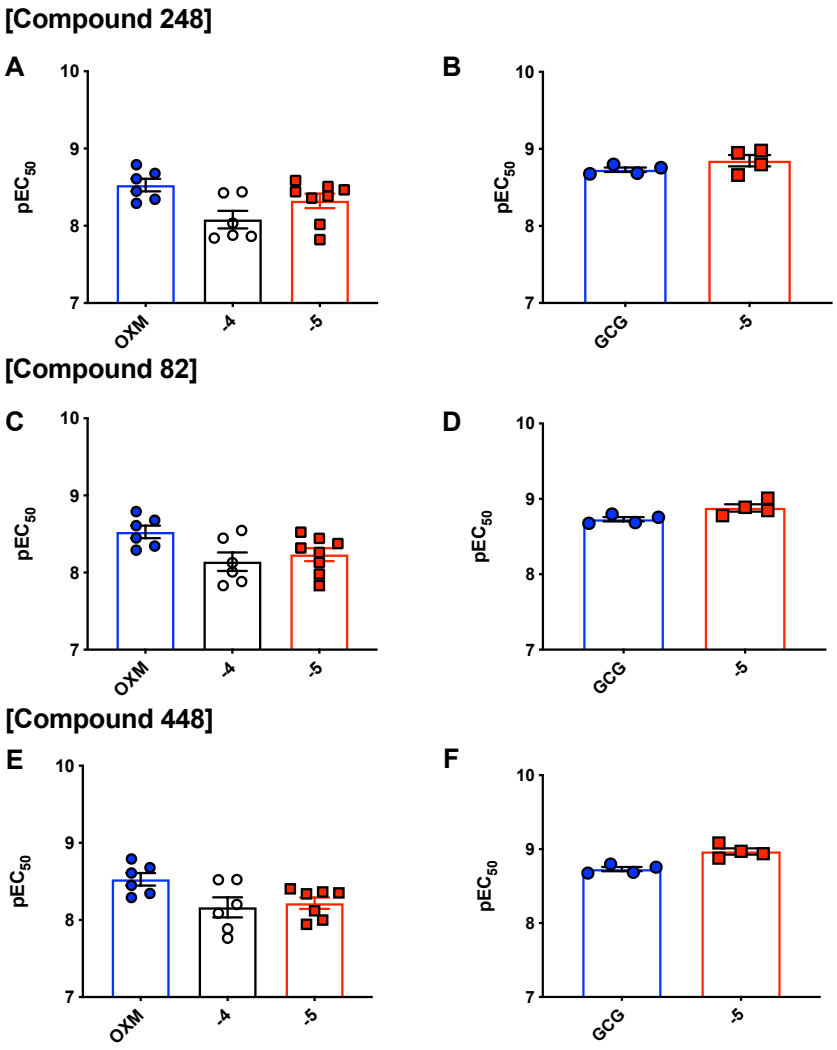

Figure B.11: **Scatter plots illustrating compound 249 analogues do not induce allosteric modulation on OXM or GCG-mediated cAMP accumulation in CHO-GLP-1R cells.** Panel A, C and E show that compound 248, 82 and 448 do not potentiate OXM-mediated cAMP accumulation even when high concentration at 10^{-4}M was applied to the CHO-GLP-1R cells. Similarly, panels B, D, and F show that these analogues are not allosteric modulators on GCG-mediated cAMP accumulation. 500 CHO-GLP-1R cells/well under 15-minute co-stimulation with peptide ligands in the presence of rolipram were used in the cAMP assays. All data were normalised to the maximum cAMP response determined by 100μM forskolin stimulation. All data are means from at least 2 independent experiments with duplicates $\pm$ S.E.M (upper error bars).

B.5 Compound 607 does not inhibit GSIS in high glucose settings

Given the interesting profile of compound 607 as a NAM of GLP-1 and OXM-mediated cAMP responses, its potential action on GLP-1 and OXM-mediated GSIS were next explored. Similar to the approach in investigating compound 249 potentiation of insulin secretion, compound 607 was also applied to low and high glucose settings.

Here compound 607 did not appear to alter the extent of insulin secretion in low glucose setting, and it also did not affect insulin secretion in high glucose settings (Fig. B.12), suggesting it did not act as a potentiator of insulin secretion in the presence of glucose stimuli alone.

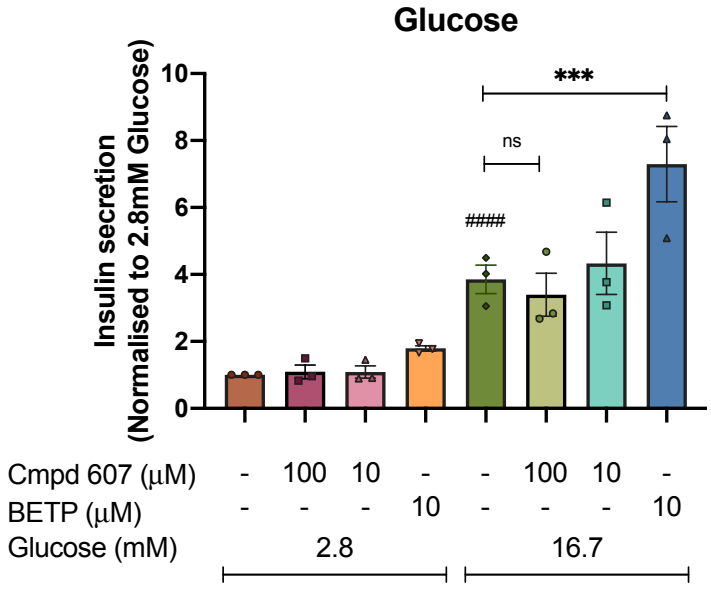

Figure B.12: **Compound 607 does not affect GSIS in INS-1 832/3 WT cells.** Compound 607 does not facilitate GSIS while BETP enhances GSIS in the presence of 16.7mM glucose in INS-1 832/3 WT cell line. Mean ± S.E.M. insulin secretion data (responses normalised to the GSIS secretion responses at 2.8mM respectively) in 3 independent experiments with quadruplicates are shown in the above scatter plots. Statistical significance compared between response at 2.8mM and 16.7mM glucose in the INS-1 832/3 WT cell lines were determined by Student's t-test with Welch's correction and are indicated by hash above the bars (####, $p<0.0001$). Statistical significance compared between responses with or without the presence of compounds at 16.7mM glucose in insulin secretion assays respectively were determined by Student's t-test with Welch's correction and are indicated by asterisks above the bars (***, $p<0.001$; ns, non-statistically significant).

B.6 Compound 607 inhibits GLP-1 and OXM-mediated GSIS

Similar to the determination of compound 249 actions on GLP-1R agonists-mediated GSIS, the INS-1 832/3 WT cells were incubated with compound 607 at both 100μM and 10μM for an hour, before insulin secretion measurement. BETP was again included as a positive control. Contrary to the action of compound 249 in enhancing GLP-1-mediated GSIS, compound 607 at 100μM illustrated inhibition of GLP-1-mediated GSIS, with a reduction of 1.43-fold ($p < 0.05$) (Fig. B.13A). Similar effect was also observed in OXM-mediated GSIS, where compound 249 at 100μM decreased GSIS by 1.21-fold ($p < 0.05$) (Fig. B.13B). Interestingly, compound 607 also did not affect Ex-4-mediated GSIS, similar to the results of compound 249. The GSIS results here also illustrated compound 607 inhibition of GSIS is ligand dependent.

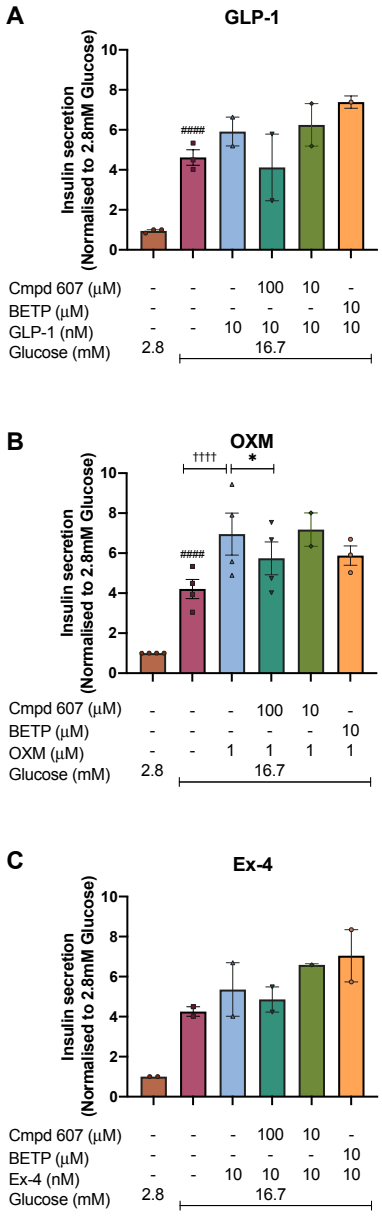

Figure B.13: **Compound 607 inhibits GSIS mediated by GLP-1 and OXM in INS-1 832/3 WT cells.** Compound 607 inhibits GSIS while BETP enhances GSIS in the presence of 16.7mM glucose in INS-1 832/3 WT cell line. Mean ± S.E.M. insulin secretion data (responses normalised to the GSIS secretion responses at 2.8mM respectively) in 1 to 3 independent experiments with quadruplicates are shown in the above scatter plots. Statistical significance compared between responses at 2.8mM and 16.7mM glucose among the INS-1 832/3 WT cell lines were determined by Student's t-test with Welch's correction and are indicated by hash above the bars (####, $p < 0.0001$). Statistical significance compared among the peptide ligand influence on GSIS in INS-1 WT cells were determined by one-way ANOVA with Bonferroni's corrections compared with the mean of the WT group and are indicated by obelisk above the bars (++++, $p < 0.0001$). Statistical significance compared between responses with or without the presence of peptide ligands at 16.7mM glucose in insulin secretion assays respectively were determined by Student's t-test with Welch's correction and are indicated by asterisks above the bars (*, $p<0.05$).

B.7 Use of NanoBiT Technology to investigate compound 249 effect on G protein dissociation

B.7.1 Principle of NanoBiT G protein dissociation assay

The NanoLuc® Binary Technology (NanoBiT) is based on NanoLuc, which is an engineered luciferase from the deep-sea shrimp Oplophorus gracilirostris. It facilitates the real-time measurement of G protein dissociation between the heterotrimeric Gα and G$\beta\gamma$ subunits upon receptor activation. The NanoBiT system consists of two small units, Large BiT (LgBiT) and Small BiT (SmBiT) of the luciferase. Here, the LgBiT component is fused to the Gα subunit while the SmBiT is fused to the G$\beta\gamma$ subunits. Whilst the receptor is at its resting state, the Gα and G$\beta\gamma$ subunits are associated, facilitating the LgBiT and SmBit subunit complementation to generate bright luminescent signal. However, when the receptor is activated (e.g. when GLP-1R is activated by GLP-1), the dissociation of the heterotrimeric Gα and G$\beta\gamma$ subunits is triggered, resulting in a lack of complementation of the two NanoLuc subunits; therefore no luminescence is resulted (Fig. B.14).

To determine the dose-dependent effect on G protein dissociation, a range of concentrations of GLP-1 is applied to the GLP-1R. The reduction in luminescence measured over time in terms of the area under the curve (AUC) of each individual GLP-1 concentration was collated and transformed into a concentration-dependent curve (Fig. B.14). The results obtained are then normalised to the AUC value of the vehicle control.

B.7.2 Methods of the NanoBiT G protein dissociation assay

The following methods were received with courtesy from Dr Matthew Harris (Department of Pharmacology, University of Cambridge). 250,000 HEK293ΔAll (a cell line with all G proteins knocked out using CRISPR-Cas9 technology) cells stably expressing GLP-1R were seeded into 10 cm dishes and cultured for 24 hours. Cells were then transiently transfected with appropriate Gα-LgBiT, Gβ_1 and Gγ_2-SmBiT at a 1:3:3 ratio (0.5μg: 1.5μg: 1.5μg). For Gα_q subunit, cells were also transfected with 1μg of RIC8A, a chaperone protein required for Gα_q family signalling [Miller et al., 2000]. 24 hours after transfection, cells were harvested and seeded at a density of 60,000 cells per well into poly-D-lysine (PDL) coated clear-bottomed 96 well plates (Corning). After a further 24 hours, media was removed, cells were washed with HBSS plus 10mM

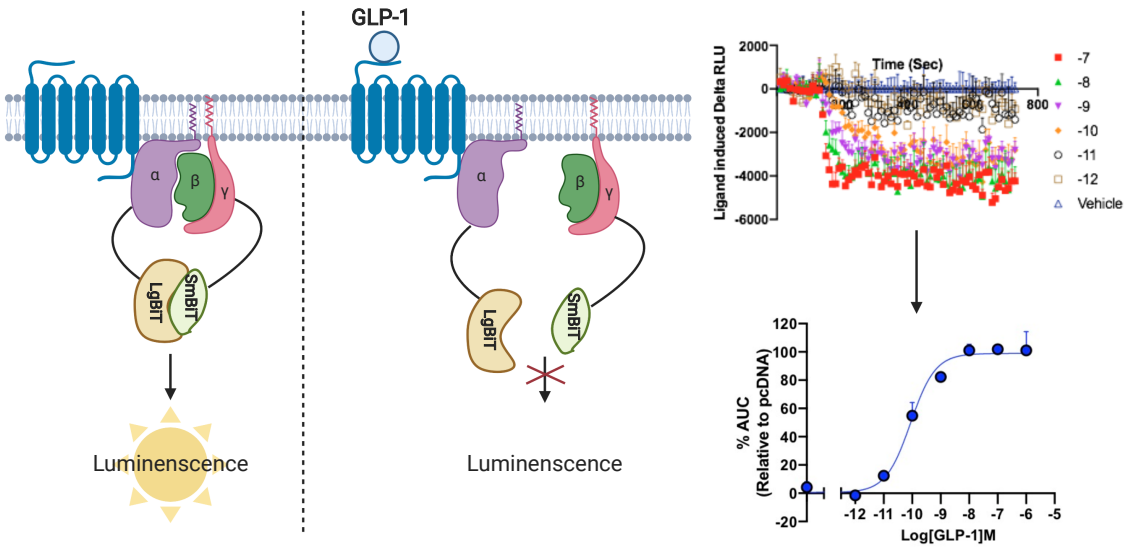

Figure B.14: **Principle of NanoBiT G protein dissociation assay.** When the receptor is at its resting state, the Gα and G$\beta\gamma$ subunits are associated, facilitating the LgBiT and SmBit subunit complementation to generate bright luminescent signal. However, when the receptor is activated, the dissociation of the heterotrimeric Gα and G$\beta\gamma$ subunits is triggered, resulting in a lack of complementation of the two NanoLuc subunits; therefore no luminescence is resulted. Schematic diagram modified from the original concept from Dr Matthew Harris (Department of Pharmacology) and was created using Biorender.

HEPES and 80μl HBSS, containing 10mM HEPES and 0.1% BSA, was added to each well. Compound 249 was diluted in HBSS, containing 10mM HEPES and 0.1% BSA, to a concentration of 10μM and 80μl added to each well. 10μl of Coelenterazine-h (diluted in HBSS, containing 10 mM HEPES, 0.1% BSA and 10μM compound 249 was then added to each well to a final concentration of 5μM, and the plate incubated for 1 hour in the dark. Ligands were diluted in HBSS, containing 10mM HEPES, 0.1% BSA and 10μM compound 249, to the desired concentration. After incubation, a baseline luminescence level was determined for 2 minutes using a Hamamatsu Functional Drug Screening System (FDSS). Ligands were then robotically added in the appropriate range and luminescence measured every 10 seconds for 10 minutes. Ligand-induced delta luminescent units were corrected to baseline and vehicle, and the AUC used to generate concentration-response curves. G protein dissociation is expressed as a percentage of the maximum response observed.

The results (Fig. B.15 and B.16) of compound 249 allosteric effect on G protein dissociation measured using the assay described above were interpreted in Section 5.8.2.

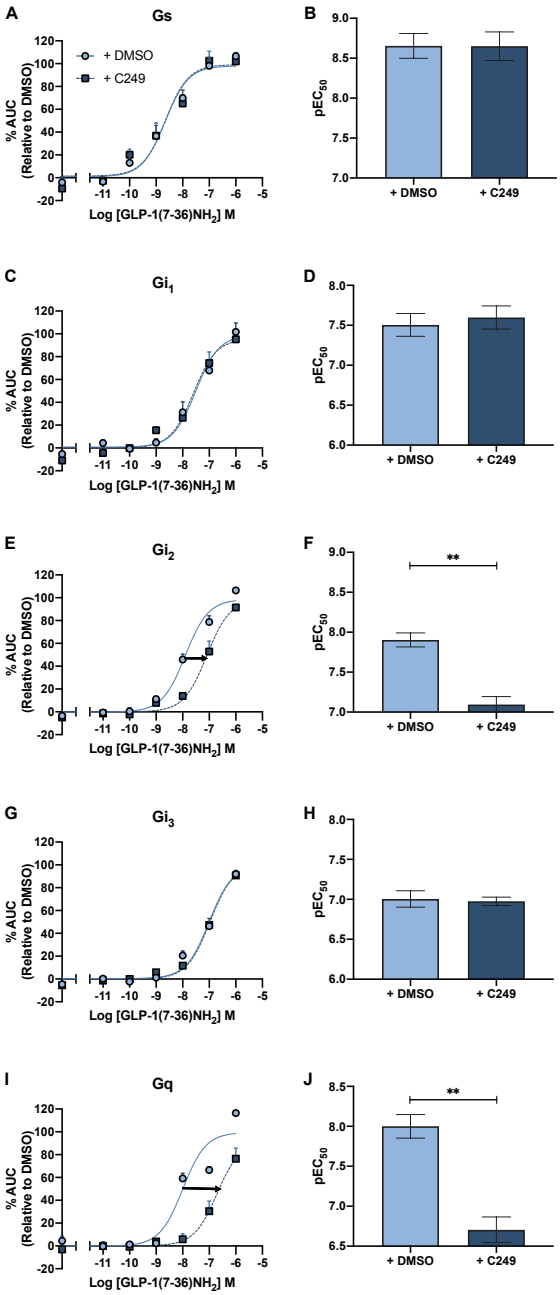

Figure B.15: **Compound 249 displays negative allosteric modulation in Gα_{i2} and Gα_q protein dissociation upon GLP-1R activation by GLP-1.** (A) Gα_s, (C) Gα_{i1}, (E) Gα_{i2}, (G) Gα_{i3} and (I) Gα_q protein dissocation upon GLP-1R activation by GLP-1 in the presence of compound 249 was investigated using the NanoBiT G protein dissociation assay, performed by Dr Matthew Harris (Department of Pharmacology, University of Cambridge). Dose response curves were generated by converting the area-under-the-curve (AUC) of each GLP-1 concentration. The AUC values were then normalised to that of DMSO control. All data are means from at least 2 independent experiments ± S.E.M. The pEC_{50} values with or without compound 249 effect on (B) Gα_s, (D) Gα_{i1}, (F) Gα_{i2}, (H) Gα_{i3} and (J) Gα_q protein dissociation were shown in the above scatter plots. Statistical significance compared the pEC_{50} responses with or without compound 249 respectively were determined by Student's t-test with Welch's correction and were indicated by asterisks above the bars (**, $p<0.01$).

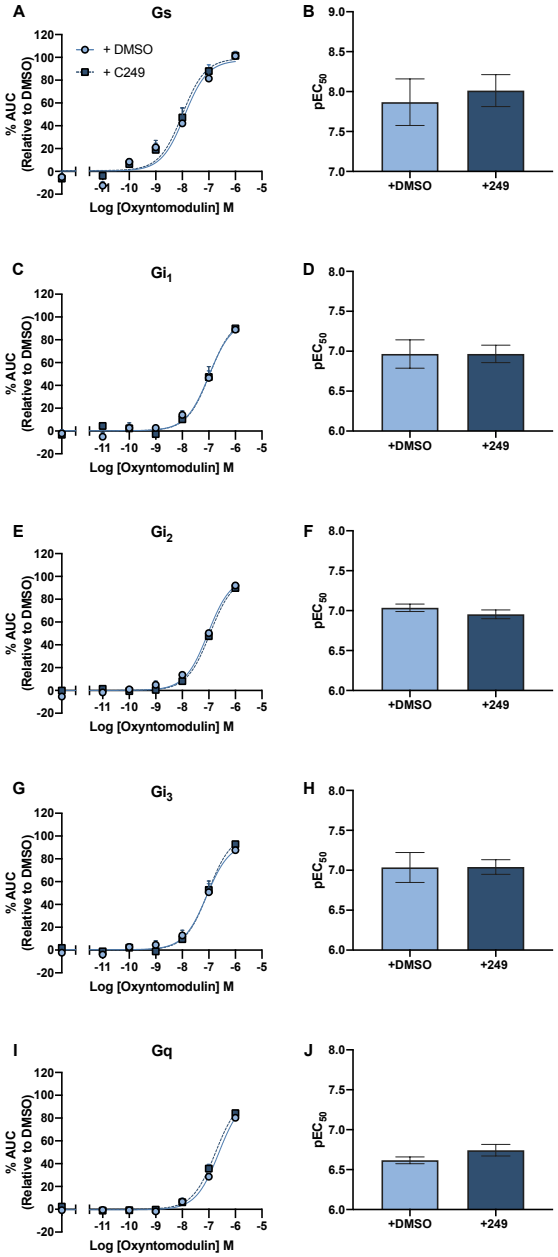

Figure B.16: **Compound 249 does not affect G protein dissociation upon GLP-1R activation by OXM.** (A) Gα_s, (C) Gα_{i1}, (E) Gα_{i2}, (G) Gα_{i3} and (I) Gα_q protein dissocation upon GLP-1R activation by OXM in the presence of compound 249 was investigated using the NanoBiT G protein dissociation assay, performed by Dr Matthew Harris (Department of Pharmacology, University of Cambridge). Dose response curves were generated by converting the area-under-the-curve (AUC) of each OXM concentration. The AUC values were then normalised to that of DMSO control. All data are means from at least 2 independent experiments $\pm$ S.E.M. The pEC_{50} values with or without compound 249 effect on (B) Gα_s, (D) Gα_{i1}, (F) Gα_{i2}, (H) Gα_{i3} and (J) Gα_q protein dissociation were shown in the above scatter plots. Statistical significance compared the pEC_{50} responses with or without compound 249 respectively were determined by Student's t-test with Welch's correction and were indicated by asterisks above the bars (**, $p<0.01$).

B.8 *In silico* docking results of compound 249 to GLP-1R

B.8.1 Sources for GLP-1R, GCGR and small molecule 3D compound structures

Structures of full-length GLP-1R crystal structures were obtained from RCSB protein data bank (PDB) (https://www.rcsb.org). The structures for GLP-1R were energy-minimised and were clear of any lipoproteins or water molecules attached to the structures before performing docking studies. The table below outlined GLP-1R (Table B.4) crystal structures used in the docking studies.

The 3D conformation of compound 249 was obtained from the NCBI PubChem inventory (https://pubchem.ncbi.nlm.nih.gov) identified by the compounds' unique Z numbers. The 3D conformation of compound 249 was converted to its lowest energy forms by using the energy minimization force field 'mmff94' option available in OpenBabel (version 2.4.0.) before docking with the refined receptor crystal structures of interests.

Table B.4: **Full-length cryo-EM crystal structures of GLP-1R used in molecular modelling.**

PDB code	Description	Reference
5NX2	Crystal structure of human GLP-1 receptor bound to the 11-mer agonist peptide 5	Jazayeri et al., 2017
5VAI	Cryo-EM structure of active rabbit GLP-1 receptor in complex with GLP-1 and Gs protein	Zhang et al., 2017

B.8.2 Methods of *in silico* docking

In silico docking were performed initially via the open-source programme Autodock Vina [Trott and Olson, 2010] by Dr Taufiq Rahman (Department of Pharmacology, University of Cambridge). Blind docking was adopted during which specific binding site on the receptor was not specified and the entire receptor models were used to predict any possible receptor-ligand interactions. The exhaustiveness for the search was set to 24 and five independent docking were performed for each compound candidate on specific receptor conformations of interest. The poses with the highest binding affinity (kcal/mol) were considered to be the final pose for each drug. The corresponding 2D ligand-protein interaction was predicted using PoseView available in the Proteins.Plus platform (https://proteins.plus).

B.8.3 Predicted binding poses of compound 249 at the GLP-1R

As stated in Section 5.8.3, three potential binding sites of compound 249 at the GLP-1R were suggested. Compound 249 was predicted to bind to the ECD and ECL1 (model 1) (Fig. B.17), ECL2 (model 2) (Fig. B.18) and TM3 and 4 core (model 3) (Fig. B.19). The implications of the predictions are discussed in Section 5.8.3. Fig. B.20 summaries the potential amino acid interactions using the snake-plot representations.

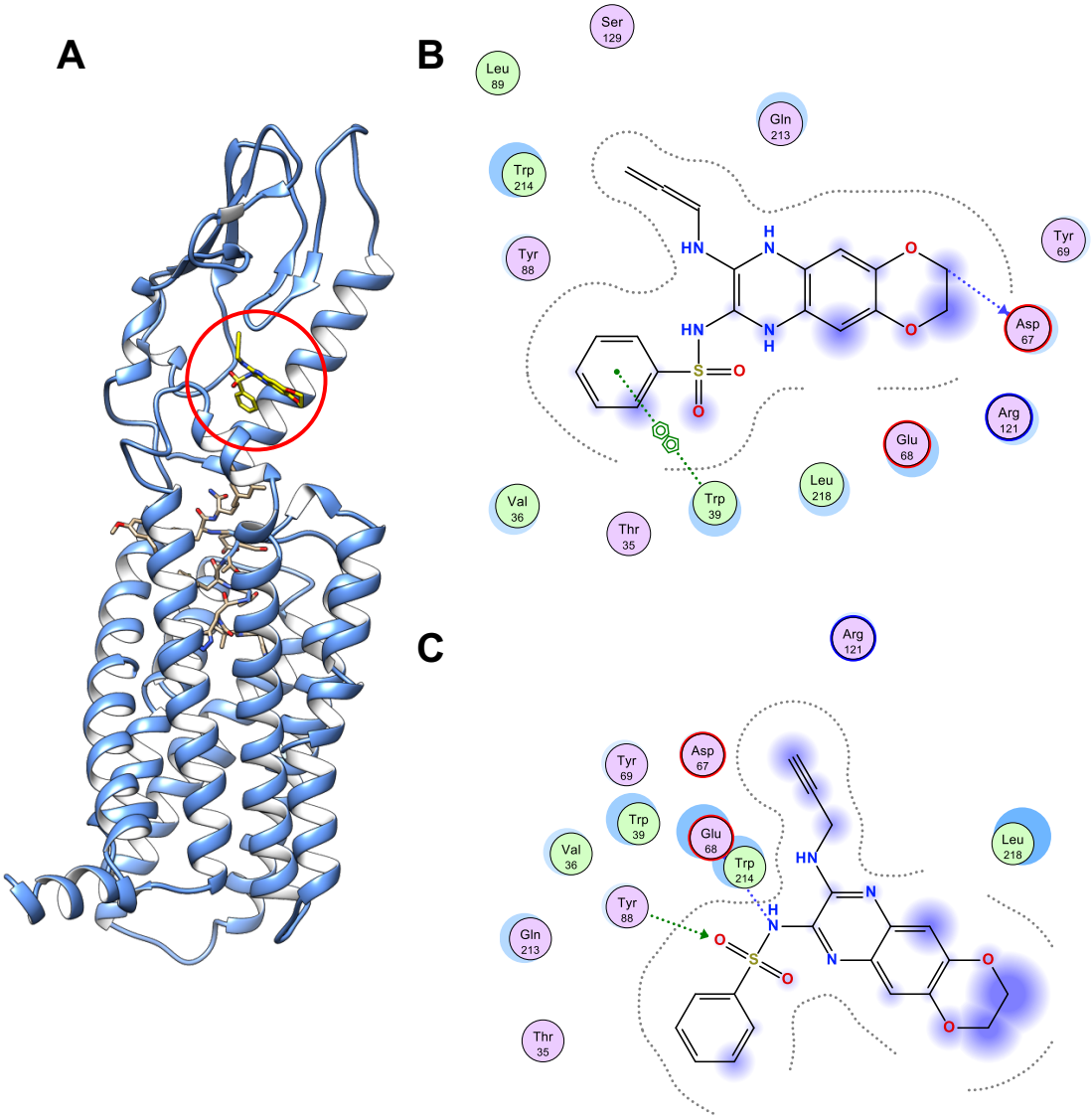

Figure B.17: **Compound 249 *in silico* docking at the GLP-1R (Pose 1).** (A) Compound 249 was docked against the full length GLP-1R crystal structures (PDB: 5NX2) with the use of ICM gold software. (B) and (C) show the prediction of potential amino acid interaction with compound 249 by the use of the Vina Pose and ICM pose software. The *in silico* docking was conducted by Dr. Taufiq Rahman.

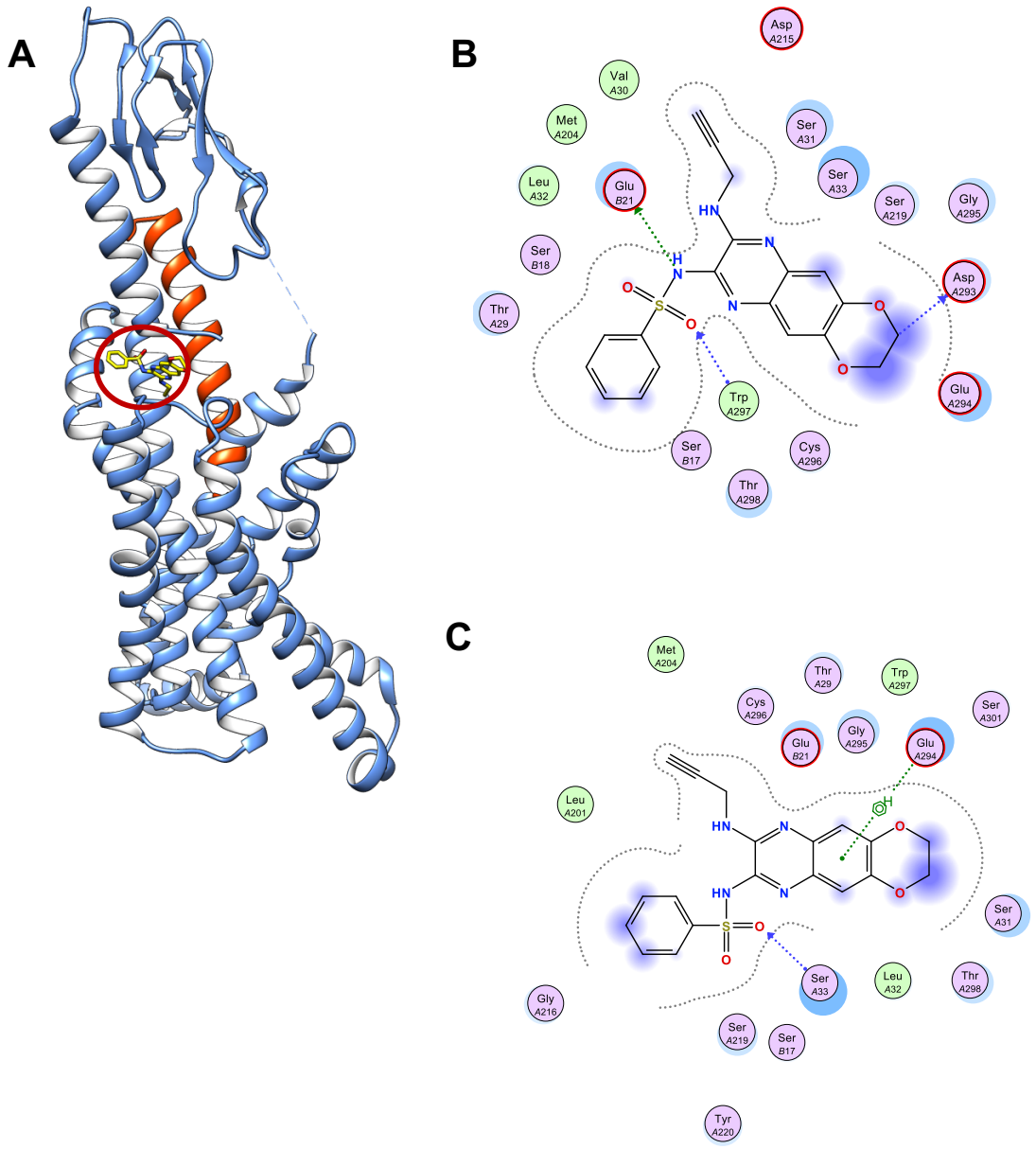

Figure B.18: **Compound 249 *in silico* docking at the GLP-1R (Pose 2).** (A) Compound 249 was docked against the full length GLP-1R crystal structures (PDB: 5VAI) with the use of ICM pose with GOLD-based refinement. (B) and (C) show the prediction of potential amino acid interaction with compound 249 by the use of the Vina Pose and ICM pose software. The *in silico* docking was conducted by Dr. Taufiq Rahman.

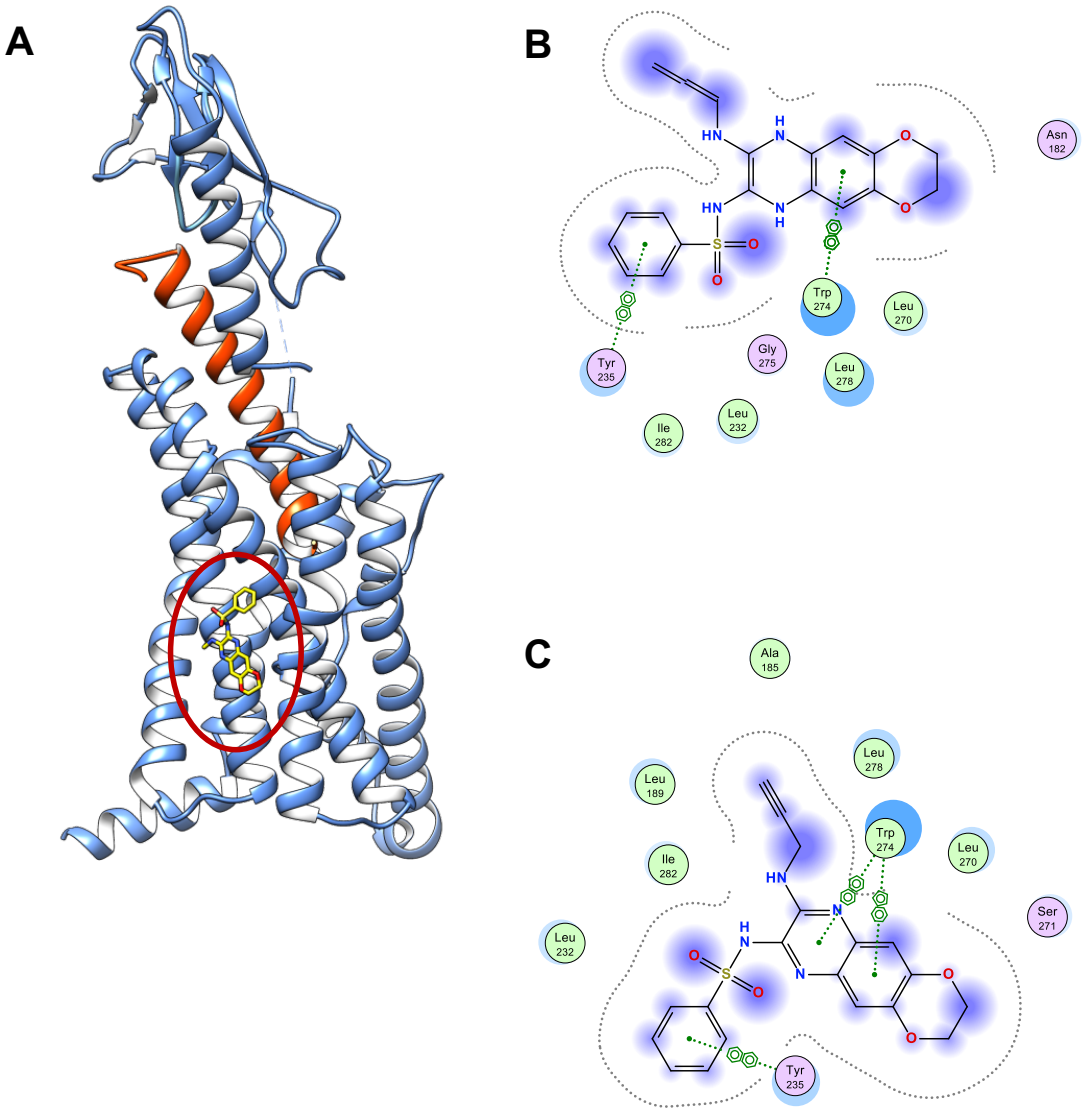

Figure B.19: **Compound 249 *in silico* docking at the GLP-1R (Pose 3).** (A) Compound 249 was docked against the full length GLP-1R crystal structures (pdb: 5VAI) with the use of VinaPose with GOLD-based refinement. (B) and (C) show the prediction of potential amino acid interaction with compound 249 by the use of the Vina Pose and ICM pose software. The *in silico* docking was conducted by Dr. Taufiq Rahman..

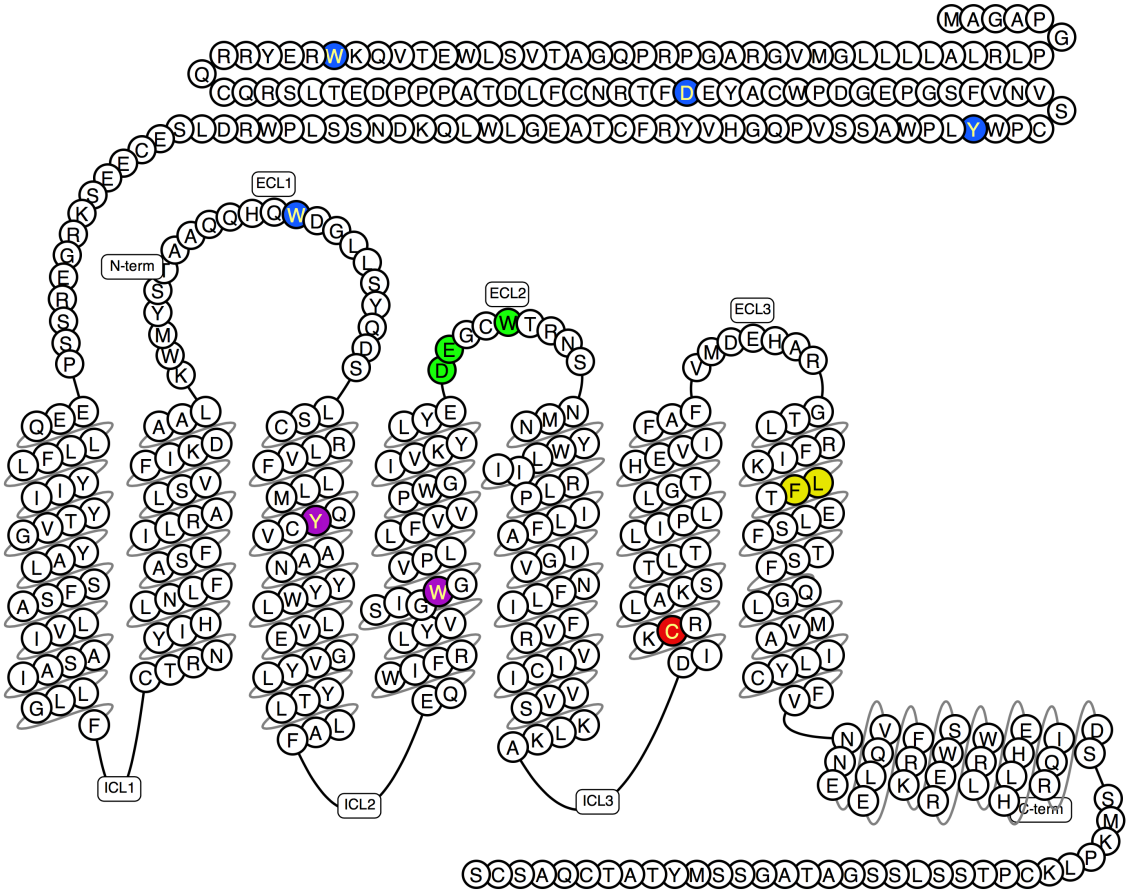

Figure B.20: **Compound 249 potential interacting residues at the GLP-1R as predicted by *in silico* docking.** The residues highlighted in blue represent the prediction using the PDB model 5NX2; the residues highlighted in purple represent the prediction using the PDB model 5VAI with the use of AutoDOCK vina followed by GOLD-based refinement. The residues highlighted in green represent the prediction using the PDB model 5VAI with the use of ICM Pro docking followed by GOLD-based refinement. The residue in red highlights the position of the C347 residue while the residues in yellow show the interacting residues on the GLP-1R with its orthosteric agonist GLP-1. All *in silico* docking were conducted by Dr Taufiq Rahman.